UNIVERSITY OF SOUTHAMPTON

FACULTY OF NATURAL AND ENVIRONMENTAL SCIENCES

School of Chemistry

Understanding Cyclobutenone Rearrangements:

An *in silico* Study

by

Théo Piechota Gonçalves

September 2014

A Thesis Submitted for the Degree of Doctor of Philosophy

UNIVERSITY OF SOUTHAMPTON

ABSTRACT

Faculty of Natural and Environmental Sciences

School of Chemistry

Doctor of Philosophy

Understanding Cyclobutenone Rearrangements:

An *in silico* study

By Théo Piechota Gonçalves

The work described in this thesis sheds new light on the mechanistic pathways followed during thermochemically and photochemically induced cyclobutenone rearrangements through an understanding of thermodynamic and kinetic aspects. The investigation applies DFT and *ab initio* methods to various rearrangements studied in the laboratory. Energy pathways for various cyclobutenone rearrangements have been developed to rationalise selectivity issues where competitive mechanisms are available. In addition, we have developed models to account for different outcomes observed for organometallic additions to cyclobutenediones. These have, in particular, led to a better understanding of the course of carbonyl addition reactions given by organoytterbium reagents.

Table of Contents

Academic Thesis: Declaration Of Authorship

I, Théo Piechota Gonçalves declare that this thesis and the work presented in it are my own and has been generated by me as the result of my own original research.

Understanding Cyclobutenone Rearrangements: An *in silico* Study

I confirm that:

1. This work was done wholly or mainly while in candidature for a research degree at this University;
2. Where any part of this thesis has previously been submitted for a degree or any other qualification at this University or any other institution, this has been clearly stated;
3. Where I have consulted the published work of others, this is always clearly attributed;
4. Where I have quoted from the work of others, the source is always given. With the exception of such quotations, this thesis is entirely my own work;
5. I have acknowledged all main sources of help;
6. Where the thesis is based on work done by myself jointly with others, I have made clear exactly what was done by others and what I have contributed myself;
7. Parts of this work have been published as:

M. Mohamed, T. P. Gonçalves, R. J. Whitby, H. F. Sneddon, D. C. Harrowven, *Chem. Eur. J.* **2011**, *17*, 13698–13705.

D. C. Harrowven, M. Mohamed, T. P. Gonçalves, R. J. Whitby, D. Bolien, H. F. Sneddon, *Angew. Chem. Int. Ed.*, **2012**, *51*. 4405–4408.

W. J. Buffham, N. A. Swain, S. L. Kostiuk, T. P. Gonçalves, D. C. Harrowven, *Eur. J. Org. Chem*. **2012**, *6*, 1217–1222.

E. Packard, D. D. Pascoe, J. Maddaluno, T. P. Gonçalves, D. C. Harrowven, *Angew. Chem. Int. Ed.*, **2013**, *49*, 13314–13317.

Signed: ……

Date: ……

Preface

The research in this thesis was carried out under the supervision of Prof. D. C. Harrowven at the University of Southampton between 2010 and 2014.

Acknowledgements

I CLAIM NOT TO HAVE CONTROLLED EVENTS,
BUT CONFESS PLAINLY THAT EVENTS HAVE CONTROLLED ME.
A. LINCOLN

I would kindly like to thank Prof. David Harrowven for the opportunity to undertake this work under his supervision at The University of Southampton. I greatly appreciate the intensive meetings, discussions and reflections on ambiguous problems and for bringing this thesis to a readable state.

Special thanks to Dr. Edmond Lee for spiritual and scientific support during times when problems seemed intractable and for his helpful suggestions in respect of this thesis. I also thank my PhD colleagues Jason Petrou, Emma Packard and Mubina Mohamed for introducing me to squarate chemistry and for their tireless experimental support on joint projects, and Zeshan Yousuf for years of discussion-debates-fights about mechanism during lunch. Thanks must also be given to Julien Marchois who shared his computational pain with me, and to Gabriella Barozzino for introducing me to some of the more exotic aspects of organolithium chemistry during my fruitful placement in France under the supervision of Jacques Maddaluno.

This work would not have been possible without the *IRIDIS High Performance Computing Facility*, which provided much of the computer power needed for the calculations. I thank the outstanding team running this facility, especially David Baker, Ivan Wolton and Elena Vataga. I am also grateful to the *EPSRC UK National Service for Computational Chemistry Software* (*NSCCS*) at Imperial College London for the computer power given and the support offered by their fantastic staff, especially Alexandra Simperler and Helen Tsui, including some very stimulating workshops and meetings.

I gratefully acknowledge ERDF for their financial support of the IS:CE-Chem project via the InterReg IVa program 4061 and The University of Southampton for addition support. I thank all my colleagues from the Harrowven laboratory who gave me companionship during the time of this work and everyone who supports/develops free of charge computational chemistry software, without which this work would be difficult. It is impossible to list you all…

Finally I must thank my Sister, Mother, Father, Pawel, Thiago and …my dog Alex

for all their support and understanding. Though non-scientific, it contributed significantly to my work. At the very end I thank all my PCs, laptops, working stations and HPCs for SURVIVING THIS …and at the same time I apologise to Mother Earth for my computational carbon footprint.

Dedication

I dedicate this work to my family.

Science is cool
like a swimming pool…

by Thiago Gonçalves-Miśkiewicz

List of abbreviations

THERE IS NOTHING IN A CATERPILLAR THAT TELLS YOU IT'S GOING TO BE A BUTTERFLY.
R. BUCKMINSTER FULLER

Ac	acetyl
AIM	the quantum theory of atoms in molecules.
aq	aqueous
Ar	aryl
B3LYP	Becke 3-Parameter, Lee, Yang and Parr DFT method
BCP	bond critical point in QTAIM
Bn	benzyl
BS	broken-symmetry
Bu	butyl
CCSD(T)	Coupled-Cluster Singles Doubles and Non-iterative Triples Correction method
CHELPG ESP	charges from electrostatic potentials using a grid based method
cm^{-1}	wavenumber
COSMO	conductor-like screening model solvation method
CPCM	conductor-like screening model implemented in the PCM framework solvation method
Δ	heat or delta
$\nabla^2\rho_{(b)}$	Laplacian of electron density at bond critical point
d.r.	diastereomeric ratio
DBU	1,8-diazabicyclo[5.4.0]undec-7-ene
DCM	dichloromethane
DFT	density functional theory
DMF	*N*,*N*-dimethylformamide
E(2)	stabilization energy from NBO analysis
equiv.	molar equivalents
ECP	effective core potential
EDG	electron donating group
EWG	electron with drawing group
$f^+(r)$	Fukui function for nucleophilic attack
FBO	Fuzzy bond order
F12-CCSD	explicitly-Correlated Coupled-Cluster
G(T)	Gibbs free energy at T temperature
GS	ground state
HF	Hartree–Fock method
HOMO	Highest occupied molecular orbital.
HMTETA	hexamethyltriethylenetetramine
i	iso
IEFPCM	integral equation formalism polarizable continuum model solvation method
IRC	intrinsic reaction coordinate calculation
LUMO	lowest unoccupied molecular orbital.
MAE	mean absolute error

MD	molecular dynamic
Me	methyl
MEP	molecular electrostatic Potential mapped onto the molecular electron density
MP2	Møller–Plesset perturbation theory second order
MUE	Mean Unsigned Error
NBO	natural bond orbital
NICS	nucleus-independent chemical shift
NMR	nuclear magnetic resonance spectroscopy
n_p	p-rich lone pair
n_s	s-rich lone pair
[O]	oxidation
ONIOM	n-layered integrated molecular orbital and molecular mechanics
PES	potential energy scan
Ph	phenyl
PMDT	bis[2-(dimethylamino)ethyl](methyl)amine
Py	pyridyl
QM	quantum mechanic
QM/MM	quantum mechanic / molecular mechanic
QM/QM	quantum mechanic / quantum mechanic
$\rho_{(b)}$	electron density at bond critical point
RDG	reduced density gradient
RI	resolution of identity
RMSE	root mean square error
RMSD	root-mean-square deviation
RT	room temperate
SEM	[2-(trimethylsilyl)ethoxy]methyl
SHOMO	second highest occupied molecular orbital
SLUMO	second lowest occupied molecular orbital.
SMD	universal solvation model base on density
SOMO	single occupied molecular orbital
t	tertiary
TBDMS	*tert*-butyldimethylsilyl
tert	tertiary
Tf	triflate
TFA	trifluoroacetic acid
TFAA	trifluoroacetic anhydride
Th	thienyl
THF	tetrahydrofuran
TMS	trimethylsilyl
TS	transition state
UBS	unrestricted broken spin-symmetry
viz.	videlicet
$V_{(r)}$	electronic potential energy at bond critical point
WFM	wavefunction method

Chapter 1: Introduction

1.1 The mechanistic course of cyclobutenone rearrangements

TRUTH IN SCIENCE CAN BE DEFINED AS THE WORKING HYPOTHESIS BEST SUITED TO OPEN THE WAY TO THE NEXT BETTER ONE.
KONRAD LORENZ

Cyclobutenone rearrangements provide a useful entry to many polyaromatic and heteroaromatic ring systems.[1] The first step usually involves a ring opening reaction leading to a vinylketene intermediate, *e.g.* **1.1** to enyne-ketene **1.2**. In the case of alkynyl cyclobutenones, this is followed by ring closure leading to diradical intermediate **1.3** and H-atom abstraction to give quinone **1.4**. As such, it belongs to a family of rearrangements that includes the Bergman (Ene-Diynes),[2] Myers (Enyne-Cumulenes)[3] Myers-Saito (Enyne-Allenes)[4, 3b] and Schmittel (Enyne-Allenes)[5] rearrangements (Figure 1.1).

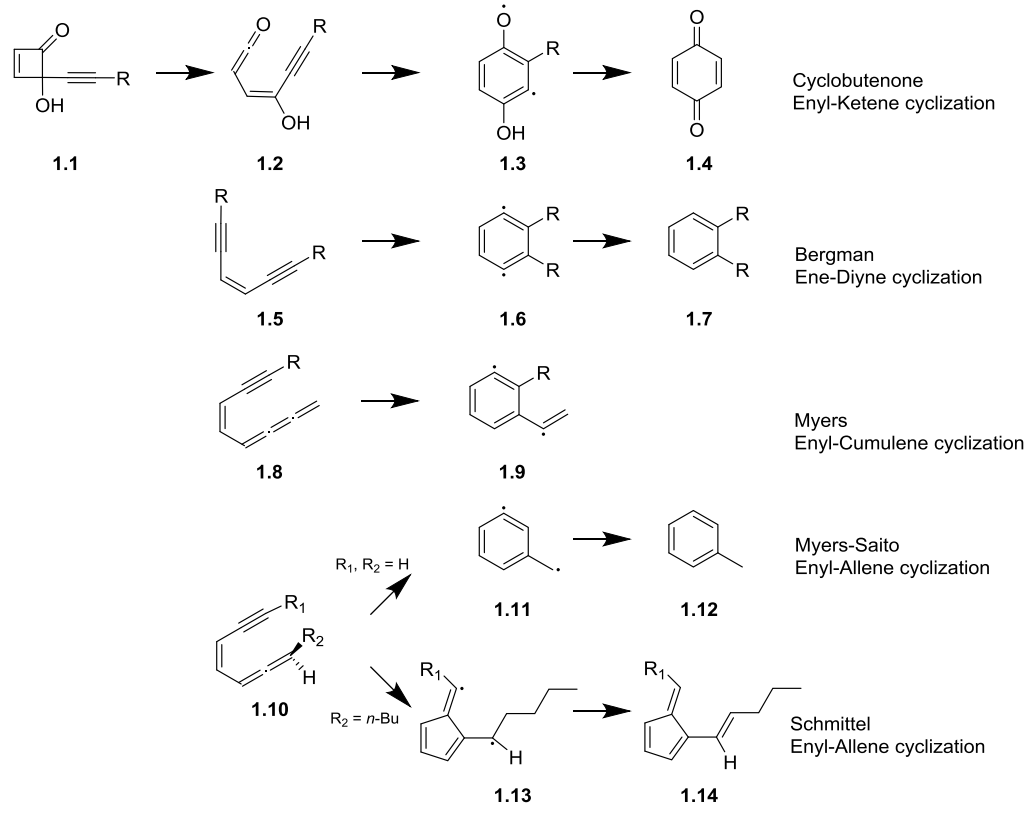

Figure 1.1. Family of thermal rearrangement reactions involving diradical intermediates.

The alkynylcyclobutenone rearrangement[6] did not gain as much attention as the Bergman and Myers-Saito rearrangement, due to the recognition that these processes

were responsible for the antibiotic activity and DNA cleavage abilities of several natural products containing the enediyne or enyneallene subunit. Nonetheless, cyclobutenone rearrangements have proven to be attractive in natural products total synthesis, particularly for the construction of compounds containing a quinone ring. Indeed, they feature as key steps in many target syntheses including mansonnone B **1.15**,[7] cribrostatin 6 **1.16**,[8] lomandrone **1.17**,[9] aristolindiquinone **1.18**,[9] (–)-colombiasin A **1.19**,[10] (–)-elisapterosin B **1.20**,[10] and khellinone[11] **1.21** (Figure 1.2).

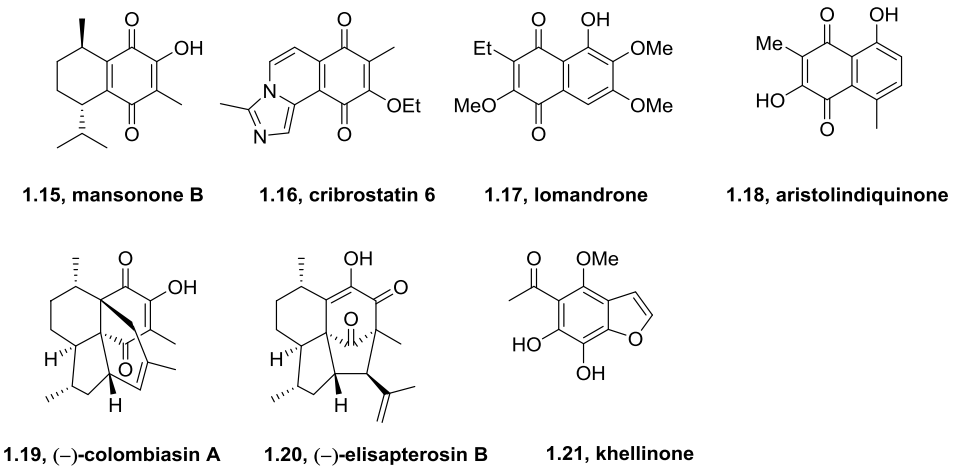

Figure 1.2. Some of the natural products synthetized by cyclobutenone rearrangement.

This atom efficient reaction generally involves thermolysis in a high boiling solvent such as 1,4-dioxane, chlorobenzene or *p*-xylene. The accepted mechanism for the alkynylcyclobutenone rearrangement first involves a torquoselective electrocyclic ring opening of the cyclobutenone **1.22** to a reactive vinylketene intermediate **1.25** (Scheme 1.1). An electrocyclic ring closure follows to give one of two possible σ,π-diradical intermediates, arene **1.26** or cyclopentadiene **1.27**. Formation of the aromatic diradical intermediate **1.26** is generally favoured when the alkyne bares an alkyl residue and is followed by an intramolecular hydrogen atom transfer leading to quinone **1.23**. However, when the alkyne bares a radical stabilising group, cyclisation favours formation of the cyclopentadiene diradical **1.27**, which goes on to form cyclopentenedione **1.24** after H-atom transfer.

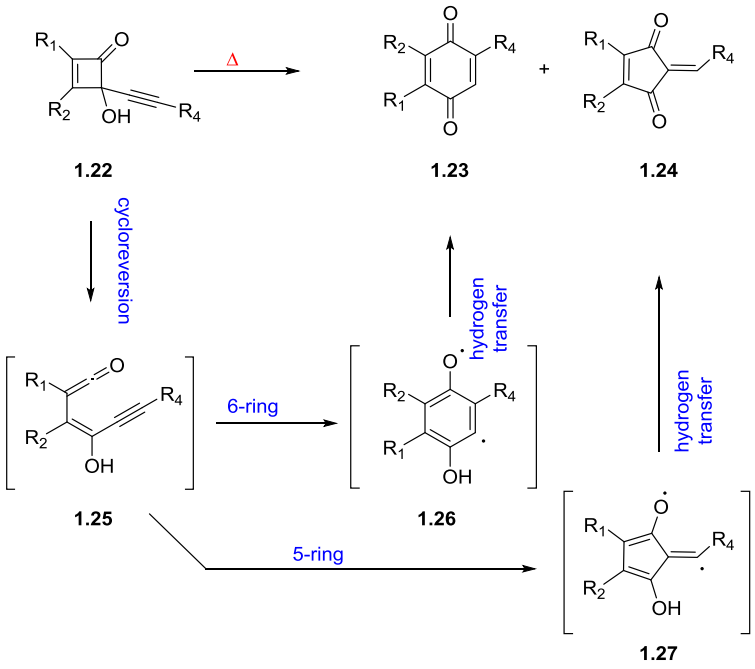

Scheme 1.1. Mechanism for the thermal rearrangement of 4-alkynylcyclobutenones.

This trend was demonstrated using various analogues of cyclobutenone **1.28** (Scheme 1.2). In each of the cases studied, alkynes with aliphatic substituents (R), led to the corresponding quinone **1.29**. By contrast, when a phenyl residue was attached to the alkyne, formation of cyclopentenedione was favoured[12a, b, 6, 12c]. The cyclopentenedione ring was also observed when **1.28** was treated with Pb^{2+} salt.[13] However, as this reaction proceeds by a different mechanistic pathway, it will not be considered in detail here.

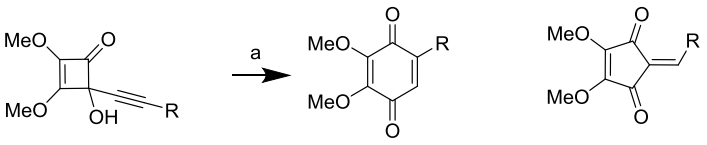

1.28a, R = n-C_4H_9 78%
1.28b, R = CH_2Ph 71%
1.28c, R = Ph 21%

46%

a) 138 °C, *p*-xylene.

Scheme 1.2. The influence of substituents on the thermal rearrangements of alkynylcyclobutenones.

Further studied performed by Zora and co-workers found that ferrocenyl substituents, such as in **1.31**, show a greater tendency for formation of five membered rings (Scheme 1.3).[14] This was explained by their greater ability to stabilise conjugated radical intermediates compared to a phenyl ring.[15] The authors investigate a range of conditions and in each case the corresponding cyclopentenedione **1.33** was provided as the major product.

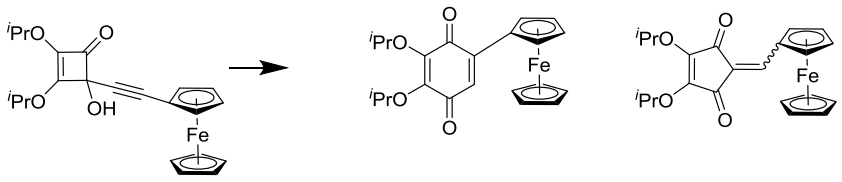

1.31 **1.32** **1.33**

Conditions:		
Dioxane, 100 °C, 4 h	2%	70%
SiO_2, 125 °C,15 min		67%
SiO_2, ethyl acetate 25 °C, 24 min		34%

Scheme 1.3. Thermolysis of 2-ferrocenylidenecyclopentenediones.

With unsymmetrical systems, such as **1.34**, the authors observed *E*-*Z* isomerisation of the alkene joining the side chain to the five membered ring (Scheme 1.4). Experiments appeared to support their hypothesis that rotation of the double bond was possible due to a high contribution from the zwitterionic mesomeric forms **1.35**/**1.36**.

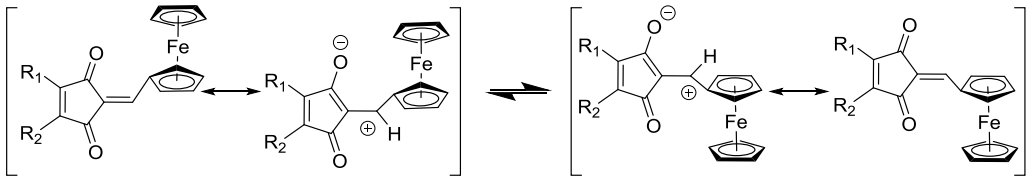

1.34 **1.35** **1.36** **1.33**

Scheme 1.4. Proposed mechanism for the (*E*)-(*Z*) isomerisation of 2-ferrocenylidenecyclopentenediones.

It is notable that a number of 2-methylene-4-cyclopentene-1,3-diones **1.37** have been found to exhibit anticancer activity (Figure 1.3). Benzylidene derivatives such as **1.38** were shown to display particularly potent antitumor activities by Inayama and co-workers.[16] Later, Hori and co-workers synthesised TX-1123 (**1.39**) and TX-1925 (**1.40**) as new antitumor agents,[17] perhaps inspired by the realisation that several natural products containing this pharmacophore displayed useful antitumor and/or antifungal activity. These include lucidone **1.42** and linderone **1.44**, their methyl derivatives methyllucidone **1.43** and methyllinderone **1.45**,[18] and coruscanone A **1.41**.[19]

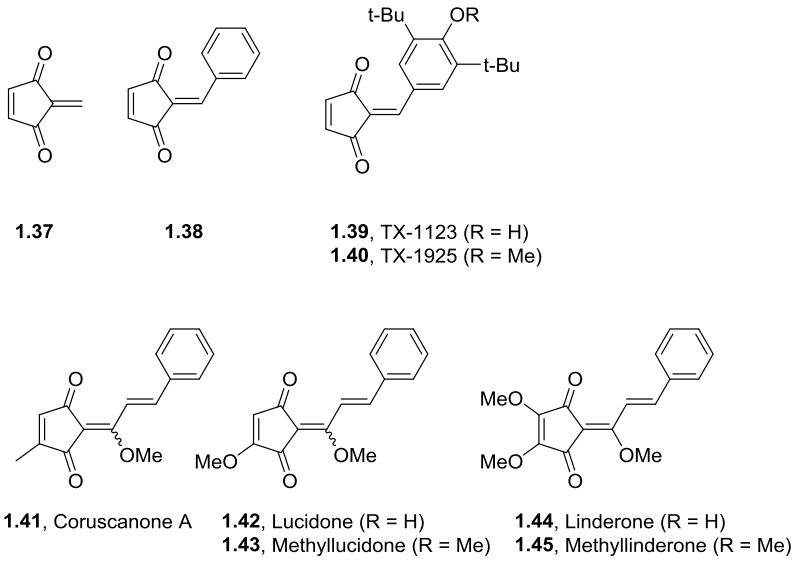

Figure 1.3. Structures of 2-ethylene-4-cyclopentene-1,3-diones and related molecules.

The influence of diradical stabilisation on the course of these reactions extends to the related rearrangements of alkynylcyclobutenimines. For example, condensed arene **1.50** was the only observed product on thermolysis of cyclobutenimine **1.46** (Scheme 1.5). This outcome was explained by the stabilisation afforded to the diradical intermediate **1.48** by the two proximal phenyl residues. The yields attained in this and related reactions were, however, low to moderate which the authors attributed to the oxidation step, **1.49** to **1.50**, which proceeded via an unknown pathway.[20]

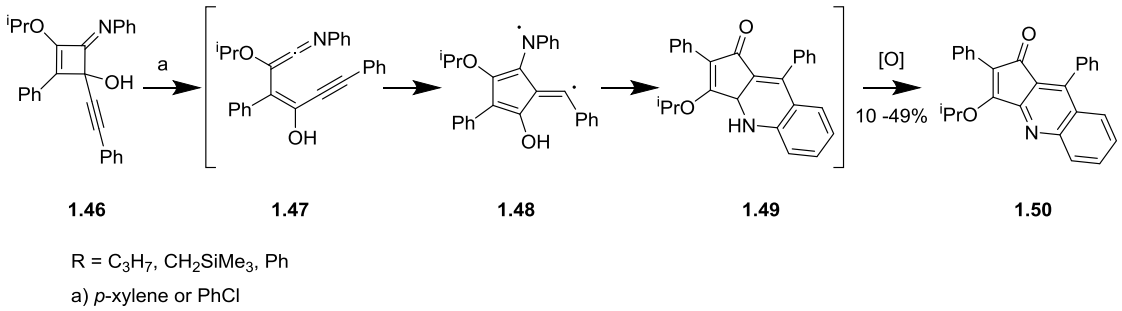

Scheme 1.5. Rearrangement of 4-alkynylcyclobutanimines.

The reactivity of diradical intermediates has also been explored as a means to trigger cascade and domino reactions. Typically, diradical intermediates akin to **1.26** and **1.27** are quenched by intramolecular H-atom transfer leading to a quinone or cyclopentenedione (Scheme 1.1). However, in some cases an alternative pathway proves more facile, as in the aforementioned rearrangement of **1.46** to **1.50** (Scheme 1.5). Alternative pathways are also followed when intramolecular H-atom transfer is blocked by substitution. Moore and co-workers were the first to exploit this tactic, with their extension of the rearrangement to allyl ethers such as **1.51**, where *O*- to *C*-allyl transfer is observed leading to tetrasubstituted quinones in high yield (Scheme 1.6).[21]

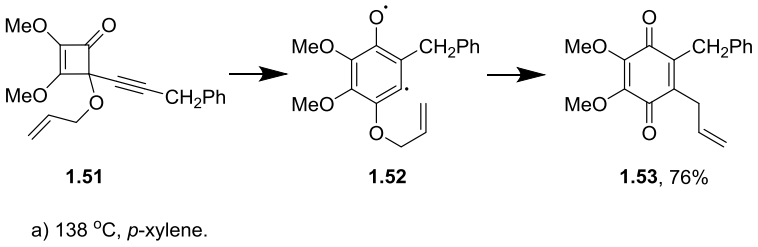

Scheme 1.6. Cyclobutenone rearrangement followed by allyl transfer.

The same group also noted that thermolysis of cyclobutenone **1.54** in the presence of Bu_3SnOMe led to the incorporation of tin in the product **1.57** (Scheme 1.7).[22] The mechanism they suggested invoked the formation of stannyl ether **1.55**. A cyclobutenone rearrangement to **1.56** then induced an intramolecular 1,3-migration to quinone **1.57**. The yield of the reaction was variable and heavily influenced by substituents. In particular, it proved more efficient when C-2 and C-3 bore alkyl residues and less efficient when they bore alkoxy substituents.

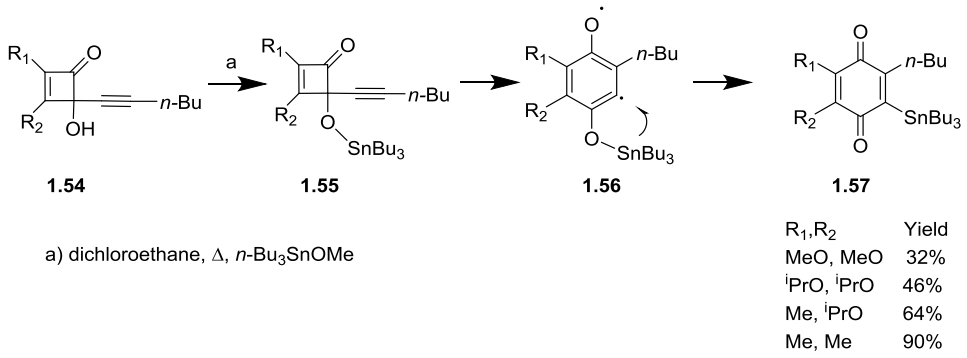

Scheme 1.7. Cyclobutenone rearrangement followed by trialkyltin transfer.

Importantly, it was found that the ring opening of **1.58** proceeded 9 times faster in the presence of Bu_3SnOMe (Scheme 1.8).

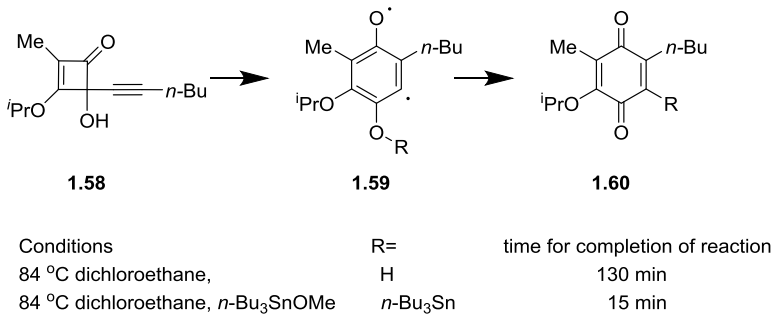

Scheme 1.8. Impact of Bu_3SnOMe on the rate of the cyclobutenone rearrangement.

Silicon too can be transferred via similar mechanism (Scheme 1.9). Thus, when the hydroxyl group is transformed into the corresponding silyl ether, as in cyclobutenones **1.61** and **1.65**, 1,3-migration is observed for both the aryl and cyclopentadienyl diradical intermediates, **1.62** and **1.66** respectively. An isotope labelling study showed that rearrangement of the silyl group did not involve exchange between molecules, suggesting an intramolecular mechanism. The involvement of zwitterionic intermediates **1.64** and **1.68** was also suggested.[3a]

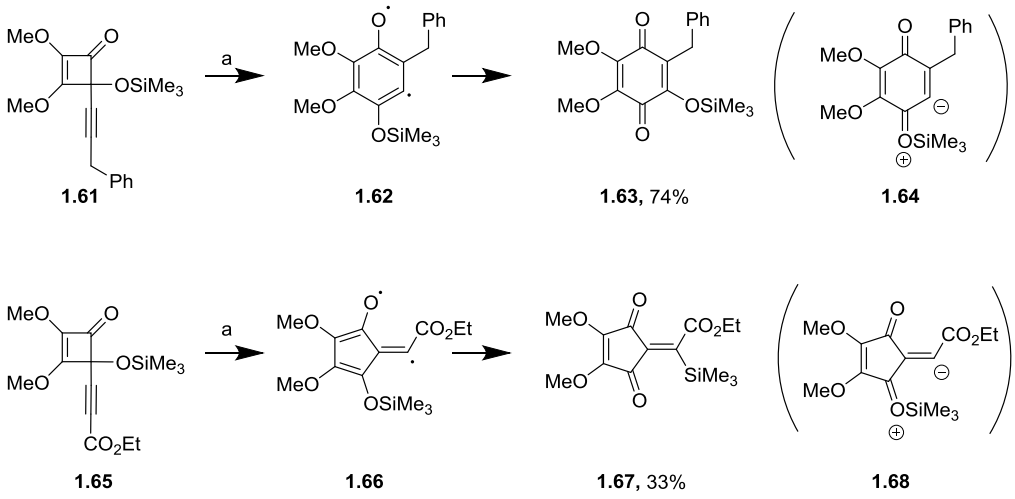

Scheme 1.9. Cyclobutenone rearrangement followed by silicon transfer.

When a TBDMS protecting group was used, as in cyclobutenone **1.69**, migration of silicon to form **1.71** was the major pathway followed. However, spirocycle **1.72** was also identified as a side product, implicating a facile 1,5-hydrogen atom abstraction (Scheme 1.10).[12a]

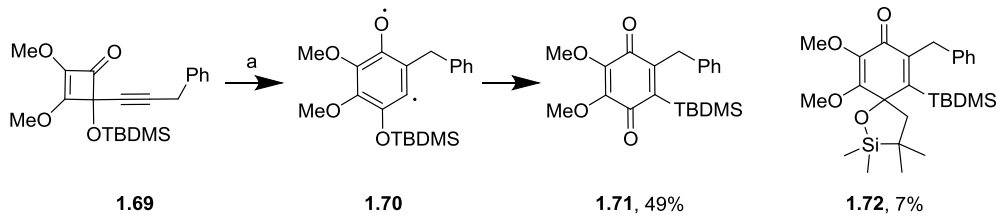

Scheme 1.10. Cyclobutenone rearrangement leading to the formation of a quinone and a spiro compound.

When the hydroxyl group is converted to the corresponding methyl ether, as in **1.73**, thermochemical rearrangement leads to spirocycle **1.76** exclusively (Scheme 1.13).

The mechanism proposed implicates diradical intermediate **1.74**. Abstraction of a hydrogen atom from the methoxy group next forms diradical intermediate **1.75**, which undergoes ring closure to epoxide **1.76**. A slow rearrangement then gives aldehyde **1.78** via the zwitterionic intermediate **1.77**. The mechanism was subjected to an isotope labelling study, which was consistent with the proposal.

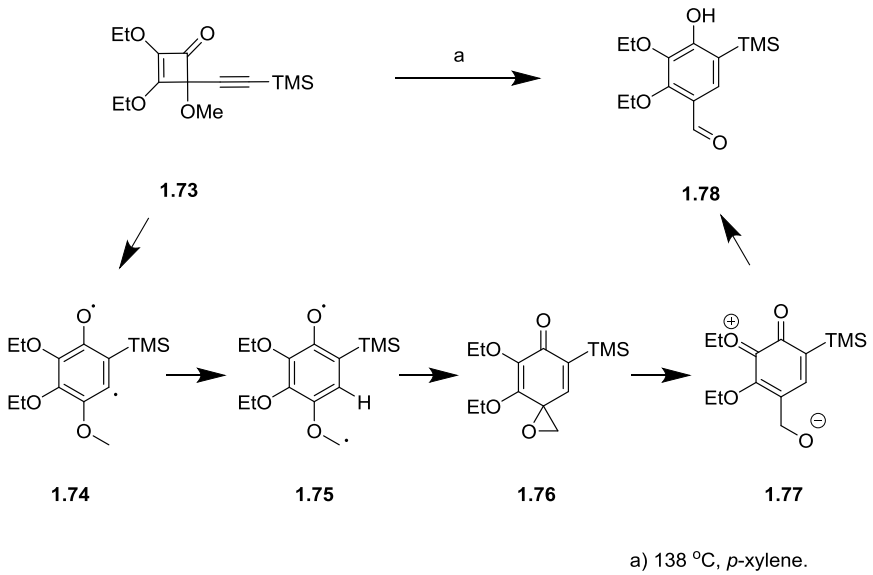

Scheme 1.11. Cyclobutenone rearrangement leading to the formation of a benzaldehyde via a spirocycle.

Such spirocyclisation reactions can also be diverted when outpaced by a competitive reaction. The thermolysis of **1.79** is a case in point as the diradical intermediate **1.80** favours 1,5-hydrogen abstraction from the proximal THP group over 1,4-hydrogen abstraction from the proximal methyl group (Scheme 1.12).[12a] The resulting diradical intermediate **1.81** then undergoes fragmentation to quinone methide **1.82** and δ-lactone **1.83**. Trimerisation of the former gives the observed product **1.84**.

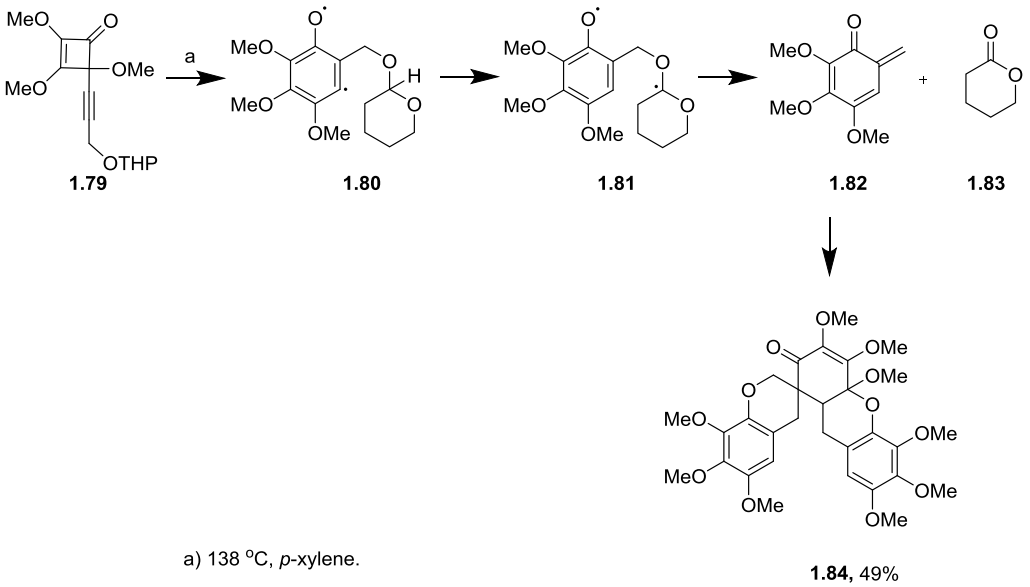

Scheme 1.12. Formation of quinone methide and δ-lactone via cyclobutenone rearrangement.

In a similar manner, the thermal rearrangement of cyclobutenone **1.85** permits generation of quinone methide **1.87** by a route involving a hydrogen abstraction pathway from **1.86** to **1.87** (Scheme 1.13). The quinone methide **1.87** cannot be isolated as it readily forms dimer **1.88**. When the reaction is conducted in the presence of butyl vinyl ether **1.89**, *in situ* capture forms chromane **1.90** in excellent yield.

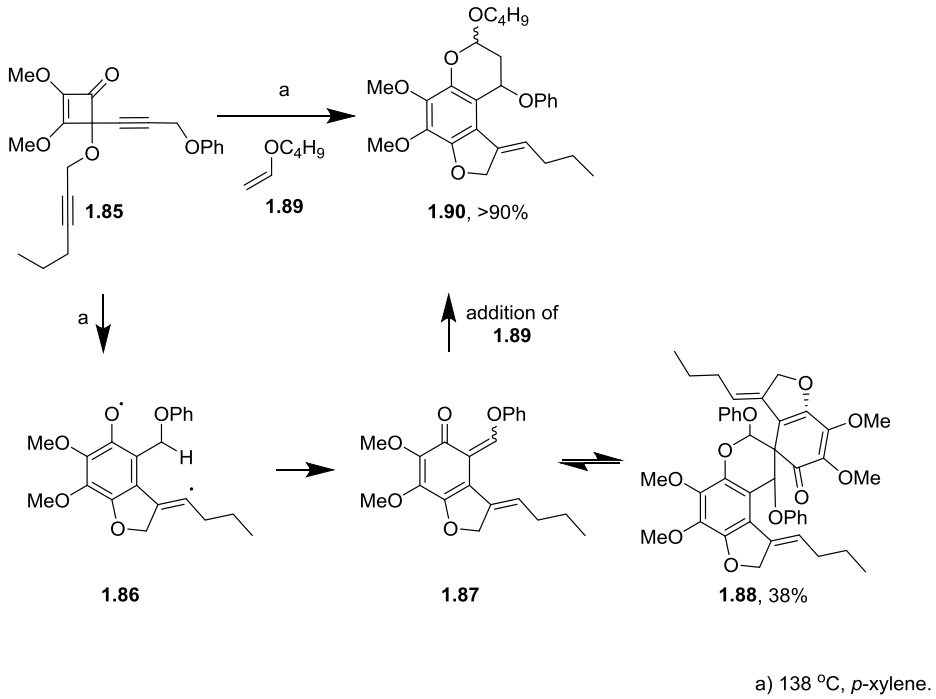

Scheme 1.13. Reaction of a quinone methide generated by cyclobutenone rearrangement.

Aryl radical addition to unsaturated bonds in the ether residue was also studied as this allows the diradical intermediate to be used in the formation of quinones with fused rings systems. The reaction of diyne **1.91** was studied by Moore and co-workers[23] and unexpectedly its outcome was found to be concentration dependent when the C-4 hydroxyl group was unprotected (Scheme 1.14). Thus, thermolysis of cyclobutenone **1.91a** gave rise to both cyclic **1.93** and acyclic **1.94** products. The proportion of each varied with concentration, with cyclisation favoured at high dilution. By contrast, when the hydroxyl group was protected as its methyl ether **1.91b**, the product given was **1.95**.[24] The authors concluded that in this case the reaction occurs via an inter- rather than an intramolecular hydrogen atom transfer.

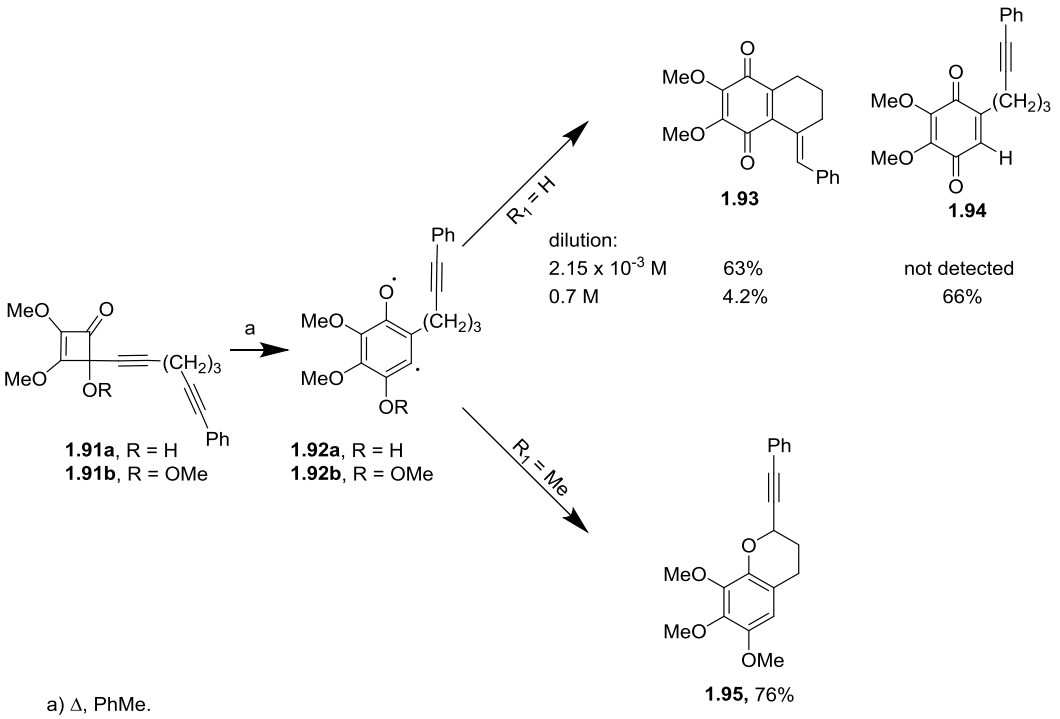

Scheme 1.14. Influence of concentration and substituents on the course of H-atom abstraction reactions.

The reaction was subsequently used a key step in a total synthesis of cribriostatin 6 **1.100** (Scheme 1.15).[8] However, it proved to be problematic and low yielding with the formation of both cyclic and acyclic products, **1.99** and **1.98** respectively. Varying the solvent, temperature and concentration failed to elevate the yield of desired intermediate **1.99**.

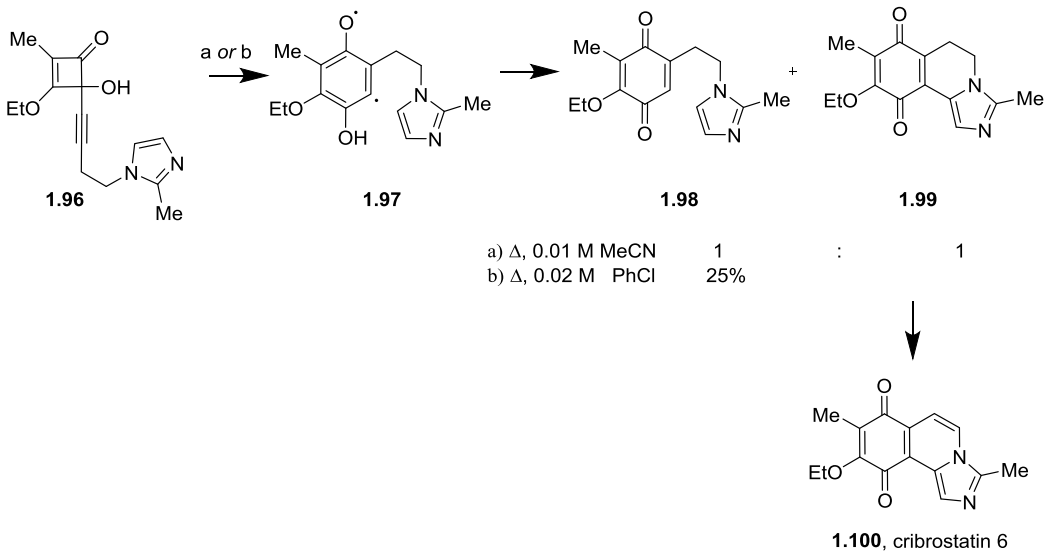

Scheme 1.15. A key step in the total synthesis of cribrostatin 6.

The nature of the diradical intermediate has attracted much attention. In particular, debate has focused on the best representation of the first formed diradical intermediate (Figure 1.4). The work of Moore *et al.*[21] has provided many insights into the reactivity of such intermediates. It has been suggested that the initial diradical intermediate is best represented as **1.103**, rather than **1.102** or the allenic species **1.101,** due to aromaticity. However, it was also recognised that substituents such as nitriles might promote a switch from a diradical intermediate such as **1.106** to a zwitterionic **1.105** or allenic **1.104** form. This question was addressed computationally by Balci and Jones[25] for 1,2-cycloheptadiene and 1,2-cyclohexadiene where the allelic **1.107**, diradical and polar **1.108** forms were discussed.

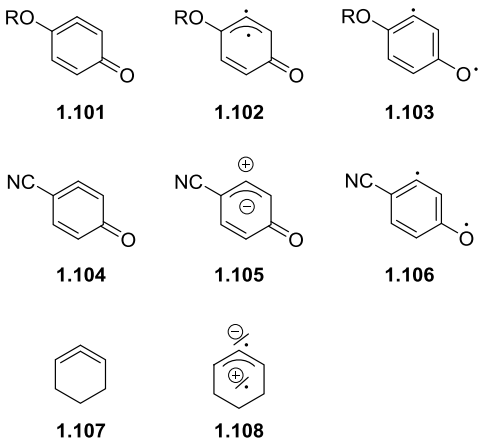

Figure 1.4. Diradical, zwitterionic and allenic representations of intermediates.

The degree of unsaturation in the C4 substituent has a significant impact on the mechanistic course of the reaction. As we have seen, the rearrangement of alkynylcyclobutenenones proceeds via a singlet open-shell diradical intermediates. By contrast, vinylcyclobutenone rearrangements proceed via closed-shell intermediates (Schemes 1.16).[26] In such cases ring opening leads to a reactive ketene, *viz.* **1.109→1.112**, which undergoes a facile 6π-electrocyclic ring closure to cyclobutenone **1.113**. Tautomerisation to hydroquinone **1.110** follows, though aerial oxidation often delivers quinone **1.111** as the isolated product.

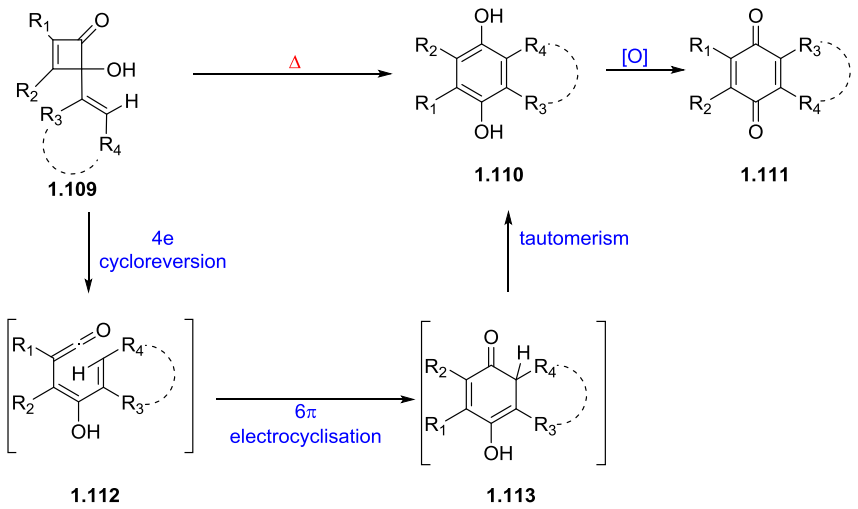

Scheme 1.16. Mechanism for the thermal rearrangement of 4-aryl and 4-vinylcyclobutenones.

When cyclobutenone **1.114** was subjected to thermolysis, the rearrangement formed tetralone **1.116**.[27] In this case the 6π-electrocyclisation reaction of **1.115** outpaced a

possible [2+2] cycloaddition between the ketene and the proximal alkene, and tautomerism to a hydroquinone was blocked by the presence of the vinyl substituent.

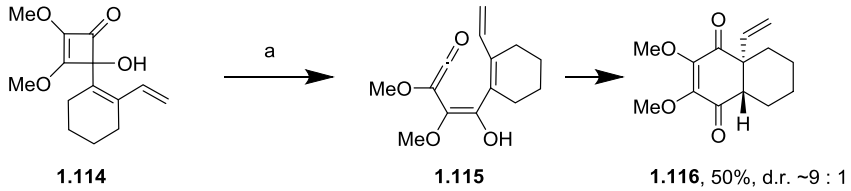

1.114 **1.115** **1.116**, 50%, d.r. ~9 : 1

a) 120 °C, THF, microwave.

Scheme 1.17. Formation of cyclohex-2-en-1,4-dione via thermolysis of cyclobutenone **1.114**.

In stark contrast, thermolysis of cyclobutenone **1.117** gave spirocycle **1.118**. This was explained by evoking a carbonyl-ene reaction of vinylketone **1.119** to **1.120** rather than the more commonly observed 6π-electrocyclic ring closure. Tautomerisation to **1.121** and air oxidation then formed spirocycle **1.118**.

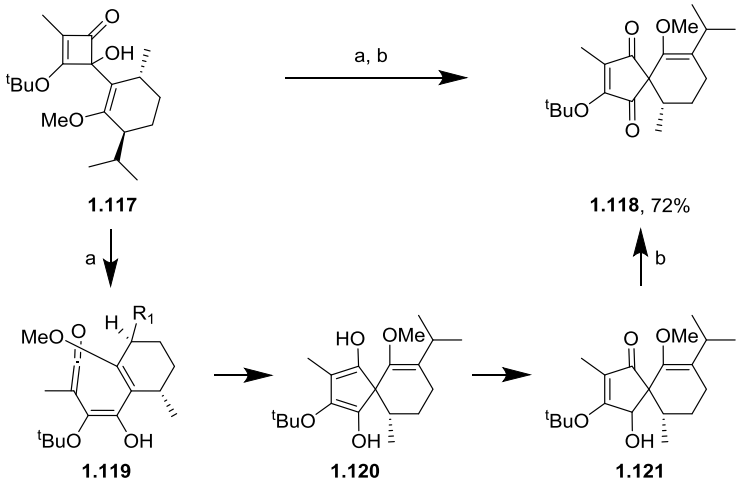

1.117 **1.118**, 72%

1.119 **1.120** **1.121**

a) THF, 120 °C, μwave, 30 min; b) Dess-Martin periodinane, DCM, 0 °C, 30 min, 72% over 2 steps.

Scheme 1.18. Thermal rearrangement of cyclobutenone **1.117** and formation of spirocycle **1.118**.

In cases where an electrocyclic ring closure reaction is not available to the ketene intermediate, other modes of ketene capture can be induced. For example, with cyclobutenone **1.122**, ring opening of the cyclobutenone gives the *E*-vinylketene **1.123**. A [2+2] cycloaddition with the proximal alkene then gives **1.124** and/or **1.125**, depending on the nature of the alkene substituents (Scheme1.19).[28]

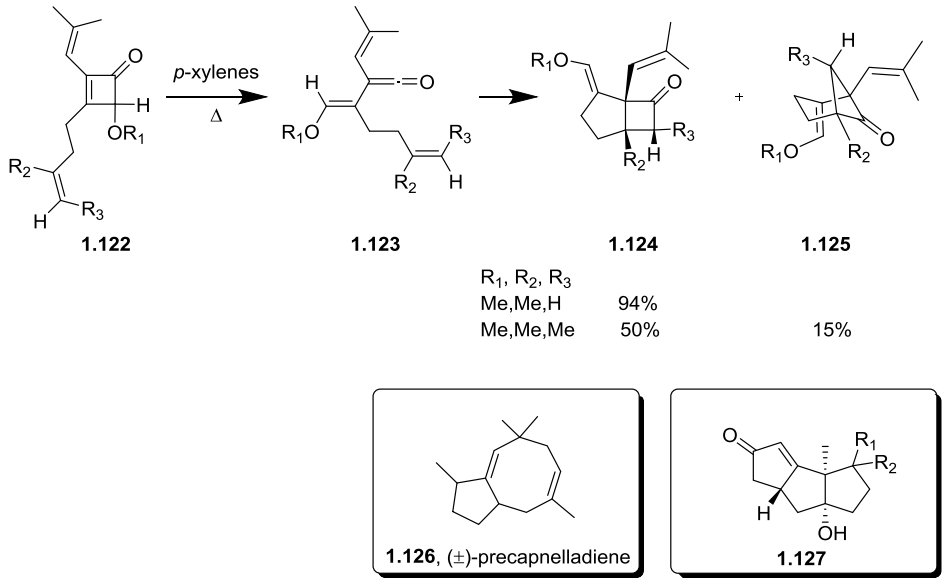

Scheme 1.19. Formation of bicycle[3.2.0] and bicycle[3.1.1] via [2+2] cyclisation of ketene.

The approach provides a versatile route to fused ring systems that are difficult to obtain by alternative means, and was used in syntheses of (±)-precapnelladiene **1.126** and **1.127**.[29] A further extension of this method was provided by Harrowven and co-workers,[27] who found that the [2+2] cycloaddition product **1.129** was formed exclusively when **1.128** was thermalized at 120 °C (Scheme 1.20).

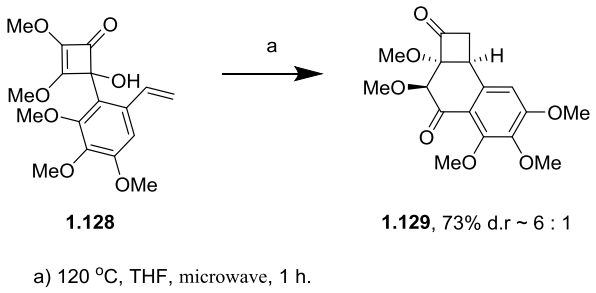

Scheme 1.20. Rearrangement of 4-(o-styryl)-cyclobutenone **1.128** to benzobicyclo[4.2.0]octenone **1.129**.

However, the course of this reaction was heavily influence by substituents on the vinyl group. For example, for substrates such as **1.130** two possible [2+2] cycloaddition reactions are possible leading to **1.133** and **1.134** (Scheme 1.21). For styrene **1.130a**, tricycle **1.133** was the only product observed. By contrast, thermolysis of *cis*-stilbene **1.130b** led to **1.138** via formation of **1.134**, homolytic bond cleavage to the diradical intermediate **1.136** and cyclisation. For *trans*-stilbene

1.130c, both **1.137** and **1.138** were formed as products, suggesting that the diradical intermediate **1.135** had time to interconvert with its rotamer **1.136**.

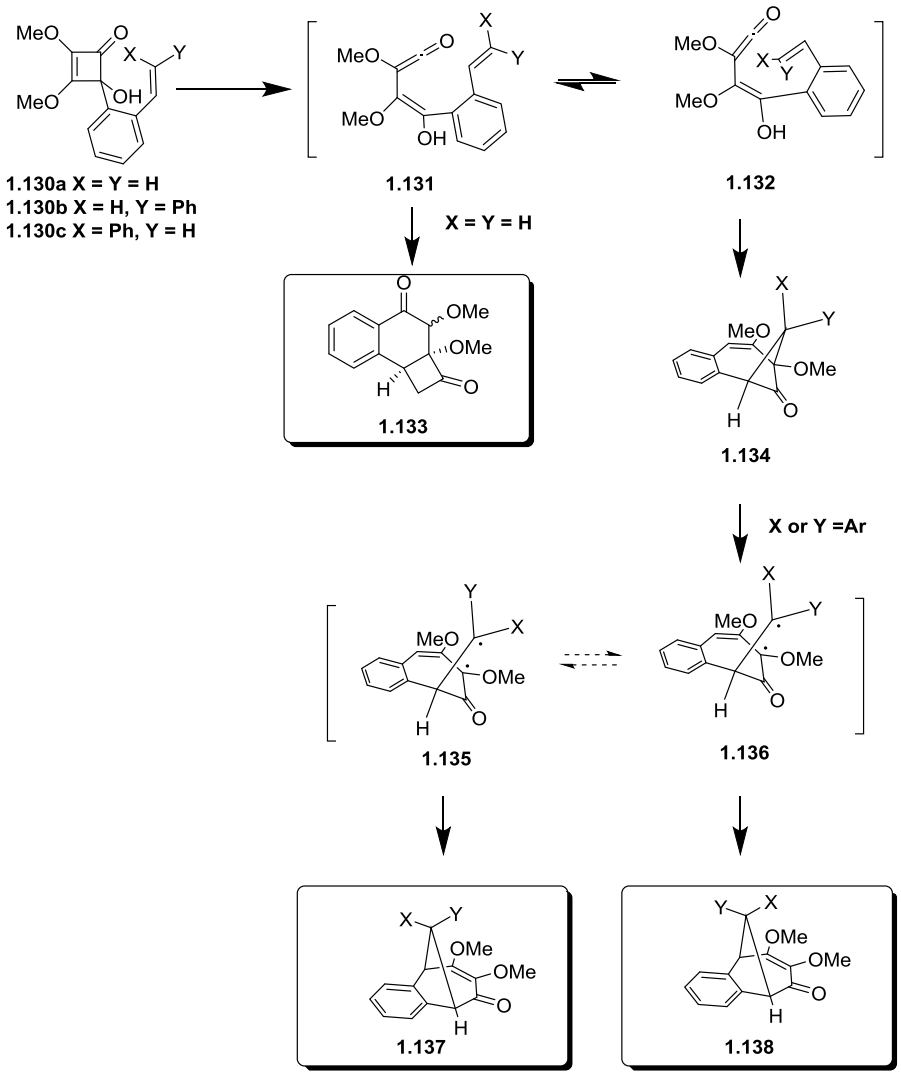

Scheme 1.21. Proposed mechanism for the thermal rearrangement of 4-(*o*-stytyl)-cyclobutenones.

The cyclobutenone rearrangement can give a variety of products if an electrocyclic ring closure step is not available. For example, ring opening of cyclobutenone **1.139** forms ketene **1.140** which is capture by sulfur to give the zwitterionic species **1.141**.[30] An elimination to **1.142** then sets up a transannular ring closure to form **1.144** or **1.146**, depending on the nature of substituent R. Interestingly, when this residue is a vinyl group the reaction leads to the formation of lactone **1.148** via dicarbonyl **1.43** and transannular ring closure to **1.45**. Heterolytic cleavage to dipolar intermediate **1.147** then sets a cyclisation to give the observed 5*H*-furanone

product **1.148**. Notably, the rearrangement has been used in a key step in total syntheses of linderaspirone A and B-linderone.[31]

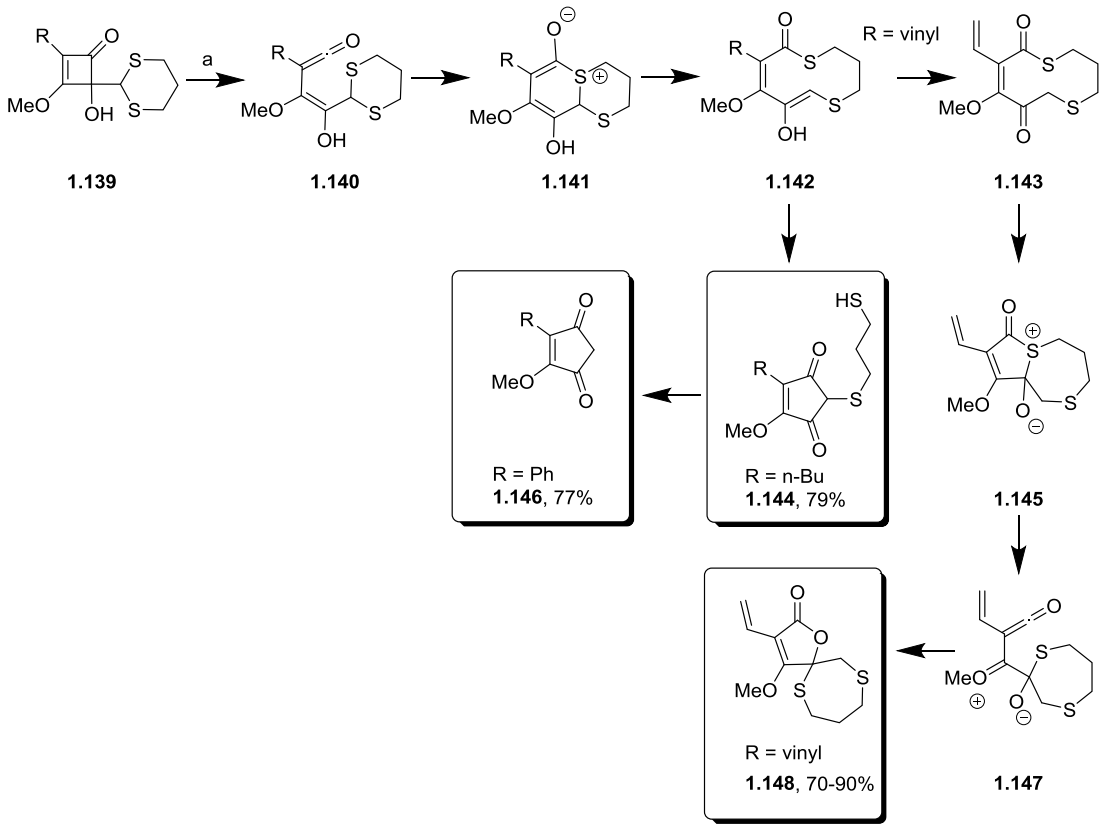

a) 138 °C, *p*-xylene, 3 h.

Scheme 1.22. Ring expansion of 4-(1,3-dithiane-2-yl)cyclobutene-1-ones.

A similar reaction was observed with epoxide **1.149**, which gave furanone **1.153** on thermolysis (Scheme 1.23). The mechanism proposed involves capture of the ketene intermediate **1.150** by the epoxide to form the ε-lactone **1.151**. Heterolytic cleavage of the C-O bond then forms zwitterionic intermediate **1.152** and triggers cyclisation to furanone **1.153**.

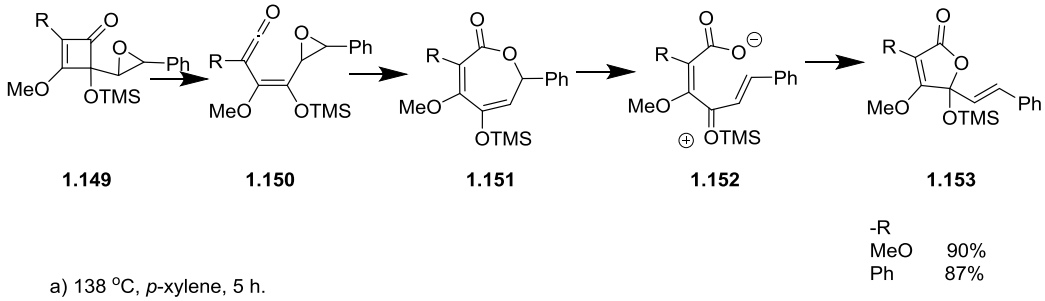

a) 138 °C, *p*-xylene, 5 h.

Scheme 1.23. Ring expansion of 4-oxiranylcyclobutene-1-ones.

A similar product was observed when water was used to quench the reaction of **1.54** with lithiated TMS acetylene (Scheme 1.24).[32] In this case, ring opening of cyclobutenone **1.154** to ketene **1.157** is believed to be involved. Hydrolysis of the ketene with water next gives carboxylic acid **1.158**, with tautomerism and cyclisation completing the sequence to yield lactones **1.155** and **1.156**.

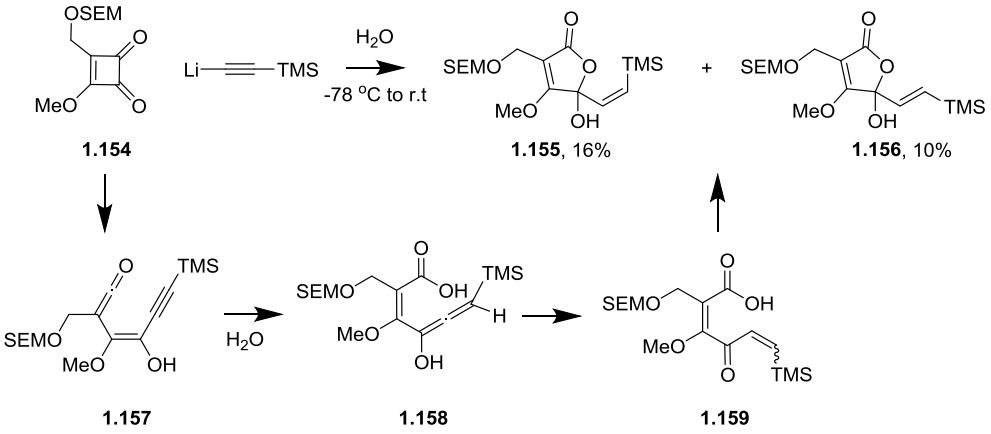

Scheme 1.24. Formation of butenolides via cyclobutenone rearrangement in water.

A lactone was also formed when cyclobutenone **1.160** was treated with lead tetraacetate in toluene at room temperature (Scheme 1.25).[13] The suggested mechanism involves ring opening with participation by an acetate ligand **1.163**, which explains why the reaction occurs at room temperature. A similar ring expansion occurs with cerium based oxidants while manganese oxidants produce acyclic products.

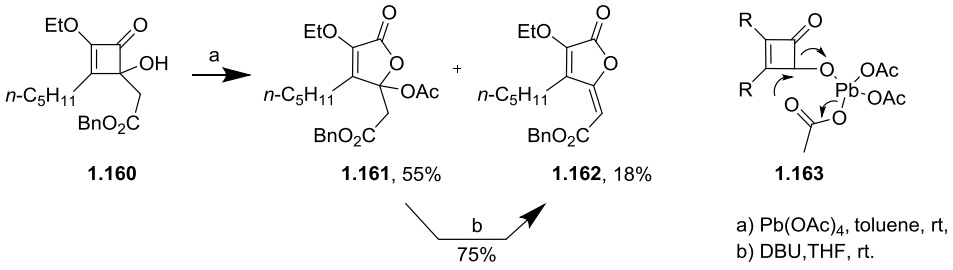

Scheme 1.25. Formation of furanones by oxidative rearrangement of 4-hydroxy-2-cyclobutenone

Lactone **1.165** can be obtained from arylcyclobutenone **1.164** because the *O,O'*-disubstituted arene ring prevents electrocyclic ring closure of the (*Z*)-vinylketene intermediate **1.166** (Scheme 1.26). As a consequence the reaction proceeds via the

(*E*)-vinylketene intermediate **1.167** which undergoes ring closure leading to γ-lactone **1.165** via **1.168**.[33]

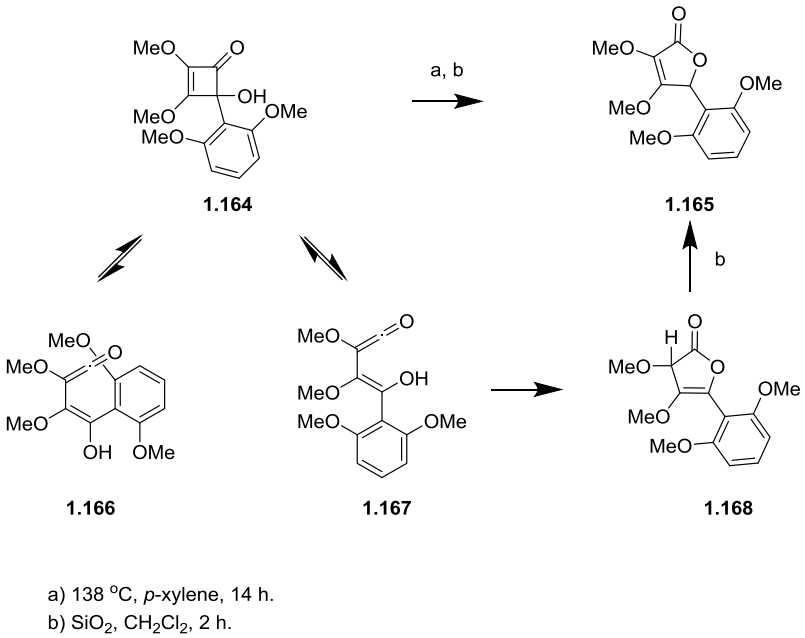

Scheme 1.26. Formation of furanones by rearrangement of hindered arylcyclobutenone.

Lactone formation is also seen with squaramides such as **1.169** (Scheme 1.27). Indeed, Liebeskind and co-worker[34] observed exclusive formation of lactone **1.172** when this compound was subjected to thermolysis. None of the expected product **1.173** was observed in the product mixture suggesting that the course of the rearrangement was switched by the formation of a strong hydrogen bond between the amide residue and the hydroxyl group.

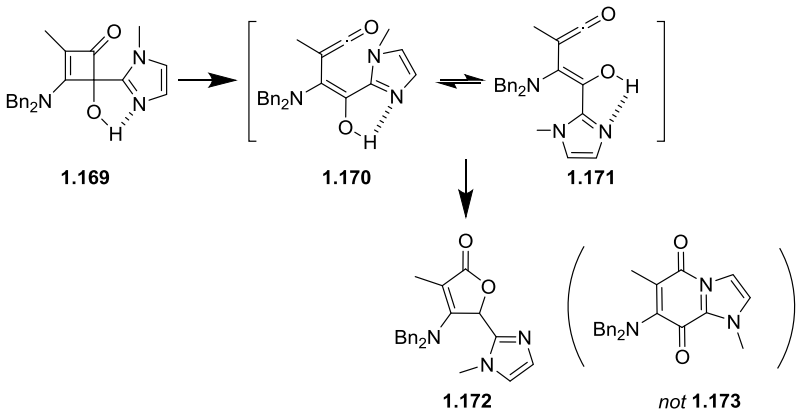

Scheme 1.27. Unexpected formation of a lactone ring via thermal rearrangement of 4-hydroxy-4-(-1-methylimidazo-2-yl)-2-cyclobutenone **1.169**.

Cyclobutenones also rearrange to lactones under photochemical irradiation. Recorded yields were low when conducted under standard photochemical conditions (though our work has led to the development of a very efficient protocol). The mechanism proposed involved a torquoselective ring opening of cyclobutenone **1.168** to (*E*)-vinylketene **1.169** with 'inward' rotation of the hydroxyl group. Ring closure then gives 5*H*-furanone **1.170** (Scheme 1.28).[12a]

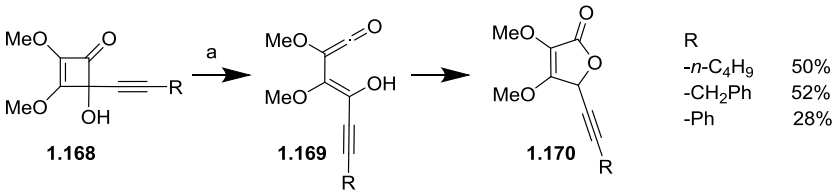

a) hν, 0 °C, THF.

Scheme 1.28. Photolysis of cyclobutenones.

It is interesting to note that some photochemical reactions involving cyclobutenes, *e.g.* **1.177** and **1.180**, are not stereospecific (Scheme 1.29). Importantly, disrotatory ring opening is always the predominant pathway.[35]

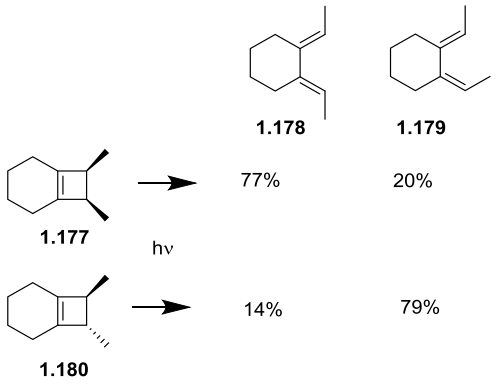

Scheme 1.29. Selectivity in the photolysis of cyclobutenes.

1.2 Computational studies on the cyclobutenone rearrangement

EXPLAINING THE UNKNOWN BY MEANS OF THE UNOBSERVABLE IS ALWAYS A PERILOUS BUSINESS.
ANON.

The first step of a cyclobutenone rearrangement involves ring opening. This opening for cyclobutenes is selective and mainly gives rise to one isomer under thermal conditions. The cyclobutene ring opening was studied experimentally more than 50 years ago by the Frey group at Southampton University (Scheme 1.30).[36] The author observed that the (*E*)-isomer **1.182** was formed after thermal ring opening of **1.181** and that none of the (*Z*)-isomer **1.183** could be detected. This preference was attributed to sterics for the studied system.

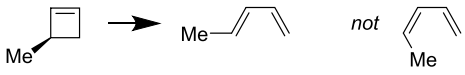

1.181 **1.182** **1.183**

Scheme 1.30. Thermolysis of the 3-methylcyclobutene.

Since then, the term torquoselectivity has been introduced to describe such stereochemical preferences in ring opening reactions.[37] This four electron reaction is dictated by molecular orbital interactions and follows a conrotatory electrocyclic ring opening pathway. In the general case **1.185** to **1.186**, this occurs via a Möbius aromatic transition state (Scheme 1.31).[38]

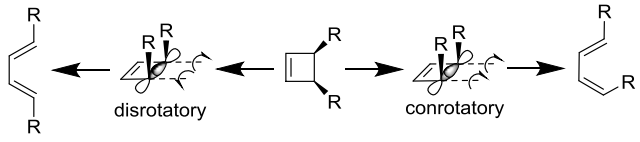

1.184 **1.185** **1.186**

Scheme 1.31. Disrotatory and conrotatory ring opening of cyclobutene.

The Woodward-Hoffmann frontier orbital correlation diagram shows the required rotation for ring opening to satisfy the phase alignment of orbitals. Indeed, this explains why ring opening is conrotatory (Figure 1.5).[39]

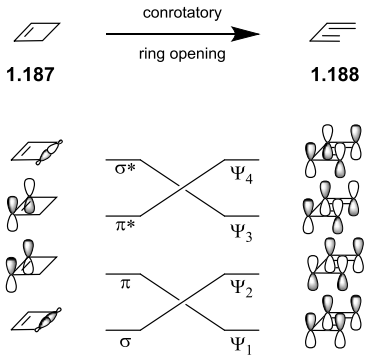

Figure 1.5. A Woodward-Hoffmann correlation diagram for the conrotatory electrocyclic opening of cyclobutene to butadiene.

However, it does not explain why some substituents favour 'inward' rotation while others favour 'outward' rotation (Scheme 1.32). It is known, for example, that methoxy groups prefer[40] to rotate 'outward' (entry 1, Scheme 1.32) while silyl groups[41] prefer to rotate 'inward' (entry 3, Scheme 1.32) when in competition with a saturated alkyl group.

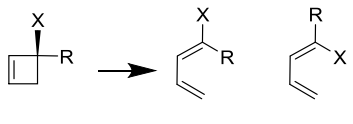

1.189 **1.190** **1.191**

entry	X	R		
1	OMe	^{t}Bu	90%	<1
2	Me	^{t}Bu	30%	70%
3	$SiMe_2Ph$	n-C_8H_{17}		100%

Scheme 1.32. Influence of substituents on the torquoselective ring opening of cyclobutenes.

To explain this phenomena various models were postulated based on orbital interactions in the transition state (Figure 1.6). The Rondan-Houk model[42] predicts that a donor substituent with a filled orbital will give rise to a more significant closed-shell interaction when that substituent rotates outward. By contrast, the interaction between the filled σ-orbital of an attached alkyl residue and the vacant π* orbital promotes inward rotation.

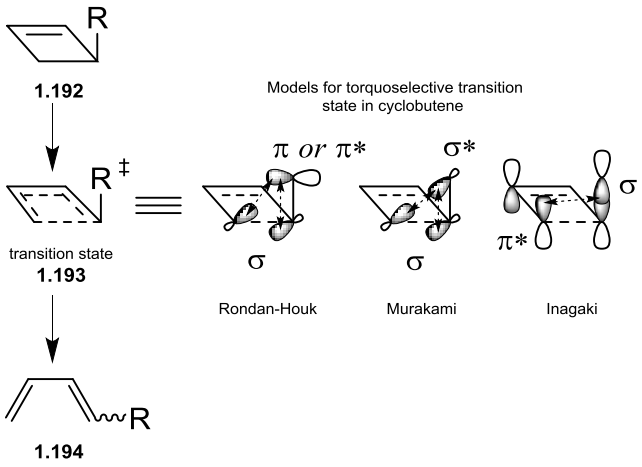

Figure 1.6. Transition state models for torquoselective ring-opening of cyclobutenes developed by various authors based on the donor and acceptor interactions of substituents.

The authors suggest that this orbital interaction accounts for the torquoselectivity observed in entry 1, Scheme 1.32, where the *tert*-butyl group prefers to rotate inward, thereby showing the dominance of electronic over steric effect. The Murakami model explains the selectivity observed with silyl substituents,[41, 43] by suggesting that an interaction between the silicon-carbon σ* orbital and the proximal carbon-carbon σ bond promotes and rotation of silyl group (entry 3, Scheme 1.32) inward.

However, Inagaki's model provides an alternative understanding of the torquoselectivity observed with silicon substituents.[44] Analysis of the electrocyclic reaction led him to conclude that orbital overlap between the high-lying C-Si σ orbital and the evolving butadiene π* orbital was key (*i.e.* Geminal Bond Participation). The interbond population was studied to support this statement. Further analysis of the allowed and forbidden torquoselective ring opening of silyl substituted cyclobutene was provided by Houk and co-workers.[45]

The 4π electrocyclic ring opening of cyclobutene occurs via a Mobius transition state.[46] A calculation of Nuclear Independent Chemical Shift (NICS) showed that the centre of the cyclobutene ring has a value of -12.3 ppm which suggests an aromatic transition state. The authors support this statement by invoking a magnetic susceptibility enhancement (Λ) for the transition structure (defined as the increase in magnetic susceptibility in going from the reactants to the transition state).

The transition state for ring opening was studied by a variety of *ab initio*[47] and DFT methods.[48] As noted by Houk and co-workers,[48] calculations of the transition state geometry show little dependence on the method used, yet only correlated methods (*i.e.* MP2 method) with tempered basis sets proved quantitatively accurate.

In a further study the ring opening of cyclobutene, cyclobutenone and cyclobutenedione were compared (Scheme 1.33).[49] For these model systems, the cyclobutenone ring opening **1.196→1.197→1.198** gave a value for $\Delta G_{(298K)}$ of 25.7 kcal/mol at MP2/6-31G(d). The cyclobutenedione ring opening (**1.199→1.200→1.201**) had a higher energy but this was still low compare to that determined for cyclobutene (**1.187→1.195→1.188**).

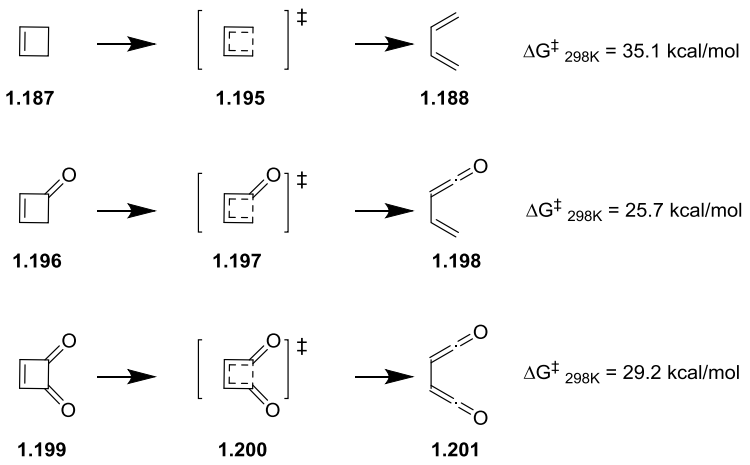

Scheme 1.33. Calculated Gibbs free energy (ΔG) values for the ring opening reactions of cyclobutene, cyclobutenone and cyclobutenedione at the MP2/6-31G(d)//MP2/6-31G(d) level.

It was suggested that the lower energy requirement for ring opening of cyclobutenones is due to the dipolar character of the transition state (Figure 1.7), where a zwitterionic mesomeric form **1.203** can contribute.[50, 49] This also helps to explain the stability of the vinylketene intermediate **1.202** (Figure 1.7).

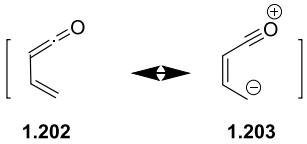

1.202 1.203

Figure 1.7. Dipolar resonance structures of vinylketene.

Houk and co-workers[51] also compared the ring opening of substituted cyclobutenes **1.205** and cyclobutenones **1.192** (Scheme 1.34) in order to gain a better understanding of torquoselectivity in each system.

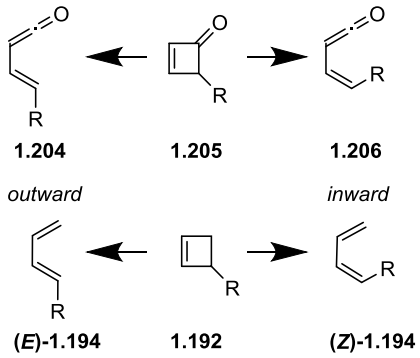

1.204 1.205 1.206

outward *inward*

(*E*)-1.194 1.192 (*Z*)-1.194

Scheme 1.34. Torquoselective ring open of cyclobutene and cyclobutenone.

They observed that substituents exhibited the same torquoselectivity preference in cyclobutenes and cyclobutenones, though the energy differences were larger in cyclobutenes than they were in cyclobutenones (Figure 1.8). Substituents such as $-BH_2$, -CHO and -NO favoured inward rotation whereas others they examined favoured outward rotation.

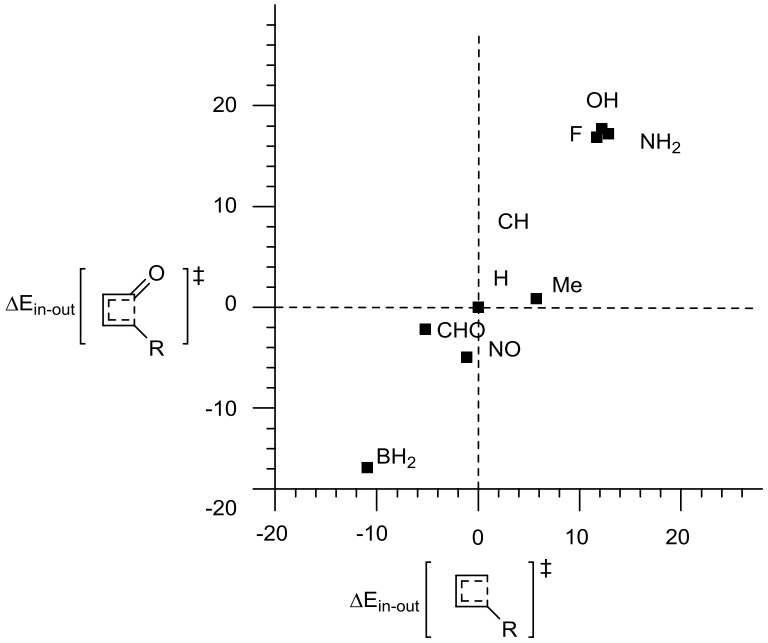

Figure 1.8. Graphical representation of the difference in activation energies for inward and outward rotation of substituents [kcal/mol] for cyclobutenones (MP2/6-31G(d)//HF/6-31G(d) and cyclobutenes (MP2/6-31G(d)//HF/3-21G).

The difference in energies between those two ring systems was explained on the basis of orbital interactions. The low-lying σ*‡ LUMO at the point of transition is responsible for stabilisation as its interaction with electron donating substituents lowers the energy barrier for ring opening (Figure 1.9). In cyclobutenes the HOMO and LUMO frontier orbitals are the σ‡ and σ*‡ of the C-C bond that brakes during the reaction. In both cases the σ*‡ HOMO are similar in energy. However, in cyclobutenone the σ*‡ has a second unoccupied molecular orbital (SLUMO) is higher in energy. The SHOMO ($\pi_{CC} + \pi_{CO}$‡) and LUMO ($\pi^*_{CC} + \pi^*_{CO}$‡) orbitals both arise from the π system. Also, participation of the carbonyl oxygen lone pairs was mentioned, as one can mix with the HOMO during the ring opening of a cyclobutenone. This difference reduces the influence of substituents on the torquoselectivity exhibited by cyclobutenones compared to cyclobutenes.

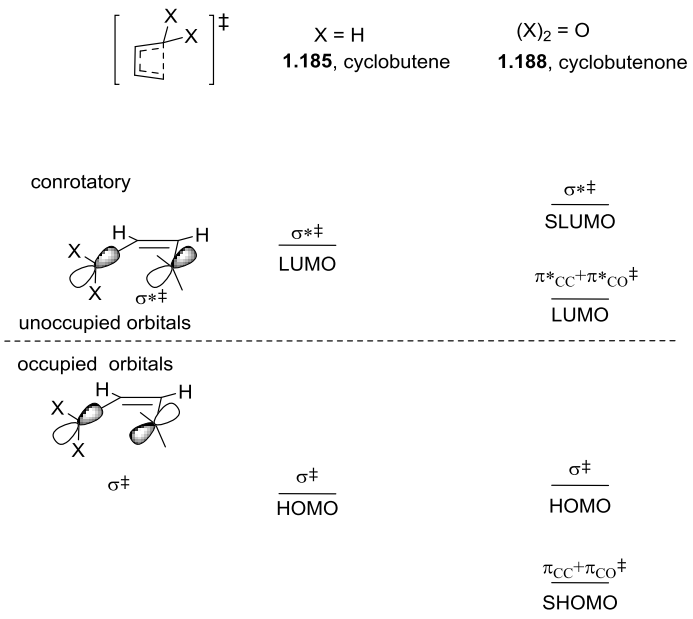

Figure 1.9. Frontier orbitals for the transition states of cyclobutene (left) and cyclobutenone (right) ring opening.

Though the ring opening reaction is torquoselective, there is growing evidence that the reaction proceed via competitive ring opening pathways. Thus, donating groups like phenyl favour outward rotation and dictate kinetics (Scheme 1.35). This was demonstrated by Danheiser and Helgason[52] in their synthesis of **1.209** from **1.207**, where kinetically favourable ring opening leads to a (*Z*)-vinylketene **1.211** that has no means of trapping. Consequently, it reverts back to **1.207**, allowing the reaction to proceed via (*E*)-vinylketene **1.208**. This reversibility was later rationalised by Houk *et al*.[51]

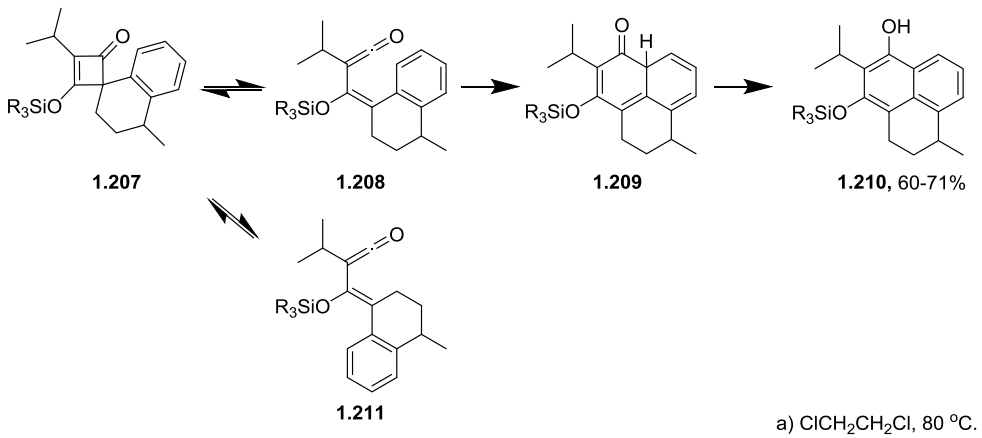

Scheme 1.35. Cyclobutenone rearrangement via the less favoured (*E*)-vinylketene intermediate.

The ring opening of cyclobutenones was also studied to explain the formation of acylallenes **1.216** in ketene-acetylene [2+2]-cycloaddition reactions (Scheme 1.36).[53] The mechanism for formation of oxetene ring **1.217** versus cyclobutenone **1.214**, and the formation of the 1,3-X shift product **1.216**, was investigated. The authors concluded that the [2+2]-cycloaddition to cyclobutenone **1.214** was faster in the majority of cases studied. They also concluded that the 1,3-X shift reaction, *viz.* **1.215** to **1.216**, was unlikely to occur via cyclobutenone **1.214** and involved a pathway via **1.217**. Their findings were confirmed by experiments conducted at elevated temperatures.[53]

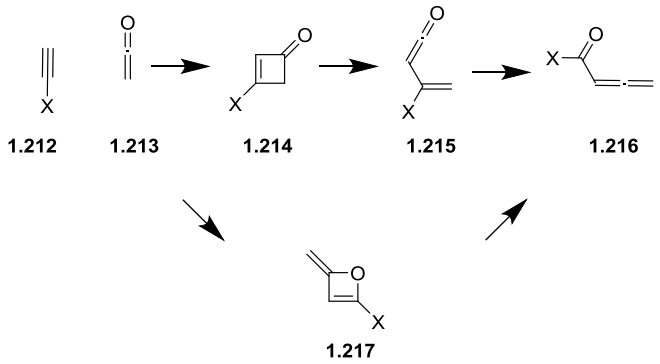

Scheme 1.36. The formation of acylallenes via ring opening of an oxetene and via a 1,3-X shift.

The enyne-ketene ring closure reactions of **1.220** were studied by Engels and co-workers (Scheme 1.37).[54] Their calculations relating to the transition state showed that 6-ring closure **1.220→1.218** was favoured over 5-ring closure **1.220→1.222** for the model system. Their CCSD(T) calculation using the double zeta basis set showed a good correlation with the computationally cheaper B3LYP method. Also, CCSD(T) found that the T1 diagnostic was low for these transition states, though the actual values were not reported. It was suggested that 5-ring closure leads to the (*E*)-isomer of diradical **1.222** rather than the (*Z*)-isomer. All of the transition states reported had no spin contamination and the BLYP method was deemed to be inappropriate.

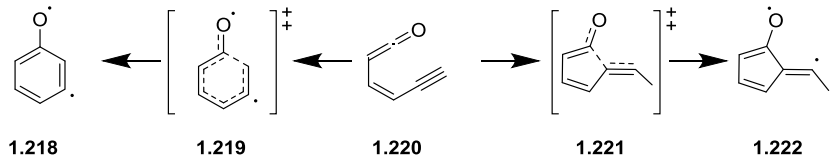

ΔE [kcal/mol]		
CCSD(T)/cc-pVDZ*	17.6	41.3
B3LYP/6-31G(d)	13.3	41.2
B3LYP/6-311G(d)	16.7	45.6

* at B3LYP/6-31G(d) geomerty

Scheme 1.37. Energy barriers for ring closure of **1.220** [kcal/mol].

Using B3LYP calculations, the authors were able to explain the selectivity observed by Moore and co-workers for the thermolysis of cyclobutenone **1.223** (Scheme 1.38).[12a] Indeed, it was not found necessary to include solvent or free energy corrections to obtain good agreement between theory and experiment. It was mentioned that 5-ring closure to **1.224** was favoured over 6-ring closure to **1.226** due to stabilisation of the vinyl radical intermediate by the phenyl ring and the influence of the two methoxy substituents.

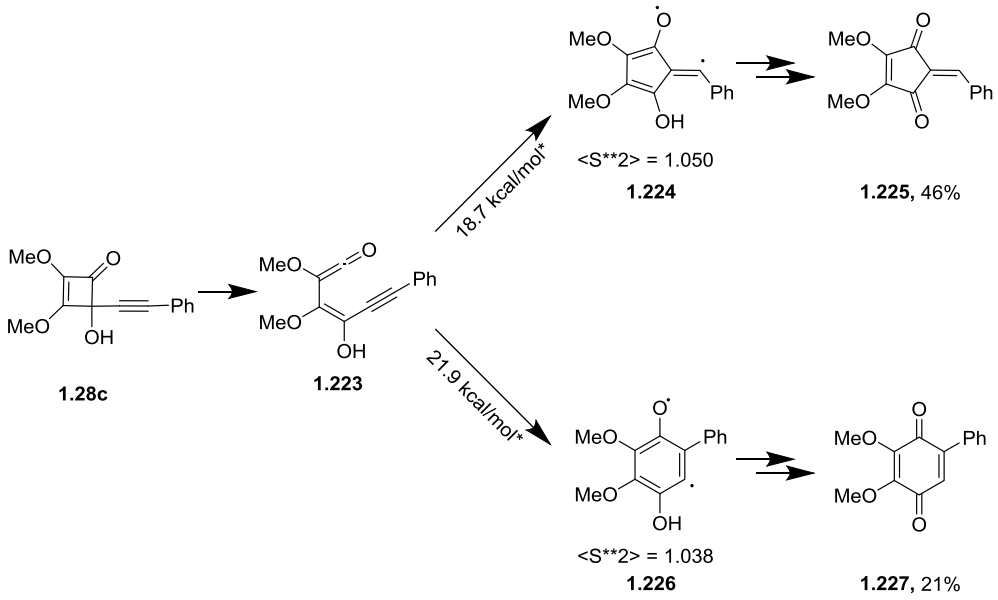

Scheme 1.38. Experimental and *in silico* predicted selectivity of ring closure. *Gibbs free energies at 25 °C from the B3LYP/6-31G(d) method.

The authors also investigated the energy of various electronic structures of the diradical intermediates. The MRCI+Q data was qualitatively reproduced by B3LYP, showing that in both cases diradical intermediates **1.222** and **1.218** were more stable than their closed-shell forms **1.228** and **1.229**. However, it was found that the

difference in energy between the diradical form **1.218** and **1.228** was only a few kcal/mol.

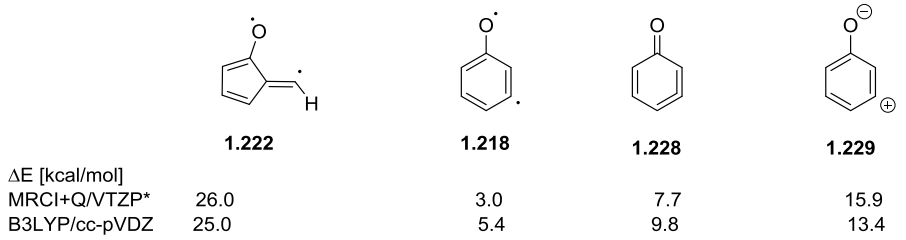

Figure 1.10. Energies of different representations of diradical intermediate.

This finding led the authors to conclude that substituent effects could shift a system from a diradical state such as **1.231** to a carbenic state such as **1.230**. In particular, strong electron donating groups (-*EDG*) or strong electron withdrawing groups (-*EWG*) could lead to a favourable orbital interaction that would switch the system towards carbene **1.230** (Figure 1.11).

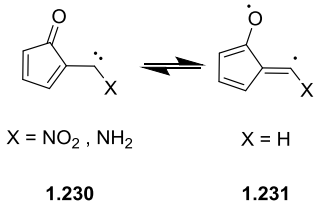

Figure 1.11. How substituent effects might bias the system towards diradical or zwitterionic intermediates.

The ring closure reaction of **1.28c** was studied by Fernandez and co-workers (Scheme 1.39) using HF at the MP2 level with the 6-31G(d,p) basis set.[55] The authors concluded that the intermediate **1.232** is allenic and not diradical **1.226** in nature, as the open-shell guess of SCF converged to a closed-shell solution. However, this statement contradicts results reported by Engels and co-workers.[54]

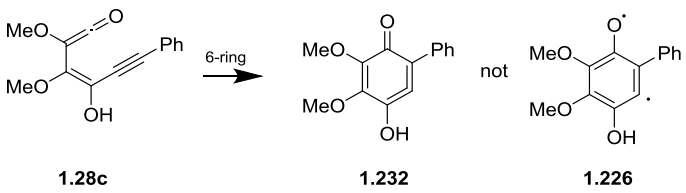

Scheme 1.39. Prediction of an allenic intermediate generated from ketene ring closure by Fernandez.

The existence of two possible electronic states was also studied for intermediates of enyne-allene reactions, which were investigated using mPWPW91/cc-pVDZ.[56] It was observed that molecules with a suitably placed oxyanion substituent, *e.g.* **1.234** ($R^3 = O^-$), prefer to give zwitterionic intermediates (**1.236** ↔ **1.237** or **1.238** ↔ **1.239**) rather than diradical intermediate **1.233** or **1.235** for both 5- and 6-ring closure (Scheme 1.40).

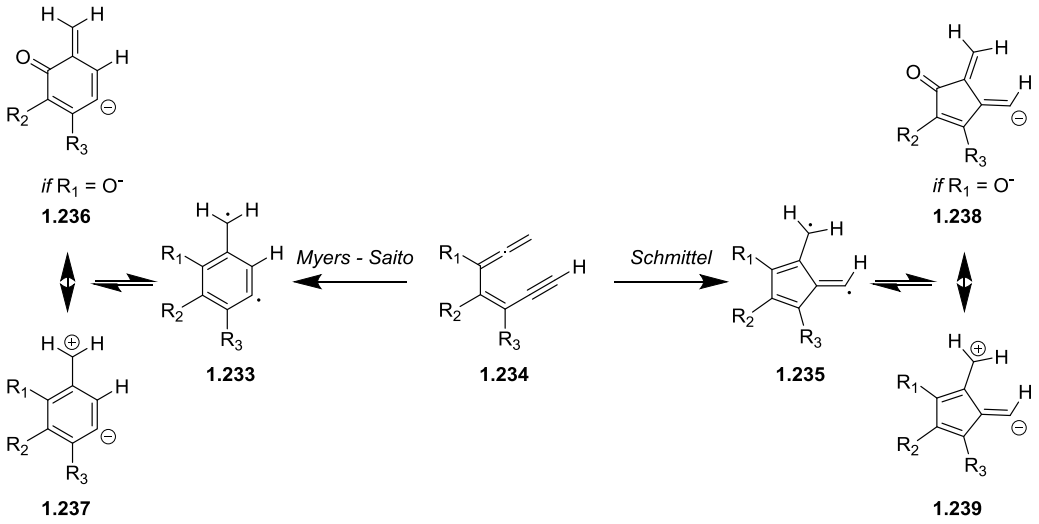

Scheme 1.40. Electronic structure of Myers-Saito and Schmittel intermediates.

Diradical and zwitterionic intermediates in cycloaromatisation reactions were subjected to a recent review[57]. Also, it was recently found that spin states of carbenes can be shifted by the formation of hydrogen bonds.[58] To describe systems where more than one electronic structure of an intermediate is possible, Dewar introduced the term '*orbital isomerism*'.[59]

Interestingly, when such systems are co-ordinated to chromium, as in **1.240**, 6-ring formation to **1.243** is favoured. Calculations at B3LYP together with the 6-31G(d) and SSD basis sets suggest both a kinetic and thermodynamic preference for closure of ketene **1.240** to **1.243**. The competitive 5-ring closure to **1.244** followed by neophyl rearrangement to **1.245**[60] was examined and found to have higher energy barrier (Scheme 1.41). Calculations were carried out on both singlet and triplet states, however triplet state calculations were used when concluding that the 6-ring closure pathway was the more favourable.[61] The authors did not report spin contamination and spin density data for any of the diradical open-shell singlet species.

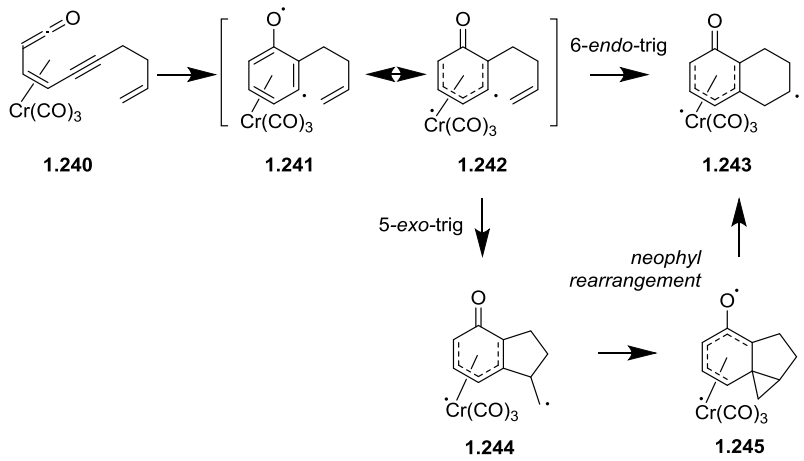

Scheme 1.41. Enyne-ketene ring closure followed by allyl addition.

1.3 Organometallic addition to cyclobutenedione

THE ONLY TROUBLE WITH A SURE THING IS THE UNCERTAINTY.
AUTHOR UNKNOWN

Cyclobutenones can be prepared in many ways.[62] The most popular means of accessing them uses commercially available squaric acid **1.246** as a starting point (Scheme 1.42). The formation of symmetric cyclobutenediones such as **1.247** can be realised by esterification. The addition of organometallic reagents to form **1.248**, followed by acidic workup, gives access to unsymmetrical cyclobutenediones such as **1.249**.

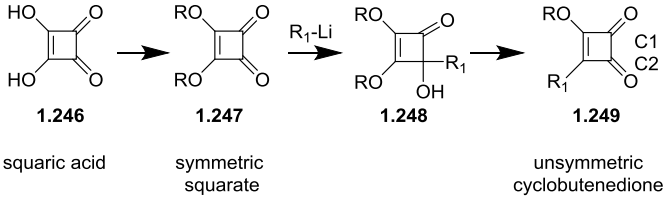

Scheme 1.42. Synthesis of cyclobutenediones from squaric acid.

For cyclobutenedione **1.243**, two 1,2-addition modes are possible (Scheme 1.43). It is known that organolithium and organomagnesium reagents favour addition to the *C*-1 carbonyl. Thus, addition of 2-lithioanisole to cyclobutenedione **1.243** gives cyclobutenone **1.244** which, on thermolysis and air oxidation, yields benzoquinone **1.246**. Access to the *C*-2 addition product **1.248** is possible through the use of protecting groups, *e.g.* **1.247**. This longer sequence gives access to the regioisomeric benzoquinone **1.250**, albeit in modest yield.[63]

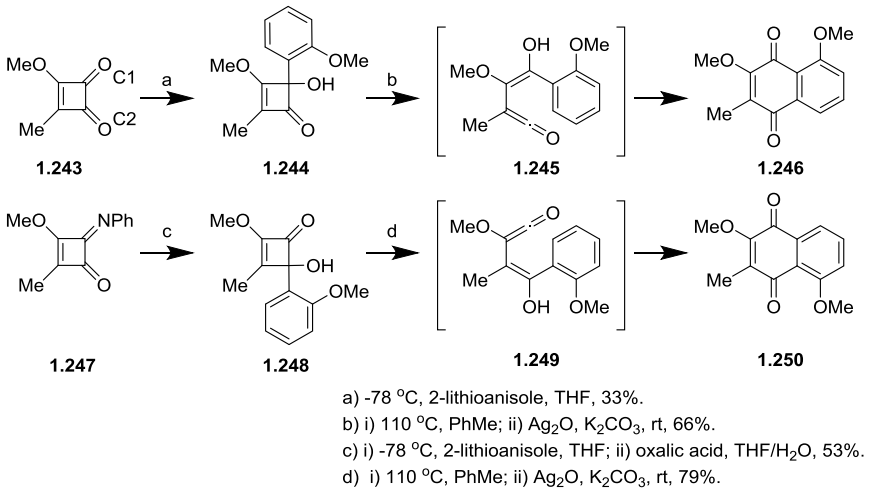

Scheme 1.43. Formation of two benzoquinone regioisomers via selective addition of an organometallic reagent followed by thermolysis.

Under specific conditions, double 1,2-addition to the carbonyl groups in **1.258** is possible (Scheme 1.44).[64] The reaction gives different outcomes when the additions are performed in a stepwise fashion using different organometallic reagents. For example, the stepwise addition of phenylmagnesium bromide to squarate **1.258** provides access to cyclobutenedione **1.260** while double addition of phenyllithium forms intermediate **1.261** and leads to 1,4-dicarbonyl **1.263**.

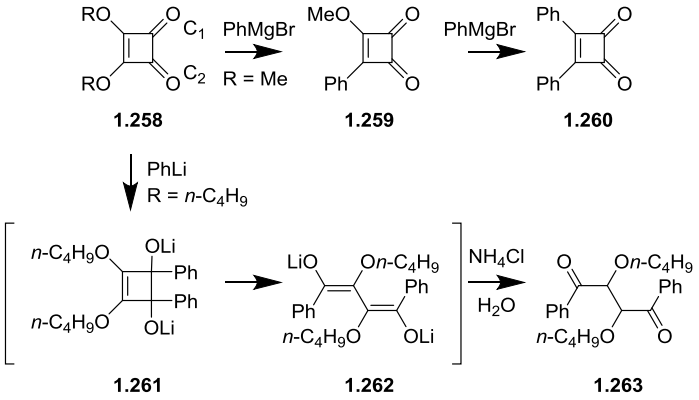

Scheme 1.44. Stepwise and double 1,2-addition to squarate **1.251**.

1,4-additions to cyclobutenediones are also possible with organocuprates (Scheme 1.45). Indeed, Liebeskind and co-workers[65] use the addition of cuprate **1.265** to squarate **1.264** to access cyclobutenone **1.266** and its thermalized product **1.263**.

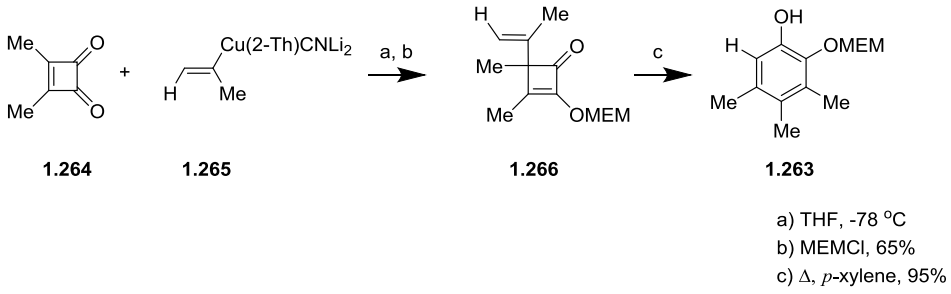

Scheme 1.45. 1,4-addition to cyclobutenedione with organocuprate.

Interestingly, with vinylcyclobutenone **1.268**, 1,6-addition of cuprates was observed.[66] The products **1.269** were formed in 43-69% yield depending on the nature of the organocuprate used (Scheme 1.46).

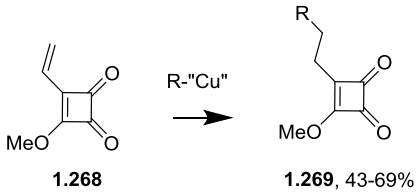

1.268 **1.269**, 43-69%

Scheme 1.46. 1,6-Addition of organocuprates to 3-vinylcyclobutenediones.

If two equivalents of vinyllithium are added to one equivalent of cyclobutenedione **1.270**, double-addition is observed (Scheme 1.47). Importantly, the second addition leads to cyclobutene **1.272**, which spontaneously ring opens to octatetraene **1.273** and triggers an 8π-electrocyclisation via a Möbius transition state to form cyclooctatriene **1.274**. Protonation next induces a transannular ring closure to give bicyclooctenone **1.275**. The course of the reaction changes when vinylmagnesium bromide is used. In this case 1,4-addition to cyclobutenone **1.271** is favoured leading to **1.276**. This triggers a similar sequence of events but gives the isomeric product **1.279**.[67]

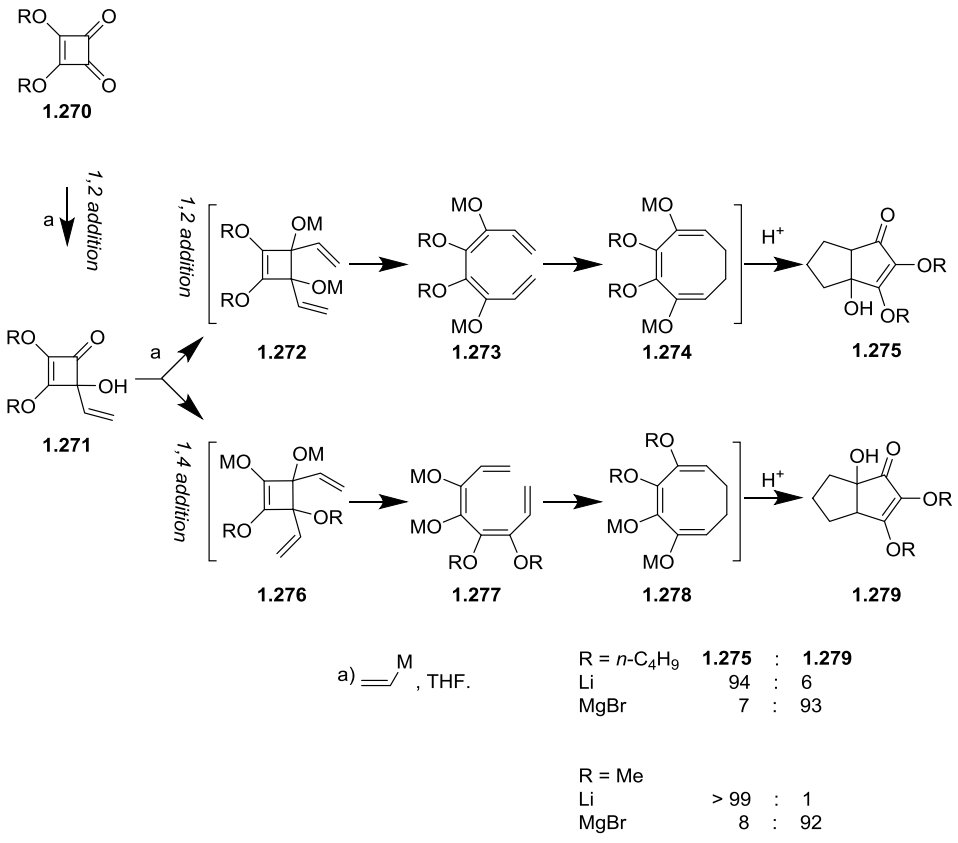

Scheme 1.47. Formation of two bicyclooctenone regioisomers via double organometallic addition reactions.

To provide a deeper understanding of these addition reactions, Varea and co-workers performed a computational study.[68] Analysis of **1.280** showed that the lowest energy conformer of cyclobutenedione is **1.280c**, though the difference between it and conformer **1.280b** was not large (Figure 1.12).

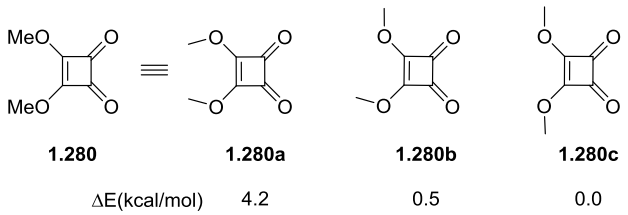

Figure 1.12. Conformations of dimethylcylobutenedione with their calculated relative energies at B3LYP/6-311++G(d,p)//B3LYP/6-31G(d).

Modelling of vinylmagnesium bromide additions to **1.280** were carried at B3LYP/6-311++G(d,p)//B3LYP/6-31G(d) using the CPCM implicit solvation model and Gibbs free energies at 195 K were determined. Calculations with both tetrahydrofuran and diethyl ether as explicit solvent were reported. These free energies (ΔG_{195K}) calculations showed that 1,2-addition of vinylmagnesium bromide to cyclobutenedione **1.280** is greatly favoured (12.4 kcal/mol) over 1,4-addition (34.7 kcal/mol), in agreement with performed experiments (Scheme 1.47). This was explained by the need to proceed via a highly strained transition state **1.286** to achieve 1,4-addition (Figure 1.13). However, modelling of second addition pathway proved more challenging.

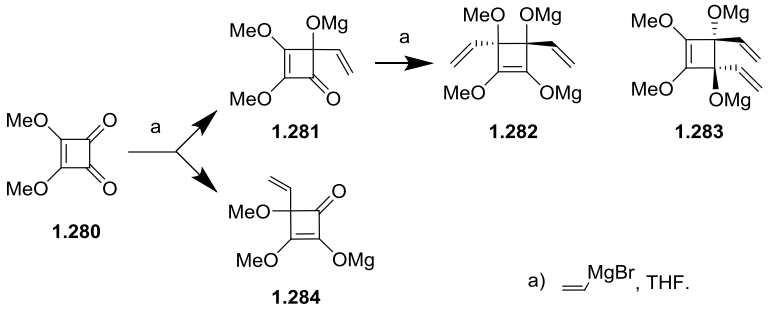

Scheme 1.48. Addition of vinylmagnesium bromide to dimethyl squarate.

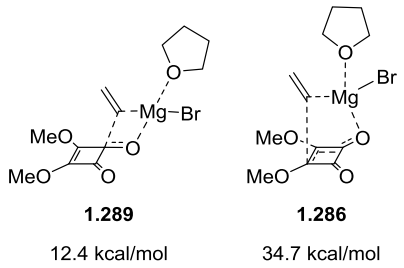

Figure 1.13. Explicit solvated transition state for 1,2- and 1,4-addition of vinylmagnesium bromide to dimethyl squarate.

In the laboratory, the addition of vinylmagnesium bromide to **1.287** or **1.288** (Scheme 1.49) shows that protection of the hydroxyl group inhibited further organometallic additions. Thus, the second organometallic requires a proximal alkoxy group. It was concluded that this was an example of a Ligand-Assisted Nucleophilic Addition (LANA).[69]

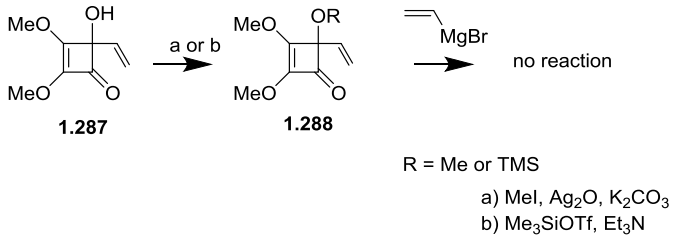

Scheme 1.49. Second addition of vinylmagnesium bromide to dimethyl squarate is inhibited by protection of the hydroxyl group.

Further investigation showed that it was necessary to consider the organomagnesium reagent as an explicitly solvated dimer at B3LYP/6-311++G(d,p) level in order to reproduce the observed experimental selectivity. This showed that the second 1,2-addition to form **1.290** was higher in energy than the 1,4-addition pathway **1.292**, which is in agreement with performed experiments (Scheme 1.50). The influence of solvent was also studied computationally using an explicit solvated transition state. From this it was note of that the reaction barrier is higher in Et_2O than in THF, while selectivity is better in THF than Et_2O. This too supports experimental findings. The facile addition of the second equivalent of Grignard reagent was rationalised with reference to the Complex Induced Proximity Effect (CIPE).[70] This explains why the second addition of a vinyl residue favours *anti*- over *syn*-addition.

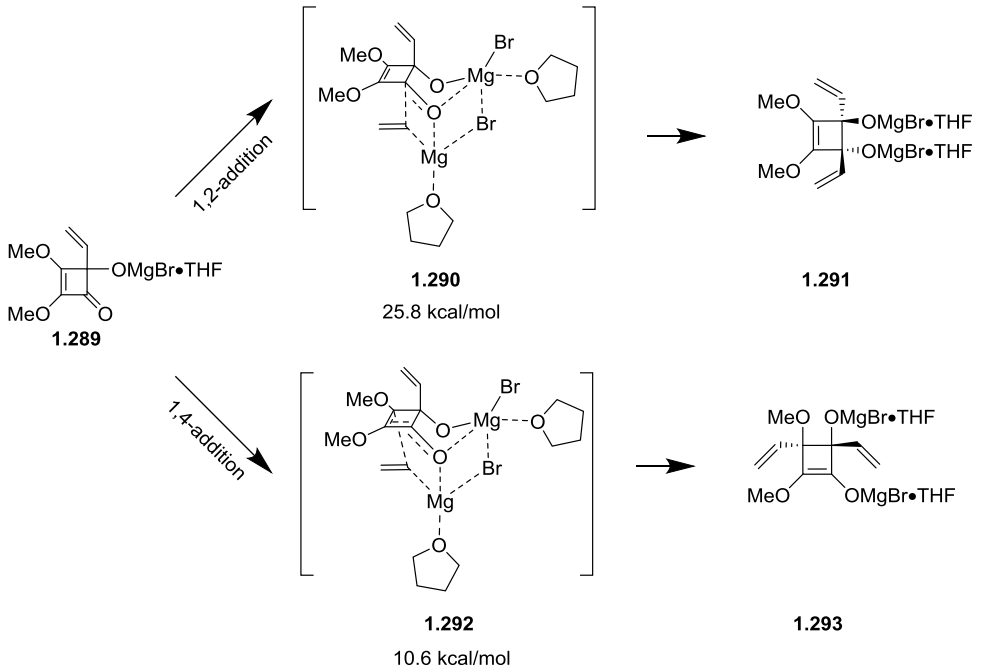

Scheme 1.50. Explicit solvated transition state for 1,2- and 1,4-addition of vinylmagnesium bromide to cyclobutenone **1.289**.

Varea and co-workers[67] also investigated the torquoselectivity of ring closure following quenching of the organometallic adduct **1.294** at low temperature (Scheme 1.51). They concluded that the ring closure of protonated **1.295** to **1.296** is favoured over an 8π electrocyclic reaction and ring closure to **1.297**.

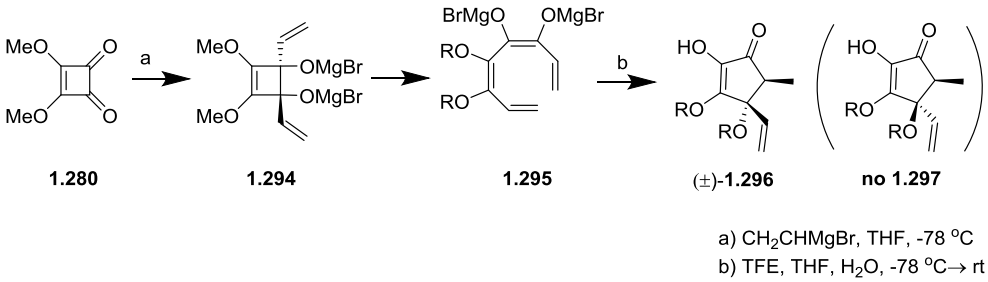

Scheme 1.51. Formation of cyclopentenones via double addition to cyclobutenediones.

The torquoselective ring closure of **1.295** to **1.296** was described as a conrotatory four-electron electrocyclic process. Calculations on the parent system **1.298** showed that the in-phase HOMO of the enolate and the LUMO of acrylic moiety interact in conrotatory fashion to form product **1.299** (Figure 1.14). A variety of related 4π-electrocyclic ring closure reactions have been studied theoretically by De Lera[71] and support this statement.

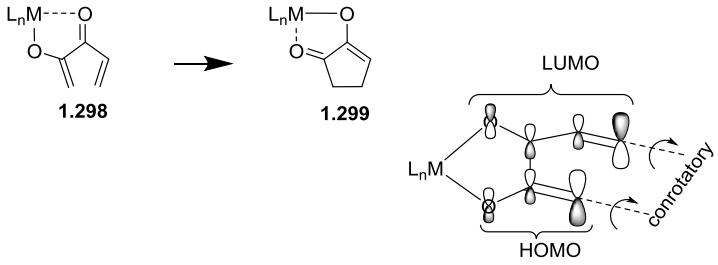

Figure 1.14. Torquoselective ring closure via a conrotatory topology of the enolate moiety and an electrophilic enone group.

Chapter 2: Thermal rearrangement of arylcyclobutenone

THERE IS NOTHING IMPOSSIBLE TO HIM WHO WILL TRY.
ALEXANDER THE GREAT

2.1 Chapter Abstract

In this project the thermal rearrangements of arylcyclobutenones (Scheme 2.1) were investigated to provide new insights into the mechanistic course of such processes.[72] High yields for this reaction were obtained when conducted under flow in dioxane. With the help of quantum mechanical calculations, a variety of possible mechanisms were examined in order to ensure the correctness of the predicted pathway. Benchmarking and validation was performed to ensure the method used provided reliable energies for the overall reaction. Calculated rate constants at 150 ^{o}C were also compared with experimentally determined values. Our theoretical investigation gave good agreement with experimental findings. The primary conclusions were published, in part, in *Chem. Eur. J.*[73] The experimental work described in that publication, and discussed herein, was conducted by Dr. Mubina Mohamed. A fuller account of that study was presented her PhD thesis.[74]

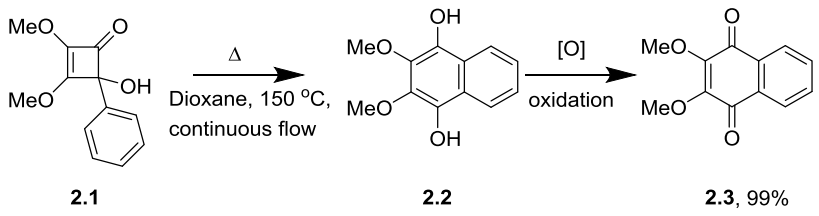

Scheme 2.1. General scheme for the phenylcyclobutenone rearrangement. In this Chapter the *in silico* modelling of the transformation of **2.1** to **2.2** is discussed.

2.1.1 Validation and Benchmark of model reaction

IT'S THE JOB THAT'S NEVER STARTED AS TAKES LONGEST TO FINISH.
J.R.R. TOLKIEN, THE LORD OF THE RINGS

2.1.1.1.1 Method impact on geometry and energy

Our investigation began by testing Moore's proposed mechanism[33] which assumes that ring opening of cyclobutenone **2.1** leads to ketene **2.4** via an electrocyclic ring opening reaction (Scheme 2.2). In the next step of the sequence an electrocyclic 6-closure to **2.5** is proposed followed by tautomerization to hydroquinone **2.2**. The geometry of all intermediates and transition states for the reaction were initially obtained with BLYP[75] and B3LYP[76] using the 6-31G(d)[77] basis set with density fitting using the Orca 2.8 package.[78] Geometries were further refined using the triple zetta basis set 6-311G(d,p)[79] with B3LYP using Gaussian 09. All ground and transition states were confirmed by calculation of the analytical Hessian. The conformational analysis performed revealed large number of transition states and ground state geometries which were relevant for this reaction pathway. The lowest energy conformers found were used for validation in benchmarking to identify the most reliable method with which to proceed.

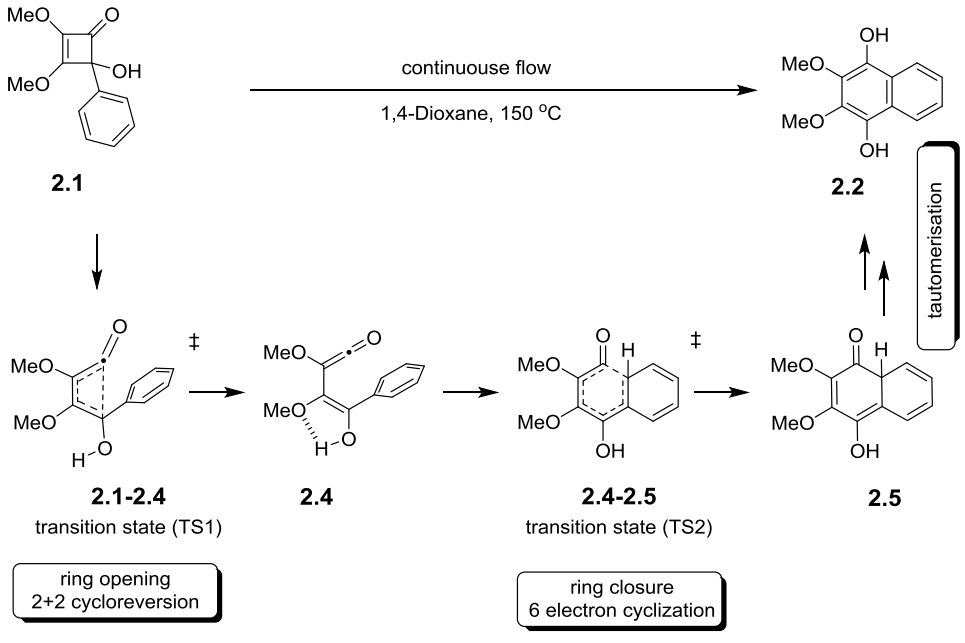

Scheme 2.2. The accepted mechanism of the Moore rearrangement of phenylcyclobutenone **2.1**.

Energetic data from ΔG B3LYP/6-311G(d,p) at 150 °C suggests that the first two steps of the reaction are of high energy, with tautomerization being a lower energy process. Consequently, those steps were used as a benchmark to establish whether

the computational method employed provided accurate energies and could correctly identify the rate-controlling step. As the most time consuming step in our computational study would be transition state optimization,[80] it was important to choose a method that gives satisfactory results with minimum computational cost.

To understand the performance of various computational methods, a study of the geometries and energies of transition states was performed (Table 2.1 and Figure 2.1). The benchmark of geometry for the two transition states (TS1 and TS2) and the ground state of **2.1** was considered with reference to bonds directly involved in the reaction. The C-C distance of the breaking and forming sigma bonds at the point of transition is method dependent and gives an insight into the geometrical accuracy (Figure 2.1). Hartree-Fock,[81] MP2,[82] Semi-empirical (AM1,[83] PM3[84], PM6,[85] RM1[86]), DFT and double hybrid DFT (DH-DFT) method using 6-311G(d,p) basis set were all examined. All data was obtained by full optimization was followed by an analytical Hessian to confirm the character of stationary point (*i.e.* ground state or transition state). From this study, the B2PLYP and MP2 methods emerged as the most reliable geometries and were taken as the reference. However, those methods are the both computational expensive.

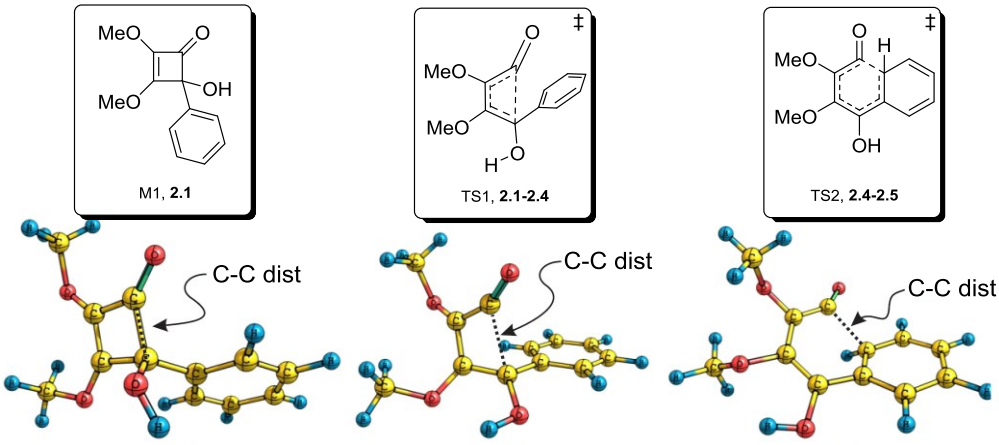

Figure 2.1. Geometries of the reactant (M1) and transition states TS1 and TS2 used for benchmarking and validation. Geometry at B3LYP/6-311G(d,p) level.

Table 2.1. Benchmarking and validation of selected methods for the calculation of geometries for the reactant (M1) and transition states TS1 and TS2. For DFT, DH-DFT and *ab initio* calculations the 6-311G(d,p) basis set was used. The imaginary frequency (ω_i) is reported as a negative value. For semi-empirical calculations, heat of formation is reported. All calculations were performed using Gaussian 09[87] except the semi-empirical methods which were performed using MOPAC 2012.[88]

			Relative Energy [kcal/mol]			C-C dist. [Å]			ω_i [cm^{-1}]	
Method		Level	M1	TS1	TS2	M1	TS1	TS2	TS1	TS2
WFM	Semi-empirical	AM1	0	14.8	10.6	1.583	2.016	2.024	-680.5	-691.6
		PM3	0	15.6	9.6	1.596	2.104	2.052	-447.9	-593.1
		PM6	0	17.4	9.5	1.605	2.073	2.001	-541.2	-725.0
		RM1	0	17.9	6.8	1.580	2.092	2.011	-445.4	-635.0
	Ab initio	HF	0	42.7	46.6	1.550	2.136	1.984	-517.0	-961.1
		MP2	0	23.4	23.4	1.566	2.160	2.091	-186.7	-366.4
DFT		BLYP	0	16.3	17.0	1.605	2.227	2.113	-186.5	-354.0
		B3LYP	0	22.9	22.9	1.579	2.189	2.072	-257.8	-454.6
		M06-2x	0	27.0	26.2	1.562	2.121	2.013	-301.2	-536.0
DH-DFT		B2PLYP	0	32.0	32.6	1.572	2.185	2.072	-240.8	-439.3

Analysing the data from Table 2.1 we can observe the following trends. Semi-empirical methods are attractive because of their speed. For the methods studied the bond length (C-C) on ground state (M1) vary from 1.580 Å (for RM1) to 1.605 Å (for PM6) with RM1 being closest to the value given by B2PLYP[89] (1.572). For the ring opening reaction, the C-C distance at the point of transition (TS1) varies from 2.016 Å (AM1) to 2.104 Å (PM3), with the latter being closest to B2PLYP (2.185 Å). For the ring closure reaction, the C-C distance at the point of transition (TS2) varies from 2.001 Å (PM6) to 2.052 Å (PM3) and again PM3 is close to B2PLYP (2.072 Å). All of these semi-empirical methods predicted that the first step is rate determining with values varying from 14.8 to 17.9 kcal/mol compared to 6.8 to 10.6 kcal/mol for second step. The magnitudes of energy barriers suggest that the reaction can occur at room temperature. However, as the experiment requires heating above ~100 ^{o}C, it was clear that all of these semi-empirical methods underestimate significantly the energy barrier to be overcome. All semi-empirical methods predict similar imaginary frequencies with the most recent methods, such as RM1 or PM6, performing no better than the older methods (AM1 and PM3). This may be due to their parameterisation for ground state rather than transition state structures. It is worth mentioning that all semi-empirical methods tested gave different conformations for the methoxy groups compared to the geometries obtained from B2PLYP and MP2.

Hartree-Fock (HF) calculations performed slightly better in respect of the geometry. The C-C distance given for the ground state (M1) was 1.550 Å, *i.e.* 0.02 Å shorter than predicted by B2PLYP. For the ring opening reaction (TS1), the C-C distance in the transition state was 2.136 Å, (0.04 Å shorter than that of the reference determined by B2PLYP). For the ring closure reaction (TS2) the C-C distance in the transition state was 1.984 Å (0.08Å shorter than that of the reference B2PLYP). The HF method also predicts that the second step of the sequence is rate determining but predicts very high energy barriers for both TS1 and TS2 (42.7 and 46.6 kcal/mol). Additionally, all imaginary frequencies were higher than those given by MP2 and B2PLYP. This is a known limitation of the method as it fails to describe the electron correlation correctly and over estimates reaction barrier.[90] Direct comparison with MP2 gives an insight into the impact of electronic correlation on both the geometry and energy barrier.

Inclusion of electron correlation via second order perturbations through use of the Møller–Plesset second order (MP2) method, improves these geometries compared with HF. The C-C distance prediction for ground state (M1) was 1.566 Å, just 0.006 Å shorter than B2PLYP. For the ring opening reaction the transition state TS1 C-C distance was 2.160 Å, some 0.028 Å shorter, while for the ring closure reaction the C-C distance in the transition state was 2.091 Å (0.02 Å shorter). MP2 gave essentially the same energy for the two transition states, being 23.4 kcal/mol. These were much lower than the value given by the HF method and more in line with the true value. However, this improvement comes at some cost in respected longer computational time compared with HF.

Pure BLYP predicted a C-C bond length in the ground state (M1) of 1.605 Å, some 0.03 Å longer than B2PLYP. For the ring opening reaction (TS1) that C-C distance in the transition state was 2.227 Å (short by 0.040 Å), while the ring closure reaction (TS2) the C-C distance at the point of transition was 2.113 Å (compared to 2.072 Å for B2PLYP). This method is known to perform poorly with transitions states. However, the possibility of using resolution of identity (RI-DFT) makes this calculation an order of magnitude faster than typical DFT methods. Like the aforementioned semi-empirical methods, it too predicted a low reaction barrier, though this time the second step was deemed to be rate determining step.

B3LYP predicted bond length comparable with B2PLYP, all being within 0.01 Å. The calculated imaginary frequencies were also close to those attained using B2PLYP. Indeed, the geometries obtained with this method at using a lower 6-31G(d) basis set had already used to study cyclobutenone diradical ring closure reactions,[54] which is why we were encourage to use the method here. Another advantage of B3LYP with the 6-311G(d,p) basis set is that unscaled frequencies are close to experimental frequency, making this method appropriate for vibrational free energy correction. The more sophisticated DFT functional M06-2x[91] predicts shorter bond lengths than the reference B2PLYP by as much a 0.04 Å, while imaginary frequencies were higher.

All calculations obtained with the 6-311G(d,p) basis set suffer from its incomplete basis set. Undoubtedly, inclusion of more tempered basis sets like MG3S, ma-TZVP, or maug-cc-pV(T+d)Z can improve geometry predictions, as recommend by

Truhlar.[80d] From a practical point of view use of less polarised and diffuse basis sets for geometry optimisation gives a much "sharper" geometry optimization due to faster gradients and Hessians, which can be a significant bottleneck for transition state searches. For that reason screening a large number of molecules with heavy basis sets are not desirable. Also, M06-2x is more sensitive to integral grid and takes longer for the geometry optimization of large molecules compared to B3LYP.[92]

The main conclusion from the aforementioned geometry benchmarking was that B3LYP with the 6-311G(d,p) basis set is a cheaper equivalent of more expensive MP2 and B2PLYP and is appropriate for the geometry optimization. RI-BLYP can be used for fast pre-optimisation and conformational screening. Semi-empirical methods gave incorrect geometries for all of the transition states so must be used with caution. The barrier height predictions vary significantly, suggesting the need for another validation method for accurate energy calculations. Additionally, 6-311G(d,p) is not able to provide quantitative energies with MP2 and B2PLYP due to slow basis set convergence. Basis set extrapolation techniques would be required.[93]

2.1.1.1.2 Method and set dependency impact on electronic energy

THE CHEMIST IS A GUEST AT THE PHYSICIST'S TABLE AND FREQUENTLY DINES WELL.
RICHARD BERSOHN

The quantitative calculation of energy barriers requires a method that is able to provide reliable predictions for the relative energy barriers presented by competitive pathways. From previous benchmarking of the at B3LYP with 6-311G(d,p) basis set we showed that this provide appropriate geometry predictions. In spite of the limited treatment of dynamic electron correlation by DFT, *ab initio* methods were applied to obtain accurate energetic values. To find the best method with respect to cost and accuracy, a range of calculations were performed (Table 2.2) to complement data from Table 2.1. The most accurate energy calculation in Table 2 was given by CCSD(T)/CBS (Table 2.2, entry 1) which is believed to get close to the basis set limit of that method. Such calculations give errors close to a limit of chemical accuracy and will be taken as reference here. For the time being CCSD(T) calculations, with its larger basis set, are not possible for large systems due to limitations in computer power.

It is clear from this approach that the ring-closure step (27.9 kcal/mol) has a higher barrier than the initial ring-opening step (26.6 kcal/mol). The CCSD(T) at 6-31G(d) (Table 2.2, entry 2) with Pople's double zeta basis set gives a similar energetic values for TS2 (28.0 kcal/mol) but is much higher by 1.8 kcal/mol for TS1 (28.4 kcal/mol). Indeed, it incorrectly predicts that the first step is rate determining which may be related to a slow basis set convergence for TS1 than TS2. The lower computational cost of the MP2 method with 6-31G(d) and cc-pVDZ basis sets (Table 1.2, entry 4 and 5) makes it attractive. Though it gave values similar to B3LYP (Table 2.2, entry 6, 7 and 8), it incorrectly predicted that the first step of the sequence was rate determining and underestimate both energy barriers. Basis set extrapolation of MP2 gives values at the basis set limit (MP2/CBS). This revision correctly predicted that the second step was rate determining by 1 kcal/mol, though the energy barrier calculated was too low by ~4 kcal/mol compared with the CCSD(T)/CBS reference method. MP2, being more expensive computationally, did not show any enhancement in performance over B3LYP for our system.

The improvement of B3LYP in respect of basis set showed that this method at 6-311G(d,p) is not able to identify the rate determining step correctly or provide quantitative values for barrier heights. Increasing the basis set from 6-311G(d,p) to 6-311+G(d,p), increased the reaction barrier for ring opening by 0.23 kcal/mol and for the ring closure by 1.00 kcal/mol (Table 2.2, entry 6 and 7). This shows the significance of adding a diffusion function to carbon and oxygen atoms. A further increase of basis set to 6-311++G(2df,2p) (Table 2.2, entry 7 and 8), led to a decreased in the calculated barrier for ring opening by 0.2 kcal/mol and an increased for the barrier for ring closure by 0.24 kcal/mol. Indeed, with this basis set the second step was correctly identified as rate determinant by 1.4 kcal/mol, in agreement with CCSD(T)/CBS. However, the reaction energies it predicted were lower, by ~3 kcal/mol. Underestimating the energies barrier for reaction is a known frailty of B3LYP which, even at the basis set limit, will not provide quantitative data. Here B3LYP gives a similar performance to MP2.

Table 2.2. Effect of Basis set on B3LYP in comparison with results attained using the coupled cluster method for the reactant (M1), transition state TS1 and TS2. All calculation were performed using the geometry form B3LYP/6-311G(d,p). The most accurate calculations are from CCSD(T)/CBS. All energies shown are in kcal/mol.

Entry	Method/Basis set	M1	TS1	TS2
1	CCSD(T)/CBS*//B3LYP/6-311G(d,p)	0.00	26.6	27.9
2	CCSD(T)/6-31G(d)//B3LYP/6-311G(d,p)	0.00	28.4	28.0
3	MP2/CBS**//B3LYP/6-311G(d,p)	0.00	22.6	23.6
4	MP2/cc-pVDZ	0.00	23.5	23.3
5	MP2/6-31G(d)	0.00	24.9	24.1
6	B3LYP/6-311++G(2df,2p)	0.00	22.7	24.1
7	B3LYP/6-311+G(d,p)	0.00	23.1	23.9
8	B3LYP/6-311G(d,p)	0.00	22.9	22.9

*energies from CCSD(T)/6-31G(d) with MP2 extrapolation with cc-pVTZ and cc-pVQZ basis sets; **energies from MP2 extrapolation with cc-pVTZ and cc-pVQZ basis sets.

As the tested methods failed to provide an accurate energy picture for this transformation we concluded that it was necessary to perform CCSD(T) calculations. It was shown[73] that the B3LYP method underestimated the reaction barrier,

predicting the reaction to be much faster than it is in reality. By contrast, the coupled cluster method, even with a medium basis set, provided more reliable data and gave energies close to the experimentally measured values.

For this reason, our modelling of the Moore rearrangement was conducted using CCSD(T)/6-31G(d) calculations performed as a single point on B3LYP/6-311G(d,p) geometries and it was designated as CCSD(T)/6-31G(d)//B3LYP/6-311G(d,p). This method was found to be robust when applied to the multistep reaction sequence. All coupled cluster calculations have a T1 diagnostic lower than 0.016, suggesting that single reference methods are appropriate. It is known that values higher than 0.02 suggest significant multi-reference character and hence require the use of multi-reference methods. [94]

2.1.1.1.3 Vibrational correction impact on the barrier heights

WELL BEGUN IS HALF DONE.
ARISTOTLE

To compare calculated values with performed experiments we employed the Eyring equation.[95] This required calculation of Gibbs free energies which includes enthalpy and entropy terms and corrections for temperature (Table 2.3).

Table 2.3. Relative zero point energy and Gibbs free energy correction at B3LYP/6-311G(d,p).

Corrections to:	**M1**	**TS1**	**TS2**
Zero Point Energies (ΔZPE)	0	-1.3	-1.1
Gibbs Free Energies (ΔG^o) at 25 ^oC	0	-0.1	1.2
Free Energies (ΔG^o) at 150 ^oC	0	0.5	2.4

All energies shown are in kcal/mol.

Corrections were performed using B3LYP/6-311G(d,p). Inclusion of Zero Point Energies (ZPE) lowered both transition state energies by more than 1.1 kcal/mol. By contrast, the Gibbs free energy correction at room temperature raised TS2 by 1.2 kcal/mol, but had a little impact on TS1. Finally Free Energy corrections for the

experimental temperature of 150 °C raised both TS1 and TS2, by 0.5 and 2.4 kcal/mol respectively. Indeed, the second step is now favourable energetically and, after correction, is implicated as rate determining step. Inclusion of a free energy correction is essential here as consideration of energies without these corrections in place can lead to misrepresentative quantitative results.[73]

2.1.1.1.4 Solvation energy impact on the barrier heights

IF YOU CAN DREAM IT, YOU CAN DO IT.
WALT DISNEY

As experiments were performed in 1,4-dioxane as solvent, it seemed sensible to see if it this had any bearing on the course of the reaction. The impact of solvation was examined using CPCM[96] and IEF-PCM[97] with both giving similar values (Figure 2.2). They indicated that the energy of the first step (**2.1-2.4)** increases by *ca.* 0.7 kcal/mol and the second (**2.4-2.5**) by 0.3-0.6 kcal/mol. These figures are not high, which is to be expected for electrocyclic reactions that do not involve charged species.

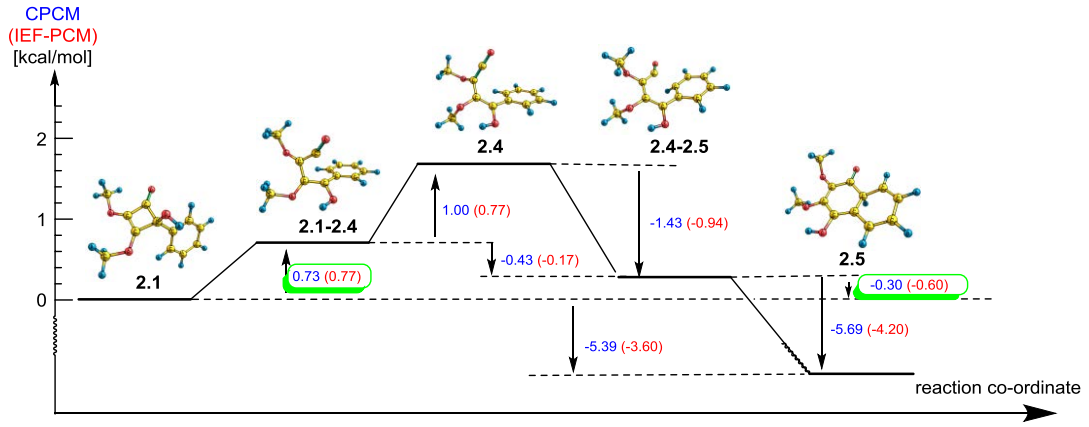

Figure 2.2. Relative solvation energies obtained by the solvation models: **CPCM** and **IEF-PCM** with 1,4-dioxane as a solvent using B3LYP/6-311G(d,p).

The performance of such solvation methods when applied with 1,4-dioxane at 150 °C is uncertain as the incompressibility approximation is not valid.[98] At such elevated temperatures one would expect less interaction than at room temperature due to higher solvent diffusion.[99] Some reports in the literature suggest that it is better to adjust the dielectric constant at high temperatures.[100]

2.1.1.1.5 Conclusions regarding our energy calculations

GOOD SENSE ABOUT TRIVIALITIES IS BETTER THAN NONSENSE
ABOUT THINGS THAT MATTER
MAX BEERBOHM

Validation and benchmarking for the first step of the arylcyclobutenone rearrangement were performed. Extensive analysis shows that B3LYP/6-311G(d,p) was an appropriate method for geometry calculations. With free energy corrections, the B3LYP method proved appropriate to provide qualitative picture of the reaction. To achieve a quantitative picture it was necessary to acquire data using complete basis set energy extrapolation at CCSD(T) level. The less demanding CCSD(T)/6-31G(d) gave a close fit to for the second step (TS2) but over estimates the first step (TS1) by ~2 kcal/mol. For that reason, further calculations used data from CCSD(T)/6-31G(d)//B3LYP/6-311G(d,p) with a Gibbs free energy correction for reactions conducted at 150 ^{o}C. The CCSD(T)/6-31G(d)//B3LYP/6-311G(d,p) approach is more appropriate for studying multistep reactions and competitive pathways when the nature of each transition state is very different.

2.1.2 Description of thermal path

... A MOLECULAR SYSTEM ... (PASSES) ... FROM ONE STATE OF EQUILIBRIUM
TO ANOTHER ... BY MEANS OF ALL POSSIBLE INTERMEDIATE PATHS,
BUT THE PATH MOST ECONOMICAL OF ENERGY WILL BE THE MORE OFTEN TRAVELED.
HENRY EYRING

Each step in the reaction pathway, from reactant to final product, for the arylcyclobutenone rearrangement reaction was studied computationally. A large number of conformers were screened to identify the lowest transition states for each step of the sequence. Gibbs free energy graphs at 150 ^{o}C reveal that the second step is rate determining (Figure 2.3). Rates calculated from B3LYP/6-311G(d,p) predict a rate constant of 0.72 s^{-1}, being ~500 times faster than that given by experiment of (0.0015 s^{-1}). Remarkably, the CCSD(T)/6-31G(d) method predicts a rate constant of 0.0016 s^{-1} which is in excellent agreement with the measured value.[73]

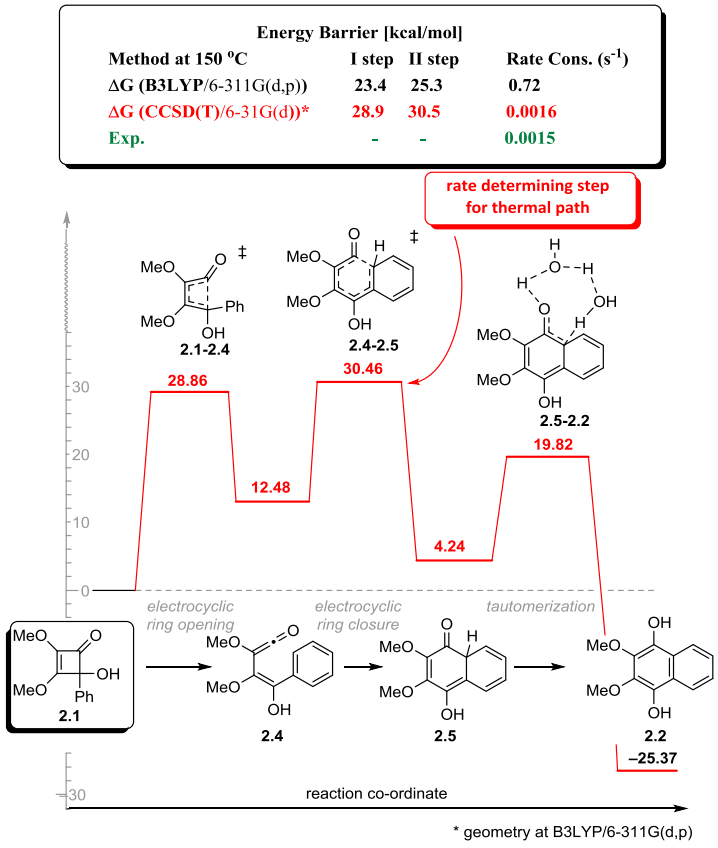

Figure 2.3. Gibbs free energy graph of the lowest path of the arylcyclobutenone rearrangement.

The calculations we undertook suggest that the reaction is a three step process with the second step being rate determinant with a barrier of 30.5 kcal/mol (Figure 2.3). Further analysis of the lowest energy pathway included a full

description of the lowest energy intermediates involved and was supported by wavefunction and density analysis. Bond order analysis was performed using Fuzzy bond order,[101] as it is more stable with respect to changes in basis-set compared to the Mayer bond order method[102] and with good correlation to measured values.[102-103] Fuzzy bond order is defined in fuzzy atomic space where any point of space may simultaneously be attributed to many atoms by a soft overlapping boundaries partitioning scheme.

Analysis using Quantum Theory of Atom in Molecule (QTAIM)[104] was used to show the existence of bond critical points (BCP) which are associated with the bond path described by electron density. All characteristics of a bond are thus reflected by the properties of the bond critical point (BCP). Importantly, negative Laplacian ($\nabla^2\rho(r)$) are given for a shared interaction while a positive value represents a closed-shell interaction. Usually, shared interactions are found for covalent bonds while a closed shell interaction indicates ionic and van der Waals' interactions. Bond strength is reflected by electron density ρ_b, Laplacian, $\nabla^2\rho_b$, and potential energy density $V(r)$ at the BCP.[105] QTAIM also allows non-covalent interactions to be studied. The Reduced Density Gradient (RDG) surface is powerful technic to analyse weak interactions.[106] This surface distinguishes between repulsive and attractive interactions with respect to the second largest eigenvalue (λ_2) of the electron density Hessian matrix. As suggested by convention, the blue area represent strong attractive interactions while red areas represent strong repulsive interactions and green area represent weak (such as van der Waals) attractive interactions in the range from -0.04 to 0.02. Thus, QTAIM analysis is based on a discrete space partition where any point can be attributed to only one atom.

Orbital analysis, such as Natural Bond Orbital (NBO),[107][108] gives information on the orbitals that are interacting and the energy of those interactions. Here we analyse F(i,j), which refers to the orbital overlap term, and E(2) which is related to the energy of that interaction. Natural Bond Orbital gives a simplistic vision of interactions as the analysis is based on localised molecular orbitals for an optimal Lewis structure.

Conformation screening of the lowest conformation of the starting material **2.1** shows that the hydroxyl group points towards the benzene ring rather than the

cyclobutenone. No hydrogen bond is evident in the lowest energy conformation. The C-C distance for bond linking the carbonyl and alcohol residues is 1.579 Å (Figure 2.4), which is longer than that in ethane by 0.05 Å. Indeed, Fuzzy bond order analysis gives a value of 0.87, compared to 1.23 for ethane **2.6**, indicating that it has far less bonding character than a normal C-C bond. Laplacian, electron density and potential energy density values at the bond critical point also show lower values than ethane. These findings support the fact that this bond is weaker than a typical single bond and is easier to break on thermolysis.

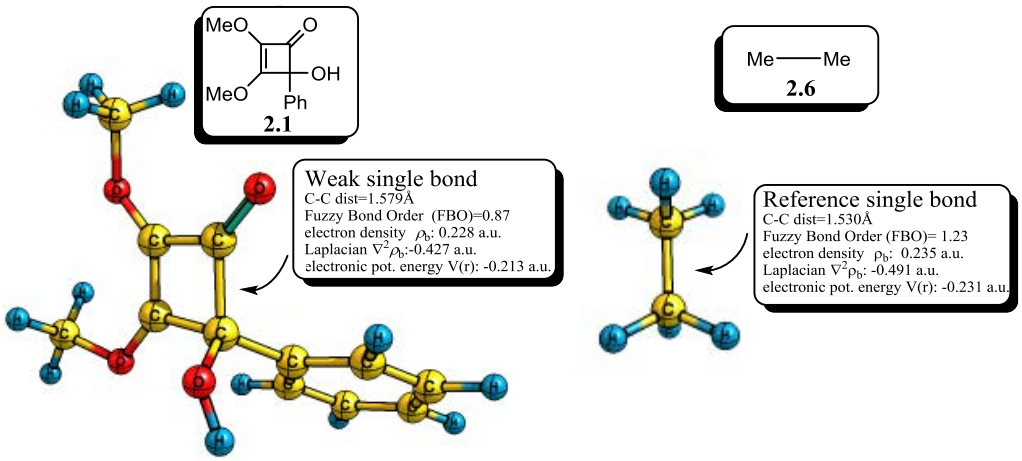

Figure 2.4. Geometry of the lowest ground state of arylcyclobutenone **2.1**. Geometry and NBO analysis at B3LYP/6-311G(d,p), Fuzzy bond order and QTAIM analysis at M062X/6-311++G(2d,2p).

Analysis of the lowest energy transition state for ring opening, **2.1-2.4**, shows that the conformation of both the hydroxy and methoxy groups are different to those in starting material (Figure 2.5). The methoxy groups are inclined out of the plane of the ring to some extent while the phenyl ring and hydroxyl groups are orthogonal to the breaking C-C sigma bond. Both assist the ring opening reaction via orbital interactions with the $\sigma^*_{C\text{-}C}$ of the breaking bond. The conformation of the hydroxyl group allows better overlap between its p-rich lone pair and the σ* of the breaking C-C bond. In this step one σ and one π bond are broken leading to two new π bonds. The transition state geometry is reached when the aforementioned C-C distance is 2.189 Å.

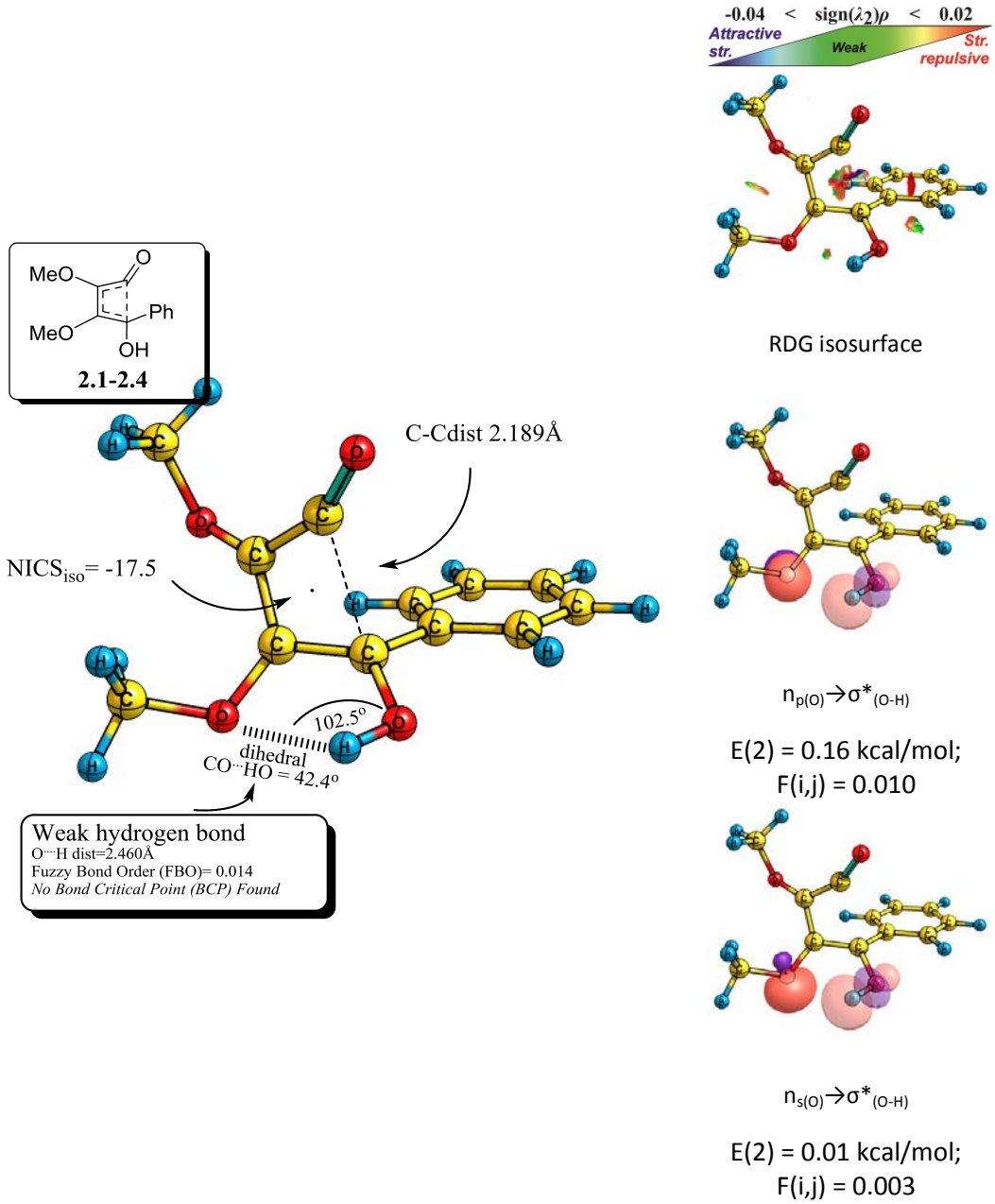

Figure 2.5. Geometry of the lowest energy transition state of ring opening of aryl-cyclobutenone. Geometry and NBO at B3LYP/6-311G(d,p), Fuzzy bond order analysis and RDG at M062X/6-311++G(2d,2p).

The hydrogen of the hydroxyl group, which in the starting material was pointing towards the phenyl ring, now points towards the proximal methoxy group. Indeed, its geometry suggests the formation a nonlinear intramolecular hydrogen bond, as the O-H-O angle is 102.5° while the C-O-H-O dihedral angle is 42.2°. A Quantum Theory of Atoms in Molecules (QTAIM) analysis of structure failed to revel bond critical point (BCP) for this hydrogen bond, which is consistent with reports for similar systems.[109] However, a reduced density gradient (RDG) analysis showed a small attractive interaction (in green-blue) close to a repulsive region (in brown-red) of the similar size. Fuzzy bond order analysis also gave a low value of 0.01. Finally, a Second Order Perturbation analysis with Natural Bond Orbital (E(2)-NBO) analysis revealed that the p-rich oxygen and s-rich lone pair do interacting with σ^*_{OH}. However, the orbital interaction has a low total value of 0.17 kcal/mol indicating poor orbital overlap, as evidenced by a low value for the orbital overlap term F(i,j) for both interactions. These findings suggest that this hydrogen bonding plays no significant role here. The ring opening reaction involves four electrons and thus obeys the rule of Möbius aromaticity. Calculation of isotropic nuclear independent chemical shift ($NICS(0)_{iso}$) gives negative value of -17.5, as would be expected for an aromatic transition state (Figure 2.5). This is consistent with values in the literature for similar cyclobutenone ring systems.[46]

The ring opening reaction gives ketene **2.4** as a reaction intermediate (Figure 2.6). This ketene is very reactive as it possesses a low energy LUMO located in ketene group. Hydrogen bonding within that molecule was also investigated and was found to be energetically significant. Indeed the hydrogen oxygen distance is short (1.96 Å) and the H-O-H angle reduces to 118.1°. Compared to that found in transition state TS1, the dihedral angle is turned to 2.1°. The energy of the hydrogen bond was estimated to be 7.8 kcal/mol using electronic potential density V(r) at the bond critical point.[105]

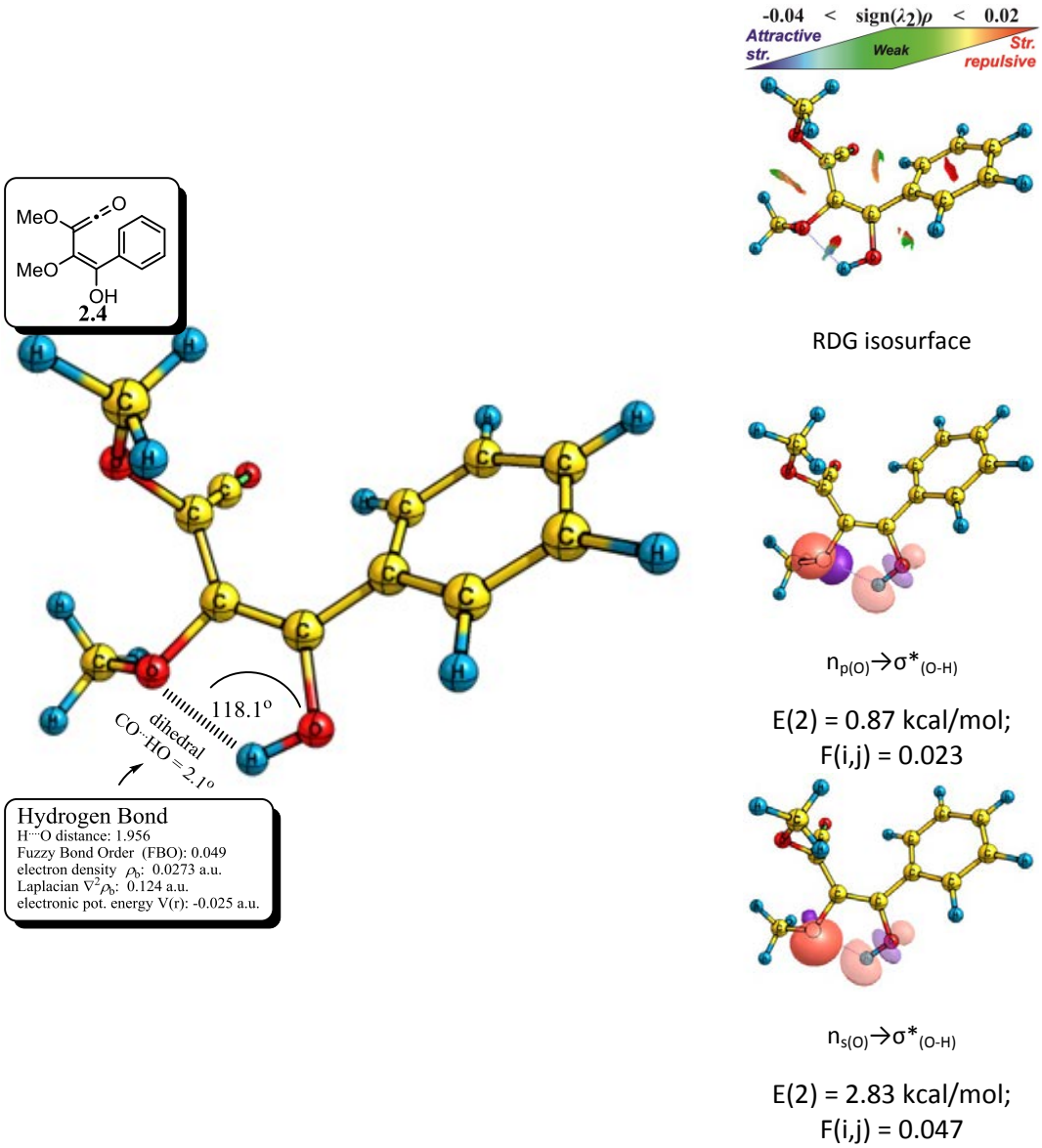

Figure 2.6. Geometry of ketenic intermediate **2.4** in the phenylcyclobutanone rearrangement pathway. Geometry and NBO at B3LYP/6-311G(d,p), Fuzzy bond order analysis and RDG at M062X/6-311++G(2d,2p).

Natural bond orbital analysis also shows a high value for the hydrogen bonding interaction. The s-rich lone pair of the proximal methoxy group interacts more strongly with the σ^*_{OH} than its p-rich lone pair, having an interaction energy of 3.70 kcal/mol. The orbital overlap term F(i,j) for both interactions is higher (0.047 and 0.023) than it is in the transition state TS1 resulting in higher interaction energies. Fuzzy bond order analysis also reflects this with a value of 0.05. Reduced density

gradient (RDG) analysis reflects this too, with the appearance of a more prominent attractive (green-blue) area than was observed for transition state TS1. All these findings suggest that hydrogen bonding is significant for the ketene intermediate **2.3** and helps to define the geometry of its lower energy conformation.

In the second step of the reaction, ketene **2.3** undergoes ring closure with the proximal arene. This is the rate determinant step and displays a late transition state **2.4-2.5** (Figure 2.7), as expected due to the loss of aromatization energy. In this step the breaking of a π bond in the aromatic system is compensated to some extend by the energy gained by formation of a sigma bond. The calculated transition state has a C-C distance of 2.07 Å for the bond being formed (Figure 2.8). The geometry of the benzene ring is distorted a little from planarity with the angle between the plane of the arene and the newly forming bond being ~40°. The methoxy groups are almost orthogonal to the plane of the 6-membered ring being formed.

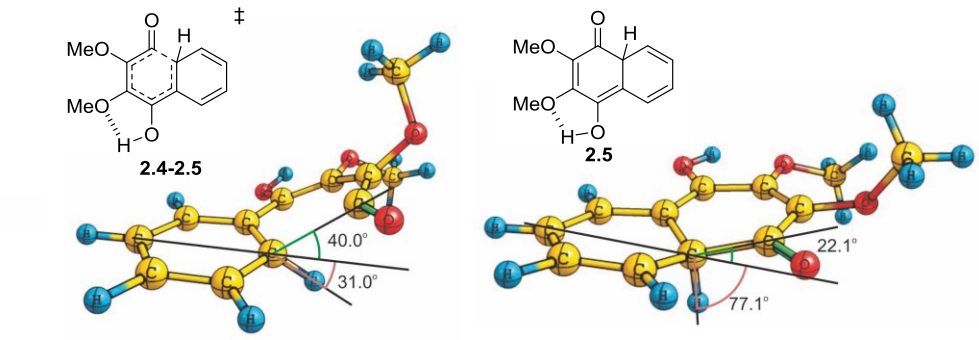

Figure 2.7. Geometry of the transition state for the second step of the sequence and the ketone intermediate at B3LYP/6-311G(d,p).

This reaction is a six electron electrocyclization reaction that obey Hückel rules of orbital overlap. The $NICS_{iso}$ gives a negative value -9.1, supporting the aromatic character of this transition state (Figure 2.8).

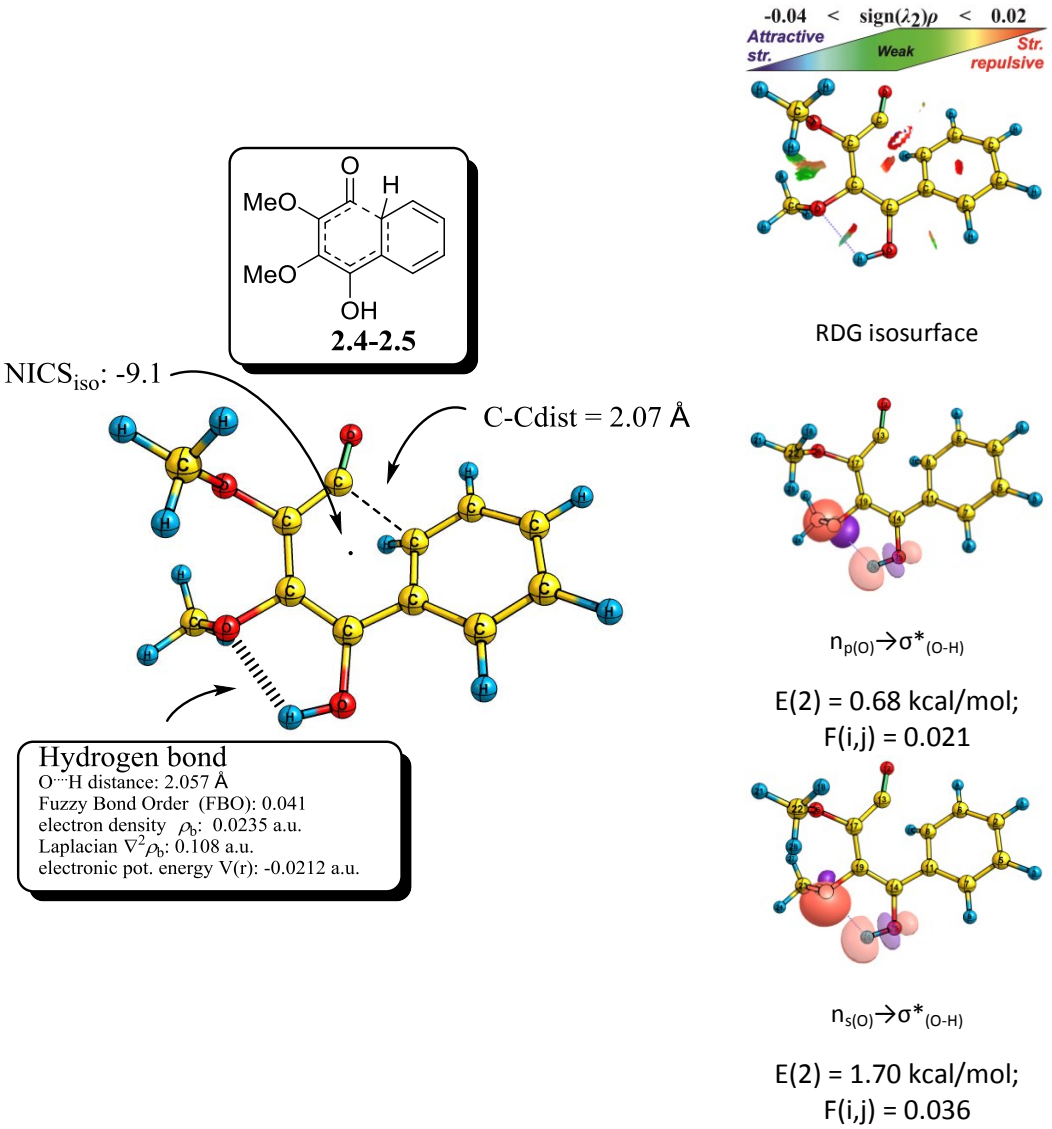

Figure 2.8. Geometry of the transition state for the ring closure step **2.4-2.5**. Geometry and NBO at B3LYP/6-311G(d,p), Fuzzy bond order analysis, AIM and RDG at M062X/6-311++G(2d,2p).

Importantly, the hydrogen bond between the -OH and -OMe residue is preserved in the transition state but has a higher O···H distance (2.06 Å) compared with the previous intermediate. The energy of that hydrogen bond is estimated to be 6.64 kcal/mol by potential energy V(r)[105] at bond critical point (BCP) and the total value of those interactions from NBO is 2.38 kcal/mol (from both LP_O-σ^*_{O-H}). Fuzzy bond order gives a value of 0.041 for the hydrogen bond. The reduced density gradient (RDG) show an attractive green-blue area and a repulsive brown-red between these

groups. Both appear smaller for **2.4-2.5** than those of the ketenic intermediate **2.4**. These findings suggest that hydrogen bonding is significant and helps to define the geometry of the lowest energy conformer.

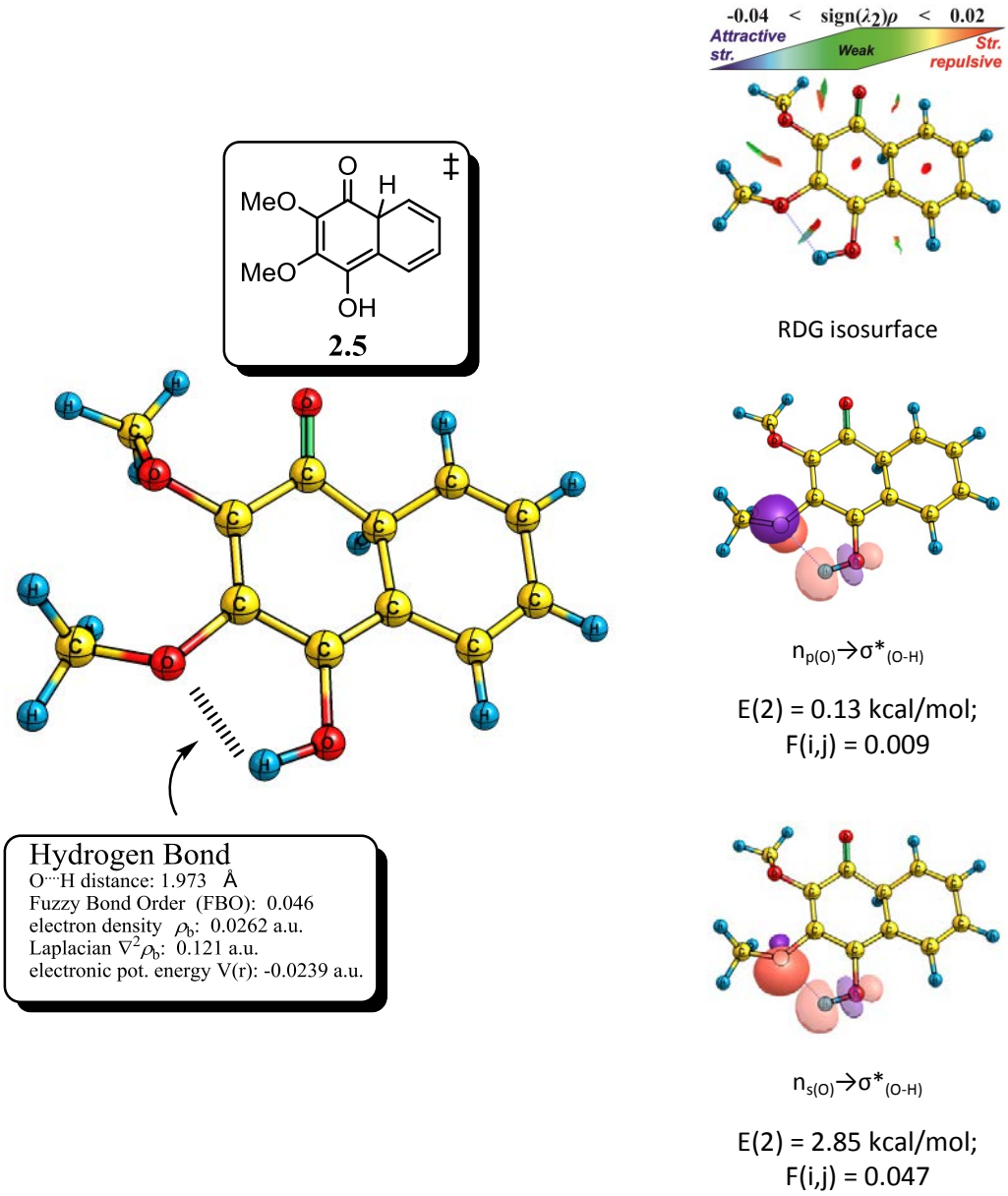

Figure 2.9. Geometry and NBO at B3LYP/6-311G(d,p), Fuzzy bond order analysis, AIM and RDG at M062X/6-311++G(2d,2p).

The ring closure reaction to form ketone **2.5** (Figure 2.9) shows that the aforementioned hydrogen bond is preserved and shortens to a distance of 1.973 Å as the reaction proceeds. Fuzzy bond order analysis gave a value of 0.045 for this interaction and its contribution was estimated by 2.98 kcal/mol from NBO orbital interaction calculations. An AIM analysis indicates that hydrogen bond is stronger and more significant than for transition state TS2.

Ketone **2.5** has a higher energy than phenylcyclobutenone **2.1** by 4.24 kcal (Figure 2.3). Indeed, the thermodynamic driving force for this reaction comes in next step where ketone **2.5** undergoes tautomerization to benzohydroxyquinone **2.2** (Figure 2.3). Calculation shows that this reaction is exergonic and favourable by -25.4 kcal/mol due to the aromatisation of both six membered rings. Indeed, this step drives the whole reaction forward. The mechanism of tautomerization was explored to provide insights to the energy barrier. Different tautomerization mechanisms, such as direct H-transfer, multiple H-transfer and bimolecular H-transfer were explored (Figure 2.10). In the literature it has been suggested that tautomerization by direct H-transfer is slow under normal conditions as it requires a disfavoured suprafacial 1,3-hydrogen shift.

A study of these different pathways (Figure 2.10) showed that direct H-transfer does indeed have a high barrier of ~47.7 kcal/mol, which is higher than exhibited by the rate determinant second step (Figure 2.3). This is to be expected as the transition state involves unfavourable suprafacial geometry (Figure 2.10). It also has a high imaginary frequency (-1976.9 cm^{-1}), suggesting a significant contribution from tunnelling.

An alternative pathway involves multiproton transfer and is reliant on the availability of hydrogen bonds.[110] It can involve any organic or inorganic molecule containing a free hydroxyl group. In our calculations water was used as the simplest canonical model, with a small number of conformers. For ketone **2.5**, addition of one water molecule lower the barrier for tautomerization to 16.4 kcal/mol.

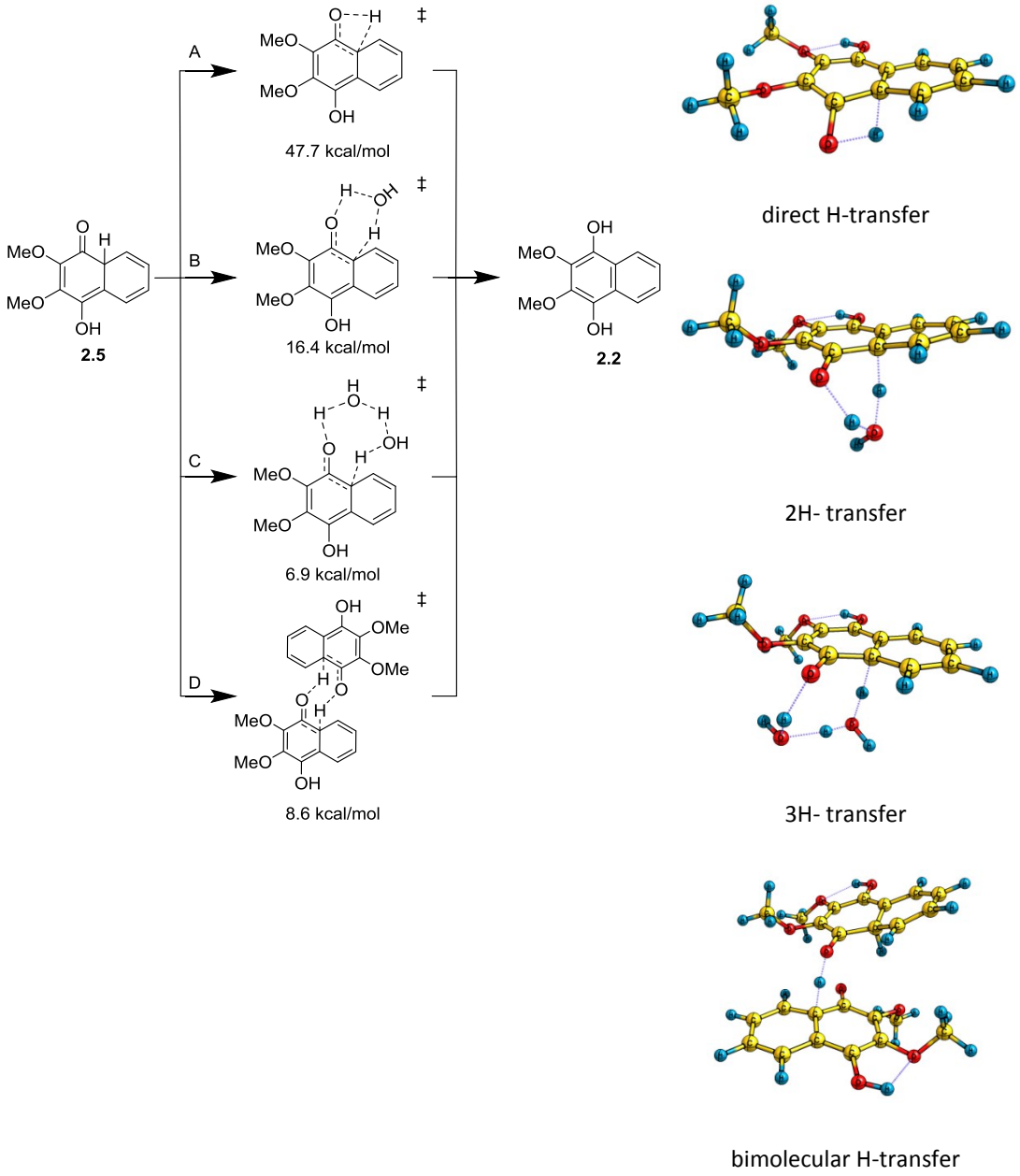

Figure 2.10. Propose mechanisms for tautomerization reaction. Electronic energy from B3LYP/6-311G(d,p) energies are reported in kcal/mol.

Inclusion of second water molecule lowered that barrier further to just 6.9 kcal/mol. Indeed, this was the lowest barrier observed of all the paths analysed using B3LYP/6-311G(d,p). The bimolecular proton-transfer involving two molecules of ketone **2.5** was also examined and found to be similar.[111] The energy barrier is slightly higher (8.6 kcal/mol). However, as the concentration of this ketone is likely to be low, it is unlikely to be an important pathway. However, in circumstances where entropic effects dominate, this channel could become significant. Proton transfer catalysed by the starting material **2.1**, product **2.2**, or Lewis acids and bases in the system, were not investigated but by implication may play a significant role.

The final product of this arylcyclobutanone rearangement is dihydrobenzoquinone **2.2**. Its lowest conformation is shown in Figure 2.11. The molecule has two fused aromatic ring systems and is much more stable than the initial arylcyclobutanone **2.1** with its high energy four membered ring. Experimentaly the corresponding benzoquinone **2.3** is often observed as the major product ot the reaction. It comes from air oxidation of **2.2** which was not modelled.

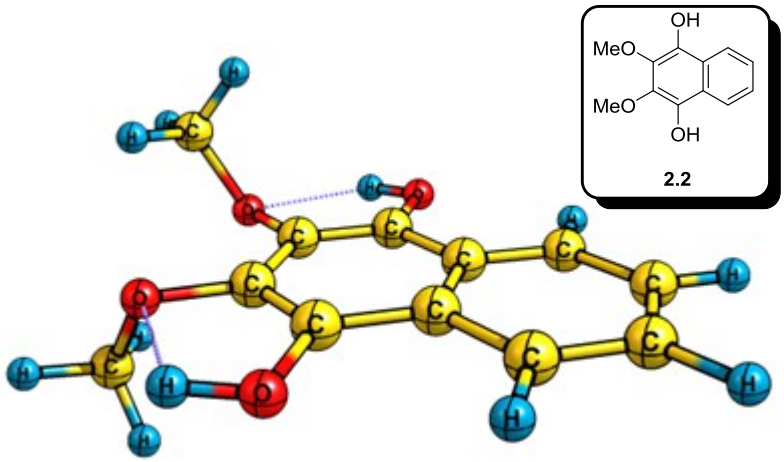

Figure 2.11. Product of arylcyclobutenone rearangement at B3LYP/6-311G(d,p).

2.2 Conclusions

SO LITTLE DONE, SO MUCH TO DO.
ALEXANDER GRAHAM BELL

The thermal rearrangement of arylcyclobutenone **2.1** was modelled *in silico*. Extensive screening of conformations with B3LYP was followed by single point calculations at CCSD(T), as recommended by our benchmarking. Calculations revealed that this rearrangement involves a three-step pathway, with the second step being rate determining. Excellent agreement between theory and experimental was observed, especially in respect of the rate constants obtained. A hydrogen bond between the hydroxyl group and a proximal methoxy residue is unimportant in the first step of the reaction involving ring opening. However it becomes more important as the reaction progresses. Modelling suggest that the final step of the sequence, tautomerization, proceeds via a transition state involving a concerted triple proton transfer (Figure 2.10, Path C) using water as a canonical model.

Chapter 3: Understanding the Torquoselectivity in Cyclobutenone Rearrangements

GET ON YOUR BIKES AND RIDE!
FREDDIE MERCURY

3.1 Chapter abstract

Our analysis of the arylcyclobutenone rearrangement next examined the question of torquoselectivity. The ring opening reaction can occur via inward or outward rotation of the hydroxy residue leading to ketenes **3.2** and **2.4** (Scheme 3.1). Further cyclisation gives furanone **3.1**. or hydroquinone **2.2**. In general, thermal rearrangement leads to the corresponding hydroquinone via the (*Z*)-vinylketene **2.4** while photochemical rearrangement gives the corresponding 5*H*-furanone[12a] via the (*E*)-vinylketene **3.2**. Both reactions display high selectivity and are high yielding when conducted under flow.[112] However, some notable exceptions to those general rules have uncovered. The aim of this project was to provide a fuller understanding of torquoselectivity under thermal and photochemical conditions through CCSD(T)/6-31G(d)//B3LYP/6-311G(d,p) analysis of their Gibbs free energies at 25 °C and 150 °C.

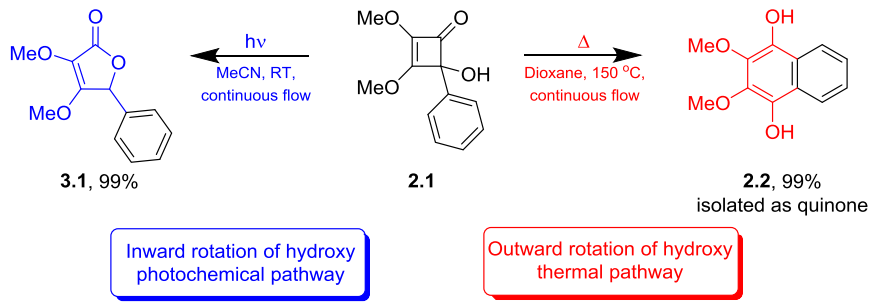

Scheme 3.1. Inward and outward pathway for ring opening for arylcyclobutenone.

The main conclusions from this Chapter, together with the associated experimental findings, have been published.[73] A fuller account of the experimental findings are reported in the PhD thesis of Dr. Mubina Mohamed.[74]

3.1.1 Pathway of aryl-cyclobutenone

SIMPLICITY IS THE KEY TO BRILLIANCE.
BRUCE LEE

The thermal rearrangement of cyclobutenone **2.1** is know to proceed via the (*Z*)-vinylketene intermediate **2.4** and its collapse to hydroquinone **2.2** (Scheme 3.2). Our calculations were thus extended to consider ring opening to (*E*)-vinylketene **3.2** leading to 5*H*-furanone **3.1** as this product is observed in the photochemical rearrangement.

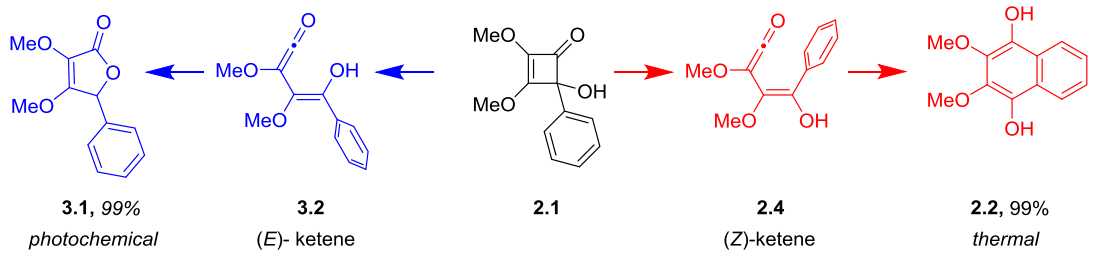

Scheme 3.2. Observed selectivity in thermal and photochemical cyclobutenone rearrangement.

The inward rotation of the hydroxyl group (Figure 3.1) occurs via a similar geometry to that seen for its outwards rotation but with the hydroxyl and phenyl groups reversed.

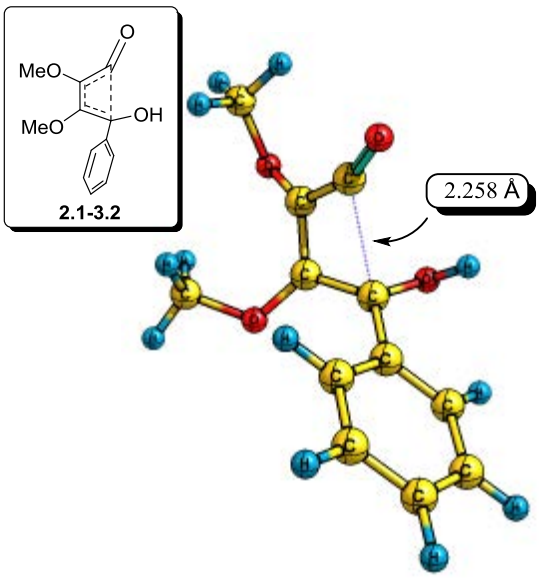

Figure 3.1. Geometry of the transition state leading to ketene (*E*)-3.2 at B3LYP/6-311G(d,p).

The breaking C-C bond lengthens to 2.258 Å as it reaches the transition state which, compared to 2.189 Å (Figure 2.5) for the transition state leading to (*Z*)-vinylketone **2.4**, suggests that the latter has an earlier transition state. Indeed, the energy barrier

is higher for the inward rotation of the hydroxyl group by around 6 kcal/mol (Figure 3.6). In contrast to its outward rotation, no hydrogen bonding is possible in this case. Inward rotation of hydroxyl moiety forms (*E*)-**3.2** and places the ketene and conjugated enol in the plane (Figure 3.2). The aromatic ring and hydroxyl group are inclined a little to minimise the steric clash between them. The geometry makes it possible for the σ-rich lone pair of the hydroxyl group to interact with the $\pi^*_{C=O}$ of the ketone moiety. The energy of this interaction (E(2)-NBO) is 4.68 kcal/mol with an oxygen-carbon distance of 2.542 Å. The positive Laplacian of BCP found between those atoms suggest an interaction and this is also evidenced by the Fuzzy bond order of 0.12 and can be seen as a blue area in the RDG isosurface.

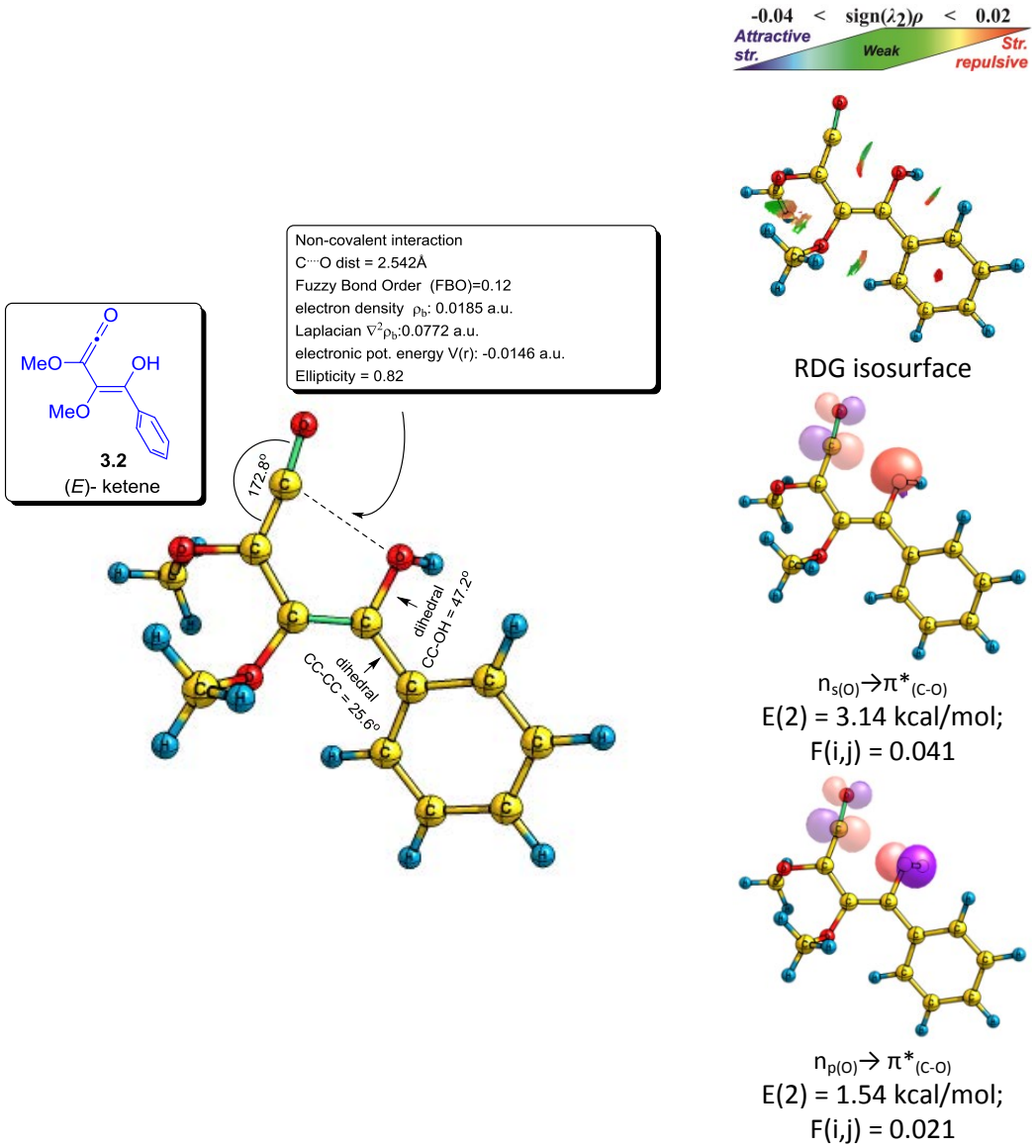

Figure 3.2. Geometry and analysis of (*E*)-ketene **3.2** at B3LYP/6-311G(d,p).

The orbital interaction and good overlap between the hydroxyl lone pair and ketene group suggests a fast ring closure reaction. However, the calculations revealed it to be a high-energy process for intramolecular transition states (Figure 3.3, Path B). All attempts to calculate the ground state for the zwitterionic structure **3.3** failed (Figure 3.3, Path A). With implicit and explicit solvation included, all of these converged to the open product **3.2** [using B3LYP, MP2 and B2PLYP at 6-311G(d,p) basis sets]. From this we can conclude that **3.3** is not a relevant intermediate in this reaction pathway. One could envision an intramolecular transition state proceeding via direct 1,2-addition of hydroxyl group to carbonyl from ketene (Figure 3.3, Path B). However, in this case transformation was shown to be a high-energy process, at 39.3 kcal/mol, as the transition state has the suprafacial rather than the antrafacial geometry needed for efficient 1,3-hydrogen transfer.

Intermolecular hydrogen transfer was examined next. Here, a hydroxyl or equivalent group can assist proton transfer via hydrogen bonding (Figure 3.3, Path C). This path was found to have a low energy barrier of 9.8 kcal/mol. The reaction proceeds via a six-membered cyclic transition state, with water or an alcohol acting as catalyst by lowering the energy barrier for proton transfer. To avoid conformational problems, water was used in these calculations. By analogy, any hydroxyl, such as those in the reactant, intermediate or product, could facilitate the reaction.

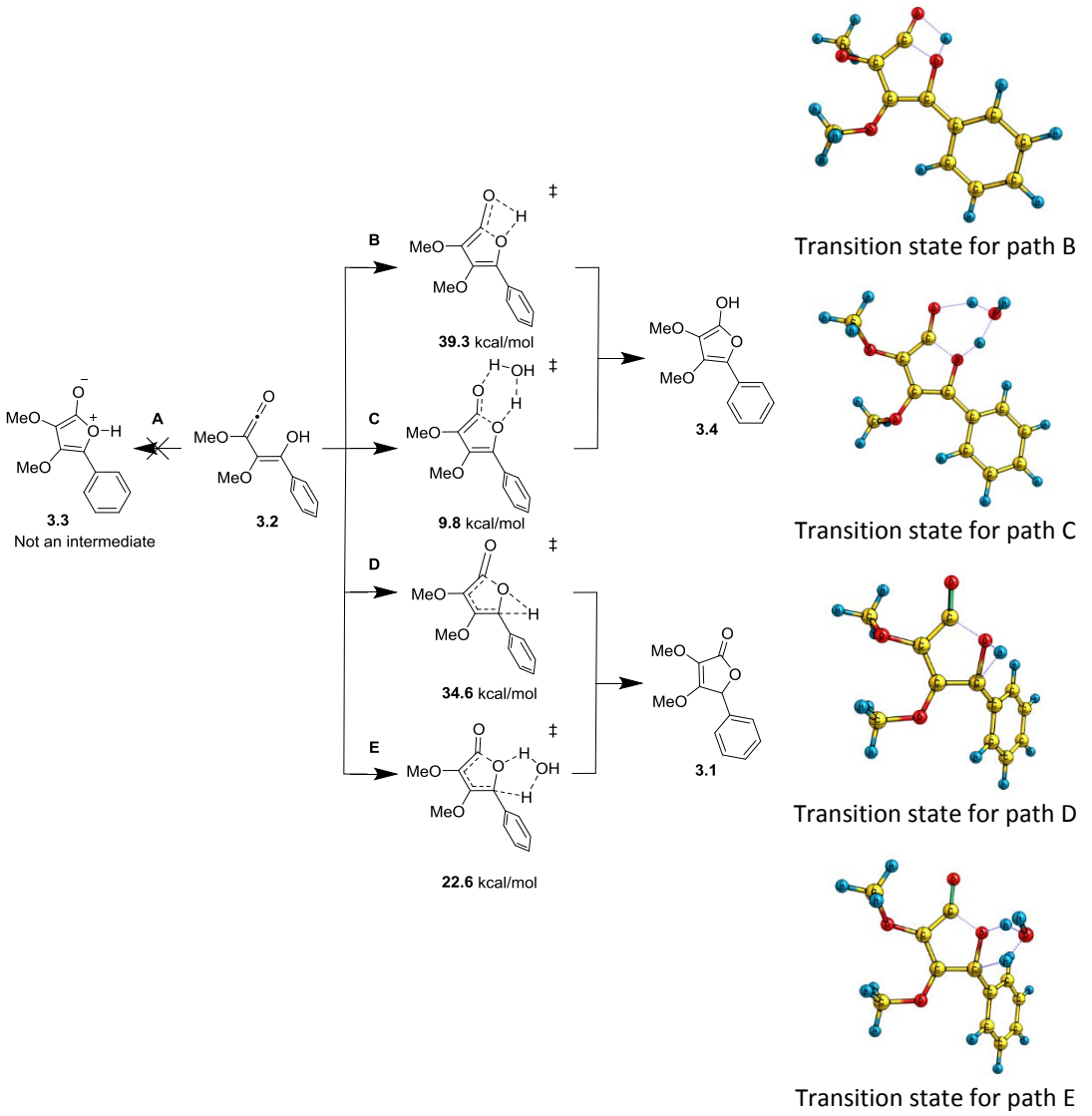

Figure 3.3. Proposed mechanisms for the lactonization step. Electronic energy from B3LYP/6-311G(d,p) energies are reported in kcal/mol.

It is also possible to envision the direct transformation of ketene 3.2 to the final product 3.1 via hydroxyl addition to the ketene with simultaneous 1,2-hydrogen transfer (Figure 3.3, Path D). This direct process was found to be high in energy, at 34.6 kcal/mol. Also, it is possible to envision an intermolecular variation involving double a hydrogen transfer reaction leading to 5H-furanone 3.1 (Figure 3.3, Path E). This competitive channel also has a high energy barrier of 22.6 kcal/mol.

Notably the aromatic furanol **3.4** is more stable than the reactant (Figure 3.6) by 3.8 kcal/mol. However, being an enol ether it tends to isomerise to the more stable 5*H*-furanone via tautomerization. As the hydrogen has to migrate over a long distance (3.5 Å) this is likely to occur via intermolecular rather than intramolecular proton transfer. Indeed all attempts to find an intramolecular transition state failed (Figure 3.4, Path A and B). Two alternative pathways were suggested for such a hydrogen transfer reactions, one via the assistance of two water molecules and the other via three molecules of water in the transition state. The lowest conformation of the transition state with two molecules of water has a barrier of 21.2 kcal/mol (Path C). With the addition of a third water molecule this rises to 28.6 kcal/mol (Path E) or 33.8 kcal/mol (Path D) if the hydrogen bond to the proximal methoxy group is absent. Finally, a transition state with four water molecules was found to have the lowest energy barrier of 12.3 kcal/mol (Path F). Thus, it seems likely that tautomerization occurs in a stepwise manner. For example, at high temperature one could envision abstraction of the acidic furanol proton in the reactant by a weak base or protonation of the electron rich furan by a weak acid. As it was clear from experimentation that tautomerization was not the rate determinant step in this sequence and has no influence on its course, we decide to spend no further time on this study.

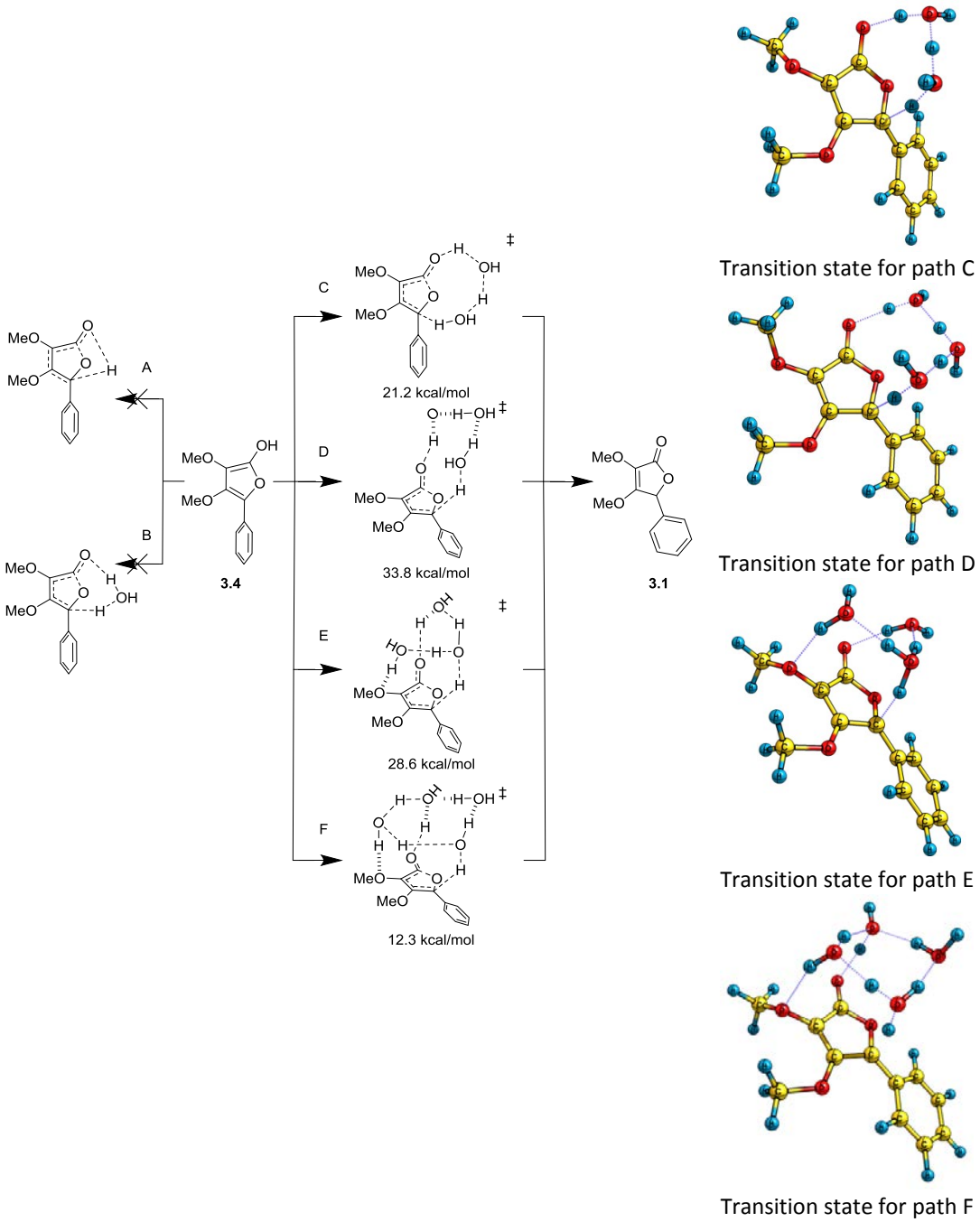

Figure 3.4. Proposed mechanisms for the tautomerization reaction of furanol **3.4** to furanone **3.1** Electronic energy from B3LYP/6-311G(d,p) energies are reported in kcal/mol. Water was used as a representation of any molecule containing hydroxyl group.

It is also possible to imagine the formation of 5*H*-furanone via (*Z*)/(*E*) isomerisation of the vinylketene intermediate (Figure 3.5), which could mask any torquoselectivity. Determining the energy required for that isomerisation step was in the scope of this study. Direct isomerisation via rotation of the double bond was modelled first (Figure 3.5, Path A). Unsurprisingly, the energy of that transformation was high at 42.0 kcal/mol. At UB3LYP/6-311G(d,p), the transition state had a spin contamination <S**2> = 1.04 suggesting diradical character, as would be expected for the rotation of a double bond. In spite of the known limitations of single reference methods for this type of calculation, the value given can be taken as reasonable estimate.[113]

A more likely mechanism for this isomerisation involves sequential tautomerization steps via dicarbonyl **3.5**. As with our previous investigation, transition states involving intra- and inter-molecular hydrogen transfer were each modelled. In common with those systems, direct proton transfer was found to have a high energy barrier of 54.1 kcal/mol (Figure 3.5, Path B). The transition state involving a double proton transfer was simulated using one molecule of water as a model catalysis. This decreased the energy barrier for ketene isomerisation to **2.4** to 35.6 kcal/mol (Figure 3.5, Path C). The transition state for triple proton transfer was also simulated by the inclusion of two water molecules and had an energy barrier of 29.9 kcal/mol (Figure 3.5, Path D).

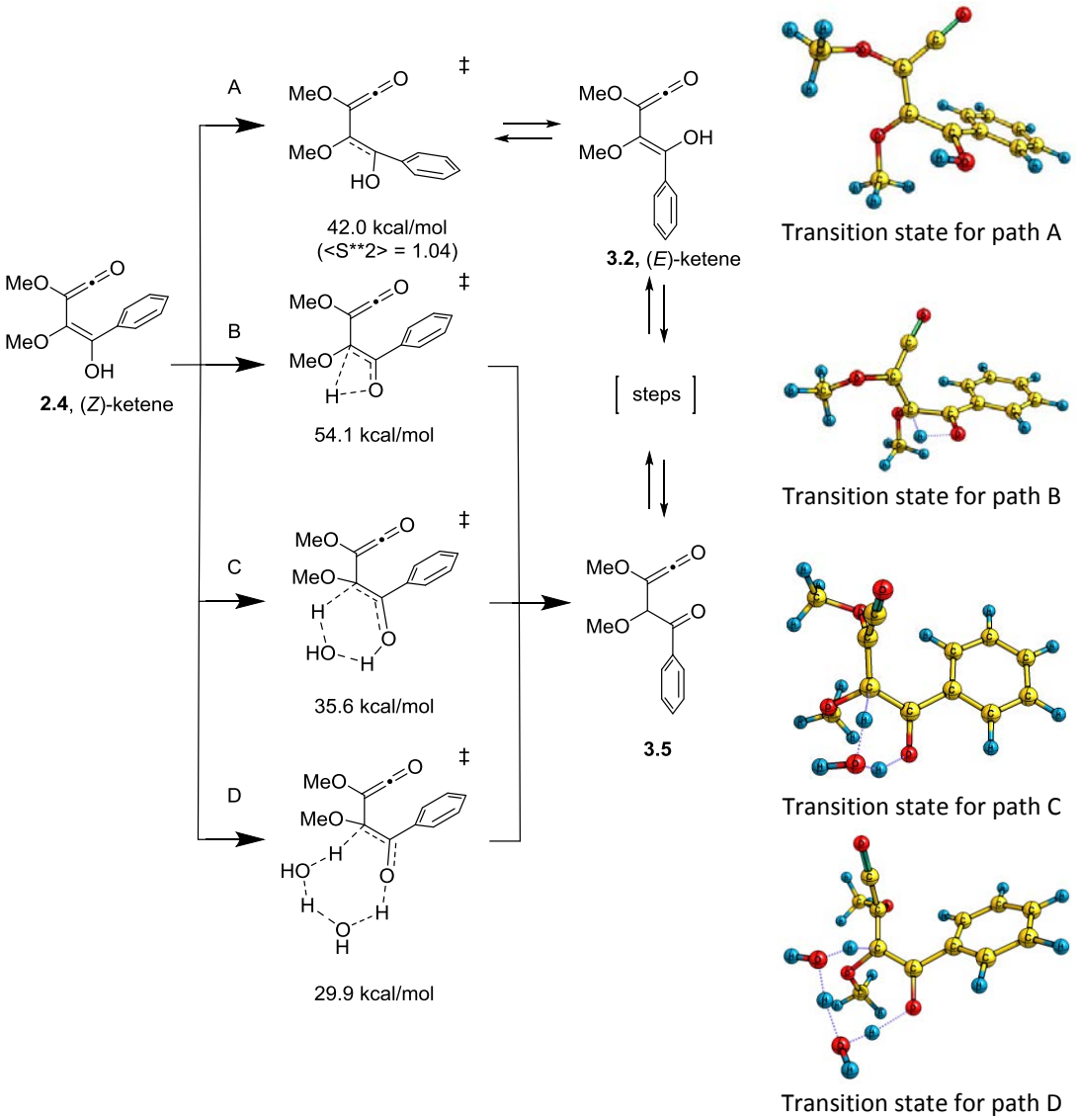

Figure 3.5. Proposed mechanisms for an isomerisation reaction from (*Z*)-ketene **2.4** to (*E*)-ketene **3.2**. Electronic energy from B3LYP/6-311G(d,p) are reported in kcal/mol.

All modelled competitive routes for the formation of (*E*)-vinylketene **2.4** from (*Z*)-vinylketene **3.2** were found to have a higher energy barrier than for inward rotation of the hydroxyl group during electrocyclic ring opening. From this we can conclude that the electrocyclic ring opening step is the likely source of the (*E*)-ketene intermediate **2.4**.

Finally the Gibbs free energy graph for all of the low-energy conformations found was calculated at 150 °C and 25 °C to provide an insight into the thermal and photochemical pathways. Having conducted extensive analysis of the pathways and conformations for both formed product a numbers conclusions can be drawn (Figure

3.6). The highest point on the graph is for the ring opening with inward rotation of the hydroxyl group. This step has a barrier of 35.0 kcal/mol and is 6.1 kcal/mol higher than the competitive ring opening leading to (*Z*)-**3.2** (at 150 °C). For (*Z*)-vinylketene **3.2**, the barrier for the ring closure to **2.4**-**2.5** (30.5 kcal/mol) is lower than that for the formation of (*E*)-vinylketene **3.2** from cyclobutenone **2.1**. Consequently, hydroquinone formation is expected in line with our experimental findings. Importantly, this explains why torquoselectivity is observed in the thermochemical rearrangement when the electrocyclic ring opening is not the rate determinant step of the sequence as a whole.

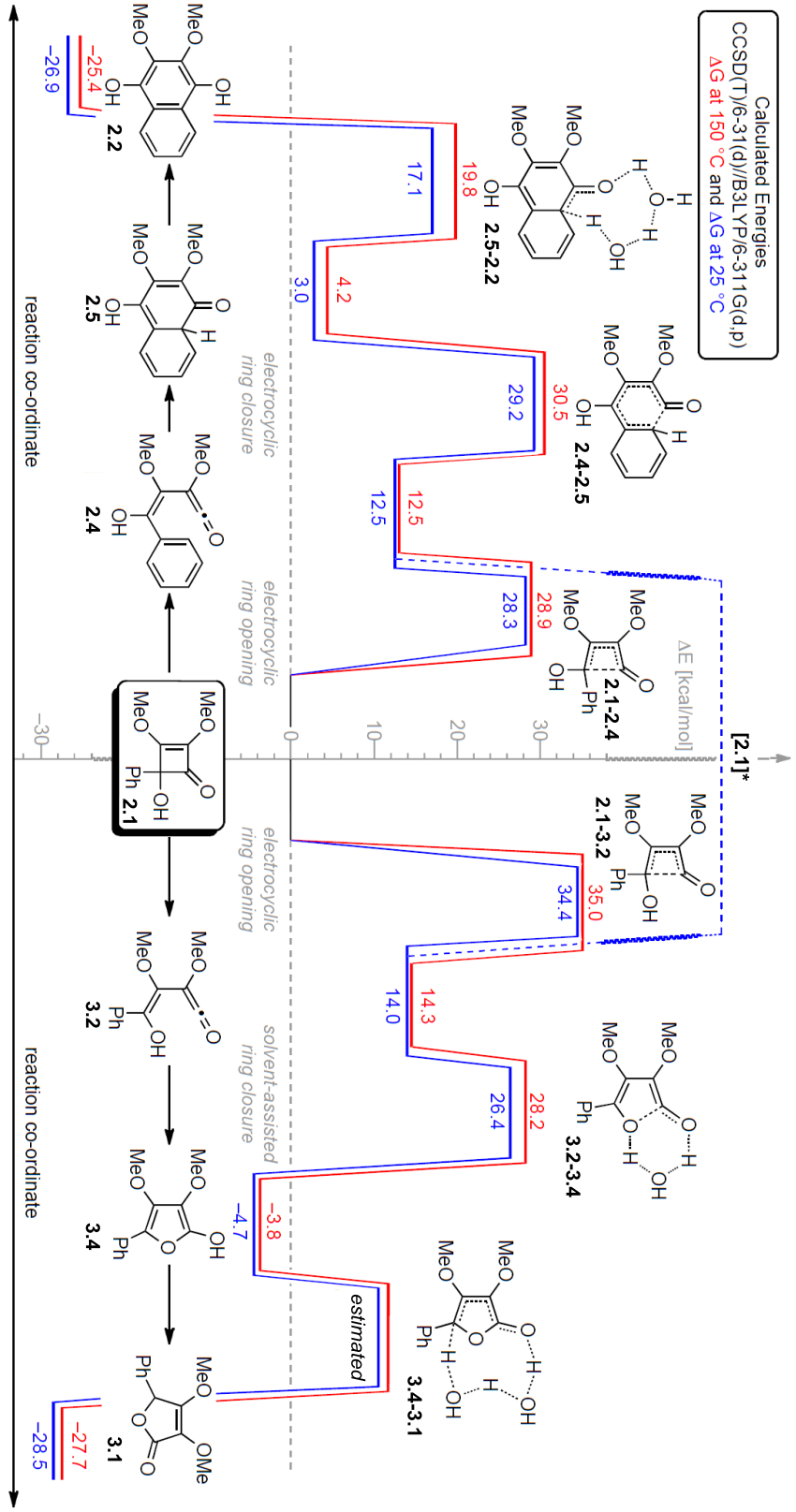

Figure 3.6. Calculated reaction pathways for the inward and outward rotation of the hydroxyl group in the arylcyclobutenone rearrangement of **2.1**.

Using this graph it is possible to understand the selectivity given in the photochemical rearrangement (Figure 3.6 and Figure 3.7). When the starting material **2.1** absorbs energy from a photon, it gives an excited intermediate [**2.1**]*. This undergoes a non-selective ring opening to form both the (*E*)- and (*Z*)-vinylketene intermediates **3.2** and **2.4**. At this stage both can give away excess energy to the solvent to relax from there excited state to the ground state. From this point their pathways are the same as those of the thermochemical reaction, albeit at 25 °C. Consequently, both the (*E*)- and (*Z*)-vinylketenes **3.2** and **2.4** can proceed to product or reverse back to the starting cyclobutenone **2.1** (Figure 3.7). For (*Z*)-vinylketene **2.4**, reversal is the favoured pathway as requires the system to overcome a 28.3 kcal/mol barrier rather than the 30.5 kcal/mol barrier leading to the hydroquinone **2.2** (Figure 3.6). For the (*E*)-vinyl ketene **3.2** the barrier to proceed to 5*H*-furanone **3.1** is 9.8 kcal/mol while to reverse to cyclobutenone **2.1** requires 34.4 kcal/mol.

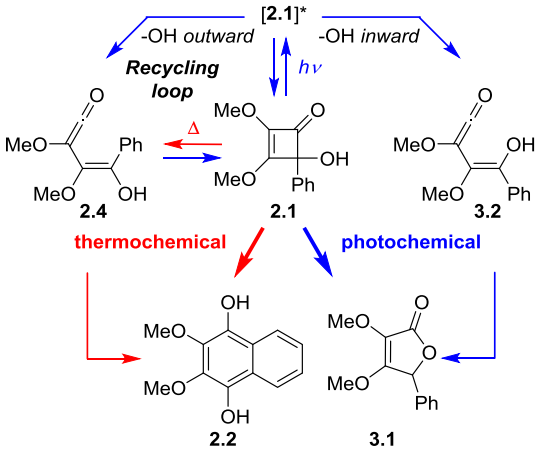

Figure 3.7. Selectivity for the photochemical and thermal rearrangement for phenylcyclobutenone **2.1.**

3.1.2 Pathway of (2-pyridyl)-cyclobutenone

SNOOPY
IT IS BETTER TO THINK YOU ARE HALF DRY
THAN TO KNOW YOU ARE ALL WET.
CHARLES MONROE SCHULZ

Having established the origin of the selectivity for both the thermal and photochemical rearrangements of phenylcyclobutenes we now needed to understand an anomaly that occurred in the case of (2-pyridyl)-cyclobutenone **3.8** (Scheme 3.3). Thus, while its thermal rearrangement gave quinolizinone **3.10** exclusively, its photochemical rearrangement gave a 1:1 mixture of **3.10** and γ-lactone **3.6**. To extend our knowledge of this system, an *in silico* study of the (2-pyridyl)-cyclobutenone rearrangement was conducted.

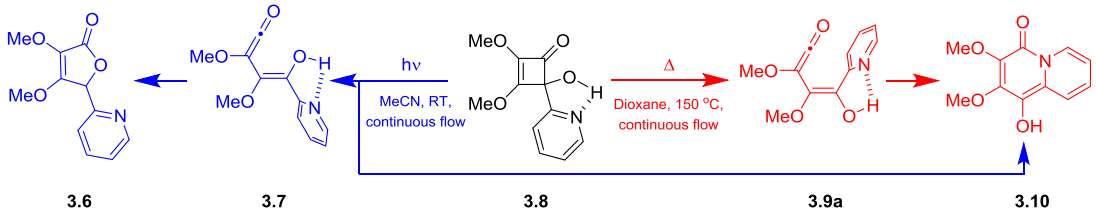

Scheme 3.3. Inward and outward pathways observed in the rearrangement of (2-pyridyl)-cyclobutenone **3.8**.

The low energy conformer of (2-pyridyl)-cyclobutenone **3.8** has a hydrogen bond between the pyridine nitrogen and the proximal hydroxyl group (Figure 3.8) which is not present in arylcyclobutenone **2.1**. Fuzzy bond order analysis of this bond gives a value of 0.072, which suggests strong hydrogen bonding. Its Laplacian, electron density and potential energy are 0.120 a.u., 0.0320 a.u. and -0.0279 a.u. respectively. These values are higher than any of the hydrogen bonds previously determined within the arylcyclobutenone rearrangement, *vide supra*. Indeed, as estimated by its potential energy ($V_{(r)}$),[105] this hydrogen bond is worth ~8.75 kcal/mol, due to good orbital overlap [F(i.j) = 0.070] and a high interaction energy of 7.44 kcal/mol between the s-rich lone pair of nitrogen ($n_{s(N)}$) and hydroxyl antibonding orbital ($\sigma^*_{(O-H)}$), as determined by NBO. A Reduced Density Gradient (RDG) calculation showed a strong interaction in the region between the hydroxyl group and the nitrogen centre, confirming that this is indeed a strong hydrogen bond (Figure 3.8).

That hydrogen bonding increases electron density on the associated oxygen atom, which in turn weakens the C-C bond to the carbonyl group in the cyclobutenone via interaction between this p-rich oxygen atom and $\sigma^*_{C\text{-}C}$. This is manifest by a lengthening of that C-C bond to 1.594 Å (by comparison, in the analogous phenylcyclobutenone **2.1** this bond length is 1.579 Å, Figure 2.4). The Fuzzy Bond Order value of 0.85 and the electron density, Laplacian and potential energy at BCP are also lower than those calculated for arylcyclobutenone **2.1**, adding further support to the suggestion that this is an easier to bond.

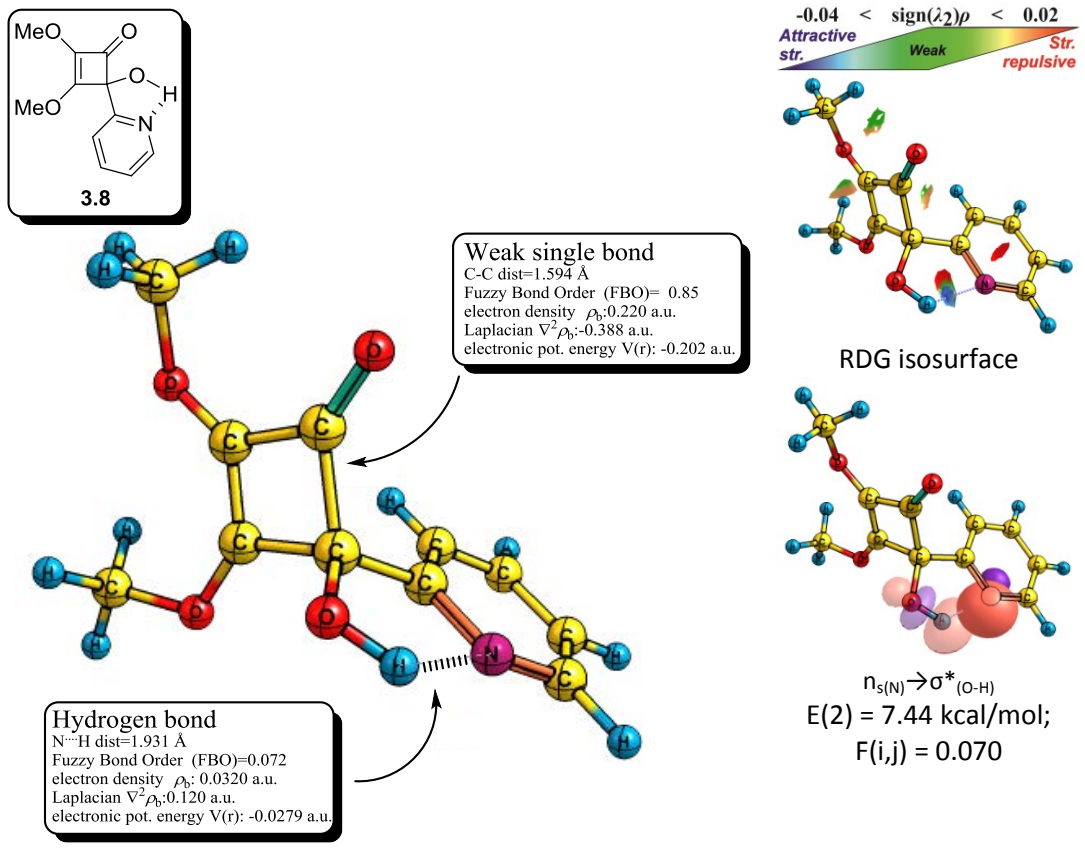

Figure 3.8. Geometry and analysis of the lowest conformation of (2-pyridyl)-cyclobutenone. Geometry and NBO analysis at B3LYP/6-311G(d,p), Fuzzy bond order and QTAIM analysis at M062X/6-311++G(2d,2p).

These orbital interactions have a significant impact on energy of ring opening. Ring opening with an outward rotation of the hydroxyl group has energy barrier of 25.7 kcal/mol (Figure 3.13) which is 3.2 kcal/mol lower that that given with phenylcyclobutenone **2.1** (Figure 2.3, 28.9 kcal/mol). Importantly, in this case the

hydrogen bond between the hydroxyl group and the pyridine accelerates ring opening (Scheme 3.4 and Figure 3.9).

This observation was used as a starting point to perform an NBO study and screening of substituent effects, which is covered in the next chapter. It supports the idea that hydrogen bonding can lower the energy needed to induced the electrocyclic ring opening of a cyclobutenone. The hydrogen bond in the transition state **3.8-3.9a** is also shorter (1.876 Å) than it is in the transition state **3.7-3.8** (1.931 Å), suggesting that it might also enhance any torquoselectivity preference.

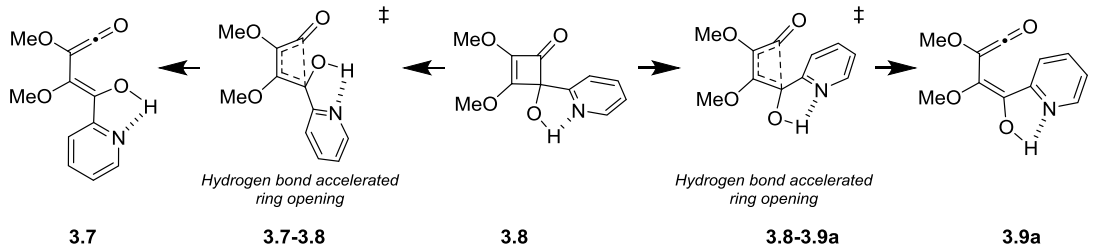

Scheme 3.4. Hydrogen bond accelerated ring opening of (2-pyridyl)-cyclobutenone **3.8**.

The strength of this hydrogen bond is reflected in the Fuzzy bond order analysis (0.085 vs. 0.072) and also by an AIM, which both show a higher barrier for transition state **3.7-3.8** over transition state **3.8-3.9a**. Furthermore, reduced density gradient analysis shows a more intense blue colour in hydrogen bonding region. Finally, NBO analysis shows that the orbital overlap term is higher in TS **3.8-3.9a** (0.081) than it is in TS **3.7-3.8** (0.070), with the energy interaction estimated to be 10.40 kcal/mol and 7.73 kcal/mol respectively. For that reason torquoselectivity is enhanced for ring opening of (2-pyridyl)-cyclobutenone **3.8** (with an energy difference of 8.2 kcal/mol, Figure 3.13) in comparison to phenylcyclobutenone **2.1** (where the energy difference is 6.1 kcal/mol, Figure 3.6).

Hydrogen bonding also makes the oxygen atom more electron rich. Consequently, it strengthens the interaction between its lone pair and the $\sigma^*_{C\text{-}C}$ of the break bond leading to an acceleration of the reaction.

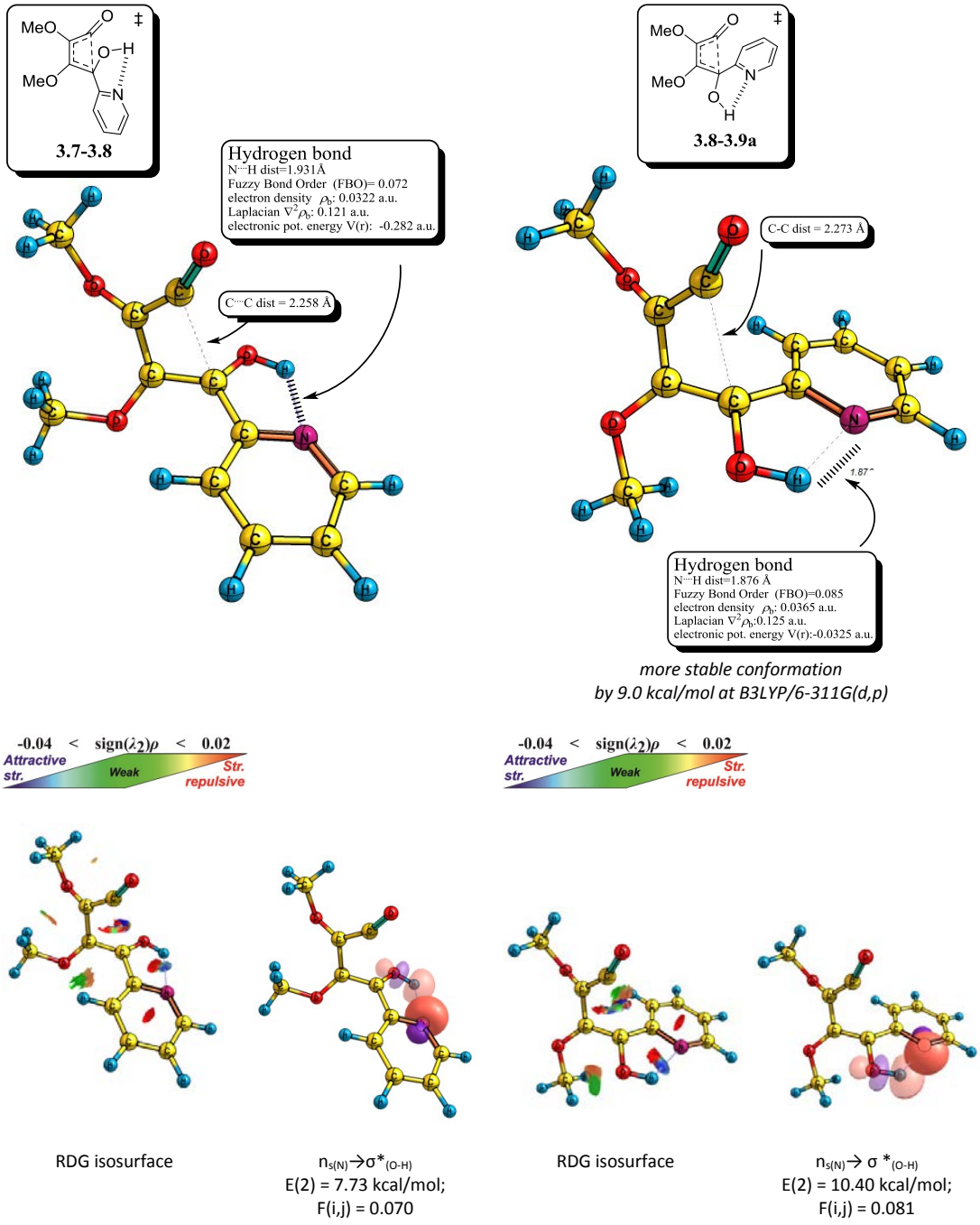

Figure 3.9. Geomerty and analysis of the lowest inward and outward transition state of (2-pyridyl)-cyclobutenone. Geometry and NBO analysis at B3LYP/6-311G(d,p), Fuzzy bond order and QTAIM analysis at M062X/6-311++G(2d,2p).

With (*Z*)-vinylketene intermediate **3.9**, two hydrogen bonding patterns are possible (Figure 3.10). The lowest energy intermediate found has a hydrogen bond between the hydroxyl group and the pyridine nitrogen **3.9a** rather than the proximal ether **3.9b**. The hydrogen bond with nitrogen has a distance of 1.859 Å while that to oxygen is 2.022 Å. The oxygen has two lone pairs with which it can form hydrogen bonds. However, the energy of the interaction is stronger for N···H (at

10.53 kcal/mol) and this also has a higher overlap term [F(i,j)] of 0.082 than that given for H···O (of 2.56 kcal/mol and F(i,j) = 0.040). Fuzzy bond order analysis reflects this trend showing 0.085 for the hydrogen bond to nitrogen and 0.043 for hydrogen bond to oxygen. Also electron density, Laplacian and potential energies are higher for the intermediate with the N···H interaction than those observed with the conformer showing the hydrogen bond to oxygen. Finally, reduced density gradient analysis shows a more intense blue colour for **3.9a** that for **3.9b**, implying a stronger hydrogen bond.

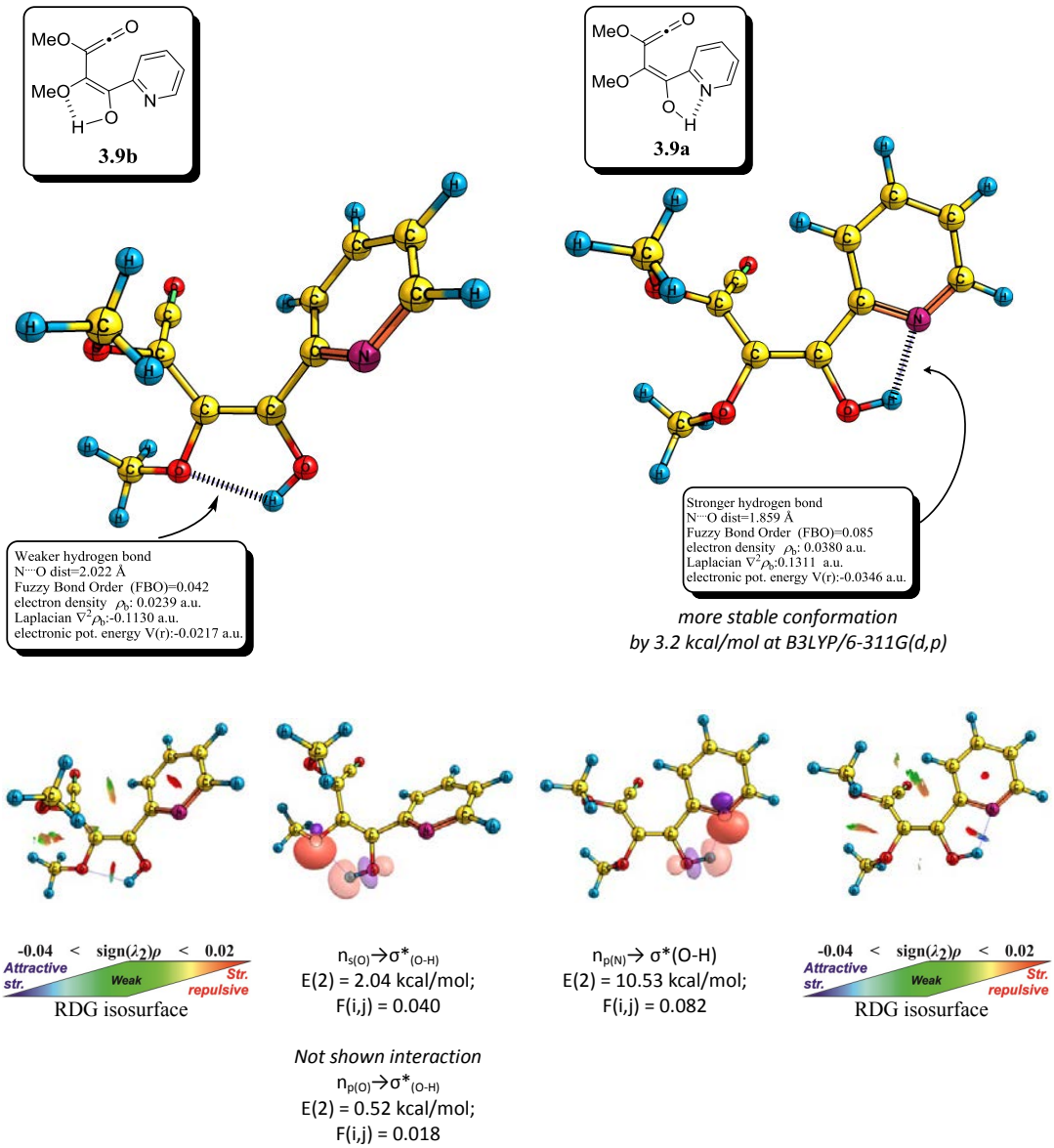

Figure 3.10. Geomerty and analysis of the lowest two distinguish hydrogen bonded conformation of (*Z*)-ketene intermediate. **3.9a** and **3.9b** conformars. Geometry and NBO analysis at B3LYP/6-311G(d,p), Fuzzy bond order and QTAIM analysis at M062X/6-311++G(2d,2p).

At this point ketene intermediate can undergo a cyclisation reaction to form quinone **3.12** (Scheme 3.5, Path A). However, this follows a high energy pathway so is not observed experimentally.[5] Indeed, this step is calculated to be higher in energy compared to closure of the phenylcyclobutenone **2.1** analogue (32.9 kcal/mol compared with 30.5 kcal/mol) which suggests that this step is slowed by the presence of the electronegative nitrogen atom. In this case the low energy cyclisation pathway involves trapping of the ketene with the pyridine nitrogen as it does not involve dearomatisation of the pyridine ring (Scheme 3.5, Path B). For this to happen the N···H hydrogen bond must break. This is compensated to some extent by the formation of the weaker O···H hydrogen bond. Calculation shows that this rotation of the pyridine ring has a barrier of 3.5 kcal/mol, which is close of energy difference between the two conformers **3.9a** and **3.9b** (Figure 3.10).

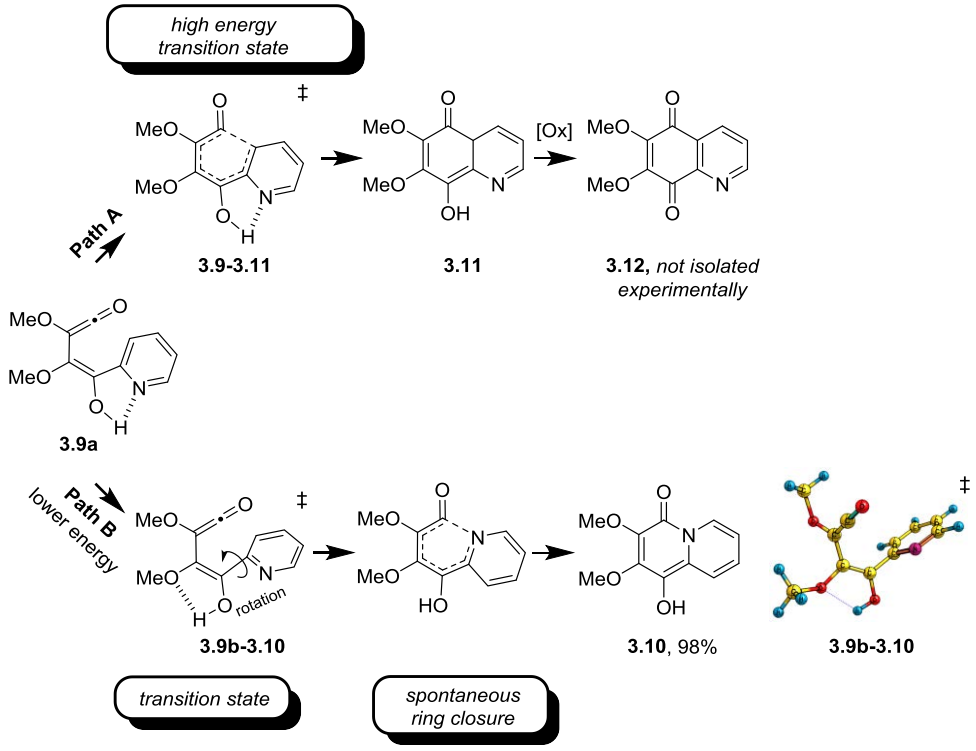

Scheme 3.5. Two possible pathways for ring closure reaction.

Following rotation, the pyridine ring spontaneously undergoes ring closure to form quinolizine **3.10**. This ring closure reaction from ketene **3.9b** to product **3.10** was confirmed using the IRC calculation at B3LYP and MP2 at 6-311G(d,p) basis sets, which confirmed that the ring closure reaction is spontaneous as does not involve a

dearomatisation step, as seen in phenylcyclobutenone **2.1**. Experimentally this is evidenced by that fact that reaction proceeds rapidly at 100 °C.[73]

The lactonization pathway for this system proceeds via (*E*)-vinylketone **3.7** and is akin to that followed by the phenyl analogue **3.2** (Figure 3.3). A key difference between the two is the strong hydrogen bond in (*E*)-vinylketene intermediate **3.7**, which ensures the planar orientation of the hydroxyl group and the arene (Figure 3.11). Fuzzy bond order analysis shows a high value of 0.072, with electron density, Laplacian and potential energy calculations at the bond critical point all supporting the presence of a strong hydrogen bond. The bond strength calculated from potential energy ($V_{(r)}$) is 9.4 kcal/mol.[105] This value is close to the that calculated for the orbital interaction from NBO analysis. The hyperconjugation energy (E(2)-NBO) between $n_{s(N)} \rightarrow \sigma^*_{(O-H)}$ has a magnitude of 9.08 kcal/mol due to the large orbital term F(i,j) of 0.076. This intermediate benefits from an orbital interaction between the s-rich lone pair on oxygen and the antibonding orbital of the ketene ($n_{s(O)} \rightarrow \pi^*_{(C=O)}$), 3.47 kcal/mol. At 2.558 Å, the C-O distance is longer than the phenyl analogues **3.2** and this is reflected by lower values for Fuzzy bond order, electron density, Laplacian and potential energy. Indeed, this interaction causes the ketene to bend, with C=C=O exhibiting a bond angle of 172.8°. Reduced Density Gradient analysis also revealed that the hydrogen bond is strong, in support of all of the listed observations.

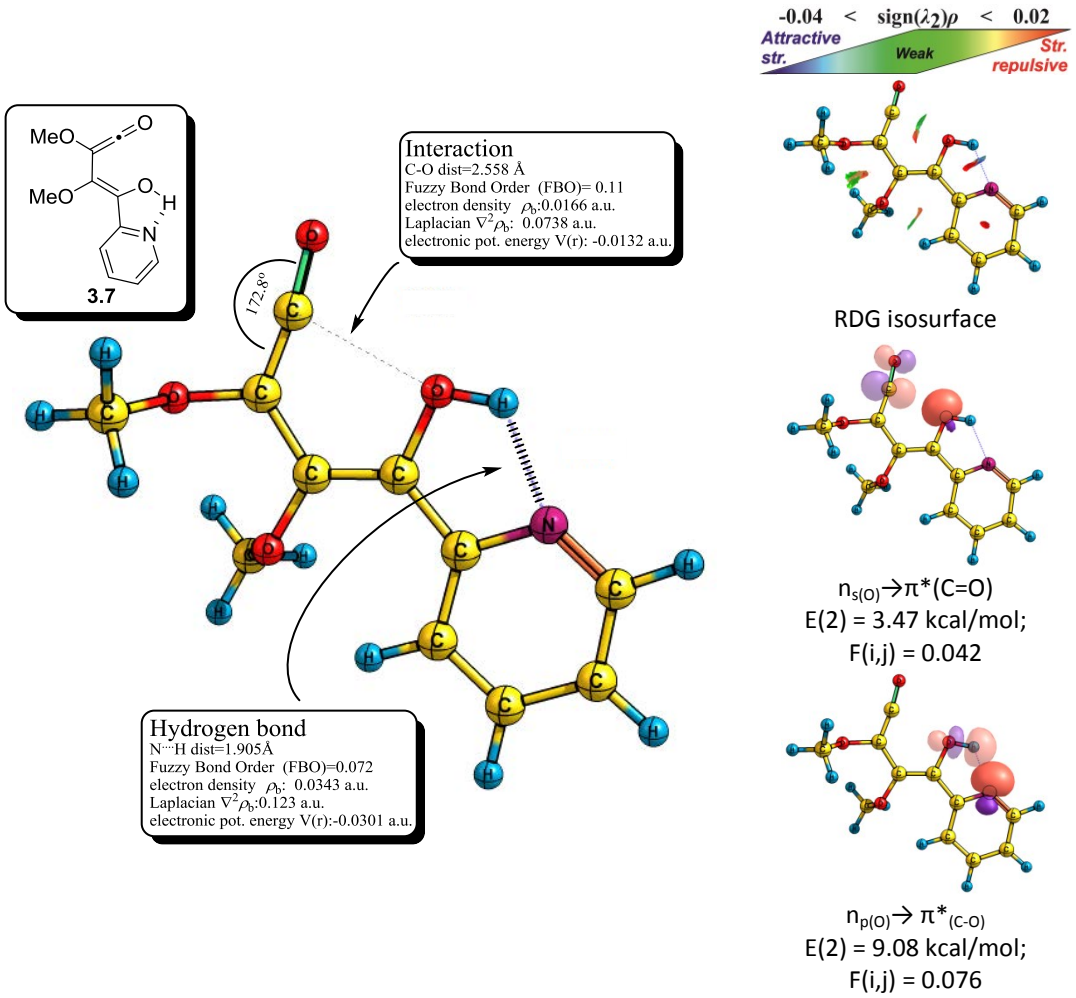

Figure 3.11. Geometry and analysis of the lowest conformation of (*E*)-vinylketene intermediate **3.7**. Geometry and NBO analysis at B3LYP/6-311G(d,p), Fuzzy bond order and QTAIM analysis at M062X/6-311++G(2d,2p).

The further ring closure reaction, **3.7-3.13/3.14**, can occur by a number of different transition states (Figure 3.12). By analogy to the rearrangement of phenylcyclobutenone **2.1**, double proton transfer stimulated by water was investigated. It had an energy barrier of 9.4 kcal/mol (Path A). Interestingly, the presence of the pyridine ring made other transition states viable. Indeed, calculation showed that the intramolecular proton transfer **3.7-3.14** (Path B) had a similar barrier (10.1 kcal/mol) via the five membered ring transition state. However, the lowest energy barrier calculated for this ring closure reaction involved a pyridine promoted proton transfer (Path C). Hence, in spite of the entropic contribution, the intramolecular reaction is likely to be faster once Gibbs free energy is considered. Notably, however, all pathways have energies barrier that are easily achieved under the experimental conditions employed.

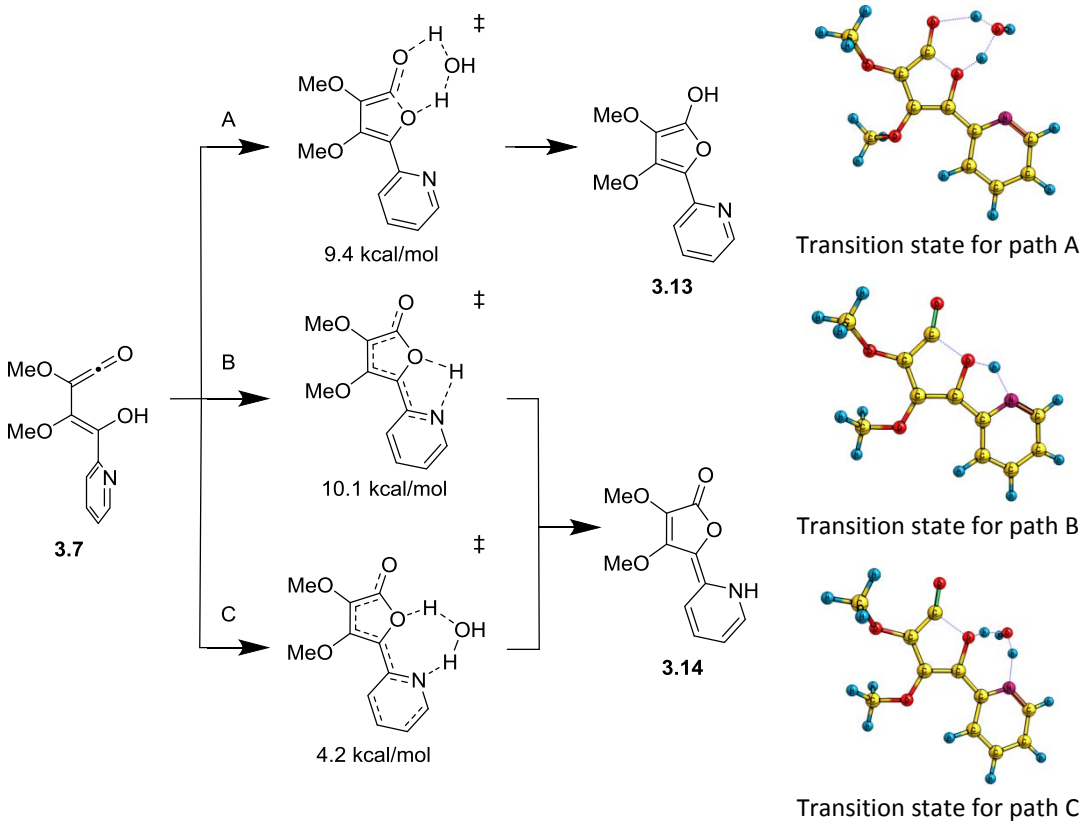

Figure 3.12. Proposed mechanisms for the ring closure of (*E*)-vinylketone intermediate **3.7**. Electronic energy from B3LYP/6-311G(d,p) with energies reported in kcal/mol.

Importantly furanone **3.13** is more stable than starting material **3.8** by -1.3 kcal/mol (Figure 3.13), though not to the same extent as was observed with the rearrangement of phenylcyclobutenone **2.1** (-3.8 kcal/mol, Figure 3.6). The 2.5 kcal/mol energy difference between these systems can be attributed to the loss of hydrogen bonding over the course of the (2-pyridyl)-cyclobutenone rearrangement. The tautomerization step, **3.13** to **3.6**, was not analysed as it is known to be a low energy processes [as shown by our studies on phenylcyclobutenone **2.1** (Figure 3.4)]. The full graph at CCSD(T)/6-31G(d)//B3LYP/6-311G(d,p) shows a similar energetic picture to that attained for the thermal rearrangement of phenylcyclobutenone **2.1**. Notably, the reaction favours ring opening occurs via inward rotation of the pyridine moiety and this is now the rate determinant state. In spite of this switch, the thermochemically and the photochemically induced ring openings to (*E*)- and (*Z*)-vinylketene (**3.7** and **3.9**) follow the same pathways overall.

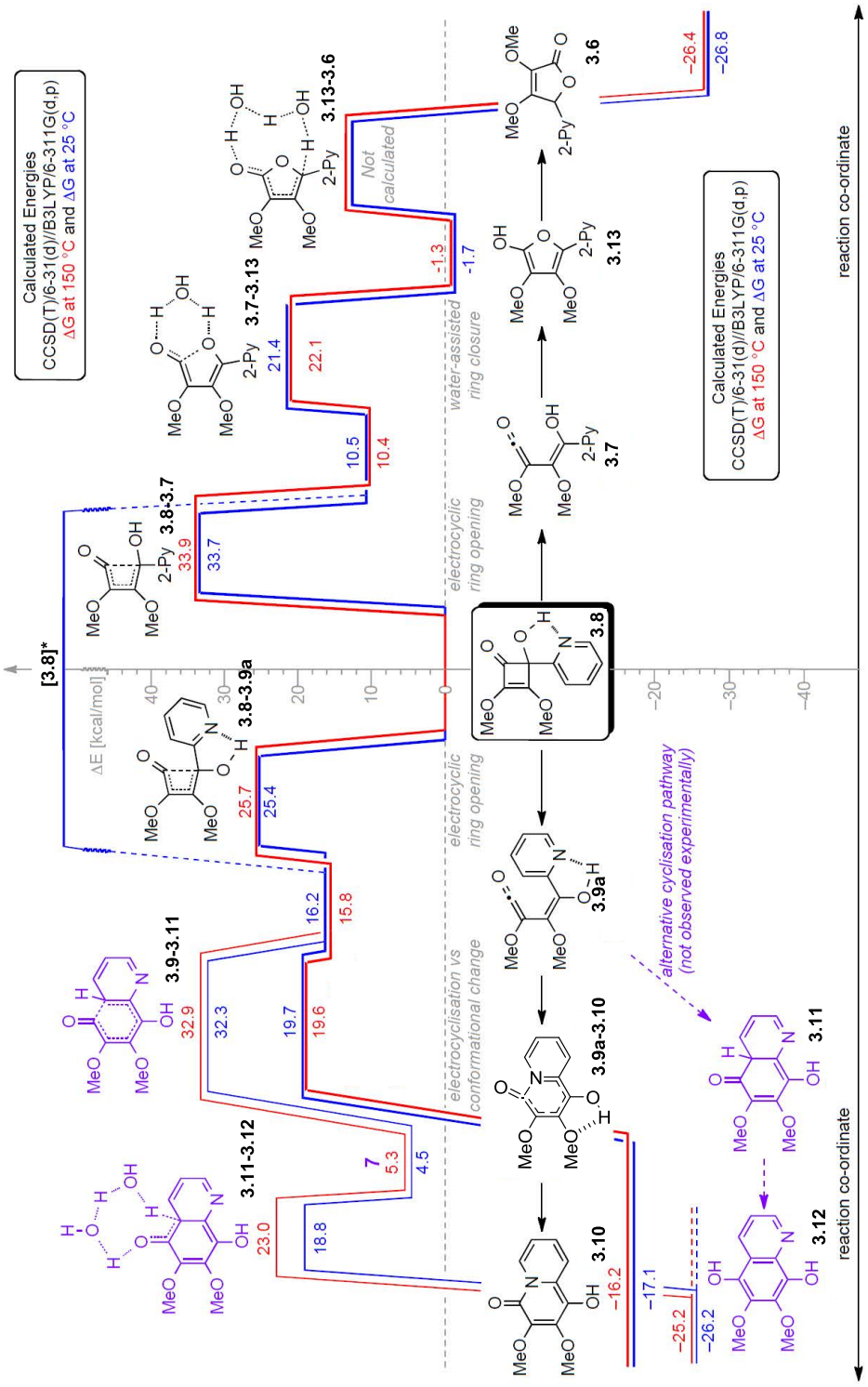

Figure 3.13. Reaction pathways for rearrangement of (2-pyridyl)-cyclobutenone **3.8**.

Importantly, when rearrangement is triggered by photon absorption, both (*E*)- and (*Z*)-vinylketenes **3.7** and **3.9** are formed. In this case both of the products of ring closure, **3.6** and **3.10**, are formed as the recycling of ketene **3.9** back to the starting material **3.8** is a higher energy process that the pathway leading to quinolizine **3.10**. This is in agreement with the performed experiment where 1:1 mixture of **3.6** and **3.10** was formed in 98% isolated yield (Figure 3.14).[73]

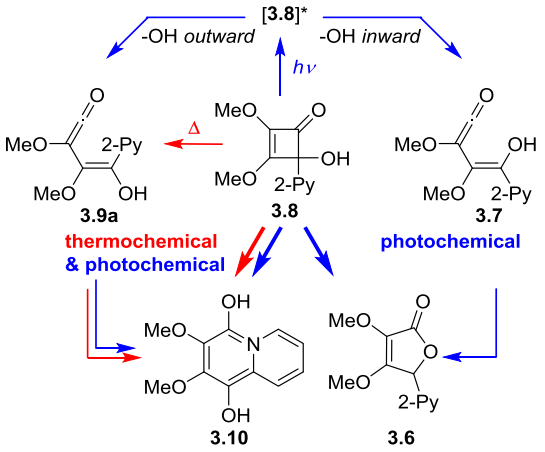

Figure 3.14. Selectivity in the photochemical and thermal rearrangement of (2-pyridyl)-cyclobutenone **3.8**.

3.2 Conclusions

IT'S MORE FUN TO ARRIVE A CONCLUSION THAN TO JUSTIFY IT.
MALCOLM FORBES

Molecular modelling of the rearrangements of cyclobutenones **2.1** and **3.8** were performed and the results attained were found to be consistent with experimental results. The rate determining step for each was different under thermal conditions though they follow a similar pathway leading to **2.2** and **3.10** respectively. For 2-pyridylcyclobutenone **3.8** (Figure 3.13), calculations showed that cyclization of vinylketene **3.9a** to quinolizinone **3.10** was spontaneous on adoption of an appropriate reactive conformer, thereby diverting it away from the usual recycling loop. In parallel, the geometric isomer **3.7** favours cyclization to furan **3.13** (10.9 kcal/mol) over 4π-electrocyclic ring closure to cyclobutenone **3.8** (23.2 kcal/mol) and gives the expected furanone **3.6**. Torquoselectivity in the thermal opening of cyclobutenone **3.8** to vinylketene **3.9a** was again evidenced, with calculations additionally indicating that a hydrogen bond between the pyridine and hydroxyl residue leads to a significant rate enhancement. This was manifest experimentally by the realization of a near quantitative yield for the thermolysis of **3.8** to **3.6** at 100 °C for 10 min under continuous flow, when related aryl- and heteroaryl-cyclobutenone rearrangements typically require prolonged heating at 150 °C to achieve a similar outcome.

Chapter 4: Torquoselectivity in Arylcyclobutenone Rearrangements

4.1 Chapter abstract

IF IT'S HARD TO REMEMBER, IT'LL BE DIFFICULT TO FORGET.
ARNOLD SCHWARZENEGGER

The thermal rearrangement of a cyclobutenone often gives a different outcome to the photochemical rearrangement. Often this can be explained using the concept of torquoselectivity, where the means of triggering the ring opening a cyclobutenone determines the isomeric ratio of vinylketene intermediates that are formed (Scheme 4.1). The difference in energy between these competitive pathways dictates the outcome of reaction. It is known that a preference for one mode over the other is due to the orbital interactions involved in a given system.[51] In this chapter the influence of substituents on the torquoselectivity of arylcyclobutenone ring opening reactions is analysed.

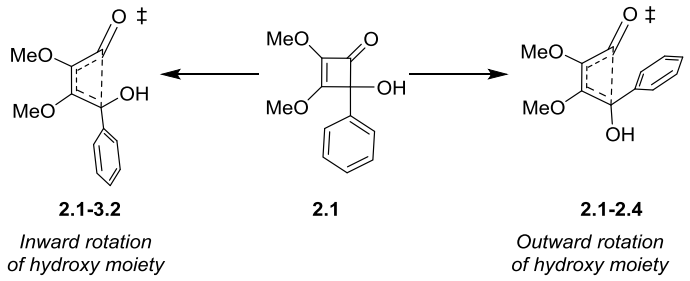

Scheme 4.1. Inward and outward rotation of a 4-hydroxy moiety in the ring opening of cyclobutenone **2.1**.

4.1.1 Natural bond orbital analysis (NBO) of transition states

THE DIFFERENCE BETWEEN FICTION AND REALITY? FICTION HAS TO MAKE SENSE.
TOM CLANCY

The difference in the electronic energy for inward and outward transition states for the opening of 4-phenyl-4-hydroxycyclobutenone **2.1** was calculated to be 5.5 kcal/mol using B3LYP (Figure 4.1). From Figure 4.1, it can be seen that the geometry of the core carbon-framework involved in bond breaking is very similar. Indeed, the only significant difference between the inward and outward ring opening

pathways is the position of the C-4 substituents and the extent to which the braking bond is lengthened (Figure 4.1, Figure 3.1 and Figure 2.5). As mentioned previously, hydrogen bonding in the outward transition state is insignificant energetically.

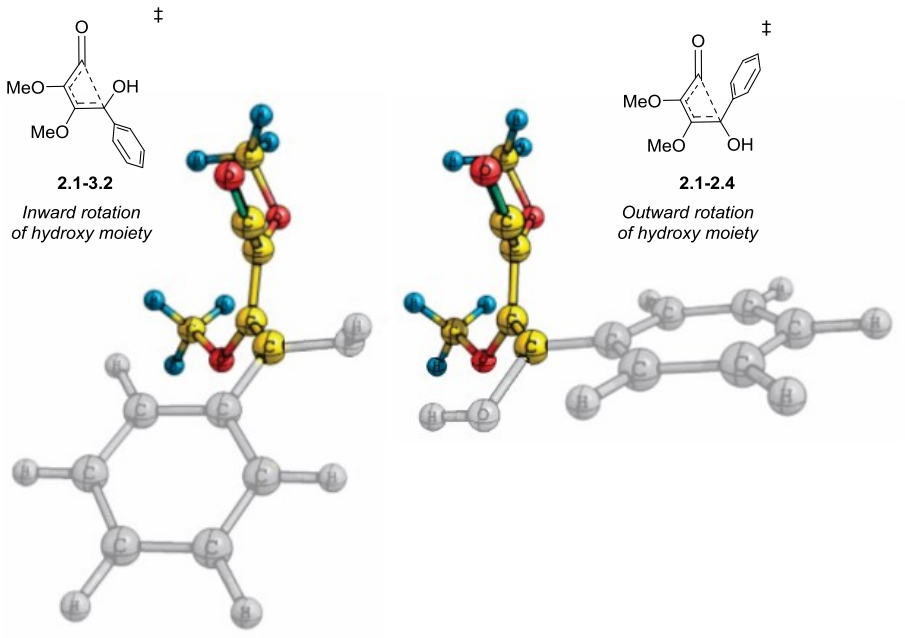

Figure 4.1. Comparison of geometries for the inward (left) and outward (right) transition states. Geometries of the transition state were obtain at the B3LYP/6-311G(d,p) level.

In order to provide a theoretical explanation of the torquoselectivity, an NBO analysis was performed. To obtain a pictorial representation of the interacting orbitals determining the torquoelectronic preference,[114] the transition state orbitals were localised with respect to the reactant resonance structure. The orbital interaction energies were obtained by the explicit deletion of the orbitals at HF/6-311G(d,p) level on a geometry determined by the B3LYP/6-311G(d,p) method. In that way it is possible to compare the relative impact of specific orbital interactions on torquoselectivity. The energy of the most relevant interactions are listed in Table 4.1.

Table 4.1. Comparison of orbital interaction energies (E(2)-NBO) for inward and outward transition states calculated by explicit deletion of orbitals involved at HF/6-311G(d,p).

Entry	**TRANSITION STATE** (2.1-3.2) **Inward rotation of hydroxy moiety**	**TRANSITION STATE** (2.1-2.4) **Outward rotation of hydroxy moiety**	**ΔE [kcal/mol]** $E_{out} - E_{inw}$
		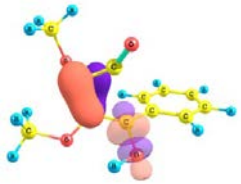	
1	E(2) $\pi_{(C-C)} \rightarrow \sigma^*_{(C-O)}$ 3.7 kcal/mol	E(2) $\pi_{(C-C)} \rightarrow \sigma^*_{(C-O)}$ 3.6 kcal/mol	-0.1
		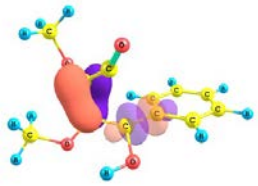	
2	E(2) $\pi_{(C-C)} \rightarrow \sigma^*_{(C-Ar)}$ 1.5 kcal/mol	E(2) $\pi_{(C-C)} \rightarrow \sigma^*_{(C-Ar)}$ 2.4 kcal/mol	0.9
	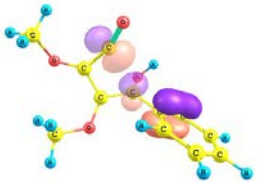	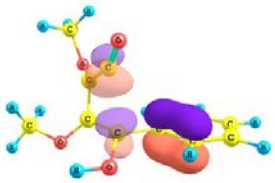	
3	E(2) $\pi_{(Ar)} \rightarrow \sigma^*_{(C-C)}$ 7.3 kcal/mol	E(2) $\pi_{(Ar)} \rightarrow \sigma^*_{(C-C)}$ 6.9 kcal/mol	-0.4
	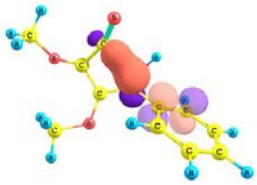	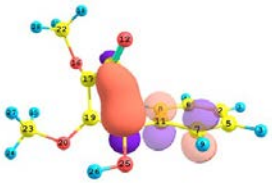	
4	E(2) $\sigma_{(C-C)} \rightarrow \pi^*_{(Ar)}$ 8.2 kcal/mol	E(2) $\sigma_{(C-C)} \rightarrow \pi^*_{(Ar)}$ 8.7 kcal/mol	0.5
	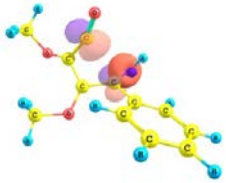	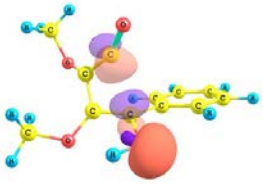	
5	E(2) $n_{s(O)} \rightarrow \sigma^*_{(C-C)}$ 1.5 kcal/mol	E(2) $n_{s(O)} \rightarrow \sigma^*_{(C-C)}$ 0.7 kcal/mol	-0.8
			
6	E(2) $n_{p(O)} \rightarrow \sigma^*_{(C-C)}$ 7.8 kcal/mol	E(2) $n_{p(O)} \rightarrow \sigma^*_{(C-C)}$ 17.1 kcal/mol	9.3
TOTAL	**30.0 kcal/mol**	**39.4 kcal/mol**	**9.4**

Entry 1 shows the stabilisation energy given by an interaction between the double bond of the enone and the carbon-oxygen antibond ($\pi_{(C\text{-}C)} \rightarrow \sigma^*_{(C\text{-}O)}$). The energy of interaction is similar for inward and outward rotation, with the inward transition state favoured by 0.1 kcal/mol. A low energy difference of 0.9 kcal/mol (Table 4.1, Entry 2) was also observed for the interaction of the enone double bond with and C-Ph antibond ($\pi_{(C\text{-}C)} \rightarrow \sigma^*_{(C\text{-}Ar)}$), making the outward transition state more favourable. Neither of these were deemed to be sufficient to be responsible for the torquoselectivity observed.

Next, orbital interactions involving the breaking bond were analysed. The π donation of the aromatic ring to the breaking C-C bond is more stabilising for inward ring opening by 0.4 kcal/mol (Table 4.1, Entry 3). However hyperconjugation from the breaking C-C bond to the antibonding orbital of the aromatic ring favours outward rotation by 0.5 kcal/mol (Table 4.1, Entry 4), so the effects cancel each other out.

Finally, interactions involving the oxygen lone pairs were analysed. The s-rich oxygen orbital in both transition states has a low energy of interaction due to its orthogonality to C-C antibond and this favour the inward transition state (Table 4.1, Entry 5). However, the p-rich lone pair and C-C antibond ($n_{p(O)} \rightarrow \sigma^*_{(C\text{-}C)}$) has the highest energy of interaction of all those studied (Table 4.1, Entry 6). For the outward transition state this interaction has a stabilising influence of 17.1 kcal/mol whereas for inward rotation this interaction only contributes 7.8 kcal/mol. Thus, this interaction is the "game changer" in orbital energy terms, pushing the system strongly towards outward rotation of the hydroxyl group during ring opening step. The difference in these interactions is due to the orbital overlap term (F(i,j)) for which outward rotation has a higher value (0.112) than inward rotation (0.070). Thus, while other orbitals play a role in lowering the energy barrier, it is this interaction that governs selectivity.[114-115]

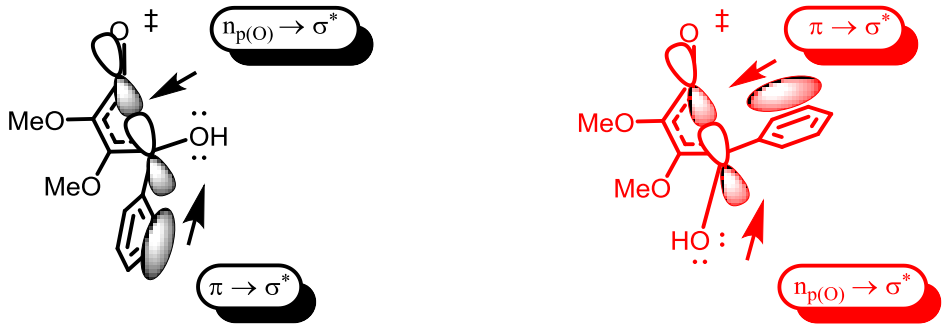

Inward rotation of hydroxy moiety

Outward rotation of hydroxy moiety

Figure 4.2. Cartoon representation of the most important interaction driving torquoselectivity in the phenylcyclobutenone rearrangement.

In conclusion, the torquoelectronic model was examined by natural orbital analysis on product-like resonance structure. The most important interaction in respect of torquoselectivity is the $n_{p(O)} \rightarrow \sigma^*_{(C\text{-}C)}$ overlap as it is this that makes outward rotation of the hydroxyl group favourable over inward rotation by 9.3 kcal/mol, which is in accordance with DFT studies.

4.1.2 Substituent effects on torquoselectivity and ring opening

CHESS IS MENTAL TORTURE.
GARRY KASPAROV

The previous study revealed how various orbital interactions influence the energy barrier for ring opening. A fuller understanding can be made by screening a range of systems with different substituents decorating the core structure as this should reveal how each impacts on the reaction barrier. The natural orbital analysis (NBO) suggests that the reaction should be highly influenced by the π donor ability of the substituent on the saturated carbon centre (Z, Scheme 4.2). In order to verify this hypothesis, the influence of substituents at C2, C3 and C4 on the transition states for ring opening was examined.

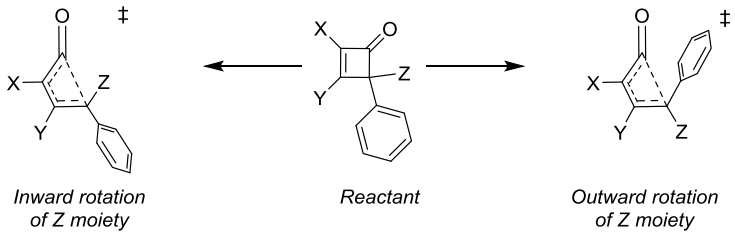

Scheme 4.2. A study on the influence of substituents (X, Y and Z) on the inward and outward transition states for the thermochemical opening of substituted cyclobutenones.

It was shown in the previous chapter that the B3LYP level of theory was not appropriate for attaining a quantitative picture, but was able to provide qualitative trends for such reactions. Moreover, B3LYP is proven to be one of the most efficient methods for the calculation of transition states, which require considerable computational effort. The reaction barrier for the ring opening of cyclobutenones via inward and outward transition states was calculated for 35 arylcyclobutenones decorated with various substituents. To achieve consistency in respect of conformation analysis, more than 130 transition states were examined. The results of these calculations are shown in Table 4.2 for the both inward and outward transition states. They are listed from lowest to highest reaction barrier for the more commonly encountered outward transition state. These data are also summarised in Graphs 4.1 and 4.2, where a plot of the energy barrier for inward versus outward rotation is given.

Table 4.2. The impact of substituents on the inward and outward ring opening reaction at B3LYP/6-311G(d,p).

Entry	X,Y,Z-substituents	barrier height[kcal/mol]			
		E_{Out*}	E_{In**}	E_{In}-E_{Out}	E_{In}/E_{Out}
1	OMe, OMe, O^-	4.9	15.2	10.3	3.1
2	NO_2, NO_2, OH	12.2	11.4	-0.8	0.9
3	NO_2, H, OH	13.4	19.6	6.2	1.5
4	F, H, OH	14.4	26.1	11.7	1.8
5	H, NO_2, OH	14.8	21.8	6.9	1.5
6	H, F, OH	15.8	20.2	4.4	1.3
7	CN, CN, OH	16.8	23.6	6.8	1.4
8	CF_3, CF_3, OH	17.1	24.1	6.9	1.4
9	F, F, OH	17.2	21.3	4.2	1.2
10	CF_3, H, OH	17.3	23.9	6.6	1.4
11	H, CF_3, OH	17.3	24.2	6.9	1.4
12	CN, H, OH	17.6	24.0	6.4	1.4
13	CF_3, OH, OH	17.7	23.3	5.6	1.3
14	H, CN, OH	17.7	24.1	6.4	1.4
15	H, H, OH	17.8	23.8	6.0	1.3
16	H, OH, OH	17.8	22.6	4.8	1.3
17	H, O^-, OH	18.2	24.6	6.3	1.3
18	OMe, OMe, OH (***)	18.2	26.8	8.6	1.4
19	CN, OH, OH	18.5	23.9	5.4	1.3
20	H, NH_2, OH	18.8	24.1	5.3	1.3
21	F, OH, OH	19.2	21.1	2.0	1.1
22	OCH_2R, OCH_2R, OH	19.9	25.6	5.7	1.3
23	OH, F, OH	20.3	24.9	4.6	1.2
24	Ph, OMe, OH	21.3	27.0	5.8	1.3
25	OMe, OMe, OH	21.6	27.1	5.5	1.3
26	OH, OH, OH	21.9	27.1	5.2	1.2
27	OH, CF_3, OH	22.1	27.5	5.4	1.2
28	OMe, OMe, OCF_3	22.3	27.2	5.0	1.2
29	OH, H, OH	22.8	28.9	6.1	1.3
30	OH, CN, OH	23.1	29.4	6.3	1.3
31	$NMeCH_2R$, $NMeCH_2R$, OH	23.4	30.4	7.1	1.3
32	OMe, OMe, H	23.9	20.7	-3.2	0.9
33	OMe, OMe, F	24.8	29.1	4.3	1.2
34	OMe , Ph, OH	25.4	32.5	7.2	1.3
35	OMe, OMe, Cl	25.9	30.5	4.6	1.2

Only the lowest conformers of each transition states are included. * Outward rotation of the Z substituent, ** inward rotation of the Z substituent, *** In this case the phenyl residue was replaced with a 2-pyridyl residue.

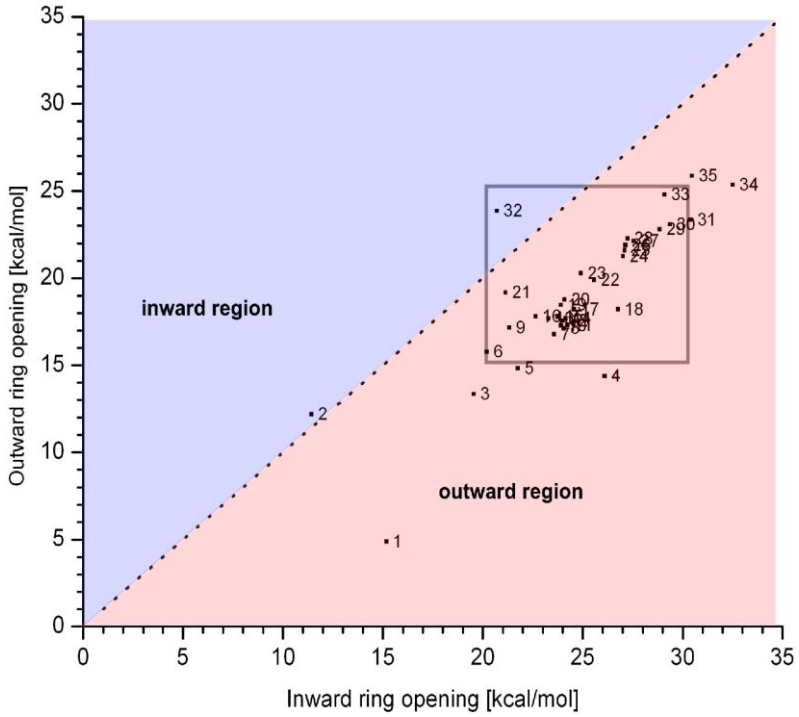

Graph 4.1. Graphical representation of results shown in Table 4.2. The dotted line separates the molecules favouring inward and outward rotation of Z. Compounds are identified by their entry number in Table 4.2.

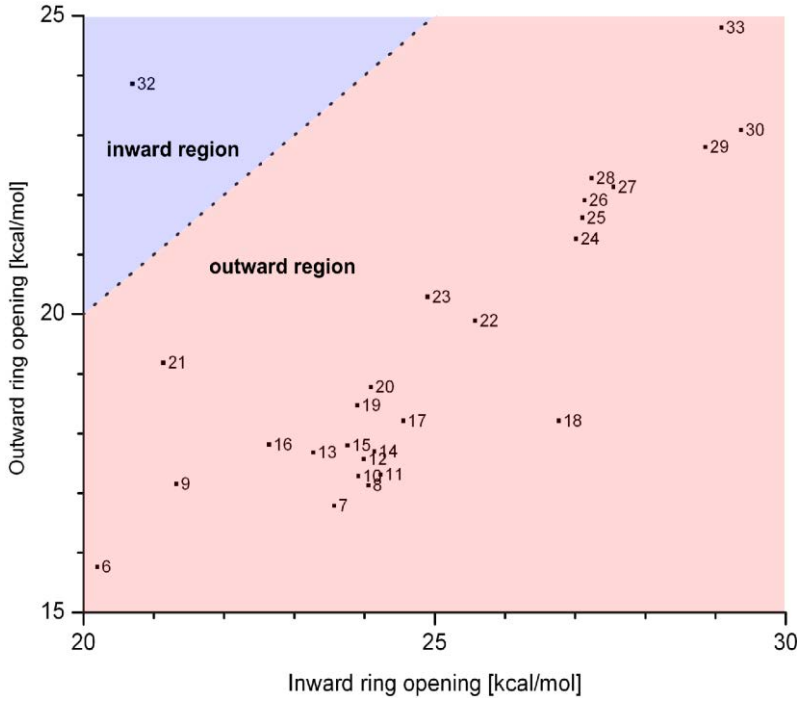

Graph 4.2. Magnification of the key 20-30 kcal/mol region of Graph 4.1. Compounds are identified by their entry number in Table 4.2.

Primary conclusions:

1. **General trends.** For the substituents studied, the energetic window for outward rotation was 20 kcal/mol (Table 4.2, Entry 1, 4.9 kcal/mol and Entry 2, 25.9 kcal/mol) and for inward rotation was 21.1 kcal/mol (Table 4.2, Entry 2 11.4 kcal/mol and Entry 34, 32.5 kcal/mol). Outward rotation was the favourable pathway in all but two cases (Table 4.2, Entry 2 and Entry 32). The average values for E_{In}/E_{Out} and E_{In}-E_{Out} were 1.2 and 5.7 kcal/mol, respectively.
2. **The Z-substituent effects.** The lowest value of energy for the outward transition state, 4.9 kcal/mol (Table 4.2, Entry 1), is with an alkoxide as the Z-substituent. This can be explained by the strong donation ability of the anion and the importance of the $n_p \rightarrow \sigma^*_{(C\text{-}C)}$ interaction. It is worth noting that E_{In}-E_{Out} for that molecule is 10.3 kcal/mol, one of the highest values attained in the study. It corroborates the conclusions drawn from our earlier natural bond orbital (NBO) study which showed the influence of the $n_p \rightarrow \sigma^*_{(C\text{-}C)}$ interaction on torquoselectivity in the ring opening step. The influence of substituents in position Z on the barrier height allows them to be ranked as follows: O^- >> OH > OCF_3 > H > F > Cl (Figure 4.3).

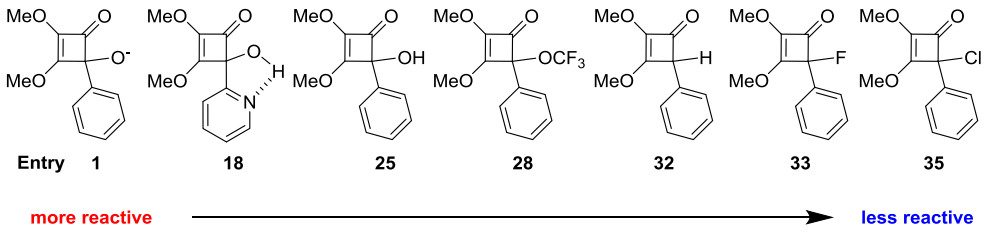

Figure 4.3. The influence of the Z substituent on reactivity. In this Figure the number below each structure refers to the entry number in Table 4.2.

The lack of a lone pair on hydrogen raises the activation energy for outward rotation and leads to a switch in torquoselectivity. Again, this is in agreement with our previous findings, when the DONOR$\rightarrow\sigma^*_{(C\text{-}C)}$ interaction was identified as the primary influence on torquoselectivity. The influence of intramolecular hydrogen bonding is also seen in Entry 18 of Table 4.2, where replacement of the phenyl residue for a 2-pyridyl substituent leads to an

enhancement in rate and torquoselectivity. The fluoro- and chloro substituents behave differently.

3. **The X-substituent effect.** The rate of the ring opening step is also influenced by the substituent X, as shown in Figure 4.4. When this is an electron withdrawing group the barrier for ring opening is reduced. By contrast, donor substituents such as a hydroxyl group raise the energy barrier. The influence of substituents in the X position can be ranked as follows: $NO_2 > F > CF_3 > CN > H > OH$.

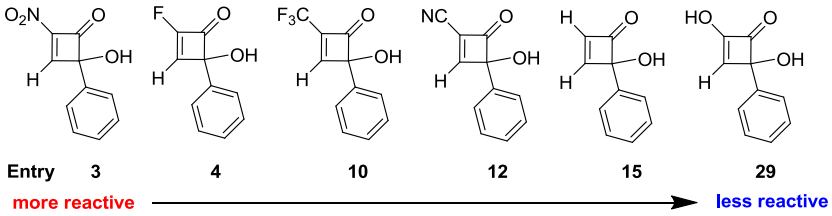

Figure 4.4. The reactivity order for substituents X. In this Figure the number below each structure refers to the entry number in Table 4.2.

This ordering is independent of the nature of the Y-substituent, as demonstrated by the examples shown in Figure 4.5.

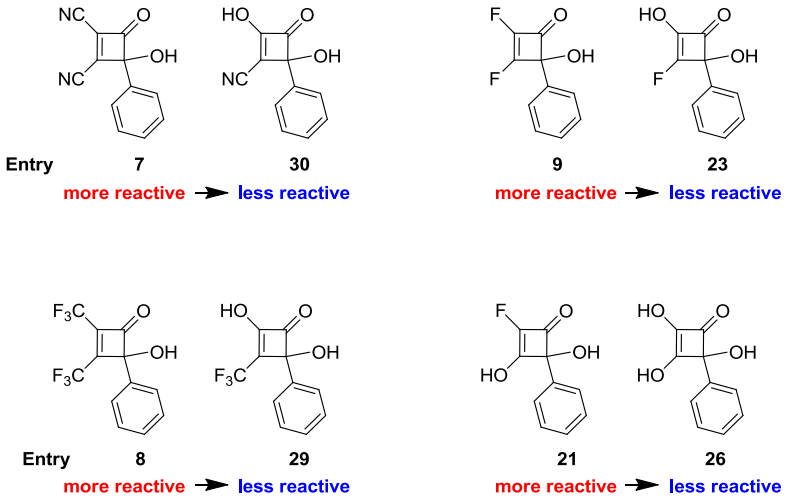

Figure 4.5. The order of reactivity for substituents X is unaltered by the nature of substituent Y. In this Figure the number below each structure refers to the entry number in Table 4.2.

4. **The Y-substituent effect.** The rate of the ring opening step is also influenced by the substituent Y. Electron withdrawing groups lower the barrier for ring opening, so the influence is akin to that of the X-substituents. They can be ranked as follows: NO_2 > F > CF_3 > CN > H > OH > O^- > NH_2.

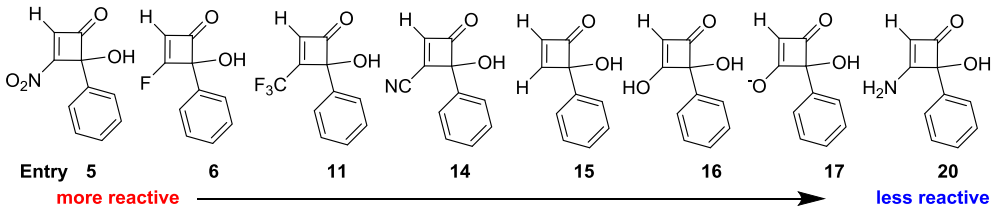

Figure 4.6. The reactivity order for substituents Y. In this Figure the number below each structure refers to the entry number in Table 3.2.

5. **The X and Y substituent effect.** Although the influence of substituents X and Y follows the same trend, the former is the dominant effect. This is exposed by comparing the barriers for various X,Y-disubstituted, X-substituted, Y-substituted and unsubstituted cyclobutenones. In most of the cases studied, these followed a general trend: X,Y-disubstituted > X-substituted > Y-substituted > unsubstituted (Figure 4.7).

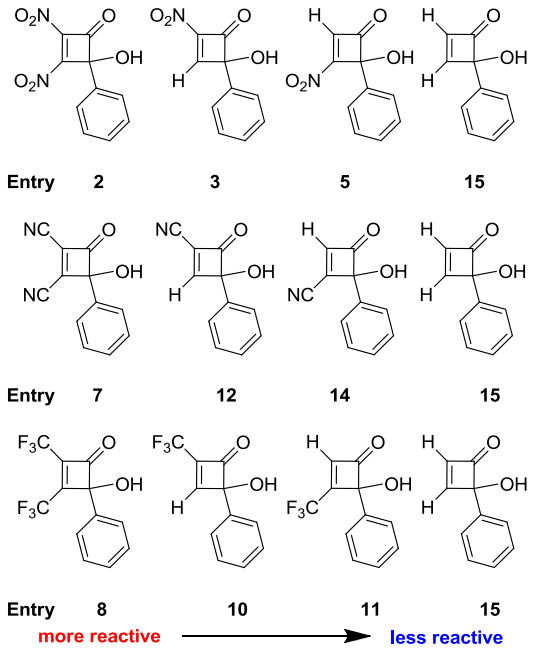

Figure 4.7. The reactivity order for -NO_2, -CN, -CF_3 substituents in X and Y position. In this Figure the number below each structure refers to the entry number in Table 4.2.

Fluoro-substituents proved anomalous as they gave: X-substituted > Y-substituted > X,Y-disubstituted > unsubstituted (Figure 4.7).

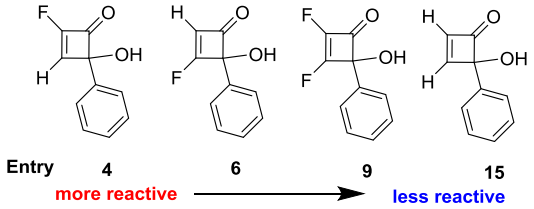

Figure 4.8. The reactivity order for -F substituent in X and Y position. In this Figure the number below each structure refers to the entry number in Table 4.2.

Hydroxyl groups also behave anomalously as they slow the reaction down relative to the parent system. As a consequence they are ordered unsubstituted > Y-substituted > X,Y-disubstituted > X-substituted (Figure 4.9).

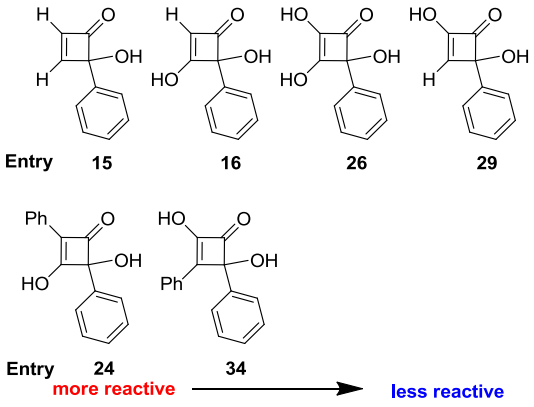

Figure 4.9. The reactivity order for systems with hydroxyl substituents in positions X and Y. In this Figure the number below each structure refers to the entry number in Table 4.2.

6. **Double substitution effects.** For the most part double substitution at X and Y follows the same trend as monosubstitution at X or Y. Notable exceptions are the substrates with cyano and fluoro substituents, which switch position in the rank order (Figure 4.10). As the energy differences are small, this is not of great significance.

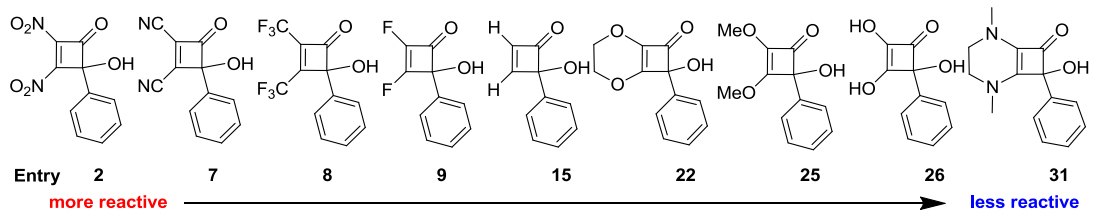

Figure 4.10. The reactivity order for -NO_2, -CN, -CF_3, -F, -H, -OC_2H_4O-, -OMe, -OH, -$N(Me)C_2H_4N(Me)$- double substitution in X, Y position. In this Figure the number below each structure refers to the entry number in Table 3.2.

4.2 Conclusions

SOME THINGS ARE EASY, THEY ARE ONLY HARD TO DO.
A. EINSTEIN

In conclusion, substituents at all positions impact on the rate of the ring opening step in thermally induced cyclobutenone rearrangements. The Z-substituent has the greatest influence. The reduction in barrier height follows the order: O^- >> OH > OCF_3 > H > F > Cl. The X- and Y- substituents influence the system less but show the opposite trend, with NO_2 > F > CF_3 > CN > H > OH > O^- > NH_2. Torquoselectivity is reversed when the Z-substituent is a hydrogen or nitro group. The barrier height is likely to impact on the stabilities of such compounds, which explains why some must be stored at low temperature and are stable for only a short period of time.

Chapter 5: Cyclobutenone Rearrangement Pathways

THE INFINITE MONKEY THEOREM STATES THAT A MONKEY HITTING KEYS AT RANDOM ON A TYPEWRITER KEYBOARD FOR AN INFINITE AMOUNT OF TIME WILL ALMOST SURELY TYPE A GIVEN TEXT, SUCH AS THE COMPLETE WORKS OF WILLIAM SHAKESPEARE.
INFINITE MONKEY THEOREM

5.1 Chapter abstract

This chapter is primarily concerned with the alkynylcyclobutenone rearrangement. Various models have been examined in an attempt to provide a general picture for the reaction and to understand experimental outcomes. Complete reaction pathways, from reactant to product, have been examined on small, model systems to delineate the impact of substituents on the course of the rearrangement. To provide a fuller picture, closed-shell and open-shell singlet diradical pathways have been considered, with all pathways calculated using the B3LYP, M06-2x and M06-L optimized geometries together with the 6-311G(d,p) basis set. It is well established that M06-2X gives better estimates of energy in general. However, UBS-M06-2X seems to overestimate the energies for some open-shell singlet diradical species.[116] Improvements through the addition of spin projection corrections,[117] have some limitations,[118] as has been noted with the spin projection corrections for enyne-ketene cyclisations[54] which worsen when these are included.

Since the aim of this study was to evaluate competitive pathways, which including diradical species, the B3LYP functional will be emphasized in the analysis. Despite the complexity involved in exploring such transition state space, interpretation will be based on results attained by DFT, within their limitation. Importantly, our preliminary studies with the multireference methods MRCI+Q and NEVPT2, show good agreement with B3LYP in line with recent studies in the literature.[54]

5.1.1 4-Ethynylcyclobut-2-en-1-one

INTEGRITY IS THE ESSENCE OF EVERYTHING SUCCESSFUL.
R. BUCKMINSTER FULLER

The simplest alkynylcyclobutenone rearrangement one can envision involves 4-ethynylcyclobut-2-en-1-one **5.1** (Scheme 5.1). The ring opening to vinylketenes **5.2** and **5.5**, together with the closure of the former to diradical intermediates **5.3** and **5.4**, has been subjected to a molecular modelling study. This pathway was previously analysed[51, 54] as isolated steps. Indeed, there have been no reports in the literature detailing *in silico* studies of the rearrangement as a whole, from **5.1** through to the projected intermediates arising from its thermolysis. Thus, our starting point was to perform such an analysis and the reaction pathways examined are summarised in Figure **5.1**.

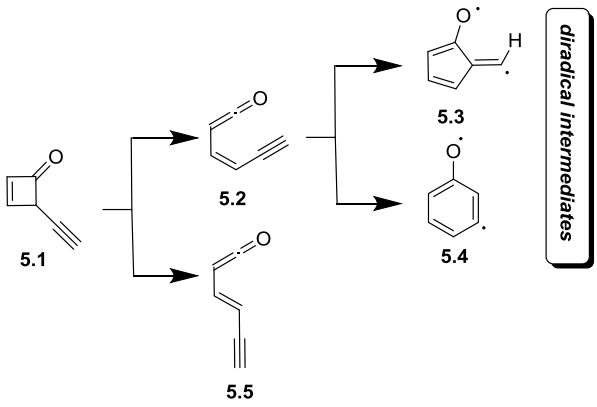

Scheme 5.1. The competitive pathways for 4-ethynylcyclobut-2-en-1-one **5.1**.

It is notable that the first step, ring opening, has a lower energy barrier for formation of the (*E*)-ketenic intermediate **5.5** than for the (*Z*)-ketene intermediate **5.2**, suggesting that (*E*)-ketene **5.5** will be formed as the kinetic product. This is in agreement with our study of the arylcyclobutenone rearrangement where substituent screening (Table 4.1 and Table 4.2, Entry 32) showed that torquoselectivity was reversed when the saturated carbon centre, C-4, bore a hydrogen atom. The (*E*)-ketenic intermediate has two conformations, **5.2** and **5.6**, with a low barrier for interconversion. It also has two competitive cyclisation pathways available to it ─ a 6-ring closure to **5.4** or a 5-ring closure to **5.3**. 6-ring closure involves 6 electrons and is the lowest energy path. Its transition state, [**5.2**-**5.4**], shows no spin contamination (<S**2> = 0.000) at the B3LYP/6-311G(d,p) level which implies a

close-shell rather than a diradical transition state. However the product of this reaction, **5.4**, is a

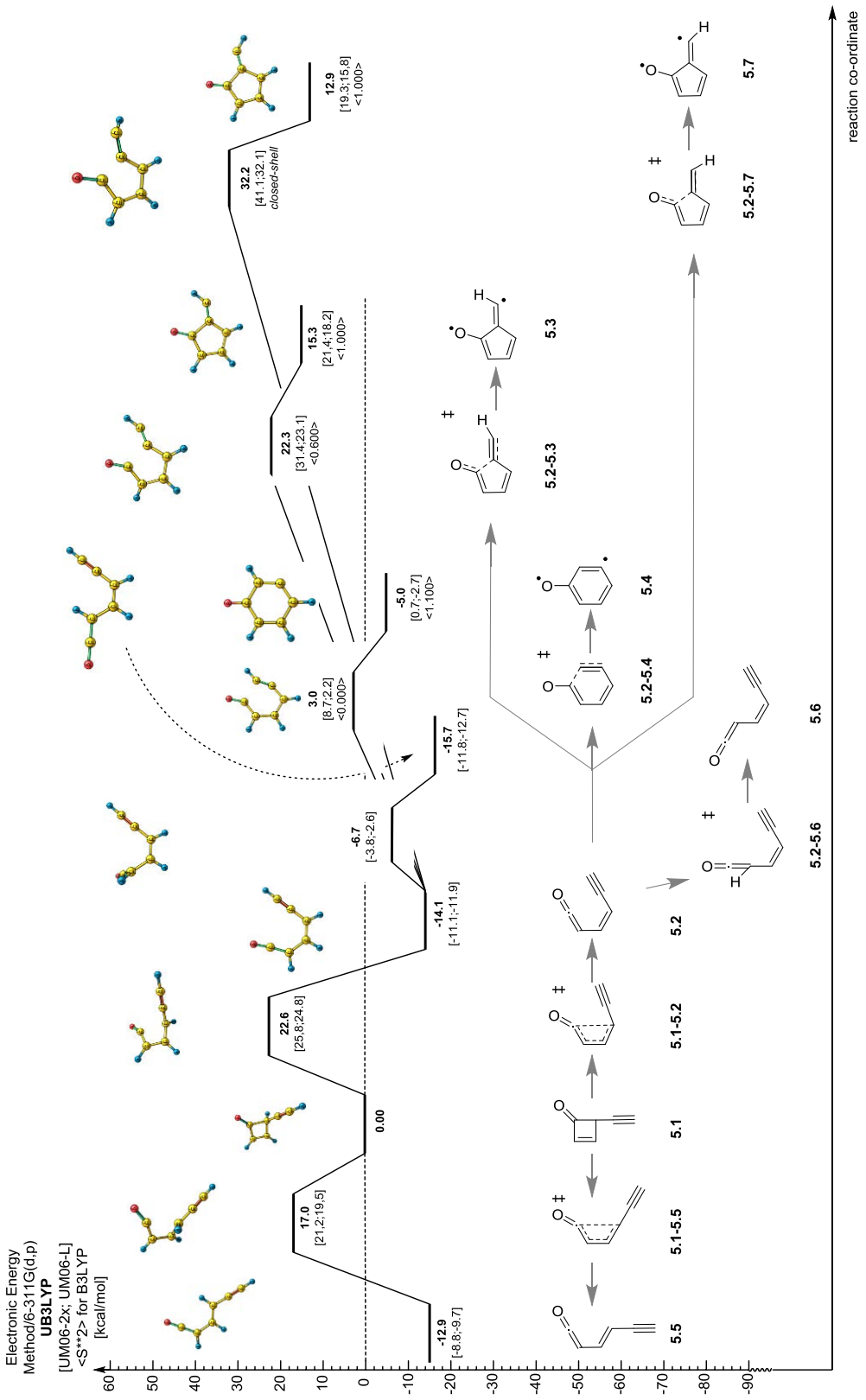

Figure 5.1. Energy graph for the competitive pathways for 4-ethynylcyclobut-2-en-1-one **5.1.**

diradical intermediate with a spin contamination of <S**2> = 1.100. This is consistent with calculations at the B3LYP/6-31G(d) level described in the literature.[54] For 5-ring closure there are two possible transition states. One of these, [**5.2**-**5.7**], proceeds via a closed-shell (CS) transition state and has been calculated with the spin-restricted formalism (R-DFT, *i.e.* <S**2> = 0.000).[54] The second proceeds via an open-shell (OS) singlet diradical transition state [**5.2**-**5.3**], which is reported here.

Calculations using the spin-unrestricted broken-symmetry (UBS-DFT) formalism showed spin contamination of <S**2> = 0.600, which was lower in energy than the reported values by some considerable margin (9.9 kcal/mol). Both transition states were followed by IRC and these interconnect the different isomers of the diradical product. If the unrestricted formalism is applied to the closed-shell transition state geometry of **5.2**-**5.7**, its collapse to **5.2**-**5.3**, the geometry obtained with the spin-unrestricted broken-symmetry formalism. Energies obtained using the M06-2x and M06-L functionals give a similar qualitative picture. The two diradical intermediates **5.4** and **5.3** have their radical centres localised in both the sigma and pi framework and are thus called σ,π-diradicals. The spin density surface shows localisation of the distinctive radical centres as depicted in Figure **5.2**.

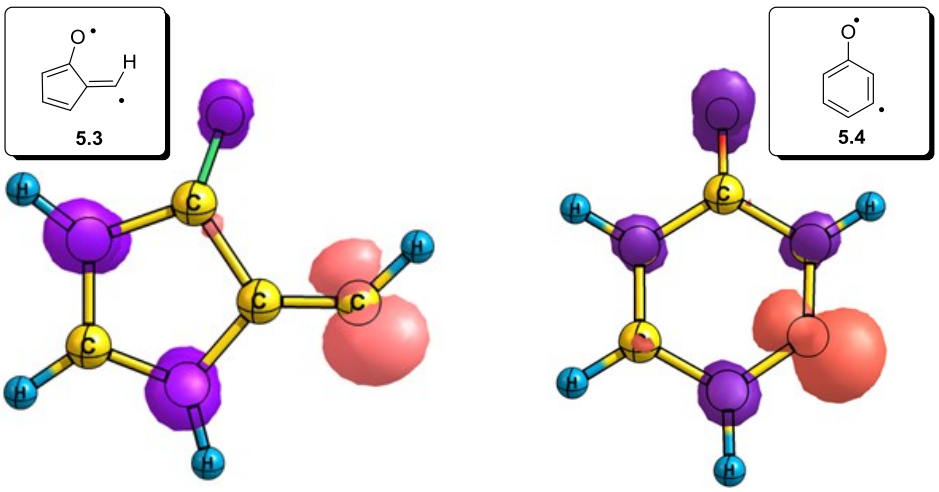

Figure 5.2. Spin-density profiles for the two σ,π-diradical intermediates **5.3** and **5.4** at the UBS-B3LYP/6-311G(d,p) level. The blue surface (positive spin-density) corresponds to an excess of α-electron density in the π-system while the orange surface (negative spin-density) corresponds to an excess of β-electron density in the σ framework.

5.1.2 4-Vinylcyclobut-2-en-1-one

IF WE KNEW WHAT IT WAS WE WERE DOING, IT WOULD NOT BE CALLED RESEARCH, WOULD IT?
ALBERT EINSTEIN

The course of such reactions is quite different when the ethynyl group is replaced by a vinyl group, as in **5.8** (Scheme 5.2). For this system only the 5-ring closure mode leads to a diradical intermediate, **5.11**, with the 6-ring closure producing cyclohexadienone **5.10**. Also, as the vinyl group is a better π electron-donor than the ethynyl group it has a stronger preference to rotate outward, as previously suggested from NBO. That said, the calculated reaction pathway shown in Figure 5.3 indicates that the energy barrier for this pathway is not very different from that given by the analogous alkynylcyclobutenone **5.1** (Figure 5.1).

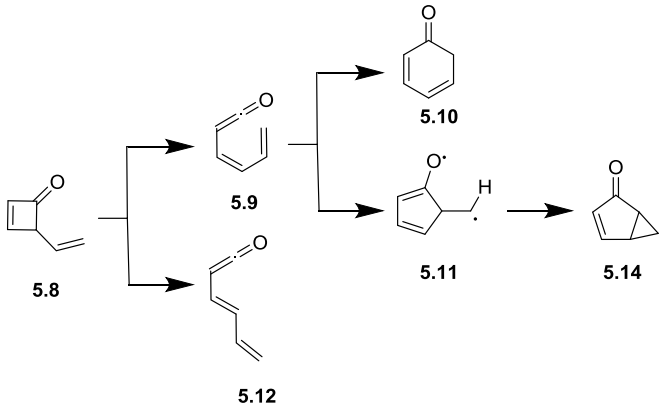

Scheme 5.2. The competitive pathways of 4-vinylcyclobut-2-en-1-one **5.8**.

The first step, ring opening, has the same preference for formation of the (*E*)-vinylketene intermediate **5.9**. However, compared with the alkynylcyclobutenone **5.1,** the energy barrier for (*Z*)-vinylketene **5.2** formation (Figure 5.1) is lowered by 1.3 kcal/mol. For the ring closure reaction the 6-*endo*-trig pathway (**5.9**-**5.10**) is more favourable as it occurs via a closed-shell singlet. This pathway involves a six electron, aromatic transition state so is energetically favourable (34.2 kcal/mol) and does not form a diradical intermediate as before. By contrast, the less favourable 5-*exo*-trig ring closure (**5.9**-**5.11**) has a much higher energy barrier and occurs via a open-shell diradical singlet with spin contamination of <S**2> = 0.600. The unstable five-membered ring diradical intermediate **5.11** spontaneously cyclises to bicyclo[3.1.0]hexenone **5.14**, in the process passing from a diradical species to a molecule with closed-shell character.

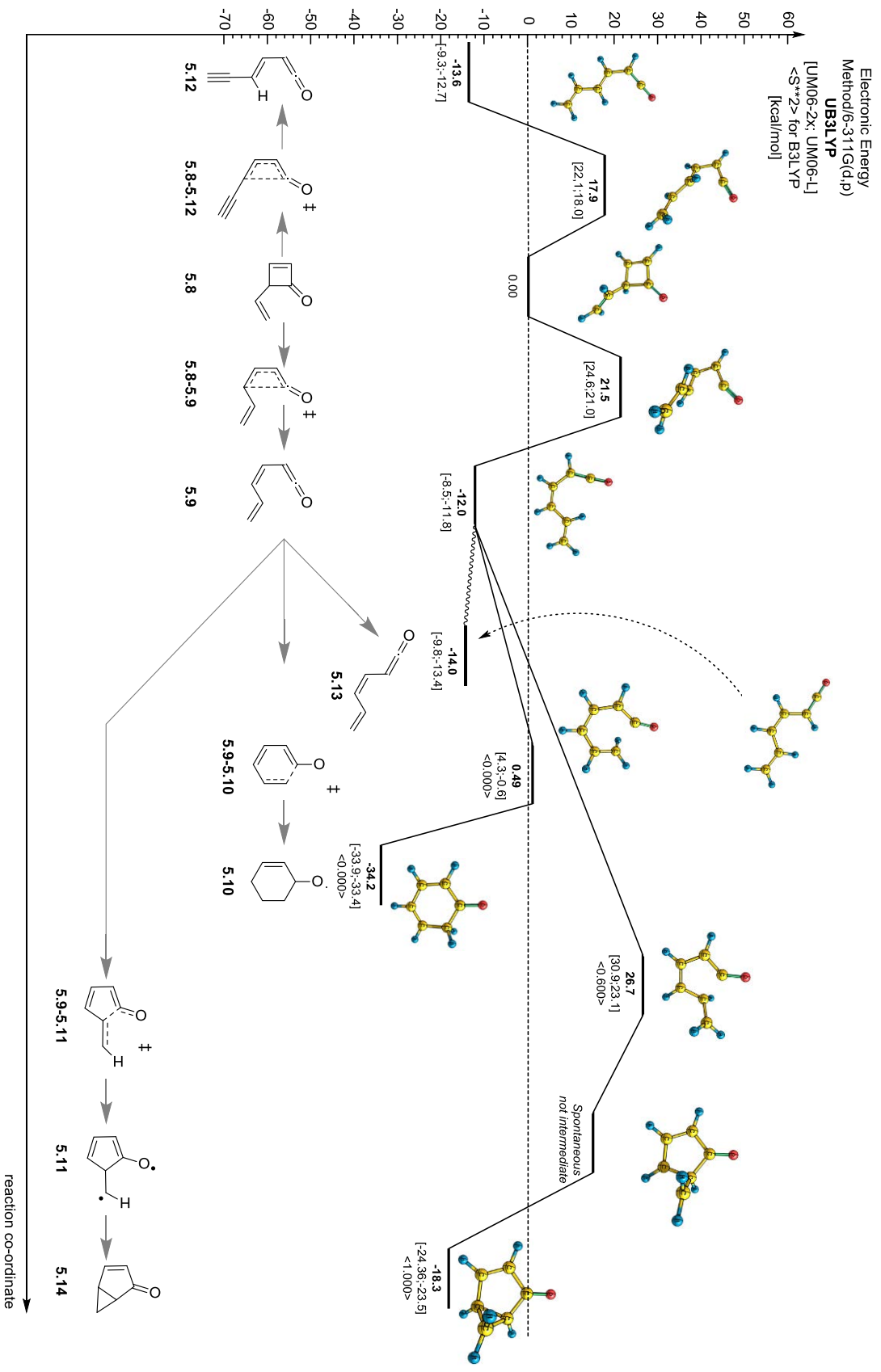

Figure 5.3. Energy graph for the competitive pathways for 4-vinylcyclobut-2-en-1-one **5.8**.

5.1.3 4-Ethynylcyclobut-2-en-1-imine

WHO WISHES TO FIGHT MUST FIRST COUNT THE COST
SUN TZU, THE ART OF WAR

To provide a fuller understanding of the trends in this type of rearrangement we next modelled 4-ethynylcyclobut-2-en-1-imine **5.15** (Scheme 5.3) to see if it would favour arene **5.17** formation. The energy picture is presented in Figure 5.4.

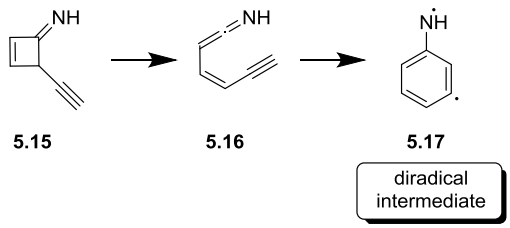

Scheme 5.3. Thermal rearrangement of 4-ethynylcyclobut-2-en-1-imine **5.15**.

The first ring opening reaction (**5.15**-**5.16**) is much higher in energy than for 4-ethynylcyclobut-2-en-1-one **5.1**, being increased by 4.35 kcal/mol due to the influence of the imine group. The ring closure step (**5.16**-**5.17**) is also higher in energy than our reference (Scheme 5.1 and Figure 5.1), indicating that the imine increases the energy barrier for both transition states and slows the reaction overall. Despite those higher energy requirements, the rearrangement has been demonstrated to be usable for some applications.[20]

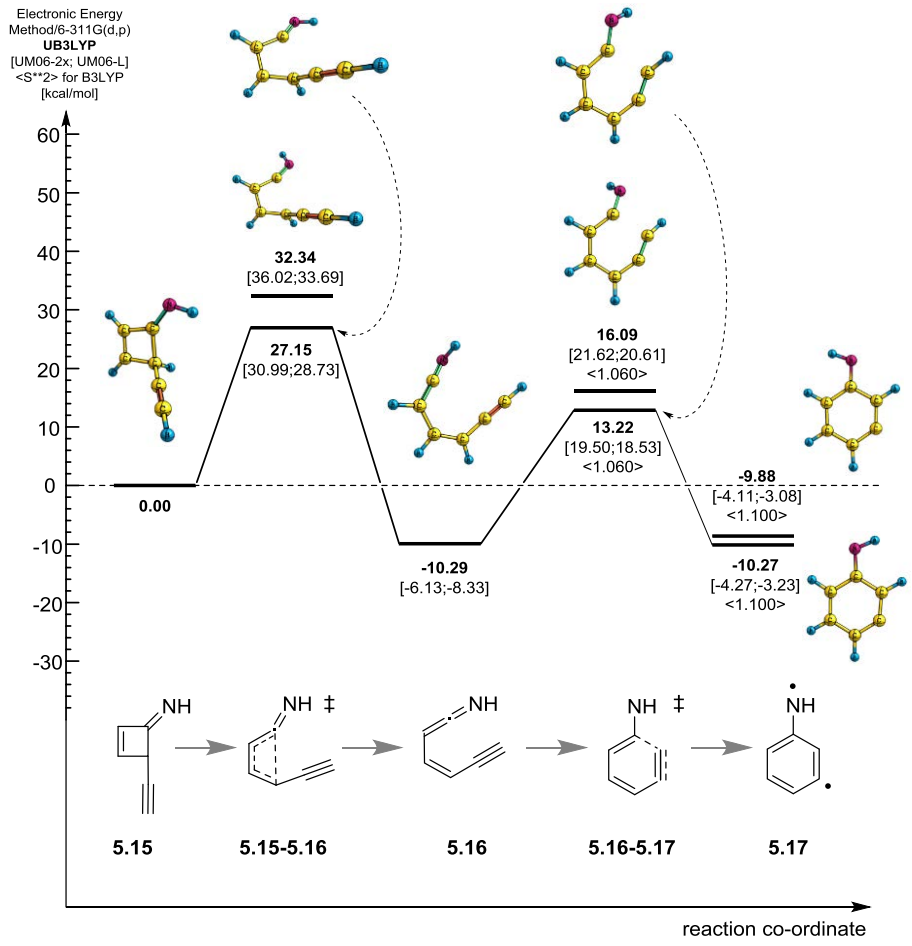

Figure 5.4. Energy graph for the thermal rearrangement of 4-ethynylcyclobut-2-en-1-imine **5.15**.

5.1.4 4-Ethynyl-4-hydroxy-3-methoxycyclobut-2-en-1-one and its thermolysis with water

BE LIKE A POSTAGE STAMP. STICK TO ONE THING UNTIL YOU GET THERE.
JOSH BILLINGS

The study was next extended to more synthetically relevant model systems, such 4-ethynyl-4-hydroxy-3-methoxycyclobut-2-en-1-one **5.18** (Scheme 5.4). Our hope was to reveal the influence of adding methoxy and hydroxy groups on reaction barriers in order to provide a fuller understanding of trends such as the torquoselectivity of ring opening. Also, the presence of the hydroxyl group at C-4 makes it possible to explore the final hydrogen transfer step from **5.20** to the observed quinone **5.21** and furanol **5.24** products or its lactone tautomer.

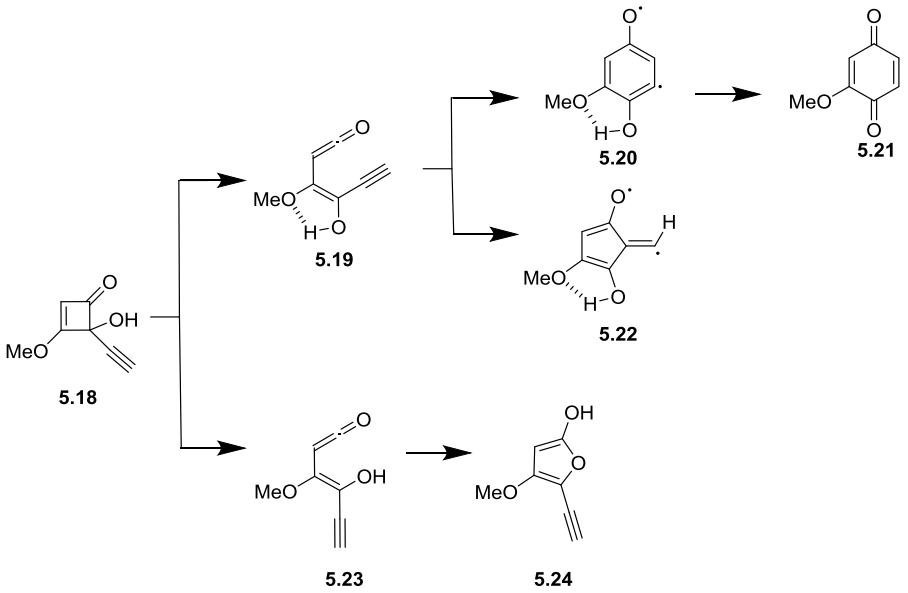

Scheme 5.4. Competitive pathways examined for 4-ethynyl-4-hydroxy-3-methoxycyclobut-2-en-1-one **5.18**.

In this example, the ring opening reaction favoured (*Z*)-vinyl ketene formation (*via* **5.18**-**5.19**) as shown in Figure 5.5. Hydrogen bonding in the transition states was seen to be insignificant and could not account for the switch in selectivity, which is driven by an $n_O \rightarrow \sigma^*$ orbital interaction. Again, the (*Z*)-ketene intermediate **5.19** can undergo two types of cyclisation. Here, the 5-ring closure transition state (**5.19**-**5.22**) has a higher energy barrier and a spin contamination of <S**2 = 0.4>, which increase further to <S**2 = 1.000> as the reaction progress to the five-membered

ring intermediate **5.22**. Moreover, as previously mentioned for 4-ethynylcyclobut-2-en-1-one (**5.1**), this intermediate **5.22** has a higher energy than the reactant **5.18**.

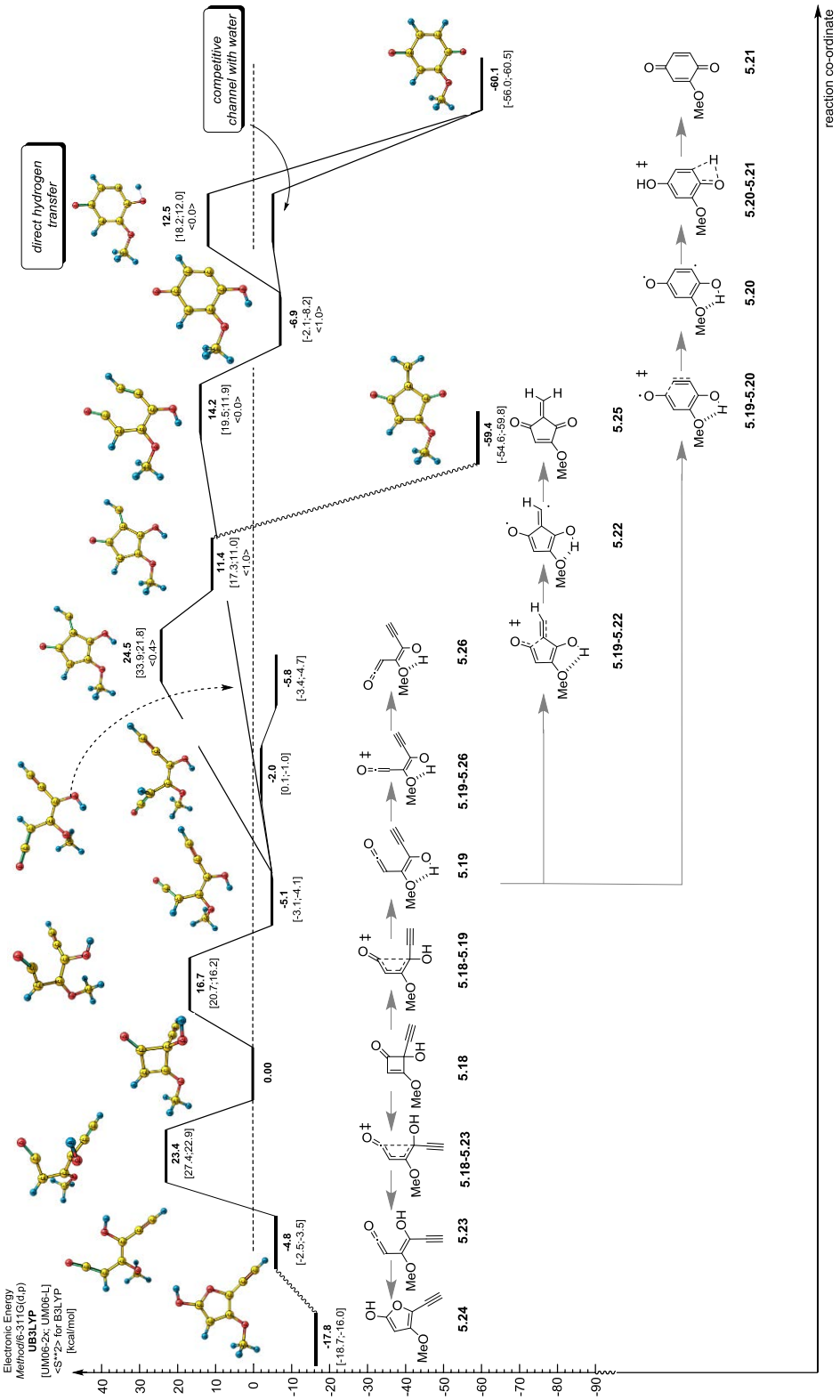

Figure 5.5. Energy graph for the competitive pathways for rearrangement of 4-ethynyl-4-hydroxy-3-methoxy-cyclobut-2-en-1-one **5.18**.

The energy barrier for 6-ring closure (**5.19**-**5.20**) is 10.3 kcal/mol lower than for 5-ring closure (**5.19**-**5.22**). Its transition state has no spin contamination, which implies it has closed-shell character. Interestingly, it leads to an aromatic intermediate **5.20** that exhibits open-shell diradical singlet character with spin contamination <S**2 = 1.000> and is more stable than the five-member ring diradical **5.22**. Formation of quinone **5.21** from **5.20** can be envisioned via two mechanisms. Calculations revealed that an intramolecular hydrogen atom transfer (**5.27**-**5.21**) represents a higher energy path (Figure 5.6). This trend was reproduced by a more tempered basis set in calculations with free energies correction at 150 ^{o}C (Figure 5.6). The transition state for the transformation is nearly planar and has no spin contamination. Indeed, it has many similarities in common with the enol-keto tautomerization mechanism discussed earlier, which also proceeded via a 1,3-hydrogen transfer. Adding a Gibbs free energy correction (ΔG, at 150 ^{o}C) to the electronic energies (ΔE) decreases the energy barrier slightly.

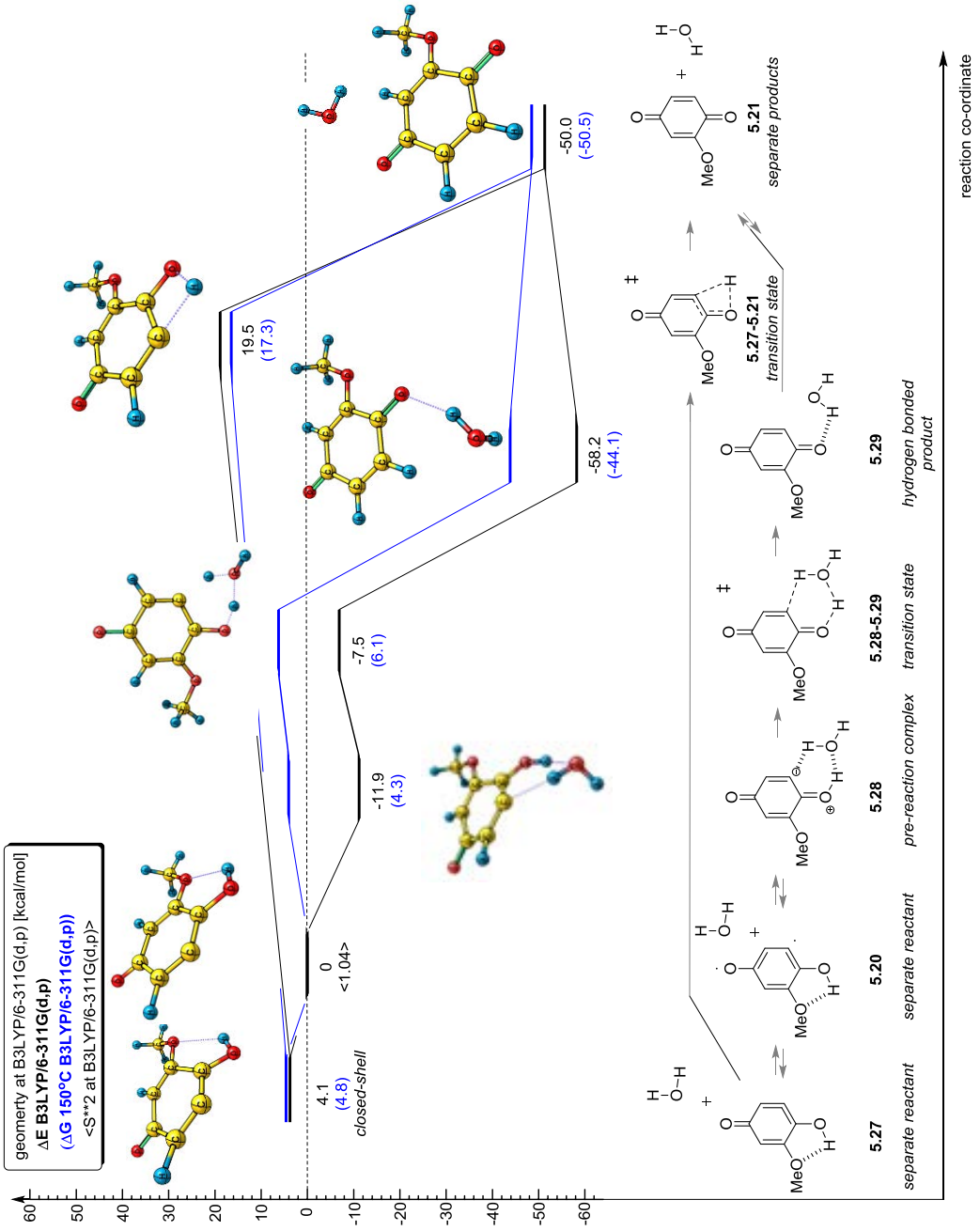

Figure 5.6. Energy graph for hydrogen transfer of diradical intermediate **5.20** promoted by water.

It was found that diradical intermediate **5.20** can form two hydrogen bonds with water and that the hydrogen-bonded adduct **5.28** has closed-shell character with no spin contamination. Thus, it seems that the character of this intermediate changes from a diradical to a closed-shell state in the presence of water (from **5.20** to zwitterionic state **5.28**), implicating a switch from one orbital isomer to another (Scheme 5.5). The allenic intermediate **5.27** has been found to have a higher energy than diradical **5.20** but the difference is only 4.1 kcal/mol (Figure 5.6). The diradical

complex with water, **5.30**, was not found as it spontaneously converges to the closed-shell singlet **5.28**. This was confirmed by a wavefunction instability test.

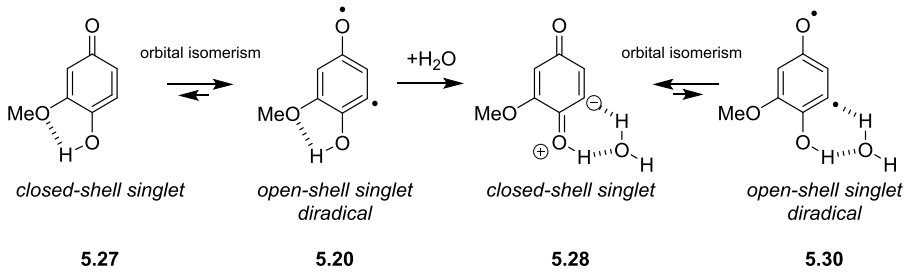

Scheme 5.5. Switch of orbital isomer promoted by water. The diradical complex with water **4.30** spontaneously converges to closed-shell singlet **5.28**.

The H···O hydrogen bond has a high Fuzzy bond order, Laplacian, potential energy density and electron density at the bond critical point (Figure 5.7). Moreover it shows great similarity to a short strong hydrogen bond (SSHB).[119] The hydrogen bond to carbon, C···H, is also important for the stability of that complex. Interestingly, the charge distribution determined by CHELPG ESP[120], calculated with MultiWFN[121], gives a high positive charge on the hydrogen in the H···O hydrogen bond and a high negative charge on the carbon involved in the C···H interaction. The reduced density gradient (RDG) surface shows this hydrogen bonding as a dark blue area.

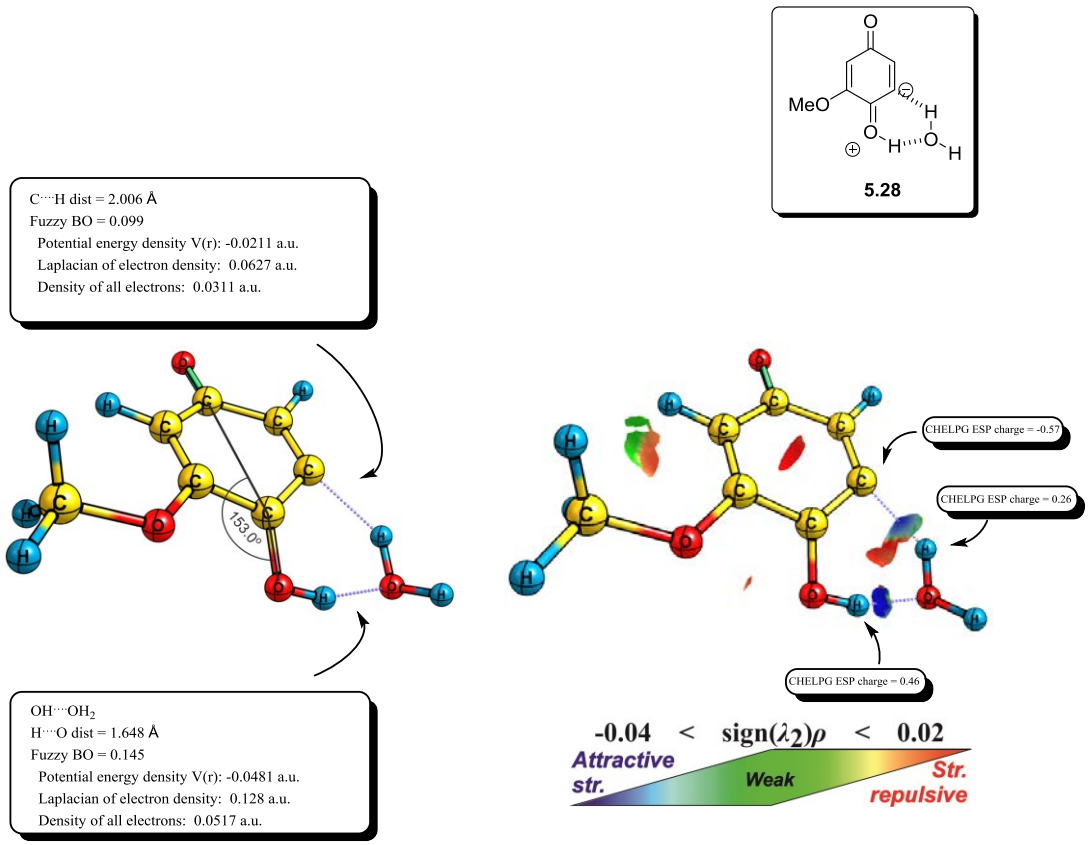

Figure 5.7. Geometrical and electronic analysis of complex **5.28**. Geometry and NBO analysis at B3LYP/6-311G(d,p), Fuzzy bond order and QTAIM analysis at M062X/6-311++G(2d,2p).

Together with the AIM and NBO analyses performed, these show that **5.28** is the best representation of this intermediate in water. The energy gained from hydrogen bonding interactions is hugely significant. Nevertheless, at 150 °C entropy effects generally promote disaggregation rather than aggregation (Figure 5.6), as observed in vacuum.

In tetrahydrofuran it is expected that entropy loss due to disaggregation of water and THF will compensate for the entropy loss when **5.28** forms an adduct. With water, after all, both the electronic energies and Gibbs free energies show that it promotes double hydrogen transfer and that that outpaces direct tautomerization even at 150 °C. The entropy effect is important but does not change the overall picture of the reaction. Indeed, the double hydrogen transfer reaction is much lower in energy than direct transfer and explains why the output of the reaction depends on the substrate concentration. The reaction can be seen as an example of fast keto-enol

tautomerization catalysed by any molecule containing a hydroxyl group. This was exemplified by the thermolysis of cyclobutenone **5.31** in dry dioxane which gives a mixture of cyclised and uncyclised products **5.33** and **5.34**. However addition of even small quantities of deuterium oxide to this reaction promoted formation of deuterated quinone **5.36** exclusively. This provides evidence for the correctness of our calculated path and the relevance of hydrogen bonding to the stability of zwitterionic intermediates such as **5.35**. These experiments were performed by Dr. Mubina Mohamed and are described in detail in her PhD thesis.[74]

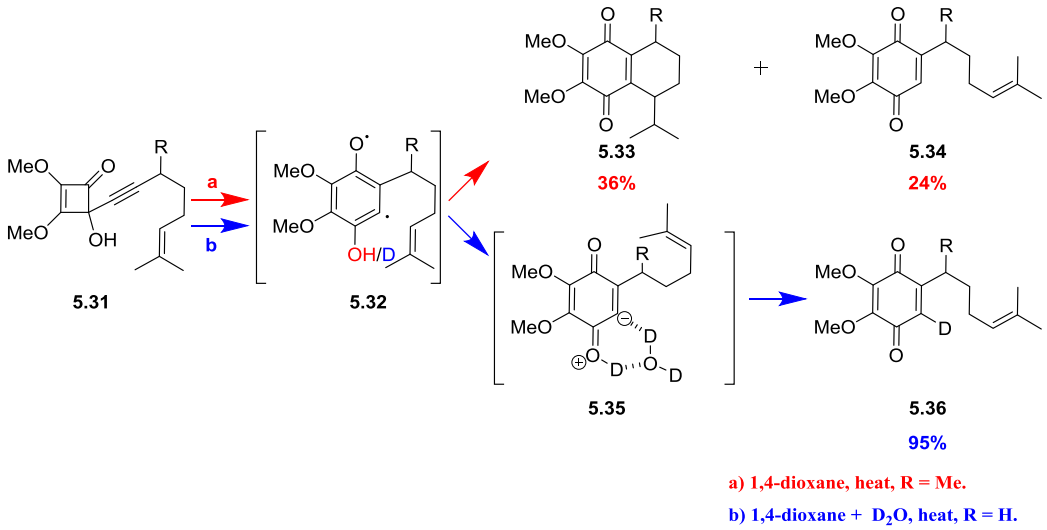

Scheme 5.6. Competitive ring closure and hydrogen transfer reactions promoted by water (experiments conducted by Dr. Mubina Mohamed).

5.1.5 Ring closure with an proximal acetate

IT IS BY LOGIC THAT WE PROVE,
BUT BY INTUITION THAT WE DISCOVER.
H. POINCARE

In the previous example, the diradical intermediate was quenched in the presence of water via an orbital isomer switch. However, if the hydroxyl group is protected, this reaction is no longer available, opening up the possibilities to access higher energy processes. To explore this possibility, molecular modelling studies were conducted with acetate **5.31**. In particular, we were interested to see if this protecting group would undergo hydrogen atom abstraction to **5.30** or ring closure leading to zwitterion **5.32A** (Scheme 5.7).

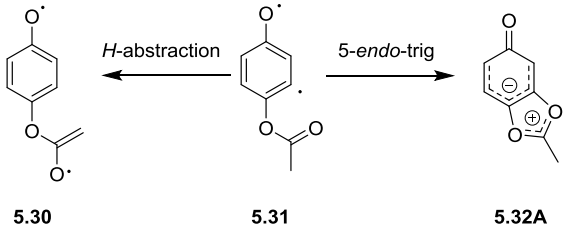

Scheme 5.7. Hydrogen abstraction and ring closure pathways available to diradical **5.31**.

Exploratory molecular modelling (Figure 5.8) showed that hydrogen atom abstraction (**5.30**-**5.31**) was the less favourable of those pathways. Were it to occur, fragmentation of the π,π-diradical **5.30** to ketene **5.37** and quinone **5.38** seems likely to occur as it can proceed via a low-energy pathway. Importantly, for this system the lower energy pathway was 5-ring closure via **5.31**-**5.32A**, where the oxygen of the acetate group adds to the proximal carbon-centred radical. Notably the transition state displayed closed-shell character, rather than the open-shell singlet character expected for a π,π-diradical **5.31** interaction. This results from the stabilisation effect of both oxygen atoms, which helps to shift the intermediate towards the more stable zwitterionic state **5.32A**. Further studies showed that various unimolecular pathways involving the breaking of sigma bonds had high energy requirements. It therefore seemed likely that zwitterion **5.32A** would hydrolyse if formed in the presence of water. [As an aside, it is worth mentioning that rearrangement of diradical intermediate **5.31** to its regioisomer **5.39** is a high-energy process.]

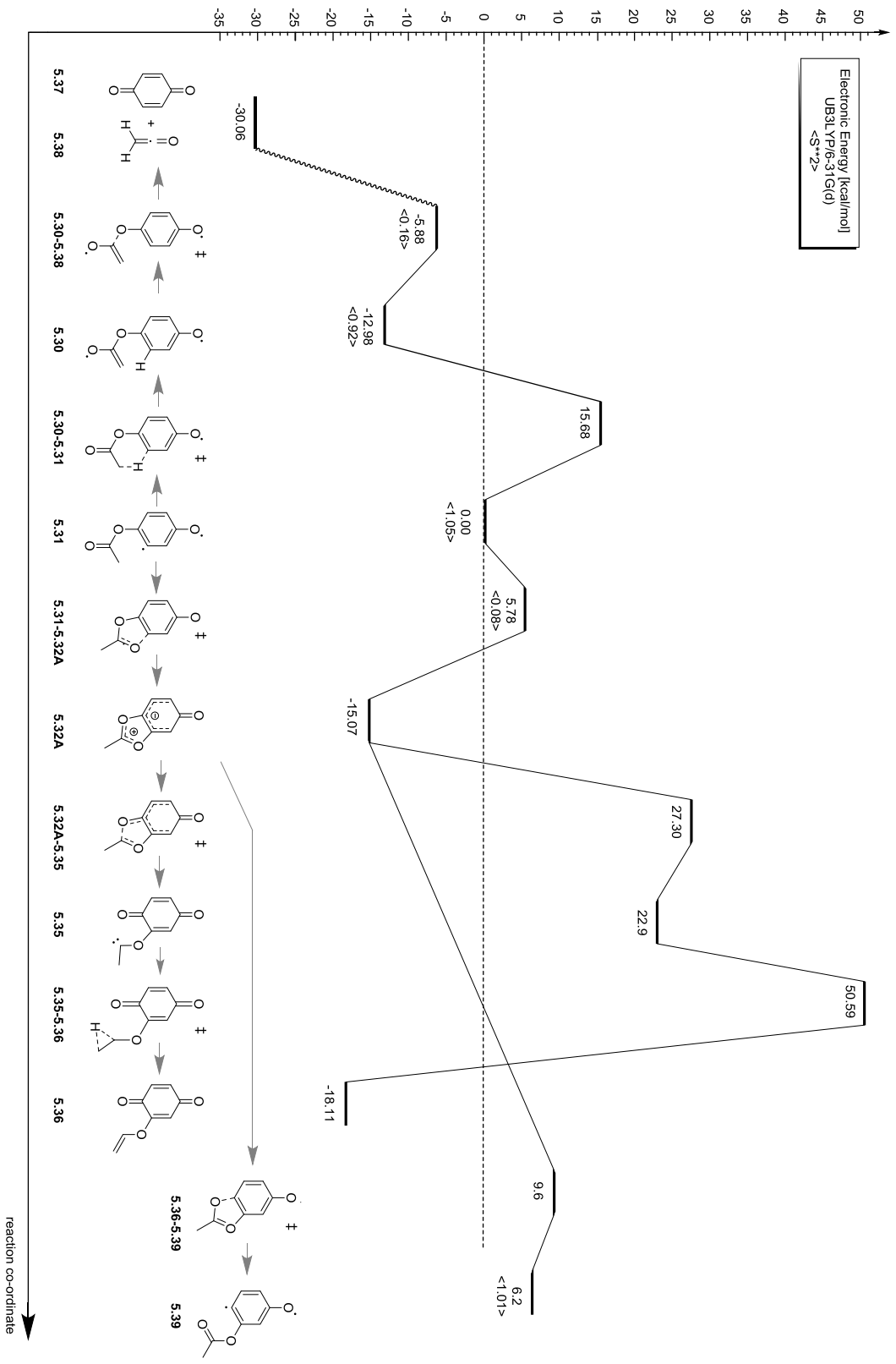

Figure 5.8. Energy graph for ring closure and hydrogen abstraction pathways of diradical **5.31**.

The zwitterionic intermediate **5.32A** can react with water to form **5.33**, which is likely to collapse to acetates **5.40** and **5.41** (Scheme 5.8). It is worth mentioning that

quinone **5.34** could also be envisioned from hydrolysis of vinyl ether **5.36**. However, as the required C-O bond breaking step **5.32A-5.35** and the 1,2-hydrogen shift **5.35-5.36** represent higher energy pathways, this was deemed an unlikely outcome (Figure 5.8).

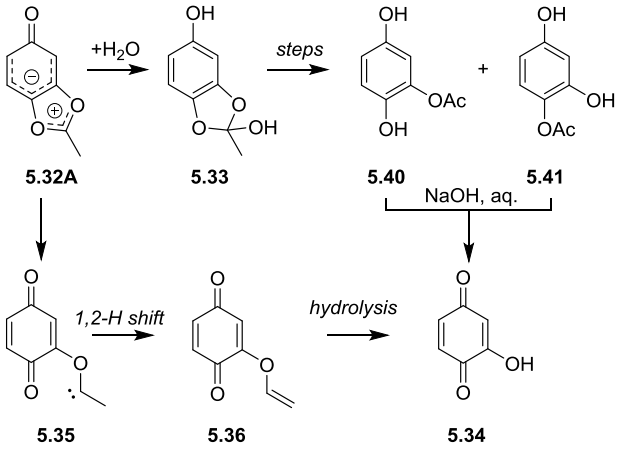

Scheme 5.8. Competitive pathways for formation of hydroxybenzoquinone **5.34** from zwitterionic intermediate **5.32**.

The experiments giving support to the existence of this reaction channel were undertaken by Dr. Mubina Mohamed and are described in details in her thesis.[74] In essence, the thermolysis of cyclobutenone **5.42** in wet dioxane gives a 1:1 mixture of acetates **5.45A** and **5.45B** in high yield (Scheme 5.9).

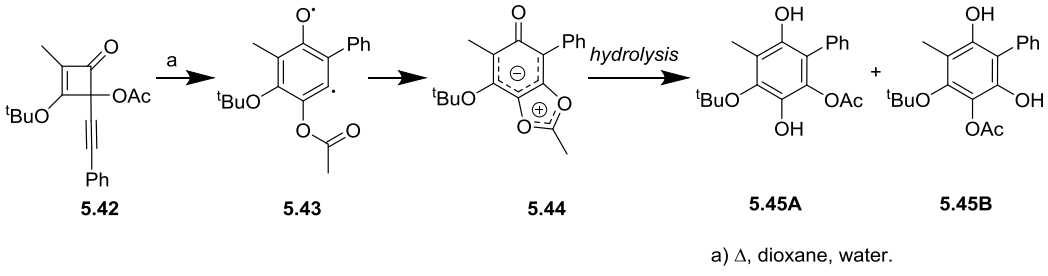

Scheme 5.9. Formation of hydroxybenzoquinone **5.43** from thermal rearrangement via hydrolysis of zwitterionic intermediate **5.42**. (Experiments by Dr. Mubina Mohamed).

To provide a better understanding of the electronic structure of intermediate **5.32A**, further analyses were performed (Figure 5.9). The planar geometry suggests a strongly delocalise π system. However, it is not clear from this what the best representation of its mesomeric structure is. The geometrical data together with

support from a Fuzzy bond order analysis, suggests that the C-O bond at C4 is best viewed as carbonyl as it is a short bond with much double bond character (FBO = 1.89, Figure 4.9). The C1-O1 bond is shorter than the C2-O2 bond but both have single bond character (FBO = 1.19 and 1.12 respectively). The C7-O1 bond is shorter than C7-O2 and both have a bond order close to 1.5. Further evidence for this was gained from ellipticity (ε) data, which are higher for C7-O1 than C7-O2. Bond ellipticity (ε) is associated with the π character of a bond and it is a measure of the double character. From CHELPG ESP analysis it is clear that oxygen O1 is more electropositive than O2 and both are negatively charged.

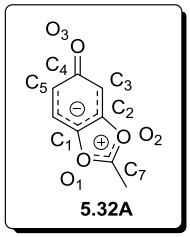

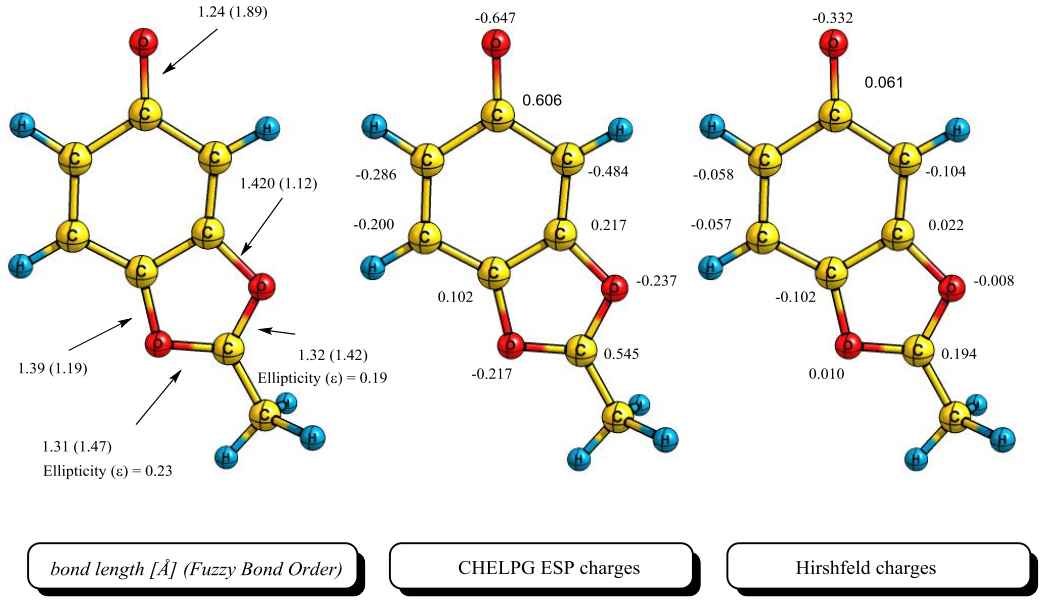

Figure 5.9. Geometry and electronic properties of zwitterionic intermediate **5.32**. Geometry at B3LYP/6-31G(d), Fuzzy bond order and charges analysis at M062X/6-311++G(2d,2p).

The carbon C2 is more electropositive than C1 and both are positively charged. The carbon C3 is more electronegative than C5 and both are negatively charged. The largest negative charge is on oxygen O3.

A Natural Resonance Theory (NRT-NBO) analysis of **5.32A** was next conducted to reveal the relative contribution of each of the primary resonance forms (Figure 5.10). It showed that **5.32B** was the most representative form, closely followed by the **5.32C** resonance form. Other resonance forms contribute less than 1% overall.

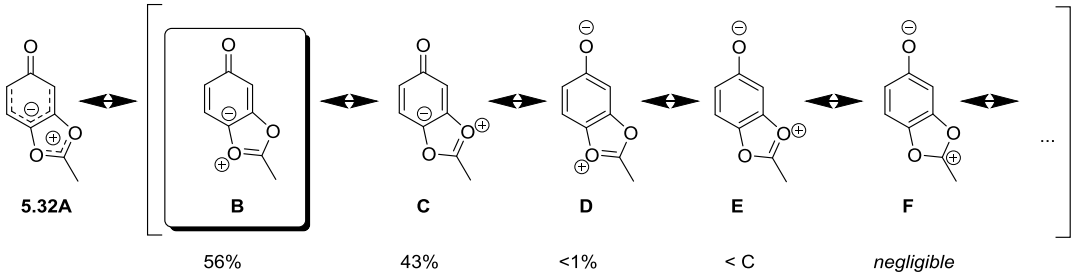

Figure 5.10. Contribution of resonance structures to zwitterionic intermediate **5.32**. NBO analysis at B3LYP/6-311G(d,p).

Interestingly, this NRT-NBO analysis does not reflect the charges obtained from CHELPG ESP. Resonance form analysis suggests that a negative charge is localised on carbon C1 and a positive charge on O1 and O2 oxygen. This differs from CHELPG ESP (Figure 5.9), which suggests that the positive charge is located on carbon C7 and the negative charge is on oxygen O3. Also, the C1 and C2 carbons have positive charges and both O1 and O2 oxygen are predicted to have negative charges, which is in stark contrast to the situation depicted by the most populated resonance forms from NRT-NBO. Charges given by Hirshfeld[122] support the resonance structures obtained from NRT-NBO. The C1 carbon has a negative charge while the adjacent C2 carbon has a positive charge. Similarly, the O1 oxygen has positive charge whereas O2 has a negative charge.

5.2 Conclusion regard model pathways

THE EARTH IS LIKE A SPACESHIP THAT DIDN'T COME WITH AN OPERATING MANUAL.
R. BUCKMINSTER FULLER

A diverse array of alkynylcyclobutenone rearrangement pathways were modelled for both closed-shell and open-shell singlet diradical reactions. The model systems studied show that ring openings of such species proceed with closed-shell character and are likely to be the rate determinant step. However, subsequent ring closure steps are highly influenced by substituents and can proceed with diradical or closed-shell character. For example, examination of the reactivity of the thus formed σ,π-diradical intermediates in vacuum showed that it was likely to give common radical reactions, such as cyclisation to a proximal alkene. By contrast, in the presence of water an intermolecular double hydrogen transfer reaction was seen to outpace such processes. Indeed, the σ,π-diradical appears to switch to a closed-shell polar orbital isomer in order to form strong hydrogen bonds with a hydroxyl containing molecule. Intramolecular cyclisation with a proximal acetate group was also shown to be a low energy process and to the best of our knowledge inspired the discovery of a hitherto unrecognized reaction pathway.

Chapter 6: Organolithium and Organoytterbium Addition to Cyclobutenediones

6.1 Chapter abstract.

LAW OF COMPENSATION:
NO CALCULATION IS EVER A COMPLETE FAILURE; IT CAN ALWAYS SERVE AS A BAD EXAMPLE.
ANON

The addition of organometallic reagents to cyclobutenediones is one of the most important reactions used for the synthesis of cyclobutenone intermediates. When unsymmetrical cyclobutenediones such as **6.2** are employed (Figure 6.1), the addition of an organolithium generally gives the *C*-1 addition product **6.1**. Indeed, the usefulness of this transformation has been demonstrated many times in the total synthesis of natural products, *e.g.* of cribriostatin 6 **6.4**.[73] However, pioneering work in the Harrowven group has shown that transmetallation of organolithium reagents by addition of ytterbium triflate can change the selectivity of such organometallic addition reactions giving access to *C*-2 adducts such as **6.3**. The methodology was exemplified in a first total synthesis of (−)-mansonone B **6.5**.[7]

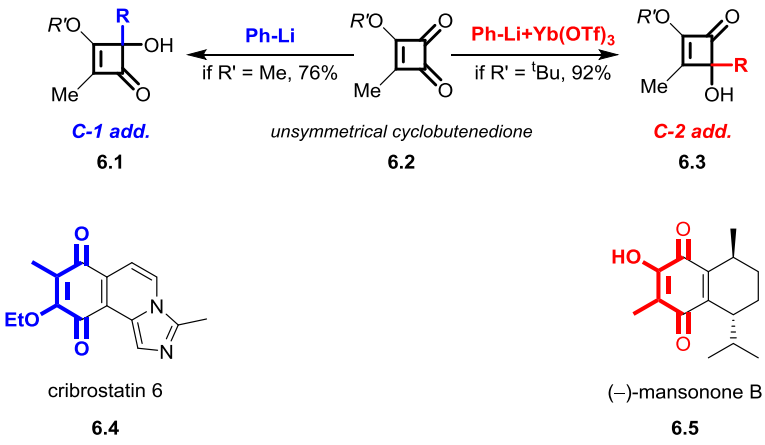

Scheme 6.1. General selectivity of organolithium and organoytterbium additions to unsymmetrical cyclobutenedione **6.2** and its application in the total syntheses of cribriostatin 6 **6.4** and (–)-mansonone B **6.5**.

Inspired by the differential selectivity observed in organolithium and organoytterbium additions to cyclobutenediones, we decided to embark on a computational study in the hope that this would help to explain their dichotomous reactivity. As the literature has limited data on the modelling of organometallic additions to cyclobutenediones,[68] this project involved i) an analysis of the intrinsic reactivity of cyclobutenediones, ii) a study on the addition of organolithium and organoytterbium reagents to acetone and iii) a study on their additions to cyclobutenediones. Part of this research has been published[7] and the experimental procedures that underpin this study are discussed in detail within the PhD thesis of Dr. David Pascoe[123] and Dr. Emma Packard.[124] The project involving methyllithium dimers was conducted in collaboration with Dr. Jacques Maddaluno and Dr. Julien Marchois at the IRCOF institute in Rouen, France.

6.2 Understanding the Intrinsic Reactivity of Unsymmetrical Cyclobutenediones

WHATEVER YOU DO WILL BE INSIGNIFICANT, BUT IT IS VERY IMPORTANT THAT YOU DO IT.
MAHATMA GANDHI

The unsymmetrical cyclobutenedione **6.6** (Figure 6.1) has two electronically non-equivalent carbonyl groups. Each is connected to a common alkene but only one benefits from conjugation to an oxygen lone pair. Conformational analysis at M06-2x/6-31G(d) revealed two low energy conformations for 3-(*tert*-butoxy)-4-methylcyclobut-3-ene-1,2-dione (Figure 6.1). In both conforms the *tert*-butoxy group sits in the plane to cyclobutenedione ring. However the S-*trans* conformer **6.6** was found to be more stable than S-*cis* conformer **6.7**. This difference is largely due to steric energy as shown by NBO pairwise steric exchange analysis,[125] where this equates to a 5.4 kcal/mol difference in energy. Similarly, the Reduced Density Gradient (RDG) analysis reveals a larger repulsion area for the less favourable S-*cis* conformation (larger brown-pink area). However, NBO analysis indicates that this is offset to some degree as the $n_{s(O)} \rightarrow \pi^*_{(C=C)}$ interaction is higher in the S-*cis* conformer than in the S-*trans* conformer, as evidenced by the higher orbital overlap term F(i,j).

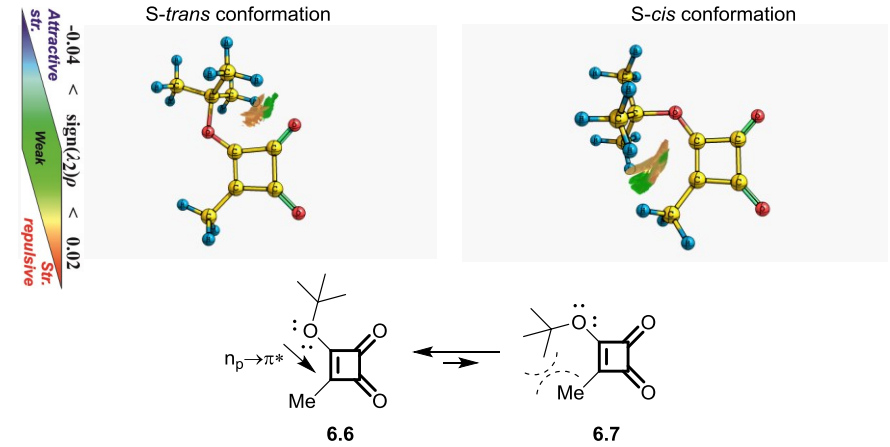

ΔE	0	4.0
$\Delta_{(NBO\ Steric\ pairwise\ exchange)}$	0	5.4
$E(2)_{[np(O)\rightarrow\sigma^*(C=C)]}$	39.2	43.6
F(i,j)	0.105	0.111

Figure 6.1. NBO and RDG analyses of the two conformations of cyclobutenone at M06-2x/6-31G(d). All energies are in [kcal/mol].

A Natural Resonance Theory (NRT)[126] analysis of the contribution of various mesomeric forms of 3-(*tert*-butoxy)-4-methylcyclobut-3-ene-1,2-dione **6.6** is presented in Figure 6.2. The mesomeric forms show that the idealized Lewis structure **6.6A** is most representative, with a contribution of 51%. The first polar resonance form **6.6B**, with an anion localised on the *C*-2 ketone (18%), and its equivalent ketonic form **6.6C** (16%) are also significant. The zwitterionic resonance structure **6.6D** has a lower contribution (15%) as the positive charge is stabilised to a lesser extent by hyperconjugation. These differences in population of the various mesomeric structures is reflected in the bond distances, bond orders and charges (Figure 6.3). The double bond in the *C*-1 carbonyl is shorter than that of the *C*-2 carbonyl, which is supported by Fuzzy bond order calculations. Also, the bond connectivity *C*2-*C*3 is shorter than that connectivity *C*4-*C*1 and has a lower Fuzzy bond order (1.004 Å compared to 1.085 Å). The CHELPG ESP charges[127] also reflect those resonance contributions. The oxygen of the *C*-2 carbonyl carries more negative charge than that at *C*1, as expected from the high contribution of the mesomeric form **6.6B**. Likewise, it also carries a higher positive charge on carbon (Figure 6.3).

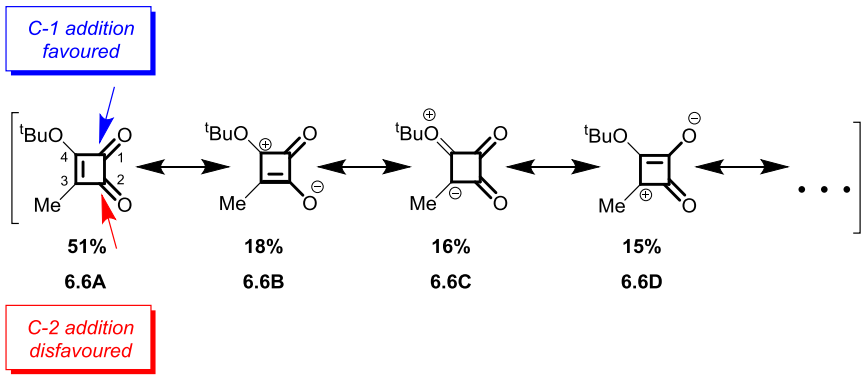

Figure 6.2. Mesomeric structure contributions to cyclobutenedione **6.6** at M06-2x/6-31G(d). The contributions from these significant resonance structures were normalise to 100%.

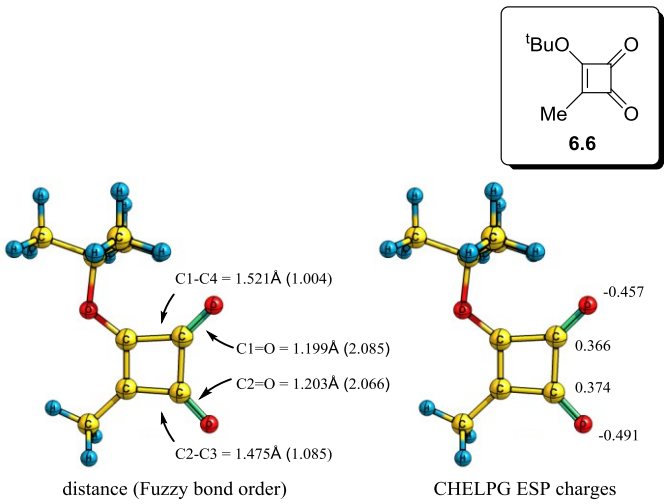

Figure 6.3. Geometric and electronic analysis of cyclobutenedione **6.6** at M06-2x/6-31+(d).

To provide complementary understanding of the intrinsic reactivity of **6.6**, a calculation of the Molecular Electrostatic Potential (MEP) surfaces mapped on total electron density was performed (Figure 6.4). The surface showed a concentrated blue area close to *C*-1 rather than *C*-2, so predicts its preferential attack by a nucleophile based on electrostatics. Also, a Fukui function for nucleophile attack, $f^{+}(r)$,[128] was performed. This revealed a higher surface concentration on *C*-1 rather than *C*-2, suggesting a higher reactivity of this carbon towards nucleophilic attack. The surface also suggests the possibility of 1,4-nucleophile addition at *C*-3, which has been observed experimentally with soft nucleophiles.[65]

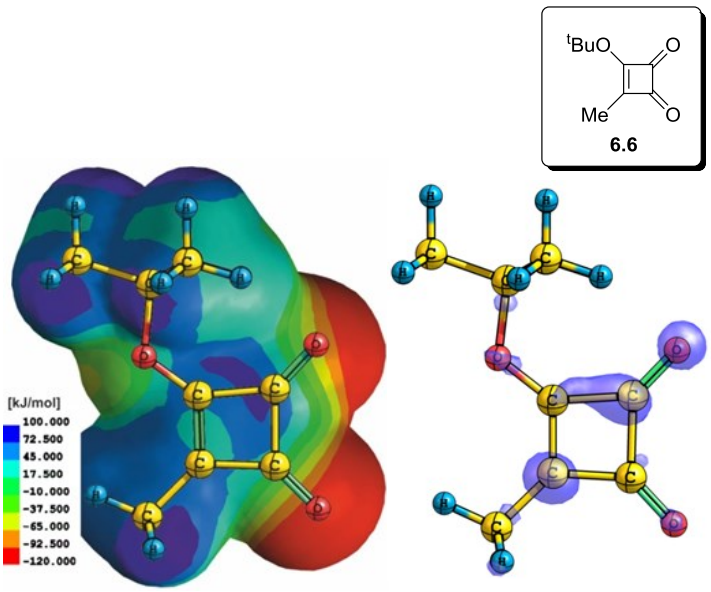

Figure 6.4. Molecular Electrostatic Potential (left) and Fukui function for nucleophile attack $f^{+}(r)$ (right) with only positive phase of surface at B3LYP/6-311G(d,p) level.

All of these analyses support the observed preference for nucleophilic attack at the *C*-1 carbonyl of 3-(*tert*-butoxy)-4-methylcyclobut-3-ene-1,2-dione **6.6**. However, they do not explain the preference for organoytterbium additions to occur at *C*-2!

6.3 Methyllithium Additions to Acetone

PEPPA:
WE'RE TRYING TO RUN AWAY FROM OUR SHADOWS.
SUZY SHEEP:
YOU CAN'T RUN AWAY FROM YOUR SHADOW. YOU NEED A SCOOTER.
FROM PEPPA PIG

6.3.1 Benchmark Study: Methyllithium Addition to Acetone

Before embarking on our investigation we decided to perform a benchmark study with calculations initiated on a simple related system – the addition of methyllithium to acetone in vacuum. The stationary points calculated for that idealise system are shown in Figure 6.5 at the M06-2x/6-31+G(d) level. For the ground state, two low energy conformers **6.8** and **6.9** were found with a 1.8 kcal/mol difference in energy. The reaction barrier for the conformation change was not calculated. Methyllithium addition to acetone has a low reaction barrier of 3.0 kcal/mol suggesting a very fast reaction in vacuum at this level of theory.

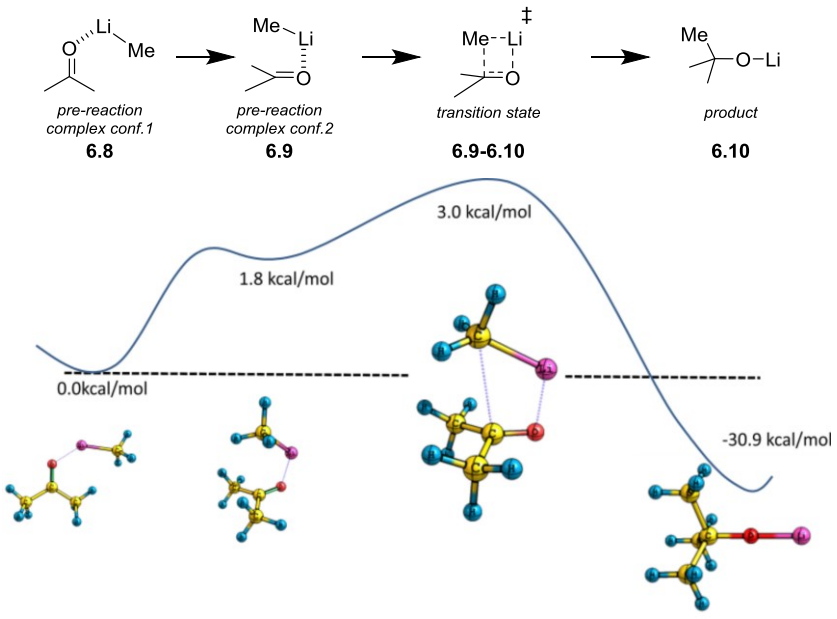

Figure 6.5. Reaction pathway for addition of methyllithium to acetone in vacuum at M06-2x/6-31+G(d).

As the description of electronic structure by the 6-31+G(d) basis set is limited, the study was extended to a more tempered basis set using the CCSD(T)/CBS method. The study sought to validate the performance of DFT for determining the transition state **6.9-6.10** and assess it against data in literature.[129] Calculations of potential electrostatic scan (PES) using M06-2x, MP2 and B3LYP, together with the recommended 6-311+G(2df,2dp) basis set, show significant discrepancies (Graph 6.1). The B3P86[76] method which was used previously on a similar systems[130] gave a flat surface and an early transition. The *ab initio* MP2 method predicted a higher energy barrier and a maximum close to that predicted by M06-2x method. To provide a final judgment, CCSD(T)/CBS energy calculations were performed on each of the principal geometries obtained. These give more accurate energies when calculated using DFT and MP2 geometries. They are represented by red triangles in Graph 6.1. The maximum point of energy from CCSD(T)/CBS was reproduced well by MP2 and M06-2x, though the energy value predicted was different. Thus, it shows the reliability of the MP2 and M06-2x methods in predicting transition state geometries for **6.9-6.10** and the failure of B3P86.

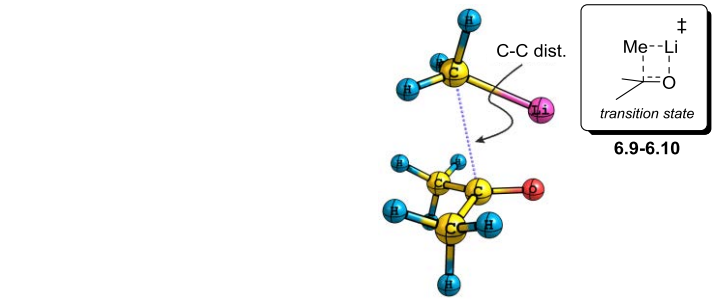

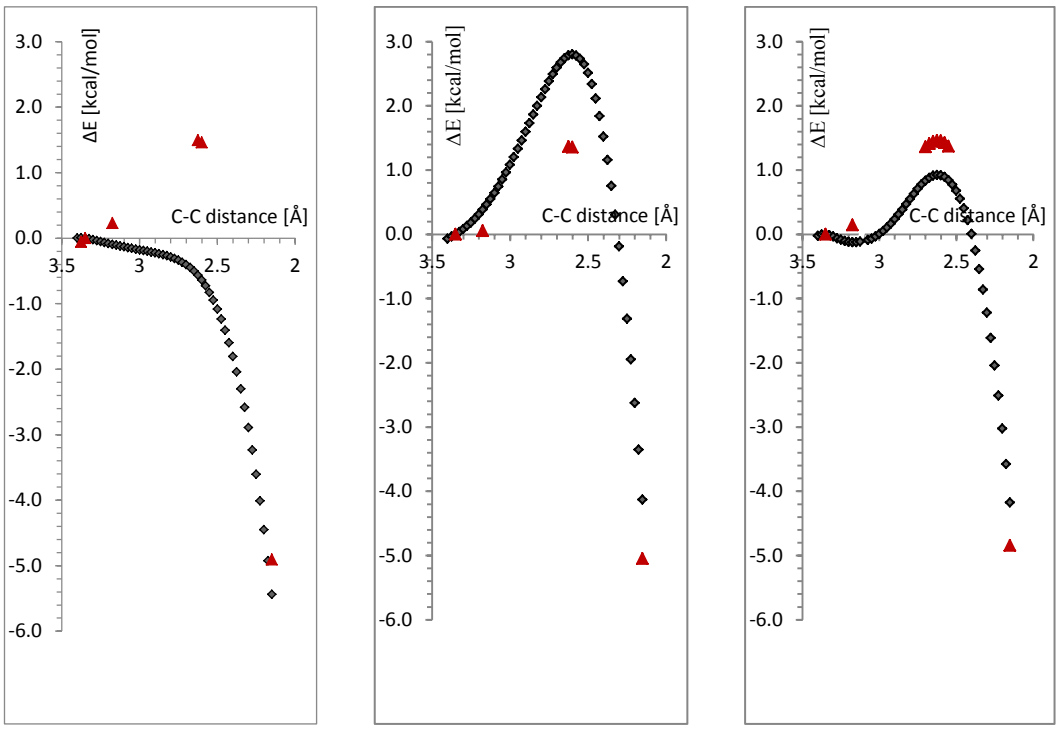

♦ B3P86/6-311+G(2df,2p) ♦ MP2/6-311+G(2df,2p) ♦ M06-2x/6-311+G(2df,2p)

Graph 6.1. Potential energy scan of the developing C-C bond close to the transition state region (3.4 Å to 2.15 Å) given by different methods. The red triangles (▲) represent single point energies by CCSD(T)/CBS extrapolation obtained by CCSD(T)/6-31G(d) and MP2 at cc-pVDZ and cc-pVTZ.

To further explore the reliability of DFT methods, a benchmark for various methods and basis sets was performed (Table 6.1 and Graph 6.2). With respect to basis set dependence, all methods showed shorter C-C distances at the point of transition state when the diffusion function was added. The M06-2x calculations predicted similar distances to those attained using B3LYP, whereas a longer distance was predicted using 6-31G and a shorter distance was predicted using 6-311G. B3P86 always predicted a distance higher than 2.9 Å, even with the large 6-311+G(2df,2p) basis set. M06-L and BLYP do not performed as badly as B3P86 but showed limited accuracy even when large basis sets were employed. These pure-DFT methods perform calculations an order of magnitude faster than the hybrid DFT methods when used in conjunction with resolution of identity (RI-DFT). This makes them attractive for very large systems and molecular dynamic applications. The CCSD(T)/CBS C-C distance, estimated by single point energies from a scan using M06-2x/6-311+G(2df,2p) geometry, was 2.605 Å and this was reproduced with M06-2x at 6-31+G(d,p) and B3LYP with the 6-31+G(d) basis set. MP2 at 6-31+G(d,p) gaves good transition state distances but this cames at a cost as the memory and CPU requirements were higher than those required by DFT making these computations impracticable for larger systems.

Table 6.1. Basis set and method dependence on C-C distance in [Å] of transition state **6.9-6.10**.

Basis\method	M06-2x	B3LYP	B3P86	M06-L	BLYP	MP2
6-31G(d)	2.630	2.618	3.403			
6-31+G(d)	2.619	2.606	3.368			
6-31+G(d,p)	2.605	2.594	2.912			2.599
6-311G(d,p)	2.622	2.630	3.326			
6-311+G(d,p)	2.621	2.632	3.351			
6-311+G(2df,2p)	2.619	2.621	3.376	2.487	2.677	

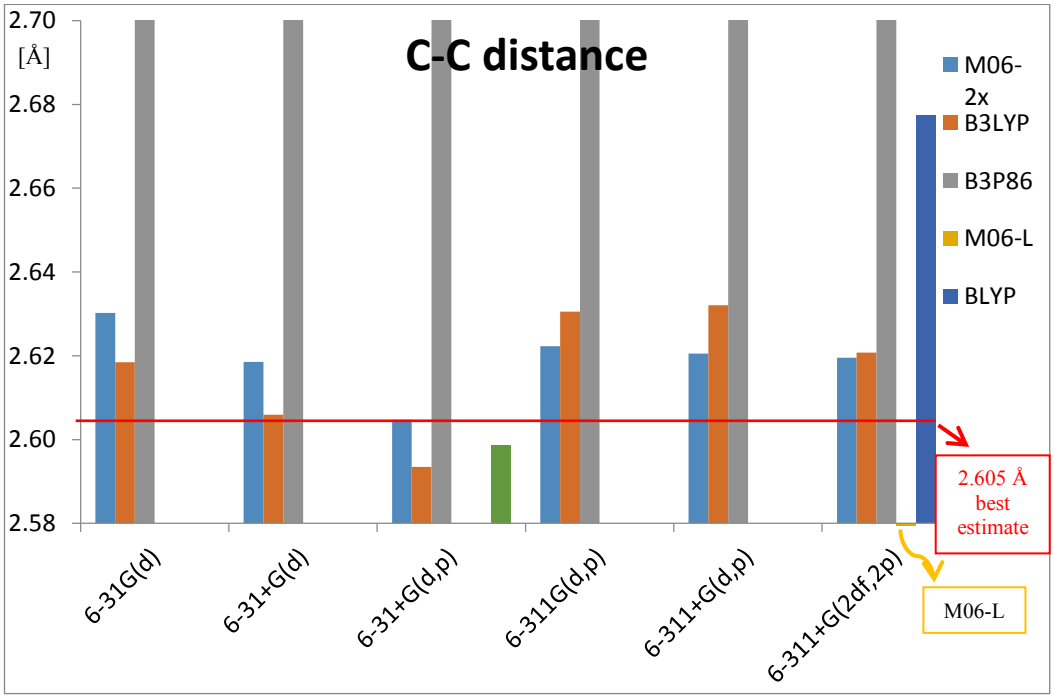

Graph 6.2. Graphical representation of Table 6.1. The red line shows the estimated C-C distance by CCSD(T)/CBS value extrapolation obtained by CCSD(T)/6-31G(d) and MP2 at cc-pVDZ and cc-pVTZ. B3P86 gives very long bond distances and M06-L gives very short bond distances so for clarity these values are not shown.

After extensive benchmarking of the transition state geometry, validation of the electronic energy was performed using *ab initio* and double hybrid DFT methods (Table 6.2). The most accurate methods in the table are CCSD(T) and are taken as reference. The coupled cluster with two point extrapolation and the explicit correlation coupled cluster (F12a-CCSD(T)) agree that the barrier height is 4.0 kcal/mol. The difference between these methods is less than 0.1 kcal/mol and is negligible for the purpose of this study. Each predicted reaction energies to be around -32 kcal/mol. The coupled cluster method without triple correction (CCSD) predicted a much higher energy of 5.3 kcal/mol. The Møller–Plesset (MP2) method extrapolated to the basis set limit underestimated the barrier value but is less than 0.4 kcal/mol from the best estimative. The double hybrid B2GP-PLYP method gave excellent agreement with the predicted value when using the cc-pVTZ basis set. No basis set dependency for that method was observed for cc-pVTZ, cc-pVQZ and Def2-QZVPP so no extrapolation to the complete basis set was needed.[131] However, addition of a dispersion correction[132] via empirical parameters underestimated the reaction barrier by more than 1 kcal/mol.

Table 6.2. Barrier heights for the reaction of acetone with methyllithium in [kcal/mol] obtained from *ab initio* and double hybrid DFT methods at M06-2x/6-31+G(d) geometry.

Method/Basis set	**pre-reaction complex (6.8)**	**transition state (6.9-6.10)**	**product (6.10)**
F12a-CCSD(T)/AVDZ	0	4.0	-32.6
CCSD(T)/CBS (AVTZ=>AVQZ)	0	4.0	-32.2
CCSD/AVTZ	0	5.3	-31.7
RI-MP2/CBS (AVTZ=>AVQZ)	0	3.7	-35.6
B2GP-PLYP/cc-pVTZ	0	4.0	-30.1
RI-B2GP-PLYP/cc-pVQZ	0	4.0	-29.8
RI-B2GP-PLYP/Def2-QZVPP	0	4.0	-30.1
RI-B2GP-PLYP-D/cc-pVQZ	0	2.8	-30.1

The accurate *ab initio* methods are attractive but, unlike DFT, are computationally too expensive to apply to larger systems. Despite the limitations, the energetic performance of various DFT methods towards the reaction of acetone and methyllithium was conducted (Table 6.3). Increasing the basis set from 6-31G(d) to 6-311+G(2df,2p) did not change the performance of these methods dramatically. M06-2x estimated the barrier to be in the range of 3.2-2.5 kcal/mol, around 1 kcal/mol lower than that given by *ab initio* calculations. B3LYP overestimated the barrier by less than 0.8 kcal/mol (against F12a-CCSD(T) as reference), with both functionals reaching their energy maximum at 6-31+G(d,p). Energy convergence of B3P86 was different, as it suffers from a bad geometry and has minimum of 2.9 kcal/mol at 6-31+G(d,p) basis set.

Table 6.3. Barrier heights for the reaction of acetone with methyllithium obtained by DFT methods. Energies from fully optimized geometries.

Method / **Basis Set**	**M062x**	**B3LYP**	**B3P86**	**M06-L**	**BLYP**	**BB1K**	**BMK**	**M06**	**HF**
6-31G(d)	3.0	4.5	3.4						
6-31+G(d)	3.0	4.6	3.4						
6-31+G(d,p)	3.2	4.8	2.9			4.1	4.0		
6-311G(d,p)	3.0	4.7	3.3						
6-311+G(d,p)	2.7	4.3	3.4				3.6	1.7	10.5
6-311+G(2df,2p)	2.5	4.2	3.4	0.6	2.7	3.6	3.4	1.6	

Energy different between reactant **6.8** and transition state **6.9-6.10** are in [kcal/mol].

Local DFT methods, like M06-L, also underestimated the energy barrier significantly due to bad geometry predictions. By contrast, HF dramatically overestimated the energy barrier. BB1K and BMK predicted energy barriers at 6-31+G(d,p) basis set were in excellent agreement with our reference value, however these functionals are not appropriate for systems where dispersion energy plays important role.

The impact of zero-point energies, Gibbs free energies and solvation energy corrections were also investigated (Table 6.4 and Figure 6.6) at the M06-2x/6-31+G(d) level. The addition of a ZPE correction for electronic energy increased the transition state energy slightly. The addition of a Gibbs free correction to the electronic energies at -78 ^{o}C further increased the energy barrier. It was observed that a smaller energy difference was predicted for separate reactants than for the pre-reaction complex, which is likely to be the result of entropy impact. The addition of solvation energy increased the energy barrier further and was more significant for separate reactants. All implicit tetrahydrofuran (THF) solvation models showed the same trend. However SMD gave higher energies than those attained using the IEF-PCM and CPCM models, which were similar.

Table 6.4. Solvation (in THF), free energy (ΔG at -78 ^{o}C) and zero point energy corrections to barrier heights for the reaction of acetone with methyllithium.

ΔE (M06-2x/6-31+G(d))	**ΔE**	**ΔE+ZPE**	**ΔG**	**ΔG +IEF-PCM**	**ΔG +CPCM**	**ΔG +SMD**
Acetone **6.12** and MeLi **6.11** in separation	22.1	20.8	14.4	0.5	0.1	7.5
pre-reaction complex **6.8** conf.1	0.0	0.0	0.0	0.0	0.0	0.0
transition state **6.9-6.10**	3.0	3.6	4.8	5.5	5.3	6.3
Product **6.10**	-30.9	-27.0	-25.8	-35.6	-35.9	-26.2

Energy different between reactant **6.8** and transition state **6.9-6.10** are in [kcal/mol].

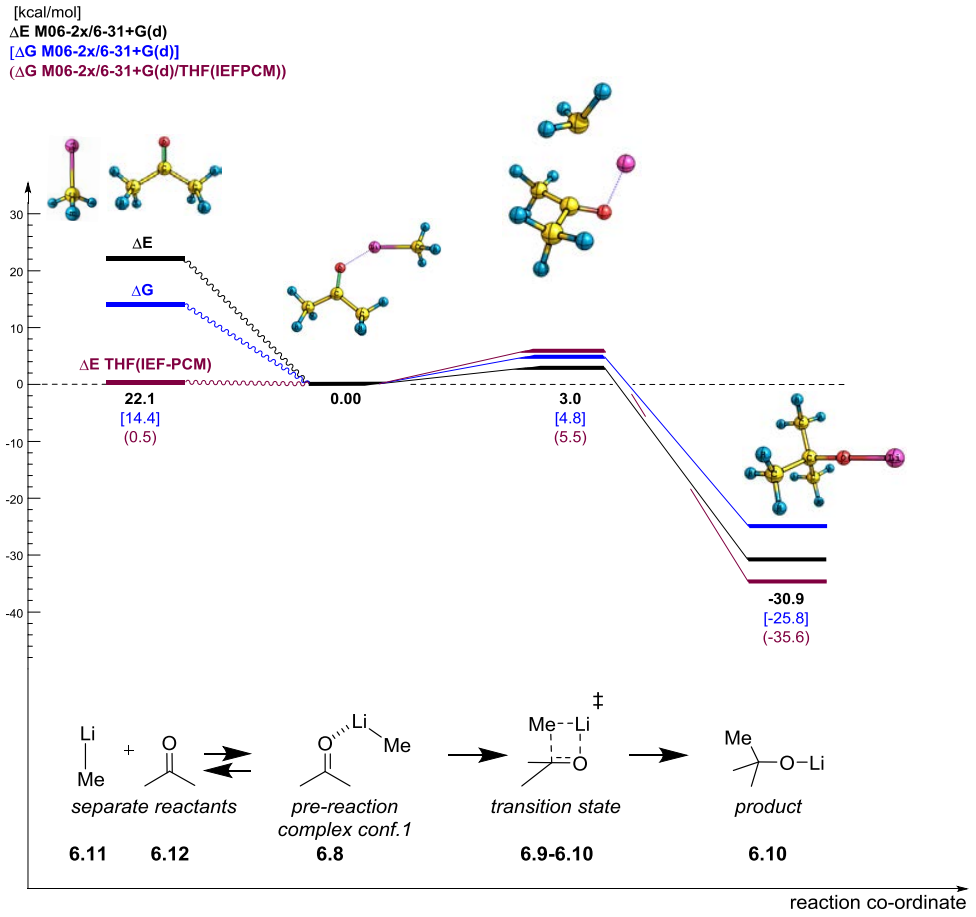

Figure 6.6. Solvation (in THF), Gibbs free energy (ΔG at -78 °C) and electronic energy for the reaction of acetone with methyllithium.

In conclusion, the M06-2x and B3LYP at 6-31+(d) or 6-31+(d,p) are appropriate for geometries and qualitative energies. However, the double hybrid B2GP-PBLYP method provided better quantitative energies for the reaction barriers. The impact of solvation energy and Gibbs free energy corrections were significant. The studies performed showed that Gibbs free energies at -78 °C from B2GP-PBLYP/cc-pVQZ//M06-2x/6-31+(d) with THF solvation energies from M06-2x/6-31+(d,p)/IEFPCM(THF) provided an appropriate qualitative picture of the reaction. M06-2x performed slightly worse than DH-DFT or CCSD(T) but was significantly faster.

6.3.2 Model Study: Methyllithium Dimer Addition to Acetone

COMMON SENSE IS NOT SO COMMON.
VOLTAIRE

The addition of methyllithium monomer to acetone in solvent is unlikely to occur as it is known that methyllithium exist in a dimeric form in tetrahydrofuran.[133a-c, 68, 133d, e] To satisfy those findings, the addition reaction was studied using explicitly solvated methyllithium dimer **6.13**, as the most representative model of experimental conditions (Figure 6.7). For these calculations, tetrahydrofuran was substituted for dimethyl ether as the latter has fewer conformations so was less costly in respect of computation time.[134]

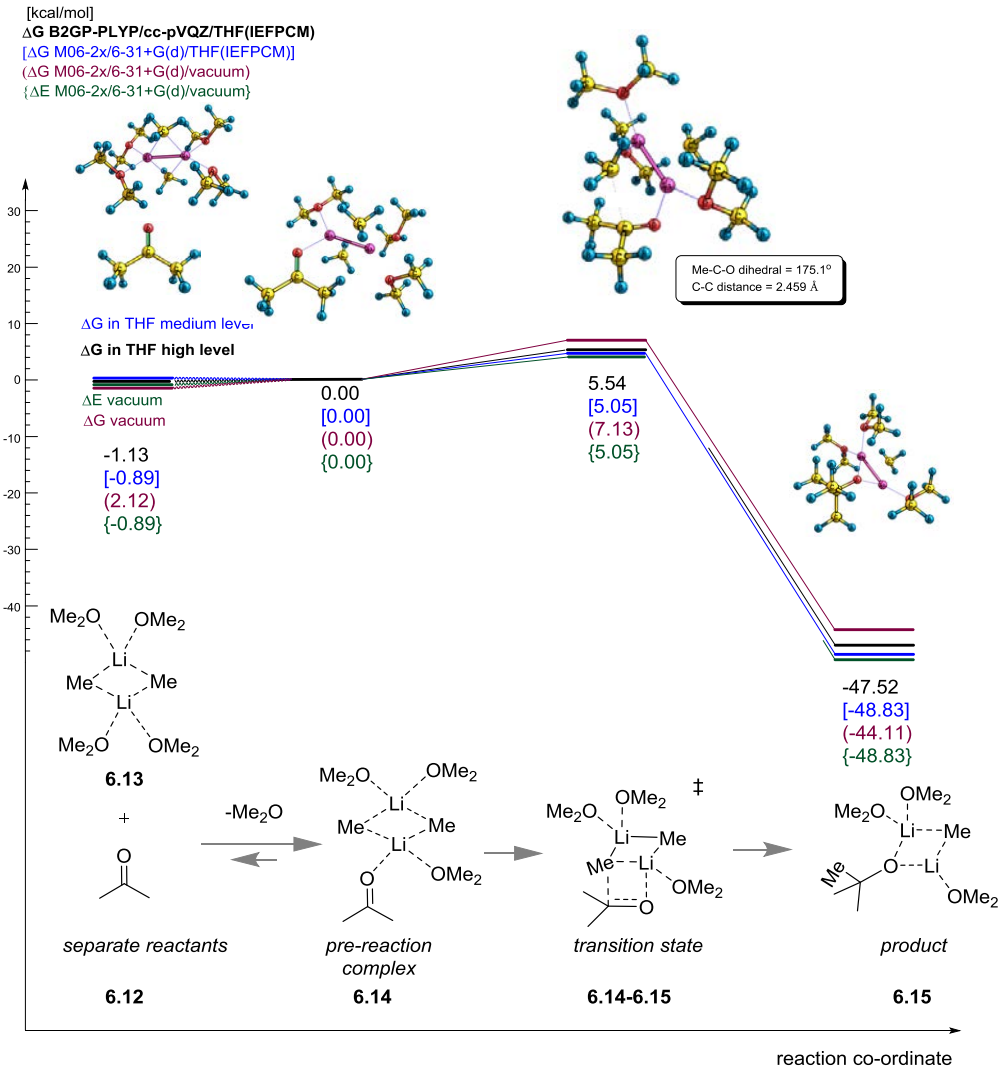

Figure 6.7. Energy graph for methyllithium dimer addition to acetone. All geometries at M06-2x/6-31+G(d). For clarity, a single bond has been drawn between the two lithium atoms.

Careful conformational analysis revealed 8 conformations for the transition state **6.14-6.15** due to the presence of solvent as ligands. The Gibbs free energy data at -78 ^{o}C on B2GP-PBLYP/cc-pVQZ//M06-2x/6-31+G(d) with implicit solvation IEF-PCM by THF showed that the reaction has a 5.5 kcal/mol barrier and is exergonic with -47.5 kcal/mol reaction energy. The formation of a pre-reaction complex by ether-acetone ligand **6.14** exchange was unfavourable by -1.13 kcal/mol when compared to separate reactants **6.12** and **6.13**. In comparison to the methyllithium-acetone system (Figure 6.6), the reaction barrier has a similar value but the geometry is very different. The reaction of the explicitly solvated methyllithium dimer with acetone has a shorter C-C distance and a different dihedral angle at the transition state. The M06-2x method reproduced the B2GP-PLYP energies to within 0.5 kcal/mol.

6.3.3 Model Study: Addition of Methyllithum Heterodimer to Acetone

CURIOUSER AND CURIOUSER
ALICE, IN WONDERLAND

The product of the previous reaction is mixed dimer **6.15** (Scheme 6.7) which can also react with acetone. It was reported in the literature that mixed dimers of this type are more stable than the corresponding homodimer. To provide some insight into the influence, nature and reactivity of the mixed dimer we next turned our attention to a computational study of its addition to acetone (Figure 6.8). The alkoxide moiety was simulated by methoxide to avoid conformational problems and reduced the computational cost. Analysis of Gibbs free energies at -78 ^{o}C showed that addition of a methoxy group (**6.17-6.18)** lowers the energy of MeLi addition to acetone, *viz.* **6.17-6.19**. However, due to the low barrier of the reverse reaction, methoxy addition is likely to be highly reversible. Formation of the methyl addition product **6.18** is highly exergonic and can be considered irreversible. In comparison with the homodimer addition (Figure 6.7), **6.14** to **6.14-6.15**, the energy barrier is slightly higher. Also, for that system the M06-2x method reproduced the value attained using B2GP-PLYP and gave energies within 0.4 kcal/mol of each other.

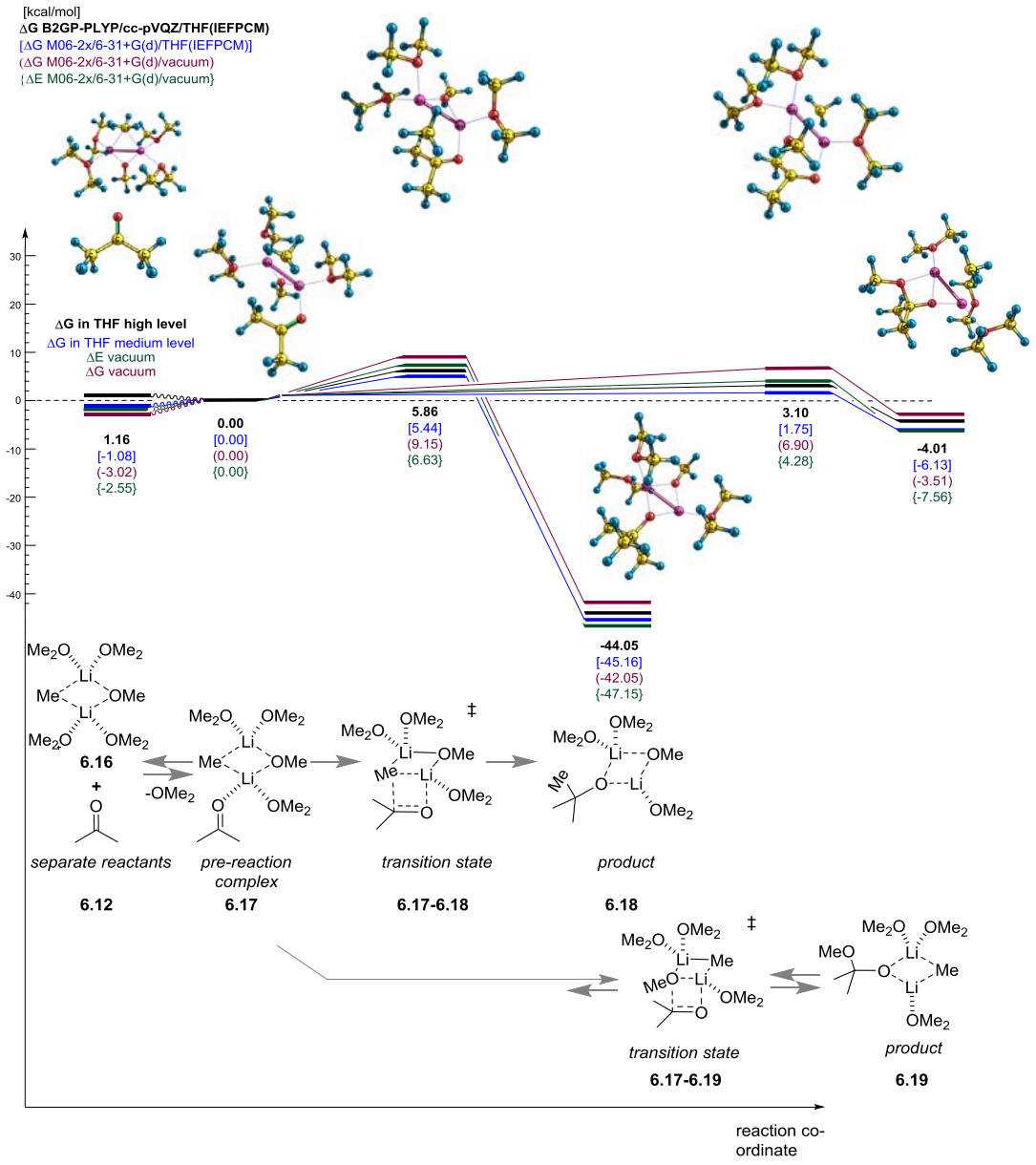

Figure 6.8. Energy graph for addition of methyllithium ─ methoxylithum heterodimer to acetone. All geometries at M06-2x/6-31+G(d). For clarity, a single bond has been drawn between the two lithium atoms.

The C-C distance for the forming bond in the transition state was shorter for the mixed dimer than for the homodimer, suggesting lower reactivity for the heterodimer. Also, it was observed that the transition states for heterodimer addition had a significant twist compared to the geometry for MeLi addition (Figure 6.6), **6.17-6.18** and **6.17-6.19**, and that the dihedral angles associated with its approach were very different (Figure 6.9).

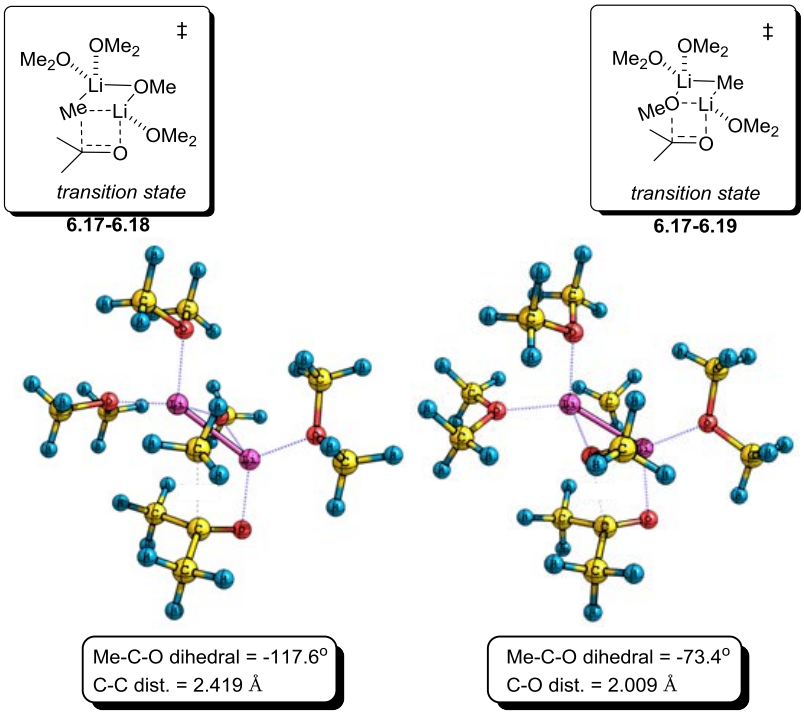

Figure 6.9. Geometries of the lowest transition states found for addition of the methyllithium─methoxylithium heterodimer to acetone. All geometries at M06-2x/6-31+G(d). For clarity, a single bond has been drawn between the two lithium atoms.

To provide further understanding of the nature of mixed dimers, our reactivity calculations were extended to the MeLi•LiCl complex (Scheme 6.2, Figure 6.10). This mixed dimer was reported to be more stable in THF solution when compared with methyllithium and lithium chloride homodimers. Indeed, experimental findings involving NMR analysis, support this hypothesis.[135]

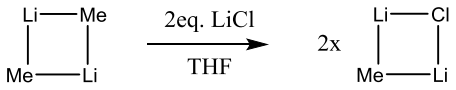

Scheme 6.2. Formation of the MeLi•LiCl from homodimer and LiCl.

As expected from experiments, the addition of lithium chloride across acetone was not observable under these simulation conditions (Figure 6.10) as it was not possible to find a transition state for **6.21-6.23** and product **6.23** at M06-2x/6-31+G(d) level.

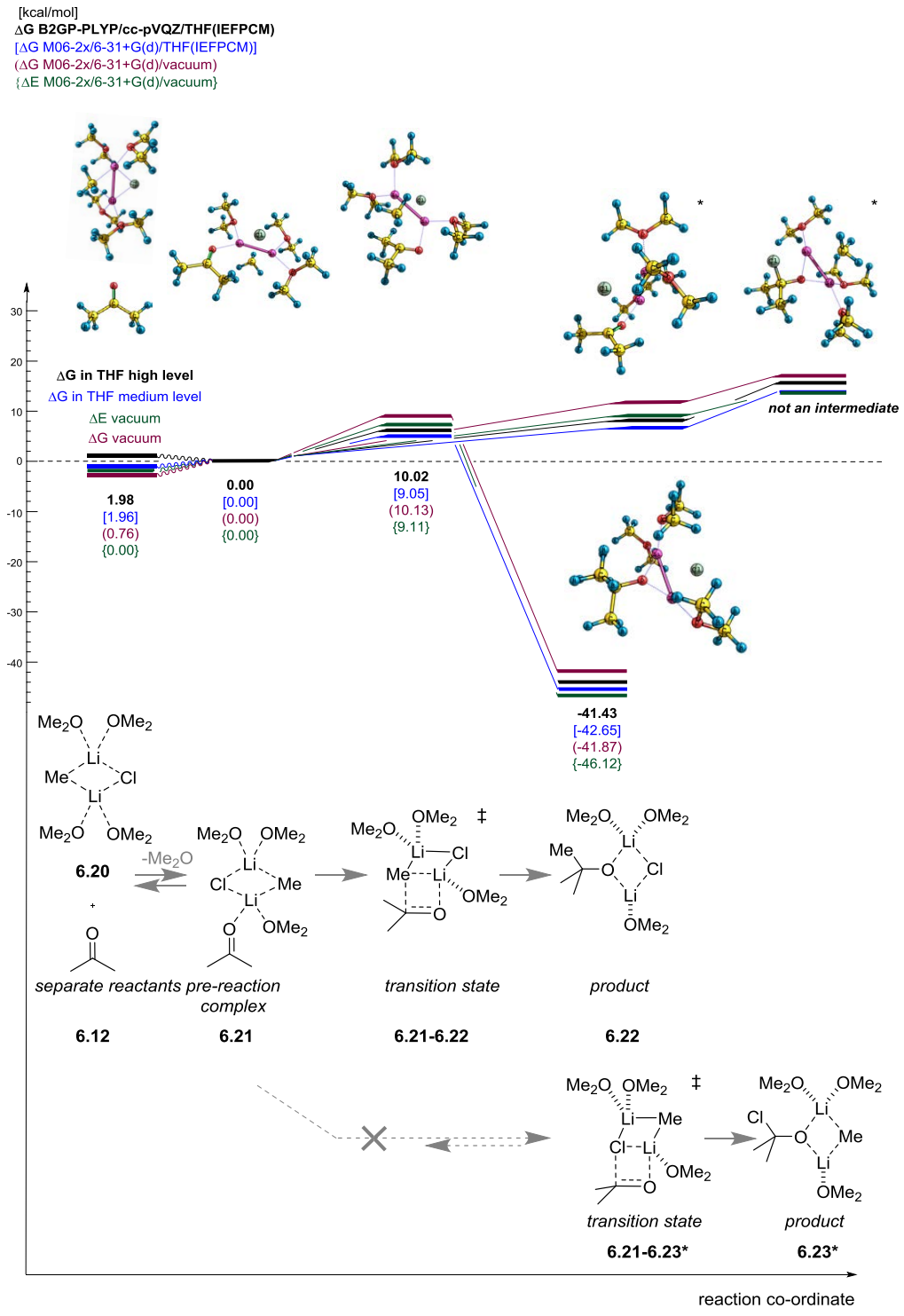

Figure 6.10. Energy graph for the addition of methyllithium─lithum chloride heterodimer to acetone. All geometries at M06-2x/6-31+G(d). For clarity, a single bond has been drawn between the two lithium atoms. (* indicate 'best guess' geometries)

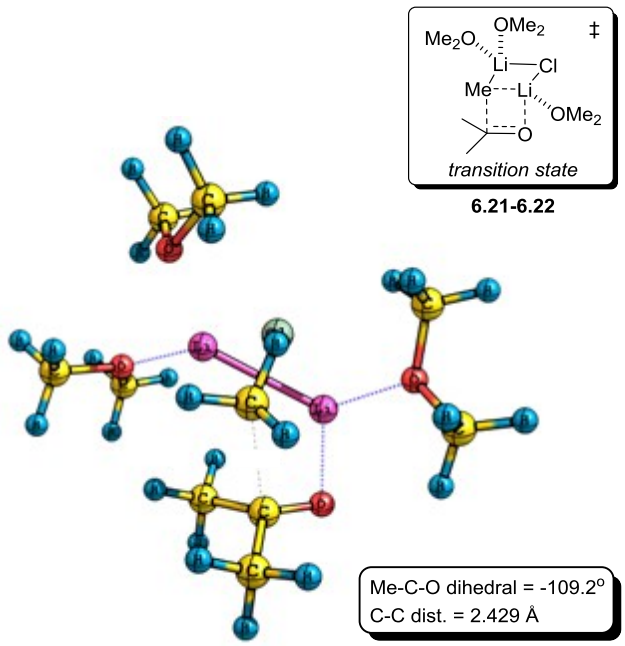

Figure 6.11. Geometry of the lowest transition states found for addition of methyllithium ─ lithium chloride heterodimer to acetone. All geometries at M06-2x/6-31+G(d). For clarity, a single bond has been drawn between the two lithium atoms.

Calculations showed that methyllithium addition to acetone **6.21-6.22** had an energy requirement of 10.0 kcal/mol, which was much higher than that observed in the previous examples. The M06-2x method reproduced the B2GP-PLYP energies within 1.0 kcal/mol. Also, the transition state geometry had a C-C distance of 2.43 Å for the developing bond, which was longer than that for the MeLi•MeOLi complex (**6.17-6.18**, Figure 6.9). It also had a narrower dihedral angle of 109.2° (Figure 6.8).

As calculations of the transition states with organolithium dimers were time consuming, hybrid ONIOM(QM/QM)[136] and semi-empirical methods were also benchmarked as they are much faster and can be applied to very large systems. The semi-empirical PM6 method predicted a Gibbs free energy barrier of 6.27 kcal/mol, which was only 0.73 kcal/mol higher than the value obtained from B2GP-PLYP (Figure 6.12).

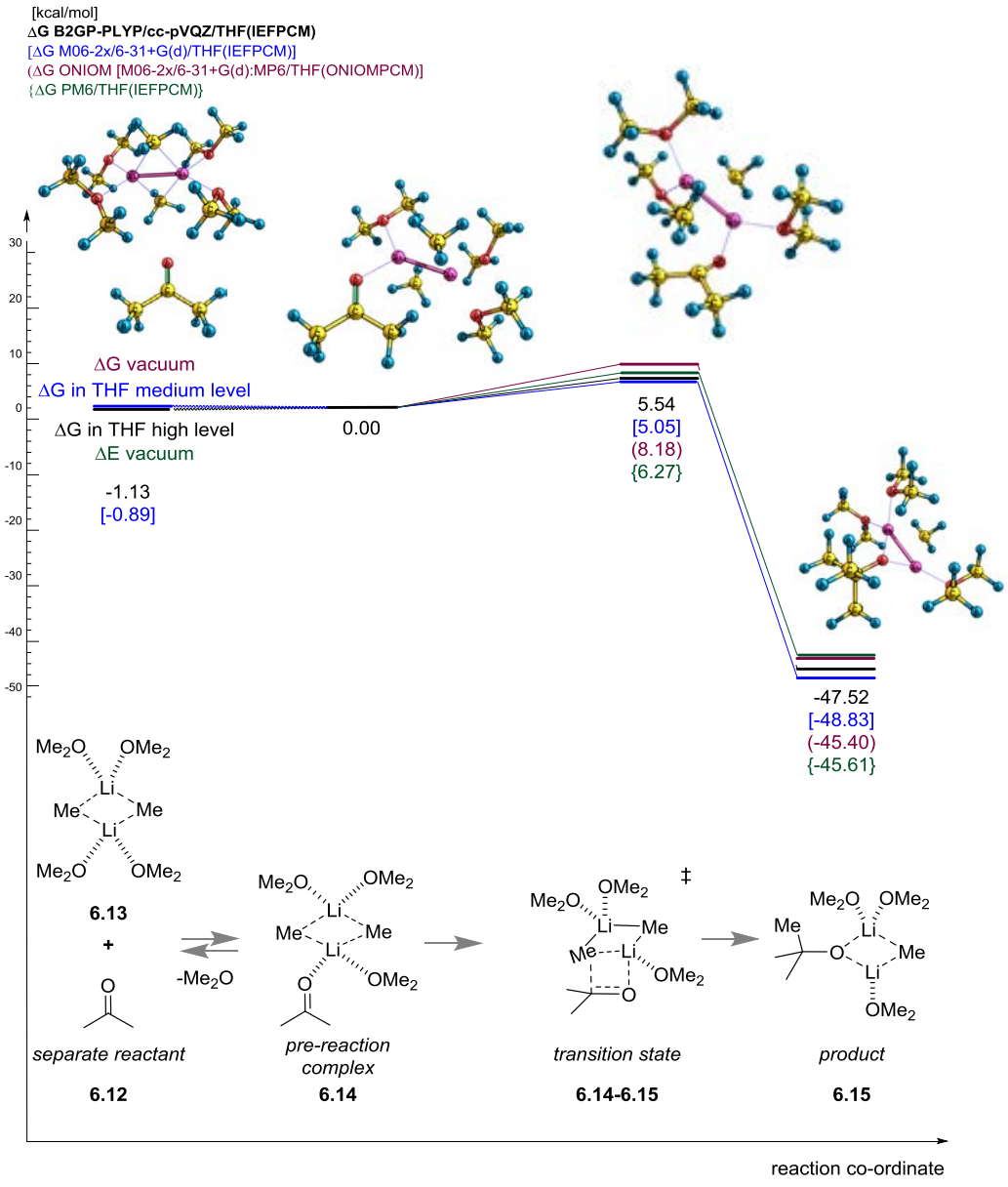

Figure 6.12. Energy graph for methyllithium dimer addition to acetone given by different models. For clarity, a single bond has been drawn between the two lithium atoms.

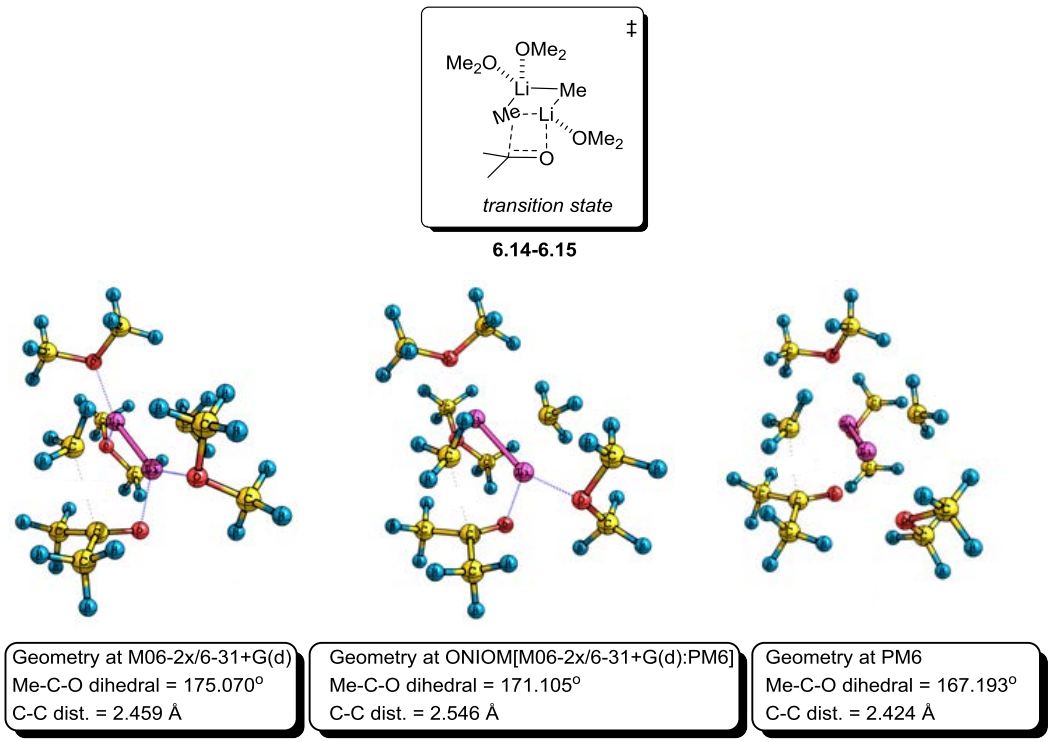

Figure 6.13. Geometry of the transition state for methyllithium dimer addition to acetone given by different models. For clarity, a single bond has been drawn between the two lithium atoms.

However, the predicted position of the lithium atoms in transition state **6.14-6.15** given by each of these methods were very different from those given by the M06-2x method (Figure 6.13). Regarding the ONIOM study, the methyl groups of dimethyl ether were placed in a lower method layer (treated by fast semi empirical PM6 method) and rest of the atoms were placed in a high method layer (treated by the more accurate M06-2x/6-31+G(d) method). This hybrid ONIOM(M06-2x:PM6) gave a Gibbs free energy barrier of 8.18 kcal/mol which is overestimated by 3.13 kcal/mol when compared with M06-2x. However, the geometry of transition state looked similar to that obtained by M06-2x, as shown in Figure 6.13.

6.3.4 Conclusion

I FIND PURER PHILOSOPHY IN A POEM THAN IN A CONCLUSION OF GEOMETRY, A CHEMICAL ANALYSIS, OR A PHYSICAL LAW.
WILFRED OWEN

Calculations in this model study, involving monomeric and dimeric methyllithium addition to acetone, were investigated. We found that the geometry of the transition states was predicted well with B3LYP/6-31+G(d) and M06-2x/6-31+G(d,p) for monomeric methyllithium addition. However, B3LYP overestimates the reaction barrier by 0.6 kcal/mol and M06-2x underestimates it by 0.8 kcal/mol compared to results obtained using *ab initio* methods. The best estimate of the energy barrier came using the coupled-cluster method and this was reproduced with BB1K, BMK and B2GP-PLYP/cc-pVTZ. We found that dispersion energy plays a significant role on the explicitly solvated dimeric methyllithium complex, so the B2GP-PLYP and M06-2x method were preferred. Inclusion of corrections for Gibbs free energy and solvent effects increase the energy barrier by ~2.5 kcal/mol and are important. The explicitly solvated methyllithium dimer is the most realistic model studied. The addition of methyllithium homodimers to acetone has a different geometry to that predicted for monomer addition. Mixed complexes of methyllithium with lithium methoxide, and with lithium chloride, have a higher energy barrier than that given by the methyllithium homodimer, suggesting that these would be more selective when competitive paths are possible. Our calculations also suggested that large systems could be simulated by an ONIOM approach with M06-2x and PM6 layers, though it is likely to over-estimate energy barriers so further validation would seem appropriate.

6.4 Addition of Methylithium Monomer, Dimer and Heterodimer to Unsymmetrical Cyclobutenediones.

THE WORLD IS NOT A HAMBURGER - YOU CAN'T HAVE IT YOUR WAY.
UNKNOWN AUTHOR

Our calculations on the systems of primary interest began with an assessment of the addition of monomeric methyllithium to the unsymmetrical cyclobutenedione **6.25** (Figure 6.14). The DFT methods B3LYP, M06-2x and BMK predicted a barrierless process. However, by applying one of the recommended geometry optimisation methods, MP2/6-31+G(d,p),[80d] four different transition states for *C*-1 and *C*-2 addition emerged.

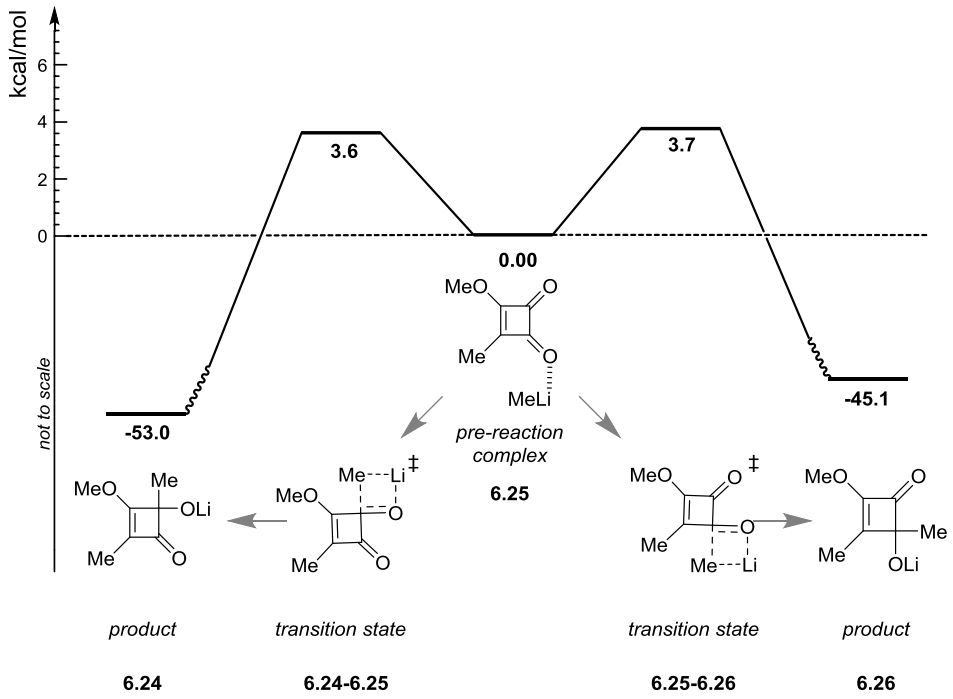

Figure 6.14. Energy graph for methyllithium additions to 3-methoxy-4-methylcyclobut-3-ene-1,2-dione **6.25** at MP2/6-31+G(d,p) in vacuum.

The transition state for *C*-1 addition **6.24-6.25** has a longer C-C distance (2.48 Å) for the developing bond compared to that for *C*-2 addition **6.25-6.26** (2.76 Å) (Figure 6.15). The *C*-1 adduct **6.24** was also found to be more thermodynamically stable than *C*-2 adduct **6.26**.

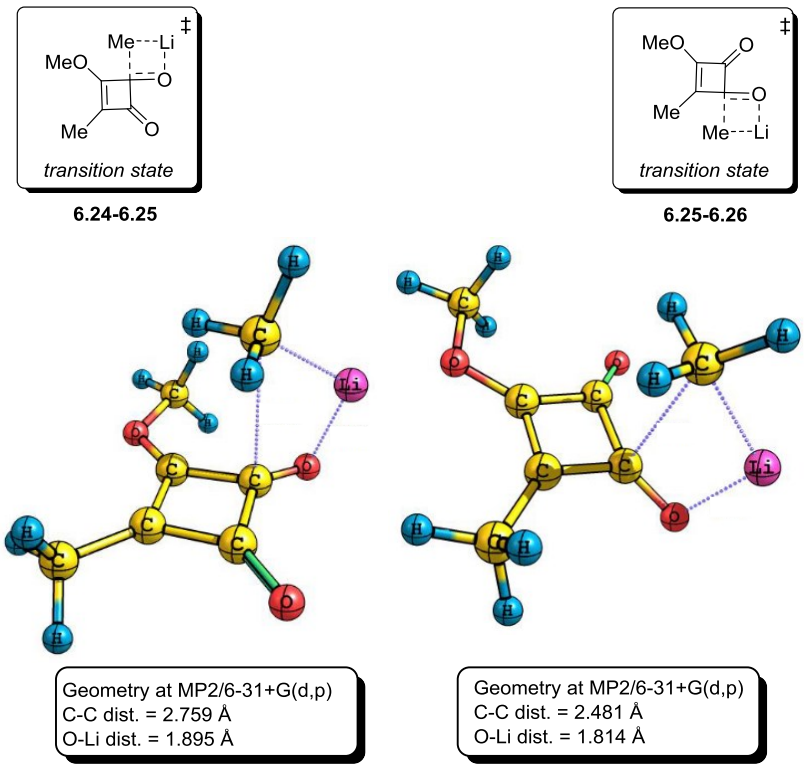

Figure 6.15. Geometry of the lowest transition states for methyllithium addition to 3-methoxy-4-methylcyclobut-3-ene-1,2-dione at MP2/6-31+G(d,p) in vacuum.

The difference in energy for these competitive pathways is just 0.1 kcal/mol. Though the method correctly predicted *C*-1 addition (Figure 6.14), the small energy difference does not reflect the near exclusive addition of MeLi to the *C*-1 carbon of cyclobutenedione **6.25** observed by experiment. Consequently, it seemed sensible to performed further calculations on the explicitly solvated methyllithium dimer **6.28** (Figure 6.16).

For each addition, 16 low energy conformations for the transition states were calculated giving a total of 32 transition state conformers. Despite the large conformational energy window for *C*-1 addition **6.27-6.28** (1.3 – 6.8 kcal/mol) and *C*-2 addition **6.28-6.29** (3.7 – 7.8 kcal/mol), calculations on all of the conformations was required to guarantee the correctness of the predicted low energy pathway. The transition state for *C*-1 addition has a longer C-C distance (2.547 Å) than for *C*-2 addition (2.505 Å) by 0.042 Å in the lowest S-*trans* conformations (Figure 6.17). The difference in energy for both competitive pathways is 2.4 kcal/mol, predicting correctly the exclusive *C*-1 addition observed by experiment.

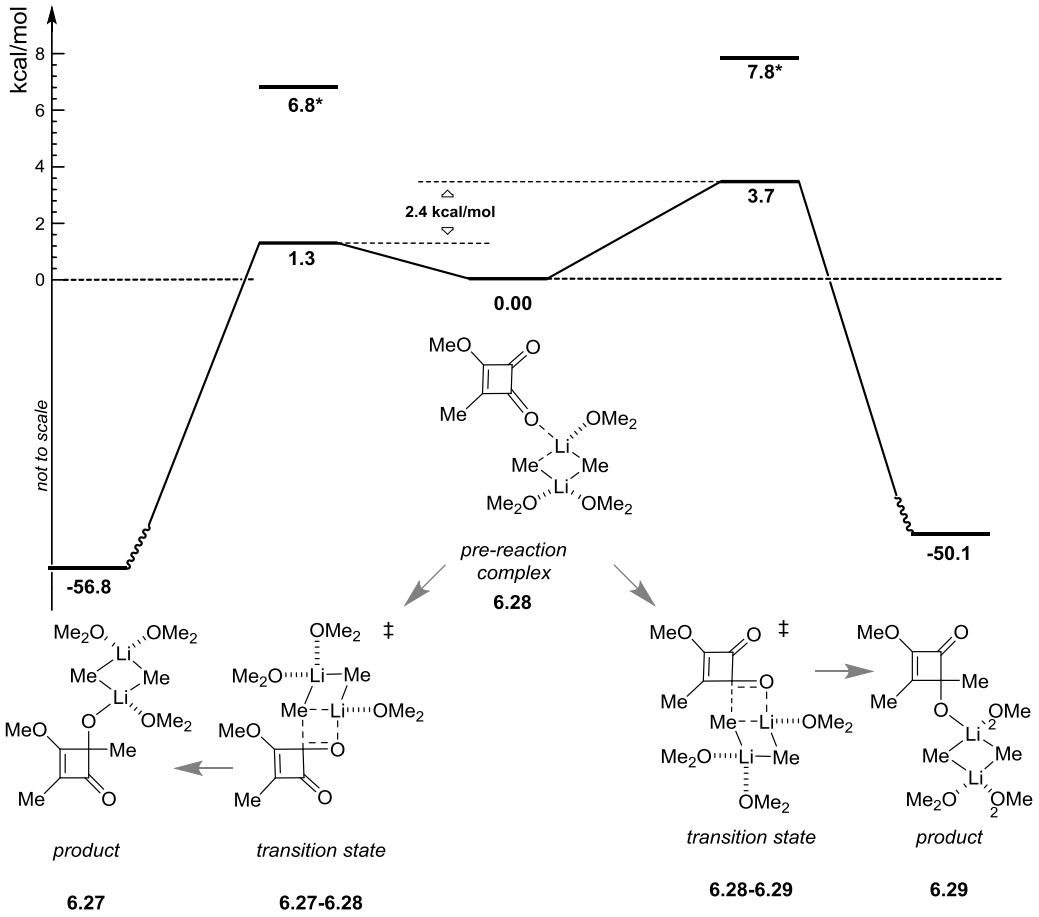

Figure 6.16. Energy graph for the addition of methyllithium homodimer-dimethyl ether complex to 3-methoxy-4-methylcyclobut-3-ene-1,2-dione at M06-2x/6-31+G(d,p) in vacuum. *The highest energy conformer found.

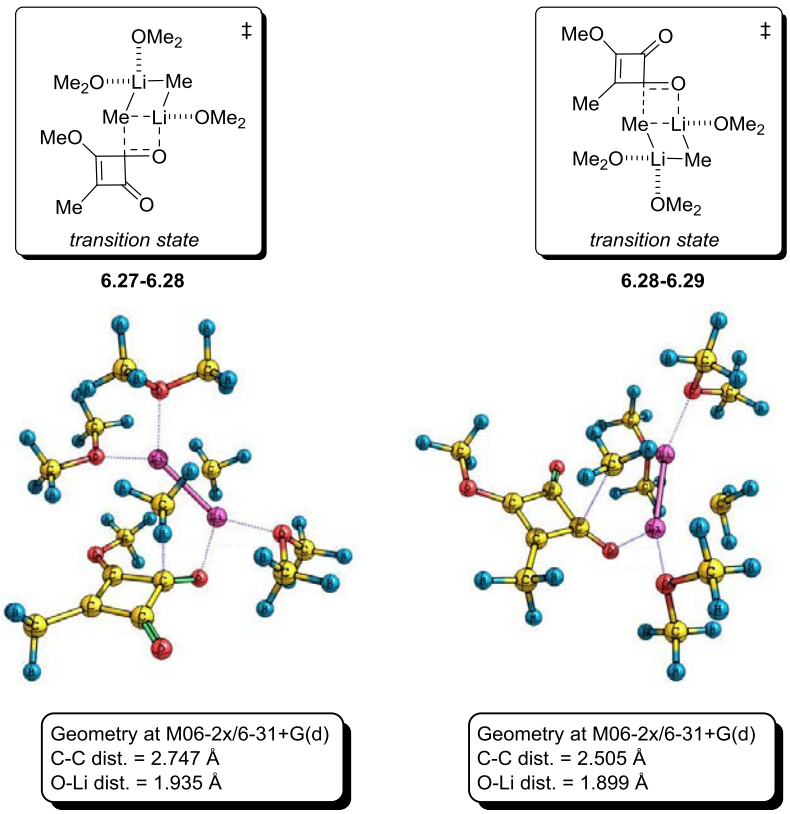

Figure 6.17. Geometry of the lowest energy transition states found for the addition of methyllithium homodimer - dimethyl ether complex to 3-methoxy-4-methylcyclobut-3-ene-1,2-dione at M06-2x/6-31+G(d,p) in vacuum. For clarity, a single bond has been drawn between the two lithium atoms.

Calculations on the related system 3-(*tert*-butoxy)-4-methylcyclobut-3-ene-1,2-dione (Figure 6.18) showed the same trend for selectivity as that described for 3-methoxy-4-methylcyclobut-3-ene-1,2-dione. However, a more pronounced steric clash between the attacking dimer and the *tert*-butoxy group at *C*-3 transition state **6.30-6.31** was evidenced. This was most pronounced in the transition state for *C*-1 addition, which had a longer C-C distance (2.655 Å) for the developing bond than for *C*-2 addition (2.501 Å) in the lowest energy S-*trans* conformations (Figure 6.19). The difference in energy for these competitive pathways was found to be 1.1 kcal/mol, predicting the favourability of *C*-1 addition observed under experimental conditions. Also, this system has a large conformational energy window for both *C*-1 addition (3.8 – 10.1 kcal/mol) and *C*-2 addition (4.9 – 12.1 kcal/mol) necessitating calculation of all conformations to guarantee the correctness of the pathway. Interestingly, the lowest energy conformation for the *C*-1 adduct transition state was

found to have a different conformations to that of the methoxy analogue **6.25** due to steric clash.

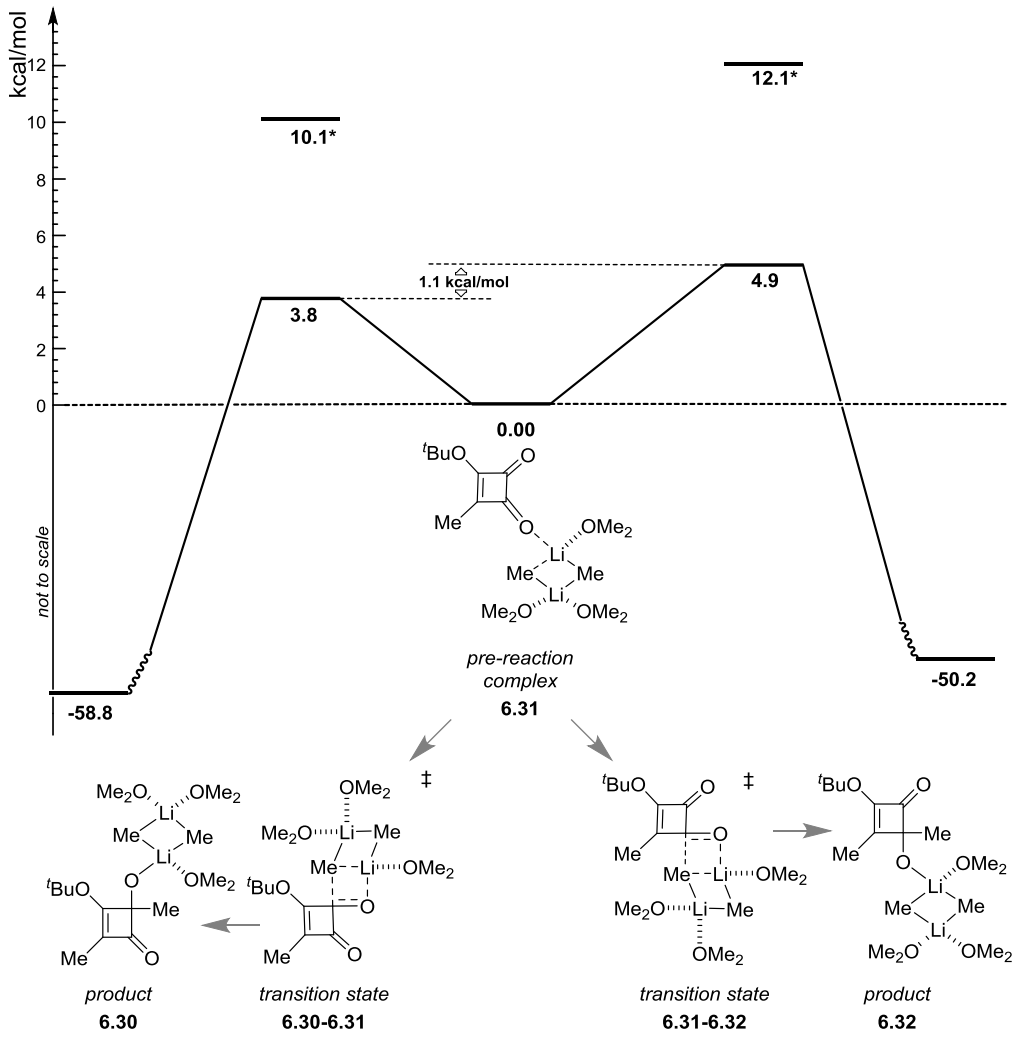

Figure 6.18. Energy graph for addition of methyllithium homodimer - dimethyl ether complex to 3-(*tert*-butoxy)-4-methylcyclobut-3-ene-1,2-dione **6.31** at M06-2x/6-31+G(d,p). *The highest energy conformer found.

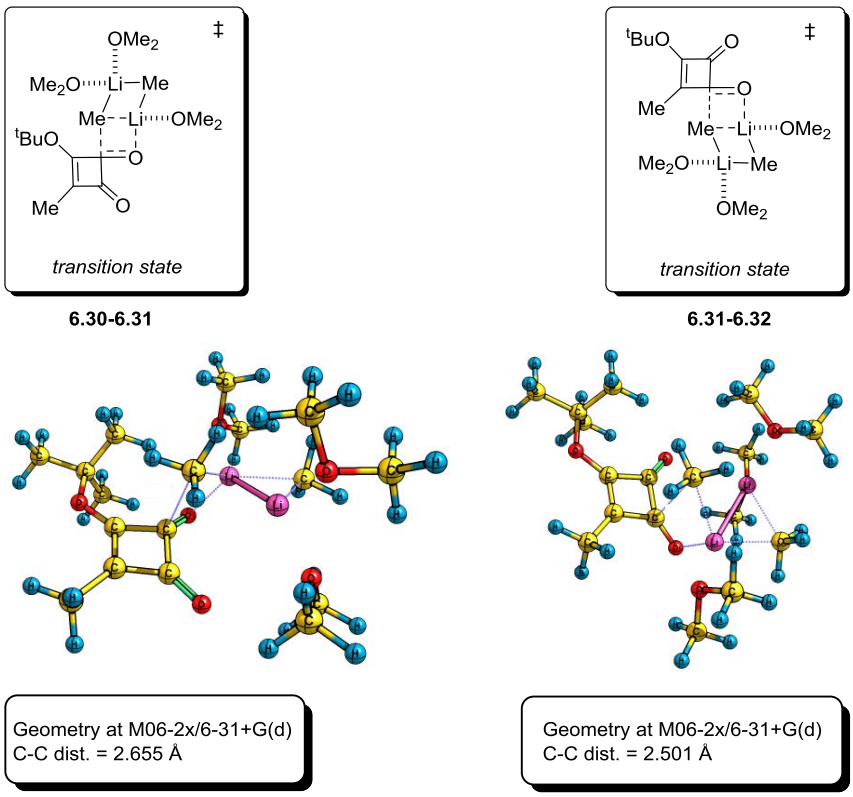

Figure 6.19. Geometry of the lowest energy transition states found for methyllithium homodimer dimethyl ether complex additions to 3-(*tert*-butoxy)-4-methylcyclobut-3-ene-1,2-dione at M06-2x/6-31+G(d,p). For clarity, a single bond has been drawn between the two lithium atoms.

Comparing the two competitive pathways with those given in the previous example, the energy difference is smaller due the steric clash. Thus, it is expected that for cyclobutenediones with large substituents at *C*-3, that addition of organolithium dimers might overcome the electronic preference for *C*-1 addition if steric demand is particularly high. This is observe experimentally in the addition of phenyllithium to **6.31**, which gives ~1:1 selectivity for the *C*-1 and *C*-2 addition products.[7]

At the beginning of a reaction between an organolithium reagent and a carbonyl group, the reaction is likely to involve the homodimer. However, as the reaction advances the more stable heterodimer with the product alkoxide is likely to dominate. To assess the impact of this heterodimer addition on selectivity and reactivity, molecular modelling of the addition of MeLi•MeOLi to **6.34** was also conducted. Lithium methoxide was used as a model alkoxide to avoid conformation problems. The difference in energy for the competitive *C*-1 and *C*-2 organolithium addition pathways for **6.34** was founded to be 3.3 kcal/mol (Figure 6.20), correctly predicting the exclusive *C*-1 addition observed under experimental conditions as this

this value is much higher than that given in the previous examples. Again, a large conformational energy window for *C*-1 (1.8 – 9.47 kcal/mol) and *C*-2 addition (5.15 – 10.15 kcal/mol) was observed.

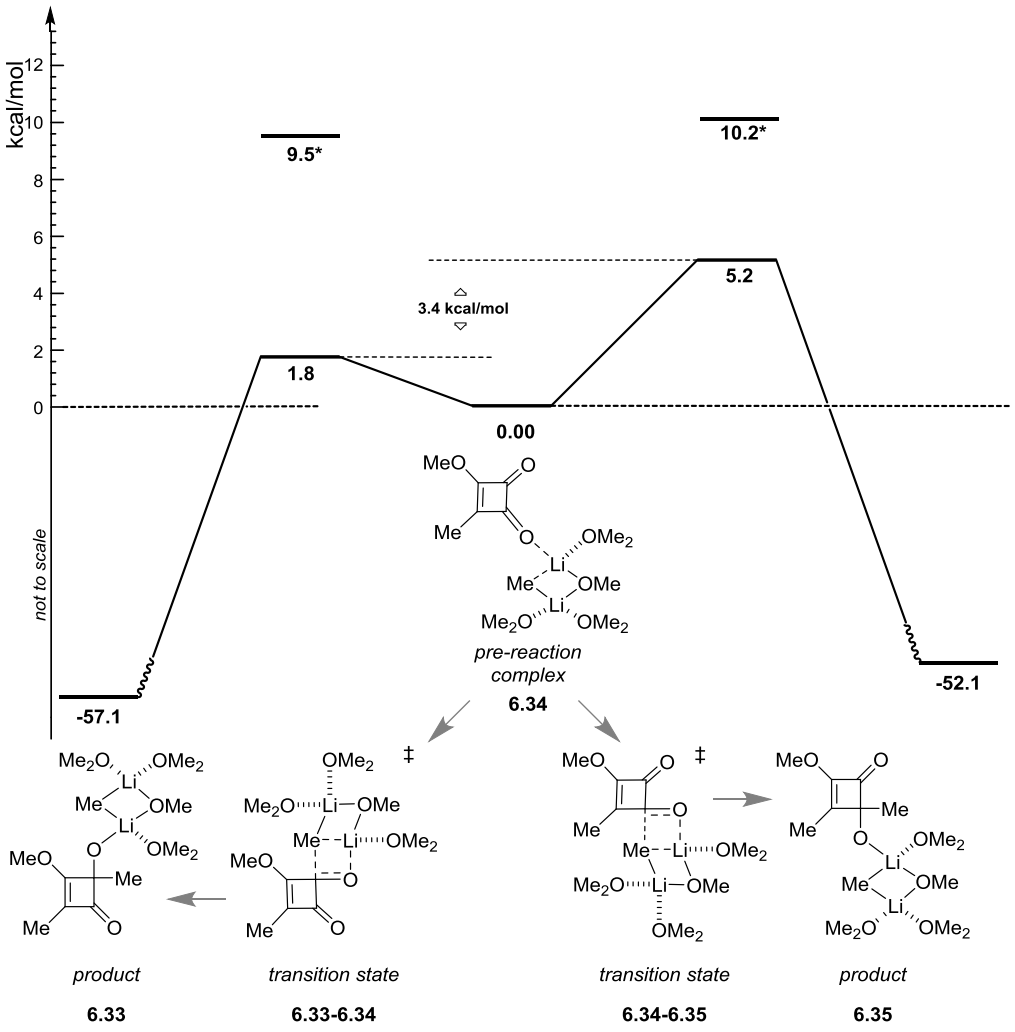

Figure 6.20. Energy graph for addition of methyllithium – methoxylithium heterodimer – dimethyl ether complex to 3-(methoxy)-4-methylcyclobut-3-ene-1,2-dione **6.34** at M06-2x/6-31+G(d,p). *The highest energy conformer found.

6.4.1 Conclusions

IF YOU DON'T WANT ANYONE TO KNOW, DON'T DO IT.
CHINESE PROVERB

Modelling of the addition of methyllithium to unsymmetrical cyclobutenediones was conducted. All addition reactions are driven by kinetics and are in agreement with performed experiments. The selectivity of *C*-1 vs. *C*-2 addition for both reactions was predicted correctly with both homodimer as the attacking organometallic species and MeLi monomer. However, neither appears to be truly representative. Rather, it seems that the addition of MeLi•MeOLi complex is more representative, certainly in the late phase of the reaction. Importantly, the trends observed with the acetone – methyllithium dimer system were mirrored by those observed with the cyclobutenediones studied.

6.5 Organoytterbium Additions to Cyclobutenediones

THE GREATER DAMAGE FOR MOST OF US IS NOT THAT OUR AIM IS TOO HIGH AND WE MISS IT, BUT THAT IT IS TOO LOW AND WE REACH IT.
MICHELANGELO

6.5.1 Model System for Organoytterbium

The addition of organoytterbium reagents to cyclobutenediones can show a different selectivity to that observed with organolithium reagents. In the presence of ytterbium triflate **6.36**, an organolithium reagent **6.37** can form the corresponding ate complex **6.38**. In turn this could release lithium triflate to form a neutral species **6.39** (Scheme 6.3).

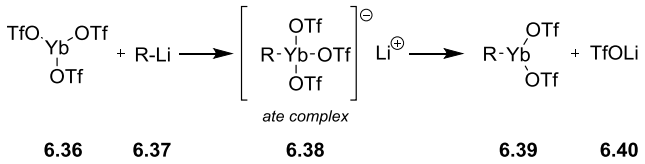

Scheme 6.3. Formation of organoytterbium species from ytterbium triflate **6.36** and an organolithium **6.37**.

In order to understand the different selectivities observed in the addition of organoytterbium and organolithium reagents to cyclobutenediones, a molecular modelling investigation was conducted. Calculations with ytterbium Yb^{+3} were modelled with a large core Stuttgart–Dresden pseudo potential, MWB59 ECP, which includes the 4f electrons in the core, in combination with their adapted basis set.[137] In this approach the 59 core electrons are replaced and the remaining 8 electrons are treated explicitly as valence electrons with the corresponding MWB59 basis set. As the contribution of the 4f orbitals to chemical bonding becomes negligible towards the end of the lanthanide row[137b] the incorporation of these f orbitals in the pseudo potential provides acceptable results in respect of geometry.[138] However, it has been pointed out that the nonparticipation of 4f electrons in chemical bonding should be considered in any study of chemical reactivity.[139] The application of this MWB59 pseudo potential has been found to be efficient and robust in SCF and geometry convergence. As the unpaired electron is treated by pseudopotential, the calculations on radical Yb^{3+} complexes benefit from a restricted rather than an

unrestricted formalism, providing efficient calculations. In this way it is possible to screen the large number of conformers and transition states required for this project.

To test the performance of the method a benchmark was performed on a model system, where the triflate was substituted with fluorine (Figure 6.21) and the lithium atom was omitted.

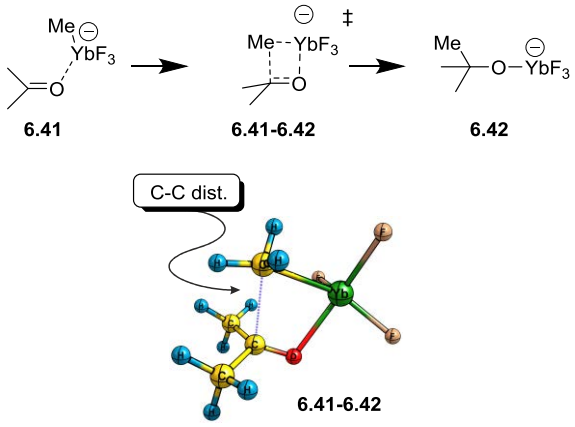

Figure 6.21. Model system for reaction of an organoytterbium ate complex with acetone.

The geometry of addition of an anionic organoytterbium fluoride to acetone was modelled by DFT and *ab initio* methods (Table 6.5). Due to the anionic character of the organometallic species, a slow basis set convergence of geometry was observed compared with our study of the methyllithium–acetone model system (Table 6.1). The most sophisticated and CPU time consuming models were B2PLYP and MP2 and those were taken as the reference for the geometry validation of the transition state. Both methods predicted a C-C distance for the developing bond in the transition state of around 2.494 - 2.516 Å. HF predicted the shortest distance (2.420 Å) and BLYP (2.588 Å) the longest distance (Table 6.5).

Table 6.5. Method and basis set dependencies on C-C distance in transition state **6.41-6.42.**

METHOD/Basis set	dist. C-C
HF/6-31G(d)	2.420
BLYP/6-311+G(2df,2p)	2.588
M06-L/6-311+G(2df,2p)	2.468
B3P86/6-311+G(2df,2p)	2.536
B3LYP/6-31G(d)	2.548
B3LYP/6-31+G(d,p)	2.524
B3LYP/6-311+G(2df,2p)	2.514
M062x/6-31G(d)	2.512
M062x/6-31+G(d,p)	2.470
M062x/6-311+G(2df,2p)	2.457
MP2/6-31+G(d,p)	2.494
B2PLYP/6-31+G(d,p)	2.516

* the MWB59 basis set was used for Yb atom.

When the basis set was increased from 6-31G(d) to 6-311+G(2df,2p) a shortening of the C-C distance from 2.548 Å to 2.514 Å for the B3LYP method was noted. The same trend was observed with M062x, where the distance decreased from 2.512 Å to 2.457 Å. The predicted C-C distances for M06-L and M062x were in close agreement (within 0.011 Å). B3P86 predicted a C-C distance of 2.536 Å and did not show any of the erroneous behaviour observed in the methyllithium–acetone model. It is difficult to draw any definitive conclusions about the C-C distance from these calculations as all used the same pseudo potential basis set for ytterbium. Also, all of the methods showed slow SCF and geometry convergence, which can be a bottleneck in larger systems, especially when a diffusion function is included in the basis set. From a practical perspective, B3LYP/6-31G(d)/MWB59 using SCF geometry showed fast convergence. For that reason it was chosen for geometry optimisations. Further refinement with a higher level of theory could then be considered if needed.

To give insights into the energy barrier, single point energy calculations were performed on the B3LYP/6-31G(d) derived geometry (Figure 6.22, Table 6.6). The most accurate data we attained came from CCSD(T)/aug-cc-pVTZ/MWB59 which predicted an energy barrier of 7.95 kcal/mol, which was close to the 8.00 kcal/mol value predicted by B2PLYP/6-311+G(2df,2d)/MWB59.

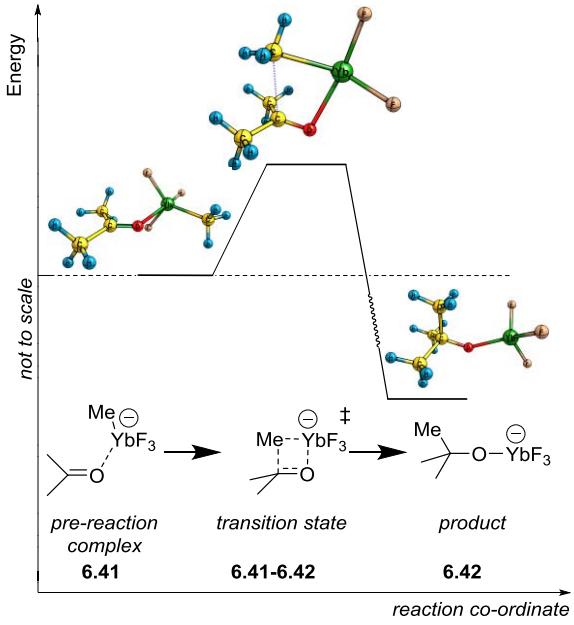

Figure 6.22. Energy graph for the model reaction of an organoytterbium ate complex with acetone.

Using the 6-311+G(2df,2d)/MWB59 basis set, BB1K performed the best of all of the DFT methods examined by predicting a value of 7.55 kcal/mol. By contrast M062X, M06 and M06HF gave values of 6.71, 5.99 and 5.46 kcal/mol respectively, underestimating the barrier by more than 1.25 kcal/mol. Using the more practical 6-311+G(d,p) basis set, B3P86 perform best giving a barrier of 8.05 kcal/mol. BB1K and M062X also performed well, giving values of 8.31 and 7.56 kcal/mol respectively. However, as M062X includes treatment of dispersion interactions, it seemed a better choice for our larger systems. Use of the lower level 6-31G(d) basis set with B3LYP predicted barrier of 7.45 kcal/mol, underestimating this by only 0.50 kcal/mol compared to the CCSD(T) results. By contrast, HF dramatically overestimates the barrier. The CCSD(T) reaction energies (-42.45 kcal/mol) were also in line with those given by B3LYP/6-31G(d) (-42.47 kcal/mol) and B2PLYP/6-

311+G(2df,2d) (-42.26 kcal/mol). M06 and M06HF/6-311+G(2df,2d) were notable outliers, predicting very low energy barriers compared to our reference.

Table 6.6. The barrier heights and reaction energies for the addition of an organoytterbium ate complex to acetone by different methods and basis set (at B3LYP/6-31G(d) geometry).

Method/Basis set	Pre-reaction complex 6.41	Transition state 6.41-6.42	Product 6.42
B3LYP/6-31G(d)	0.00	7.45	-42.47
HF/6-31G(d)	0.00	12.97	-43.27
BB1K/6-311+G(d,p)	0.00	8.31	-43.28
M062X/6-311+G(d,p)	0.00	7.56	-41.09
B3P86/6-311+G(d,p)	0.00	8.05	-46.44
M062X/6-311+G(2df,2d)	0.00	6.71	-41.38
M06/6-311+G(2df,2d)	0.00	5.99	-39.85
M06HF/6-311+G(2df,2d)	0.00	5.46	-48.47
BB1K/6-311+G(2df,2d)	0.00	7.55	-43.62
B2PLYP/6-311+G(2df,2d)	0.00	8.00	-42.26
MP2/cc-pVTZ	0.00	7.24	-45.63
CCSD(T)/aug-cc-pVTZ	0.00	7.95	-42.45

* the MWB59 basis set was used for Yb atom.

The inclusion of tetrahydrofuran solvation energy (Table 6.7) via implicit solvation models increased the reaction barrier from 7.45 kcal/mol to 8.15-8.59 kcal/mol. The CPCM, IEFPCM and SMD[140] implicit solvation models all agreed within 0.44 kcal/mol. Inclusion of solvent also decreased the reaction energy to -39.22 and -39.51 kcal/mol for CPCPM and IEFPCM respectively with a somewhat higher value of -37.90 kcal/mol given for SMD.

Table 6.7. The barrier heights and reaction energies for addition of an organoytterbium ate complex to acetone corrected for solvation using different implicit models (at B3LYP/6-31G(d) geometry).

Solvation methods	Pre-reaction complex 6.41	Transition state 6.41-6.42	Product 6.42
THF(CPCM)	0.00	8.15	-39.51
THF(IEFPCM)	0.00	8.24	-39.22
THF(SMD)	0.00	8.59	-37.90

* the B3LYP/6-31G(d)/MWB59/MWB59 method was used.

6.5.2 Conclusions

SUCCESS IS HAVING TO WORRY ABOUT EVERY DAMN THING IN THE WORLD, EXCEPT MONEY.
JOHNNY CASH

Benchmarking for geometry and energy in a model system for an organoytterbium addition to acetone was performed. The anionic system shows slow basis convergence with respect to geometry and energy. In spite of this it was deemed inappropriate to apply a diffusion function so B3LYP/6-31G(d) was identified as our method of choice for the optimization of large systems. Better energies were obtained using the M06-2x/6-311+G(d,p) level of theory. Reoptimization at B3LYP/6-31+G(d,p) or M06-2x/6-31+G(d,p) can be envisioned in cases where there is uncertainly the about the geometry. The B2PLYP double hybrid DFT was able to reproduce CCSD(T) values with reasonable accuracy, as they had with the organolithium model system. The inclusion of solvation energies increased the energy barrier in all the tested implicit methods. However the IEFPCM method was preferred to achieve consistency with the organolithium addition study.

6.6 Real System with Ytterbium

QUEEN GERTRUDE
MORE MATTER, WITH LESS ART.
SHAKESPEARE, HAMLET

Based on the conclusions drawn in our geometric and energetic benchmark calculations, those methods were next applied to the system of interest (Figure 6.23). The organoytterbium species were modelled as neutral and anionic species to provide insights into the selectivity of addition and the nature of the organoytterbium reagent. After an extensive conformational study was performed the following conclusions can be drawn from the Gibbs free energies at -78 ^{o}C in tetrahydrofuran as solvent. Formation of ate complex $[PhYb(OTf)_3]^-$ is more favourable than the species $PhYb(OTf)_2 + TfO^-$ by 25.2 kcal/mol. The addition of $PhYb(OTf)_2$ to **5.6** is predicted to favour reaction at the ketonic *C*-1 carbonyl (*i.e.* $\Delta G_A < \Delta G_D$, Figure 6.23), which is contrary to experimental findings. However the reaction of $[PhYb(OTf)_3]^-$ with **5.6** is predicted by modelling to favour *C*-2 carbonyl addition (i.e. $\Delta G_H < \Delta G_E$, Figure 6.23). In contrast to the analogous organolithium additions, which are largely driven by electronic effects, the selectivity of organoytterbium additions is strongly influenced by steric effects. The cyclobutenedione **6.6** has to change from an S-*trans* conformation to the higher energy S-*cis* conformation to achieve the less encumbered transition state **H**. Higher negative charge separation on the *C*-2 carbonyl (CHELPG ESP Figure 6.4), together with the oxophilic character of organoytterbium reagents, leads to its preferential interaction with the *C*-2 carbonyl over the *C*-1 carbonyl. The strength of those interactions has an impact on the regiochemical course of addition, as ΔG_G is less than ΔG_F by about 2.5 kcal/mol.

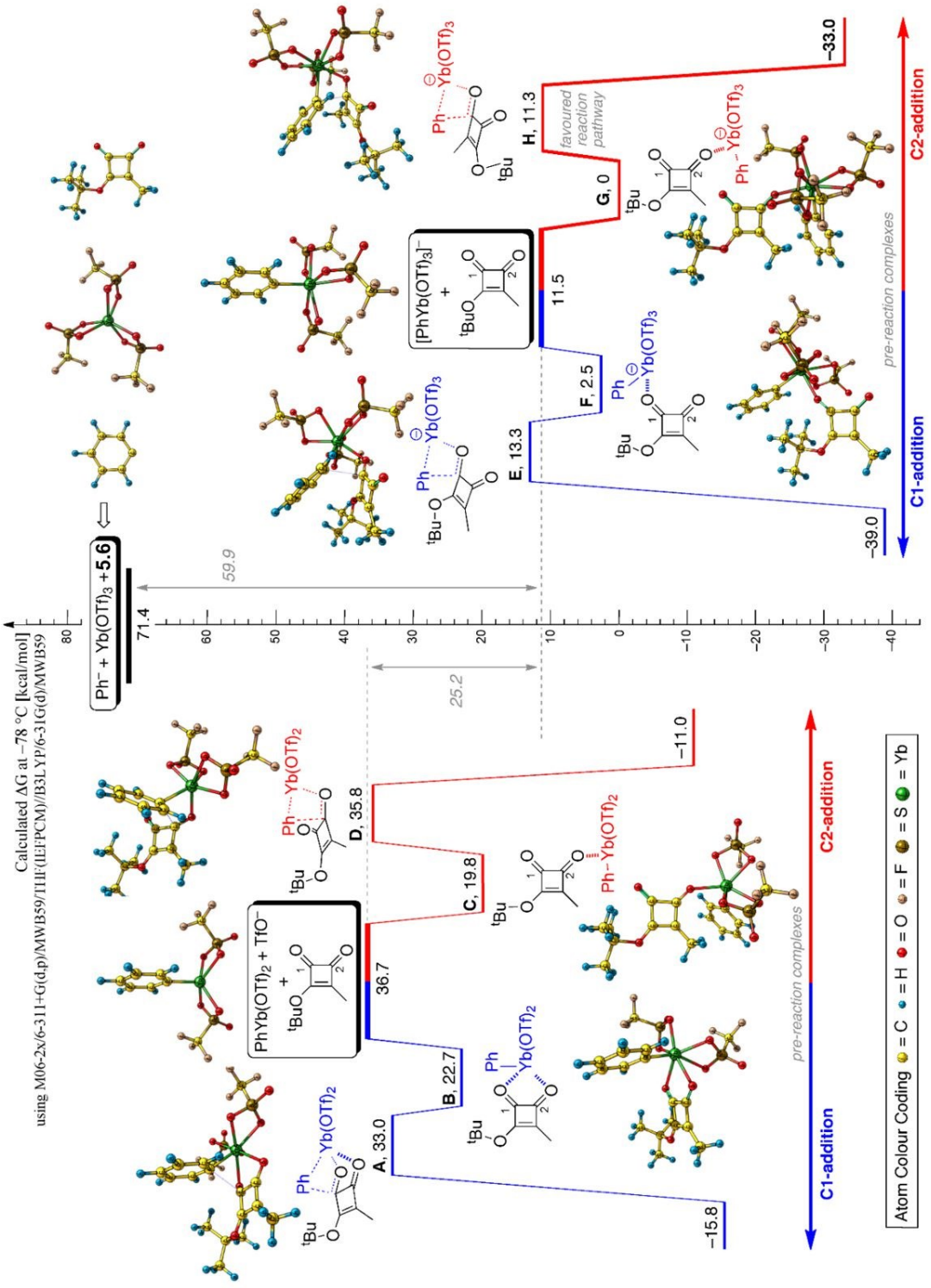

Figure 6.23. Selectivity of organoytterbium addition to cyclobutenedione **5.6** for neutral organoytterbium reagents and the corresponding ate complex

6.7 Potential Mimics of the Ytterbium System

EXPERIENCE IS WHAT YOU GET WHEN YOU DON'T GET WHAT YOU WANT.
DAN STANFORD

The conclusions drawn from the addition reactions of organoytterbium reagents to cyclobutenedione can, in principle, be used to design reactions with organolithium reagents to achieve a similar switch in selectivity. Screening a variety of ligands revealed that PMDETA **6.44** (*N,N,N′,N″,N″*-pentamethyldiethylenetriamine, Figure 6.24) and HMTETA **6.45** (1,1,4,7,10,10-Hexamethyltriethylenetetramine) have the potential to switch the regioselectivity of organolithium additions to cyclobutenone **6.6**. By contrast, our calculations with the 12-crown-4•MeLi complex indicated that it would behave in a similar fashion to the methyllithium dimer.

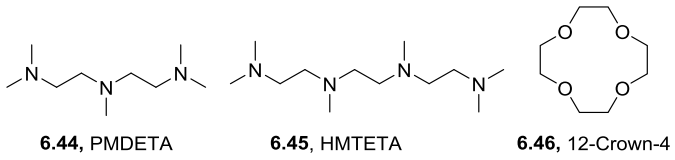

6.44, PMDETA **6.45**, HMTETA **6.46,** 12-Crown-4

Figure 6.24. Chelating ligands for organolithium reagents.

In contrast to other popular additives, the PMDETA•PhLi complex has a monomeric structure.[141] Exploratory molecular modelling calculations on the MeLi•PMDETA complex **6.47** showed a preference for *C*-2 addition to **6.6** (via **6.47**-**6.49**) over *C*-1 addition (via **6.47**-**6.48**) by 2.7 kcal/mol (Figure 6.25). The electronic energy calculated at the M06-2x/6-31+G(d) level agreed with the free energy calculations at B2GP-PLYP/cc-pVQZ with THF as solvent.

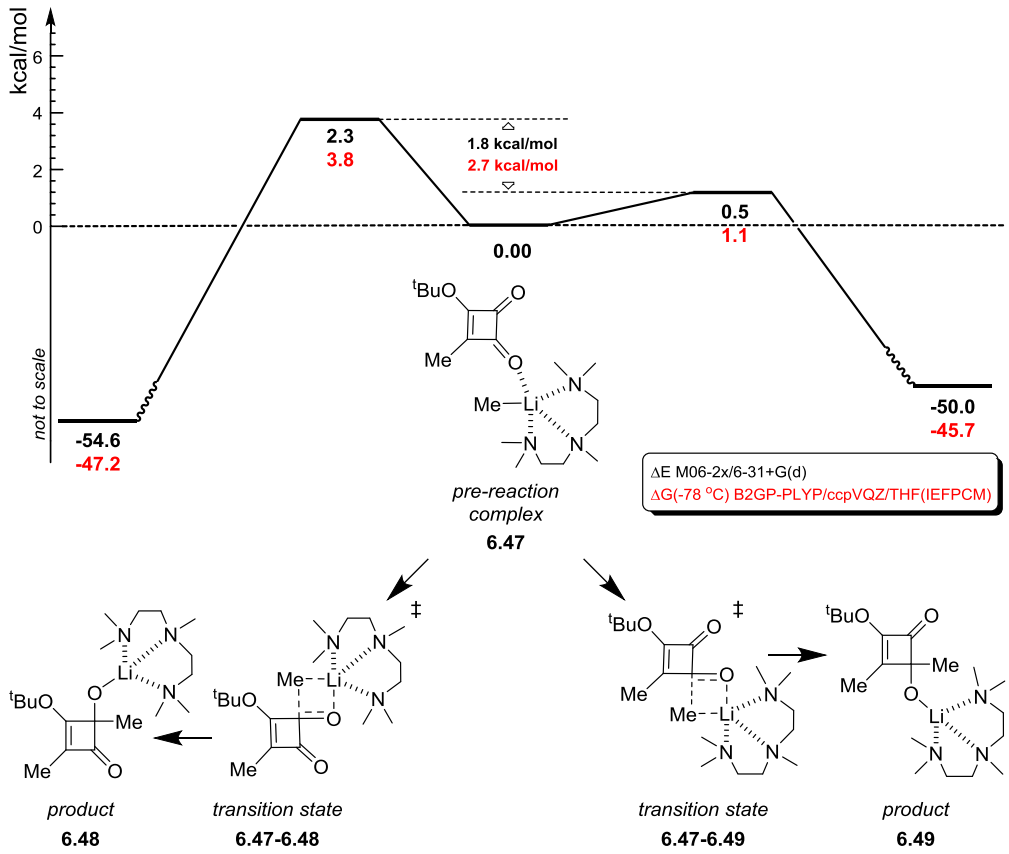

Figure 6.25. Energy graph for methyllithium-PMDETA complex addition to 3-(*tert*-butoxy)-4-methylcyclobut-3-ene-1,2-dione using the M06-2x/6-31+G(d) geometry.

This organolithium complex follows the less hindered pathway so mimics the course followed by organoytterbium ate complexes. However, no S-*trans* to S-*cis* conformational change is observed as both transition states have longer C-C distances for the forming bond in the transition state (Figure 6.26).

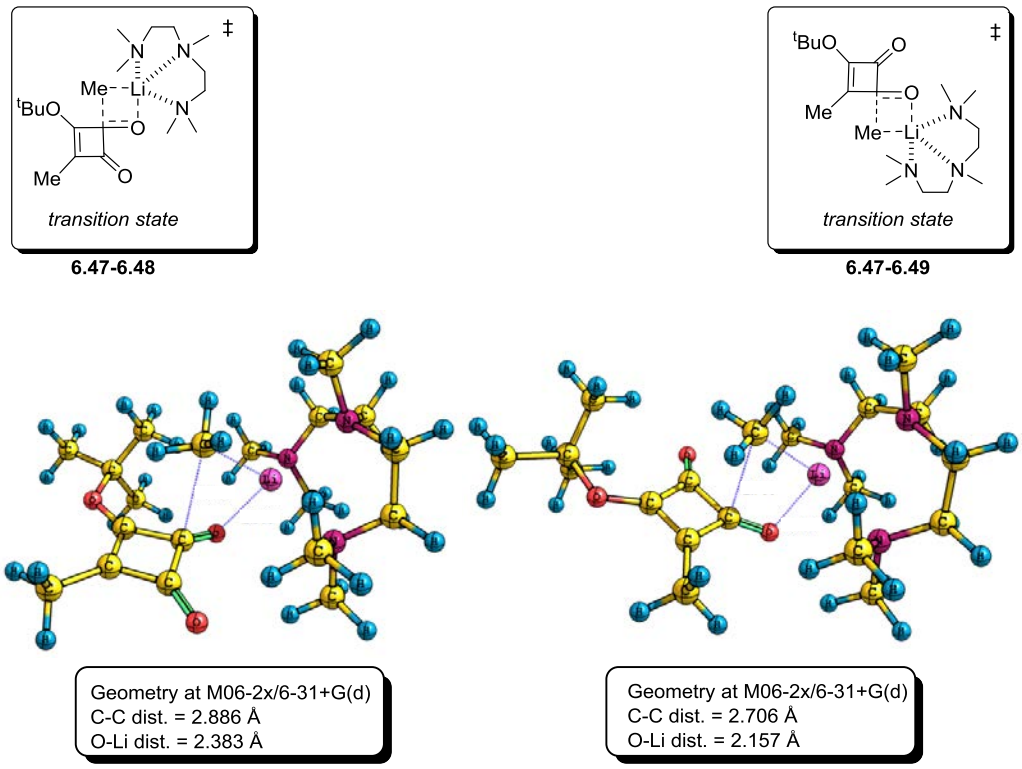

Figure 6.26. Geometry of the lowest energy transition states found for addition of methyllithium homodimer-dimethyl ether complex to 3-(*tert*-butoxy)-4-methylcyclobut-3-ene-1,2-dione **6.6** using the M06-2x/6-31+G(d,p) geometry.

If phenyllithium is use instead of methyllithium, a further boost in selectivity can be expected. Alas, at the time of writing, we have no experimental work to back-up this postulate.

6.8 Conclusions

YOU MAY HAVE TO FIGHT A BATTLE MORE THAN ONCE TO WIN IT.
MARGARET THATCHER

The computational study presented above shows that the addition of methyllithium to a cyclobutenedione involves dimeric species while for organoytterbium additions the corresponding ate complex is involved. The intrinsic reactivity of cyclobutenediones suggests that addition to the *C*-1 carbonyl of **6.28** is favoured over *C*-2 addition due to electronic effects. This pathway is observed for most organolithium reagents, and is supported by DFT calculations and laboratory experiments. However, the character of an organometallic reagent in respect of its ligands can influence the course of such reactions. This is especially true of organoytterbium additions to cyclobutenediones, were electronic effects can be overwhelmed by steric effects leading to a switch in selectivity. Thus, it should be possible to mimic the course of organoytterbium additions with organolithium reagents. In particular, calculations suggest that chelation by ligands such as PMDETA and HMTETA might allow this to be realised, even with 2-(*tert*-butoxy)cyclobutene-1,2-dione **6.6**. We await experimental conformation of that finding.

Chapter 7: Side Project: Formation of Tetrahydropyran rings via boat transition states.

OF COURSE IN THE FIRST MATCHES YOU ARE MORE CAREFUL, PERHAPS MORE CAREFUL THAN YOU SHOULD BE.
DIEGO MARADONA

7.1 Chapter abstract

This side project was conducted to explain an unexpected selectivity issue that arose during the formation of a central building block of the natural product onnamide F **7.4**,[142] pederin **7.5**,[143] and psymberin **7.3**[144] (Scheme 7.1). The key step of the synthesis involved formation of tetrahydropyran ring **7.2** from γ-lactone **7.1** which was triggered by the addition of ammonia.[145]

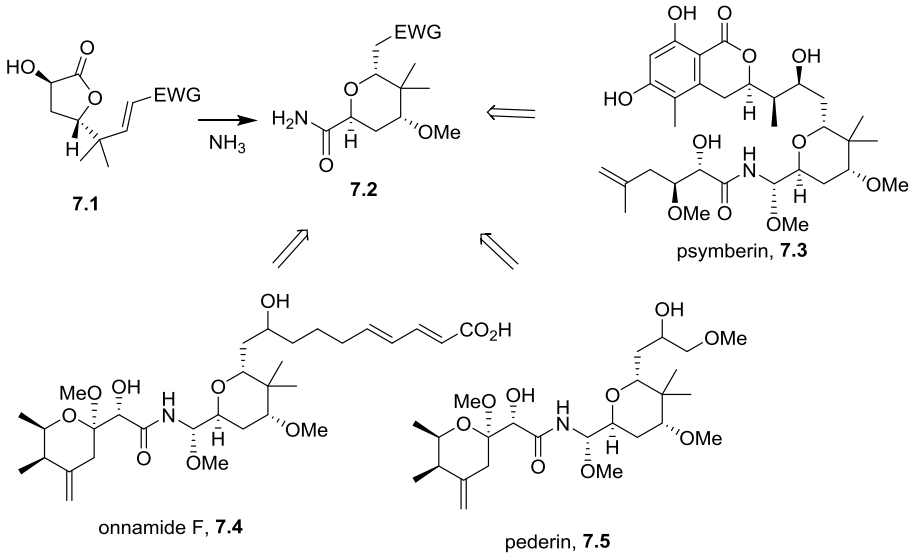

Scheme 7.1. The synthesis of tetrahydropyran **7.2** as a central building block for the natural products onnamide F **7.4**, pederin **7.5**, and psymberin **7.3**.

In the conversion of γ-lactone **7.1** to tetrahydropyran **7.2**, cyclisation occurs via the acyclic diol **7.6**. However, the reaction also gives diasteroisomer **7.7** in proportions dependent on the nature of the electron-withdrawing group -*EWG* (Scheme 7.2). If a cyano group (-CN) is present, selectivity was poor with similar quantities of **7.2** and **7.7** given. However, with an ester group (-CO_2Et) attached a 14 : 1 selectivity in favour of the desired outcome was given. The choice of solvent also had an impact on selectivity.

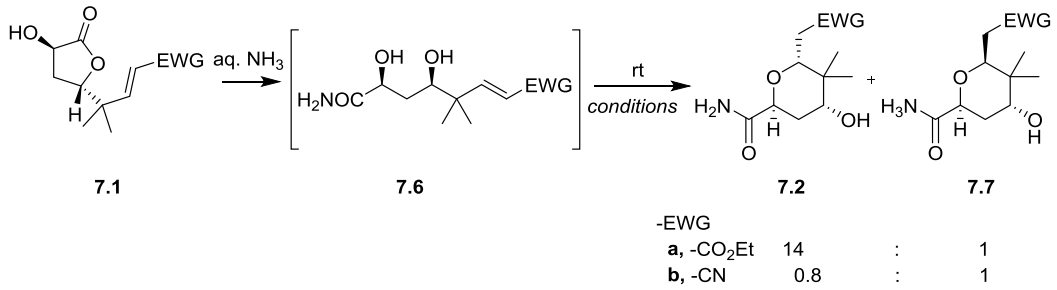

Scheme 7.2. Expansion of furanone **7.1** to tetrahydropyrans **7.2** and **7.7**.

To provide some insights on the course of the reaction and the observed selectivity, a molecular modelling study was conducted. To avoid conformational problems, all calculations were carried out on anionic intermediates. Geometries were obtained at M62x/6-31+G(d,p) following single point energy calculations at M06-2x/6-311+G(2df,2p). Solvent effects were incorporate at the M06-2x/6-311+G(2df,2p) level with the implicit IEFPCM solvation model. The Gibbs free energy graphs at 25 ^{o}C were also calculated with THF, DMSO, MeOH and DMF as solvents for the transformation of **7.6** to **7.2** and **7.7**. The deprotonation reaction was modelled with 1,8-diazabicycloundec-7-ene (DBU). For simplicity, discussion here will focus on ΔG values obtained at vacuum and with MeOH as solvent, as this was found to reflect all relevant trends for that system.

7.2 Study on model systems

IF I HAVE A THOUSAND IDEAS AND ONLY ONE TURNS OUT TO BE GOOD, I AM SATISFIED.
ALFRED NOBEL

To ensure that there are no barrierless steps in the sequence, we first performed a model study with alkyne **7.12** as a weak electron withdrawing (-*EWG*) group. As shown in Scheme 7.3, the simple model reaction showed that a chair like transition state **7.9-7.10** was lower in energy than a boat-like transition state **7.8-7.9**, by 1.54 kcal/mol in vacuum and 3.85 kcal/mol in methanol. The thus formed anionic intermediates, **7.8** and **7.10**, can easily reverse to the reactant due to the low energy barrier. The inclusion of solvent increased the energy of the transition state and increased the energy difference between them. However, the deprotonation step decreased from 122.40 kcal/mol in vacuum to 27.20 kcal/mol in methanol. The reaction is exergonic and kinetically favoured leading to a chair conformation **7.13** via the chair-like transition state **7.9-7.10**. This model was taken as an unperturbed system as it has no substituent effects.

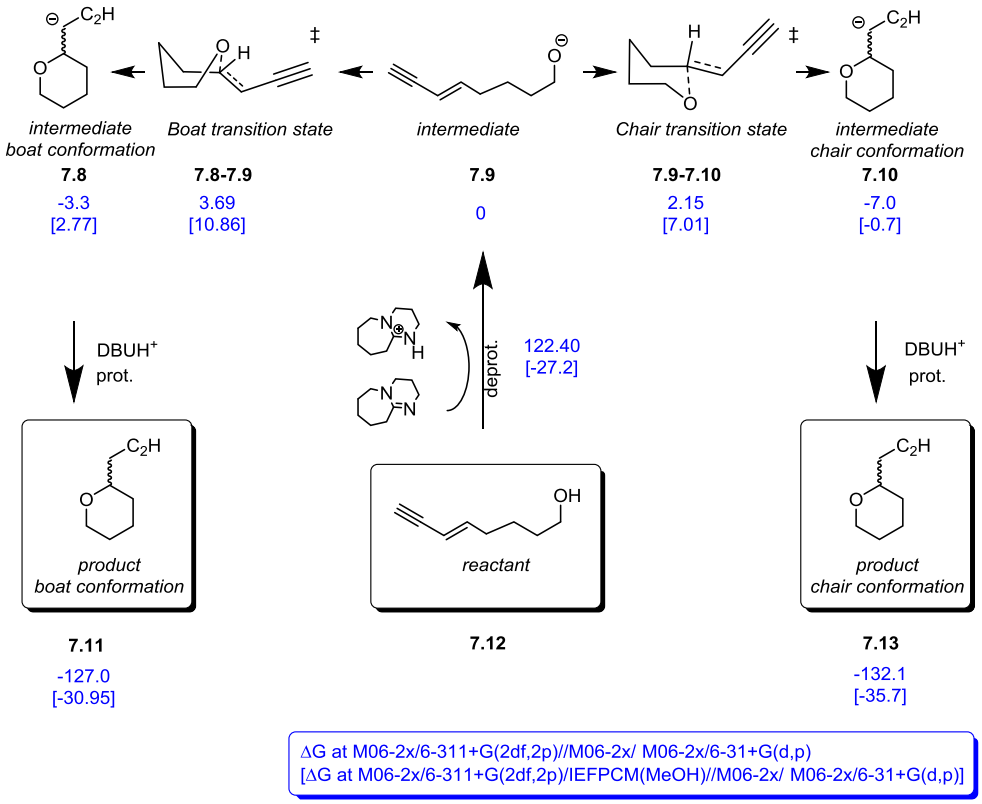

Scheme 7.3. Competitive pathways for ring closure of simplest model system of (*E*)-oct-5-en-7-yn-1-ol **7.12**.

The chair transition state **7.9-7.10** has a longer O-C distance at the point of transition than that observed in the boat transition state **7.8-7.9** (Figure 7.1) which implies that early transition state is the favourable pathway.

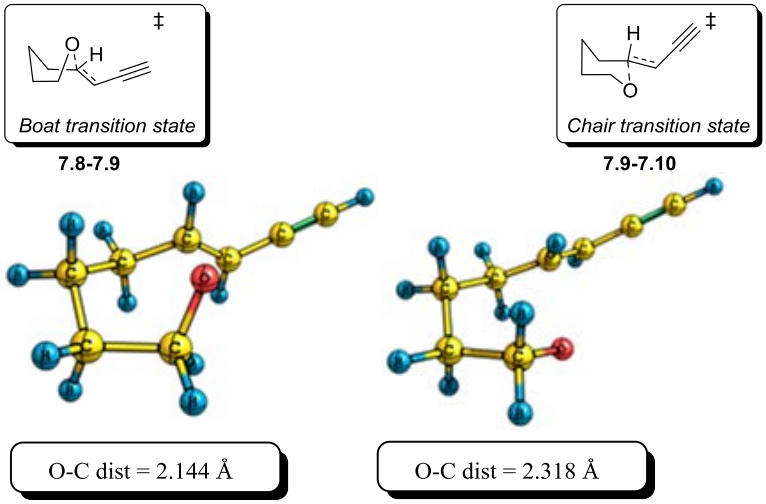

Figure 7.1. The geometry of transition states for the ring closure reaction of (*E*)-oct-5-en-7-yn-1-ol 7.12 at M06-2x/6-31+G(d,p).

Importantly, the picture changes if a hydroxyl group is added to the tethering chain in our model system, *e.g.* **7.18**. It allows formation of a hydrogen bond in the "boat-like" transition state **7.14-7.15** (Scheme 7.4).

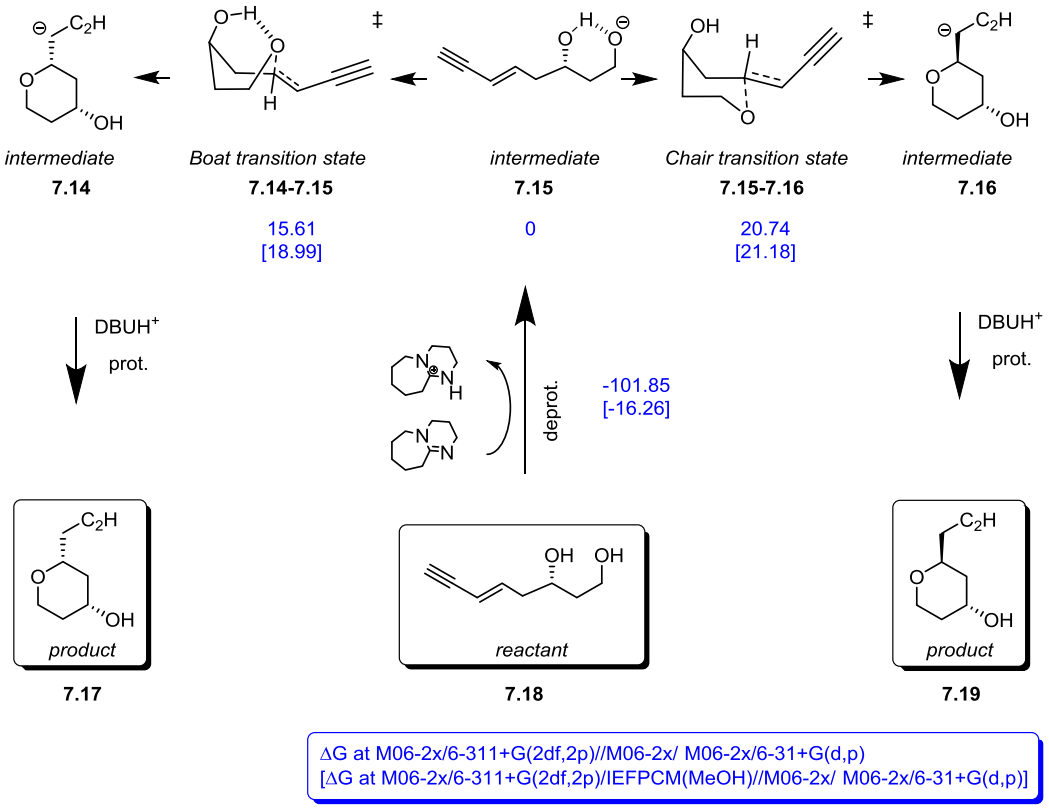

Scheme 7.4. Competitive pathways for ring closure of the simple model system of (*S,E*)-oct-5-en-7-yne-1,3-diol **7.18**.

The energy barriers are much higher for both transition states but importantly the boat transition state **7.1-7.15** is now lower in energy by 5.13 kcal/mol in vacuum and decreasing to 2.19 kcal/mol in methanol solvent. The boat transition state also has a shorter carbon-oxygen bond distance at the point of transformation suggesting a later transition state compared to that found in the chair transition state **7.15-7.16** (Figure 7.2). The energy gained from stabilisation by the hydrogen bond makes this the lower energy pathway. For all transition state analyses the lower energy conformation has the hydroxyl group in an axial position. Comparison with the previous systems shows that the presence of the hydroxyl group also decreases the energy of deprotonation, in vacuum and in methanol, by stabilizing the intermediate alkoxide **7.15**.

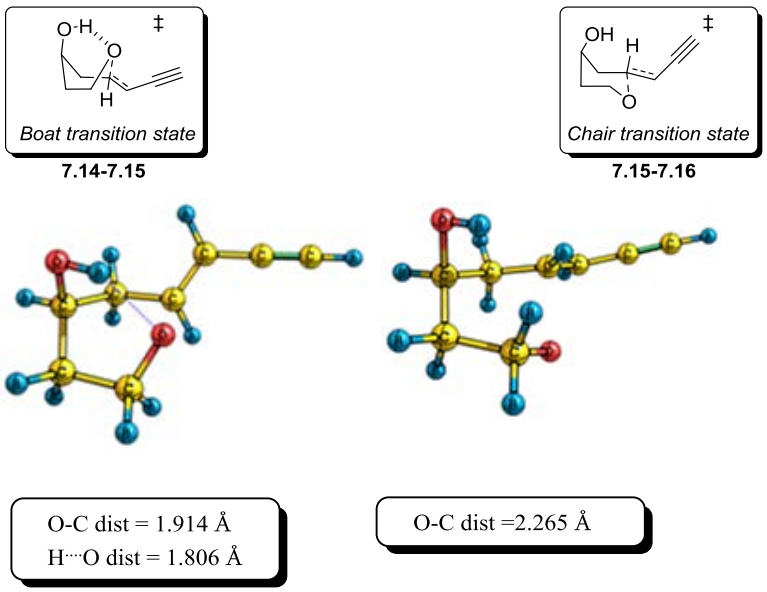

Figure 7.2. The geometry of transition states of ring closure reaction of (*E*)-oct-5-en-7-yn-1-ol **7.18** at M06-2x/6-31+G(d,p).

When an amide and two methyl groups were added to the unperturbed system the preference for proceeding via chair-like transition state was again evidenced (Scheme 7.5). The energies barrier were now higher for both transition states (5.83 and 8.68 kcal/mol) due to steric effects in spite of the availability of hydrogen bonding to the amide. The chair transition state **7.21-7.22** has a lower in energy barrier than the boat transition state **7.20-7.21** by 2.85 kcal/mol in vacuum and this decreased to 1.56 kcal/mol in methanol. This is expected as the lack of a hydroxyl group in the tethering chain means that there is no advantage gained by proceeding via boat pathway. As seen in the previous example (Scheme 7.4) the presence of an additional hydrogen bond decreases the energy of deprotonation in vacuum and methanol when compared with unperturbed system (Scheme 7.3).

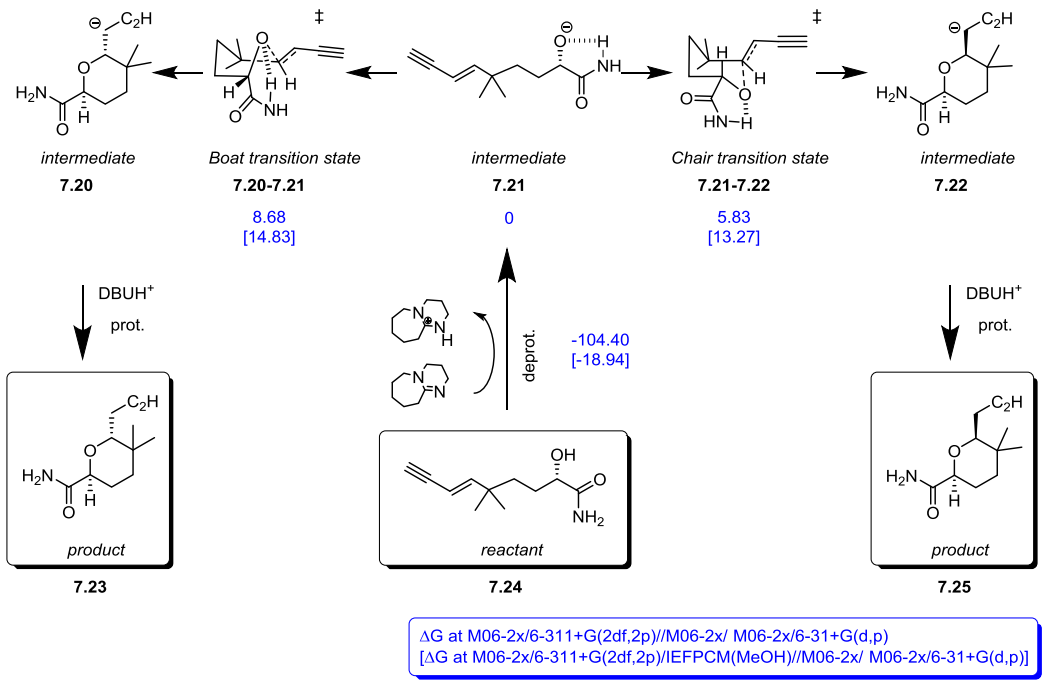

Scheme 7.5. Competitive pathways for ring closure of simple model system of (*S,E*)-2-hydroxy-5,5-dimethylnon-6-en-8-ynamide **7.24**.

The impact of the amide moiety and methyl groups on the geometry of transition states **7.21-7.22** and **7.20-7.21** is demonstrated in Figure 7.3. Both have a shorter C-O bond distance at the point of transition due to hydrogen bond stabilization from the amide moiety. In contrast to the previously reported models, the boat-like transition state here **7.20-7.21** has a shorter distance than in the chair-like transition state **7.20-7.22**.

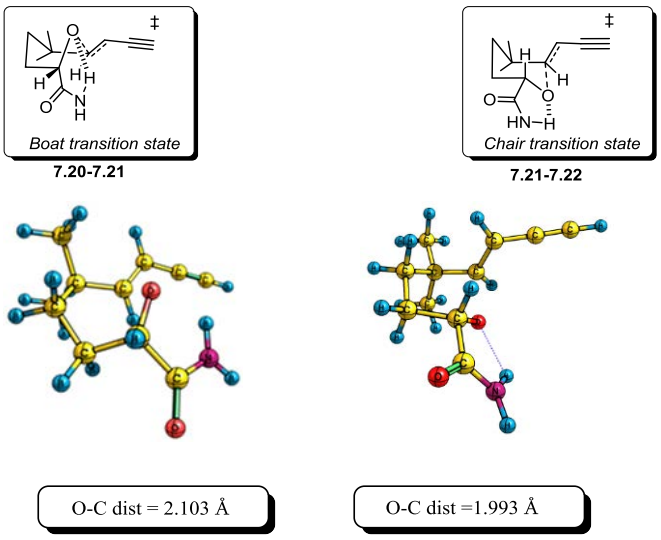

Figure 7.3. The geometry of transition states for the ring closure reaction of of (*S,E*)-2-hydroxy-5,5-dimethylnon-6-en-8-ynamide **7.24** at M06-2x/6-31+G(d,p).

We now added the critical hydroxy group to the previous model (Scheme 7.6) and were pleased to note that selectivity was again reversed. The boat transition state **7.26c-7.27c** was now lower in energy than the chair transition state **7.27c-7.28c**, by 1.79 kcal/mol in vacuum and 0.83 kcal/mol in methanol. As expected, the key difference is the availability of a hydrogen bond in the boat pathway, though in protic solvent this interaction is weaker. Anionic intermediates **7.26c** and **7.28c** also have a lower energy barrier for reversal back to the anionic intermediate **7.27c**. Deprotonation is also lowered in energy compared to that observed in previous examples (-89.03 kcal/mol in vacuum and 9.2 kcal/mol in methanol) as a result of having two hydrogen bonds available to stabilise **7.27c**. This system is similar to real system, but instead of a cyano or ester group, the CCH group is present (Scheme 7.2).

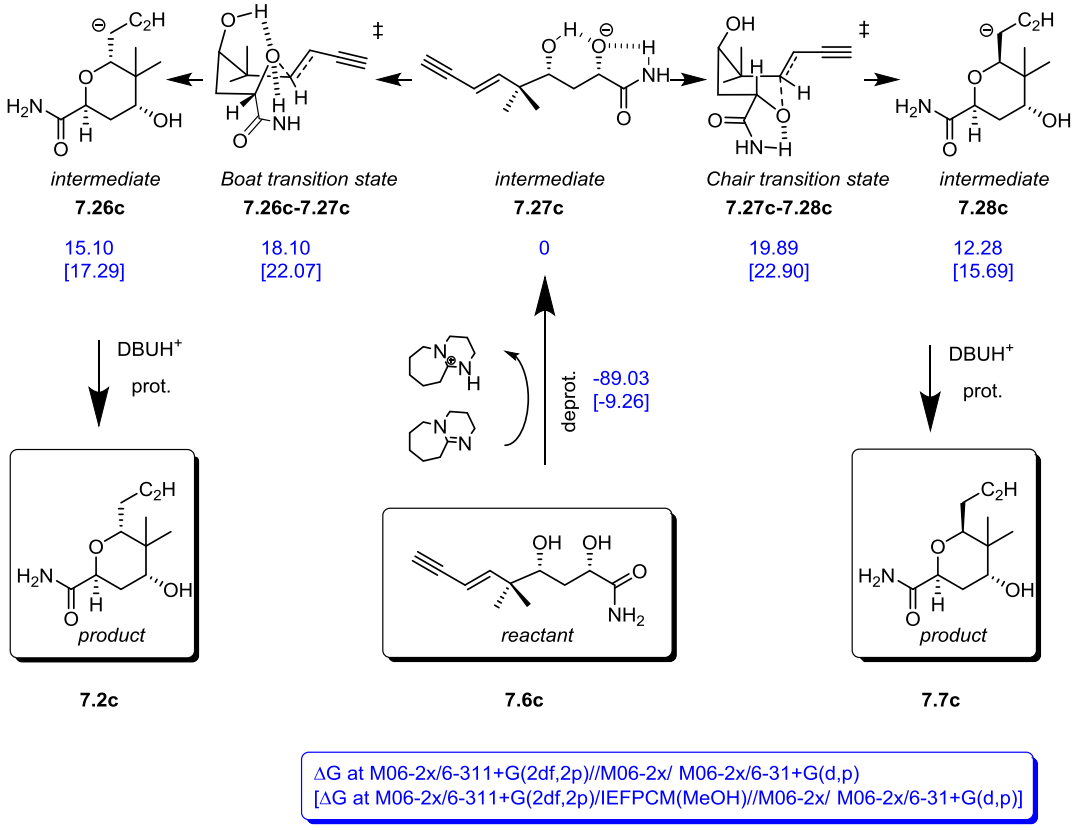

Scheme 7.6. Competitive pathways for ring closure of our simple model system of (*S,E*)-2-hydroxy-5,5-dimethylnon-6-en-8-ynamide **7.6c**.

As before, the kinetically favourable boat transition state **7.26c-7.27c** has a shorter C-O distance than the unfavoured chair transition state **7.27c-7.28c** (Figure 7.4). The

hydrogen bond in the transition state geometry **7.26c-7.27c** is nonlinear.[146] An NBO analysis of the hydrogen bond revealed a strong orbital interaction, with the large overlap term of F(i,j) = 0.071 being confirmed by a Fuzzy bond order of 0.072 (Figure 7.5).

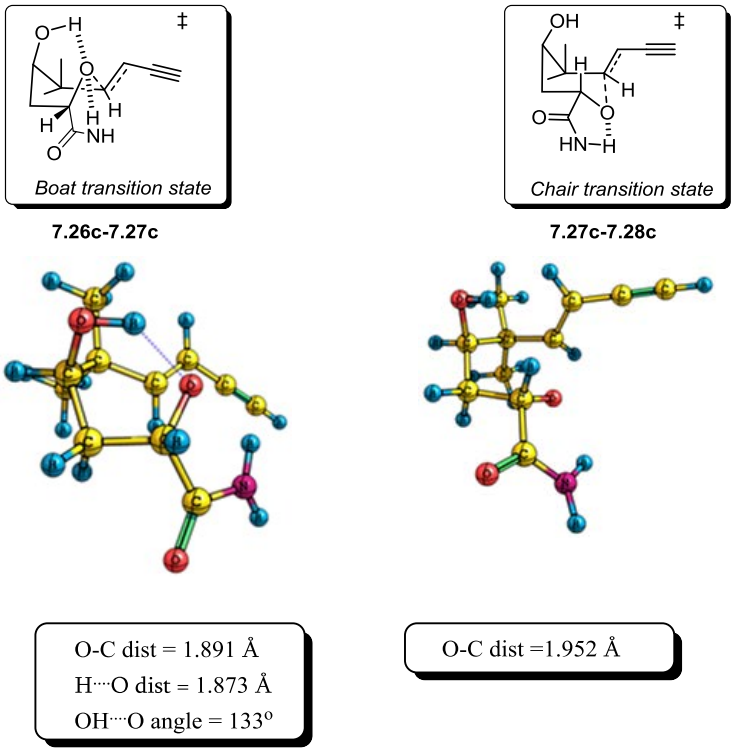

Figure 7.4. The geometry of the transition states for the ring closure reaction of (*S,E*)-2-hydroxy-5,5-dimethylnon-6-en-8-ynamide **7.24** at M06-2x/6-31+G(d,p).

The hydrogen bond strength calculated with potential energy density (V(r))[105] is 9.6 kcal/mol, which is close to the value calculated using NBO (E(2) = 9.0 kcal/mol, Figure 7.5). The hydrogen bond with the amide has a length of 2.12 Å length and angle of 107.6°. Energetically it has less impact on the geometry of the transition state. However, this hydrogen bond removes electron density from oxygen and makes the reaction more selective.

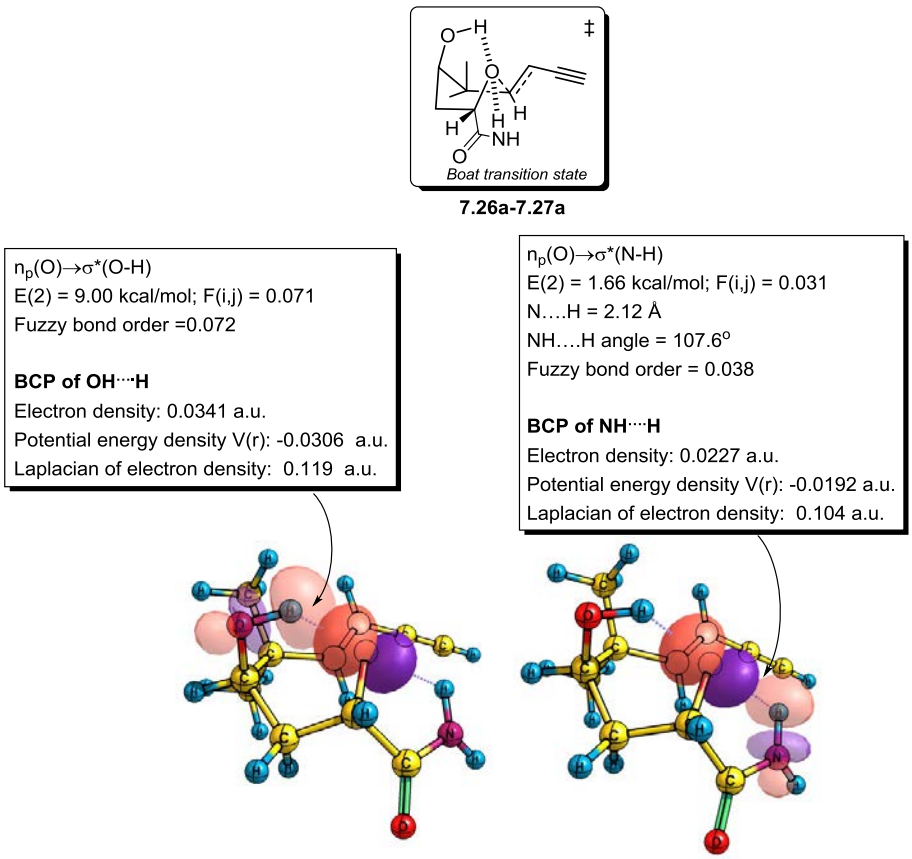

Figure 7.5. Geometry and electronic properties of the hydrogen bonds in the boat transition state model for ring closure of (*S,E*)-2-hydroxy-5,5-dimethylnon-6-en-8-ynamide **7.6c**. Geometry and NBO analysis at M06-2x/6-31+G(d,p), Fuzzy bond order and QTAIM analysis at M062X/6-311++G(2d,2p).

7.3 Modelling real system and trends observed

JUST REMEMBER, WHEN YOU'RE OVER THE HILL, YOU BEGIN TO PICK UP SPEED.
CHARLES SCHULZ

Finally our attention turned to the synthetically relevant molecules **7.6** and their transformation to tetrahydropyrans **7.2** and **7.7** (Scheme 7.7). The pathway graphs for the two competitive pathways with ester and nitrile electron withdrawing groups were both modelled. For both groups the boat transition state **7.26-7.22** was found to be lower in energy due to hydrogen bonding. The energy difference between the two transition states is higher for the ester group (2.60 kcal/mol) than for nitrile group (0.71 kcal/mol).

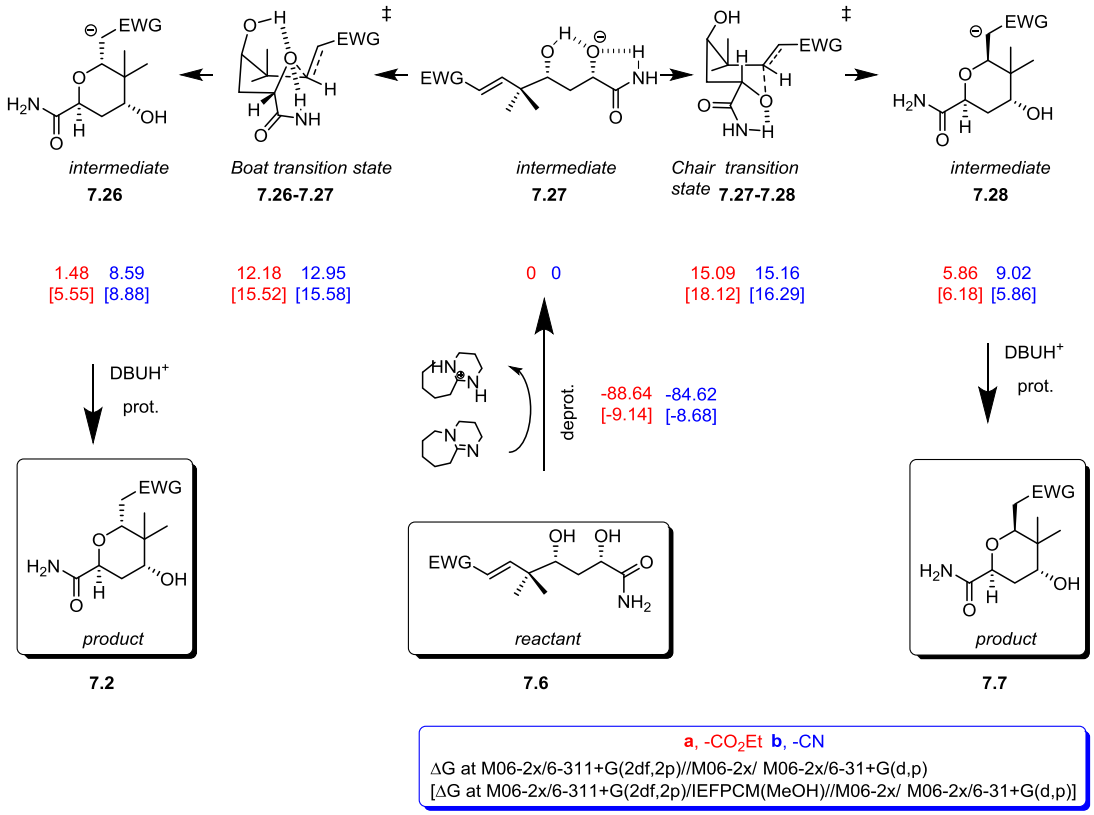

Scheme 7.7. Competitive pathways for ring closure of **7.27**.

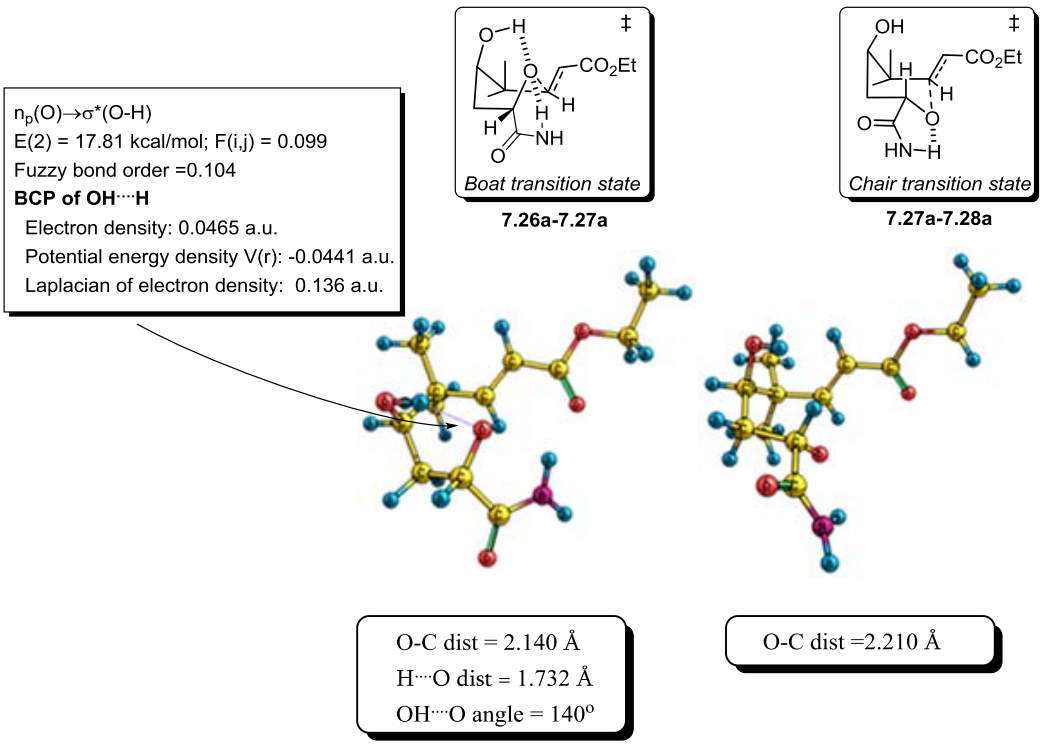

Figure 7.6. The geometry of transition states for the ring closure reaction of **7.26a**. Geometry and NBO analysis at M06-2x/6-31+G(d,p), Fuzzy bond order and QTAIM analysis at M062X/6-311++G(2d,2p).

When compared with the alkynyl group (Scheme 7.6), similar reactivity trends are observed. Selectivity shows a good correlation to the calculated carbon-oxygen distance at the point of transition and follows the electron withdrawing capacity of the group attached to the Michael acceptor leading to the order CCH < -CN < CO_2Et (Figure 7.4, 7.5, 7.6, 7.7).

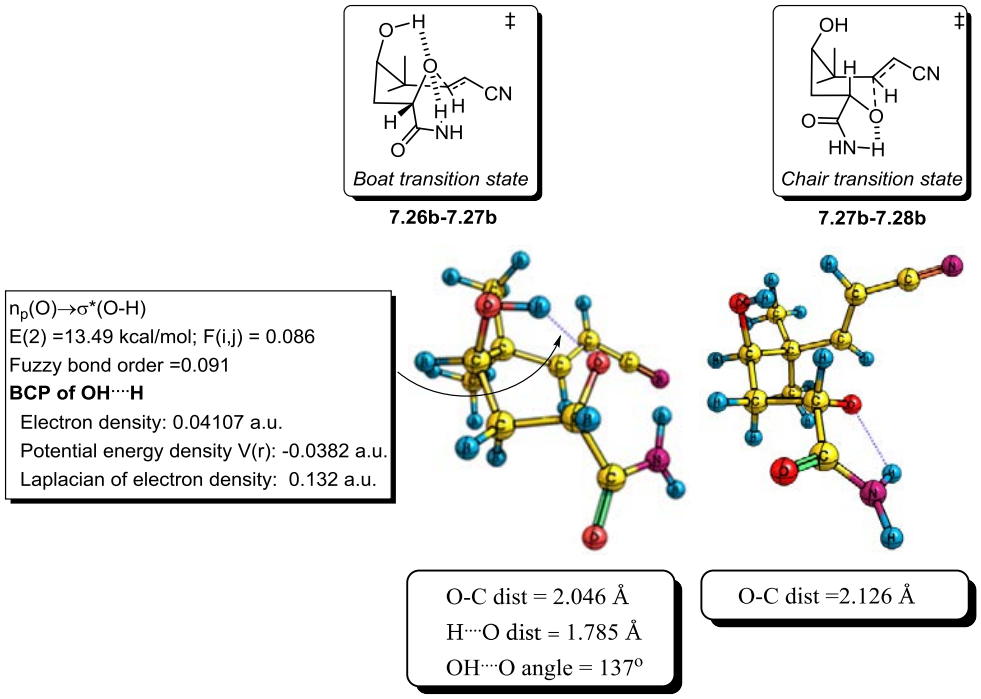

Figure 7.7. The geometry of transition states for the ring closure reaction of **7.26b**. Geometry and NBO analysis at M06-2x/6-31+G(d,p), Fuzzy bond order and QTAIM analysis at M062X/6-311++G(2d,2p).

Selectivity also increases with a shortening of the hydrogen bond H···O distance in the transition state, which reflects the impact of the electron withdrawing group on the transition state geometry. The short C-O distances in the transition state lead to a lowering of the orbital overlap term F(i,j), Fuzzy bond order and the E(2)-NBO stabilisation energy for hydrogen bonding.

The lowest energy boat transition state observed with the –CN group does not explain why so much product is derived via the chair transition state **7.27b-7.28b** (Scheme 7.2). However the stability of the formed intermediates **7.26** and **7.28** shows that this step is reversible (Scheme 7.8). In the anionic intermediate **7.27,** the alkoxide is stabilised by hydrogen bonding by both the amide and the hydroxyl group. By contrast, in intermediate **7.26** the anion is only stabilised by the electron withdrawing group. Thus, for weak and intermediate *–EWGs* cyclisation is a reversible reaction. The reaction rate for this recycling loop follows the order -CO_2Et < -CN < -CCH, as shown in show in Scheme 7.8. Due to hydrogen bonding,

the reverse reaction is faster via the boat transition state than it is via the chair transition state.

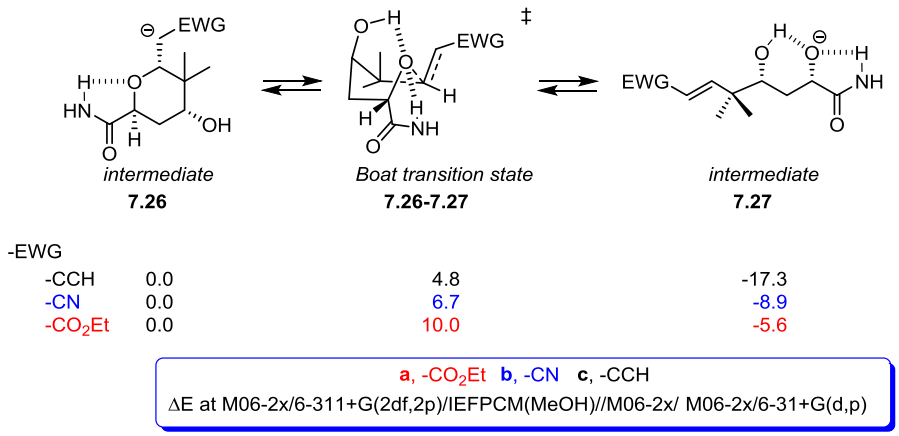

-EWG			
-CCH	0.0	4.8	-17.3
-CN	0.0	6.7	-8.9
$-CO_2Et$	0.0	10.0	-5.6

a, $-CO_2Et$ **b**, -CN **c**, -CCH

ΔE at M06-2x/6-311+G(2df,2p)/IEFPCM(MeOH)//M06-2x/ M06-2x/6-31+G(d,p)

Scheme 7.8. The influence of substituents on the recycling loop for intermediate **7.26**.

Indeed, we believe that this is situation reflected in the associated experimental outcomes, namely that the nitrile group gives more of the thermodynamic product, whereas the ester group promotes the kinetic pathway so gives that product in preference.

7.4 Conclusions

IF MATHEMATICALLY YOU END UP WITH THE INCORRECT ANSWER,
TRY MULTIPLYING BY THE PAGE NUMBER.
ANONYMOUS MURPHY'S LAW

DFT modelling of various model and real systems were performed with extensive conformational analysis. Calculations revealed that the presence of a hydroxyl group in the tethering chain leads to short strong hydrogen bonding[119] and this promotes boat rather than chair-like transition states (Scheme 7.9). The energy barrier for cyclisation depends of the nature of the electron withdrawing group (*–EWG*), decreasing in order of their electron withdrawing abilities: $–C_2H$ < –CN < $–CO_2Et$. The same trend is observed for hydrogen bond distance and selectivity increases in the same order. This link between the energy of hydrogen bonding and selectivity can be attributed to its interrelationship with the lateness of the transition state. The bond order, Laplacian, electron density, orbital overlap term (F(i,j)) and orbital interaction energy of the hydrogen bond increase in the following order –CCH < –CN < $–CO_2Et$ in the respective transition states.

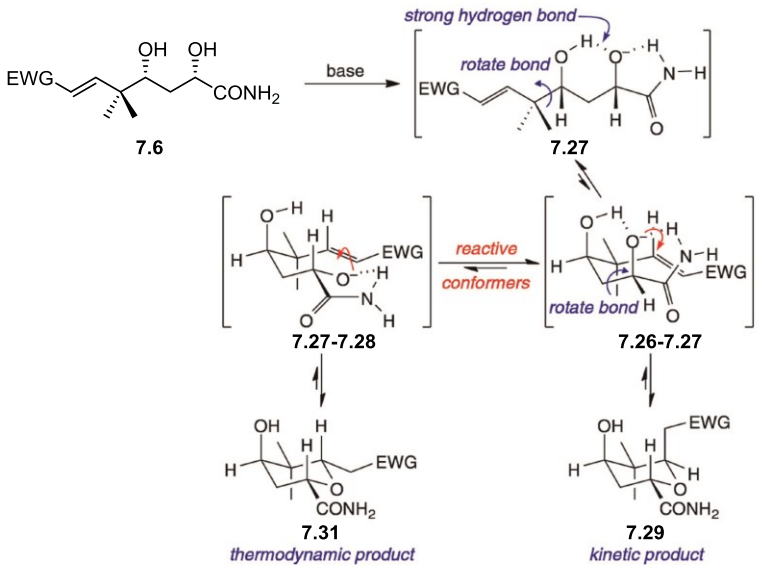

Scheme 7.9. Explanation of the stereochemical course of the **7.6** cyclization base on DFT calculations.

The outcome of the reaction is also influenced by thermodynamic factors as the reversing loop is faster for weaker electron withdrawing groups. This explains why the cyano group shows much lower selectivity than expected from kinetic barriers. Solvent effects increase the reaction barrier and decrease selectivity slightly. The

methyl and amide groups make the reaction slower and more selective. For all modelled examples of the transition states, the lower energy conformer has the hydroxyl group in the axial rather than an equatorial position.

Chapter 8: Further Work

THE BEST TIME TO PLANT A TREE WAS FORTY YEARS AGO. THE SECOND BEST TIME IS TODAY.
CHINESE PROVERB

The presented work can be extended as follows:

- Our studies on the alkynylcyclobutenone rearrangement have shown that the alkyne residue (–R_1) is not the only substituent to influence the mode of ring closure (Scheme 8.1). Indeed, substituents at *C*-2 and *C*-3 (–X and –Y) and groups attached to the *C*-4 oxygen (–P) can all bias the reaction towards five- or six-ring closure to **8.3** and **8.4** (Scheme 8.1). As we have seen, the selectivity achieved when the *C*-4 hydroxyl is protected by an acetate group, is quite remarkable as no five ring products are observed in the product mixture. It is plausible that modelling could identify other means of selectively promoting either the 5- or 6-ring closure pathway.

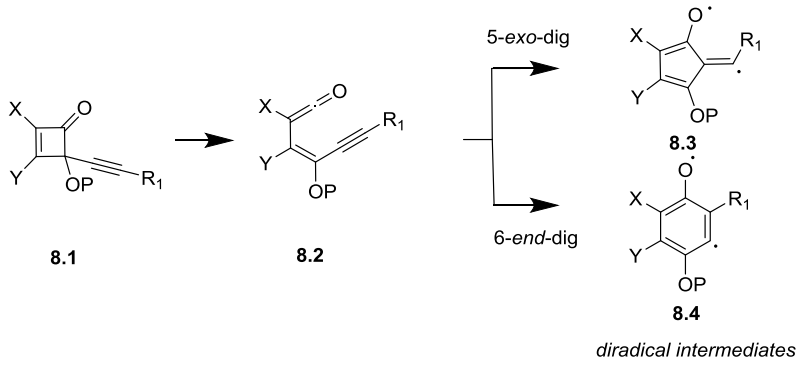

Scheme 8.1. A study of the influence of substituents on the formation of five and six membered rings.

- The aforementioned reaction also has great potential for the development of new cascade reaction sequences. Many complex diradical cascade transformations can be designed using DFT method from the outset to confirm their likely course. These could provide useful routes to rare fused ring skeletons.
- For example, preliminary calculations show that a substrate such as **8.9** could lead to diradical intermediate **8.8**. Cyclisation of the carbon-centred radical

to the proximal alkene then sets up two ring closures give tetracycle **8.5** (Scheme 8.2).

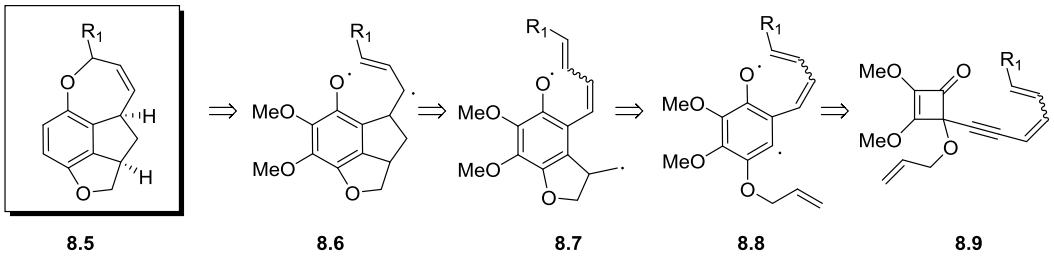

Scheme 8.2. Cascade rearrangement via diradical intermediate.

- Our computational studies on the switch between diradical and zwitterionic orbital isomers can be extended, allowing the discovery of other useful reactions. For example, different groups attached to the *C*-4 hydroxyl and the cyclobutenone could be screened to see if solvolysis of the zwitterionic orbital isomer could be realised with water, an alcohol or an amine. It could also be examined to see if, for example, triethyl orthoacetate protected cyclobutenone **8.14** can give fused ring systems such as **8.11** (Scheme 8.3).

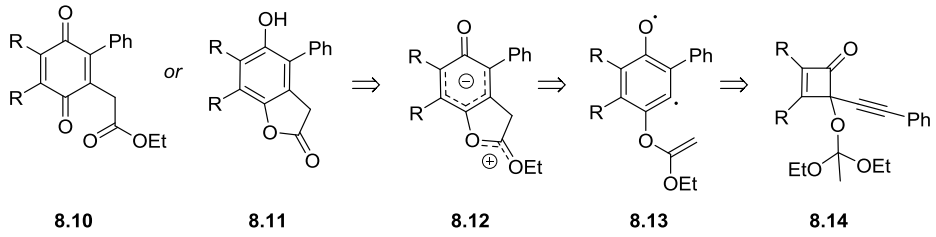

Scheme 8.3. Investigation of new reactions involving the orbital isomer switch from diradical to zwitterionic intermediates.

- The selectivity of organolithium additions to cyclobutenediones could be extended to larger systems such as the addition of phenyllithium to cyclobutenones. Further calculations of free Gibbs energies at -78 ^{o}C could provide a deeper understanding of factors that influence selectivity in the addition of nucleophiles. In the laboratory, experiments using PMDT and HMTETA as additives to organolithium reagents could also prove the value

and applicability of DFT predictions in designing new organometallic reactions.

Chapter 9: Description of Computational Methods

LIVE PURE, SPEAK TRUE, RIGHT WRONG, FOLLOW THE KING...
ELSE, WHEREFORE BORN.....
ALFRED TENNYSON

Molecular properties like geometries, energies, and frequencies can be calculated mathematically based on traditional quantum chemical methods, ranging from semi-empirical to sophisticated and expensive post Hartree-Fock methods. In these methods an electronic wavefunction which depends on 4N coordinates (3N spatial and N spin) for an N-electron system is used as a basic variable. However, many times being inapplicable for real-world problems as desired, accuracy can only be achieved for small systems. To model larger systems an alternative less expensive approaches were developed from which functional theory (DFT) has been found to be useful as a general tool in organic reactions study. In DFT, the electron density function $\rho(r)$ is used to calculate the properties of the system as it depends on only three spatial coordinates. In this thesis, mainly the hybrid DFT functionals B3LYP[147a, 75b, 76, 147b] and M06-2x[91] were used in most reaction mechanism calculations. A brief discussion of HF, post-HF and DFT will be presented in this chapter. A more comprehensive description of quantum chemical methods is available in standard textbooks.[148]

9.1 General overview of quantum mechanical methods

9.1.1 The Schrödinger equation

The Schrödinger equation is the fundamental equation of quantum mechanics.[149] This equation establishes a link between the energy and the wavefunction of the system and can be written as eigenvalue equation:

$$\hat{H}\Psi = E\Psi.$$

[Equation 1]

For a molecular system, the Hamilton operator $\hat{H}$ contains kinetic and potential energy terms for the nuclei (α, β) and electrons (i, j), and is represented by:

$$\hat{H} = -\sum_i \frac{\hbar^2}{2m_e}\nabla_i^2 - \sum_\alpha \frac{\hbar^2}{2m_\alpha}\nabla_\alpha^2 - \frac{1}{4\pi\varepsilon_0}\sum_{i,\alpha}\frac{eZ_\alpha}{r_{i,\alpha}} + \frac{1}{4\pi\varepsilon_0}\sum_{i>j}\frac{e^2}{r_{i,\alpha}} + \frac{1}{4\pi\varepsilon_0}\sum_{\alpha>\beta}\frac{Z_\alpha Z_\beta}{r_{i,\alpha}}.$$

[Equation 2]

However, for solving the Schrödinger equation for a system with more than two particles, specific approximations are needed. In 1927 Born and Oppenheimer suggested an approximation based on adiabatic separation of electronic and nuclear part.[150] This approach generalized later by Born and Huang[151] is based on large mass difference between the nuclei compared to the electrons, though electrons can be treated as moving in a fixed nuclear framework. This simplifies Hamilton operator and the interactions between the electrons and the nuclei are treated as a static external potential (V_N). This approach simplify the electronic Schrödinger equation of Eqn. 1 and can be written as

$$\left(\hat{H} + \mathrm{V}_N\right)\Psi_{el}(r_i; R_i) = E_{el}\Psi_{el}(r_i; R_i)$$

[Equation 3]

which depends on the electrons (r_i) and where the coordinates of the electrons depend only parametrically on the nuclear coordinates R_i. The Born-Oppenheimer is a good approximation to the molecular electronic Schrödinger. Moreover, it provides practically the only way to calculate a molecular potential energy surface and molecular structure. However this approximation is not appropiate in case of proton tunneling and excited state dynamics, which play an important role in chemical reactions.[152]

9.1.2 The Hartree-Fock method

The electronic Hamiltonian can be described by a sum of one-electron Hamiltonians

$$\widehat{\boldsymbol{H}} = \sum_{\boldsymbol{i}}^{\boldsymbol{N}} \widehat{\boldsymbol{h}}_{\boldsymbol{i}}.$$

[Equation 4]

Then the electron-electron repulsion is neglected or included in some average way. The one-electron Hamiltonians $\hat{h}_i$ would then satisfy the corresponding one-electron Schrödinger equation:

$$\widehat{\boldsymbol{h}}_{\boldsymbol{i}}\boldsymbol{\psi}_{\boldsymbol{i}} = \boldsymbol{\varepsilon}_{\boldsymbol{i}}\boldsymbol{\psi}_{\boldsymbol{i}}.$$

[Equation 5]

Inserting these conditions in the Schrödinger equation gives for the wave-functions

$$\boldsymbol{\Phi}(\boldsymbol{x}_1, \boldsymbol{x}_2, \dots, \boldsymbol{x}_N) = \boldsymbol{\Phi}(\boldsymbol{x}_1)\boldsymbol{\Phi}(\boldsymbol{x}_2), \dots, \boldsymbol{\Phi}(\boldsymbol{x}_N).$$

[Equation 6]

This many-electron wave-function is denoted as the Hartree product.[153] In the Hartree method[153] the energy is acquired by variationally minimizing Φ,

$$\boldsymbol{E} = \frac{\int \boldsymbol{\Phi}^* \widehat{\boldsymbol{H}} \boldsymbol{\Phi} \boldsymbol{dx}}{\int \boldsymbol{\Phi}^* \boldsymbol{\Phi}\, \boldsymbol{dx}}.$$

[Equation 7]

The weakness of the Hartree product is that it violates a property of fermionic particles. The wave-function of fermions is antisymmetric with respect to interchange of two electrons, which is known as the Pauli exclusion principle.[154] In order to satisfy that antisymmetric nature J.C. Slater introduced a determinant relation[155]

$$\boldsymbol{\Phi(x_1, x_2, \dots, x_N)} = \frac{\mathbf{1}}{\sqrt{N!}} \begin{vmatrix} \chi_1(x_1) & \chi_2(x_1) & \dots & \chi_N(x_1) \\ \chi_1(x_2) & \chi_2(x_2) & \dots & \chi_N(x_2) \\ . & . & . & . \\ . & . & . & . \\ \chi_1(x_N) & \chi_2(x_N) & \dots & \chi_N(x_N) \end{vmatrix}.$$

[Equation 8]

In this determinant the electrons are described by the spin-orbitals χi, which are products of space and spin parts of the electrons and are represented by the columns. The coordinates of a particular electron is represented by the rows. Thus antisymmetric nature is satisfied by an interchange of two electrons corresponding to the interchange of two rows of the determinant, which consequently changes the sign of the wave-function.

The Hartree-Fock method employs the Slater determinant[156] and resultant nonlinear equations are solved iteratively in the self-consistent field (SCF) procedure. The initial guess orbitals can be obtained from semi-empirical approaches. The Hartree-Fock equation can be written as

$$\hat{\boldsymbol{F}}(\mathbf{1})\boldsymbol{\Phi_i}(\mathbf{1}) = \boldsymbol{\varepsilon_i}\boldsymbol{\Phi_i}(\mathbf{1}),$$

[Equation 9]

in which the employed effective one-electron Fock operator is expressed as

$$\hat{\boldsymbol{F}}(\mathbf{1}) = \hat{\boldsymbol{h}}(\mathbf{1}) + \sum_{\boldsymbol{i}}^{\boldsymbol{N/2}} \left[2\hat{\boldsymbol{J}}_{\boldsymbol{i}}(\mathbf{1}) - \boldsymbol{K_i}(\mathbf{1})\right]$$

[Equation 10]

and

$$\hat{h}(1) = -\frac{1}{2}\nabla_1^2 - \sum_M \frac{Z_M}{r_{1M}}$$

[Equation 11]

$$\hat{J}(1)\chi_a(1) = \frac{\int dx_2 \chi_b^*(2)\chi_b(2)}{r_{12}}\chi_a(1)$$

[Equation 12]

$$\hat{K}(1)\chi_a(1) = \frac{\int dx_2 \chi_b^*(2)\chi_a(2)}{r_{12}}\chi_b(1)$$

[Equation 13]

were $\hat{J}$ and $\hat{K}$ are the Coulomb and exchange operators, respectively. The Coulomb operator $\hat{J}$ describes the Coulombic interaction between electrons. The exchange operators $\hat{K}$ is a non-local operator considering the exchange of two particles describing the interaction which has no classical analogue. Hartree-Fock theory is able to describe 99% of the total energy. This is due to main field approximation were HF-method describes only average interaction of the electrons with each other. Unfortunately the remaining energy is critical for achieving required chemical accuracy (1 kcal/mol). Moreover, the method fails to describe the reduced probability of finding one electron in the neighbourhood of another electron, so-called the Coulomb cusp of the wave-function. This lost by HF-method energy which is a difference between the HF-method and the exact energy is referred to as the correlation energy.[157] Moreover, this energy can refer to the dynamic correlation energy which is due to the correlated movement of electrons and static correlation energy which is due to limitation of the single determinant description of the wave-function.

It is possible to introduce empirically parameters to Hartree-Fock formalism. The use of proper training set and further approximations allow employing less demanding basis set and some inclusion of electron correlation effects. The advantage of this method is the ability to treat large systems where the Hartree-Fock method even with modest basis set is beyond reach.

9.1.3 Beyond HF-theory

The way to improve the HF-method is to include electron excitations perturbatively. This approach assumes that the HF wave-function is relatively close to the exact wave-function. The second-order energy correction, according to Møller-Plesset perturbation theory[82] can be written as

$$E_{MP2}^{(2)} = \frac{1}{4} \sum_{i,j,a,b} \frac{|\langle ab||ij\rangle|^2}{\epsilon_i + \epsilon_j - \epsilon_a - \epsilon_b}.$$

[Equation 14]

The i, j refer to occupied orbitals and a, b refer to unoccupied orbitals. The $|\langle ab||ij\rangle|$ is equivalents to $|\langle ab|ij\rangle| - |\langle ab|ji\rangle|$, which corresponds to the effect of Coulomb and exchange operators. In the MP2 theory only two-electron excitations contribute to total energy.

In order to increase performance, the computational cost can be reduced by including only excitations in the valence orbitals as the core excitations have minor contribution to total energy. The higher order MP*n* series introduces a significant higher computational cost.[158] In addition, some properties such as dispersion forces, which are important in van der Waals interaction, are described reasonably well with MP2 theory which is a known failure of DFT methods. However higher computational cost of MP2 make this approach less attractive than DFT.

A higher accuracy of method can be achieved when description of the electron correlation includes singly, doubly, triply, ..., etc. excited determinants in the calculation. However the gain accuracy came with higher computational cost which is a bottleneck for many chemical problems. The Configuration Interaction (CI)[159] approach is based on a linear combination of the excited determinants. Second approach Coupled Cluster (CC)[160] is based on an exponential ansatz and is widely used due to its size-consistency.[161] Special attention gain the CCSD(T) method including single, double excitations with perturbation triples correction.[162] This method is considered as gold standard and gives good certainty of chemical accuracy at complete basis set limit i.e. CCSD(T)/CBS.[163] It can be however unreliable if the

system possesses a significant multi-configurational character which can be verified by inspection of T1 diagnostic.[94]

The high quality CCSD(T) data at complete basis set limit (CBS) are computer time consuming tasks. In order to improve performance of basis set convergence, explicit correlation methods were developed. Those so-called CCSD(T)-F12x approaches are able to yield complete basis set quality data.[164] This approach is able to produce reaction energies with chemical accuracy using only valence-double-ζ basis sets. Further method performance can be achieved by localisation of molecular orbitals. For example so-called DF-LCCSD(T0)-F12 method is applicable to molecules with up to 61 atoms with chemical accuracy.[165]

When the molecular system is a combination of several important electronic configurations i.e. with a significant multi-configurational character, the methods described above will fail. For those systems, the Multi-Configurational Self-Consistent Field (MCSCF) approach should be employed. In that method, the orbital coefficients are optimized simultaneously in addition to the CI coefficients. The most important MCSCF method is the Complete Active Space SCF (CASSCF), in which the orbitals (space) are divided into inactive, which are fully occupied, virtual orbitals, and active orbitals, with vary occupation. With that defined orbital space a full CI-calculation is performed.[166] This approach provides the appropriate treatment of system with static correlation. The dynamical electron correlation can be recovered in CASSCF by including electron excitations perturbatively. This is achieved in the CAS second order perturbation theory (CASPT2) method.[167] This is analogous to the MP2 perturbation for the HF-wave function, but instead of the HF-wave function, a CASSCF wave function is employed. There are also different approaches to treat dynamical electron correlation formulation in multireference methods known like MRMP2[168] MRCI and NEVPT.[169]

9.1.4 Density functional theory (DFT)

9.1.4.1.1 Hohenberg-Kohn theorems

Employing electron density rather than wavefunction is appealing due to its much less coordinate dependence. However, only after the paper written by Hohenberg and Kohn in 1964[170] a unique relationship between the electron density ρ(r) and all fundamental properties of a given system was formulated. Within the Born-Oppenheimer approximation, the electronic Schrodinger equation is written as below:

$$\widehat{\boldsymbol{H}}_{\boldsymbol{elec}}\boldsymbol{\psi}_{\boldsymbol{elec}}(\boldsymbol{r}_{\boldsymbol{i}},\boldsymbol{R}_{\boldsymbol{A}}) = \boldsymbol{\varepsilon}_{\boldsymbol{elec}}\boldsymbol{\psi}_{\boldsymbol{elec}}(\boldsymbol{r}_{\boldsymbol{i}},\boldsymbol{R}_{\boldsymbol{A}})$$

[Equation 15]

where the Hamiltonian is the operator corresponding to the total energy of the system is expressed as:

$$\widehat{\boldsymbol{H}}_{\boldsymbol{elec}} = -\sum_{\boldsymbol{i=1}}^{\boldsymbol{N}}\frac{\mathbf{1}}{\mathbf{2}}\boldsymbol{\nabla}_{\boldsymbol{i}}^{\mathbf{2}} - \sum_{\boldsymbol{i=1}}^{\boldsymbol{N}}\sum_{\boldsymbol{A=1}}^{\boldsymbol{M}}\frac{\boldsymbol{Z}_{\boldsymbol{A}}}{\boldsymbol{r}_{\boldsymbol{iA}}} + \sum_{\boldsymbol{i=1}}^{\boldsymbol{N}}\sum_{\boldsymbol{j>1}}^{\boldsymbol{N}}\frac{\mathbf{1}}{\boldsymbol{r}_{\boldsymbol{ij}}}.$$

[Equation 16]

The second term in the Hamiltonian (external potential v(r)) is the one that is system-dependent. For known v(r), then $\widehat{H}_{elec}$ and ψ_{elec} are determined, and ρ(r) is obtained as integral which represents a functional of v(*r*) and ψ_{elec}:

$$\boldsymbol{\rho}(\mathbf{r}) = \boldsymbol{N}\int \ldots \int |\boldsymbol{\Psi}(\boldsymbol{x}_{\mathbf{1}},\boldsymbol{x}_{\mathbf{2}} \ldots \boldsymbol{x}_{\boldsymbol{N}})|^{\mathbf{2}}\boldsymbol{dx}_{\mathbf{1}}\,\boldsymbol{dx}_{\mathbf{2}} \ldots \boldsymbol{dx}_{\boldsymbol{N}}.$$

[Equation 17]

Hohenberg and Kohn[170] proved in the first theorem that v(*r*) and ψ_{elec}. are unique functionals of ρ(*r*) by so-called *reductio ad absurdum*. It was shown that two external potentials, differing by more than one additive constant, cannot give the same ground state electron density. Strictly speaking the external potential v(*r*) is a unique potential of ρ(*r*). Consequently, the ground state electron density $\rho_0(r)$

determines all ground state properties, like N, v(r), ψ_0 and E0. The ground state electronic energy can be expressed as

$$\mathbf{E[\rho] = V_{ne}[\rho] + T[\rho] + V_{ee}[\rho]}$$

[Equation 18]

where V_{ee}, V_{ne}, T are terms from electron-electron interactions, nuclear potential, and kinetic energy, respectively. The second theorem proves that for any trial, electron density function ρ(r), satisfied conditions $\rho(r) \geq 0$, $\int \rho(r)dr = N$ and:

$$\boldsymbol{E_0 \leq E[\rho(r)]}.$$

[Equation 19]

where E_0 is the true ground state energy. The second theorem delivers the energy variation principle. These two theorems provide the theoretical establishment of using ρ(r) rather than ψ to calculate all ground state properties. However, they do not define a mathematical form of the universal functional.

9.1.4.1.2 Kohn-Sham approach

The universal functional was proposed in 1965 by Kohn and Sham.[171] They approach the unknown universal functional by introducing the concept of a non-interacting reference system constructed from a set of one-electron orbitals, so-called Kohn-Sham orbitals ϕ_i^{KS}. In this approach, the kinetic energy term T is expressed by the kinetic energy (T_S) of a non-interacting reference system (with the same density as the real system) and a small correction term T_C due to electron-electron interaction:

$$\boldsymbol{T[\rho] = T_s[\rho] + T_c[\rho]}$$

[Equation 20]

Also the electron-electron repulsion term (V_{ee}) can also be divided into two parts: the classical charge-cloud coulomb repulsion (J) and a non-classical electron-electron repulsion (E_{ncl}), containing exchange and correlation:

$$\boldsymbol{V_{ee}[\rho] = J[\rho] + E_{ncl}[\rho]}$$

[Equation 21]

where charge-cloud coulomb repulsion (*J*) is described by:

$$\boldsymbol{J[\rho] = \frac{1}{2}\iint \frac{\rho(r_1)\rho(r_2)}{r_{12}} dr_1 dr_2.}$$

[Equation 22]

In the Kohn-Sham scheme, the two unknown terms ($T_c[\rho]$ and $E_{ncl}[\rho]$) are incorporated as exchange-correlation functional $E_{xc}[\rho]$ as follow:

$$\boldsymbol{E_{xc}[\rho] = T_c[\rho] + E_{ncl}[\rho],}$$

[Equation 23]

which is then divided into two parts, exchange $E_x[\rho]$ and correlation $E_c[\rho]$ leading to:

$$\boldsymbol{E_{xc}[\rho] = E_x[\rho] + E_c[\rho].}$$

[Equation 24]

In that way combining equations 20 to 24, gives us energy expressed as:

$$\mathrm{E}[\rho] = \mathrm{V_{ne}}[\rho] + \mathrm{T}[\rho] + \mathrm{V_{ee}}[\rho]$$
$$= \mathrm{V_{ne}}[\rho] + (T_s[\rho] + T_c[\rho]) + (J[\rho] + E_{ncl}[\rho])$$
$$= T_s[\rho] + J[\rho] + E_{xc}[\rho] + \mathrm{E_{ne}}[\rho]$$
$$= T_s[\rho] + \frac{1}{2}\iint \frac{\rho(r_1)\rho(r_2)}{r_{12}} dr_1 dr_2 + E_{xc}[\rho] + \int V_{Ne}\rho(r)dr =$$

$$= -\frac{\boldsymbol{1}}{\boldsymbol{2}}\sum_{\boldsymbol{i}}^{\boldsymbol{N}} \langle \boldsymbol{\varphi_i^{KS}} | \boldsymbol{\nabla^2} | \boldsymbol{\varphi_i^{KS}} \rangle$$
$$+ \frac{\boldsymbol{1}}{\boldsymbol{2}}\sum_{\boldsymbol{i}}^{\boldsymbol{N}}\sum_{\boldsymbol{j}}^{\boldsymbol{N}} \iint \left|\boldsymbol{\phi_i^{KS}(r_1)}\right|^2 \frac{\boldsymbol{1}}{\boldsymbol{r_{12}}} \left|\boldsymbol{\phi_i^{KS}(r_2)}\right|^2 \boldsymbol{dr_1 dr_2}$$
$$+ \boldsymbol{E_{xc}[\rho]} - \sum_{\boldsymbol{i}}^{\boldsymbol{N}} \int \sum_{\boldsymbol{i}}^{\boldsymbol{N}} \frac{\boldsymbol{Z_A}}{\boldsymbol{r_{1A}}} \left|\boldsymbol{\varphi_i^{KS}(r_1)}\right|^2 \boldsymbol{dr_1}.$$

[Equation 25]

Constructing a Slater determinant from $\varphi_i^{KS}$and minimizing the total energy under the normalization constraint of $\langle \varphi_i^{KS} | \varphi_i^{KS} \rangle = \delta_{ij}$ leads to the Kohn-Sham equation:

$$\left(-\frac{1}{2}\nabla^2 + V_{eff}(r_1)\right)\phi_i^{KS} = \varepsilon_i \phi_i^{KS}$$

[Equation 26]

where

$$V_{eff}(r_1) = \int \frac{\rho(r_2)}{r_{12}} dr_2 + V_{XC(r_1)} - \sum_A^M \frac{Z_A}{r_{1A}}$$

[Equation 27]

and

$$V_{XC} = \frac{\delta E_{XC}}{\delta \rho}.$$

[Equation 28]

The $V_{eff}(r_1)$ is dependent of electron density and thus equation 26 can be solved iteratively. This equation would yield the exact energy and electron density in case the exact mathematical form of the V_{XC} is known. The approximations of The Kohn-Sham method, which is in principle exact, come from the formulation of exchange-correlation functional. There is no systematic strategy to improve approximate functionals and new better functionals are in constant development.

Initially introduced local density approximation (LDA) is based on assumption that the exchange-correlation energy at any point is only the electron density dependent at that point.[172] This assumption is appropriate for systems with gradually varying densities. Moreover overestimates binding energies and thus their performance are inappropriate to use when studying chemical reactions.

Next step in functional ladder (so-called Rung 2) is generalized gradient approximation (GGA) which introduces the dependence on the gradient of the density in the exchange correlation energy:

$$\boldsymbol{E_{xc} = \int F(\rho, \nabla\rho)\, dr.}$$

[Equation 29]

Introducing a higher order density gradient leads to the meta-GGA (so-called Rung 3) methods.[173a, b, 75b, 173c] This provides a better description for real systems, as those always have a spatially varying density.[174] Significant improvement was suggested in 1993, when Becke suggested a hybrid functional. This approach mixes a fractional of the exact exchange from Hartree-Fock and introduces three empirical parameters. This hybrid GGA functional, named B3LYP[147a, 75b, 76, 147b] is usually expressed as:

$$\boldsymbol{E_{XC}^{B3LYP} = (1-a)E_X^{Slater} + aE_X^{HF} + bE_X^{B88} + (1-c)E_C^{VWN} + cE_C^{LYP}.}$$

[Equation 30]

Slater E_X^{Slater} is the Dirac-Slater exchange corresponding to the uniform electron gas, E_X^{HF} is the Hartree-Fock exchange, $E_X^{B88}$is the gradient correction to exchange,[173b] E_C^{VWN} and E_C^{LYP} are the correlation functionals of Vosko, Wilk and Nusair[147a] and Lee, Yang, and Parr[75b] respectively. The three parameters a, b and c are 0.20, 0.72 and 0.81, respectively. Generally hybrid functionals represents substantial improvement for description of chemical thermodynamic and kinetics.

Another functional widely used in this thesis is more sophisticated M06-2X from family of Minnesota Functionals.[91] This meta-hybrid GGA functional has high exchange 54% of Hartree-Fock exchange and 35 parameters. It introduces the Laplacian dependencies in the exchange correlation energy:

$$\boldsymbol{E_{xc} = \int F(\rho, \nabla\rho, \nabla^2\rho)\, dr.}$$

[Equation 31]

However, evaluation of the Laplacian is numerically challenging. For that reason the tau (τ) was introduced which represents kinetic energy density for the occupied Kohn-Sham orbitals ϕ_i^{KS}:

$$\boldsymbol{\tau_\sigma(r) = \frac{1}{2}\sum_i^{occ.} \left|\nabla\phi_i^{KS}\right|^2.}$$

[Equation 32]

The M06-2X represent substantial improvement over B3LYP and is recommended for applications involving main-group thermochemistry, kinetics, non-covalent interactions, and electronic excitation. The M06-2X has a very good response under dispersion forces, which is remarkable improvement over DFT methods like B3LYP. However its performance comes together with greater computational cost and larger sensibility to integration grid than B3LYP.[92]

9.1.5 Basis set

In general, a basis set is used to perform a quantum chemical calculation and represent a mathematical description of the orbitals within a molecular system. In a Linear Combination of Atomic Orbital (LCAO) approximation the molecular orbitals Ψ_i are expressed as a linear combination of functions known as basis functions $\phi_\mu = (1,2,\dots \mathrm{N})$. Generally those are pre-defined set of one-electron functions and are nuclear cantered:

$$\boldsymbol{\Psi = \sum_{\mu=1}^{N} c_\mu \phi_\mu}\,.$$

. **[Equation 33]**

Each atom within a molecule has basis functions assigned to approximate its orbitals. The best fitting for that purpose are Slater type (STOs) functions which are characterized by exponential $-\xi r$ term:

$$\boldsymbol{\phi_\mu = N_j(x,y,z)e^{-\xi r}}$$

. **[Equation 34]**

However, Gaussian type functions (GTF) were introduced instead of Slater type (STO) for the electronic orbital in LCAO wave function to improve the molecular integral calculations. Gaussian type functions are characterized by exponential $-\alpha r^2$ term:

$$\boldsymbol{\phi_\mu = N_j(x,y,z)e^{-\alpha r^2}},$$

[Equation 35]

even though the Gaussian type functions do not describe atomic orbitals as good as STOs. To overcome such limitation, individual basis functions are constructed from a linear combination of Gaussian type functions:

$$\phi_\mu = \sum_k d_{\mu k}\, g_k$$

[Equation 36]

where the $d_{\mu k}$ represents fixed coefficients and g_k represents the individual functions, which are all of the same type. Basis functions ϕ_μ constructed in that way are known as "contracted" Gaussians and individual Gaussian functions g_k are known as primitives. "uncontracted" is referred to a basis function consisting of a single Gaussian function. Considering number and types of Gaussian functions range of basis sets may be classified, as follows: (1) Minimal basis set (2) Split valence basis set (3) Polarized basis set (4) Diffuse function.

9.1.5.1.1 Minimal Basis Sets

Minimal basis set uses fixed atomic-type orbitals with the minimum number of AO basis functions and maintaining the overall spherical symmetry. The widely used minimal basis set STO-3G[175] employs three Gaussian primitives (3G) per basis functions and "STO" stands for Slater-type atomic. However, this does not give an even satisfying accuracy and further improvement is needed.

9.1.5.1.2 Split Valence Basis Sets

In split valence basis sets additional basis functions are assigned to each valence atomic orbital. Split valence basis sets are characterized by the number of functions allocated to valence orbitals. The popular double zeta basis set proposed by Pople *et al.*[175] is typically designated as X-YZ*G*, where X is the number of primitive Gaussians describing the core orbitals and, Y and Z numbers are representing the valence orbitals. The *G* stands for Gaussian type basis functions. The example of that is double zeta basis set like 6-31G.[176] Variation with three numbers representing the valence orbitals, indicate triple zeta basis set. The variety of split

valence basis sets was developed in base of different philosophy. Further flexibility of basis set towards better performance is achieved by addition of polarization functions.

9.1.5.1.3 Polarized Basis Sets

Split valence basis set allows orbitals to adjust their size, but does not allow to change shape. Polarized basis set overcame this limitation by adding orbitals with an angular momentum beyond what is required for the description of each atom. This allows distorting orbitals in molecular environment from their original atomic shape. Polarization functions are important to describe bonds because they provide flexibility needed to describe regions between bonded atoms. Popular, 6-31G(d) basis set, is formed by adding d polarization function to all the heavy atoms (i.e. non-hydrogen atoms). The 6-31G(d,p)[176-177] extension, is formed from the 6-31G(d) basis set plus addition of p polarization functions to hydrogen atoms. This polarisation scheme can be expanded to high angular momentum basis set like 6-311G(2df,2pd),[178] which represent triple zeta basis set and besides the (311) valence functions two d functions and one f functions are added to heavy atoms, and two p and two d function are added to the hydrogen atom. Some special basis sets like correlation consistent basis sets were designed to converge systematically to the complete basis set (CBS) limit. This is achieved by extrapolation techniques using empirical parameters.[179] Those basis sets are cc-pVNZ where N=D,T,Q,5,6,... (D=double, T=triples, etc.). The cc stands for correlation-consistent, p stands for polarized and the V indicates they are valence-only basis sets.

9.1.5.1.4 Diffuse Basis Sets

To properly described electron density far away from the nuclear centres (e.g. anions, lone pairs, and excited states) diffuse functions are required. They allow orbitals to relax and occupy a larger region of space in order to improve description of weakly bounded electrons. Diffuse basis sets are recommended for calculations of electron affinities, proton affinities, inversion barriers, bond angles and anions. The addition of diffusion function to heavy atoms in popular, 6-311G(d,p) basis set, is designated by addition of plus symbol "+" to form 6-311+G(d,p) basis set. The

addition of diffusion function to all atoms is represent by two "+"symbols, like in 6-311++G(d,p) basis set.[178]

9.1.5.1.5 Final considerations regarding basis sets

A sufficiently large basis set should always be considered in energy calculations. In order to reduce the computational cost, many times smaller basis sets are employed, principally for geometry optimization. For DFT calculations the basis set convergence is reached usually quite fast. Correlated calculations such as MP2, coupled-cluster (CC) and double hybrid DFT (DH-DFT) often require a much larger basis set to reach their potential.

9.1.6 Transition state theory

Transition state theory (TST)[95] was developed by Eyring, Polanyi, and Evans. It is a statistical mechanical theory of reaction rate constants used in the interpretation of elementary chemical reactions. The TST is also referred to as "activated-complex theory," "absolute-rate theory" and "theory of absolute reaction rates". The theory was derived based on the following assumptions: (1) The reaction proceed via lowest energetic path with its energetic maximum called transition state, (2) The transition state species are in equilibrium with reactants and follows the Boltzmann distribution law, (3) The nuclear motion along the reaction coordinate is electronically adiabatic and can be described by classical mechanics and kinetic theory can be used to calculate the rate of this conversion.[180] The reaction rate constant (k) can than be expressed as:

$$\boldsymbol{k = \frac{k_b T}{h} e^{-\frac{\Delta G^{\ddagger}}{RT}}}$$

[Equation 37]

where $k_b, h, R, \Delta G$ and T are Boltzmann constant (3.2983×10^{-27} kcal/mol), Planck's constant (1.58365×10^{-37} kcal/s), gas constant (1.987207×10^{-3} kcal mol^{-1} K^{-1}), Gibbs free energy change from reactant to transition state (in kcal/mol) and absolute temperature (in Kelvin), respectively. At room temperature (298.15 K) a 1st order reaction rate constant of 1 s^{-1} corresponds to a Gibbs free energy barrier of 17.4 kcal/mol. However the reaction rate constant decreases by an order of magnitude (~10 times) if this $\Delta G^{\ddagger}$ barrier is increased by 1.4 kcal/mol. This equation has similar formula to earlier proposed Arrhenius equation and moderately agrees with its rule of thumb that the reaction rate doubles for every 10 ^{o}C increase in temperature. For reactions in room temperature the calculated *in silico* reaction rate constant can be compared with the experimental measured kinetic data, if available. A too high calculated Gibbs free energy often implies that either the assumed mechanism is wrong or that the considered model is not appropriate. Generally, the Gibbs free energy barrier $\Delta G^{\ddagger} = \Delta H^{\ddagger} - T\Delta S^{\ddagger}$ is used to derive the reaction rate constant. However, in some parts of this work only the electronic energy was taken

into account. The entropy and enthalpy effects cannot be calculated accurately with the cluster model which uses mixture of explicit and implicit solvent.

Further insights to understanding of transition state geometry was postulated by George S. Hammond.[181] The hypothesis helps to understand the structure of transition state which cannot be directly characterized. The postulate states that species with close energies along the reaction co-ordinate will have close structures. This permits to discuss the structure of the transition state in terms of the reactants, intermediates or products. In the case where the transition state closely looks like reactants, the transition state is called "early" while a "late" transition state is the one that is similar to the intermediate or the product.[182]

Also related, the Hammond postulate Curtin–Hammett principle is useful in qualitative analysis of multistep chemical reactions.[183] It applies for a reaction which has a pair of reactive intermediates or reactants that fast interconvert and both go irreversibly to a distinctive product. The equilibrium distribution of the two intermediates will not necessarily govern the product ratio. Though, the observed product ratio will depend on the difference in energy between the energy of the transition state to form each product.

9.2 Practical consideration of quantum mechanical methods in calculations

9.2.1 Techniques involved in locating transition state

One of the most challenging tasks in reaction mechanism studies is to find the transition state which connects desired reactant with appropriate product. The task turns to be more complicated if reaction occurs via unknown path and involved range of possible conformations. One simple approach is based on the Synchronous Transit-Guided Quasi-Newton method.[184] This applies a linear synchronous transit or quadratic synchronous transit approach to guess an initial structure close to the transition state. Then attempt with quasi-Newton optimizations algorithm is used to locate transition state geometry. In this method, the reactant and product geometries are used to generate the guess of transition state geometry. This scheme has good performance for simple reactions, however is problematic to apply for complex transformations. Moreover, it cannot guarantee that the geometry found is the right one, i.e. which connects the reactant and product via the lowest energy path. An alternative method is focused on a main reaction coordinate, like bond distances, bond angles, or dihedral angles. In that way reaction energy profile can be plotted as a function of the reaction coordinate and related energy. The point with the highest energy is believed to be close to transition state though can be used as a starting point for transition state searching. Usually a Hessian is needed to guarantee smooth and successful transition state optimizations. It is preferable to calculated it in analytically rather than numerically fashion to avoid numerical artefact. These calculations can be very time consuming or prohibited for large systems. For that reason usually optimization of transition state geometry is performed stepwise, refining geometry from low to higher level of theory. Furthermore if guess transition state geometry for large systems contains number of low or imaginary frequency modes this approach can be challenging. An alternative cheaper approach requires calculation of local Hessian, in which the second derivatives of energy are calculated numerically on pre-defined fragment of molecule.

In order to confirm character of transition state, intrinsic the reaction coordinate (IRC) calculation has to be performed.[185] This is special case of the minimum

energy path (MEP) calculations in which it is possible to verify reaction path from reactant, transition state, to product. Such approach uses Hessian at transition state and is computational expensive.

9.2.2 Performance of DFT methods

In this thesis, the popular hybrid functionals B3LYP[147a, 75b, 76, 147b] and M06-2x[91] are used to investigate the reaction mechanisms. Various assessments have been reported in the literature addressing the accuracy and performance of both methods. A study of reaction mechanisms requires accurate the two crucial properties: geometries and energies. The geometry is one of the most important as on larger system and generally DFT methods are applied. This is due to the large computational cost of gradients and Hessians calculation. If required, an accurate energy can be obtained by more sophisticated methods on geometry from DFT. In this chapter the performance of DFT and some *ab-initio* methods are discussed towards application to organic reaction mechanisms.

9.2.2.1.1 Know limitations of DFT

The density functionals have widespread popularity but, as *ab-initio* method, possess some shortage. Origins of some artefacts are known which can yield large errors. The three main recognized deficiencies are self-interaction error, near-degeneracy error and lack of dispersion treatment. Yang and co-workers proposed that delocalization errors and static correlation errors lead to the failures of approximate density functionals.[186] Their performed study on system, such as H_2^+ where functionals failed to describe properly dissociation path. For system with one electron, exchange energy is expected to cancel the Coulomb energy as electron-electron interaction is absent. When H_2^+ dissociates, the system converges to artificial delocalized state with each centre holding half electron ($H^{0.5+}$ + $H^{0.5+}$), rather than the correct localized state ($H + H^+$). This wrong behaviour of DFT was attributed to fact that the delocalized state is favoured, as displays less self-interaction, which is repulsive. This creates the error of bond dissociation energy of 55 kcal/mol at the B3LYP/6-311G(d,p) level. For systems with many-electrons, this tendency to *spread out* the electron density artificially is called delocalization error.

This causes inappropriate description of systems with fractional charges and respectively wrong dissociation curve. Most approximate functionals yield an incorrect convex behaviour of dissociation curve. From the other side HF method gives an opposite concave comportment and suffers from localization error instead. As in the transition state geometries have electrons delocalized over more than one centre the delocalization error leans towards lower transition state energies. Therefore, generally DFT underestimates barrier heights. However, hybrids functional like B3LYP with additional HF exchange benefit from some error cancellation and improve barrier height calculations.

Because of the sing-determinant nature of approximate functionals covalent bonds are well described; however the bond dissociation energy is always overestimated. The exchange-correlation functional is local, thus it is unsuitable for accounting the long range static correlation. In contrast to delocalization error which lowers barrier heights, this error tends to raise barrier heights. It appears in many cases that some hybrid functional methods like B3LYP benefit from balancing those two errors. It should be noted that correct dissociation curve can be obtained from high level multi reference methods. Also known deficiency of B3LYP is a lack of description of van der Waals interaction. Due to this, for example π-stacking, like in DNA, cannot be accurately treated.[187] This deficiency pronounces in tendency for exaggerated repulsion. To address this problem an empirical correction has been suggested together with new DFT methods. These failures are not break-downs of the theory itself but show deficiencies of the present exchange-correlation functionals which are improving over time. The useful accuracy is still with range of present DFT functionals.

9.2.2.1.2 DFT performance towards geometries of organic compounds

The B3LYP usually performs well in the prediction of geometrical parameters. At B3LYP/6-311+G(3df,2p) level of theory within the G2 database set (55 small molecules, 71 bond lengths, 26 bond angles, and 2 dihedral angles) the average errors are 0.008 Å for bond lengths, 0.61^{o} for bond angles, and 3.66^{o} for dihedral angles.[188] According to the authors, at the modest 6-31G(d) basis set B3LYP yields better geometry than given by more computationally expensive MP2. Additionally

increasing the basis set improves results further. On the other hand it was noted that improving the basis set increases the error for the B3LYP approach for the dihedral angle in H_2O_2. This was rationalised by small errors in the energy which causes larger errors for the dihedral angles than it is observed for the bond lengths or bond angles. Moreover employing big, more tempered basis set than the 6-31G(d) is costly and does not dramatically improve the geometries.[189] Their study show that frequency acquired from B3LYP/6-31G(d) method need only 0.989 scaling factor to reproduce zero-point energies (ZPE).

Further extensive study on B3LYP in the course of development of composite complete basis set model chemistry, CBS-QB3 method,[190] shows that B3LYP yield good geometries for high accuracy methods. The benchmark including bond length (H_2, HF, OH, NH, N_2, CH, CO, O_2, CF and F_2) shows that performance B3LYP at 6-311G(d,p) yield RMS errors of only 0.0049 Å compared with more computationally expensive MP2 and QCISD which gives 0.0091 Å and 0.0052 Å RMS errors respectively. It was also noted that the B3LYP geometries do not improve significantly with larger basis sets like 6-311+G(2df,2pd). However errors at lower basis sets are significant for B3LYP, though still better than from MP2 and QCISD methods. Also their study show that frequency need to be scaled only by 0.99 to obtain appropriate ZPE with B3LYP at 6-311G(d,p). The study carried out during formulation of Gaussian-3 reveals that B3LYP/6-31G(d) geometry yields similar results as MP2 geometries compared with QCISD/6-31G(d).[191] Moreover compared to MP2 it improves the geometry of CN and O_2^+ but fails with species like CH_4^+, BF_3^+ and BCl_3^+.

In more recent studies from Gaussian-4 theory it was found that B3LYP with 6-31G(2df,p) is able to deliver appropriate value for ZPE when frequencies are scaled by 0.9854.[192] This differs from the original Gaussian-3 theory in which the geometries are calculated at the MP2 including all electron and 6-31G(d) basis set. In development of Gaussian-3X theory,[193] the use of the B3LYP geometries leads to an improvement in overall results compared to the MP2 geometries, which were previously used in initial formulation of Gaussian-1,[194] Gaussian-2,[195] and Gaussian-3[77] theories. Authors observed improvement of absolute deviation from 1.13 to 1.06 kcal/ which was related to better geometries overall. Nonetheless the poor performance for set of molecules with hydrogen bond was attributed to failure

of B3LYP/6-31G(2df,p) in predicting this geometries. In consequence average absolute deviation of 1.12 kcal/mol at the Gaussian-4 (B3LYP geometry) level increases compared to 0.60 kcal/mol at the Gaussian-3 (MP2 geometries) level for hydrogen bonded set. To heal that deficiency, addition of diffusion function (B3LYP/6-31+G(2df,p) geometries) reduces errors to 0.47 kcal/mol. Inappropriate geometries with B3LYP/6-31G(2df,p),[193] were also found for the Jahn-Teller distortions in the ions, as this also was observed for B3LYP/6-31G(d) geometries.[191]

The B3LYP geometry based composite method like Gaussian-3 (B3LYP/6-31G(d) geometry) and CBS-QB3 (B3LYP/6-311G(d,p) geometry) methods are able to predict the BDE with an accuracy of about 8.4 kJ/mol and therefore being a useful theoretical tool for BDE.[196] This value is close to 8.6 kJ/mol from MP2 based geometry composite methods which is for Gaussian-3 ((U)MP2(full)/6-31G(d) level geometry opt) and CBS-Q (U)MP2(FC)/6-31G* level optimization).[197] From other side, substantial improvement of bond dissociation energies (BDE) was observed when BMK geometries were employed in Gaussian-3 method instead of B3LYP.[198]

The benchmark performed during the development of W1 an W2 theory by Martin and Oliveira shows that B3LYP/VTZ+1 yields geometries are close enough to CCSD(T) geometry and do not cause a major effect on the final computed result.[199] The VTZ+1 differs from VTZ by an additional single high-exponent of d-type function for all second-row atoms. The CCSD(T) optimizations compared to B3LYP is extremely costly for larger molecules. However the situation changes if good geometry is required for radical or diradical were more computational expensive methods are required to appropriate treat dynamic and static correlation effects.[200]

The study performed by Zhao and Truhlar towards validation of M06 functional family shows that B3LYP can perform poorly with organometallic and metalorganic which is partially due to lack of dispersion.[91] This dispersion effect are necessary to properly describe large system like proteins and it is very important for larger system.[201] To address that deficiency Grimme and Steinmetz propose inclusion of dispersion effects to B3LYP/6-31+G(d,p) method via empirical parameters which can deliver geometrical data in agreement to CCSD(T).[202]

This conclude that, B3LYP is generally good for achieving required structural accuracy. In order to obtain very accurate, higher than CCSD(T), geometries multilevel geometry optimization were suggested. However due to larger computational cost their application lay within benchmarking rather that chemical applications.[203]

Interesting criticisms of B3LYP method were addressed in work of Grimme and co-workers were authors provide argument against application of B3LYP in thermochemistry.[204] Authors heal the B3LYP deficiencies with corrections for missing London dispersion and basis set superposition error (BSSE). New presented B3LYP-gCP-D3/6-31G(d) scheme is in the same black-box as previous B3LYP at similar computational cost with improved performance. In addition it was shown that the partial error compensation effects in the plain B3LYP/6-31G(d) model chemistry are unsystematic and strongly depend on the chemical nature of the molecular test set. The B3LYP-gCP-D3/6-31G(d) found to improve the transition state region analysed by PES. Similar strategy of additional correction was applied to Hartree–Fock in HF-3c scheme. In order to get accurate results three correction terms are applied for London dispersion interactions (D3 scheme), basis set superposition error (gCP scheme) and basis set incompleteness effects.[205] This method shows accurate geometries at low basis set and root-mean-square deviation (RMSD) errors were substantially improved over Hartree–Fock.

The ground state geometries are benchmarked to known experimentally values. Achieving accurate transition state geometries is a more challenging task as this cannot be directly measured by experiments. In studies performed by Lynch and Truhlar, high-level calculations of saddle point geometries were used to benchmark performance of DFT methods.[206] The performed study for four small transition state reactions:

$$Cl + H_2 \rightarrow HC1 + H$$

$$H + H_2 \rightarrow H_2 + H$$

$$H + ClH \rightarrow HC1 + H$$

$$OH + H \rightarrow H_2 + O.$$

shows that the B3LYP/6-31+G(d,p) performed poorly on geometry with RMSD of 0.12 Å compared with 0.06 Å, 0.06 Å, 0.03 Å, 0.02 Å from BH&HLYP

mPW1PW91 MPW1K and MP2 methods respectively. In addition it was found that B3LYP and mPW1PW9 methods tend to overestimate the sum of the bond distances for the forming and breaking bonds at the saddle point, so-called "looser saddle point". This is in contrast to MP2 which has the opposite trend.

Later Truhlar and co-workers[207] suggest the BB1K method, a 1-parameter model for kinetics which can give excellent saddle point geometries and barrier heights, better than competitive MPW1K. This performance is observed even at modest 6-31+G(d,p) basis set.

Further study of Truhlar and co-workers[80c] for transition states geometries and donor-acceptor distances show that *ab-initio* multi reference MRMP2 with active space from nominal correlated participating orbitals (nom-CPO) was performing remarkably. The MRMP2/nom-CPO with mean unsigned error (MUE) of 0.007 Å as compared to 0.018 Å for CCSD was the most recommended for such propose. From computationally cheaper methods the excellent MUE of 0.019 Å was observed for M06-2X, and 0.039 Å for MP2 and B3LYP.

Later Truhlar and co-workers performed extensive systematic study on 48 transition state geometries of small reactions with variety of the methods.[80d] It was observed that:

1) The MC3BB and MC3MPW doubly hybrid functionals and the M08-HX and M06-2X hybrid meta-GGAs are the best performing
2) M08-HX is the most recommended having a lower cost when compared to some best performing doubly hybrid functionals
3) The performance for barrier heights usually is related to accurate prediction of transition state geometries and respectively the bad performance for barrier heights is associated with less reliable prediction of transition state structures
4) A minimally augmented triple-ζ basis set, such as MG3S, ma-TZVP is recommended for all DFT methods
5) Due to a cancellation of errors, MP2 at 6-31+G(d,p) basis set gives better results than large basis sets
6) Tested methods like HF, BLYP, PM3, AM1, B97-D, B3LYP, B1LYP, B98, and M05 are not recommended for transition state geometry due to large errors

7) MP2 provides good geometry at modest 6-31+G(d,p) basis set due to cancellation of errors and systematic improvement is not observed if large basis set is employed
8) Desired higher accuracy for small transition states geometries can be acquired with BMC-CCSD and MRMP2/nom-CPO methods, however at substantial higher computational cost

Further insights towards reliability of transition structures geometries from DFT methods to organic chemical reaction were addressed by Simon and Goodman.[92c] This study differs significantly from previously discussed as it includes medium to large (>40 heavy atoms) geometries of nineteen covalent-bond forming transition state structure. Comparison of the results from HF, GGA, hybrid-GGA and hybrid meta-GGA leads to conclusion that B3LYP is only slightly less accurate than computationally more expensive alternatives. Their study also shows that B3LYP is less sensitive to choice of integration grid, being an appropriate method for studies of organic mechanism although more accurate energies can be obtained by hybrid meta-GGA functional.

9.2.2.1.3 Accurate energies

The DFT method was excessively benchmarked in the past. Having similar speed of Hartree–Fock at much higher accuracy it gained general interest. Various DFT methods were developed for calculation to aim specific molecular property. In calculation of reaction mechanism, accurate reaction barrier energies are more challenging than accurate reaction energies. In the past, few DFT functionals were developed for kinetics like BMK,[208] BB1K[208] and MPW1K[209] which overperform the B3LYP for energy barriers.

The Truhlar and co-workers show in *ab-initio* and DFT study for small (up to 3 heavy atoms) 19 non-hydrogen-transfer reactions that popular B3LYP method has a mean unsigned error of energy four times larger than BB1K.[210] Surprisingly more expensive *ab-initio*, QCISD method is outperformed by the BB1K, MPWB1K, MPWKCIS1K and MPW1K DFT methods and the QCISD(T) is the best *ab-initio* method for barrier height calculations. The best performing BB1K and MPWB1K are recommended for calculations of barrier height with MUEs of 1.3 and 1.4

kcal/mol, respectively. In their benchmark MPW1K is having mean unsigned error (MUEs) of 1.6 kcal/mol where B3LYP MUE of 4.4 kcal/mol systematically underestimate the energies.

In another study performed by Korth and Grimme[211] for thermodynamic benchmarking of B3LYP MAD of 6.6 kcal/mol is produced. The best performance (MAD of 4.1-4.2 kcal/mol) was found for double hybrid functionals (B2-PLYP-D and B2GP-PLYP-D), followed by the meta-hybrid M06-2X method (MAD of 4.8 kcal/mol). The CCSD(T)/cc-pV(D/T)Z method yield MAD of 2.8 kcal/mol compared with highly accurate all electron CCSD(T)/CBS estimates. Authors also pointed out that CCSD/cc-pVQZ is not better than the best meta-hybrids.

In another benchmark performed by Zhao and Truhlar addressed to exploration of the limit of accuracy of the density functionals for thermochemistry, kinetics, and non-covalent interaction, the new M08-HX functional, from Minnesota functional family, showed the best overall performance. This was tested with several databases considering: main-group atomization energies, large-molecule atomization energies, electron affinities, hydrogen-transfer barrier heights, heavy-atom transfer barrier heights, new benchmark barrier heights, non-covalent interaction energies in uracil trimers and multiplicity-changing excitation energies. The authors note that all new M08-2X, M08-SO, M06-2X, and M05-2X methods from Minnesota functional family show dramatic improvement on geometries. However none of those methods showed improvement upon B3LYP for frequencies. In the study M08-HX and M06-2X has MUE of only 0.79 and 0.87 kcal/mol where B3LYP has large 3.15 kcal/mol error in conformational energies performance. Also their study performed on barrier highs energies for small reactions took high accurate CCSD(T)/CBS data and focal point calculations as reference. Within the database M08-HX and M06-2X has MUE of 0.86 and 1.08 kcal/mol where B3LYP has 3.49 kcal/mol.

Some authors, because of poor performance, lead to the conclusion that B3LYP method should be abandoned.[212] The authors state that the “no-questions-asked” B3LYP status appears to be now dead and buried and should be replaced by new DFT methods.

In conclusion range of argument towards success and failure of the “zoo” of DFT methods was discussed. In this thesis application of DFT for geometry and energies

calculation was validated with support of high accuracy methods like *gold standard* CCSD(T) to guarantee correctness of computational predictions within present-day methods and hardware limits.

9.3 Practical description of methods in this thesis

9.3.1 Wavefunction and density analysis employed in this thesis

In this chapter brief introduction to computation analysis is reported. The relevant computational details and keywords description are provided. Additionally some short overview of application is discussed.

9.3.1.1 Natural Bond Orbital analysis

The analysis of orbitals can provide useful information about the system reactivity. However direct analysis can be complicated as orbitals tend to be delocalised. The Natural Bond Order (NBO)[107a] procedure localise orbitals and forms one or two centres localised orbitals which are easier to analyse. This approach was found to be very useful to analyse variety properties of electronic structures. Normally more than one set of NBO orbitals is possible, which represent resonance (mesomeric) forms. The most populated is associated with the optimal Lewis structure representation. Moreover contribution of less populated resonance forms can be studied by Natural Resonance Theory (NRT-NBO).[213, 126] Within NBO framework it is possible to estimate interaction energy between two orbitals (so called: energy of hyperconjugation). The stabilisation energy between filled orbital (donor) Lewis-type NBO and empty orbital (acceptor) non-Lewis NBOs, is estimated by 2nd-order perturbation theory. These "delocalisation" corrections to the *0*th-order natural Lewis structure rise from donation of occupancy from the localized NBOs into the empty non-Lewis orbitals and is expressed as:

$$\boldsymbol{E(2) = \Delta E_{ij} = q_i \frac{F(i,j)^2}{\varepsilon_j - \varepsilon_i}.}$$

[Equation 38]

For respectively donor NBO (*i*) and acceptor NBO (*j*), the interaction energy *E(2)* (E(2)-NBO), in kcal/mol) related to orbital interaction (delocalisation) $i \rightarrow j$ is function of donor orbital occupancy (q_i), orbital energies ε_I and ε_j (diagonal elements) and the off-diagonal NBO Fock matrix element *F(i,j)*. The F(i,j) reflects the orbital overlap between orbitals i and j and is referred in the text as orbital overlap therm. Except Table 4.1 and NRT-NBO analysis, all Natural Bond Orbital (NBO) calculations were performed with Gaussian 09 at B3LYP/6-311G(d,p) level. The data in table 4.1 were obtained with FireFly[214] package as it allows better estimation of orbital interaction via explicit deletion of interacting orbitals at suggested HF/6-311G(d,p) level. All transition state NBO calculations use orbitals localized in respect to reactant Lewis resonance structure. All Natural Resonance Theory (NRT) and steric analysis was performed within FireFly at B3LYP1 with 6-311G(d,p) basis set. The B3LYP1 uses *VWN* (Vosko-Wilk-Nusair) formula I parameterisation. This slightly differs from B3LYP implanted Gaussian 09 which uses *VWN* formula III, sometimes denoted as B3LYP3. Contour value of 0.1 was employed for visualisation of all NBO orbitals.

9.3.1.2 The Atoms in Molecules analysis

The Quantum Theory of Atom in Molecule (QTAIM)[215] analysis is a tool to analyse atoms, bonds and in general molecular structure based on electron density. QTAIM defines chemical bonding and structure of a chemical system based on the topology of the electron density. According to QTAIM, molecular structure is revealed by the stationary points of the electron density together with the gradient paths of the electron density that originate and terminate at these points. The criteria of stationary points are determined by two parameters: *r* and *s*. The *r* represents *rank* of the critical point (CP) and it is a number of non-zero eigenvalues of the spectrum (Hessian matrix of density). The *signature* (*s*) of the CP is defined as a sum of three eigenvalue signs. The number -1 is assigned to a negative eigenvalue and +1 to a positive eigenvalue of the spectrum (Hessian matrix of density). In that way the critical points are conventionally expressed as (*r,s*). Assuming those criteria with $r = 3$ it is possible to identify four types of critical points: Cage Critical Point CCP (3,+3), Ring Critical Point RCP (3,+1), Bond Critical Point BCP (3,-1) and (Non-) nuclear attractor (N)NA (3,-3). Critical point with $r < 3$ is called degenerate and has at least one zero curvature and it is topologically unstable. The search of CP is a

demanding task however it is possible to check topological consistency by The *Poincaré–Hopf* equation:

$$\boldsymbol{n - b + r - c = 1} \qquad \textbf{[Equation 39]}$$

where *n, b, r* and *c* are representing number of (Non)-nuclear attractor ((N)NA), Bond Critical Point (BCP), number of Ring Critical Point (RCP) and number of Cage Critical Point (CCP) respectively. This relationship only applies to non-periodic systems and never proves the completeness of set of CPs. In other words it can only point out inconsistency and therefore incompleteness of CP. In QTAIM chemical bond is associated with a bond path which connects two nuclear attractor NA with obligatory bond critical point BCP between them. The bond path is not necessarily a straight line and all characteristics of a bond are reflected by the properties of bond critical point (BCP). Importantly, negative Laplacian ($\nabla^2\rho(r)$) of electron density is given for a shared interaction while a positive value represents a closed-shell interaction. Usually, shared interactions are found for covalent bonds while closed shell indicates ionic and van der Waals' interactions. This is of high importance as BCP can be used for characterised interatomic interactions. It was found that bond strength is proportional to electron density ρ_b, Laplacian $\nabla^2\rho_b$, local electronic potential energy density $V(r)$ at BCP.[105]

Using QTAIM formalism, non-covalent integration can be studied. The sign of Laplacian together with density value ($\Omega(r)$) mapped onto reduced density gradient ($RDG(r)$) surface reveals week interactions. Those two functions are expressed as

$$\boldsymbol{RDG(r) = \frac{1}{2(3\pi^2)^{1/3}} \frac{|\nabla\rho(r)|}{\rho(r)^{4/3}}}$$

[Equation 40]

and

$$\boldsymbol{\Omega(r) = Sign(\lambda_2(r))\rho(r)}$$

[Equation 41]

where $\nabla\rho(r)$, $\rho(r)$ an $\mathrm{Sign}(\lambda_2(r))$ represents the Laplacian of electron density at position **r,** electron density at position **r** and sign of the second largest eigenvalue of Hessian matrix of electron density at position **r**, respectively.

The Ellipticity is another property of electron density. At BCP its represent the measure of distortion of electron density in the directions perpendicular to the bond. The ellipticity of the electron density is proposed as a convenient tool to monitor the π character of double bonds and is defined as:

$$\epsilon = \frac{\lambda_1}{\lambda_2} - 1$$

[Equation 42]

where λ_1 and λ_2 are the negative eigenvalues of the Hessian of the electron density ρ_b at bond critical point (BCP), which are in $\lambda_1 < \lambda_2 < 0 < \lambda_3$ order. It is worth to mention that due to cylindrical symmetry the ellipticity is zero in ethyne and ethane. Some authors suggest ellipticity scan as a better measure of double bond character or hyperconjugation.[216]

All AIM calculations in this thesis were performed with MultiWFN.[121] All density proprieties are listed at Bond Critical Points (BCP) and all values are reported in atomic units (a.u.). The *wavefunction files* (*.wfn) from M062X/6-311++G(2d,2p) level was obtained from Gaussian 09 calculation with ultra fine grid.

The RDG surface was obtained with contour value of 0.5 and colorized with Ω(r) function between -0.04 to 0.02 a.u. range. The cut-off value of electron density $\rho(r)$ was set to 0.1 a.u.

The hydrogen bond strength was calculated using electronic potential density (V(r) in a.u.) at BCP by equation:[105]

$$\boldsymbol{E_{HB}[kcal/mol] = -0.5 * V(r) * 627.51[\frac{kcal}{mol \cdot a.u.}]}.$$

[Equation 43]

9.3.1.3 Fuzzy bond order (FBO) analysis

Fuzzy bond order[101] has been chosen for bond order analysis as more stable with respect to the change in basis-set compared with Mayer bond order method[102]. However magnitude of Fuzzy bond order is close to Mayer bond order, especially for low-polar bonds.[217] The calculation of FBO requires numerical integration of

Becke's DFT, due to which the computational cost is larger in comparison to Mayer bond order. It has been found that it provides good correlation to measured values.[102-103] Fuzzy bond order is defined in fuzzy atomic space where any point of space may simultaneously be attributed to many atoms by a soft overlapping boundaries partitioning scheme.

In this thesis all Fuzzy bond order calculations were performed with MultiWFN program with *wavefunction files* (*.wfn) file from M062X/6-311++G(2d,2p) level obtained from Gaussian 09 calculation employing ultra fine integration grid (via *Integrals(=UltraFine)* keywod). The numerical grid for Becke's DFT integration included 40 radial points and 230 angular points as recommended.[218] The bond order analysis generally is used to characterise single, double or triple bond. However in this thesis it has been also used to characterise hydrogen bond which was found to be in agreement with trends from AIM, RDG and NBO analysis, at lower computational cost.

*9.3.1.4 **Molecular Electrostatic Potential (MEP) analysis***

The molecular electrostatic potential (MEP) at a given point close to molecule is the interaction energy acting between a positive unit test charge and charge distribution of the molecule. The molecular charge distribution remains unperturbed through the external positive test charge. The MEP is a good guide in assessing the molecules reactivity towards positively or negatively charged reactants. The MEP is typically visualized through mapping its values onto the molecules boundaries surface while it can be obtain from overlapping vdW radii of all atoms, solvent accessible surface areas (SASA) or through a constant value of electron density.

The Molecular Electrostatic Potential (MEP) in this thesis was calculated with Spartan'10[219] at B3LYP/6-311G(d,p) level. To obtain this 3D surface electron density surface, isodensity surface value of 0.002 au, was colorized with the molecular electrostatic potential. By convention blue regions represents strong interaction with negative charges species and red regions represents strong affinity to positive charge species.

9.3.1.5 Fukui function surface for nucleophilic attack analysis

The Fukui function surface is an intrinsic reactivity concept which predicts reactive site towards nucleophilic, electrophilic or radical.[128] Fukui function surface, in its general form is defined as:

$$\boldsymbol{f(r) = \left[\frac{\partial \rho(r)}{\partial N}\right]_v}$$

[Equation 44]

where N and ρ represent number of electrons in present system and electron density, respectively. The constant term v in the partial derivative is external potential, such as nuclear charges for isolated system. As it is not possible to evaluate the partial derivative, the equation in finite difference approximation can be calculated unambiguously. In that way Fukui function surface for nucleophilic attack is given by difference between neutral and anionic density of system and is expressed as:

$$\boldsymbol{f^{+}(r) = \rho_{N+1}(r) + \rho_{N}(r)}$$

[Equation 45]

where $\rho_N(r)$ and $\rho_{N+1}(r)$ represent electronic density and electronic density of system with one additional electron respectively. The positive phase of this 3D function describes the region of predicted nucleophilic attack and its preference given by size. The Fukui function has also its simplified variation, so-called condensed Fukui function, formula employ atomic charges rather than densities.

In this thesis the Fukui surface for nucleophilic attack was calculated with MultiWFN program together with calculation from Gaussian 09 at B3LYP/6-311G(d,p) level. The wavefunction file (*.wfn) was generated by Gaussian program employing *UltraFine* grid. Visualisation with ChemCraft[220] was realized with surface contour value of 0.005.

9.3.1.6 **Nucleus Independent Chemical Shift (NICS)** ***analysis***

Nucleus-independent chemical shifts (NICS) have been used for the evaluation of aromaticity, antiaromaticity, non-aromaticity of single-ring systems and individual

rings in polycyclic systems such as local aromaticities. Since their introduction[221] those have been used extensively to asses such properties of the neutral molecules, ions, intermediates, and transition states.[222] This method was successfully applied to 4n+2 and 4n-electron systems at singlet and triplet electronic states. It is also shown that relative aromaticities of rings in polycyclic systems (local aromaticities) cannot be estimated by direct comparing NICS values.[223] The method is generally accepted and widely used and showed agreement with other indices of aromaticity,[224] however it has also received some criticism.[214b, 225] This approach is based on measuring the NICS value at previously added ghost atoms (*Bq*) in positions of interest. Initially, probes (*Bq*) were placed at the centres of systems (NICS(0)) and later, 1 Å above the molecular planes (so-called NICS(1)). Also the NICS-scan approach was also suggested.[223]

All Nucleus Independent Chemical Shift (NICS) calculation reported in this thesis were obtained by the negative value of isotropic magnetic shielding calculated with Gaussian 09 at B3LYP/6-311G(d,p) level. The ghost atom (Bq) was located at geometrical centre of the analysed ring. This calculation are referred as $NICS(0)_{iso}$.

9.3.2 General description of calculation procedures employed in this thesis

This chapter provides computation details of performed calculations. The relevant computational detail and keywords description is provided. Additionally some short overview of keyword is discussed.

9.3.2.1 General procedure for calculation of ground states

All geometries calculations presented in this thesis were obtained from Gaussian 09,[226] with symmetry unconstrained (*C1* symmetry) geometry optimizations and singlet spin states. Additionally range of pre-optimization and single point energies were carried out with MOPAC,[227] ORCA,[228] GAMESS(US),[214a] NWChem[229] and MolPro.[230] The geometries of all ground states were confirmed by convergence of SCF and the absence of imaginary frequencies. The converged geometries confirmed acceptable low value of force and displacement in internal and Cartesian

coordinates. In some rare cases new internal coordination system was obtained from Gaussian 03[231] or generated by hand. All transition state geometry optimizations and frequency calculations were calculated with ultra fine numerical grid to obtain reliable energies, gradients and Hessians. This requests (99,590) grid which has 99 radial shells and 590 angular points is recommended for systems containing tetrahedral centres and low frequency modes, larger molecules and some DFT methods (like M062x from Minnesota family).[91] Molecules which possibly could have lower electronic state were submitted to wavefunction instability test[232] at the same method level as geometry was obtained. The geometry was re-optimized with new orbital guess if instability was encountered. All energies are reported in kcal/mol which was obtained by multiplying in Hartree energy (Eh) by 627.51 kcal $mol^{-1}Eh^{-1}$. For all reaction pathways lower energy conformer from conformation analysis was taken into account by mean of electronic energies. Frequencies for the Zero-point energy correction and Gibbs free energy corrections were not scaled. All Gibbs free energy are reported as standard Gibbs energy (ΔG^{o}). The IEFPCM, CPCM and SMD implicit solvents were invoke by appropriate keywords with default parameter as implanted in Gaussian 09.

9.3.2.2 General procedure for calculation of transition states

Calculation of transition states were in general performed in similar way as ground state. The saddle point geometries were found by Synchronous Transit-Guided Quasi-Newton (QST2 or QST3) and relaxed scans from Gaussian 09 and ORCA. However, all final geometries were obtained with Gaussian 09 with analytical gradient and Hessian calculations. The converged geometries were confirmed by low value of force and displacement in internal and Cartesian coordinates. The character of transition state was confirmed by Intrinsic Reaction Coordinate (IRC) in mass-weighted Cartesian coordinates in both directions.

9.3.2.3 Calculation with MOPAC program

MOPAC2012 (Molecular Orbital PACkage)[227] is a semi-empirical quantum chemistry program based on NDDO approximation. This semi-empirical calculation is fast on PC computer and benefits from robust implantations. In this thesis it is

widely used to perform preliminary calculations. This program includes semi-empirical methods like AM1,[83, 233] PM3,[84] PM6,[85] PM7,[234] RM1[86] and numerical gradients and Hessian implantation. To guarantee required accuracy, all criteria for optimizations, electronic and geometric were increased by 100 times by inclusion of *PRECISE* keyword. Transition state optimization was carried out with eigenvector following routine invoked by *TS* keyword.[235] Some transition states calculations were invoked by *SADDLE* keyword which locates transition state geometry by transforming geometry of reactant to product geometry. In some problematic cases *BAR* parameter was set to 0.001 which represents a maximum rate of reduction of 0.1 percent per step. Calculation with Yb^{+3} atom were carried at PM7 level and were invoked with *SPARKLE* keyword. This treats lanthanide atom as +3 charged sparkles with no basis set associated.[236] Those geometries of the lanthanides complexes were found to be with good accuracy to experimental values. However it is known that heats of formation and electronic properties are not accurate. For that reason range of calculations were performed to obtain good guess geometries which were further refined by DFT.

9.3.2.4 CCSD(T) calculations

Restricted CCSD(T) were performed using Gamess(US).[214a] Starting *GUESS* orbitals were generated by *HUCKEL* and SCF convergence was performed together with *DAMP* function and *DIIS* accelerator. All calculations were checked towards low T1 diagnostic.[94] In some cases SCF convergent problems were overcame by using starting guess from previous Gaussian 09 calculation at the HF/6-31G(d). Except the Graph 6.1, all CCSD(T) calculations were performed with Gamess(US). The F12a-CCSD(T) were carried out with MolPro.[230]

9.3.2.5 Calculation with ORCA program

ORCA[78c] was used for pre-optimisation and scans with DFT methods, mainly BLYP and B3LYP. The local DFT method, BLYP was used together with resolution of identity approximation (RI or density fitting) with automatically assignment of auxiliary basis set invoked by keywords *RI* and *AutoAux*. The hybrid DFT like B3LYP was used with keyword *RIJCOSX* which uses chain of sphere

approximation for efficient approximations to the Hartree-Fock exchange term.[227b] This approximation leads to large speed up where induces small error.[237]

The RI-B2-GPLYP (so called double hybrid DFT method, DH-DFT) calculations were carried out with *RIJONX* approximation. This uses the RI method for the Coulomb term and the standard treatment for the exchange term. The second-order perturbation is treated with resolution of identity (RI) and Frozen Core (FC) approximations. Those approximation make calculation accessible for systems with more than 25 heavy atoms together with large cc-pVQZ (or even Def2-QZVPP) basis set.

The *Møller–Plesset* second order (MP2) calculation was achieved with resolution of identity (*RI* keyword) and frozen core (FC, as default) approximations. The automatically assignment of auxiliary basis set was invoked by *AutoAux* keyword. All MP2/CBS are obtained with RI approximation and energies were obtained by two basis sets invoked by keyword *RI-MP2*, *ExtrapolateEC(X/Y)* and *AutoAux* were X and Y denotes cardinal number of correlation consistent cc-pV*n*Z[179] basis set.

The CCSD(T)/CBS energies in Graph 6.1 were obtained with keyword line: CCSD(T) *RI-MP2 ExtrapolateEC(2/3) TightSCF* which extrapolate CCSD(T)/cc-pVDZ energies to CBS limit using MP2 calculation at cc-pVDZ and cc-pVTZ.

All CCSD(T)/CBS energies are based on RI-MP2/CBS calculations from ORCA program and CCSD(T) from GAMESS(US) program using equation:

$$\boldsymbol{E_{total}^{(CCSD(T)/CBS)} \approx E_{SCF}^{\left(\frac{HF}{B3}\right)} + E_{corr}^{\left(\frac{CCSD(T)}{B1}\right)} + E_{corr}^{\left(\frac{MP2}{CBS(B2\rightarrow B3)}\right)} - E_{corr}^{\left(\frac{MP2}{B1}\right)}}.$$

[Equation 46]

The RI-MP2/CBS energies are calculated with cc-pVTZ (B2) and cc-pVQZ (B3) basis sets and CCSD(T) correction was calculated with 6-31G(d) basis set[227a] B1 and called CCSD(T)/CBS[B1, B2=>B3]

9.3.2.6 Graphical post-processing

All images and surface rendering in this thesis were obtained with ChemCraft[232a] program. Some addition processing was handled by Gabedit[238] and

SPARTAN'10,[219] GaussView,[239] Molekel,[240] Avogadro,[241] VMD,[242] Maestro[227a] and Discovery Studio.[243]

Appendix

A PICTURE IS WORTH A THOUSAND WORDS.
ATTRIBUTED TO NAPOLEON BONAPARTE

This section includes some complementary information in addition to that described in the main text. The material is presented in a sequence following the order of previous chapters. Section 10.5 contains supplementary information relating to the analysis of various small molecules.

10.1 Supporting Information for chapter 4

SI Table 10.1. Energy decomposition analysis of transition states **2.1-2.4** and **2.1-3.2** for the ring opening of phenylcyclobutenones.

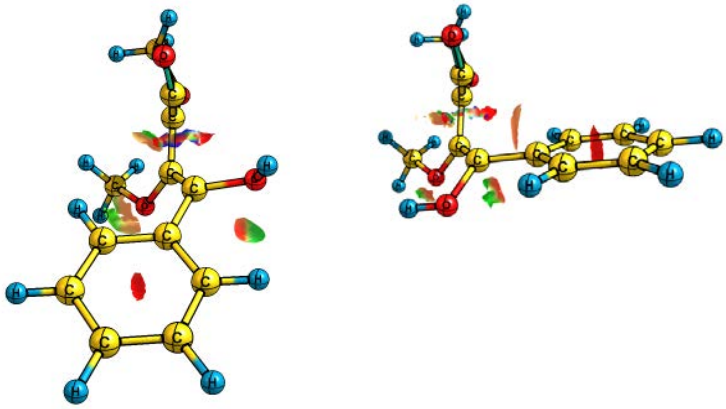

ΔE (M06-2x/6-311G(d,p))	33.80	27.40
Steric energy (Es)*	5771.17	1038.01
Quantum energy (Eq)*	-5798.48	-1063.35
Electrostatic energy (Ee)*	52.74	60.39
Steric from NBO*	425.73 (510.21**)	483.53 (495.56**)
Steric from NBO***	855.06 (1342.28**)	943.14 (934.30 **)

All values are in [kcal/mol]. *Energy of decomposition proposed by Shubin Liu.[244] Es, Ee, and Eq represent energetic contributions from: steric, electrostatic, and quantum effects, respectively were ΔE = ΔEs + ΔEe + ΔEq and ΔE = ΔTs + ΔEe + ΔExc (Ts, Ee, and Exc are the noninteracting kinetic, the electrostatic, and the exchange-correlation energy). In this definition the energy contribution from the steric effect are expressed by the Weizsäcker kinetic energy calculated with MultiWFN. ** Total disjoint NLMO steric exchange energy from pairwise sum. ***Localized in respect of product resonance structure rather than reactant. ****Total steric exchange energy.

10.2 Supporting Information for chapter 5

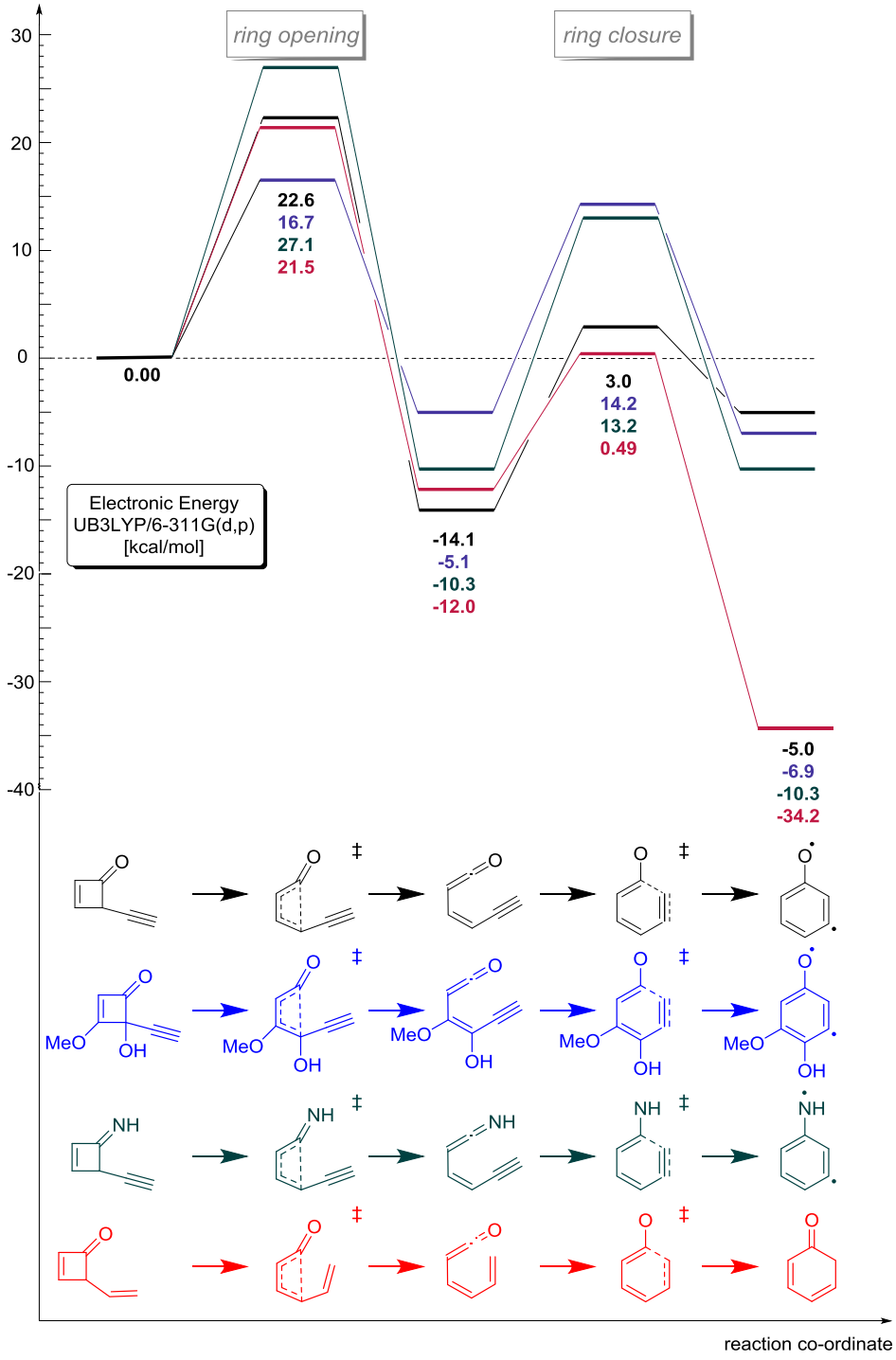

SI Figure 10.1. Competitive pathways for 4-ethynylcyclobut-2-en-1-one **5.1**, 4-vinylcyclobut-2-en-1-one **5.8** and 4-ethynylcyclobut-2-en-1-imine **5.15** from B3LYP/6-311G(d,p) method.

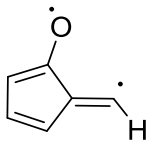

5.7

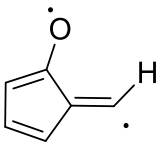

5.3

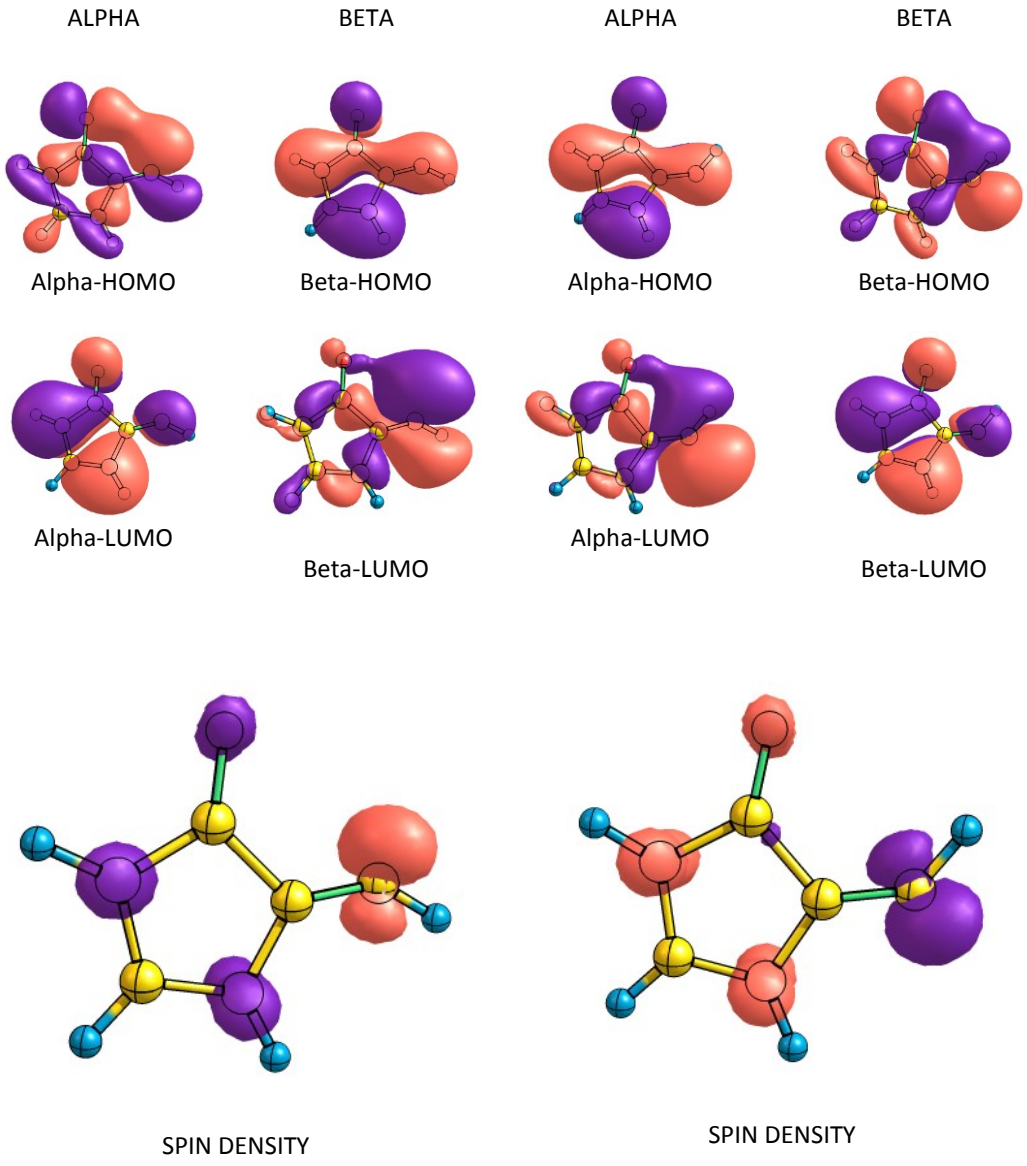

SI Figure 10.2. Graphic representation of orbitals and spin density for intermediates **5.3** and **5.7** from B3LYP/6-311G(d,p). HOMO and LUMO refers to the highest and lowest Kohn-Sham orbitals.

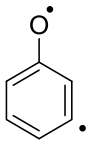

5.4

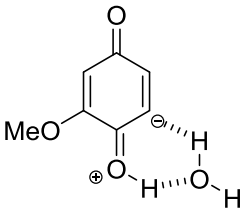

5.28

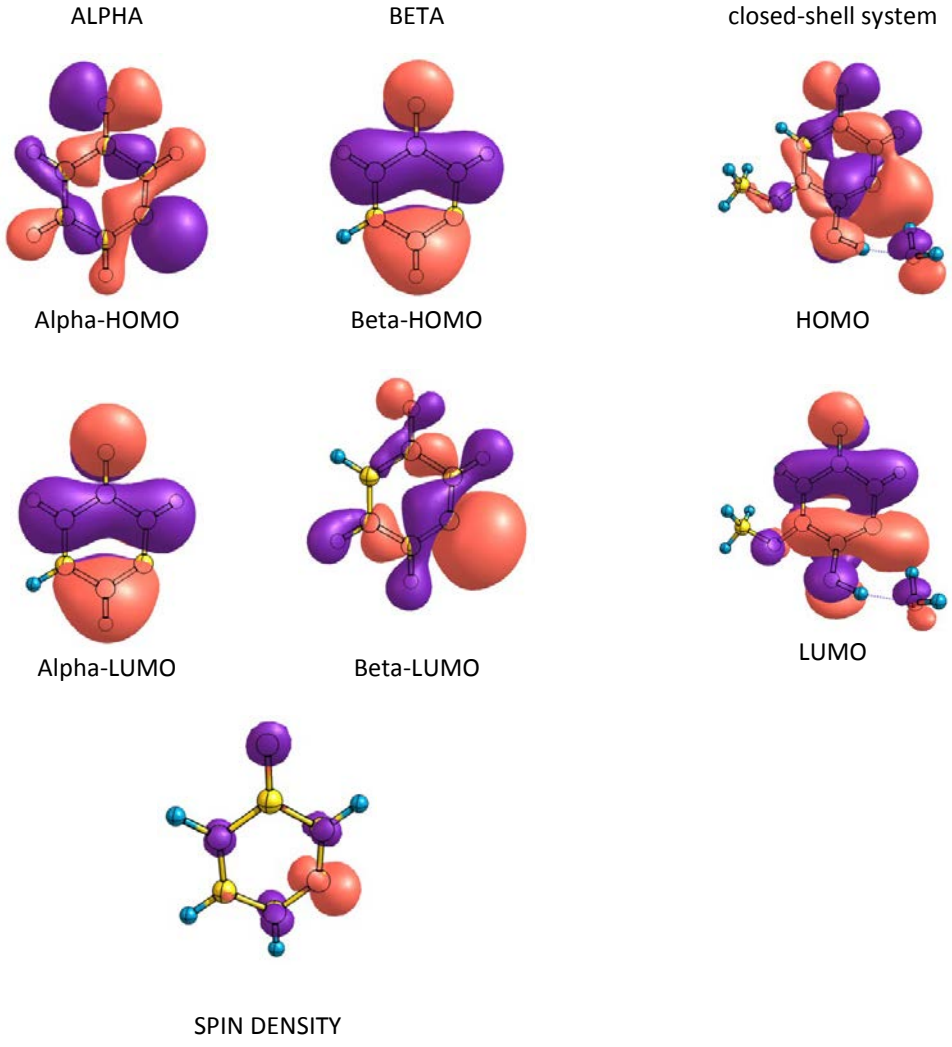

SI Figure 10.3. Graphic representation of orbitals and spin density for intermediates **5.4** and **5.28** from B3LYP/6-311G(d,p).

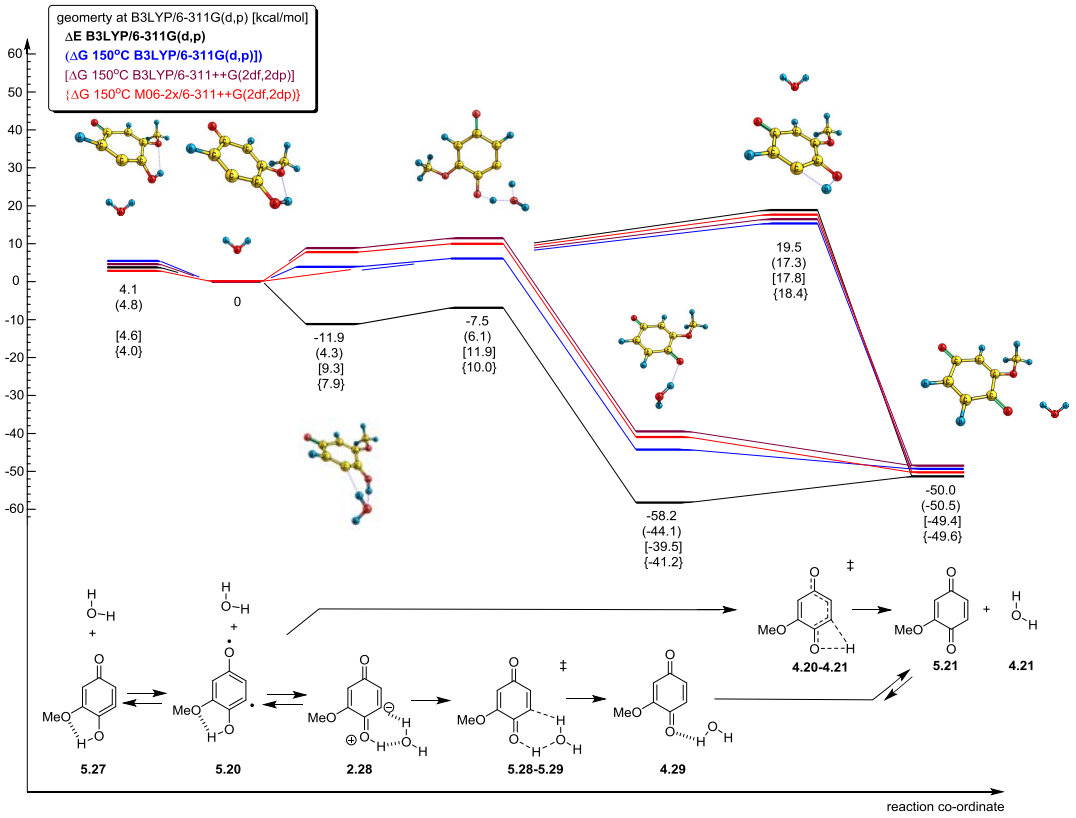

SI Figure 10.4. Energy graph for the hydrogen transfer of diradical intermediates promoted by water with energies determined by the B3LYP and M062X methods.

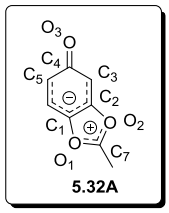

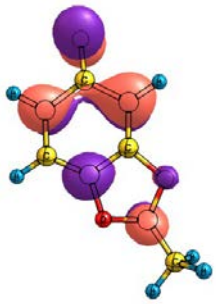

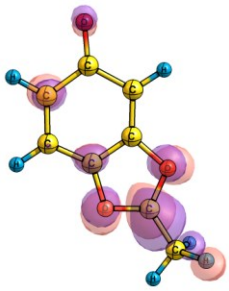

HOMO LUMO

SI Figure 10.5. Graphical representation of orbitals for intermediate **5.32** from B3LYP/6-31G(d).

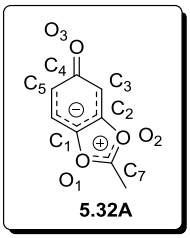

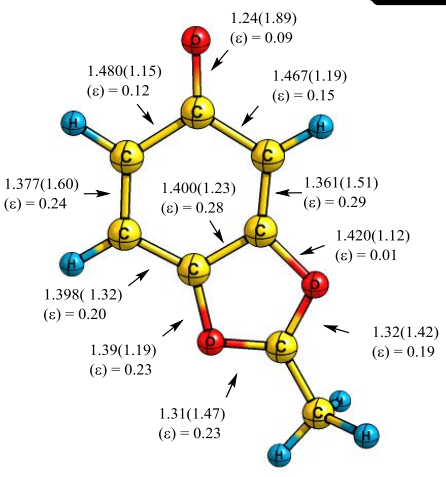

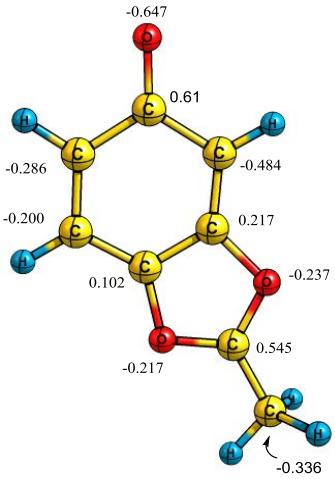

bond length [Å] (Fuzzy Bond Order)

CHLPEG ESP charge

M062x/6-311++G(2d,2p)//B3LYP/6-31G(d)

SI Figure 10.6. Geometric representation of intermediate **5.32A** at B3LYP/6-31G(d) and its electronic properties at M062X/6-311++G(2d,2p).

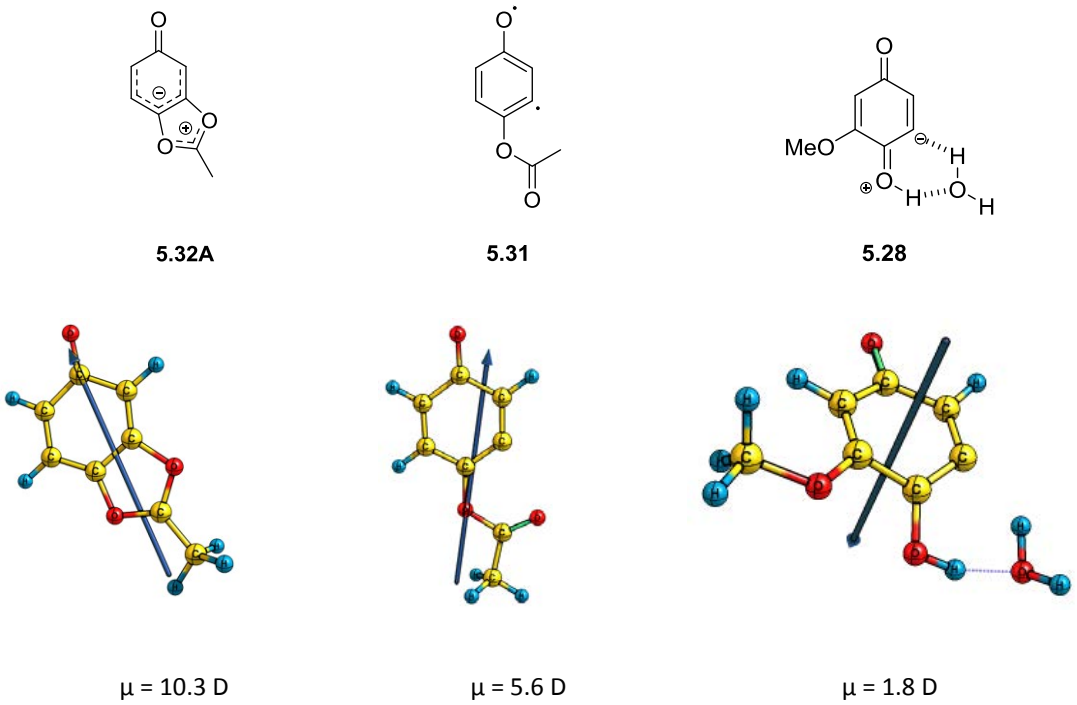

SI Figure 10.7. Dipole moments of intermediates **5.32A**, **5.31** and **5.28** at B3LYP/6-31G(d).

10.3 Supporting Information for chapter 6

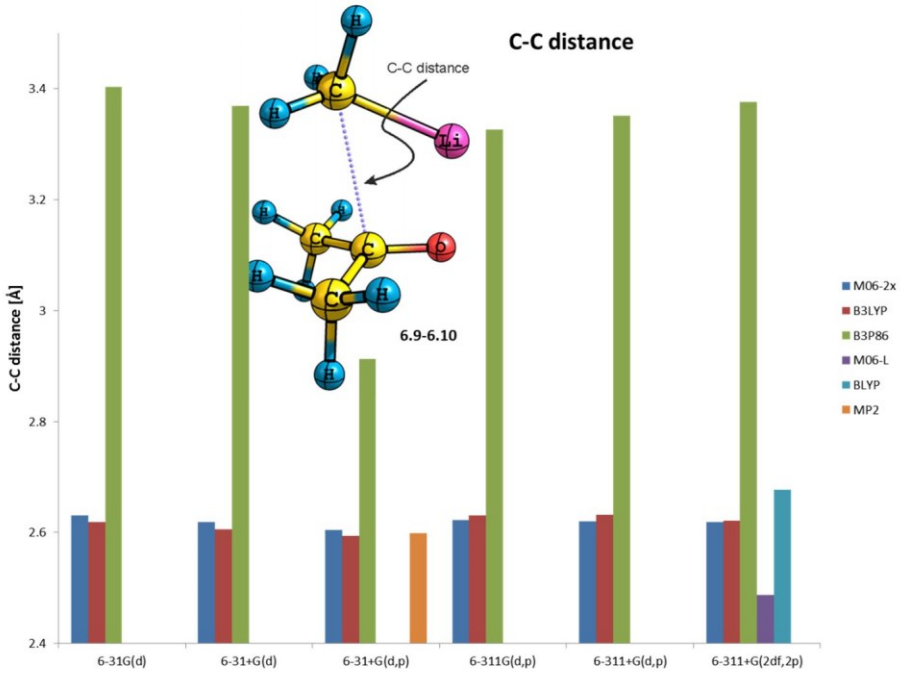

SI Figure 10.8. Basis set and method dependence on C-C distance [in Å] for transition state **6.9-6.10**.

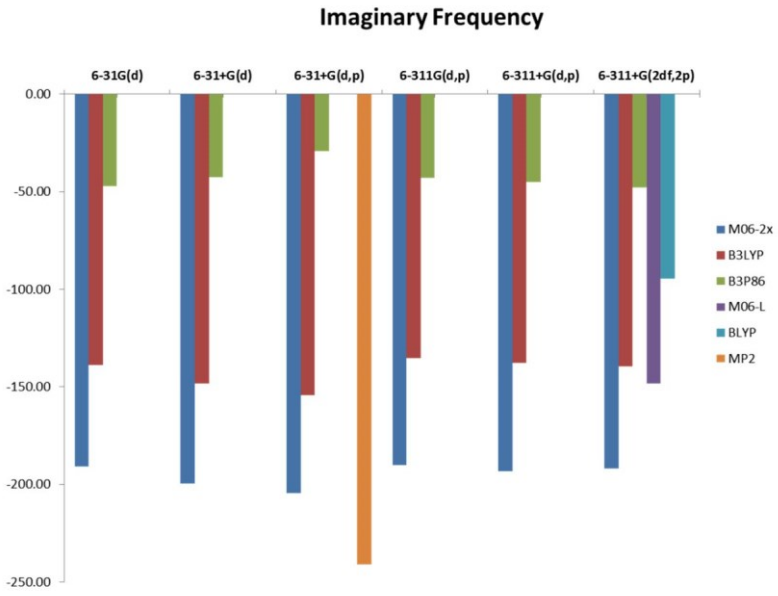

SI Figure 10.9. Basis set and method dependence on the imaginary frequencies [in cm^{-1}] of transition state **6.9-6.10**. For clarity, imaginary frequencies are reported as negative values.

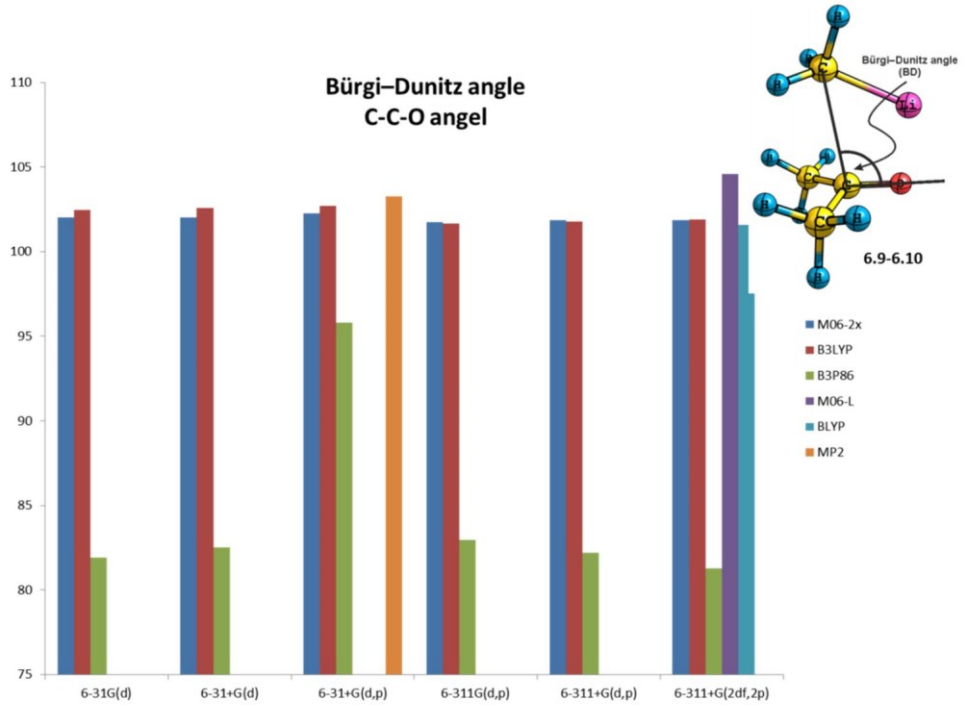

SI Figure 10.10. Basis set and method dependence on the Bürgi–Dunitz angle [in °] in transition state **6.9-6.10**.

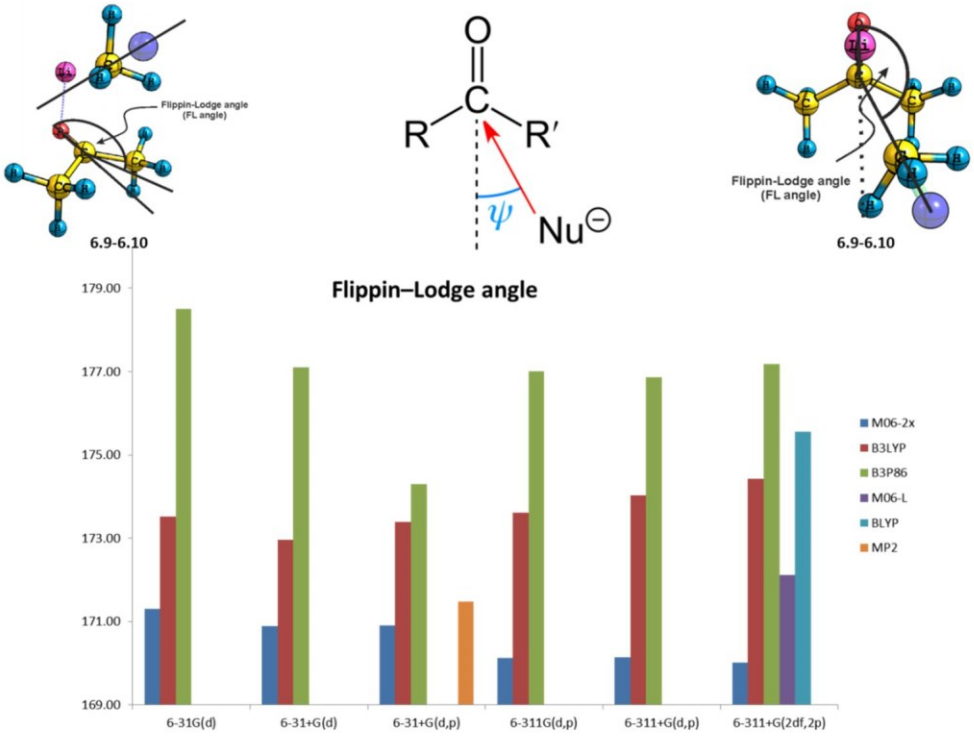

SI Figure 10.11. Basis set and method dependence on the Flippin–Lodge angle [in °] in transition state **6.9-6.10**.

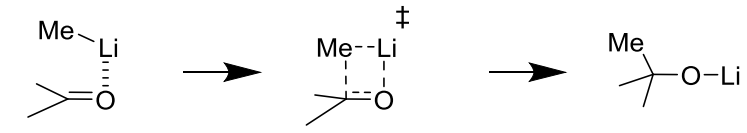

pre-reaction complex conf.2 **6.9** | *transition state* **6.9-5.10** | *product* **6.10**

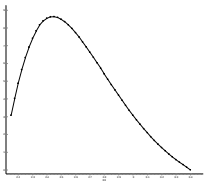

HF/3-21G*

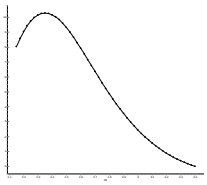

HF/6-311+G(2df,2p)

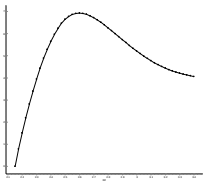

MP2/6-31+G(d,p)

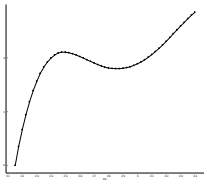

M06L/6-311+G(2df,2p)

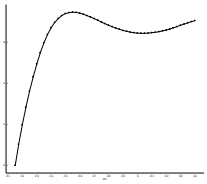

M06/6-311+G(2df,2p)

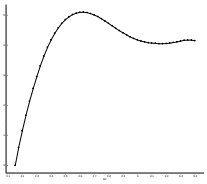

M06-2x/6-311+G(2df,2p)

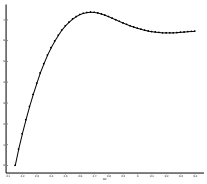

M06HF/6-311+G(2df,2p)

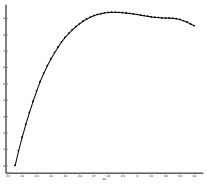

M062x/3-21G*

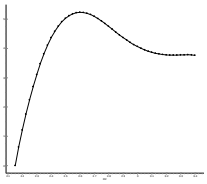

M062x/6-31+G(d,p)

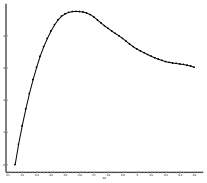

BMK/6-31+G(d,p)

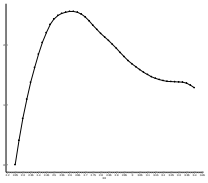

BMK/6-311+G(2df,2p)

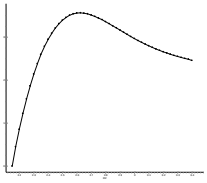

B3LYP/6-311+G(2df,2p)

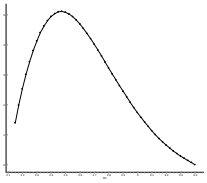

mPW2PLYP/6-31+G(d,p)

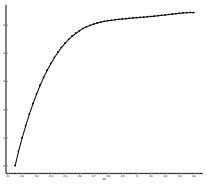

B3P86/6-311+G(2df,2p)

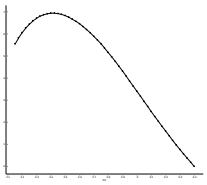

MOHLYP2/6-311+G(2df,2p)

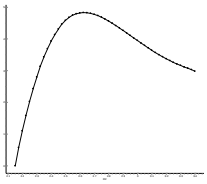

B2PLYP/6-31+G(d,p)

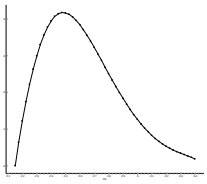

B2PLYP-D/6-31+G(d,p)

SI Table 10.2. Potential energy scan of the developing C-C bond close to the transition state region (from 2.15 Å to 3.4 Å) given by different methods.

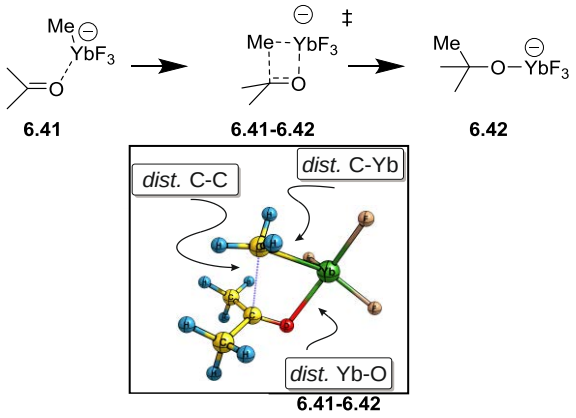

METHOD	dist. C-C	C-Yb	O-Yb
HF/6-31G(d)	2.420	2.635	2.361
BLYP/6-311+G(2df,2p)	2.588	2.601	2.435
M06-L/6-311+G(2df,2p)	2.468	2.554	2.379
B3P86/6-311+G(2df,2p)	2.536	2.528	2.413
B3LYP/6-31G(d)	2.558	2.547	2.437
B3LYP/6-31+G(d,p)	2.524	2.580	2.407
B3LYP/6-311+G(2df,2p)	2.514	2.576	2.398
M062x/6-31G(d)	2.512	2.519	2.414
M062x/6-31+G(d,p)	2.470	2.545	2.389
M062x/6-311+G(2df,2p)	2.457	2.542	2.378
MP2/6-31+G(d,p)	2.494	2.554	2.417
B2PLYP/6-31+G(d,p)	2.516	2.568	2.409

SI Figure 10.12. Geometrical benchmark on the geometry of transition state **6.41-6.42**.

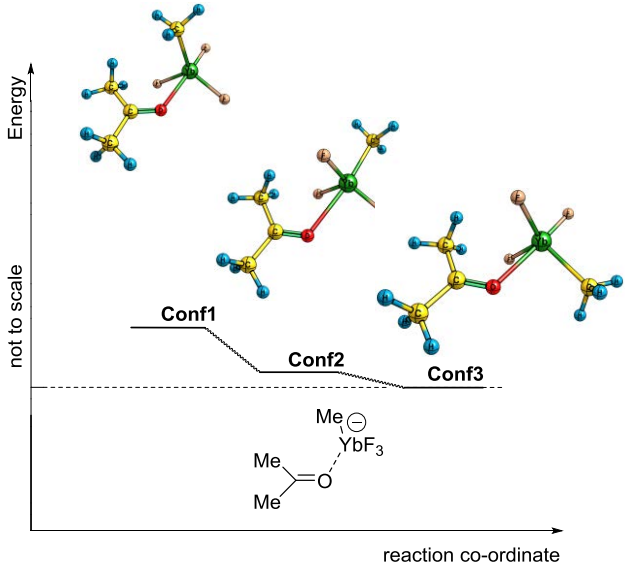

	Relative energy [kcal/mol] at B3LYP/6-31G(d)/MWB59 level		
conformation	**ΔE**	**ΔG(-78°C)**	**Δ[G(-78°C)+IEFPCM(THF)]**
Conf1	1.70	1.55	1.40
Conf2	0.10	0.08	0.10
Conf3	0.00	0.00	0.00

SI Figure 10.13. Relative energies for conformers of **6.41**.

10.4 Supporting Information for chapter 7

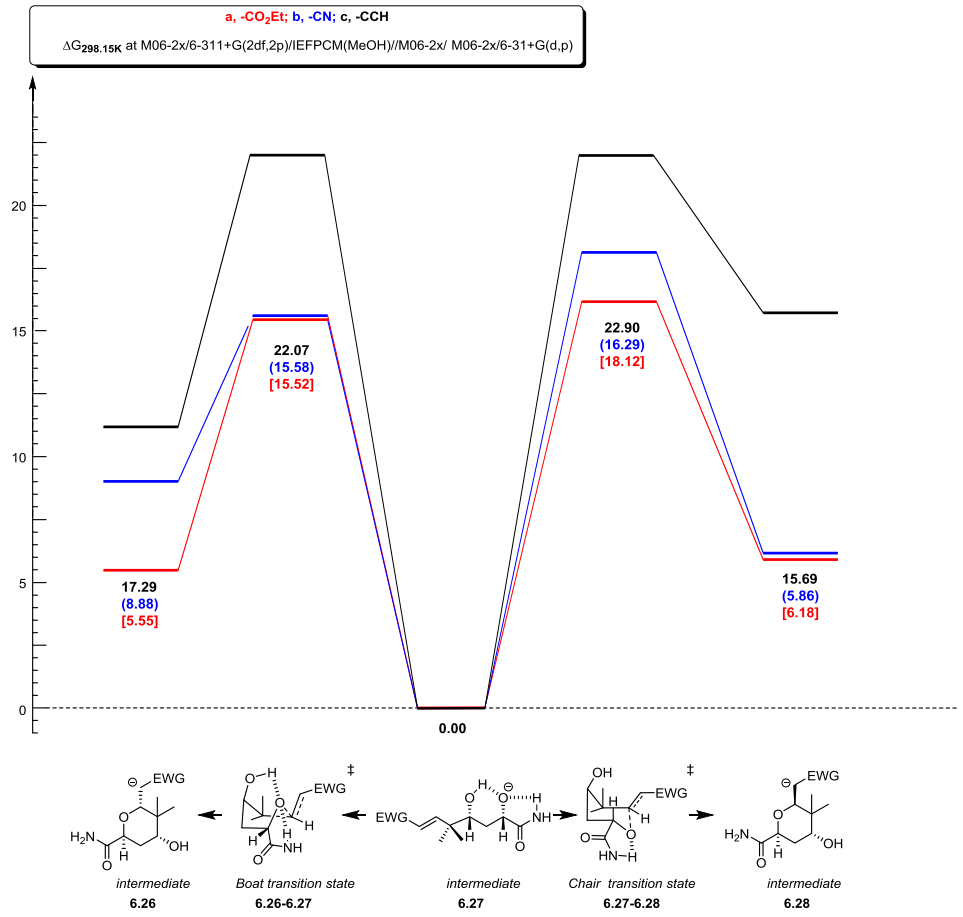

SI Figure 10.14. Ring closure reactions for **7.27a, 7.27b** and **7.27c**.

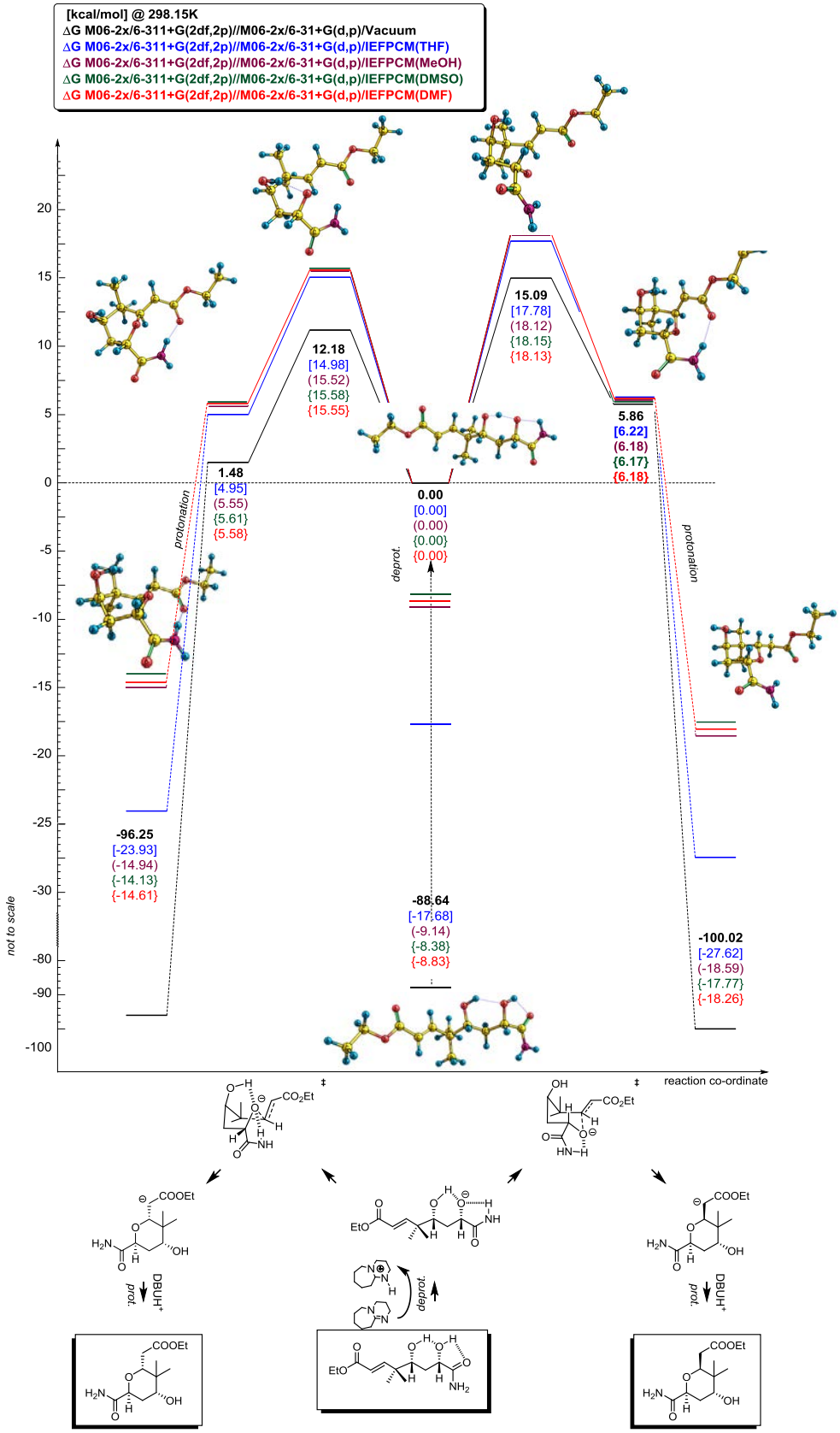

SI Figure 10.15. Ring closure reactions for **7.27a.**

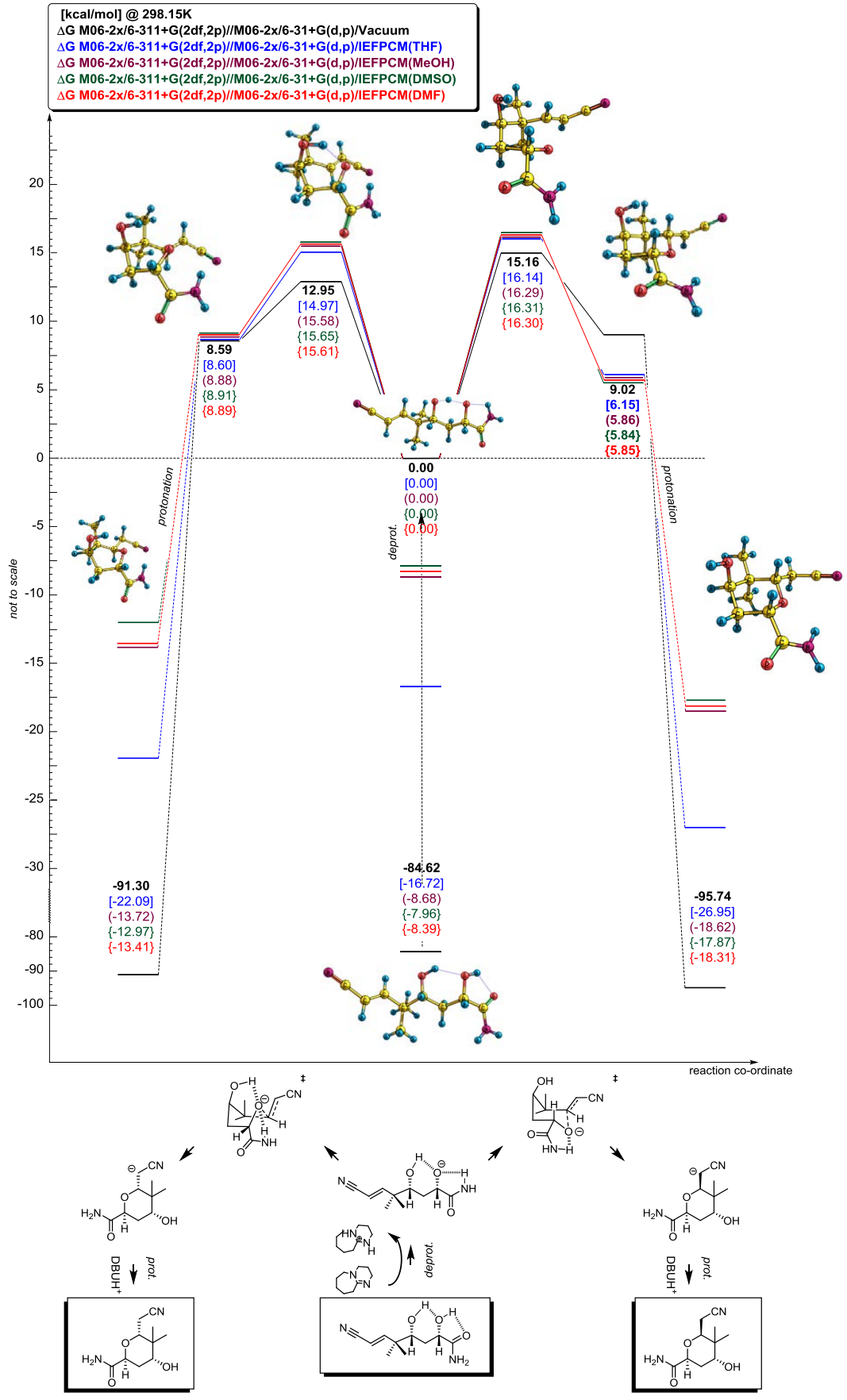

SI Figure 10.16. Ring closure reactions for **7.27b.**

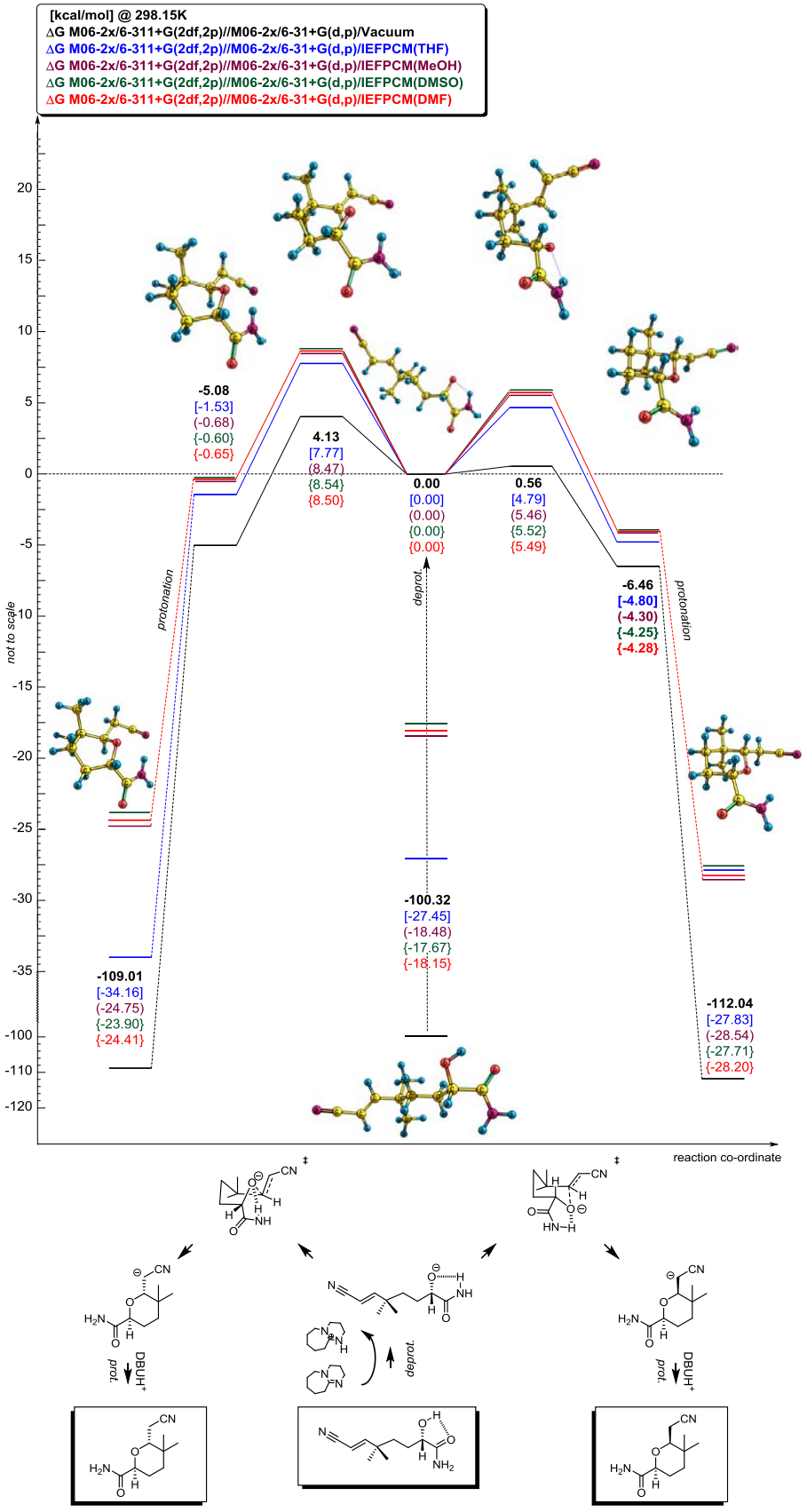

SI Figure 10.17. Ring closure reactions for (*S,E*)-7-cyano-2-hydroxy-5,5-dimethylhept-6-enamide.

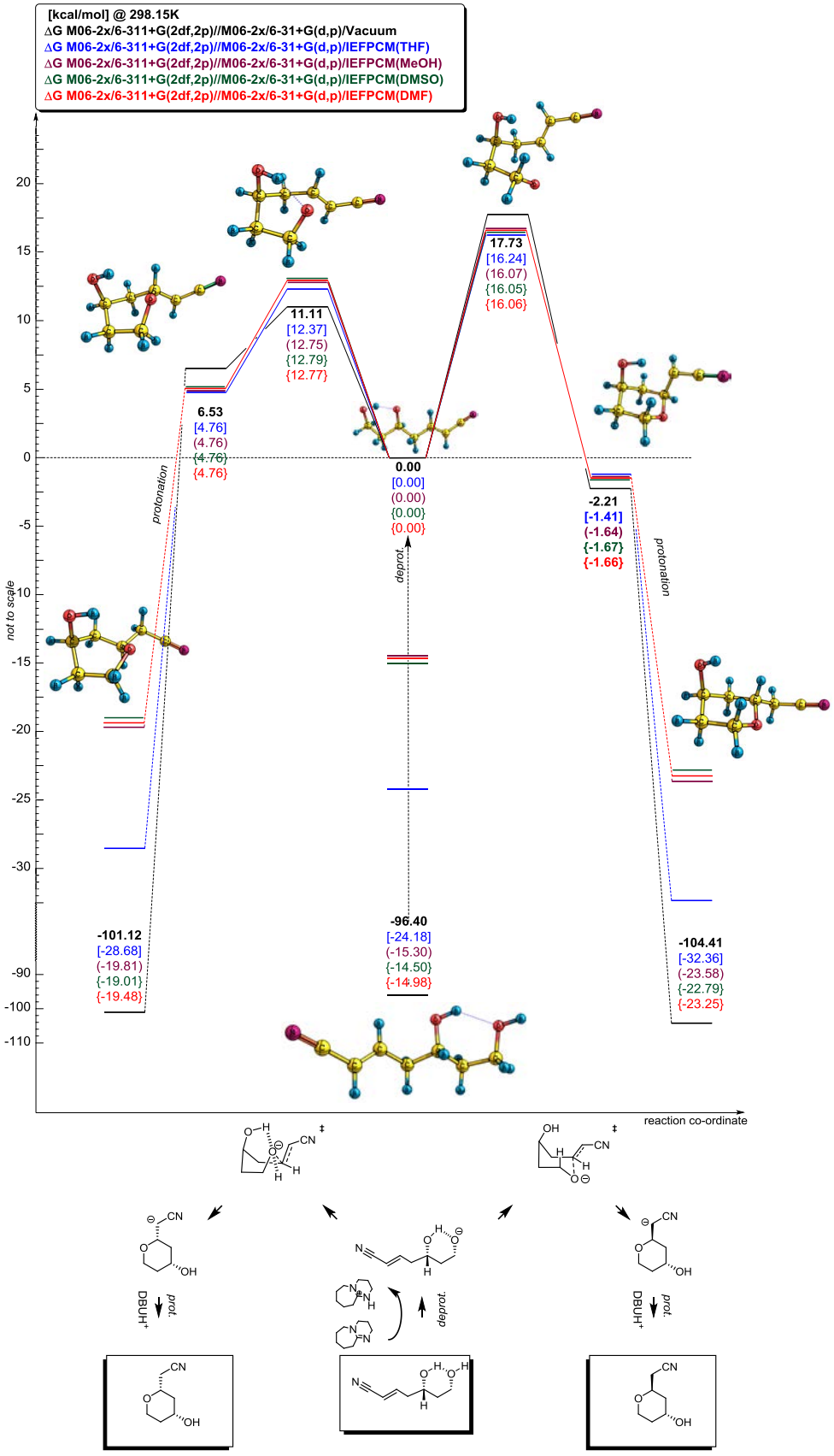

SI Figure 10.18. Ring closure reactions for (*S,E*)-5,7-dihydroxyhept-2-enenitrile.

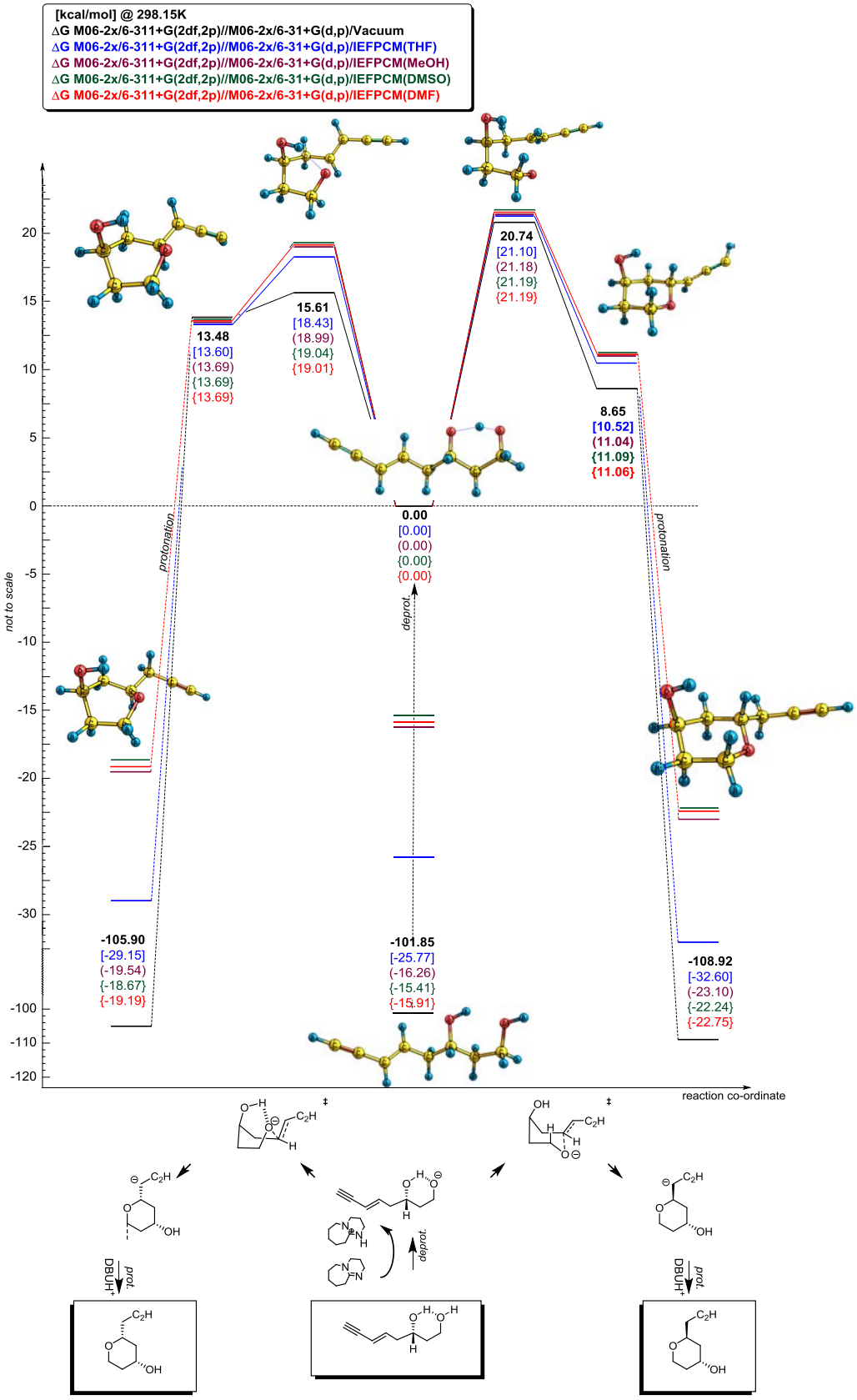

SI Figure 10.19. Ring closure reactions for (*S,E*)-oct-5-en-7-yne-1,3-diol.

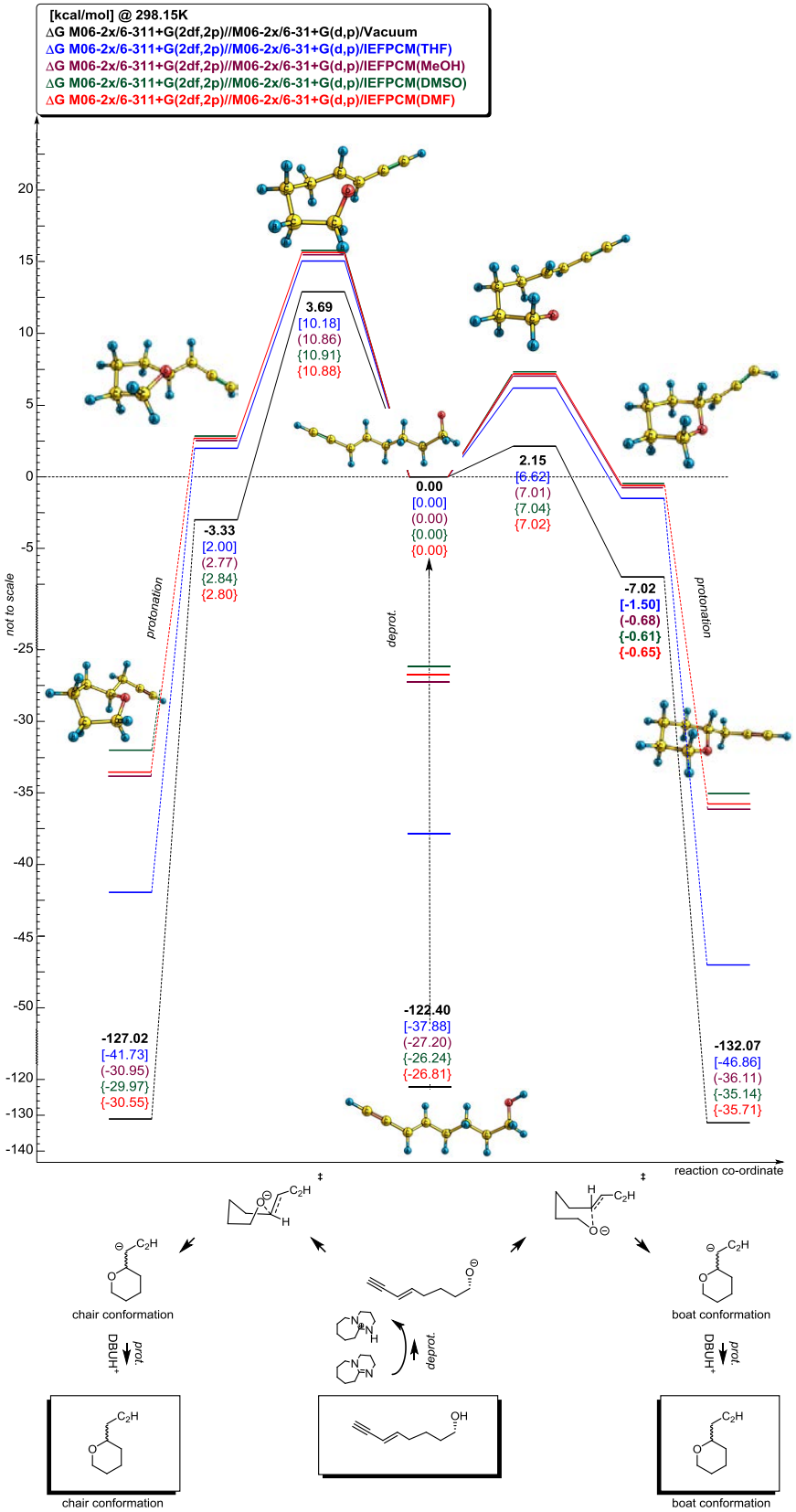

SI Figure 10.20. Ring closure reactions for **7.12.**

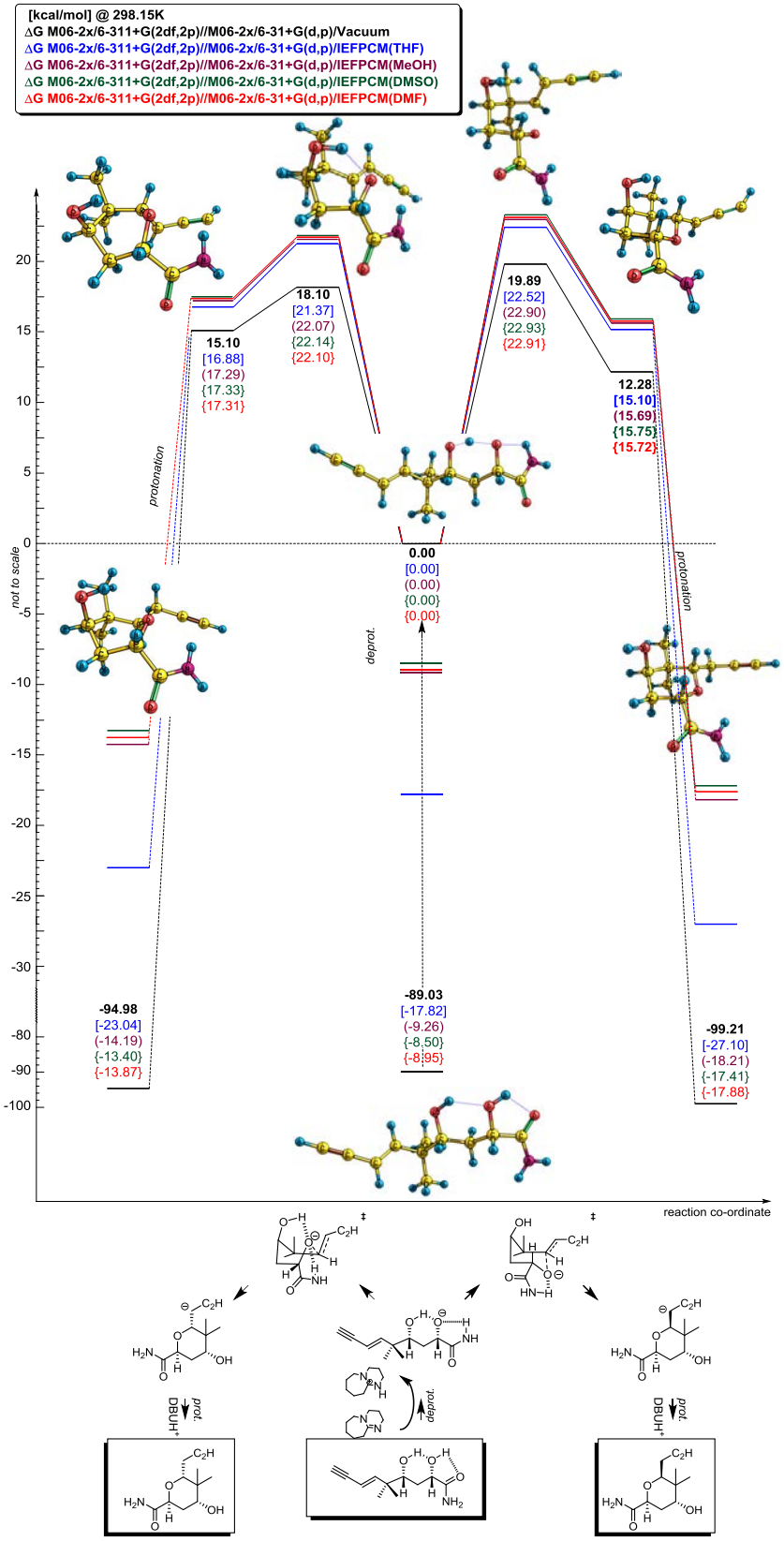

SI Figure 10.21. Ring closure reactions for **7.27c.**

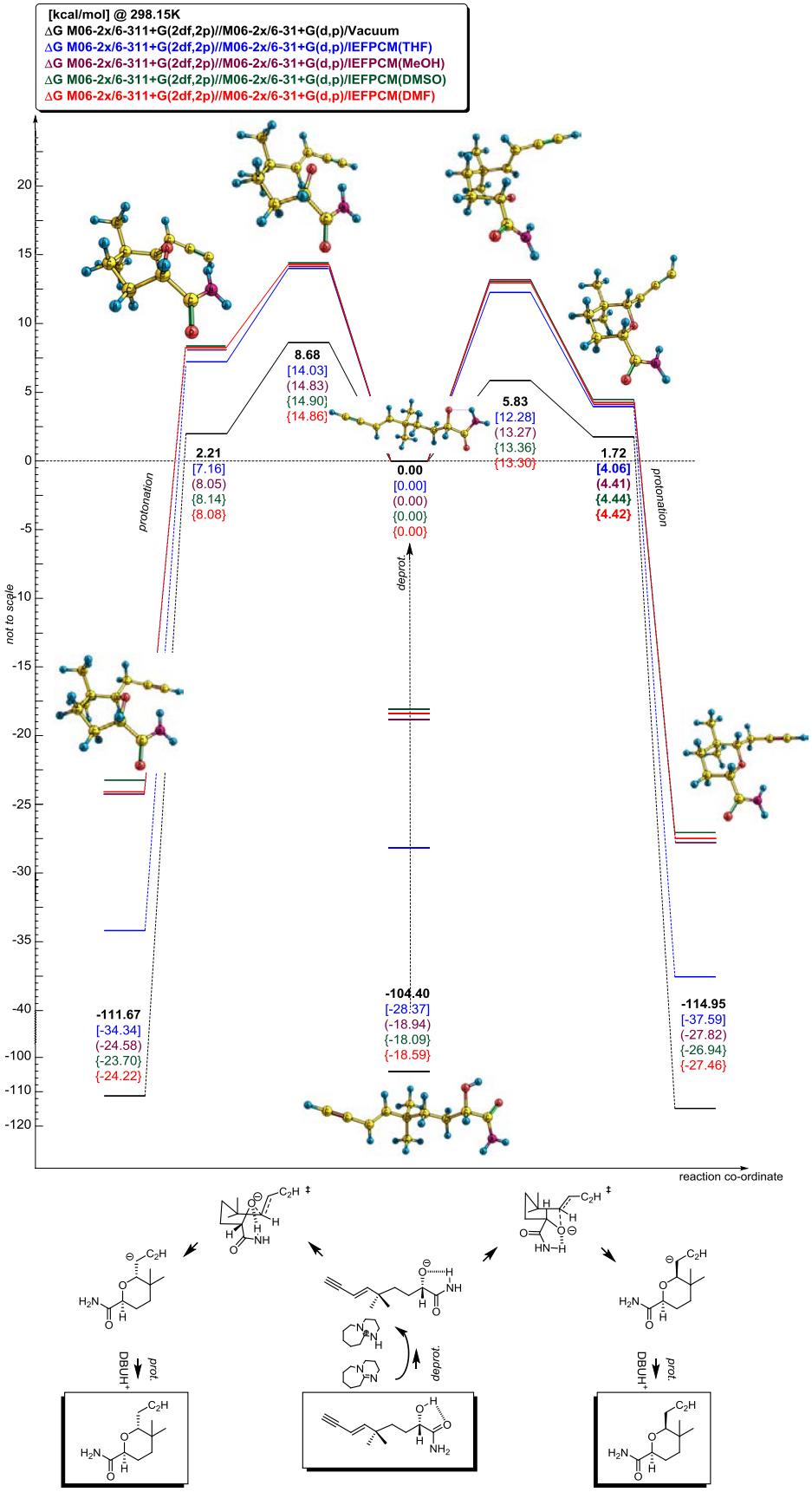

SI Figure 10.22. Ring closures reaction for **7.24.**

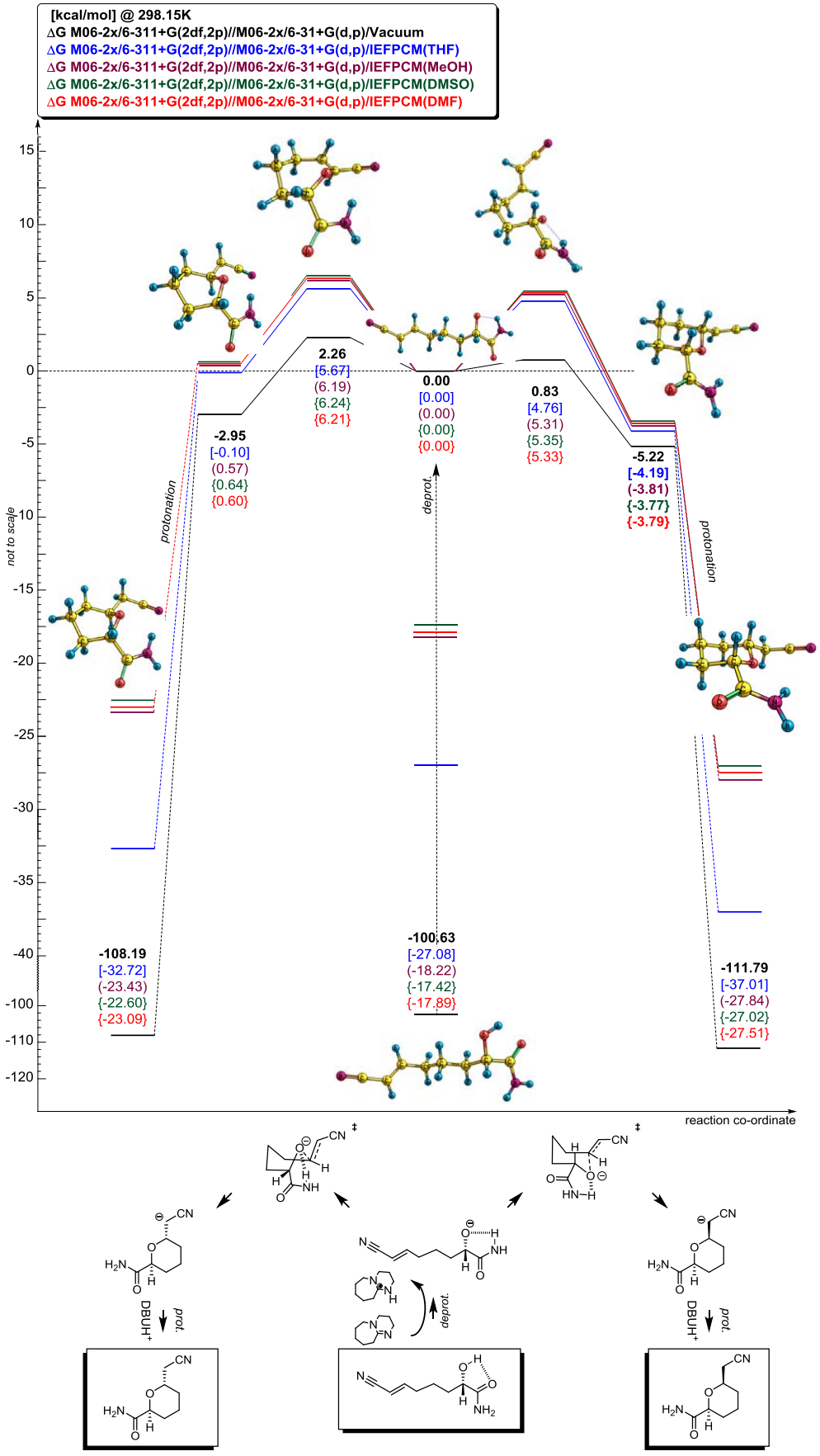

SI Figure 10.23. Ring closure reactions for (*S,E*)-7-cyano-2-hydroxyhept-6-enamide.

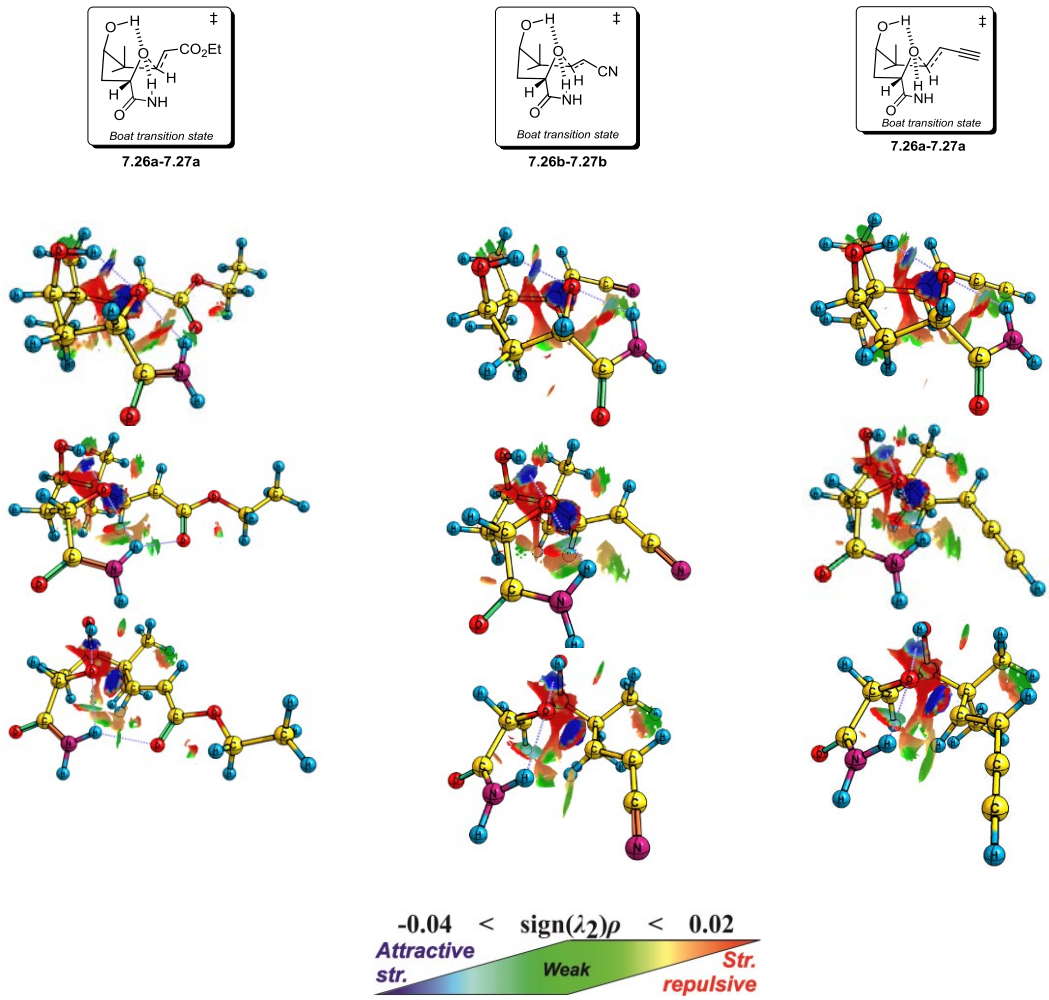

SI Figure 10.24. RDG surface of transition states **7.26-7.27**, **7.26b-7.27b** and **7.26a-7.27a**. Geometry at M06-2x/6-31+G(d,p), RDG surface at M062X/6-311++G(2d,2p).

10.5 Supporting Information for analysis

This section contains some NBO, QTAIM, CHELPG ESP charges and Fuzzy bond order analyses performed on small molecules. These provide a complementary picture of trends presented in this thesis.

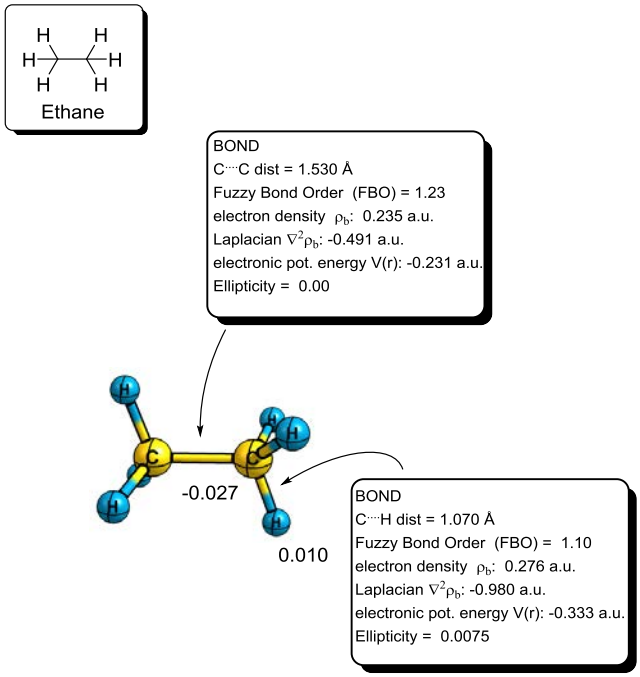

SI Figure 10.25. Geometric and electronic properties of ethane. Geometry and NBO analysis at B3LYP/6-31G(d), AIM, CHELPG ESP charges and Fuzzy bond order analysis at M062X/6-311++G(2d,2p). The geometry on Figure 2.4 was optimised at B3LYP/6-311G(d,p) level, however C-C distance obtained (1.53042 Å) was only 0.0001 Å shorter than at B3LYP/6-31G(d) level.

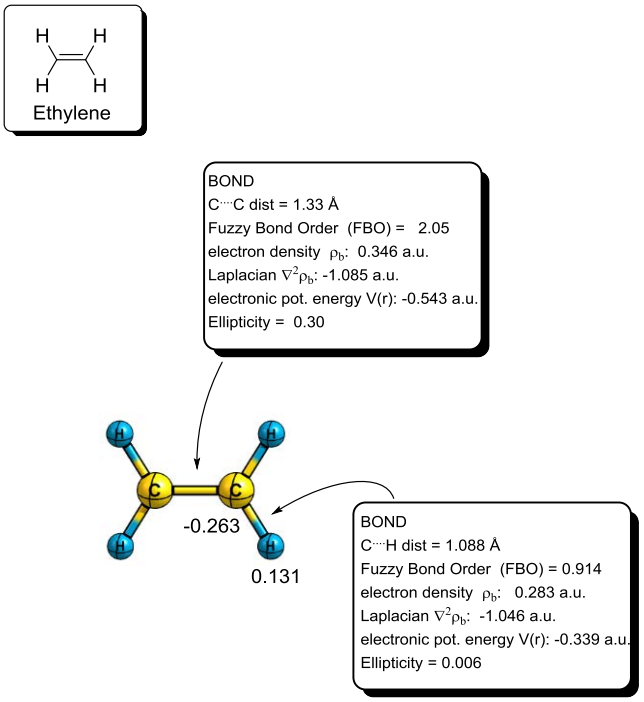

SI Figure 10.26. Geometric and electronic properties of ethylene. Geometry and NBO analysis at B3LYP/6-31G(d), AIM, CHELPG ESP charges and Fuzzy bond order analysis at M062X/6-311++G(2d,2p).

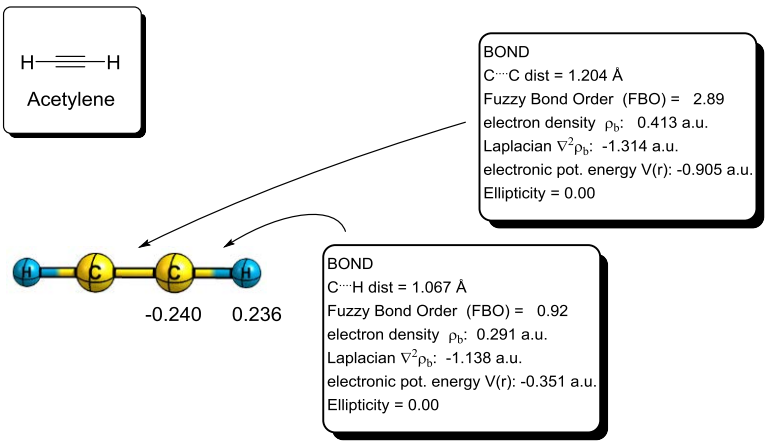

SI Figure 10.27. Geometric and electronic properties of acetylene. Geometry and NBO analysis at B3LYP/6-31G(d), AIM, CHELPG ESP charges and Fuzzy bond order analysis at M062X/6-311++G(2d,2p).

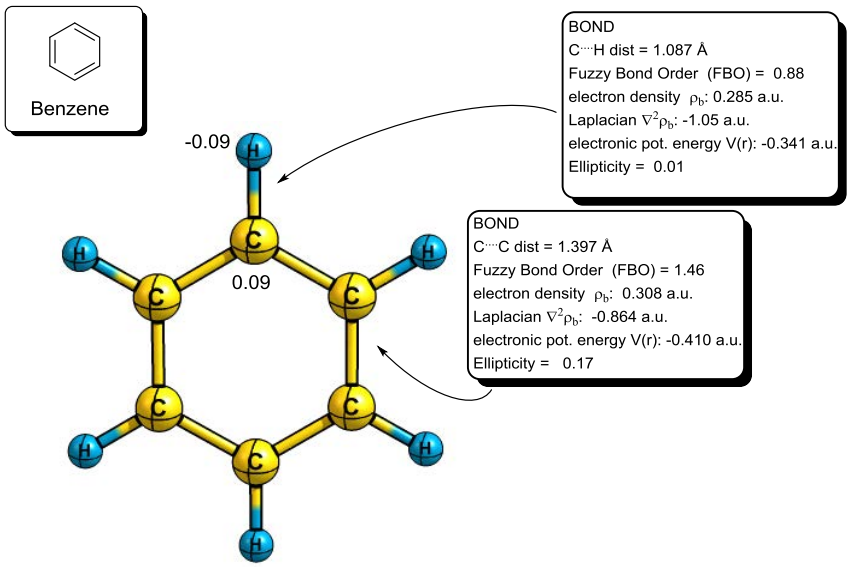

SI Figure 10.28. Geometric and electronic properties of benzene. Geometry and NBO analysis at B3LYP/6-31G(d), AIM, CHELPG ESP charges and Fuzzy bond order analysis at M062X/6-311++G(2d,2p).

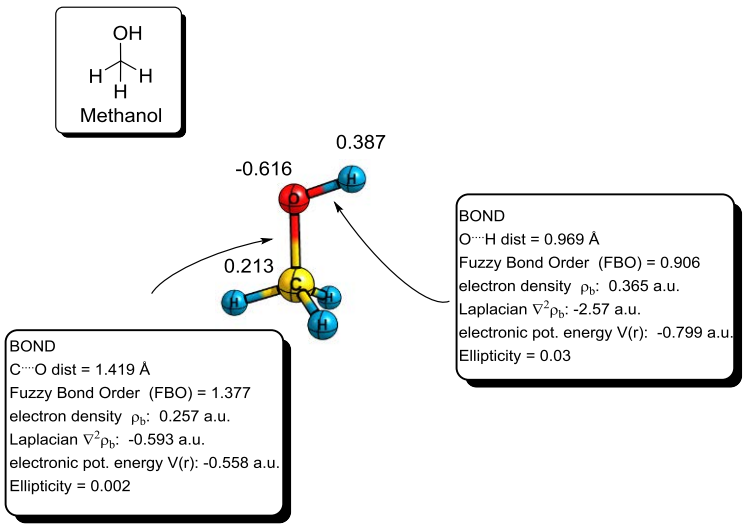

SI Figure 10.29. Geometric and electronic properties of methanol. Geometry and NBO analysis at B3LYP/6-31G(d), AIM, CHELPG ESP charges and Fuzzy bond order analysis at M062X/6-311++G(2d,2p).

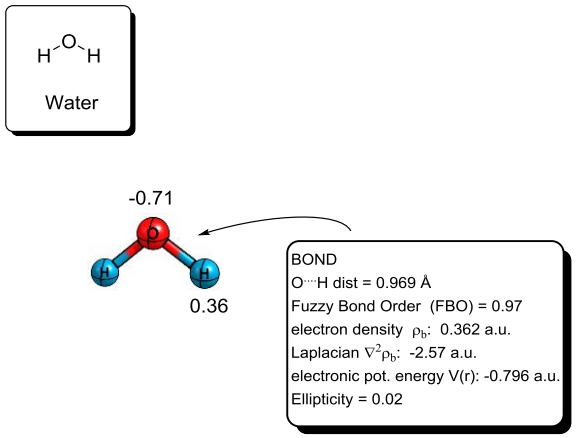

SI Figure 10.30. Geometric and electronic properties of water. Geometry and NBO analysis at B3LYP/6-31G(d), AIM, CHELPG ESP charges and Fuzzy bond order analysis at M062X/6-311++G(2d,2p).

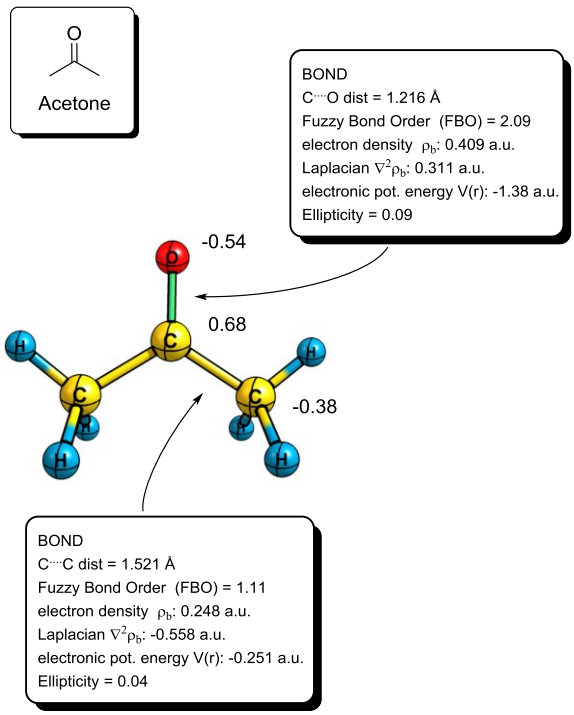

SI Figure 10.31. Geometric and electronic properties of acetone. Geometry and NBO analysis at B3LYP/6-31G(d), AIM, CHELPG ESP charges and Fuzzy bond order analysis at M062X/6-311++G(2d,2p).

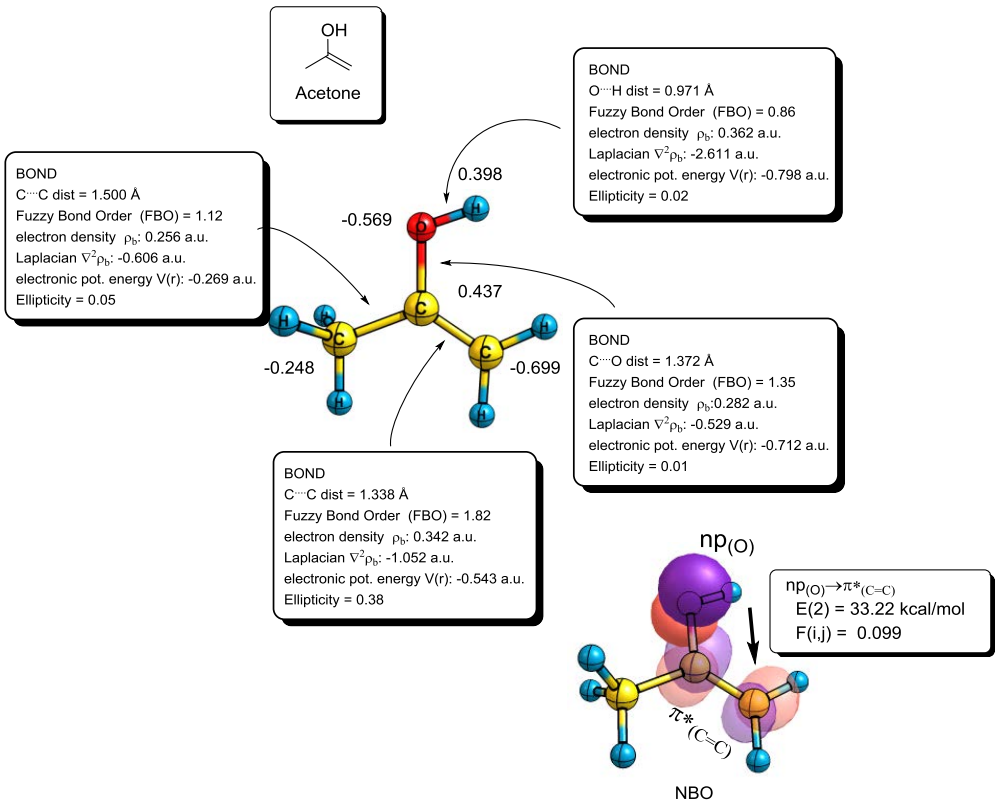

SI Figure 10.32. Geometric and electronic properties of the enol form of acetone. Geometry and NBO analysis at B3LYP/6-31G(d), AIM, CHELPG ESP charges and Fuzzy bond order analysis at M062X/6-311++G(2d,2p).

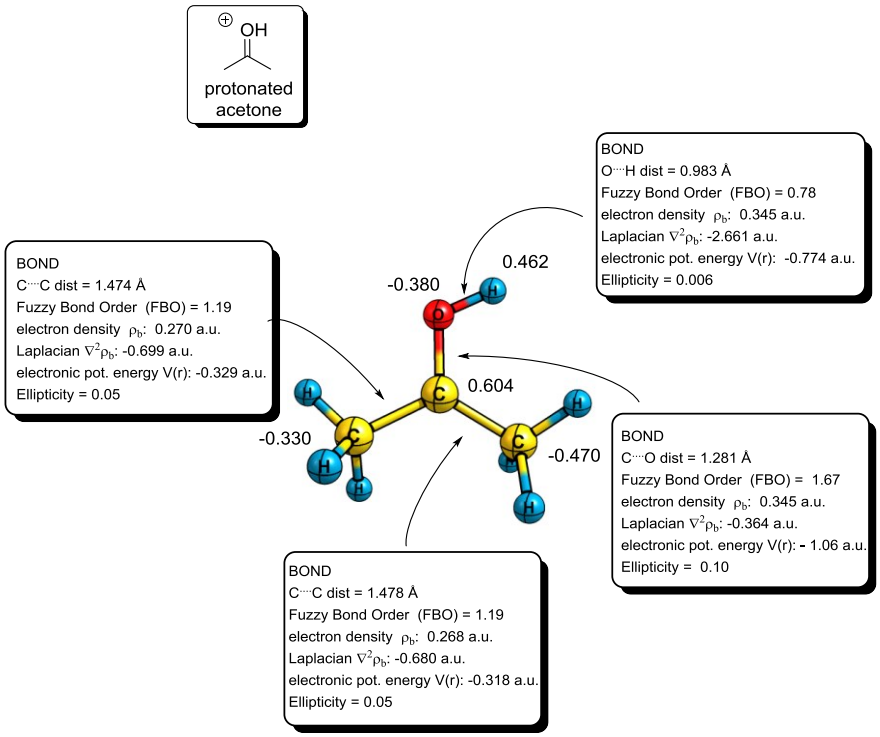

SI Figure 10.33. Geometric and electronic properties of protonated acetone. Geometry and NBO analysis at B3LYP/6-31G(d), AIM, CHELPG ESP charges and Fuzzy bond order analysis at M062X/6-311++G(2d,2p).

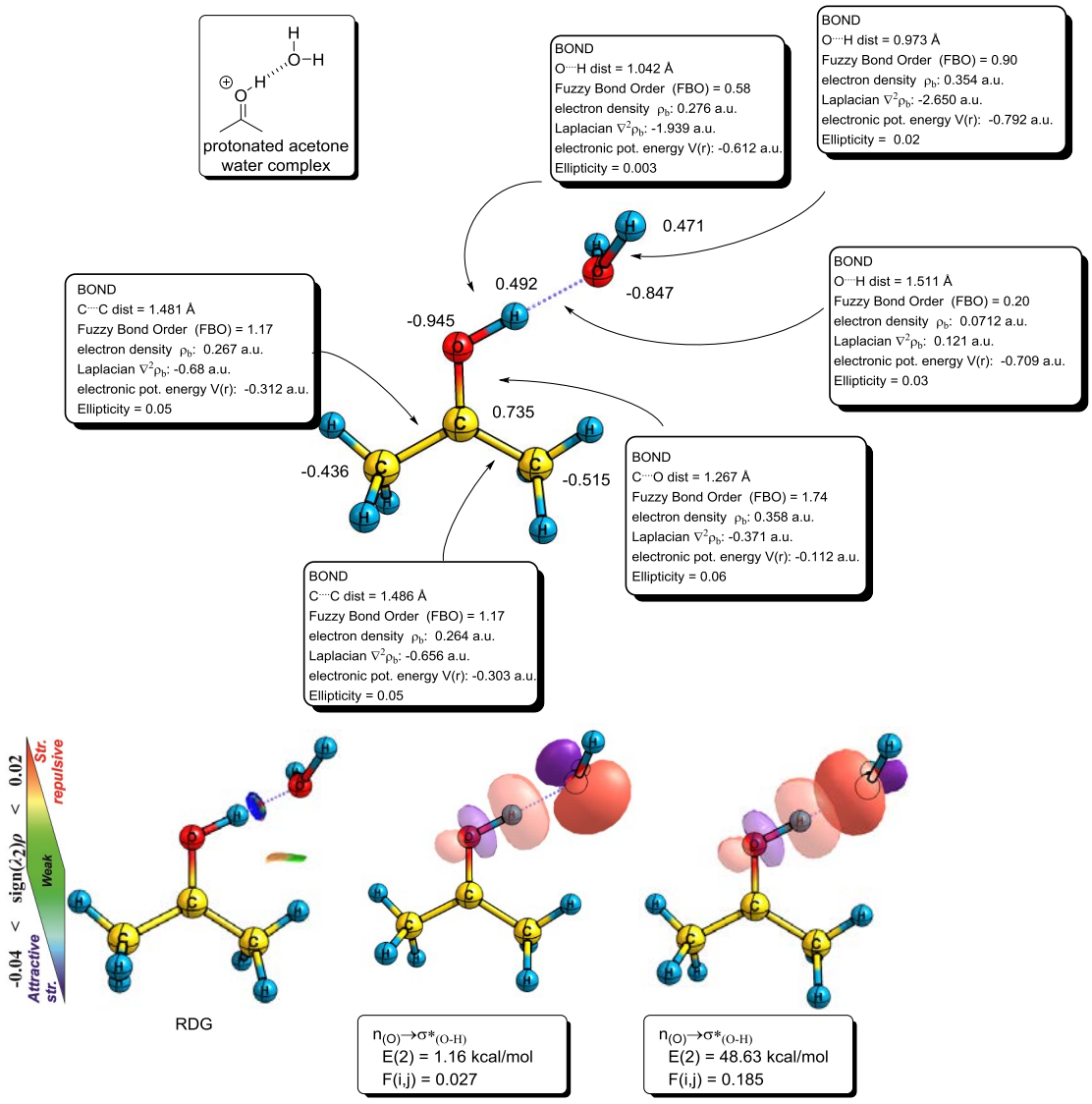

SI Figure 10.34. Geometric and electronic properties of a protonated acetone – water complex. Geometry and NBO analysis at B3LYP/6-31G(d), AIM, CHELPG ESP charges and Fuzzy bond order analysis at M062X/6-311++G(2d,2p).

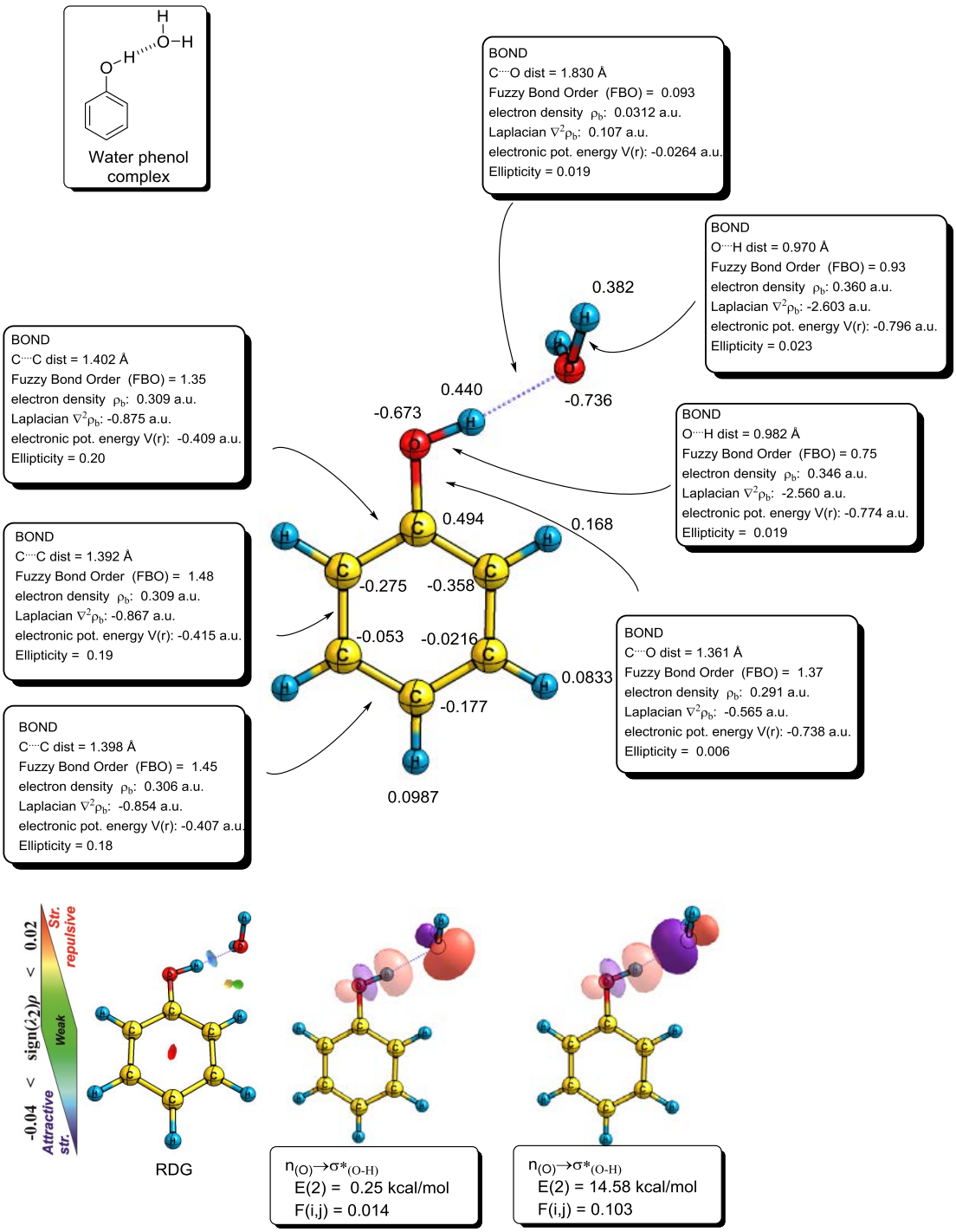

SI Figure 10.35. Geometric and electronic properties of a phenol - water complex. Geometry and NBO analysis at B3LYP/6-31G(d), AIM, CHELPG ESP charges and Fuzzy bond order analysis at M062X/6-311++G(2d,2p).

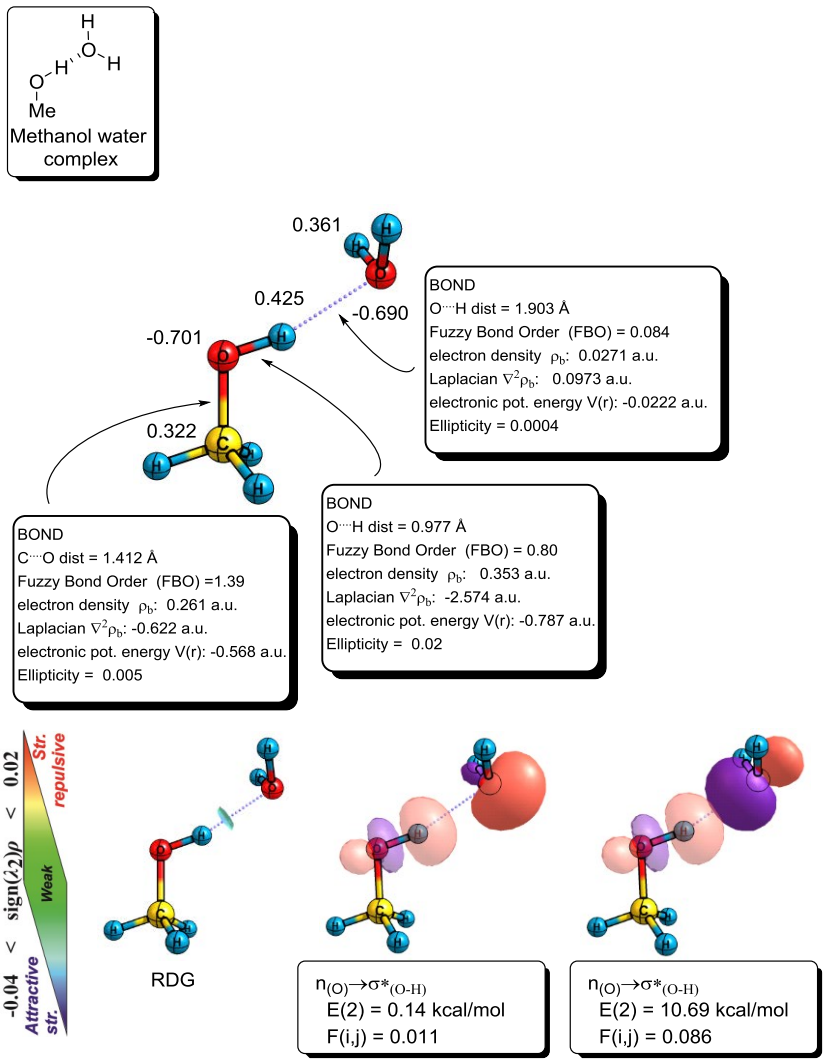

SI Figure 10.36. Geometric and electronic properties of a methanol - water complex. Geometry and NBO analysis at B3LYP/6-31G(d), AIM, CHELPG ESP charges and Fuzzy bond order analysis at M062X/6-311++G(2d,2p).

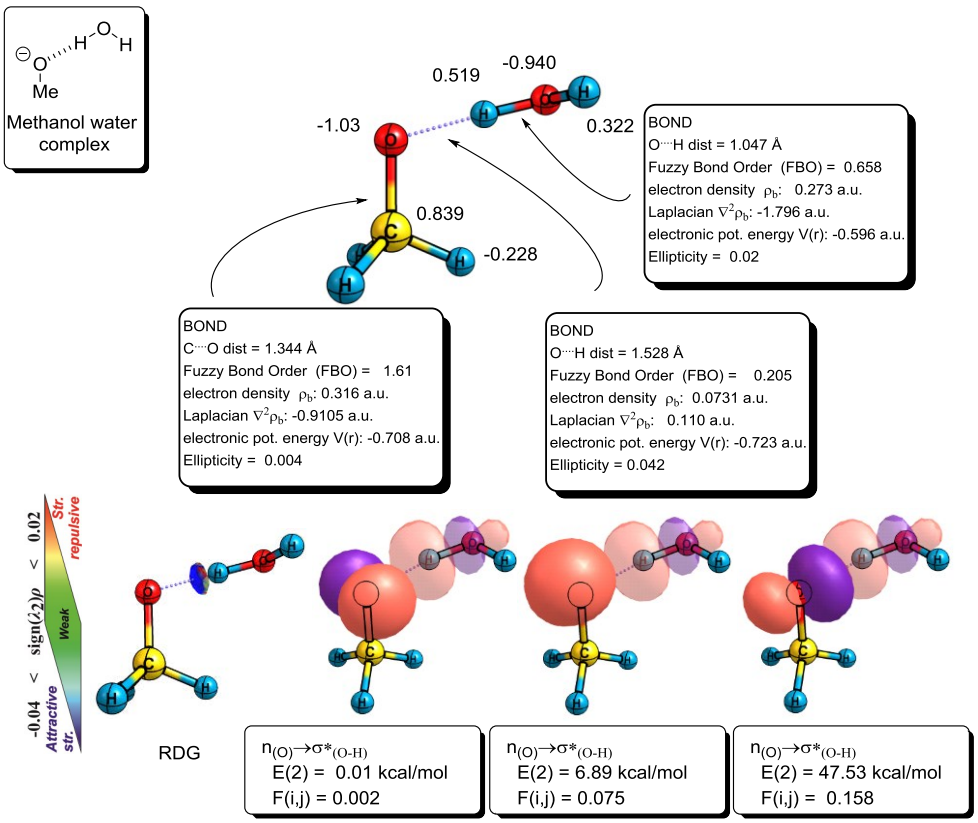

SI Figure 10.37. Geometric and electronic properties of a methoxide-water complex. Geometry and NBO analysis at B3LYP/6-31G(d), AIM, CHELPG ESP charges and Fuzzy bond order analysis at M062X/6-311++G(2d,2p).

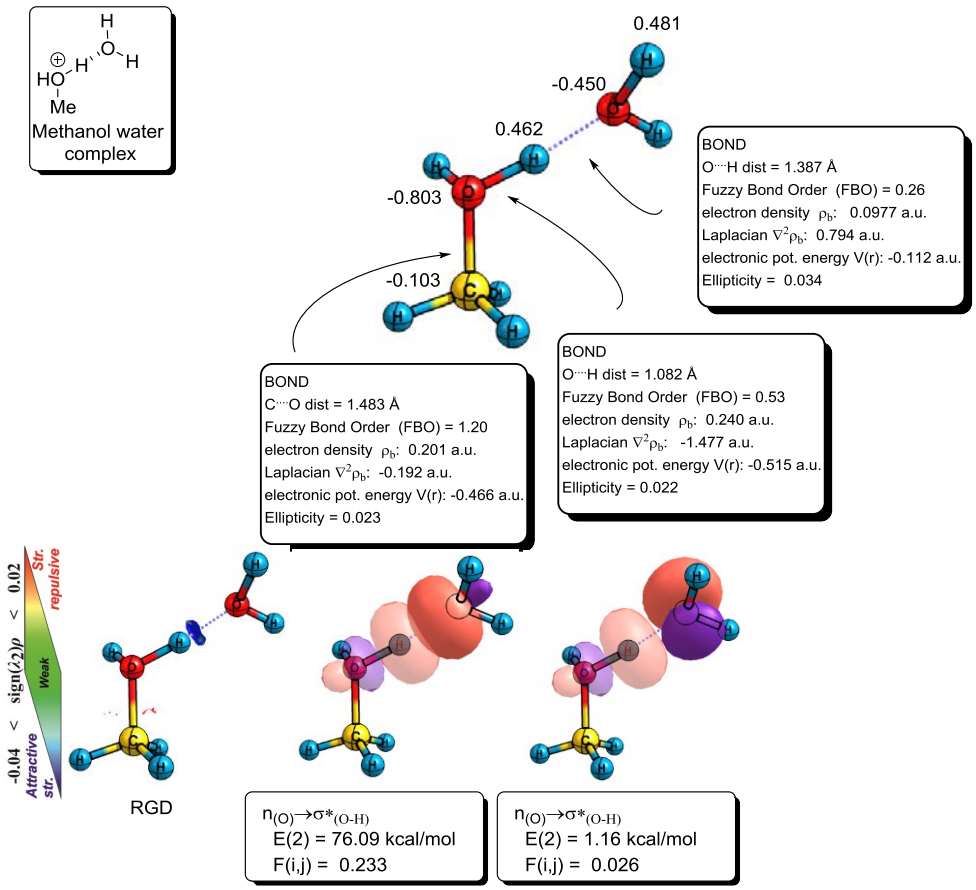

SI Figure 10.38. Geometric and electronic properties of a protonated methanol-water complex. Geometry and NBO analysis at B3LYP/6-31G(d), AIM, CHELPG ESP charges and Fuzzy bond order analysis at M062X/6-311++G(2d,2p).

Reference

THERE ARE TWO THINGS THAT EVERYBODY THINKS THEY CAN DO BETTER THAN ANYONE ELSE
PUNCH THE FIRE, AND EDIT A DAILY PAPER.
UNCLE ESEK

[1] a) S. T. Perri, H. J. Dyke, H. W. Moore, *J. Org. Chem.* **1989**, *54*, 2032-2034; b) A. Enhsen, K. Karabelas, J. M. Heerding, H. W. Moore, *J. Org. Chem.* **1990**, *55*, 1177-1185; c) J. M. Heerding, H. W. Moore, *J. Org. Chem.* **1991**, *56*, 4048-4050; d) M. P. Winters, M. Stranberg, H. W. Moore, *J. Org. Chem.* **1994**, *59*, 7572-7574; e) L. J. Sun, L. S. Liebeskind, *J. Org. Chem.* **1995**, *60*, 8194-8203; f) F. Q. Liu, L. S. Liebeskind, *J. Org. Chem.* **1998**, *63*, 2835-2844; g) J. E. Ezcurra, K. Karabelas, H. W. Moore, *Tetrahedron* **2005**, *61*, 275-286.

[2] R. R. Jones, R. G. Bergman, *J. Am. Chem. Soc.* **1972**, *94*, 660-661.

[3] a) J. O. Karlsson, N. V. Nguyen, L. D. Foland, H. W. Moore, *J. Am. Chem. Soc.* **1985**, *107*, 3392-3393; b) R. Nagata, H. Yamanaka, E. Okazaki, I. Saito, *Tetrahedron Lett.* **1989**, *30*, 4995-4998.

[4] A. G. Myers, E. Y. Kuo, N. S. Finney, *J. Am. Chem. Soc.* **1989**, *111*, 8057-8059.

[5] a) M. Schmittel, M. Strittmatter, S. Kiau, *Tetrahedron Lett.* **1995**, *36*, 4975-4978; b) M. Schmittel, M. Strittmatter, S. Kiau, *Angew. Chem. Int. Ed.* **1996**, *35*, 1843-1845.

[6] R. W. Sullivan, V. M. Coghlan, S. A. Munk, M. W. Reed, H. W. Moore, *J. Org. Chem.* **1994**, *59*, 2276-2278.

[7] E. Packard, D. D. Pascoe, J. Maddaluno, T. P. Goncalves, D. C. Harrowven, *Angew. Chem. Int. Ed.* **2013**, *52*, 13076-13079.

[8] D. Knueppel, S. F. Martin, *Angew. Chem. Int. Ed.* **2009**, *48*, 2569-2571.

[9] K. H. Lee, H. W. Moore, *Tetrahedron Lett.* **1993**, *34*, 235-238.

[10] D. C. Harrowven, D. D. Pascoe, D. Demurtas, H. O. Bourne, *Angew. Chem. Int. Ed.* **2005**, *44*, 1221-1222.

[11] M. W. Reed, H. W. Moore, *J. Org. Chem.* **1987**, *52*, 3491-3492.

[12] a) L. D. Foland, J. O. Karlsson, S. T. Perri, R. Schwabe, S. L. Xu, S. Patil, H. W. Moore, *J. Am. Chem. Soc.* **1989**, *111*, 975-989; b) A. Padwa, D. J. Austin, U. Chiacchio, J. M. Kassir, A. Rescifina, S. L. Xu, *Tetrahedron Lett.* **1991**, *32*, 5923-5926; c) K. K. Wang, *Chem. Rev.* **1996**, *96*, 207-222.

[13] Y. Yamamoto, M. Ohno, S. Eguchi, *J. Org. Chem.* **1994**, *59*, 4707-4709.

[14] M. Zora, M. Kokturk, T. Eralp, *Tetrahedron* **2006**, *62*, 10344-10351.

[15] a) E. W. Baxter, D. Labaree, S. Chao, P. S. Mariano, *J. Org. Chem.* **1989**, *54*, 2893-2904; b) X. Creary, *Org. Lett.* **2000**, *2*, 2069-2072.

[16] S. Inayama, K. Mamoto, T. Shibata, T. Hirose, *J. Med. Chem.* **1976**, *19*, 433-436.

[17] a) H. Hori, H. Nagasawa, M. Ishibashi, Y. Uto, A. Hirata, K. Saijo, K. Ohkura, K. L. Kirk, Y. Uehara, *Bioorgan. Med. Chem.* **2002**, *10*, 3257-3265; b) H. Hori, H. Nagasawa, Y. Uto, *Cell. Mol. Biol. Lett.* **2003**, *8*, 528-530; c) H. Hori, H. Nagasawa, Y. Uto, K. Ohkura, K. L. Kirk, Y. Uehara, M. Shimamura, *Bba-Proteins Proteom.* **2004**, *1697*, 29-38.

[18] a) M. Takai, S. Y. Liu, Y. Ogihara, Y. Iitaka, *Chem. Pharm. Bul.l* **1977**, *25*, 1404-1407; b) Y. W. Leong, L. J. Harrison, G. J. Bennett, A. A. Kadir, J. D. Connolly, *Phytochemistry* **1998**, *47*, 891-894; c) Y. Aoyama, T. Konoike, A. Kanda, N. Naya, M. Nakajima, *Bioorg. Med. Chem. Lett.* **2001**, *11*, 1695-1697; d) H. M. Oh, S. K. Choi, J. M. Lee, S. K. Lee, H. Y. Kim, D. C. Han, H. M. Kim, K. H. Son, B. M. Kwon, *Bioorgan. Med. Chem.* **2005**, *13*, 6182-6187.

[19] X. C. Li, D. Ferreira, M. R. Jacob, Q. F. Zhang, S. I. Khan, H. N. ElSohly, D. G. Nagle, T. J. Smillie, I. A. Khan, L. A. Walker, A. M. Clark, *J. Am. Chem. Soc.* **2004**, *126*, 6872-6873.

[20] G. Oppermann, M. Stranberg, H. W. Moore, E. Schaumann, G. Adiwidjaja, *Synthesis-Stuttgart* **2010**, 2027-2038.

[21] L. D. Foland, O. H. W. Decker, H. W. Moore, *J. Am. Chem. Soc.* **1989**, *111*, 989-995.

[22] L. S. Liebeskind, B. S. Foster, *J. Am. Chem. Soc.* **1990**, *112*, 8612-8613.

[23] H. J. Xia, H. W. Moore, *J. Org. Chem.* **1992**, *57*, 3765-3766.

[24] Y. F. Xiong, H. J. Xia, H. W. Moore, *J. Org. Chem.* **1995**, *60*, 6460-6467.

[25] M. Balci, W. M. Jones, *J. Am. Chem. Soc.* **1980**, *102*, 7607-7608.

[26] L. S. Liebeskind, S. Iyer, C. F. Jewell, *J. Org. Chem.* **1986**, *51*, 3065-3067.

[27] D. C. Harrowven, D. D. Pascoe, I. L. Guy, *Angew. Chem. Int. Ed.* **2007**, *46*, 425-428.

[28] J. M. MacDougall, P. Turnbull, S. K. Verma, H. W. Moore, *J. Org. Chem.* **1997**, *62*, 3792-3793.

[29] a) J. M. MacDougall, V. J. Santora, S. K. Verma, P. Turnbull, C. R. Hernandez, H. W. Moore, *J. Org. Chem.* **1998**, *63*, 6905-6913; b) S. K. Verma, Q. H. Nguyen, J. M. MacDougall, E. B. Fleischer, H. W. Moore, *J. Org. Chem.* **2000**, *65*, 3379-3386.

[30] K. H. Lee, H. W. Moore, *J. Org. Chem.* **1995**, *60*, 735-738.

[31] H. B. Tan, C. Zheng, Z. Liu, D. Z. Wang, *Org. Lett.* **2011**, *13*, 2192-2195.

[32] K. H. Lee, H. W. Moore, *J. Kor. Chem. Soc.* **2003**, *47*, 229-236.

[33] H. W. Moore, S. T. Perri, *J. Org. Chem.* **1988**, *53*, 996-1003.

[34] A. G. Birchler, F. Q. Liu, L. S. Liebeskind, *J. Org. Chem.* **1994**, *59*, 7737-7745.

[35] W. J. Leigh, J. A. Postigo, *J. Am. Chem. Soc.* **1995**, *117*, 1688-1694.

[36] H. M. Frey, *Trans. Faraday Soc.* **1964**, *60*, 83-87.

[37] Web of Science return more than 50 results with torquoselectivity in the title and 134 results in the topic at the time of writing this thesis, viewed on **8.08.2014**.

[38] W. R. Dolbier, H. Koroniak, K. N. Houk, C. M. Sheu, *Acc. Chem. Res.* **1996**, *29*, 471-477.

[39] W. R. Dolbier, H. Koroniak, D. J. Burton, P. L. Heinze, A. R. Bailey, G. S. Shaw, S. W. Hansen, *J. Am. Chem. Soc.* **1987**, *109*, 219-225.

[40] K. N. Houk, D. C. Spellmeyer, C. W. Jefford, C. G. Rimbault, Y. Wang, R. D. Miller, *J. Org. Chem.* **1988**, *53*, 2125-2127.

[41] M. Murakami, Y. Miyamoto, Y. Ito, *Angew. Chem. Int. Ed.* **2001**, *40*, 189-190.

[42] a) W. Kirmse, N. G. Rondan, K. N. Houk, *J. Am. Chem. Soc.* **1984**, *106*, 7989-7991; b) N. G. Rondan, K. N. Houk, *J. Am. Chem. Soc.* **1985**, *107*, 2099-2111; c) K. Nakamura, K. N. Houk, *J. Org. Chem.* **1995**, *60*, 686-691.

[43] M. Murakami, Y. Miyamoto, Y. Ito, *J. Am. Chem. Soc.* **2001**, *123*, 6441-6442.
[44] a) S. Inagaki, H. Ikeda, *J. Org. Chem.* **1998**, *63*, 7820-7824; b) H. Ikeda, Y. Naruse, S. Inagaki, *Chem. Lett.* **1999**, 363-364; c) H. Ikeda, T. Kato, S. Inagaki, *Chem. Lett.* **2001**, 270-271.
[45] P. S. Lee, S. Sakai, P. Horstermann, W. R. Roth, E. A. Kallel, K. N. Houk, *J. Am. Chem. Soc.* **2003**, *125*, 5839-5848.
[46] H. J. Jiao, P. V. Schleyer, *J. Phys. Org. Chem.* **1998**, *11*, 655-662.
[47] D. C. Spellmeyer, K. N. Houk, *J. Am. Chem. Soc.* **1988**, *110*, 3412-3416.
[48] O. Wiest, K. N. Houk, K. A. Black, B. Thomas, *J. Am. Chem. Soc.* **1995**, *117*, 8594-8599.
[49] M. A. Mcallister, T. T. Tidwell, *J. Am. Chem. Soc.* **1994**, *116*, 7233-7238.
[50] L. Gong, M. A. Mcallister, T. T. Tidwell, *J. Am. Chem. Soc.* **1991**, *113*, 6021-6028.
[51] S. Niwayama, E. A. Kallel, C. M. Sheu, K. N. Houk, *J. Org. Chem.* **1996**, *61*, 2517-2522.
[52] R. L. Danheiser, A. L. Helgason, *J. Am. Chem. Soc.* **1994**, *116*, 9471-9479.
[53] R. Koch, C. Wentrup, *Org. Biomol. Chem.* **2004**, *2*, 195-199.
[54] P. W. Musch, C. Remenyi, H. Helten, B. Engels, *J. Am. Chem. Soc.* **2002**, *124*, 1823-1828.
[55] M. R. Fernández, A. Hernández, R. Ordóñez M. , *J. Mexi. Chem. Soc.* **2002**, *46*, 136-139.
[56] C. J. Cramer, B. L. Kormos, M. Seierstad, E. C. Sherer, P. Winget, *Org. Lett.* **2001**, *3*, 1881-1884.
[57] a) M. Abe, *Chem. Rev.* **2013**, *113*, 7011-7088; b) R. K. Mohamed, P. W. Peterson, I. V. Alabugin, *Chem. Rev.* **2013**, *113*, 7089-7129.
[58] P. Costa, W. Sander, *Angew. Chem. Int. Ed.* **2014**, *53*, 5122-5125.
[59] a) M. J. S. Dewar, Kirschne.S, H. W. Kollmar, *J. Am. Chem. Soc.* **1974**, *96*, 5240-5242; b) M. J. S. Dewar, Kirschne.S, H. W. Kollmar, L. E. Wade, *J. Am. Chem. Soc.* **1974**, *96*, 5242-5244.
[60] A. N. Abeywickrema, A. L. J. Beckwith, S. Gerba, *J. Org. Chem.* **1987**, *52*, 4072-4078.
[61] J. E. Baldwin, *J. Chem. Soc. Chem. Comm.* **1976**, 734-736.
[62] a) G. B. Chai, S. Z. Wu, C. L. Fu, S. M. Ma, *J. Am. Chem. Soc.* **2011**, *133*, 3740-3743; b) A. G. Ross, X. H. Li, S. J. Danishefsky, *J. Am. Chem. Soc.* **2012**, *134*, 16080-16084.
[63] B. M. Trost, O. R. Thiel, H. C. Tsui, *J. Am. Chem. Soc.* **2003**, *125*, 13155-13164.
[64] L. A. Paquette, *Eur J. Org. Chem.* **1998**, 1709-1728.
[65] A. Gurski, L. S. Liebeskind, *J. Am. Chem. Soc.* **1993**, *115*, 6101-6108.
[66] S. Xu, B. R. Yerxa, R. W. Sullivan, H. W. Moore, *Tetrahedron Lett.* **1991**, *32*, 1129-1132.
[67] T. Varea, A. Alcalde, C. L. de Dicastillo, C. R. de Arellano, F. P. Cossio, G. Asensio, *J. Org. Chem.* **2012**, *77*, 6327-6331.
[68] T. Varea, A. Alcalde, A. Grancha, J. Lloret, G. Asensio, A. Lledos, *J. Org. Chem.* **2008**, *73*, 6521-6533.
[69] M. Solomon, W. C. L. Jamison, M. Mccormick, D. Liotta, D. A. Cherry, J. E. Mills, R. D. Shah, J. D. Rodgers, C. A. Maryanoff, *J. Am. Chem. Soc.* **1988**, *110*, 3702-3704.
[70] P. Beak, A. I. Meyers, *Acc. Chem. Res.* **1986**, *19*, 356-363.

[71] a) O. Nieto Faza, C. Silva López, R. Álvarez, Á. R. de Lera, *Chem– Eur. J.* **2004**, *10*, 4324-4333; b) O. N. Faza, C. S. López, R. Álvarez, Á. R. de Lera, *Chem– Eur. J.* **2009**, *15*, 1944-1956.
[72] S. T. Perri, L. D. Foland, O. H. W. Decker, H. W. Moore, *J. Org. Chem.* **1986**, *51*, 3067-3068.
[73] M. Mohamed, T. P. Goncalves, R. J. Whitby, H. F. Sneddon, D. C. Harrowven, *Chem-Eur. J.* **2011**, *17*, 13698-13705.
[74] M. Mohammed, PhD thesis, Southampton University (UK), **2013**.
[75] a) A. D. Becke, *Phys. Rev. A* **1988**, *38*, 3098-3100; b) C. T. Lee, W. T. Yang, R. G. Parr, *Phys. Rev. B* **1988**, *37*, 785-789.
[76] A. D. Becke, *J. Chem. Phys.* **1993**, *98*, 5648-5652.
[77] L. A. Curtiss, K. Raghavachari, P. C. Redfern, V. Rassolov, J. A. Pople, *J. Chem. Phys.* **1998**, *109*, 7764-7776.
[78] a) F. Neese, *J. Comput. Chem.* **2003**, *24*, 1740-1747; b) F. Neese, F. Wennmohs, A. Hansen, U. Becker, *Chem. Phys.* **2009**, *356*, 98-109; c) F. Neese, *Wires Comput. Mol. Sci.* **2012**, *2*, 73-78.
[79] R. Krishnan, J. S. Binkley, R. Seeger, J. A. Pople, *J. Chem. Phys.* **1980**, *72*, 650-654.
[80] a) J. Z. Pu, D. G. Truhlar, *J. Phys. Chem. A* **2005**, *109*, 773-778; b) A. Tarnopolsky, A. Karton, R. Sertchook, D. Vuzman, J. M. L. Martin, *J. Phys. Chem. A* **2008**, *112*, 3-8; c) O. Tishchenko, J. J. Zheng, D. G. Truhlar, *J. Chem. Theory. Comput.* **2008**, *4*, 1208-1219; d) X. F. Xu, I. M. Alecu, D. G. Truhlar, *J. Chem. Theory. Comput.* **2011**, *7*, 1667-1676.
[81] a) C. C. Roothaan, *J. ReV. Mod. Phys.* **1951**, *23*, 69-89; b) J. A. Pople, R. K. Nesbet, *J. Chem. Phys.* **1954**, *22*, 571–572.
[82] C. Møller, M. S. Plesset, *Phys. ReV.* **1934**, *46*, 618–622.
[83] M. J. S. Dewar, E. G. Zoebisch, E. F. Healy, J. J. P. Stewart, *J. Am. Chem. Soc.* **1985**, *107*, 3902-3909.
[84] J. J. P. Stewart, *J. Comp. Chem.,* **1989**, *10*, 209-220.
[85] J. J. P. Stewart, *J. Mol. Model.* **2007**, *13*, 1173-1213.
[86] G. B. Rocha, R. O. Freire, A. M. Simas, J. J. P. Stewart, *J. Comput. Chem.* **2006**, *27*, 1101-1111.
[87] Gaussian 09, Rev. A.02, M. J. Frisch, G. W. Trucks, H. B. Schlegel, G. E. Scuseria, M. A. Robb, J. R. Cheeseman, G. Scalmani, V. Barone, B. Mennucci, G. A. Petersson, H. Nakatsuji, M. Caricato, X. Li, H. P. Hratchian, A. F. Izmaylov, J. Bloino, G. Zheng, J. L. Sonnenberg, M. Hada, M. Ehara, K. Toyota, R. Fukuda, J. Hasegawa, M. Ishida, T. Nakajima, Y. Honda, O. Kitao, H. Nakai, T. Vreven, J. A. Montgomery, Jr., J. E. Peralta, F. Ogliaro, M. Bearpark, J. J. Heyd, E. Brothers, K. N. Kudin, V. N. Staroverov, R. Kobayashi, J. Normand, K. Raghavachari, A. Rendell, J. C. Burant, S. S. Iyengar, J. Tomasi, M. Cossi, N. Rega, J. M. Millam, M. Klene, J. E. Knox, J. B. Cross, V. Bakken, C. Adamo, J. Jaramillo, R. Gomperts, R. E. Stratmann, O. Yazyev, A. J. Austin, R. Cammi, C. Pomelli, J. W. Ochterski, R. L. Martin, K. Morokuma, V. G. Zakrzewski, G. A. Voth, P. Salvador, J. J. Dannenberg, S. Dapprich, A. D. Daniels, O. Farkas, J. B. Foresman, J. V. Ortiz, J. Cioslowski, and D. J. Fox, Gaussian, Inc., Wallingford CT, **2009**.
[88] MOPAC2012, J. J. P. Stewart, Stewart Computational Chemistry, Version 12.301M web: HTTP://OpenMOPAC.net viewed on **10.08.2014**
[89] S. Grimme, *J. Chem. Phys.* **2006**, *124,* 034108-034124.

[90] a) J. Zheng, Y. Zhao, D. G. Truhlar, *J. Chem. Theory Comput.* **2003**, *3*, 569-582; b) J. Zheng, Y. Zhao, D. G. Truhlar, *J. Chem. Theory Comput.* **2009**, *5*, 808-821.
[91] Y. Zhao, D. G. Truhlar, *Theor. Chem. Acc.* **2008**, *120*, 215-241.
[92] a) B. N. Papas, H. F. Schaefer, *J. Mol. Struct. Theochem* **2006**, *768*, 175-181; b) S. E. Wheeler, K. N. Houk, *J. Chem. Theory. Comput.* **2010**, *6*, 395-404; c) L. Simon, J. M. Goodman, *Org. Biomol. Chem.* **2011**, *9*, 689-700.
[93] a) A. Halkier, T. Helgaker, P. Jorgensen, W. Klopper, H. Koch, J. Olsen, A. K. Wilson, *Chem. Phys. Lett.* **1998**, *286*, 243-252; b) Y. Y. Chuang, S. M. Chen, *J. Comput. Chem.* **2011**, *32*, 1671-1679.
[94] T. J. Lee, P. R. Taylor, *Int. J. Quantum. Chem.* **1989**, 199-207.
[95] H. Eyring, *J. Chem. Phys.* **1935**, *3*, 107-115.
[96] a) V. Barone, M. Cossi, *J. Phys. Chem. A* **1998**, *102*, 1995-2001; b) M. Cossi, N. Rega, G. Scalmani, V. Barone, *J. Comput. Chem.* **2003**, *24*, 669-681.
[97] a) S. Miertus, E. Scrocco, J. Tomasi, *Chem. Phys.* **1981**, *55*, 117-129; b) S. Miertus, J. Tomasi, *Chem. Phys.* **1982**, *65*, 239-245.
[98] J. Tomasi, B. Mennucci, R. Cammi, *Chem. Rev.* **2005**, *105*, 2999-3093.
[99] K. Yoshida, N. Matubayasi, M. Nakahara, *J. Chem. Phys.* **2008**, *129*, 214501-214511.
[100] a) J. Tomasi, B. Mennucci, R. Cammi, *Chem. Rev.* **2005**, *105*, 2999-3093; b) T. L. Fonseca, K. Coutinho, S. Canuto, *J. Chem. Phys.* **2007**, *126*, 34502-34512.
[101] I. Mayer, P. Salvador, *Chem. Phys. Lett.* **2004**, *383*, 368-375.
[102] I. Mayer, *Chem. Phys. Lett.* **1983**, *97*, 270-274.
[103] L. Guillaumes, P. Salvador, S. Simon, *J. Phys. Chem. A* **2014**, *118*, 1142-1149.
[104] a) Bader, R. F. W. Atoms in Molecules: A Quantum Theory; The International Series of Monographs on Chemistry: No. 22; Oxford University Press: New York, **1990**; b) Popelier, P. L. Atoms in Molecules: An Introduction; Pearson Education: Harlow, U.K., **2000**.
[105] E. Espinosa, E. Molins, C. Lecomte, *Chem. Phys. Lett.* **1998**, *285*, 170-173.
[106] E. R. Johnson, S. Keinan, P. Mori-Sanchez, J. Contreras-Garcia, A. J. Cohen, W. T. Yang, *J. Am. Chem. Soc.* **2010**, *132*, 6498-6506.
[107] a) J. P. Foster, F. Weinhold, *J. Am. Chem. Soc.* **1980**, *102*, 7211-7218; b) A. E. Reed, R. B. Weinstock, F. Weinhold, *J. Chem. Phys.* **1985**, *83*, 735-746.
[108] for a current overview, see F. Weinhold, C. R. Landis, Discovering Chemistry with Natural Bond Orbitals, Wiley: Hoboken NJ, 2012.
[109] J. R. Lane, J. Contreras-Garcia, J. P. Piquemal, B. J. Miller, H. G. Kjaergaard, *J. Chem. Theory. Comput.* **2013**, *9*, 3263-3266.
[110] O. Takahashi, K. Kobayashi, A. Oda, *Chem. Biodivers.* **2010**, *7*, 1349-1356.
[111] J. M. Tadic, L. Xu, *J. Org. Chem.* **2012**, *77*, 8621-8626.
[112] D. C. Harrowven, M. Mohamed, T. P. Goncalves, R. J. Whitby, D. Bolien, H. F. Sneddon, *Angew. Chem. Int. Ed.* **2012**, *51*, 4405-4408.
[113] a) D. Cremer, *Mol. Phys.* **2001**, *99*, 1899-1940; b) E. R. DAVIDSON, A. E. CLARK, *Int. J. Quant. Chem.* **2004**, *103*, 1-9; c) M. J. McGuire, P. Piecuch, *J. Am. Chem. Soc.* **2005**, *127*, 2608-2614; d) Y. Kitagawa, T. Saito, Y. Nakanishi, Y. Kataoka, T. Matsui, T. Kawakami, M. Okumura, K. Yamaguchi, *J. Phys. Chem. A* **2009**, *113*, 15041–15046; e) T. Saito, S. Nishihara, Y. Kataoka, Y. Nakanishi, Y. Kitagawa, T. Kawakami, S.

Yamanaka, M. Okumura, K. Yamaguchi, *J. Phys. Chem. A* **2010**, *114*, 7967–7974.
[114] R. Lopez, T. L. Sordo, J. A. Sordo, J. Gonzalez, *J. Org. Chem.* **1993**, *58*, 7036-7037.
[115] a) M. Yasui, Y. Naruse, S. Inagaki, *J. Org. Chem.* **2004**, *69*, 7246-7249; b) T. Yoshikawa, S. Mori, M. Shindo, *J. Am. Chem. Soc.* **2009**, *131*, 2092-2093.
[116] a) S. N. Pieniazek, F. R. Clemente, K. N. Houk, *Angew. Chem. Int. Ed.* **2008**, *47*, 7746-7749; b) N. C. James, J. M. Um, A. B. Padias, H. K. Hall, K. N. Houk, *J. Org. Chem.* **2013**, *78*, 6582-6592.
[117] K. Yamaguchi, Y. Yoshioka, T. Fueno, *Chem. Phys. Lett.* **1977**, *46*, 360-365.
[118] a) J. M. Wittbrodt, H. B. Schlegel, *J. Chem. Phys.* **1996**, *105*, 6574-6577; b) D. H. Ess, T. C. Cook, *J. Phys. Chem. A* **2012**, *116*, 4922-4929.
[119] a) J. G. Chen, M. A. McAllister, J. K. Lee, K. N. Houk, *J. Org. Chem.* **1998**, *63*, 4611-4619; b) M. E. Green, *J. Phys. Chem. B* **2001**, *105*, 5298-5303; c) M. E. Green, *J. Phys. Chem. A* **2002**, *106*, 11221-11226.
[120] C. M. Breneman, K. B. Wiberg, *J. Comput. Chem.* **1990**, *11*, 361–373.
[121] T. Lu, F. W. Chen, *J. Comput. Chem.* **2012**, *33*, 580-592.
[122] F. L. Hirshfeld, *Theoret. Claim. Acta (Berl.)* **1977**, *44*, 129-138.
[123] D. Pascou, PhD thesis, Southampton University (UK), **2006**.
[124] E. Packard, PhD thesis, Southampton University (UK), **2013**.
[125] J. K. Badenhoop, F. Weinhold, *J. Chem. Phys.* **1997**, *107*, 5406-5421.
[126] E. D. Glendening, F. Weinhold, *J. Comput. Chem.* **1998**, *19*, 610-627.
[127] C. M. Breneman, K. B. Wiberg, *J. Comput. Chem.* **1990**, *11*, 361-373.
[128] R. G. Parr, W. T. Yang, *J. Am. Chem. Soc.* **1984**, *106*, 4049-4050.
[129] a) L. M. Pratt, I. M. Khan, *J. Comput. Chem.* **1995**, *16*, 1067-1080; b) O. Kwon, F. Sevin, M. L. McKee, *J. Phys. Chem. A* **2001**, *105*, 913-922; c) L. M. Pratt, N. Van Nguyen, B. Ramachandran, *J. Org. Chem.* **2005**, *70*, 4279-4283.
[130] a) A. Harrison-Marchand, J. Y. Valnot, A. Corruble, N. Duguet, H. Oulyadi, S. Desjardins, C. Fressigne, J. Maddaluno, *Pure. Appl. Chem.* **2006**, *78*, 321-331; b) H. Oulyadi, C. Fressigne, Y. Yuan, J. Maddaluno, A. Harrison-Marchand, *Organometallics* **2012**, *31*, 4801-4809.
[131] Z. H. Che, H. S. Wang, C. L. Chuang, *Expert. Syst. Appl.* **2010**, *37*, 7189-7199.
[132] a) A. D. Becke, E. R. Johnson, *J. Chem. Phys.* **2005**, *122*; b) E. R. Johnson, A. D. Becke, *J. Chem. Phys.* **2005**, *123*, 024101-024103; c) E. R. Johnson, A. D. Becke, *J. Chem. Phys.* **2006**, *124*, 174104-117414; d) S. Grimme, J. Antony, S. Ehrlich, H. Krieg, *J. Chem. Phys.* **2010**, *132*, 154104-154108; e) S. Grimme, S. Ehrlich, L. Goerigk, *J. Comput. Chem.* **2011**, *32*, 1456-1465.
[133] a) C. Fressigne, J. Maddaluno, A. Marquez, C. Giessner-Prettre, *J. Org. Chem.* **2000**, *65*, 8899-8907; b) C. Fressigne, A. Lautrette, J. Maddaluno, *J. Org. Chem.* **2005**, *70*, 7816-7828; c) L. M. Pratt, D. G. Truhlar, C. J. Cramer, S. R. Kass, J. D. Thompson, J. D. Xidos, *J. Org. Chem.* **2007**, *72*, 2962-2966; d) L. M. Pratt, D. Jones, A. Sease, D. Busch, E. Faluade, S. C. Nguyen, B. T. Thanh, *Int. J. Quantum. Chem.* **2009**, *109*, 34-42; e) C. Fressigne, J. Maddaluno, *J. Org. Chem.* **2010**, *75*, 1427-1436.
[134] V. M. Rayon, J. A. Sordo, *J. Chem. Phys.* **2005**, *122*, 204303-204312.
[135] a) T. Fox, H. Hausmann, H. Gunther, *Magn. Reson. Chem.* **2004**, *42*, 788-794; b) B. Lecachey, H. Oulyadi, P. Lameiras, A. Harrison-Marchand, H. Gerard, J. Maddaluno, *J. Org. Chem.* **2010**, *75*, 5976-5983.

[136] S. Dapprich, I. Komaromi, K. S. Byun, K. Morokuma, M. J. Frisch, *J. Mol. Struct. Theochem* **1999**, *461*, 1-21.
[137] a) M. Dolg, H. Stoll, A. Savin, H. Preuss, *Theor. Chim. Acta.* **1989**, *75*, 173-194; b) M. Dolg, H. Stoll, H. Preuss, *Theor. Chim. Acta.* **1993**, *85*, 441-450.
[138] For review articles see: a) Perrin, L.; Maron, L.; Eisenstein, O. *Faraday Discuss.* **2003**, *124*, 25-39; b) Eisenstein, O.; Maron, L. *J. Organomet. Chem.* **2002**, *647*, 190-197; c) L. Maron, O. Eisenstein, *J. Phys. Chem. A* **2000**, *104*, 7140-7143; d) A.Villa, U. Cosentino, D. Pitea, G. Moro, A. Maiocchi, *J. Chem. Phys. A* **2000**, 3421-3429. e) L. Joubert, B. Silvi, G. Picard, *Theo. Chem. Acc.* **2000**, *104*, 109-115.
[139] a) L. Maron, O. Eisenstein, *J. Phys. Chem. A* **2000**, *104*, 7140-7143; b) D. L. Clark, J. C. Gordon, P. J. Hay, R. Poli, *Organometallics* **2005**, *24*, 5747-5758; c) C. Clavaguera, J. P. Dognon, P. Pyykko, *Chem. Phys. Lett.* **2006**, *429*, 8-12; d) S. Schinzel, M. Bindl, M. Visseaux, H. Chermette, *J. Phys. Chem. A* **2006**, *110*, 11324-11331; e) E. Furet, K. Costuas, P. Rabiller, O. Maury, *J. Am. Chem. Soc.* **2008**, *130*, 2180-2183.
[140] A. V. Marenich, C. J. Cramer, D. G. Truhlar, *J. Phys. Chem. B* **2009**, *113*, 6378-6396.
[141] U. Schumann, J. Kopf, E. Weiss, *Angew. Chem. Int. Ed.* **1985**, *24*, 215-216.
[142] a) S. Sakemi, T. Ichiba, S. Kohmoto, G. Saucy, T. Higa, *J. Am. Chem. Soc.* **1988**, *110*, 4851-4853; b) S. Matsunaga, N. Fusetani, Y. Nakao, *Tetrahedron* **1992**, *48*, 8369-8376; c) D. Vuong, R. J. Capon, E. Lacey, J. H. Gill, K. Heiland, T. Friedel, *J. Nat. Prod.* **2001**, *64*, 640-642.
[143] a) C. Cardani, D. Ghiringhelli, R. Mondelli, A. Quilico, *Tetrahedron Lett.* **1965**, *6*, 2537–2545; b) A. Furusaki, T. Watanabé, *Tetrahedron Lett.* **1968**, *9*, 6301–6304; c) T. Matsumoto, M. Yanagiya, S. Maeno, S. Yasuda, *Tetrahedron Lett.* **1968**, *9*, 6297–6300.
[144] a) R. H. Cichewicz, F. A. Valeriote, P. Crews, *Org. Lett.* **2004**, *6*, 1951-1954; b) G. R. Pettit, J. P. Xu, J. C. Chapuis, R. K. Pettit, L. P. Tackett, D. L. Doubek, J. N. A. Hooper, J. M. Schmidt, *J. Med. Chem.* **2004**, *47*, 1149-1152.
[145] W. J. Buffham, N. A. Swain, S. L. Kostiuk, T. P. Goncalves, D. C. Harrowven, *Eur. J. Org. Chem.* **2012**, 1217-1222.
[146] a) A. C. Legon, *Faraday Discuss.* **1994**, *97*, 19-33; b) A. C. Legon, *Chem. Phys. Lett.* **1995**, *247*, 24-31.
[147] a) S. H. Vosko, L. Wilk, M. Nusair, *Can. J. Phys.* **1980**, *58*, 1200-1211; b) P. J. Stephens, F. J. Devlin, C. F. Chabalowski, M. J. Frisch, *J. Phys. Chem.* **1994**, *98*, 11623-11627.
[148] a) R. G. Parr, W. Yang, *Density-Functional Theory of Atoms and Molecules*, Oxford University Press, New York, **1989**; b) A. Szabo, N. S. Ostlund, *Modern Quantum Chemistry*, Dover Publication, New York, **1989**; c) W. Koch, M. C. Holthausen, *A Chemist's Guide to Density Functional Theory*, John Wiley & Sons Ltd., Weiheim, **2000**; d) D. C. Young, *Computational Chemistry: A Practical Guide for Applying Techniques to Real World Problems*, John Wiley & Sons Ltd., New York, **2001**; e) C. J. Cramer, *Essentials of Computational Chemistry*, John Wiley & Sons Ltd., New York, **2002**; f) E. Lewars, *Computational Chemistry*, Kluwer Academic Publishers, New York, **2004**; g) F. Jensen, *Introduction to Computational Chemistry*, John Wiley & Sons Ltd., New York, **2007**; h) L. Piela, *Ideas of Quantum Chemistry*, Elsevier B. V., Oxford, **2007**.

[149] E. Schrödinger, *Ann. Phys.* **1926**, *79*, 361-376.
[150] J. R. Oppernheimer, M. Born, *Ann. Phys.* **1927**, *389*, 457-484.
[151] K. Huang, M. Born, *Dynamical theory of lattices*, University Press, Oxford, **1954**.
[152] J. Lobaugh, G. A. Voth, *Chem. Phys. Lett.* **1992**, *198*, 311-315.
[153] D. R. Hartree, *Proc. Cambridge Phil. Soc.* **1928**, *24*, 89-110.
[154] W. Pauli, *Z. Phys.* **1925**, *31*, 765-783.
[155] J. C. Slater, *Phys. Rev.* **1929**, *34*, 1293-1322.
[156] a) V. Z. Fock, *Z. Physik.* **1930**, *61*, 126-146; b) J. C. Slater, *Phys. Rev.* **1930**, *35*, 210-211.
[157] P. O. Löwdin, *Rev. Mod. Phys.* **1962**, *34*, 80-87.
[158] J. Olsen, O. Christiansen, H. Koch, P. Jorgensen, *J. Chem. Phys.* **1996**, *105*, 5082-5090.
[159] C. C. J. Roothaan, *Rev. Mod. Phys.* **1951**, *23*, 69-89.
[160] J. Cizek, *J. Chem. Phys.* **1966**, *45*, 4256-4266.
[161] a) J. A. Pople, J. S. Binkley, R. Seeger, *Int. J. Quantum. Chem.* **1976**, *Y10*, 1-19; b) R. J. Bartlett, G. D. Purvis, *Int. J. Quantum. Chem.* **1978**, *14*, 561-581.
[162] K. Raghavachari, G. W. Trucks, J. A. Pople, M. Head-Gordon, *Chem. Phys. Lett.* **1989**, *157* 479-483.
[163] J. Rezac, P. Hobza, *J. Chem. Theory. Comput.* **2013**, *9*, 2151-2155.
[164] a) T. B. Adler, G. Knizia, H. J. Werner, *J. Chem. Phys.* **2007**, *127*; b) G. Knizia, T. B. Adler, H. J. Werner, *J. Chem. Phys.* **2009**, *130*.
[165] T. B. Adler, H. J. Werner, *J. Chem. Phys.* **2011**, *135*.
[166] B. O. Roos, P. R. Taylor, P. E. M. Siegbahn, *Chem. Phys.* **1980**, *48*, 157-173.
[167] K. Andersson, P. A. Malmqvist, B. O. Roos, *J. Chem. Phys.* **1992**, *96*, 1218-1226.
[168] H. Nakano, *J. Chem. Phys.* **1993**, *99*, 7983-7992.
[169] C. Angeli, R. Cimiraglia, S. Evangelisti, T. Leininger, J. P. Malrieu, *J. Chem. Phys.* **2001**, *114*, 10252-10264.
[170] P. Hohenberg, W. Kohn, *Phys. Rev.* **1964**, *136,* B864-B871.
[171] W. Kohn, L. J. Sham, *Phys. Rev.* **1965**, *140*, A1133-A1138.
[172] a) P. A. M. Dirac, *Proc. Cambridge Philos. Soc.* **1930,** , *26*, 376-385; b) J. C. Slater, *Phys. Rev.* **1951**, *81*, 385-390; c) S. H. Vosko, L. Wilk, M. Nusair, *Can. J. Phys.* **1980**, *58*, 1200-1211.
[173] a) A. D. Becke, *J. Chem. Phys.* **1986**, *84*, 4524-4529; b) A. D. Becke, *J. Chem. Phys.* **1988**, *88*, 1053-1062; c) J. P. Perdew, K. Burke, M. Ernzerhof, *Phys. Rev. Lett* **1996**, *77*, 3865-3868.
[174] a) A. D. Becke, *J. Chem. Phys.* **1996**, *104*, 1040-1046; b) J. M. Tao, J. P. Perdew, V. N. Staroverov, G. E. Scuseria, *Phys. Rev. Lett* **2003**, *91*.
[175] W. J. Hehre, R. F. Stewart, J. A. Pople, *J. Chem. Phys.* **1969**, 2657
[176] W. J. Hehre, Ditchfie.R, J. A. Pople, *J. Chem. Phys.* **1972**, *56*, 2257-2261.
[177] P. C. Hariharan, J. A. Pople, *Theoret. Chimica. Acta.* **1973**, *28*, 213-222
[178] R. Krishnan, J. S. Binkley, R. Seeger, J. A. Pople, *J. Chem. Phys.* **1980**, *72*, 650-654.
[179] T. H. Dunning, *J. Chem. Phys.* **1989**, *90*, 1007-1023.
[180] D. G. Truhlar, B. C. Garrett, S. J. Klippenstein, *J. Phys. Chem.* **1996**, *100*, 12771-12800.
[181] G. S. Hammond, *J. Am. Chem. Soc.* **1955**, *77*, 334-338.

[182] a) J. E. Leffler, *Science* **1953**, *117*, 340-341; b) J. E. Meany, V. Minderhout, Y. Pocker, *J. Chem. Educ.* **2001**, *78*, 204-207.
[183] J. I. Seeman, *Chem. Rev.* **1983**, *83*, 83-134.
[184] a) C. Y. Peng, H. B. Schlegel, *Israel J. Chem.* **1993**, *33*, 449-454; b) C. Y. Peng, P. Y. Ayala, H. B. Schlegel, M. J. Frisch, *J. Comput. Chem.* **1996**, *17*, 49-56.
[185] K. Fukui, *Acc. Chem. Res.* **1981**, *14*, 363-368.
[186] a) P. Mori-Sanchez, A. J. Cohen, W. T. Yang, *J. Chem. Phys.* **2006**, *125*; b) A. J. Cohen, P. Mori-Sanchez, W. T. Yang, *Science* **2008**, *321*, 792-794; c) A. J. Cohen, P. Mori-Sanchez, W. T. Yang, *J. Chem. Phys.* **2008**, *129*; d) P. Mori-Sanchez, A. J. Cohen, W. T. Yang, *Phys. Rev. Lett* **2008**, *100*.
[187] Y. Zhao, D. G. Truhlar, *Acc. Chem. Res.* **2008**, *41*, 157-167.
[188] C. W. Bauschlicher, *Chem. Phys. Lett.* **1995**, *246*, 40-44.
[189] C. W. Bauschlicher, H. Partridge, *J. Chem. Phys.* **1995**, *103*, 1788-1791.
[190] J. A. Montgomery, M. J. Frisch, J. W. Ochterski, G. A. Petersson, *J. Chem. Phys.* **1999**, *110*, 2822-2827.
[191] A. G. Baboul, L. A. Curtiss, P. C. Redfern, K. Raghavachari, *J. Chem. Phys.* **1999**, *110*, 7650-7657.
[192] L. A. Curtiss, P. C. Redfern, K. Raghavachari, *J. Chem. Phys.* **2007**, *126,* 084108- 084120.
[193] L. A. Curtiss, P. C. Redfern, K. Raghavachari, J. A. Pople, *J. Chem. Phys.* **2001**, *114*, 108-117.
[194] a) J. A. Pople, M. Headgordon, D. J. Fox, K. Raghavachari, L. A. Curtiss, *J. Chem. Phys.* **1989**, *90*, 5622-5629; b) L. A. Curtiss, C. Jones, G. W. Trucks, K. Raghavachari, J. A. Pople, *J. Chem. Phys.* **1990**, *93*, 2537-2545.
[195] L. A. Curtiss, K. Raghavachari, G. W. Trucks, J. A. Pople, *J. Chem. Phys.* **1991**, *94*, 7221-7230.
[196] X. J. Qi, Y. Feng, L. Liu, Q. X. Guo, *Chinese J. Chem.* **2005**, *23*, 194-199.
[197] a) J. W. Ochterski, G. A. Petersson, K. B. Wiberg, *J. Am. Chem. Soc.* **1995**, *117*, 11299-11308; b) L. A. Curtiss, K. Raghavachari, P. C. Redfern, J. A. Pople, *J. Chem. Phys.* **2000**, *112*, 7374-7383.
[198] W. R. Zheng, Y. Fu, Q. X. Guo, *J. Chem. Theory. Comput.* **2008**, *4*, 1324-1331.
[199] J. M. L. Martin, G. de Oliveira, *J. Chem. Phys.* **1999**, *111*, 1843-1856.
[200] a) P. M. Mayer, C. J. Parkinson, D. M. Smith, L. Radom, *J. Chem. Phys.* **1998**, *108*, 9598-9598; b) P. M. Mayer, C. J. Parkinson, D. M. Smith, L. Radom, *J. Chem. Phys.* **1998**, *108*, 604-615.
[201] X. He, L. Fusti-Molnar, G. L. Cui, K. M. Merz, *J. Phys. Chem. B* **2009**, *113*, 5290-5300.
[202] S. Grimme, M. Steinmetz, *Phys. Chem. Chem. Phys. PCCP* **2013**, *15*, 16031-16042.
[203] J. M. Rodgers, P. L. Fast, D. G. Truhlar, *J. Chem. Phys.* **2000**, *112*, 3141-3147.
[204] H. Kruse, L. Goerigk, S. Grimme, *J. Org. Chem.* **2012**, *77*, 10824-10834.
[205] H. Kruse, S. Grimme, *J. Chem. Phys.* **2012**, *136,* 154101-154116.
[206] B. J. Lynch, D. G. Truhlar, *J. Phys. Chem. A* **2001**, *105*, 2936-2941.
[207] Y. Zhao, D. G. Truhlar, *J. Phys. Chem. A* **2004**, *108*, 6908-6918.
[208] A. D. Boese, J. M. L. Martin, *J. Chem. Phys.* **2004**, *121*, 3405-3416.
[209] B. J. Lynch, P. L. Fast, M. Harris, D. G. Truhlar, *J. Phys. Chem. A* **2000**, *104*, 4811-4815.

[210] Y. Zhao, N. Gonzalez-Garcia, D. G. Truhlar, *J. Phys. Chem. A* **2005**, *109*, 2012-2018.
[211] M. Korth, S. Grimme, *J. Chem. Theory. Comput.* **2009**, *5*, 993-1003.
[212] S. F. Sousa, P. A. Fernandes, M. J. Ramos, *J. Phys. Chem. A* **2007**, *111*, 10439-10452.
[213] a) E. D. Glendening, J. K. Badenhoop, F. Weinhold, *J. Comput. Chem.* **1998**, *19*, 628-646; b) E. D. Glendening, F. Weinhold, *J. Comput. Chem.* **1998**, *19*, 593-609.
[214] a) M. W. Schmidt, K. K. Baldridge, J. A. Boatz, S. T. Elbert, M. S. Gordon, J. H. Jensen, S. Koseki, N. Matsunaga, K. A. Nguyen, S. J. Su, T. L. Windus, M. Dupuis, J. A. Montgomery, *J. Comput. Chem.* **1993**, *14*, 1347-1363; b) J. Aihara, S. Oe, *Bull. Chem. Soc. Jpn.* **2003**, 1363-1364
[215] a) Bader, R. F. W. Atoms in Molecules: A Quantum Theory; The International Series of Monographs on Chemistry: No. 22; Oxford University Press: New York, **1990**; b) Popelier, P. L. Atoms in Molecules: An Introduction; Pearson Education: Harlow, U.K., **2000**.
[216] a) J. R. Cheeseman, M. T. Carroll, R. F. W. Bader, *Chem. Phys. Lett.* **1988**, *143*, 450-458; b) M. Tafipolsky, W. Scherer, K. Ofele, G. Artus, B. Pedersen, W. A. Herrmann, G. S. McGrady, *J. Am. Chem. Soc.* **2002**, *124*, 5865-5880.
[217] E. Matito, J. Poater, M. Sola, M. Duran, P. Salvador, *J. Phys. Chem. A* **2005**, *109*, 9904-9910.
[218] As recomended by MultiWFN manual ver. 3.2.1,page 66, **2014**.
[219] Y. Shao, L. F. Molnar, Y. Jung, J. Kussmann, C. Ochsenfeld, S. T. Brown, A. T. B. Gilbert, L. V. Slipchenko, S. V. Levchenko, D. P. O'Neill, R. A. DiStasio, R. C. Lochan, T. Wang, G. J. O. Beran, N. A. Besley, J. M. Herbert, C. Y. Lin, T. Van Voorhis, S. H. Chien, A. Sodt, R. P. Steele, V. A. Rassolov, P. E. Maslen, P. P. Korambath, R. D. Adamson, B. Austin, J. Baker, E. F. C. Byrd, H. Dachsel, R. J. Doerksen, A. Dreuw, B. D. Dunietz, A. D. Dutoi, T. R. Furlani, S. R. Gwaltney, A. Heyden, S. Hirata, C. P. Hsu, G. Kedziora, R. Z. Khalliulin, P. Klunzinger, A. M. Lee, M. S. Lee, W. Liang, I. Lotan, N. Nair, B. Peters, E. I. Proynov, P. A. Pieniazek, Y. M. Rhee, J. Ritchie, E. Rosta, C. D. Sherrill, A. C. Simmonett, J. E. Subotnik, H. L. Woodcock, W. Zhang, A. T. Bell, A. K. Chakraborty, D. M. Chipman, F. J. Keil, A. Warshel, W. J. Hehre, H. F. Schaefer, J. Kong, A. I. Krylov, P. M. W. Gill, M. Head-Gordon, *Phys. Chem. Chem. Phys.* **2006**, *8*, 3172-3191.
[220] G. A. Zurko, http://www.chemcraft.com viewed on **10.08.2014**.
[221] a) M. Buhl, C. Vanwullen, *Chem. Phys. Lett.* **1995**, *247*, 63-68; b) P. V. Schleyer, C. Maerker, A. Dransfeld, H. J. Jiao, N. J. R. V. Hommes, *J. Am. Chem. Soc.* **1996**, *118*, 6317-6318.
[222] a) P. Lazzeretti, *Prog Nucl Mag Res Sp* **2000**, *36*, 1-88; b) J. A. Gomes, R. B. Mallion, *Chem. Rev.* **2001**, *101*, 1349-1383; c) T. M. Krygowski, M. K. Cyranski, *Phys. Chem. Chem. Phys.* **2004**, *6*, 249-255; d) Z. F. Chen, C. S. Wannere, C. Corminboeuf, R. Puchta, P. V. Schleyer, *Chem. Rev.* **2005**, *105*, 3842-3888.
[223] A. Stanger, *J. Org. Chem.* **2006**, *71*, 883-893.
[224] D. Moran, F. Stahl, H. F. Bettinger, H. F. Schaefer, P. V. Schleyer, *J. Am. Chem. Soc.* **2003**, *125*, 6746-6752.
[225] a) J. Ahira, *Bull. Chem. Soc. Jpn.* **2004**, *77*, 101-102; b) J. Poater, M. Sola, R. G. Viglione, R. Zanasi, *J. Org. Chem.* **2004**, *69*, 7537-7542; c) F. Faglioni,

A. Ligabue, S. Pelloni, A. Soncini, R. G. Viglione, M. B. Ferraro, R. Zanasi, P. Lazzeretti, *Org. Lett.* **2005**, *7*, 3457-3460.

[226] Gaussian 09, Revision D.01, M. J. Frisch, G. W. Trucks, H. B. Schlegel, G. E. Scuseria, M. A. Robb, J. R. Cheeseman, G. Scalmani, V. Barone, B. Mennucci, G. A. Petersson, H. Nakatsuji, M. Caricato, X. Li, H. P. Hratchian, A. F. Izmaylov, J. Bloino, G. Zheng, J. L. Sonnenberg, M. Hada, M. Ehara, K. Toyota, R. Fukuda, J. Hasegawa, M. Ishida, T. Nakajima, Y. Honda, O. Kitao, H. Nakai, T. Vreven, J. A. Montgomery, Jr., J. E. Peralta, F. Ogliaro, M. Bearpark, J. J. Heyd, E. Brothers, K. N. Kudin, V. N. Staroverov, R. Kobayashi, J. Normand, K. Raghavachari, A. Rendell, J. C. Burant, S. S. Iyengar, J. Tomasi, M. Cossi, N. Rega, J. M. Millam, M. Klene, J. E. Knox, J. B. Cross, V. Bakken, C. Adamo, J. Jaramillo, R. Gomperts, R. E. Stratmann, O. Yazyev, A. J. Austin, R. Cammi, C. Pomelli, J. W. Ochterski, R. L. Martin, K. Morokuma, V. G. Zakrzewski, G. A. Voth, P. Salvador, J. J. Dannenberg, S. Dapprich, A. D. Daniels, Ö. Farkas, J. B. Foresman, J. V. Ortiz, J. Cioslowski, and D. J. Fox, Gaussian, Inc., Wallingford CT, **2009**.

[227] a) Schrödinger Release 2013-1: Maestro, version 9.4, Schrödinger, LLC, New York, NY, **2013**; b) R. Izsak, F. Neese, *J. Chem. Phys.* **2011**, *135*.

[228] F. Neese, *Wiley Interdiscip. Rev.: Comput. Mol. Sci.* **2012**, *2*, 73-78.

[229] M. Valiev, E. J. Bylaska, N. Govind, K. Kowalski, T. P. Straatsma, H. J. J. Van Dam, D. Wang, J. Nieplocha, E. Apra, T. L. Windus, W. de Jong, *Comput Phys Commun* **2010**, *181*, 1477-1489.

[230] a) MOLPRO, version 2012.1, a package of ab initio programs, H.-J. Werner, P. J. Knowles, G. Knizia, F. R. Manby, M. Schütz, P. Celani, T. Korona, R. Lindh, A. Mitrushenkov, G. Rauhut, K. R. Shamasundar, T. B. Adler, R. D. Amos, A. Bernhardsson, A. Berning, D. L. Cooper, M. J. O. Deegan, A. J. Dobbyn, F. Eckert, E. Goll, C. Hampel, A. Hesselmann, G. Hetzer, T. Hrenar, G. Jansen, C. Köppl, Y. Liu, A. W. Lloyd, R. A. Mata, A. J. May, S. J. McNicholas, W. Meyer, M. E. Mura, A. Nicklass, D. P. O'Neill, P. Palmieri, D. Peng, K. Pflüger, R. Pitzer, M. Reiher, T. Shiozaki, H. Stoll, A. J. Stone, R. Tarroni, T. Thorsteinsson, and M. Wang, http://www.molpro.net viewed on **10.08.2014**; b) H. J. Werner, P. J. Knowles, G. Knizia, F. R. Manby, M. Schutz, *Wires Comput. Mol. Sci.* **2012**, *2*, 242-253.

[231] M. J. Frisch, G. W. Trucks, H. B. Schlegel, G. E. Scuseria, M. A. Rob, J. R. Cheeseman, J. A. Montgomery Jr., T. Vreven, K. N. Kudin, J. C. Burant, J. M. Millam, S. S. Iyengar, J. Tomasi, V. Barone, B. Mennucci, M. Cossi, G. Scalmani, N. Rega, G. A. Petersson, H. Nakatsuji, M. Hada, M. Ehara, K. Toyota, R. Fukuda, J. Hasegawa, M. Ishida, T. Nakajima, Y. Honda, O. Kitao, H. Nakai, M. Klene, X. Li, J. E. Knox, H. P. Hratchian, J. B. Cross, V. Bakken, C. Adamo, J. Jaramillo, R. Gomperts, R. E. Stratmann, O. Yazyev, A. J. Austin, R. Cammi, C. Pomelli, J. W. Ochterski, P. Y. Ayala, K. Morokuma, G. A. Voth, P. Salvador, J. J. Dannenberg, V. G. Zakrzewski, S. Dapprich, A. D. Daniels, M. C. Strain, O. Farkas, D. K. Malick, A. D. Rabuck, K. Raghavachari, J. B. Foresman, J. V. Ortiz, Q. Cui, A. G. Baboul, S. Clifford, J. Cioslowski, B. B. Stefanov, G. Liu, A. Liashenko, P. Piskorz, I. Komaromi, R. L. Martin, D. J. Fox, T. Keith, M. A. Al-Laham, C. Y. Peng, A. Nanayakkara, M. Challacombe, P. M. W. Gill, B. Johnson, W. Chen, M. W. Wong, C. Gonzalez, and J. A. Pople, Gaussian 03 (Gaussian, Inc., Wallingford, CT, **2003**).

[232] a) R. Seeger, J. A. Pople, *J. Chem. Phys.* **1977**, *66*, 3045-3050; b) R. Bauernschmitt, R. Ahlrichs, *J. Chem. Phys.* **1996**, *104*, 9047-9052.
[233] M. J. S. Dewar, E. G. Zoebisch, E. F. Healy, J. J. P. Stewart, *J. Am. Chem. Soc.* **1993**, *115*, 5348-5348.
[234] J. J. P. Stewart, *J. Mol. Model.* **2013**, *19*, 1-32.
[235] J. Baker, *J. Comput. Chem.* **1986**, *7*, 385-395.
[236] J. D. L. Dutra, M. A. M. Filho, G. B. Rocha, R. O. Freire, A. M. Simas, J. J. P. Stewart, *J. Chem. Theory. Comput.* **2013**, *9*, 3333-3341.
[237] S. Kossmann, F. Neese, *Chem. Phys. Lett.* **2009**, *481*, 240-243.
[238] A. R. Allouche, *J. Comput. Chem.* **2011**, *32*, 174-182.
[239] GaussView, Version 5, Dennington, R.; Keith, T.; Millam, J. Semichem Inc., Shawnee Mission KS, **2009**.
[240] Ugo Varetto, MOLEKEL 5.3; Swiss National Supercomputing Centre: Lugano (Switzerland).
[241] a) Avogadro: an open-source molecular builder and visualization tool. Version 1.1.1 http://avogadro.openmolecules.net/ viewed on **10.08.2014**; b) M. D. Hanwell, D. E. Curtis, D. C. Lonie, T. Vandermeersch, E. Zurek, G. R. Hutchison, *J. Cheminform.* **2012**, *4,* 1-17.
[242] W. Humphrey, A. Dalke, K. Schulten, *J. Mol. Graph. Model* **1996**, *14*, 33-38.
[243] Accelrys Software Inc., Discovery Studio Modelling Environment, Release 4.0, San Diego: Accelrys Software Inc., **2013**.
[244] S. B. Liu, *J. Chem. Phys.* **2007**, *126*, 244103-244108.

Attached publications

EVEN THE WORST BOOK CAN GIVE US SOMETHING TO THINK ABOUT.
WISLAWA SZYMBORSKA

TO READ TOO MANY BOOKS IS HARMFUL.
MAO ZEDONG

CHEMISTRY
A EUROPEAN JOURNAL

DOI: 10.1002/chem.201102263

New Insights into Cyclobutenone Rearrangements: A Total Synthesis of the Natural ROS-Generating Anti-Cancer Agent Cribrostatin 6**

Mubina Mohamed,[a] Théo P. Gonçalves,[a] Richard J. Whitby,[a] Helen F. Sneddon,[b] and David C. Harrowven*[a]

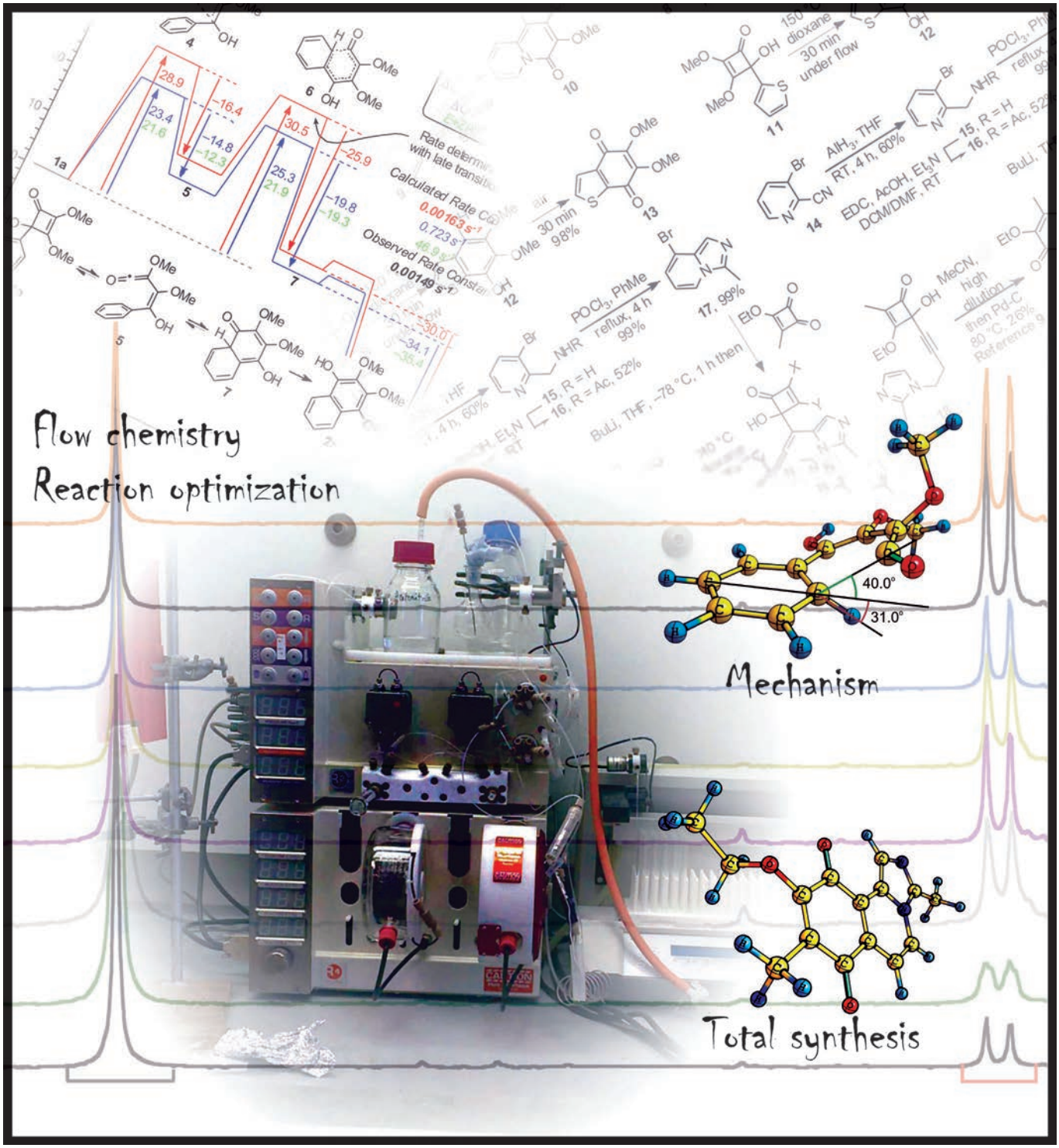

Abstract: Aryl- and heteroarylcyclobutenone rearrangements proceed in excellent yield under continuous-flow conditions. The former shows a Hammett correlation with σ_I providing strong evidence that electrocyclisation is the rate-determining step and has a late transition state. The reaction has been modelled by using DFT and CCSD(T) methods, with the latter giving excellent correlation with the experimental rate constant. A short and efficient total synthesis of cribrostatin 6, an anti-neoplastic and anti-microbial agent, provides a topical demonstration of the value of this method.

Keywords: density functional calculations · flow chemistry · Hammett correlation · reaction mechanisms · thermochemistry

Introduction

Thermal rearrangements of aryl- and heteroarylcyclobutenones have become established as useful methods for the de novo synthesis of many polyaromatic and heteroaromatic ring systems, especially those with dense substitution patterns.[1–3] Though widely used, little is known about the factors that influence the course of these reactions, or indeed the optimal conditions for effecting them. Herein we present a detailed study of the rearrangement and show how it is possible to achieve near-quantitative conversions under continuous flow. In turn, this has allowed us to establish a Hammett relationship for the reaction which,[4] in conjunction with an in silico study, provides new insights into the mechanistic course. Extensions to heteroarylcyclobutenone rearrangements include a short and efficient total synthesis of the marine natural product cribrostatin 6,[5–9] which displays useful anti-microbial and anti-cancer activity through a reactive-oxygen species (ROS)-generating mechanism.[5,7]

Results and Discussion

Reaction optimization under continuous flow and establishment of a Hammett relationship: Our investigation began with a survey of the arylcyclobutenone rearrangement, **1**→**2**+**3** (Scheme 1).[1] In batch, reactions of this type are usually conducted in xylenes at reflux (ca. 135 °C) and typically give yields of 70–85 % after 2–10 h.[1–3] By contrast, under continuous flow on a Vapourtec R4/R2+ instrument with stainless-steel tubing of 1 mm diameter,[10] it was possible to employ dioxane as the solvent at 150 °C to induce rearrangement of cyclobutenone **1a** to benzohydroquinone **2a** in 99 % isolated yield in less than 1 h.

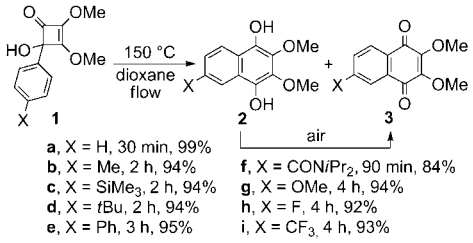

Scheme 1. Arylcyclobutenone rearrangements under continuouse flow (with isolated yields quoted for the formation of **3** from **1**).

By reasoning that the marked improvement in efficiency was due to a tight control of temperature across the narrow tubing, we were pleased to observe similar results for the rearrangement of a range of related substrates **1b–i** (Scheme 1). In each case, reactions took longer to proceed to completion than the parent compound **1a**, with electron-withdrawing substituents (F, CF_3, amide) and some electron donors (OMe) slowing the reaction down significantly. To delineate the nature of substituent effects, the progress of each reaction was determined at various residence times by using ^{1}H NMR analysis to assess the extent of conversion.[11] Though complicated by incomplete aerial oxidation of the product hydroquinones **2** to the respective benzoquinones **3**, the method proved reliable in establishing that each rearrangement exhibited first-order kinetics (Figure 1).

With these data a Hammett relationship for the reaction was sought. No correlation was evident with either the σ_m or σ_p parameter sets, as would be expected if the electrocyclic opening of the cyclobutenone were involved in the rate-determining step (Figure 2, **1a**→**5**). A reasonable correlation was given with the σ_I (inductive) parameter set (R^2=0.8584, Figure 3, grey line),[4b] with the parent compound **1a** (X= H) and those with large substituents (*t*Bu, Me_3Si, CF_3) showing greatest deviation from the line of best fit. This suggested a significant steric component to the reaction.[4,12] Indeed, by introducing a small steric correction factor (σ_I−6 % E_s) the correlation was improved to R^2=0.989 (Figure 3, bold line).[4,12]

Computational studies on the reaction mechanism: The Hammett relationship observed suggests that the electrocyc-

[a] M. Mohamed, T. P. Gonçalves, Prof. R. J. Whitby, Prof. D. C. Harrowven
Chemistry, University of Southampton
Highfield, Southampton, Hampshire, SO17 1BJ (UK)
Fax: (+44) 23-8059-6805
E-mail: dch2@soton.ac.uk

[b] Dr. H. F. Sneddon
c/o GlaxoSmithKline Medicines Research Centre
Gunnels Wood Road, Stevenage, SG1 2NY (UK)

[**] ROS = reactive-oxygen species

Supporting information for this article is available on the WWW under http://dx.doi.org/10.1002/chem.201102263.

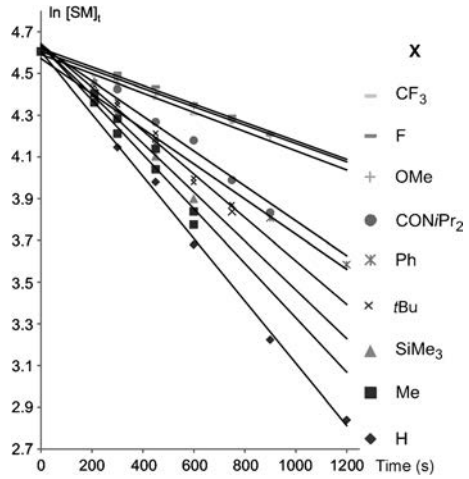

Figure 1. Determination of rate constants for **1**→**2**+**3**. X=CF_3: $k=4.4\times10^{-4}\,s^{-1}$, $R^2=0.96$; X=F: $k=4.6\times10^{-4}\,s^{-1}$, $R^2=0.98$; X=OMe: $k=6.6\times10^{-4}\,s^{-1}$, $R^2=0.99$; X=CONiPr_2: $k=8.0\times10^{-4}\,s^{-1}$, $R^2=0.98$; X=Ph: $k=8.2\times10^{-4}\,s^{-1}$, $R^2=1.00$; X=*t*Bu: $k=10.2\times10^{-4}\,s^{-1}$, $R^2=0.99$; X=$SiMe_3$: $k=12.1\times10^{-4}\,s^{-1}$, $R^2=0.98$; X=Me: $k=13.1\times10^{-4}\,s^{-1}$, $R^2=0.97$; X=H: $k=14.9\times10^{-4}\,s^{-1}$, $R^2=1.00$. $[SM]_t$=concentration of starting material at a given time.

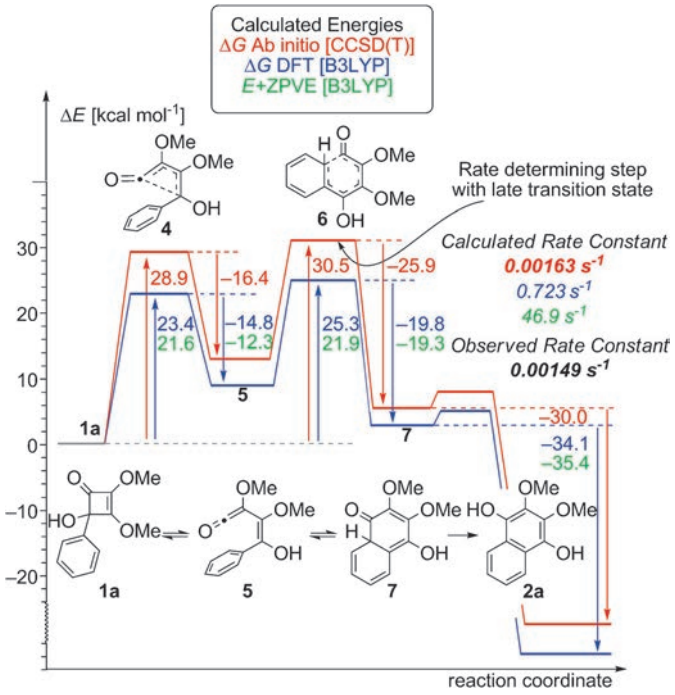

Figure 2. Summary of the energies calculated for the rearrangement **1a**→**2a** in the gas phase at 150°C computed by Δ(*E*+ZPE) UB3LYP/6-311G(d,p) (in green), Δ*G*(UB3LYP/6-311G(d,p)) (in blue) and Δ*G*(RCCSD(T)/6-31G(d)//UB3LYP/6-311G(d,p)) (in red) as well as associated rate constants.[15–18]

lisation of ketene **5** to bicyclic ketone **7** is rate determining and has a late transition state (i.e., **6** is more akin to intermediate **7** than precursor ketene **5**, Figure 2). The rate of reaction is thus dictated by the ease with which the sigma

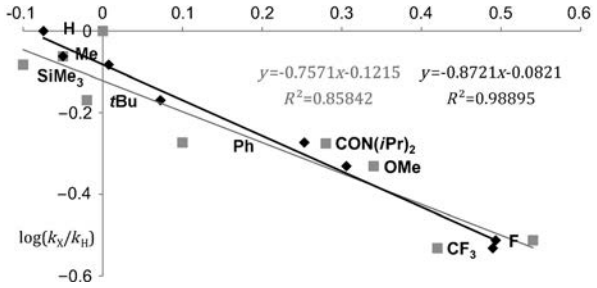

Figure 3. Hammett plot for the arylcyclobutenone rearrangement **1**→**2**+**3** with the σ_I parameter set (■) and with a steric correction (σ_I–6% E_s, ◆).[13]

bond, which is developing between the arene and the carbonyl in **6**, is established; this explains the observed influence of inductive rather than resonance effects. To test this hypothesis, the course of the reaction was modelled by DFT calculations at the UB3LYP/6-311G(d,p) level with the Gaussian 09 program.[14,15] The estimated *E*+ZPVE values (Figure 2, in green) were interesting in that they showed little difference between the activation barrier for electrocyclic ring opening (21.6 kcal mol^{-1}) and ring closing (21.9 kcal mol^{-1}). However, when these were corrected to reflect free energy, the calculated values for Δ*G* at 150°C (23.4 and 25.3 kcal mol^{-1}, respectively) supported our postulate that electrocyclisation of vinylketene **5**→**7** is rate determining. Importantly, they also showed the electrocyclic opening of **1a**→**5** to be reversible with the equilibrium favouring the cyclobutenone rather than the ketene.

A limitation of the DFT method was exposed when we sought to relate the predicted Δ*G* values to the reaction rates observed experimentally for the rearrangement **1a**→**2a**. The calculated values implied a reaction rate substantially faster than the observed one, underestimating the energy requirements by nearly 5 kcal mol^{-1}. Consequently, we refined our analysis further by employing high ab initio single-point energy calculations [RCCSD(T)/6-31G(d)] with the GAMESS(US) package.[17,18] The results attained predicted a rate constant for the rearrangement of **1a**→**2a** of 0.0016 s^{-1} after correction for the free energy at 150°C; this is in excellent agreement with the observed value (0.00149 s^{-1}). In addition, these calculations reaffirmed that the electrocyclic closure **5**→**7** is rate limiting (30.5 kcal mol^{-1} compared with 28.9 kcal mol^{-1} for **1a**→**5**).

The calculated geometry for transition-state **6** (Figure 4) is also instructive as it shows an angle of incidence of 40.0° between the developing σ bond and the plane of the arene. The angle is reduced to 22.1° as the reaction progresses to intermediate **7**. Thus, interaction between this nascent σ bond and the residual π system is limited as it develops to become part of the σ framework—an observation that is consistent with a late transition state under the influence of inductive rather than resonance effects.

Further exemplifications of the method and a total synthesis of cribrostatin 6: Our attention next turned to the rear-

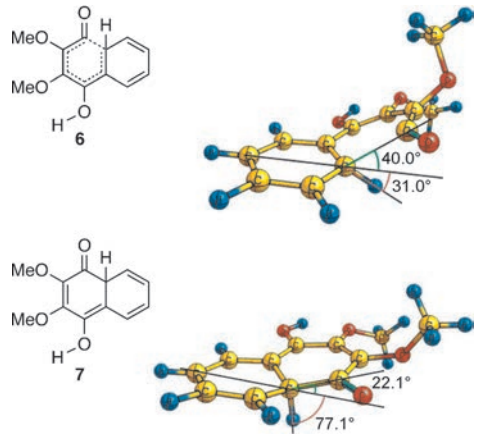

Figure 4. Calculated structures for the transition state **6** and intermediate **7**.[16]

rangement of heteroarylcyclobutenones. With a myriad of options available, we limited our study to representative electron-rich (thiophene) and electron-poor (pyridine) systems, and an exemplification through total synthesis. The thermolysis of (2-pyridyl)cyclobutenones provides rapid access to quinolizidones,[2a] for example, **9**→**10**, which are used widely in medicinal chemistry as isosteres for naphthalenes. In spite of this, the reaction has found little favour, perhaps due to modest yields (29–60%) and a need to protect the alcohol moiety formed on addition of a 2-lithiopyridine to a cyclobutendione. Under continuous-flow conditions, the thermal rearrangement of pyridylcyclobutenone **9** in dioxane at 100°C gave quinolizidone **10** in quantitative yield after a residence time of just 10 min without the need for alcohol protection (Scheme 2). Although the related synthesis of quino[*b*]thiophene **13** from thiophene **11** required a higher temperature (150°C) and an aerial oxidation, it too proceeded efficiently, to give a 98% yield over the two steps (Scheme 2).[19]

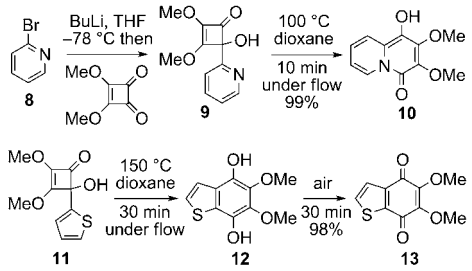

Scheme 2. Representative heteroarylcyclobutenone rearrangements under continuous-flow conditions.[17,18]

To demonstrate the value of the method, we chose to tackle the synthesis of the marine natural product cribrostatin 6 (**19**), a popular target since it was identified by Pettit et al. in 2003, that exhibits useful anti-neoplastic and antimicrobial activity.[5,6] In 2010, cribrostatin 6 was reported to induce death in cancer cells by inducing oxidative stress and the build-up of ROS.[20] As an approach to cancer chemotherapy, ROS-inducing therapies are still in their infancy. Esclomol, for example, was recently advanced to phase III clinical trials in combination with taxol, though these were halted because of increased mortality.[20] To date, four total syntheses of **19** have been reported.[6–9,20] The shortest, by Knueppel and Martin, was reported in 2009 and featured an alkynylcyclobutenone rearrangement as a key step, namely, **18**→**19**.[9] Although this step gave a low yield (26%), it allowed the total synthesis to be completed in just five linear steps.

Our plan was to achieve a synthesis of cribrostatin 6 in a similar step count, but with greater efficiency. To that end, nitrile **14** was reduced to the corresponding amine **15** with alane (AlH_3) (Scheme 3).[21] Acylation to **16** was followed by cyclisation with $POCl_3$ to give imidazopyridine **17** in a near-quantitative yield. Halogen–lithium exchange then facilitated the union of **17** and 2-ethoxy-3-methylcyclobutendione, to give a separable 3:1 mixture of adduct **20** and a regioisomer **20a** derived from addition to the vinylogous ester carbonyl. Finally, thermolysis of **20** in dioxane for 1 h at 110°C under continuous flow, followed by exposure to air for a further 45 min, gave **19** in 90% yield after purification by column chromatography.

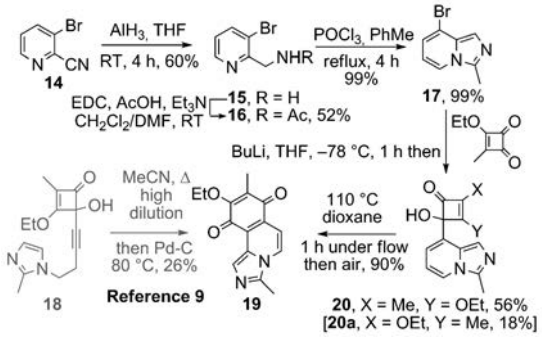

Scheme 3. A short total synthesis of cribrostatin 6 (**19**). EDC = 1-ethyl-3-(3-dimethylaminopropyl)carbodiimide.

Conclusion

In conclusion, we have shown that aryl- and heteroarylcyclobutenone rearrangements can be conveniently performed under continuous flow in dioxane at 150°C and proceed with excellent yields. The approach has allowed us to determine a Hammett relationship for the reaction. This, in conjunction with DFT and ab initio modelling,[11] provides strong evidence that the electrocyclisation of ketene **5** to bicyclic ketone **7** is rate determining in arylcyclobutenone rearrangements and has a late transition state. From a computational perspective, the excellent performance of RCCSD(T)/6-31G(d)//UB3LYP/6-311G(d,p) in predicting reaction kinetics is notable. The short and efficient total syn-

thesis of cribrostatin 6 (**19**), a useful anti-neoplastic and anti-microbial agent, provides a topical demonstration of the value of the method for the rapid construction of condensed quinones.

Experimental Section

General procedure for continuous-flow reactions: Aliquots of **1a–i** (2 mL) in dioxane were taken from bulk solutions (0.25 g in 25 mL) and heated at 150 °C under continuous flow in stainless-steel tubing (internal diameter 1 mm, capacity 10 mL) for the stated residence time by using a Vapourtec R4/R2+ device. The resulting solutions were concentrated in vacuo then analyzed by ^{1}H NMR to determine the composition (**1**, **2** and **3**) by comparison of the respective integrals as indicated in the Supporting Information.

*2,3-Dimethoxynaphthalene-1,4-dione (**3a**)*:[1a,f] Compound **3a** could be formed in a near-quantitative yield by using the general procedure with a residence time of 30 min and stirring the resulting solution in air for 1 h. M.p.: 116–118 °C (Et_2O/petroleum ether; previously reported: 115–117 °C (Et_2O));[1a,f] ^{1}H NMR (300 MHz, $CDCl_3$): δ = 7.71 (m, 2H), 8.07 (m, 2H), 4.13 ppm (s, 6H); ^{13}C NMR (75 MHz, $CDCl_3$): δ = 182.0 (2×C), 147.5 (2×C), 133.8 (2×CH), 130.8 (2×C), 126.3 (2×CH), 61.5 ppm (2×CH_3); IR ($CHCl_3$): $\tilde{\nu}$ = 3385, 2954, 1772, 1601, 1468, 1337, 1047, 994, 858 cm^{-1}; MS (ES$^+$): *m/z* (%): 241 $[M+Na]^+$ (46), 219 $[M+H]^+$ (16). See Figure 5 and Table 1.

*2,3-Dimethoxy-6-methylnaphthalene-1,4-dione (**3b**)*:[1a] Compound **3b** could be formed in 94% yield by using the general procedure with a residence time of 2 h and stirring the resulting solution in air for 3 h. M.p.: 89–91 °C (MeOH; previously reported: 90–92 °C (aq MeOH));[1a] ^{1}H NMR (400 MHz, $CDCl_3$): δ = 7.96 (d, J = 7.8 Hz, 1H), 7.87 (brs, 1H), 7.53–7.47 (ddq, J = 7.8, 1.5, 0.8 Hz, 1H), 4.12 (s, 3H), 4.10 (s, 3H), 2.48 ppm (brs, 3H); ^{13}C NMR (100 MHz, $CDCl_3$): δ = 182.3 (C), 181.8 (C), 147.6 (C), 144.9 (C), 134.4 (C), 130.8 (CH), 128.6 (C), 126.7 (CH), 126.4 (CH), 119.7 (C), 61.4 (2×CH_3), 21.8 ppm (CH_3); IR ($CHCl_3$): $\tilde{\nu}$ = 2950, 1659, 1611, 1600, 1306, 1269, 1040 cm^{-1}; MS (ES$^+$): *m/z* (%): 482 $[2M+NH_4]^+$ (60), 233 $[M+H]^+$ (100). See Scheme 4, Figure 6 and Table 2.

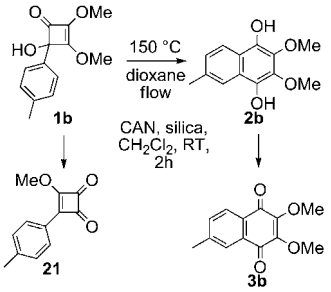

Scheme 4. Synthesis of **3b**. CAN = ceric ammonium nitrate.

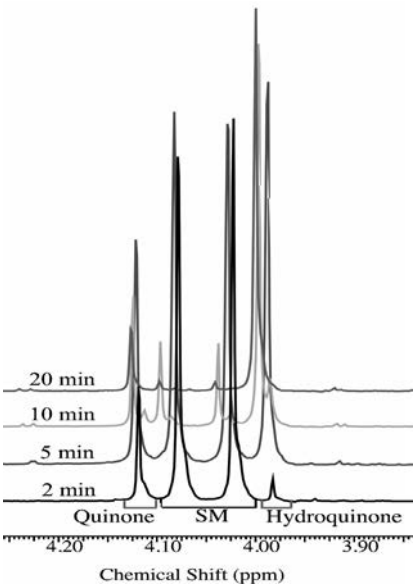

Figure 5. NMR spectra used to extract data presented in Table 1.

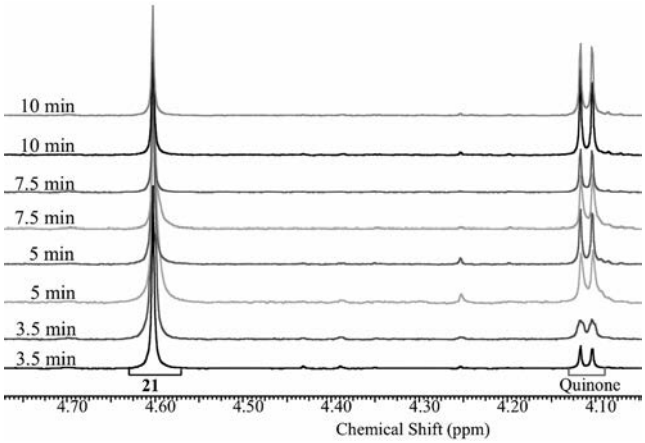

Figure 6. NMR spectra used to extract data presented in Table 2.

Table 1. Concentration of **1a** after thermolysis in dioxane at 150 °C for the stated residence time, as determined by NMR integration.

Time [s]	**1a** [%]	ln[SM]
0	100	4.61
300	63.2	4.15
450	53.5	3.98
600	39.6	3.68
900	25.1	3.22
1200	17.1	2.84

Table 2. Concentration of **1b** after thermolysis in dioxane at 150 °C for the stated residence time, as determined by NMR integration; the reactions were run in duplicate.

Time [s]	**1b** [%]	ln[SM]
0	100	4.61
	100	4.61
210	81.9	4.41
	78.4	4.36
300	72.4	4.28
	67.5	4.21
450	62.7	4.14
	56.9	4.04
600	46.5	3.84
	43.7	3.78

As an alternative to the general method, the crude reaction mixture could be concentrated in vacuo, dissolved in CH_2Cl_2 then exposed to 23% CAN on silica. The procedure facilitates the quantitative oxidation of the benzohydroquinone **2b** to benzoquinone **3b** with remaining starting-material **1b** converted to 3-methoxy-4-(4-methylphenyl)cyclobuten-1,2-dione (**21**). ^{1}H NMR (400 MHz, $CDCl_3$): $\delta = 7.94$ (d, $J = 8.1$ Hz, 2H), 7.32 (d, $J = 8.1$, Hz, 2H), 4.60 (3H, s), 2.44 ppm (s, 3H); ^{13}C NMR (100 MHz, $CDCl_3$): $\delta = 193.8$ (C), 184.7 (C), 174.9 (C), 143.9 (C), 129.9 (2×CH), 127.9 (2×CH), 125.0 (C), 116.3 (C), 61.6 (CH_3), 22.0 ppm (CH_3); IR ($CHCl_3$): $\tilde{\nu} = 1784$, 1595, 1369 cm^{-1}; MS (ES$^+$): *m/z* (%): 266 $[M+\mathrm{MeCN}+\mathrm{Na}]^+$ (100), 203 $[M+\mathrm{H}]^+$ (2).[22]

*4-Hydroxy-2,3-dimethoxy-4-(pyridin-2-yl)cyclobut-2-enone (**9**)*: *n*BuLi (3.52 mL, 2.40 M solution in hexane, 8.45 mmol) was added to a solution of 2-bromopyridine (0.82 mL, 8.45 mmol) in THF (30 mL) at −78 °C over 5 min. After 15 min the resulting solution was added, through a cannula, to a solution of dimethyl squarate (1.00 g, 7.04 mmol) in THF (10 mL) at −78 °C, giving a red solution. After 30 min, saturated NH_4Cl (20 mL) was added. The reaction mixture was allowed to warm to RT then extracted with CH_2Cl_2 (50 mL×3). The combined organic layers were washed with brine (50 mL×2), dried ($MgSO_4$), filtered, concentrated in vacuo and purified by flash column chromatography (5%→50% EtOAc/petroleum ether with 2% NEt_3) to afford the title-compound **9** as a pale brown oil (0.97 g, 4.37 mmol, 62%). ^{1}H NMR (400 MHz, $CDCl_3$): $\delta = 8.62$ (d+fine splitting, $J = 4.5$ Hz, 1H), 7.77 (td, $J = 7.5$, 1.5 Hz, 1H), 7.48 (d, $J = 7.5$ Hz, 1H), 7.30 (ddd, $J = 7.5$, 4.5, 1.0 Hz, 1H), 6.07 (s, 1H), 4.09 (s, 3H), 3.98 ppm (s, 3H); ^{13}C NMR (75 MHz, $CDCl_3$): $\delta = 182.6$ (C), 164.4 (C), 154.6 (CH), 148.3 (C), 137.6 (C), 137.4 (CH), 123.2 (CH), 120.0 (CH), 80.0 (C), 59.9 (CH_3), 58.8 ppm (CH_3); IR ($CHCl_3$): $\tilde{\nu} = 3463$, 2951, 1776, 1632, 1468, 1337, 1061 cm^{-1}; MS (ES$^+$): *m/z* (%): 222 $[M+\mathrm{H}]^+$ (100); HRMS (ES$^+$): *m/z*: calcd for $C_{11}H_{12}NO_4$: 222.0775 $[M+\mathrm{H}]^+$; found: 222.0766.

*1-Hydroxy-2,3-dimethoxy-4H-quinolizin-4-one (**10**)*: A solution of **9** (5.0 mg, 0.023 mmol) in dioxane (2 mL) was heated at 100 °C in stainless-steel tubing for a residence time of 10 min with a Vapourtec R4/R2+ device. The resulting solution was stirred in air for 1 h and then concentrated in vacuo to give **10** as a pale brown solid (4.9 mg, 0.022 mmol, 99%). M.p.: 110–112 °C (EtOAc/petroleum ether); ^{1}H NMR (400 MHz, [D$_6$]DMSO): $\delta = 8.88$ (s, 1H), 8.70 (d, $J = 7.6$ Hz, 1H), 7.73 (d, $J = 9.0$ Hz, 1H), 7.16 (dd, $J = 8.0$, 6.6 Hz, 1H), 6.86–6.97 (m, 1H), 4.03 (s, 3H), 3.87 ppm (s, 3H); ^{13}C NMR (100 MHz, [D$_6$]DMSO): $\delta = 152.1$ (C), 150.2 (C), 131.7 (C), 127.2 (C), 126.7 (C), 125.4 (CH), 125.2 (CH), 120.0 (CH), 114.0 (CH), 60.9 (CH_3), 59.3 ppm (CH_3); IR ($CHCl_3$): $\tilde{\nu} = 2955$, 2925, 1733, 1634, 1595, 1457, 1288, 1122 cm^{-1}; MS (ES$^+$): *m/z* (%): 222 $[M\mathrm{H}]^+$ (100); HRMS (ES$^+$): *m/z*: calcd for $C_{11}H_{12}NO_4$: 222.0775 $[M+\mathrm{H}]^+$; found: 222.0766.

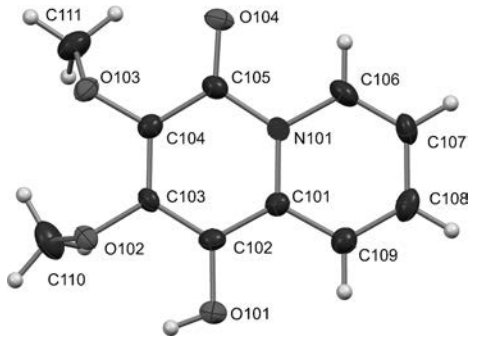

*4-Hydroxy-2,3-dimethoxy-4-(thiophen-2-yl)cyclobut-2-en-1-one (**11**)*:[1a] 2-Bromothiopene (0.376 mL, 3.87 mmol) was added to a solution of *n*BuLi (2.42 mL, 1.6 M solution in hexane, 3.87 mmol) in THF (15 mL) over 5 min at −78 °C. After 15 min, a solution of dimethyl squarate (0.50 g, 3.52 mmol) in THF (10 mL) was added over 5 min, giving an orange solution. After 1 h, saturated NH_4Cl (20 mL) was added. The reaction mixture was allowed to warm to RT then extracted with CH_2Cl_2 (20 mL×3). The combined organic layers were washed with brine (20 mL×2), dried ($MgSO_4$), filtered, concentrated in vacuo and purified by flash column chromatography (5%→40% EtOAc/petroleum ether with 2% NEt_3) to afford the title-compound **11** as a white solid (0.257 g, 1.14 mmol, 32%). M.p.: 66–68 °C (Et_2O/petroleum ether; previously reported: 68–69 °C (Et_2O));[1a] ^{1}H NMR (400 MHz, $CDCl_3$): $\delta = 7.33$ (dd, $J = 5.0$, 1.3 Hz, 1H), 7.11 (dd, $J = 3.5$, 1.3 Hz, 1H), 7.02 (dd, $J = 5.0$, 3.5 Hz, 1H), 4.11 (s, 3H), 4.02 (s, 3H), 3.56 ppm (s, 1H); ^{13}C NMR (100 MHz, $CDCl_3$): $\delta =$ 183.1 (C), 166.0 (C), 140.7 (C), 135.2 (C), 127.2 (CH), 126.2 (CH), 125.0 (CH), 85.7 (C), 60.3 (CH_3), 58.8 ppm (CH_3); IR ($CHCl_3$): $\tilde{\nu} = 3400$, 3008, 2956, 1781, 1644, 1635, 1470, 1348, 1040 cm^{-1}; MS (ES$^+$): *m/z* (%): 227 $[M+\mathrm{H}]^+$ (100).

*5,6-Dimethoxybenzo[b]thiophene-4,7-dione (**13**)*:[1a] A solution of **11** (5.0 mg, 0.022 mmol) in dioxane (2 mL) was heated at 150 °C in stainless-steel tubing for a residence time of 30 min by using a Vapourtec R4/R2+ device. The resulting solution was stirred in air for 1 h then concentrated in vacuo to give the title-compound **13** as an orange solid (4.9 mg, 0.022 mmol, 98%). M.p.: 169–172 °C (Et_2O/petroleum ether; previously reported: 171.5–173 °C (CH_2Cl_2/petroleum ether));[1a] ^{1}H NMR (400 MHz, $CDCl_3$): $\delta = 7.63$ (d, $J = 5.0$ Hz, 1H), 7.50 (d, $J = 5.0$ Hz, 1H), 4.09 ppm (apparent s, 6H); ^{13}C NMR (100 MHz, $CDCl_3$): $\delta = 178.0$ (C), 176.6 (C), 147.2 (C), 146.7 (C), 141.4 (C), 139.5 (C), 133.4 (CH), 125.9 (CH), 61.5 (CH_3), 61.6 ppm (CH_3); IR ($CHCl_3$): $\tilde{\nu} = 3033$, 3008, 2929, 1651, 1340, 1292, 858 cm^{-1}; MS (ES$^+$): *m/z* (%): 225 $[M+\mathrm{H}]^+$ (100).

*(3-Bromopyridin-2-yl)methanamine (**15**)*:[21] To a cooled (0 °C) solution of 3-bromo-2-cyanopyridine (0.100 g, 0.546 mmol) in toluene (20 mL) was added alane·Me_2NEt complex (0.5 M solution in toluene, 2.2 mL, 1.093 mmol) over 4 min. The resulting mixture was warmed to RT and then, after 16 h, was re-cooled to 0 °C. Methanol (10 mL) and saturated sodium potassium tartare (50 mL) were cautiously added, then the aqueous phase was separated and extracted with $CHCl_3$ (20 mL×3). The combined organic phases were then washed with brine (20 mL×2), dried ($MgSO_4$), filtered and concentrated in vacuo to afford the title-compound **15** as an yellow oil (60.5 mg, mmol, 60%). ^{1}H NMR (300 MHz, $CDCl_3$): $\delta = 8.52$ (dd, $J = 5.0$, 1.5 Hz, 1H), 7.85 (dd, $J = 7.9$, 1.5 Hz, 1H), 7.11 (dd, $J = 7.9$, 5.0 Hz, 1H), 4.14 (s, 2H), 2.77 ppm (s, 2H); ^{13}C NMR (75 MHz, $CDCl_3$): $\delta = 162.4$ (C), 150.2 (CH), 145.2 (CH), 123.1 (C), 115.9 (CH), 45.2 ppm (CH_2); MS (ES$^+$): *m/z* (%): 189 $[M(^{81}\mathrm{Br})+\mathrm{H}]^+$ (100), 187 $[M(^{79}\mathrm{Br})+\mathrm{H}]^+$ (100).

*N-((3-Bromopyridin-2-yl)methyl)acetamide (**16**)*:[21] Acetic acid (0.850 mL, 14.83 mmol) and triethylamine (4.13 mL, 29.7 mmol) were added sequentially to a solution of *N*-(3-dimethylaminopropyl)-*N*′-ethylcarbodiimide hydrochloride (2.84 g, 14.83 mmol) in dichloromethane (30 mL) at RT. After 1 h, a solution of **15** (1.422 g, 5.93 mmol) in DMF (15 mL) and CH_2Cl_2 (10 mL) was added, followed by 2 M sodium carbonate (30 mL) after an additional 1 h. The aqueous phase was separated and extracted with dichloromethane (3×20 mL) and then the organic phases were dried ($MgSO_4$), concentrated in vacuo and purified by column chromatography (EtOAc) to give the title-compound **16** as a white solid (0.730 g, 3.187 mmol, 52%). M.p.: 62–64 °C (EtOAc); ^{1}H NMR (400 MHz, $CDCl_3$): $\delta = 8.50$ (d, $J = 4.4$, 1.3 Hz, 1H), 7.89 (d, $J =$ 7.9, 1.3 Hz, 1H), 7.18 (brs, 1H), 7.16 (dd, $J = 7.9$, 4.4 Hz, 1H), 4.62 (d, $J = 4.3$, 2H), 2.13 ppm (s, 3H); ^{13}C NMR (100 MHz, $CDCl_3$): $\delta = 170.0$ (C), 153.7 (C), 146.9 (CH), 140.4 (CH), 123.5 (C), 120.3 (CH), 44.1 (CH_2), 23.3 ppm (CH_3); IR ($CHCl_3$): $\tilde{\nu} = 3314$, 1642, 1560, 812 cm^{-1}; MS (ES$^+$): *m/z* (%): 231 $[M(^{81}\mathrm{Br})+\mathrm{H}]^+$ (100), 229 $[M(^{79}\mathrm{Br})+\mathrm{H}]^+$ (100).

*8-Bromo-3-methylimidazo[1,5-a]pyridine (**17**)*: Phosphorus oxychloride (1.07 mL, 11.5 mmol) was added to a solution of acetamide **16** (0.730 g, 3.19 mmol) in toluene (10 mL) at RT over 5 min. The reaction mixture was heated at reflux for 4 h then cooled to 0 °C and saturated sodium bicarbonate (30 mL) was added. The aqueous phase was separated and extracted with ethyl acetate (10 mL×3), then the combined organic phases were washed with water (10 mL×2), dried ($MgSO_4$) and concentrated to give the title-compound **17** as a brown oil (0.680 g, 3.222 mmol, 99%, ca. 98% purity). ^{1}H NMR (400 MHz, $CDCl_3$): $\delta = 7.68$ (d, $J = 7.3$ Hz, 1H), 7.46 (s, 1H), 6.92 (d, $J = 6.8$ Hz, 1H), 6.47 (apparent t, $J = 7.1$ Hz, 1H), 2.69 ppm (s, 3H); ^{13}C NMR (100 MHz, $CDCl_3$): $\delta = 179.0$ (C), 136.6 (C),

130.0 (C), 120.8 (CH), 119.8 (CH), 119.5 (CH), 112.7 (CH), 12.6 ppm (CH_3); IR ($CHCl_3$): $\tilde{\nu}$ = 3314, 1642, 1560, 812 cm^{-1}; MS (ES^+): *m/z* (%): 213 [$M(^{81}Br)+H]^+$ (100), 211 [$M(^{79}Br)+H]^+$ (100).

*3-Ethoxy-4-hydroxy-2-methyl-4-(3-methylimidazo[1,5-a]pyridin-8-yl)cyclobut-2-enone (**20**)*: *n*BuLi (1.6 M in hexane, 0.79 mL, 1.26 mmol) was added to a solution of imidazo[1,5-*a*]pyridine **17** (242 mg, 1.15 mmol) in THF (5 mL) at −78 °C. After 30 min a solution of 3-ethoxy-4-methyl-3-cyclobutene-1,2-dione (0.161 g, 1.147 mmol)[1,9] in THF (5 mL) was added over 4 min, followed by saturated NH_4Cl (20 mL) after an additional 1 h. After warming to RT the aqueous phase was separated and extracted with dichloromethane (20 mL × 3). The combined organic phases were washed with brine (20 mL × 2), dried ($MgSO_4$), concentrated in vacuo and purified by flash column chromatography (0% → 5% methanol/dichloromethane with 1% NEt_3) gave firstly **20a** (59 mg, 0.204 mmol, 18%) then the title-compound **20** as a pale orange oil (175 mg, 0.642 mmol, 56%). ^1H NMR (400 MHz, $CDCl_3$): δ = 7.64 (d, *J* = 7.0 Hz, 1H), 7.39 (s, 1H), 6.97 (d, *J* = 6.8 Hz, 1H), 6.60 (t, *J* = 6.9 Hz, 1H), 4.45 (dq, *J* = 9.8, 7.1 Hz, 1H), 4.26 (dq, *J* = 9.9, 7.1 Hz, 1H), 2.66 (s, 3H), 1.85 (s, 3H), 1.36 ppm (t, *J* = 7.1 Hz, 3H); ^{13}C NMR (100 MHz, $CDCl_3$): δ = 189.5 (C), 182.2 (C), 135.5 (C), 127.8 (C), 127.6 (C), 125.2 (C), 120.7 (CH), 118.5 (CH), 116.5 (CH), 112.0 (CH), 91.6 (C), 69.2 (CH_2), 15.0 (CH_3), 12.6 (CH_3), 6.9 ppm (CH_3); IR ($CHCl_3$): $\tilde{\nu}$ = 2928, 2861, 1715, 1731, 1617, 1332, 1135, 1078 cm^{-1}; MS (ES^+): *m/z* (%): 273 $[M+H]^+$ (100); HRMS (ES^+): *m/z*: calcd for $C_{15}H_{17}N_2O_3$: 273.1161 $[M+H]^+$; found: 273.1232.

*9-Ethoxy-3,8-dimethylimidazo[5,1-a]isoquinoline-7,10-dione (**19**, Cribrostatin 6)*: Cyclobutenone **20** (59 mg, 0.217 mmol) in dioxane (2 mL) was heated at 110 °C in stainless-steel tubing for a residence time of 1 h by using a Vapourtec R4/R2+ device. The resulting solution was stirred in air for 30 min then concentrated in vacuo and purified by chromatography (2% MeOH in CH_2Cl_2) to give **19** as a light-blue solid (52 mg, 0.193 mmol, 90%). M.p.: 167–169 °C (acetone at −4 °C; previously reported: 165–167 °C (acetone)[8,9], 169–171 °C (acetone)[5], 171–172 °C (acetone)[6,7]); ^1H NMR (400 MHz, $CDCl_3$): δ = 8.52 (s, 1H); 8.10 (d, *J* = 7.6 Hz, 1H), 7.62 (d, *J* = 7.6 Hz, 1H), 4.49 (q, *J* = 6.8 Hz, 2H), 3.09 (br s, 3H), 2.13 (s, 3H), 1.45 ppm (t, *J* = 7 Hz, 3H); ^{13}C NMR (100 MHz, $CDCl_3$): δ = 184.9 (C), 180.7 (C), 156.2 (C), 137. 7 (C), 130.1 (C), 125.9 (C), 125.0 (C), 124.7 (C), 123.9 (CH), 123.5 (CH), 107.6 (C), 69.6 (CH_2), 16.0 (CH_3), 12.6 (CH_3), 9.2 ppm (CH_3); IR ($CHCl_3$): $\tilde{\nu}$ = 2925, 1662, 1626, 1611, 1527, 1172 cm^{-1}; MS (ES^+): *m/z* (%): 271 $[M+H]^+$ (100).

CCDC-808547 contains the supplementary crystallographic data for this paper. These data can be obtained free of charge from The Cambridge Crystallographic Data Centre via www.ccdc.cam.ac.uk/data_request/cif.

Acknowledgements

We gratefully acknowledge GSK, ERDF (IS:CE-Chem & InterReg IVa program 4061) and the EPSRC for funding, and for the support of the Iridis 3 cluster. Rob Wheeler and Dr. Andy Craven are thanked for valuable advice and Dr. M. E. Light for the X-ray analysis.

[1] a) H. W. Moore, S. T. Perri, *J. Org. Chem.* **1988**, *53*, 996–1003; b) S. T. Perri, H. J. Dyke, H. W. Moore, *J. Org. Chem.* **1989**, *54*, 2032–2034; c) A. Enhsen, K. Karabelas, J. M. Heerding, H. W. Moore, *J. Org. Chem.* **1990**, *55*, 1177–1185; d) J. M. Heerding, H. W. Moore, *J. Org. Chem.* **1991**, *56*, 4048–4050; e) M. P. Winters, M. Stranberg, H. W. Moore, *J. Org. Chem.* **1994**, *59*, 7572–7574; f) H. W. Moore, O. H. W. Decker, *Chem. Rev.* **1986**, *86*, 821–830; g) M. W. Reed, D. J. Pollart, S. T. Perri, L. D. Foland, H. W. Moore, *J. Org. Chem.* **1988**, *53*, 2477–2482.

[2] a) A. G. Birchler, F. Liu, L. S. Liebeskind, *J. Org. Chem.* **1994**, *59*, 7737–7745; b) D. Zhang, I. Llorente, L. S. Liebeskind, *J. Org. Chem.* **1997**, *62*, 4330–4338; c) S. Zhang, L. S. Liebeskind, *J. Org. Chem.* **1999**, *64*, 4042–4049.

[3] For an excellent review see a) R. L. Danheiser, G. B. Dudley, W. F. Austin in *Science in Synthesis, Vol. 23*, (Ed.: R. Danheiser), Thieme Chemistry, Stuttgart, **2006**, pp. 493–568; see also b) D. C. Harrowven, D. D. Pascoe, D. Demurtas, H. O. Bourne, *Angew. Chem.* **2005**, *117*, 1247–1248; *Angew. Chem. Int. Ed.* **2005**, *44*, 1221–1222; c) D. C. Harrowven, D. D. Pascoe, I. L. Guy, *Angew. Chem.* **2007**, *119*, 429–432; *Angew. Chem. Int. Ed.* **2007**, *46*, 425–428.

[4] a) L. P. Hammett, *Physical Organic Chemistry*, 2nd ed., McGraw-Hill, New York, **1970**; b) O. Exner, *Correlation Analysis of Chemical Data*, Plenum Press, New York, **1988**.

[5] G. R. Pettit, J. C. Collins, J. C. Knight, D. L. Herald, R. A. Nieman, M. D. Williams, R. K. Pettit, *J. Nat. Prod.* **2003**, *66*, 544–547; R. K. Pettit, B. R. Fakoury, J. C. Knight, C. A. Weber, G. R. Pettit, G. D. Cage, S. Pon, *J. Med. Microbiol.* **2004**, *53*, 61–65.

[6] S. Nakahara, A. Kubo, *Heterocycles* **2004**, *63*, 2355–2362.

[7] S. Nakahara, A. Kubo, Y. Mikami, J. Ito, *Heterocycles* **2006**, *68*, 515–520.

[8] M. D. Markey, T. R. Kelly, *J. Org. Chem.* **2008**, *73*, 7441–7443.

[9] D. Knueppel, S. F. Martin, *Angew. Chem.* **2009**, *121*, 2607–2609; *Angew. Chem. Int. Ed.* **2009**, *48*, 2569–2571.

[10] The flow system employed is shown in Figure 2 of S. V. Ley, I. R. Baxendale, *Chimia* **2008**, *62*, 162–168. Further details may be found on the manufacturer's web site http://www.vapourtec.co.uk/products/rseriessystem accessed 21/7/2011.

[11] a) A. Odedra, P. H. Seebergera, *Angew. Chem.* **2009**, *121*, 2737–2740; *Angew. Chem. Int. Ed.* **2009**, *48*, 2699–2702; b) F. E. Valera, M. Quaranta, A. Moran, J. Blacker, A. Armstrong, J. Cabral, D. G. Blackmond, *Angew. Chem.* **2010**, *122*, 2530–2537; *Angew. Chem. Int. Ed.* **2010**, *49*, 2478–2485.

[12] a) V. P. Andreev, *Chem. Heterocycl. Compd.* **2010**, *46*, 184–195; b) E. Kutter, C. Hansch, *J. Med. Chem.* **1969**, *12*, 647–651; c) T. Fujita, C. Takayama, M. Nakajima, *J. Org. Chem.* **1973**, *38*, 1623–1630; d) G. Ananchenko, E. Beaudoin, D. Bertin, D. Gigmes, P. Lagarde, S. R. A. Marque, E. Revalor. P. Tordo, *J. Phys. Org. Chem.* **2006**, *19*, 269–275.

[13] As the value of σ_I for CON*i*Pr_2 is not known, we used as an estimate, namely, the known value for $CONH_2$.

[14] Gaussian 09, Revision A.02, M. J. Frisch, G. W. Trucks, H. B. Schlegel, G. E. Scuseria, M. A. Robb, J. R. Cheeseman, G. Scalmani, V. Barone, B. Mennucci, G. A. Petersson, H. Nakatsuji, M. Caricato, X. Li, H. P. Hratchian, A. F. Izmaylov, J. Bloino, G. Zheng, J. L. Sonnenberg, M. Hada, M. Ehara, K. Toyota, R. Fukuda, J. Hasegawa, M. Ishida, T. Nakajima, Y. Honda, O. Kitao, H. Nakai, T. Vreven, J. A. Montgomery, Jr., J. E. Peralta, F. Ogliaro, M. Bearpark, J. J. Heyd, E. Brothers, K. N. Kudin, V. N. Staroverov, R. Kobayashi, J. Normand, K. Raghavachari, A. Rendell, J. C. Burant, S. S. Iyengar, J. Tomasi, M. Cossi, N. Rega, N. J. Millam, M. Klene, J. E. Knox, J. B. Cross, V. Bakken, C. Adamo, J. Jaramillo, R. Gomperts, R. E. Stratmann, O. Yazyev, A. J. Austin, R. Cammi, C. Pomelli, J. W. Ochterski, R. L. Martin, K. Morokuma, V. G. Zakrzewski, G. A. Voth, P. Salvador, J. J. Dannenberg, S. Dapprich, A. D. Daniels, Ö. Farkas, J. B. Foresman, J. V. Ortiz, J. Cioslowski, D. J. Fox, Gaussian, Inc., Wallingford CT, 2009.

[15] a) P. W. Musch, C. Remenyi, H. Helten, B. Engels, *J. Am. Chem. Soc.* **2002**, *124*, 1823–1828; b) P. R. Schreiner, B. H. Bui, *Eur. J. Org. Chem.* **2006**, 1162–1165; c) P. W. Musch, B. Engels, *J. Am. Chem. Soc.* **2001**, *123*, 5557–5562.

[16] All calculations were performed at the B3LYP/6–311G(d,p) level with Gaussian 09,[14] with GAMESS(US)[17] used for all RCCSD(T)/6–31G(d) calculations.[18] For each optimized structure an analytical Hessian was calculated to obtain vibrational frequencies, zero-point energies and thermodynamic corrections at 423 K, additionally confirming each as a minimum or transition-state structure. Post-processing visualization was carried out with the ChemCraft (G. A. Zhurko, *ChemCraft version 1.6*; http://www.chemcraftprog.com) and Gabedit programs (A. R. Allouche, *J. Comput. Chem* **2011**, *32*, 174–182).

[17] Programme used: GAMESS(US), ver. 1-Oct-2010 (R1): M. W. Schmidt, K. K. Baldridge, J. A. Boatz, S. T. Elbert, M. S. Gordon,

J. H. Jensen, S. Koseki, N. Matsunaga, K. A. Nguyen, S. Su, T. L. Windus, M. Dupuis, J. A. Montgomery, *J. Comput. Chem.* **1993**, *14*, 1347–1363.

[18] P. Piecuch, S. A. Kucharski, K. Kowalski, M. Musial, *Comp. Phys. Commun.* **2002**, *149*, 71–96.

[19] S. T. Perri, L. D. Foland, O. H. Decker, H. W. Moore, *J. Org. Chem.* **1986**, *51*, 3067–3068.

[20] M. T. Hoyt, R. Palchaudhuri, P. J. Hergenrother, *Invest. New Drugs* **2010**, DOI: 10.1007 s10637–010–9390-x, accessed 1/12/2010.

[21] This reduction is reported to proceed in >80% yield with the borane·THF complex (a) Z. Jiajie *Chinese Pat.* CN101239978(A); b) S. Ramsbeck, U. Heiser, M. Buchholz, A. J. Niestroj, US Pat. US2008/234313 A1, **2008**). In our hands, isolation of amine **15** from that reaction proved difficult, prompting a switch to alane.

[22] A. H. Schmidt, G. Kircher, S. Maus, H. Bach, *J. Org. Chem.* **1996**, *61*, 2085–2094.

Received: July 22, 2011
Published online: November 14, 2011

VIP Photochemistry

DOI: 10.1002/ange.201200281

An Efficient Flow-Photochemical Synthesis of 5*H*-Furanones Leads to an Understanding of Torquoselectivity in Cyclobutenone Rearrangements**

David C. Harrowven, Mubina Mohamed, Théo P. Gonçalves, Richard J. Whitby, David Bolien, and Helen F. Sneddon*

Dedicated to Professor Philip Parsons on the occasion of his 60th birthday

Thermal rearrangements of cyclobutenones give access to numerous ring systems and have proven especially valuable for the de novo synthesis of quinones, benzoquinones, and related heteroaromatics with dense substitution.[1–3] A classic example is the rearrangement of arylcyclobutenone **1a**→**3a**,[1a] where the emergence of a protocol to realize this transformation in near quantitative yield means it achieves many of the ideals for a green-chemical reaction.[2,4] In principle, such criteria could also be met by the related photochemical rearrangement of **1a** to 5*H*-furanone **4a**, yet this reaction has lain almost dormant since its introduction by Moore et al. in 1988 because of the low yields attained in each of the published examples (27–51%, Scheme 2).[5]

Herein we show how the photochemical rearrangement of 4-hydroxycyclobutenones can be realized in near quantitative yield under continuous flow using a simple, low-cost device with an interchangeable low-energy light source.[6,7] In addition, our results challenge the long-established view that the electrocyclic opening of cyclobutenones is a torquoselective process, with the thermochemical and photochemical rearrangements displaying complimentary torquoselectivity,[1e] as implicated by the aforementioned examples (Scheme 1).

Before our investigation could begin, we needed to construct a photochemical reactor for use under flow. Taking inspiration from the pioneering work of Booker-Milburn and co-workers,[6] we assembled the apparatus depicted in Figure 1.[8] A key difference between this and the published setup was our use of inexpensive, low-energy 9 W lamps in place of the more conventional 400–600 W medium-pressure mercury discharge lamps. While recognizing that this might limit the throughput of material, we hoped

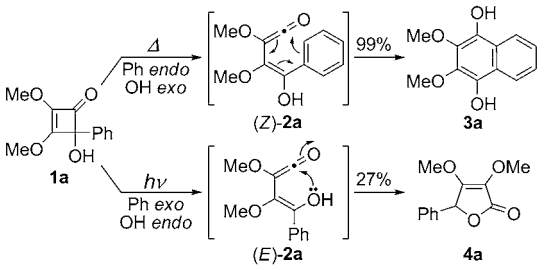

Scheme 1. Thermal and photochemical rearrangements of 4-hydroxycyclobutenone **1**.

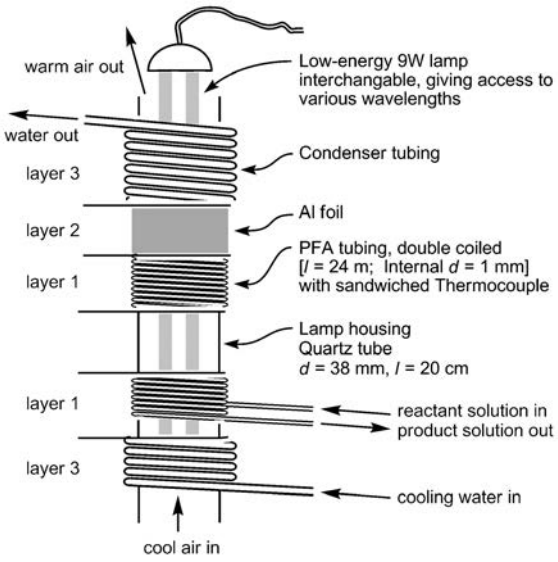

Figure 1. Flow photochemical reactor (cut-away between grey lines). PFA = perfluoroalkoxy.

that it would allow optimization for the wavelength to become "as simple as changing a light bulb", since lamps spanning a wide spectrum of wavelengths have become available at low cost in recent years.[8]

Our study began with an investigation of the rearrangement of phenylcyclobutenone **1a** to 5*H*-furanone **4a** as the reported yield of 27% was among the lowest disclosed in the original study.[5] When conducted under flow using tetrahydrofuran (THF) as solvent, a 9 W broad-spectrum UVB lamp

[*] Prof. D. C. Harrowven, M. Mohamed, T. P. Gonçalves, Prof. R. J. Whitby, D. Bolien
Chemistry, University of Southampton
Highfield, Southampton, SO17 1BJ (UK)
E-mail: dch2@soton.ac.uk
Dr. H. F. Sneddon
GlaxoSmithKline, Stevenage, Hertfordshire, SG1 2NY (UK)

[**] Financial support from GlaxoSmithKline, the ERDF (IS:CE-Chem & InterReg IVa) and the EPSRC (including support for the Iridis cluster) are gratefully acknowledged. Rob Wheeler and Andy Craven are thanked for valuable advice.

Supporting information for this article is available on the WWW under http://dx.doi.org/10.1002/anie.201200281.

(280–370 nm)[8] and a residence time of 120 min, we were pleased to attain 5*H*-furanone **4a** in 54% isolated yield, double that given using a conventional photochemical setup. NMR analysis of crude product mixtures given at various residence times showed many side products, with the ratio of product to by-products worsening as the residence times were increased. In seeking to eliminate side reactions involving the product, a comparison was made between its UV–visible spectrum and that of the starting material. Each showed strong absorbance below 275 nm, with cyclobutenone **1a** exhibiting additional absorbance bands at 295 and 315 nm. A switch to a 9 W UVB narrow-spectrum lamp giving greatest intensity in the region 310–320 nm was therefore implicated and, in the event, this did lead to a modest improvement in yield to 65%.

The step-change in performance we sought was realized with a switch of solvent from THF to acetonitrile. Indeed, through this simple expedient the rearrangement of cyclobutenone **1a** to furanone **4a** was achieved in 97% isolated yield at 0.05 M concentration with a residence time of 1 h. Interestingly, under irradiation from a UVA lamp (350–395 nm) the rearrangement was clean but proceeded at a much slower rate (< 10% conversion after 1 h). The broad-spectrum UVB lamp (280–370 nm) proved as effective as the narrow band lamp, while irradiation for 1 h using a UVC lamp (254 nm) gave complete conversion but the product **4a** was heavily contaminated with by-products which accounted for around 5% of the total mass balance.[8]

To explore the generality of the method, a range of 4-hydroxycyclobutenones **1b–h** were prepared by the addition of alkyl-, aryl-, alkyny-, and heteroaryl-lithium reagents to dimethyl squarate.[1–3] Pleasingly, under the aforementioned conditions, each underwent smooth rearrangement to the corresponding furanones **4b–h** in excellent yield (Scheme 2).

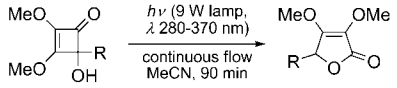

1	yield,	lit. yield	4
a, R = Ph	99%	[27%]	**a**, R = Ph
b, R = *n*Bu	95%		**b**, R = *n*Bu
c, R = *t*Bu	96%	[39%]	**c**, R = *t*Bu
d, R = Ph-CC	95%	[28%]	**d**, R = Ph-CC
e, R = *o*-MeOC$_6$H$_4$	97%	[51%]	**e**, R = *o*-MeOC$_6$H$_4$
f, R = *p*-Me$_3$SiC$_6$H$_4$	93%		**f**, R = *p*-Me$_3$SiC$_6$H$_4$
g, R = *p*-*t*BuC$_6$H$_4$	92%		**g**, R = *p*-*t*BuC$_6$H$_4$
h, R = 3-Pyridyl	94%		**h**, R = 3-Pyridyl

Scheme 2. Photochemically induced cyclobutenone rearrangements of **1a–h** [in a flask] and under continuous flow.

Our survey revealed a striking anomaly in respect of the (2-pyridyl)-cyclobutenone **1i**. In this case the photochemical rearrangement took longer to run to completion and gave a 1:1 mixture of furanone **4i** and quinolizinone **5** (Scheme 3). This anomalous result casts doubt on the view that rearrangements of 4-hydroxycyclobutenones **1** each proceed by torquoselective opening to a vinylketene, with thermolysis giving (*Z*)-**2** and photolysis giving its geometric isomer (*E*)-**2**

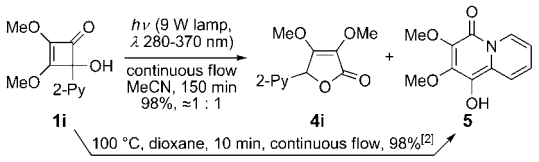

Scheme 3. Photochemical rearrangement of (2-pyridyl)-cyclobutenone **1i** under continuous flow.

(Scheme 1).[1e] Rather, it suggests that the photoinduced electrocyclic opening of **1** gives rise to a mixture of (*E*)- and (*Z*)-vinylketenes **2**, with (*E*)-**2** giving cyclization to furan **6** en route to furanone **4** while (*Z*)-**2** reverts back to cyclobutenone **1** unless it too can be captured by an internal nucleophile (Scheme 4).

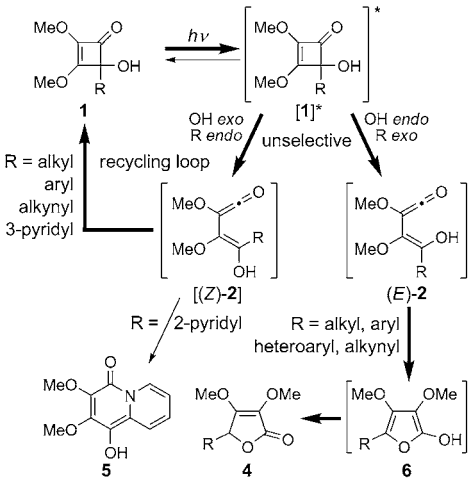

Scheme 4. Revised mechanism for the photochemical rearrangement of 4-hydroxycyclobutenones.

To explore this hypothesis we decided to model the available cyclization pathways for the intermediate (*E*)- and (*Z*)-vinylketenes, **2a** and **2i**, bearing phenyl- and (2-pyridyl)-residues, respectively. The method chosen used DFT calculations at the B3LYP/6-311G(d,p) level to establish the course of the reaction (Gaussian 09),[9–11] with energies refined for required points using the coupled cluster method CCSD(T)/6-31G(d) (GAMESS(US), Schemes 5 and 6).[2,12] Notably, the calculated barrier for 6π-electrocyclic closure of vinylketene (*Z*)-**2a** to **7** at 25 °C (16.7 kcal mol^{-1}) exceeded that for 4π-electrocyclic closure to the starting material **1a** (15.8 kcal mol^{-1}), consistent with the recycling of this intermediate. The situation was reversed for its geometric isomer (*E*)-**2a**, where the calculated barrier for returning cyclobutenone **1a** (20.4 kcal mol^{-1}) exceeded that for cyclization to furan **6a** (12.4 kcal mol^{-1} [13]) leading to the observed product **4a**. For the thermal rearrangement of cyclobutenone **1a** torquoselective opening was evidenced by the calculated activation energies for formation of vinylketenes (*E*)-**2a** (35.0 kcal mol^{-1}) and (*Z*)-**2a** (28.9 kcal mol^{-1}), respectively, at 150 °C.

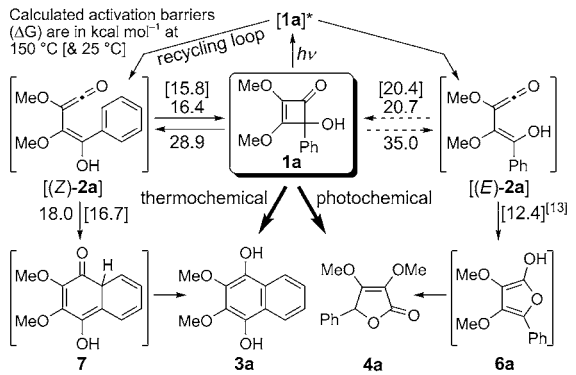

Scheme 5. Calculated energy barriers in photo- and thermochemical rearrangements of cyclobutenone **1b**.

For 2-pyridylcyclobutenone **1i** (Scheme 6), calculations showed that cyclization of vinylketene (*Z*)-**2i** to quinolizinone **5** was spontaneous on adoption of an appropriate reactive conformer, thereby diverting it away from the usual

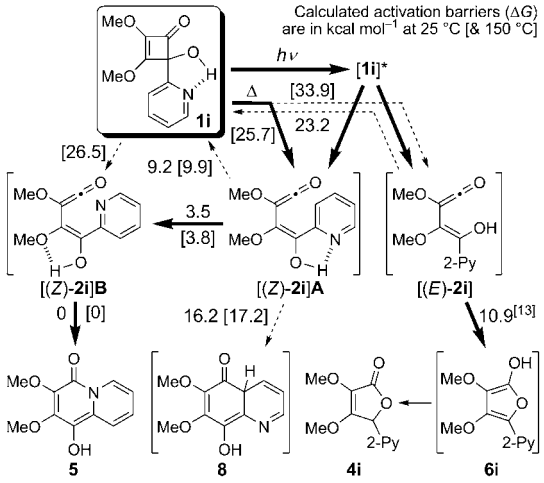

Scheme 6. Calculated activation energies in the photo- and thermochemical rearrangement of cyclobutenone **1i**.

recycling loop. In parallel, the geometric isomer (*E*)-**2i** favors cyclization to furan **6i** (10.9 kcal mol^{-1})[13] over 4π-electrocyclic closure to cyclobutenone **1i** (23.2 kcal mol^{-1}) and gives the expected furanone **4i**. Torquoselectivity in the thermal opening of cyclobutenone **1i** to vinylketene (*Z*)-**2i** was again evidenced, with calculations additionally indicating that a hydrogen bond between the pyridine and hydroxyl residues leads to a significant rate enhancement. This is manifest experimentally by the realization of a near quantitative yield for the thermolysis of **1i** to **5** at 100 °C for 10 min under continuous flow (Scheme 3), when related aryl- and heteroaryl-cyclobutenone rearrangements typically require prolonged heating at 150 °C to achieve a similar outcome.[2] Further observations relating to torquoselectivity in the thermochemical rearrangements of cyclobutenones are given in the Supporting Information.

In conclusion, we have shown that many 4-hydroxycyclobutenones can be transformed into 5*H*-furanones in near quantitative yield using an inexpensive flow-photochemical setup. The results attained challenge a long-held view that the thermal and photochemical rearrangements of cyclobutenones display complementary torquoselectivity in their electrocyclic opening to a vinylketene.[1e] Indeed, they provide a detailed mechanistic understanding of both the thermal and photochemical rearrangements of 4-hydroxycyclobutenones giving valuable insights into their scope and limitations.

Received: January 11, 2012
Revised: March 6, 2012
Published online: March 22, 2012

Keywords: cyclobutenones · density functional calculations · photochemistry · rearrangements · small ring systems

[1] a) S. T. Perri, H. W. Moore, *J. Org. Chem.* **1988**, *53*, 996–1003; b) S. T. Perri, H. J. Dyke, H. W. Moore, *J. Org. Chem.* **1989**, *54*, 2032–2034; c) A. Enhsen, K. Karabelas, J. M. Heerding, H. W. Moore, *J. Org. Chem.* **1990**, *55*, 1177–1185; d) J. M. Heerding, H. W. Moore, *J. Org. Chem.* **1991**, *56*, 4048–4050; e) M. P. Winters, M. Stranberg, H. W. Moore, *J. Org. Chem.* **1994**, *59*, 7572–7574; f) H. W. Moore, O. H. W. Decker, *Chem. Rev.* **1986**, *86*, 821–830; g) A. G. Birchler, F. Liu, L. S. Liebeskind, *J. Org. Chem.* **1994**, *59*, 7737–7745; h) D. Zhang, I. Llorente, L. S. Liebeskind, *J. Org. Chem.* **1997**, *62*, 4330–4338; i) S. Zhang, L. S. Liebeskind, *J. Org. Chem.* **1999**, *64*, 4042–4049.

[2] M. Mohamed, T. P. Gonçalves, R. J. Whitby, H. F. Sneddon, D. C. Harrowven, *Chem. Eur. J.* **2011**, *17*, 13698–13705.

[3] a) D. C. Harrowven, D. D. Pascoe, D. Demurtas, H. O. Bourne, *Angew. Chem.* **2005**, *117*, 1247–1248; *Angew. Chem. Int. Ed.* **2005**, *44*, 1221–1222; b) D. C. Harrowven, D. D. Pascoe, I. L. Guy, *Angew. Chem.* **2007**, *119*, 429–432; *Angew. Chem. Int. Ed.* **2007**, *46*, 425–428.

[4] P. T. Anastas, J. C. Warner, *Green Chemistry: Theory and Practice*, OUP, New York, **1998**, p. 30.

[5] a) S. T. Perri, L. D. Foland, H. W. Moore, *Tetrahedron Lett.* **1988**, *29*, 3529–3532; See also b) Y. Yamamoto, M. Ohno, S. Eguchi, *Tetrahedron* **1994**, *50*, 7783–7798.

[6] a) B. D. Hook, W. Dohle, P. R. Hirst, M. Pickworth, M. B. Berry, K. I. Booker-Milburn, *J. Org. Chem.* **2005**, *70*, 7558–7564; See also b) F. Lévesque, P. H. Seeberger, *Angew. Chem.* **2012**, *124*, 1738–1741; *Angew. Chem. Int. Ed.* **2012**, *51*, 1706–1709; c) M. Nettekoven, B. Püllmann, R. E. Martin, D. Wechsler, *Tetrahedron Lett.* **2012**, *53*, 1363–1366; d) A. C. Gutierrez, T. F. Jamison, *Org. Lett.* **2011**, *13*, 6414–6417; e) F. Lévesque, P. H. Seeberger, *Org. Lett.* **2011**, *13*, 5008–5011; f) T. Fukuyama, Y. Kajihara, Y. Hino, I. Ryu, *J. Flow Chem.* **2011**, *1*, 40–45; g) A. Vasudevan, C. Villamil, J. Trumbull, J. Olson, D. Sutherland, J. Pan, S. Djuric, *Tetrahedron Lett.* **2010**, *51*, 4007–4009; h) M. D. Lainchbury, M. I. Medley, P. M. Taylor, P. Hirst, W. Dohle, K. I. Booker-Milburn, *J. Org. Chem.* **2008**, *73*, 6497–6505.

[7] For excellent recent reviews on photochemical reactions see a) N. Hoffmann, *Chem. Rev.* **2008**, *108*, 1052–1103; b) T. Bach, J. P. Hehn, *Angew. Chem.* **2011**, *123*, 1032–1077; *Angew. Chem. Int. Ed.* **2011**, *50*, 1000–1045, and references therein.

[8] Further details of the photochemical apparatus and lamps used are provided in the Supporting Information.

[9] a) W. Kirmse, N. G. Rondan, K. N. Houk, *J. Am. Chem. Soc.* **1984**, *106*, 7989–7991; b) K. N. Houk, Y. Li, J. D. Evanseck, *Angew. Chem.* **1992**, *104*, 711–739; *Angew. Chem. Int. Ed. Engl.* **1992**, *31*, 682–708; c) R. Ponec, G. Yuzhakov, J. Pecka, *J. Math.*

Chem. **1996**, *20*, 301 – 310; d) P. S. Lee, X. Zhang, K. N. Houk, *J. Am. Chem. Soc.* **2003**, *125*, 5072 – 5079; e) M. Yasui, Y. Naruse, S. Inagaki, *J. Org. Chem.* **2004**, *69*, 7246 – 7249; f) J. M. Um, H. Xu, K. N. Houk, W. Tang, *J. Am. Chem. Soc.* **2009**, *131*, 6664 – 6665.

[10] Gaussian 09, Revision A.02, M. J. Frisch, G. W. Trucks, H. B. Schlegel, G. E. Scuseria, M. A. Robb, J. R. Cheeseman, G. Scalmani, V. Barone, B. Mennucci, G. A. Petersson, H. Nakatsuji, M. Caricato, X. Li, H. P. Hratchian, A. F. Izmaylov, J. Bloino, G. Zheng, J. L. Sonnenberg, M. Hada, M. Ehara, K. Toyota, R. Fukuda, J. Hasegawa, M. Ishida, T. Nakajima, Y. Honda, O. Kitao, H. Nakai, T. Vreven, J. A. Montgomery, Jr., J. E. Peralta, F. Ogliaro, M. Bearpark, J. J. Heyd, E. Brothers, K. N. Kudin, V. N. Staroverov, R. Kobayashi, J. Normand, K. Raghavachari, A. Rendell, J. C. Burant, S. S. Iyengar, J. Tomasi, M. Cossi, N. Rega, N. J. Millam, M. Klene, J. E. Knox, J. B. Cross, V. Bakken, C. Adamo, J. Jaramillo, R. Gomperts, R. E. Stratmann, O. Yazyev, A. J. Austin, R. Cammi, C. Pomelli, J. W. Ochterski, R. L. Martin, K. Morokuma, V. G. Zakrzewski, G. A. Voth, P. Salvador, J. J. Dannenberg, S. Dapprich, A. D. Daniels, Ö. Farkas, J. B. Foresman, J. V. Ortiz, J. Cioslowski, D. J. Fox, Gaussian, Inc., Wallingford CT, **2009**.

[11] All calculations were performed at the B3LYP/6-311G(d,p) level using Gaussian 09,[10] with GAMESS(US) used for all RCCSD(T)/6-31G(d) calculations.[12] For each optimized structure an analytical Hessian was calculated to obtain vibrational frequencies, zero-point energies and thermodynamic corrections at 298 and 423 K, additionally confirming each as a minimum or transition-state structure. Post-processing visualization was carried out using the ChemCraft (G. A. Zhurko, *ChemCraft version 1.6*; http://www.chemcraftprog.com) and Gabedit programs (A. R. Allouche, *J. Comput. Chem.* **2011**, *32*, 174 – 182).

[12] a) GAMESS(US), ver. 1-Oct-2010 (R1): M. W. Schmidt, K. K. Baldridge, J. A. Boatz, S. T. Elbert, M. S. Gordon, J. H. Jensen, S. Koseki, N. Matsunaga, K. A. Nguyen, S. Su, T. L. Windus, M. Dupuis, J. A. Montgomery, *J. Comput. Chem.* **1993**, *14*, 1347 – 1363; b) P. Piecuch, S. A. Kucharski, K. Kowalski, M. Musial, *Comput. Phys. Commun.* **2002**, *149*, 71 – 96.

[13] For reactions involving proton transfer the calculated ΔG presented assumes this to be solvent accelerated: O. Takahashi, K. Kobayashi, A. Oda, *Chem. Biodiversity* **2010**, *7*, 1349 – 1356. See the Supporting Information for details as to how these were estimated.

Synthetic Methods

DOI: 10.1002/ange.201307193

Organoytterbium Ate Complexes Extend the Value of Cyclobutenediones as Isoprene Equivalents**

*Emma Packard, David D. Pascoe, Jacques Maddaluno, Théo P. Gonçalves, and David C. Harrowven**

In memory of Margaret Harrowven

3-Methyl-4-methoxycyclobuten-1,2-dione (**1a**) has long been recognized as a valuable isoprene equivalent in natural products total synthesis, particularly for the preparation of hydroquinones, quinones, and their benzannulated analogues (e.g. Scheme 1).[1,2a] It is readily introduced to a substrate as the electrophilic component in organolithium or Grignard addition reactions, for example, **1a**→**2**. Here, the differential reactivity of the C1 and C2 carbonyl groups in **1a** adds to its value as a synthon by providing a reliable and predictable means of achieving the ubiquitous head to tail connectivity of isoprene units.[1,2a]

Though regiocontrol in the addition of Grignard and organolithium reagents to **1a** is of critical importance, it also imposes a severe limitation. As evidenced by the example in Scheme 1, while the method is convenient for the synthesis of benzohydroquinones such as **3**, it proves cumbersome when targeting the regioisomeric series **7**. In this case addition of a carbon nucleophile to the vinylogous ester carbonyl (C2) of **1a** is required to achieve the desired outcome. Consequently, a protecting group strategy must be invoked to mask the more reactive C1 carbonyl (e.g. **1a**→**4**).[2] Addition of the Grignard or organolithium reagent to C1 is then followed by deprotection (e.g. **5**→**6**), which can be difficult to achieve efficiently because of the presence of the acid sensitive tertiary alcohol and enol ether functions.

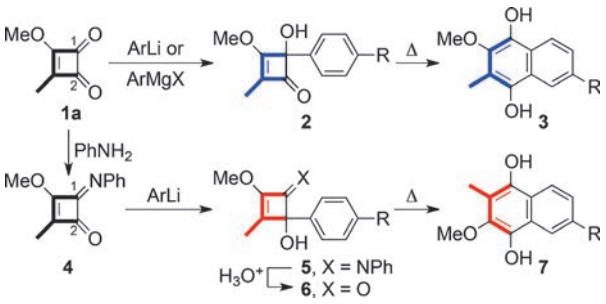

Scheme 1. Use of **1a** as an isoprene equivalent in the synthesis of benzohydroquinones.

Herein we report an expedient solution to that long-standing problem and reveal some hitherto unknown facets of organoytterbium reactivity. In essence, while organolithium and Grignard reagents favor addition to the C1 carbonyl of cyclobutenedione (**1a**), the corresponding organoytterbium reagents give exclusive addition to the C2 carbonyl of **1b** (Scheme 2).[3]

The discovery was made during an optimization study aimed at reducing side reactions resulting from deprotonation of the C3 methyl substituent in **1a**. In the addition of PhLi, for example (Scheme 3), these appeared to limit the yield of the

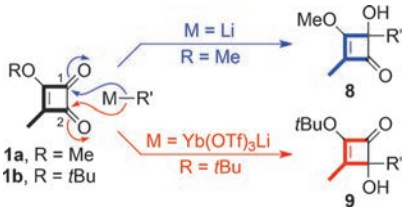

Scheme 2. Dichotomous regioselectivity in the addition of organolithium and organoytterbium reagents to cyclobutenediones. Tf = trifluoromethanesulfonyl.

1a, PhLi, THF, −78 °C	76%	–
1a, PhLi/Yb(OTf)$_3$, THF, −78 °C	50%	41%
1b, PhLi, THF, −78 °C	48%	41%
1b, PhMgBr, THF, −78 °C	22%	67%
1b, PhLi/CeCl$_3$, THF, −78 °C	31%	6% (+ **1b**, 19%)
1b, PhLi/Yb(OTf)$_3$, THF, −78 °C	–	92%

Scheme 3. Regioselectivity in the additions of various phenyl organometallics to **1a** and **1b**. THF = tetrahydrofuran.

[*] E. Packard, Dr. D. D. Pascoe, T. P. Gonçalves, Prof. D. C. Harrowven
Chemistry, University of Southampton
Highfield, Southampton, SO17 1BJ (United Kingdom)
E-mail: dch2@soton.ac.uk
Dr. J. Maddaluno
FR CNRS 3038, IRCOF, Université de Rouen
76821 Mont St. Aignan Cedex (France)

[**] Financial support from the EPSRC and ERDF (IS:CE-Chem & InterReg IVa program 4061) is gratefully acknowledged. We would also like to acknowledge Dr. Edmund Lee, the IRIDIS High Performance Computing Facility, the EPSRC National Service for Computational Chemistry Software (NSCCS), and their associated support staff for help in the completion of this work.

Supporting information for this article is available on the WWW under http://dx.doi.org/10.1002/anie.201307193.

adduct **2a** to approximately 70–80% when employing standard protocols (e.g. THF at −78°C).[4] Inspired by reports from the groups of Molander and Procter on the efficient addition of organoytterbium reagents to carbonyl compounds,[5] we decided to examine the addition of phenylytterbium triflate to **1a**.[2] The result we attained was quite unexpected, as the reaction led to the formation of both C1 and C2 adducts, **2a** and **11a**, respectively, in the corresponding yields of 50% and 41% (Scheme 3). Having noted similar anomalies in the additions of PhLi and PhMgBr to **1b**, we were delighted to find that the addition of phenylytterbium triflate to **1b** resulted in a complete reversal of the normal regiochemical course, thus giving the C2 adduct **12a** in a remarkable 92% yield upon isolation.[5,6]

To demonstrate the value of the method, a series of arylytterbium reagents were prepared and reacted with **1b**. These included *ortho*-,[7] *meta*-,[7] and *para*-substituted aromatics with a variety of substituents (+I, −I, and +M), and a heteroaromatic example[7] (see Scheme 4 and the Supporting Information). In each case the C2 adducts **12** were formed

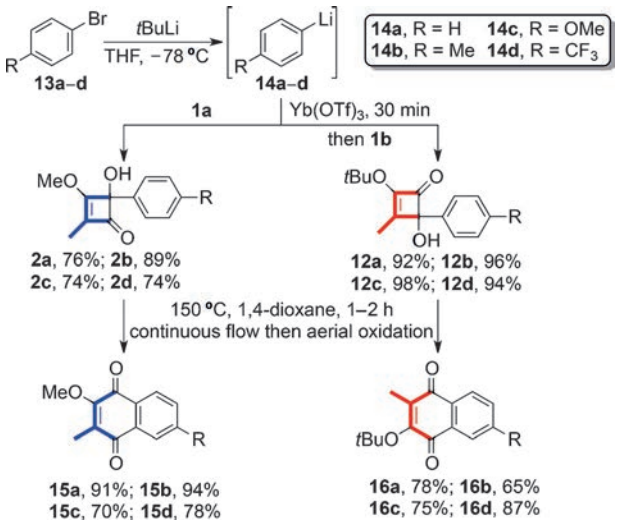

Scheme 4. Synthesis of regioisomeric series of benzoquinones using aryllithium and arylytterbium additions to **1a** and **1b**.

in excellent yield. This result was in stark contrast to the corresponding organolithium additions to **1a** where the major product **2** resulted from addition to the C1 carbonyl.[7] For completeness, all adducts were subjected to thermolysis and aerial oxidation, thus leading to the complementary series of benzoquinones **15** and **16**.

The complementary reactivity extended to vinyllithium and vinylytterbium triflate additions to **1a** and **1b** as demonstrated by the syntheses of the hydroquinones **23**–**25** and **27** (Scheme 5).[1] Notably, vinylytterbium triflate derived from vinylmagnesium bromide displayed the same regiochemical preference as those derived from vinyllithium intermediates. Interestingly, the addition of the vinyllithium **18** to **1a** proved unusual in that it gave **27** directly after a bicarbonate quench at −78°C and warming to ambient temperature. The minor product of the reaction was the C2 adduct **21b**,[7] rather than the corresponding hydroquinone.

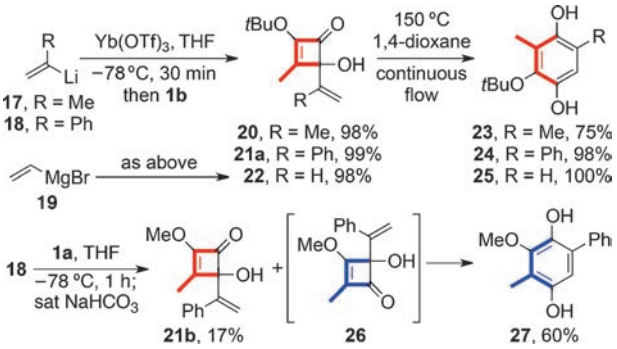

Scheme 5. Synthesis of regioisomeric series of hydroquinones by vinyllithium and vinylytterbium additions to **1a** and **1b**.

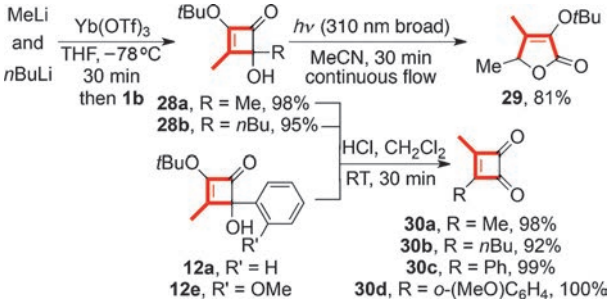

Scheme 6. Alkylytterbium additions to **1b** for the synthesis of 5*H*-furanones and diorganylcyclobutenediones.

The addition of methylytterbium triflate to **1b** also proved facile (Scheme 6). In contrast, the analogous sequence with *n*BuLi required a 2:1 equivalence with ytterbium(III) triflate to achieve a high yield of the C2 adduct **28b**.[8] The photochemical rearrangement of the adduct **28a** into the furanone **29**,[9] and the facile generation of the diorganylcyclobutendiones **30** by exposure of these adducts to acid, provide further illustrations of the method's utility.

For completeness, the addition of phenylalkynylytterbium triflate to **1b** was examined (Scheme 7). The reaction proved sluggish (9 h at −78°C) in comparison with other additions and regioselectivity was attenuated, with the formation of cyclobutenones **34** and **33** in 69% and 15% yield, respectively. In contrast, the addition of the organolithium **31** to **1a** gave the cyclobutenone **32** as the sole isolated product.

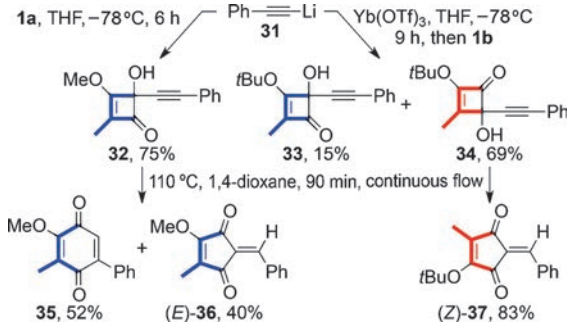

Scheme 7. Phenylalkynyllithium and ytterbium additions to **1a** and **1b**, respectively.

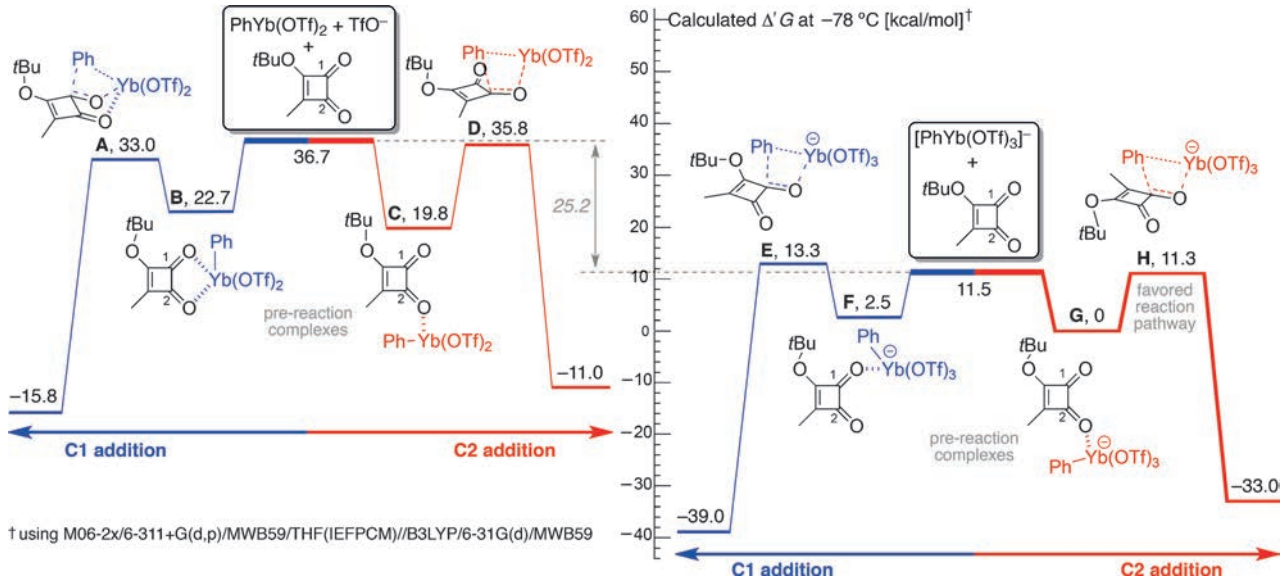

Figure 1. Calculated free energy barriers for C1 and C2 addition in the reactions of **1b** with $PhYb(OTf)_2$ and $[PhYb(OTf)_3]^-$ in THF.

Thermolyses of the adduct **32** and **34** exposed a further anomaly, with the former giving a 5:4 mixture of the quinone **35** and cyclopentenedione (*E*)-**36**, while the a latter gave only the cyclopentenedione (*Z*)-**37**.

To gain insights into the mechanistic course of organoytterbium addition reactions we decided to initiate a computational study of the reaction of $PhYb(OTf)_2$ with **1b**. However, these investigations proved fruitless, with DFT calculations predicting a preference for reaction at the ketonic C1 carbonyl (i.e. $\Delta G^{\ddagger}_{A} < \Delta G^{\ddagger}_{D}$, Figure 1).[10] The results led us to question the nature of the organometallic reagent. Based on limited literature precedent,[11] we had assumed that the reaction of PhLi with $Yb(OTf)_3$ would first give the ate complex $PhYb(OTf)_3Li$, which in turn would collapse to $PhYb(OTf)_2$ and LiOTf. When this premise was tested computationally, our calculations indicated that loss of a triflate ligand from the ate complex would cost approximately 25 kcal mol^{-1} at −78 °C! Moreover, when the reactivity of $[PhYb(OTf)_3]^-$ towards **1b** was examined, the predicted outcome mirrored our experimental findings by revealing a kinetic preference for phenyl addition to the C2 carbonyl (i.e. $\Delta G^{\ddagger}_{H} < \Delta G^{\ddagger}_{E}$, Figure 1).

The modeling also exposed some seminal facets of organoytterbium reactivity (Figure 1). In particular, the pre-reaction complexes of $[PhYb(OTf)_3]^-$·**1b** (**F** and **G**) each showed single ytterbium–carbonyl interactions leading to trapezoidal transition states. The strength of those interactions was a key factor in determining the regiochemical course of addition, with ΔG_G less than ΔG_F by about 2.5 kcal mol^{-1}. Additionally, steric interactions in the addition phase play an important role, as evidenced by 1) the need to rotate the *t*Bu ether during C1 addition (**F**→**E**, Figure 1) at a cost of about 2.6 kcal mol^{-1} [12] and 2) the low selectivity observed for addition of $[PhYb(OTf)_3]^-$ to **1a** compared to that for **1b** (Scheme 3).

Finally, to demonstrate the method's potential in terpenoid synthesis we decided to target mansonone B, a natural product whose identity has yet to be determined with rigor but seemed likely to be as depicted in **43**.[13] Our synthesis began with (−)-menthone (**39**; Scheme 8), which was readily

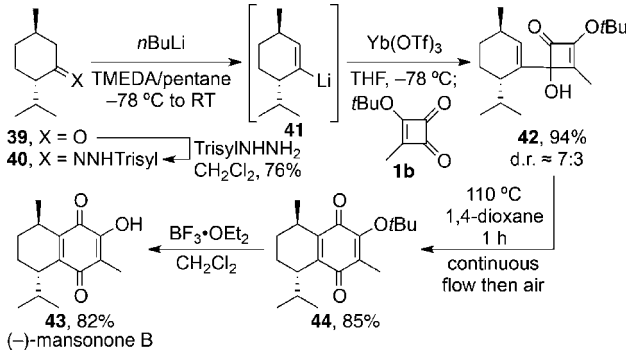

Scheme 8. First total synthesis of (−)-mansonone B. TMEDA = *N*,*N*,*N*′,*N*′-tetramethylethylenediamine, Trisyl = 2,4,6-triisopropylphenylsulfonyl.

transformed into the required vinyllithium reagent **41** by means of a Shapiro reaction.[14] Transmetallation with ytterbium triflate, and subsequent addition of the resulting vinylytterbium intermediate to **1b**, gave a 7:3 diastereomeric mixture of the C2 adduct **42** in 94 % yield. Thermolysis of that mixture under continuous flow at 110 °C with concomitant aerial oxidation, gave the quinone **44**, from which our target **43** was readily derived. Pleasingly, the physical and spectral characteristics displayed by our synthetic sample (−)-**43** matched those reported for mansonone B in its isolation paper,[13a] thus confirming the regiochemical and relative stereochemical identity of the natural product. Its absolute configuration remains uncertain because of a lack of available optical rotation data for comparison.

In conclusion, we have shown that organoytterbium additions to **1b** are easy to effect, proceed in excellent

yield, and follow a complementary regiochemical course to related organolithium additions to **1a**. Alkyl, aryl, hetaryl, vinyl, and alkynyl ytterbium reagents participate in the reaction, greatly extending the utility of cyclobutenone rearrangements by providing a predictable means of introducing this isoprene unit in a regioselective manner. High-level computational studies have provided seminal insights into the nature of organoytterbium intermediates and their reactivity. Of particular note is the realization that reactions proceed via ytterbium ate complexes.

Received: August 15, 2013
Published online: October 23, 2013

Keywords: density functional calculations · flow chemistry · natural products · rearrangement · ytterbium

[1] a) M. Mohamed, T. P. Goncalves, R. J. Whitby, D. C. Harrowven, H. F. Sneddon, *Chem. Eur. J.* **2011**, *17*, 13698 – 13705; b) D. Knueppel, S. F. Martin, *Tetrahedron* **2011**, *67*, 9765 – 9770; c) E. Peña-Cabrera, L. S. Liebeskind, *J. Org. Chem.* **2002**, *67*, 1689 – 1691. See also d) A. Padwa, M. J. Chughtai, J. Boonsombat, P. Rashatasakhon, *Tetrahedron* **2008**, *64*, 4758 – 4767; e) D. C. Harrowven, D. D. Pascoe, I. L. Guy, *Angew. Chem.* **2007**, *119*, 429 – 432; *Angew. Chem. Int. Ed.* **2007**, *46*, 425 – 428; f) D. C. Harrowven, D. D. Pascoe, D. Demurtas, H. O. Bourne, *Angew. Chem.* **2005**, *117*, 1247 – 1248; *Angew. Chem. Int. Ed.* **2005**, *44*, 1221 – 1222; g) S. K. Verma, E. B. Fleischer, H. W. Moore, *J. Org. Chem.* **2000**, *65*, 8564 – 8573; see the Supporting Information for additional references.

[2] a) B. M. Trost, O. R. Thiel, H.-C. Tsui, *J. Am. Chem. Soc.* **2003**, *125*, 13155 – 13164; b) B. M. Trost, O. R. Thiel, H.-C. Tsui, *J. Am. Chem. Soc.* **2002**, *124*, 11616 – 11617; See also c) G. Oppermann, E. Schaumann, M. Stranberg, H. W. Moore, *Synthesis* **2010**, 2027 – 2038; d) E. Schaumann, G. Oppermann, M. Stranberg, H. W. Moore, *Aust. J. Chem.* **2010**, *63*, 1656 – 1664; e) M. P. Winters, M. Stranberg, H. W. Moore, *J. Org. Chem.* **1994**, *59*, 7572 – 7574.

[3] The cyclobutenediones **1a** and **1b** were each prepared in two steps from squaric acid using literature methods: a) M. W. Reed, D. J. Pollart, S. T. Perri, L. D. Foland, H. W. Moore, *J. Org. Chem.* **1988**, *53*, 2477 – 2482; b) A. Enhsen, K. Karabelas, J. M. Heerding, H. W. Moore, *J. Org. Chem.* **1990**, *55*, 1177 – 1185. $Yb(OTf)_3 \cdot x H_2O$ was dried by heating it at 240 °C in a Kugelrohr oven for 4 d under high vacuum.

[4] a) S. L. Xu, H. W. Moore, *J. Org. Chem.* **1992**, *57*, 326 – 338; b) L. S. Liebeskind, S. Iyer, C. F. Jewell, *J. Org. Chem.* **1986**, *51*, 3065 – 3067.

[5] a) G. A. Molander, E. R. Burkhardt, P. Weinig, *J. Org. Chem.* **1990**, *55*, 4990 – 4991; b) G. A. Molander, A. M. Estévez-Braun, *Bull. Soc. Chim. Fr.* **1997**, *134*, 275 – 282; c) G. A. Molander, C. Köllner, *J. Org. Chem.* **2000**, *65*, 8333 – 8339; d) D. Johnston, N. Francon, J. J. Edmonds, D. J. Procter, *Org. Lett.* **2001**, *3*, 2001 – 2004; e) D. Johnston, E. Couché, D. J. Edmonds, K. W. Muir, D. J. Procter, *Org. Biomol. Chem.* **2003**, *1*, 328 – 337; f) G. A. Molander, D. J. St Jean, J. Haas, *J. Am. Chem. Soc.* **2004**, *126*, 1642 – 1643. See the Supporting Information for additional references.

[6] At the request of a reviewer, the reactivity of $PhLi/CeCl_3$ towards **1b** was examined and shown to favor C1 addition (Scheme 3).

[7] Additions of *ortho*-, *meta*-, and hetero-arylytterbium reagents to **1b** are detailed in the Supporting Information along with further examples of organolithium additions to **1a** and **1b** and the thermal rearrangements of **21b** and **33**.

[8] For a possible explanation of 2:1 stoichiometry required with alkyl Yb reagents see: S.-i. Fukuzawa, K. Mutoh, T. Tsuchimoto, T. Hiyama, *J. Org. Chem.* **1996**, *61*, 5400 – 5405, and references therein.

[9] D. C. Harrowven, M. Mohamed, T. P. Gonçalves, R. J. Whitby, D. Bolien, H. F. Sneddon, *Angew. Chem.* **2012**, *124*, 4481 – 4484; *Angew. Chem. Int. Ed.* **2012**, *51*, 4405 – 4408.

[10] DFT calculations were performed using B3LYP with a mixed basis set of MWB59 for Yb. Pre-optimization was carried out with MOPAC PM7/SPARKLE [a) J. J. P. Stewart, *J. Mol. Model.* **2013**, *19*, 1 – 32; b) J. D. L. Dutra, M. A. M. Filho, G. B. Rocha, R. O. Freire, A. M. Simas, J. J. P. Stewart, *J. Chem. Theory Comput.* **2013**, *9*, 3333 – 3334]. Single-point energies were calculated at the M06-2x/6-311 + G(d,p)/MWB59 level [c) Y. Zhao, D. Truhlar, *Theor. Chem. Acc.* **2008**, *120*, 215 – 241] using the IEFPCM solvation model (THF) [d) S. Miertuš, E. Scrocco, J. Tomasi, *Chem. Phys.* **1981**, *55*, 117 – 129] on optimized geometries [e) M. J. Frisch, et al., Gaussian09 A. 02, see Supporting Information for full reference]. ChemCraft was used for visualization: G. A. Zhurko, http://www.chemcraftprog.com

[11] A. Dzudza, T. J. Marks, *J. Org. Chem.* **2008**, *73*, 4004 – 4016.

[12] This estimate is based on the analogous rotamers of the vinyl ether **1b**, which differ in energy by 2.6 kcal mol^{-1} (see the Supporting Information).

[13] a) G. B. Marini Bettòlo, C. G. Casinovi, C. Galeffi, *Tetrahedron Lett.* **1965**, *6*, 4857 – 4864; b) E. Garcia, V. Mendoza, J. A. Guzman, *Nat. Prod. Lett.* **1997**, *11*, 67 – 72.

[14] R. H. Shapiro, M. F. Lipton, K. J. Kolonko, R. L. Buswell, L. A. Capuano, *Tetrahedron Lett.* **1975**, *16*, 1811 – 1814. For a review see A. R. Chamberlin, S. H. Bloom, *Org. React.* **1990**, *39*, 1 – 83.

DOI: 10.1002/ejoc.201101543

An Ammonia-Triggered Stereocontrolled Conversion of a γ-Lactone to the Central Tetrahydropyran of Pederin, Psymberin, and Onnamides D–F

William J. Buffham,[a] Nigel A. Swain,[b] Sarah L. Kostiuk,[a] Théo P. Gonçalves,[a] and David C. Harrowven*[a]

Dedicated to Professor Philip Kocienski, FRS

Keywords: Lactones / Oxygen heterocycles / Ring expansion / Cyclization / Synthesis design

The onnamides, pederin, and psymberin have each attracted attention because of their potent biological activity and interesting structural features. A short (eight steps) and efficient stereocontrolled route to the central tetrahydropyran ring in these natural products has been developed from (*S*)-malic acid. The key sequence involves the conversion of a γ-lactone to a tetrahydropyran structure triggered by the addition of ammonia.

Introduction

The onnamides (e.g., **1**),[1,2] pederin (**2**),[3] and psymberin (**3**)[4] have each attracted the attention of synthetic and medicinal chemists because of their potent biological activity and interesting structural features. Pederin, for example, is produced as a defense agent by the Paederus beetle, and man has exploited its potent toxicity in weaponry over many centuries.[5] Causing vesicular lesions on contact with the skin, pederin has been used in folkloric medicine for the treatment of boils, ringworm, and nasal polyps.[6] Importantly, it has also been shown to block mitosis at levels as low as 1 ng/mL.[7] Psymberin and the onnamides, from the marine sponges *Psammocinia sp.* and *Theonella swinhoei*, respectively, also display antitumor activity at nanomolar concentrations[4,8] whereas onnamide F (**1**), from the southern Australian sponge *Trachycladus laevisirulifer*, displays promising antifungal and nematocidal activity.[1]

From a structural perspective, the group shares the common feature of the tetrahydropyran ring at the heart of each compound (highlighted in blue, see Scheme 1), which differs from what is found in the related mycalamides, theopederins, icadamides, and onnamides A–C. Its synthesis poses a number of synthetic challenges, particularly with respect to the stereocontrol of the substituents attached to the ring. Many approaches have been developed to tackle the problem, but with varying degrees of success.[9–11] Herein, we describe a short entry to key building block **4** where an ammonia-triggered stereocontrolled conversion of a γ-lactone to a tetrahydropyran ring features as a key step, that is, **5** → [**6**] → **4**.

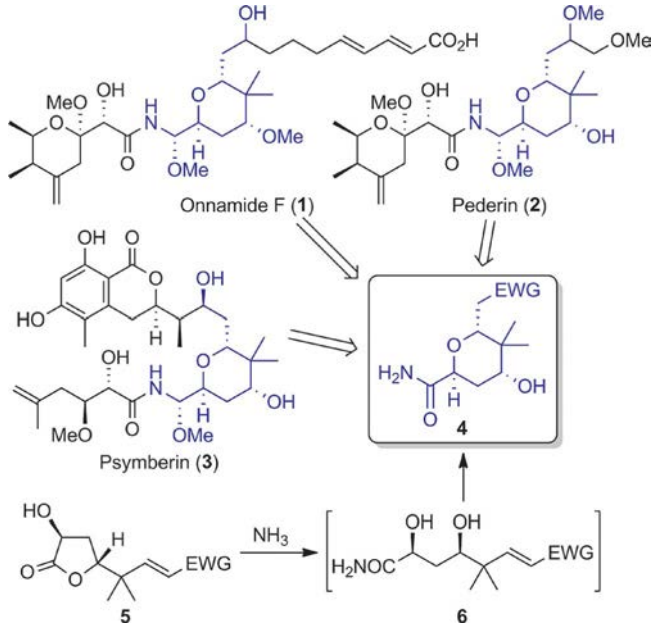

Scheme 1. Our synthetic strategy.

Results and Discussion

Our synthesis of the requisite precursor **5a** [EWG (electron-withdrawing group) = CN] began with (*S*)-malic acid (**7**) which was transformed into aldehyde **11** by sequential

[a] Chemistry, University of Southampton,
Highfield, Southampton, Hampshire, SO17 1BJ, UK
Fax: +44-23-8059-6805
E-mail: dch2@soton.ac.uk
[b] Pfizer Ltd.,
Ramsgate Road, Sandwich, Kent, CT13 9NJ, UK
Supporting information for this article is available on the WWW under http://dx.doi.org/10.1002/ejoc.201101543.

protection with cyclohexanone to give **8**, borane reduction to yield **9**, and TEMPO/TCCA [(2,2,6,6-tetramethylpiperidin-1-yl)oxidanyl/trichloroisocyanuric acid] oxidation to give **11** (Scheme 2).[12] Pleasingly, treatment of **11** with prenyl bromide and zinc dust yielded lactone **10** after an acidic workup, though this success was tempered by the lack of stereocontrol during the formation of the new stereogenic center. The diastereoselectivity was improved from 1:1 to 6:1 in favor of the desired (3*S*,5*R*)-dihydrofuran-2(3*H*)-one **10** by employing Brown's reagent in conjunction with a basic hydrogen peroxide workup,[13] though this proved to be highly capricious with yields ranging from 10 to 39%. A survey of various workup procedures was rewarded when switch was made to using sodium perborate as the oxidant. In this case (3*S*,5*R*)-**10** was furnished in a reproducible 60% yield after acidic workup followed by chromatographic separation from the (3*S*,5*S*) diastereoisomer and other impurities (analysis of the crude reaction mixture indicated a *dr* of 6:1). Next, we attempted to effect the direct conversion of (3*S*,5*R*)-**10** to unsaturated nitrile **5a** using a cross-metathesis reaction. When this proved intractable, a classic two-step ozonoloysis and Wittig olefination sequence was adopted, giving α,β-unsaturated nitrile **5a** as an inseparable 5:1 mixture of (*E*)/(*Z*) isomers.

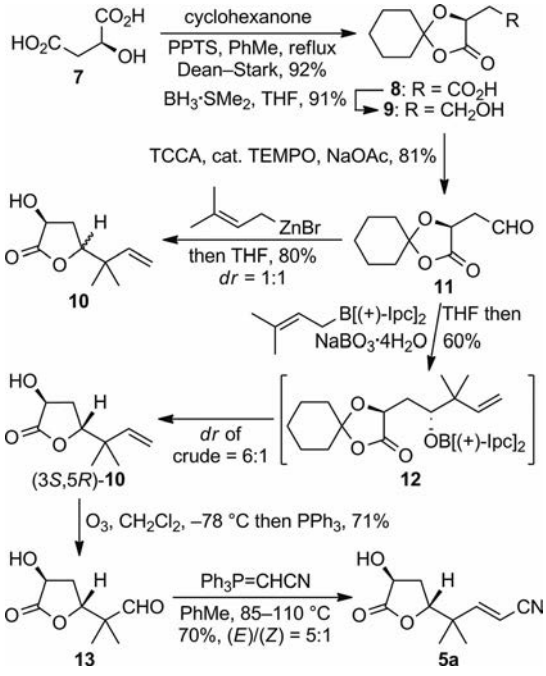

Scheme 2. Synthesis of furanone precursor **5a**. Ipc = 2,6,6-trimethylbicyclo[3.1.1]hept-3-yl.

As a key step we envisioned the direct conversion of lactone **5a** to amide **4a** through the action of ammonia (Scheme 3). Initial results were promising, as treatment of **5a** with a methanolic solution of aqueous ammonia gave a separable product mixture comprised of diol **6a** (29%) and the isomeric tetrahydropyrans **4a** (11%) and **14a** (13%). However, optimization of the reaction to give the targeted kinetic diastereoisomer **4a** proved intractable. A near quantitative yield of diol **6a** was realized by treatment of lactone **5a** with liquid ammonia in THF (tetrahydrofuran),[14] but its subsequent exposure to DBU (1,8-diazabicyclo[5.4.0]undec-7-ene) gave the thermodynamic tetrahydropyran **14a** as the sole isolated product in 95% yield. All other bases examined proved ineffective or gave product mixtures favoring tetrahydropyran **14a** over the desired diastereoisomer **4a**.[15]

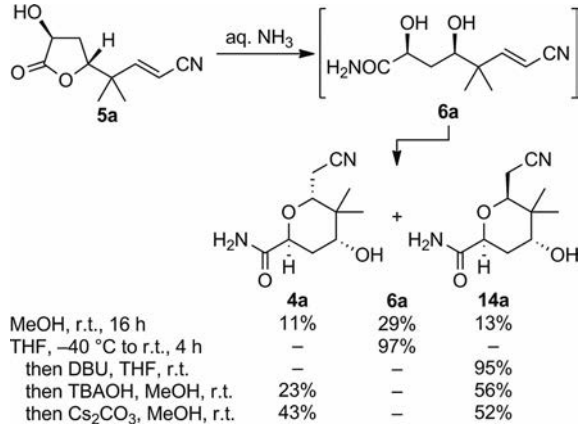

Scheme 3. Expansion of furanone **5a** to tetrahydropyrans **4a** and **14a**.

Our inability to optimize the reaction conditions for the kinetic tetrahydropyran **4a** prompted an examination of the analogous reaction with furanone **5b** (EWG = CO_2Et) which was prepared in 72% yield from lactone **10** by sequential ozonolysis and Wittig reactions (see Scheme 4). In this case, aqueous ammonia in dioxane proved a convenient and reliable method for preparing diol **6b**. Though treatment of **6b** with NaH or KO*t*Bu in THF failed to induce appreciable ring closure, cyclization with KOH in DMSO (dimethyl sulfoxide) was realized in 10 min to give the desired tetrahydropyran **4b** in 72% yield. Upon scale-up, we found that DBU in DMF (*N*,*N*-dimethylformamide) was a more reliable protocol, giving a separable 14:1 mixture of diastereoisomers with **4b** isolated in 73% yield.

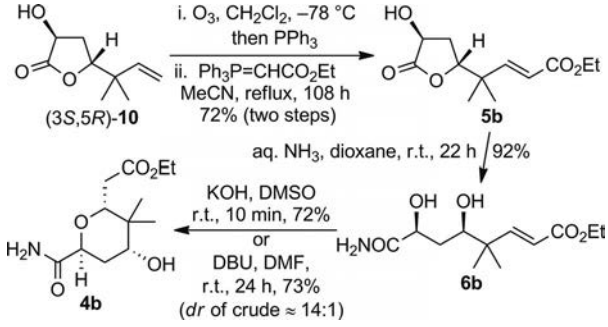

Scheme 4. Expansion of furanone **5b** to tetrahydropyran **4b**.

We believe that the stereochemical course of the kinetic cyclization is likely governed by a hydrogen bond between the proximal alkoxide and alcohol groups, as this would be much stronger in **15** than in its precursor diol **6**.[16] Thus, following the deprotonation of **6** to **15** (Scheme 5), the lowest-energy conformer **15A** will benefit from two hydrogen bonds to the alkoxide residing between the alcohol and

amide moieties. These remain intact in reactive conformer **15B**, which is accessible from **15A** by rotation of a single bond and leads to the kinetic product **4**. By contrast, adoption of the prototypical chair-like conformer **15C**, which requires greater conformational change and rupture of the strong hydrogen bond between the alkoxide and alcohol groups, leads to the thermodynamic product **14**.

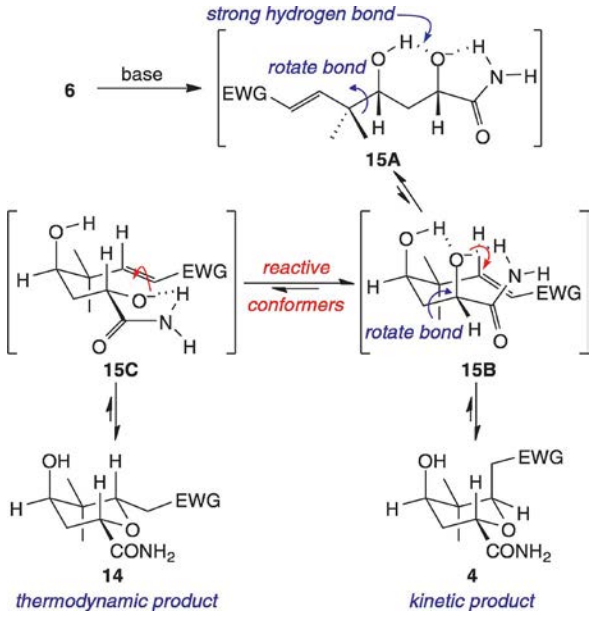

Scheme 5. Explanation of the stereochemical course of the cyclization.

The different stereochemical outcomes observed in the nitrile and ester series (Schemes 3 and 4, respectively) can be rationalized by considering the relative stabilities of the anionic intermediates formed in the course of the cyclization reactions. In DMSO, the pK_a of an ester (pK_a ≈ 29.5) is lower than that of a secondary alcohol (pK_a ≈ 30.5), which in turn is lower than that of a nitrile (pK_a ≈ 31.5).[17,18] Consequently, alkoxide additions to α,β-unsaturated esters will be more facile than the analogous additions to α,β-unsaturated nitriles and less prone to the reverse reaction. This may account for the ease with which a kinetic cyclization was realized in the ester series (**6b** to **4b**, see Scheme 4) and a thermodynamic cyclization was realized in the nitrile series (**6a** to **14a**, see Scheme 3).

Conclusions

A short (eight steps) and efficient route to the central tetrahydropyran of pederin, psymberin, and onnamides D–F has been developed from (*S*)-malic acid (**7**). The key sequence involves conversion of a γ-lactone to a tetrahydropyran ring by addition of ammonia. Notably, for α,β-unsaturated nitrile **5a**, cyclization of intermediate diol **6a** to the thermodynamic tetrahydropyran **14a** could be accomplished in high yield through the action of DBU in THF (Scheme 3). In this case, optimization to produce the kinetic tetrahydropyran **4a** proved intractable. However, through the simple expedient of switching the nitrile moiety for an ethyl ester (Scheme 4), the desired stereochemical outcome, that is, **5b** → **6b** → **4b**, was readily achieved.

Experimental Section

[(2*S*)-3-Oxo-1,4-dioxaspiro[4.5]dec-2-yl]acetic Acid (8):[19] A solution of (*S*)-malic acid (**7**, 40.0 g, 298 mmol), cyclohexanone (73.0 g, 78.0 mL, 744 mmol), and pyridinium *p*-toluenesulfonate (1 mol-%, 740 mg) in toluene (250 mL) was heated at reflux by using a Dean–Stark trap for 16 h. The mixture was then cooled to room temp. and concentrated in vacuo, and then petroleum ether (250 mL) was added. The resulting precipitate was collected by filtration, washed with petroleum ether, and dried under high vacuum to give compound **8** as a white solid (58.6 g, 274 mmol, 92%). $[\alpha]_D^{26}$ = +11.3 (*c* = 0.5, $CHCl_3$, *l* = 2); ref.[19] $[\alpha]_D^{26}$ = +7.18 (*c* = 1, $CHCl_3$). M.p. 100–106 °C (*n*-heptane); ref.[13] m.p. 104–105 °C. ^{1}H NMR (400 MHz, $CDCl_3$): δ = 10.81 (br. s, 1 H), 4.72 (dd, *J* = 6.0, 4.0 Hz, 1 H), 3.00 (dd, *J* = 17.3, 4.0 Hz, 1 H), 2.85 (dd, *J* = 17.3, 6.5 Hz, 1 H), 1.90–1.79 (m, 2 H), 1.78–1.57 (m, 6 H), 1.54–1.34 (m, 2 H) ppm. ^{13}C NMR (100 MHz, $CDCl_3$): δ = 175.2 (C), 172.0 (C), 112.2 (C), 70.0 (CH), 36.2 (CH_2), 35.3 (CH_2), 24.3 (CH_2), 22.9 (CH_2) ppm. IR (solid): $\tilde{\nu}$ = 3187, 2950, 2921, 2860, 1786, 1729, 1698 cm^{-1}. MS (ESI–): *m*/*z* (%) = 213 (100) [M – H]$^-$, 449 (20) [2 M – 2 H + Na]$^-$.

(3*S*)-3-(2-Hydroxyethyl)-1,4-dioxaspiro[4.5]decan-2-one (9):[19] Prepared according to the method by Burton et al.[20] To a solution of acid **8** (1.00 g, 4.67 mmol) in THF (15 mL) at 0 °C under nitrogen was added BH_3·SMe_2 (10 M, 0.70 mL, 7.00 mmol) dropwise, which resulted in H_2 evolution. After 30 min at 0 °C followed by 20 h at room temp., the mixture was cooled again to 0 °C, and then methanol (4 mL) was added slowly, which resulted in further H_2 evolution. The reaction mixture was warmed to room temp., stirred for 30 min, and then concentrated in vacuo. Purification by rapid column chromatography (silica, Et_2O) afforded compound **9** as a colorless oil (850 mg, 4.24 mmol, 91%). $[\alpha]_D^{26}$ = –3.0 (*c* = 0.525, $CHCl_3$, *l* = 2); ref.[19] not reported. ^{1}H NMR (300 MHz, $CDCl_3$): δ = 4.57 (dd, *J* = 6.8, 5.2 Hz, 1 H), 3.85 (m, 2 H), 2.16 [app. (apparent) ddt, *J* = 14.6, 7.0, 5.2 Hz, 1 H], 2.02 (app. dtd, *J* = 14.6, 6.7, 4.7 Hz, 1 H), 1.94–1.59 (m, 8 H), 1.57–1.35 (m, 2 H) ppm. ^{13}C NMR (100 MHz, $CDCl_3$): δ = 173.8 (C), 112.1 (C), 72.3 (CH), 59.4 (CH_2), 37.1 (CH_2), 35.8 (CH_2), 34.8 (CH_2), 24.8 (CH_2), 23.4 (CH_2) ppm. IR (oil): $\tilde{\nu}$ = 3427, 2937, 2864, 1782, 1451 cm^{-1}. MS (ESI+): *m*/*z* (%) = 223 (50) [M + Na]$^+$, 201 (50) [M + H]$^+$. HRMS (ESI+): calcd. for $C_{20}H_{32}O_8Na$ [2M + Na]$^+$ 423.1989; found 423.1985.

[(2*S*)-3-Oxo-1,4-dioxaspiro[4.5]dec-2-yl]acetaldehyde (11):[21] Prepared according to the general methods by De Luca and Jenny.[12] To a solution of alcohol **9** (3.40 g, 17.0 mmol) in CH_2Cl_2 (40 mL) at 0 °C were added TEMPO (1 mol-%, 27 mg) and trichloroisocyanuric acid (3.95 g, 17.0 mmol). The reaction mixture was stirred at 0 °C for 2 h, warmed to room temp., and then filtered through Celite. The filtrate was diluted with CH_2Cl_2 (50 mL), and the resulting solution was washed with saturated Na_2CO_3 (20 mL), HCl (0.1 M, 2 × 20 mL), and brine (2 × 15 mL). The organic layer was dried with $MgSO_4$, filtered, and concentrated to give a colorless oil (2.74 g, 13.8 mmol, 81%). $[\alpha]_D^{26}$ = +1.1 (*c* = 0.51, $CHCl_3$, *l* = 2); ref.[21] $[\alpha]_D^{26}$ = +2.5 (*c* = 0.7, $CHCl_3$). ^{1}H NMR (400 MHz, $CDCl_3$): δ = 9.78 (t, *J* = 1.0 Hz, 1 H), 4.80 (dd, *J* = 7.0, 3.7 Hz, 1 H), 3.08 (ddd, *J* = 18.2, 3.7, 1.0 Hz, 1 H), 2.91 (ddd, *J* = 18.2, 7.0, 1.0 Hz, 1 H), 1.94–1.84 (m, 2 H), 1.82–1.60 (m, 6 H), 1.55–1.40 (m, 2 H) ppm. ^{13}C NMR (100 MHz, $CDCl_3$): δ = 196.8 (CH), 172.3 (C), 112.3 (C), 68.4 (CH), 44.9 (CH_2), 36.2 (CH_2), 35.2 (CH_2), 24.4

(CH_2), 23.0 (CH_2) ppm. IR (oil): $\tilde{\nu}$ = 2937, 1865, 1791, 1727, 1451 cm^{-1}. MS (ESI+): *m*/*z* (%) = 253 (63) $[M + Na + MeOH]^+$, 221 (50) $[M + Na]^+$.

(3*S*,5*R*)-5-(1,1-Dimethylprop-2-en-1-yl)-3-hydroxydihydrofuran-2(3*H*)-one [(3*S*,5*R*)-10] and (3*S*,5*S*)-5-(1,1-Dimethylprop-2-en-1-yl)-3-hydroxydihydrofuran-2(3*H*)-one [(3*S*,5*S*)-10]: Prepared according to the method by Brown et al.[13] To a stirred solution of $BH_3{\cdot}SMe_2$ (10 M, 0.6 mL, 1.20 mmol) in THF (2.5 mL) at 0 °C under argon was added (+)-(1*R*)-α-pinene (1.96 g, 14.4 mmol) dropwise. After 1 h at 0 °C followed by 24 h at room temp., the resulting suspension was cooled again to 0 °C, and 3-methyl-1,2-butadiene (0.64 mL, 6.5 mmol) was added. The mixture was warmed to room temp., and – after 24 h – it was cooled to –78 °C. A precooled (–78 °C) solution of aldehyde **11** (1.00 g, 5.03 mmol) in THF (7 mL) was then added, and – after 1 h – the solution was warmed to room temp. over 2 h. Then, $NaBO_3{\cdot}4H_2O$ (1.85 g, 12.0 mmol) was added as a solid. After an additional 2 h, the reaction mixture was partitioned between water (25 mL) and EtOAc (20 mL). The aqueous phase was separated and extracted with EtOAc (2 × 20 mL). The combined organic phases were washed with water (15 mL) and brine (2 × 15 mL), dried with $MgSO_4$, filtered, and concentrated in vacuo. The residue was taken up with CH_2Cl_2 (60 mL) and TFA (trifluoroacetic acid, 0.5 mL), and the resulting mixture was heated to reflux for 2 h. Upon cooling to room temp., Et_3N (1 mL) was added, and the solvent was removed in vacuo. The ^1H NMR spectrum of this crude product showed **10** was formed as an approximate 6:1 mixture of diastereoisomers. Purification by column chromatography (silica, 30% EtOAc/petroleum ether) first afforded compound (3*S*,5*R*)-**10** as a colorless oil (500 mg, 2.99 mmol, 60%) followed by (3*S*,5*S*)-**10** as a white solid (58 mg, 0.35 mmol, 7%). Data for (3*S*,5*R*)-**10**: $[\alpha]_D^{26}$ = +8.6 (*c* = 0.5, $CHCl_3$, *l* = 2). ^1H NMR (400 MHz, $CDCl_3$): δ = 5.75 (dd, *J* = 17.5, 11.0 Hz, 1 H), 5.15 (dd, *J* = 11.0, 1.1 Hz, 1 H), 5.11 (dd, *J* = 17.5, 1.1 Hz, 1 H), 4.41 (dd, *J* = 8.8, 6.4 Hz, 1 H), 4.40 (dd, *J* = 8.3, 4.9 Hz, 1 H), 3.23 (br. s, 1 H), 2.33 (ddd, *J* = 14.2, 8.8, 4.9 Hz, 1 H), 2.17 (ddd, *J* = 14.2, 8.3, 6.4 Hz, 1 H), 1.10 (s, 3 H), 1.07 (s, 3 H) ppm. ^{13}C NMR (100 MHz, $CDCl_3$): δ = 177.8 (C), 141.6 (CH), 115.4 (CH_2), 85.5 (CH), 67.9 (C), 40.4 (C), 31.6 (CH_2), 23.0 (CH_3), 22.97 (CH_3) ppm. IR (oil): $\tilde{\nu}$ = 2937, 1865, 1791, 1727, 1451 cm^{-1}. MS [CI (chemical ionization)]: *m*/*z* (%) = 188 (100) $[M + NH_4]^+$, 171 (22) $[M + H]^+$, 125 (20%). HRMS (ESI+): calcd. for $C_9H_{14}O_3$ $[M]^+$ 170.0943; found 170.0937. Data for (3*S*,5*S*)-**10**: $[\alpha]_D^{28}$ = –38.7 (*c* = 0.3, $CHCl_3$, *l* = 2). M.p. 65–67 °C (EtOAc). ^1H NMR (300 MHz, $CDCl_3$): δ = 5.81 (dd, *J* = 17.4, 10.9 Hz, 1 H), 5.15 (dd, *J* = 10.9, 1.2 Hz, 1 H), 5.11 (dd, *J* = 17.4, 1.2 Hz, 1 H), 4.53 (dd, *J* = 11.1, 8.6 Hz, 1 H), 4.15 (dd, *J* = 11.1, 5.2 Hz, 1 H), 3.18 (br. s, 1 H), 2.50 (ddd, *J* = 12.5, 8.6, 5.2 Hz, 1 H), 1.96 (dt, *J* = 12.5, 11.1 Hz, 1 H), 1.12 (s, 3 H), 1.08 (s, 3 H) ppm. ^{13}C NMR (75 MHz, $CDCl_3$): δ = 177.5 (C), 141.8 (CH), 114.9 (CH_2), 83.2 (C), 68.9 (CH), 39.7 (C), 32.7 (CH_2), 23.0 (CH_3), 22.4 (CH_3) ppm. IR (solid): $\tilde{\nu}$ = 3391, 2972, 2930, 2869, 1749, 1642, 1460, 1419 cm^{-1}. MS (CI): *m*/*z* (%) = 171 (20) $[MH]^+$, 155 (10) $[MH - CH_4]^+$, 125 (25) $[M - CO_2]^+$, 95 (25), 82 (65), 69 (55) $[C_5H_9]^+$, 55 (35), 41 (100). HRMS (ESI+): calcd. for $C_8H_{11}O_3$ $[M + H - CH_4]^+$ 155.0708; found 155.0711.

2-[(2*R*,4*S*)-4-Hydroxy-5-oxotetrahydrofuran-2-yl]-2-methylpropanal (13): Ozone (1–2% in oxygen) was passed through a solution of lactone (3*S*,5*R*)-**10** (1.00 g, 5.88 mmol) in CH_2Cl_2 (50 mL) and EtOAc (50 mL) at –78 °C until a blue color persisted (25 min). The mixture was purged with oxygen for 20 min, then Me_2S (1.10 g, 17.6 mmol) was added. After 24 h at room temp., additional Me_2S (2.57 g, 41.2 mmol) was added, followed by PPh_3 (308 mg, 1.18 mmol) after 20 h. After another 1 h, the reaction mixture was washed with water (30 mL) and brine (2 × 30 mL), and the organic layers were dried with $MgSO_4$ and concentrated in vacuo. Purification by column chromatography (silica, Et_2O) afforded compound **13** as a colorless oil (715 mg, 4.15 mmol, 71%). $[\alpha]_D^{28}$ = –81.1 (*c* = 0.27, $CHCl_3$, *l* = 2). ^1H NMR (400 MHz, $CDCl_3$): δ = 9.54 (s, 1 H), 4.78 (dd, *J* = 7.7, 6.2 Hz, 1 H), 4.50 (dd, *J* = 7.8, 5.8 Hz, 1 H), 2.35 (ddd, *J* = 14.2, 7.8, 6.2 Hz, 1 H), 2.32 (ddd, *J* = 14.2, 7.7, 5.8 Hz, 1 H), 1.15 (s, 6 H) ppm. ^{13}C NMR (100 MHz, $CDCl_3$): δ = 203.0 (CH), 176.7 (C), 81.5 (CH), 67.7 (CH), 49.3 (C), 31.5 (CH_2), 18.3 (CH_3), 17.9 (CH_3) ppm. IR (oil): $\tilde{\nu}$ = 2937, 1865, 1791, 1727, 1451 cm^{-1}. MS (CI): *m*/*z* (%) = 190 (100) $[M + NH_4]^+$, 72 (57), 58 (65), 44 (68). HRMS (ESI+): calcd. for $C_8H_{11}O_3$ $[M + H - CH_4]^+$ 172.0733; found 172.0736.

(*E*)- and (*Z*)-4-[(2*R*,4*S*)-4-Hydroxy-5-oxotetrahydrofuran-2-yl]-4-methylpent-2-enenitrile (5a): A mixture of aldehyde **13** (97 mg, 0.56 mmol) and $Ph_3P{=}CHCN$ (374 mg, 1.24 mmol) in toluene (10 mL) was heated to 85 °C for 16 h and then cooled to room temp. Additional ylide (187 mg, 0.62 mmol) was added, and the resulting mixture was heated at reflux for 20 h, cooled, and then concentrated. Purification by column chromatography (silica, Et_2O) afforded compound **5a** (76 mg, 0.39 mmol, 70%) as a viscous oil and an inseparable 5:1 mixture of (*E*)/(*Z*) diastereoisomers. $[\alpha]_D^{28}$ = –36.9 (*c* = 0.415, MeOH, *l* = 2), for the mixture. ^1H NMR (300 MHz, $CDCl_3$): δ[(*E*) isomer] = 6.68 (d, *J* = 16.6 Hz, 1 H), 5.42 (d, *J* = 16.6 Hz, 1 H), 4.50 (t, *J* = 7.0 Hz, 1 H), 4.41 (dd, *J* = 7.5, 5.3 Hz, 1 H), 2.30–2.14 (m, 2 H), 1.16 (s, 3 H), 1.11 (s, 3 H) ppm; additional signals attributed to the (*Z*) isomer: δ = 6.33 (d, *J* = 12.4 Hz, 1 H), 5.47 (d, *J* = 12.4 Hz, 1 H) ppm. ^{13}C NMR (75 MHz, $CDCl_3$): δ[(*E*) isomer] = 176.5 (C), 158.1 (CH), 117.1 (C), 100.8 (C), 84.0 (C), 67.8 (CH), 41.5 (C), 31.8 (CH_2), 22.7 (CH_3), 21.4 (CH_3) ppm; additional signals attributed to the (*Z*) isomer: δ = 156.3 (CH), 99.7 (C), 84.7 (C), 23.3 (CH_3), 21.9 (CH_3) ppm. IR (CH_2Cl_2): $\tilde{\nu}$ = 3426, 3056, 2972, 2925, 2864, 1770, 1630 cm^{-1}. MS (ESI+): *m*/*z* (%) = 250 (27) $[M + Na + MeOH]^+$, 218 (100) $[M + Na]^+$. HRMS (ESI+): calcd. for $C_{10}H_{13}NNaO_3$ $[M + Na]^+$ 218.0787; found 218.0788.

(2*S*,4*R*,6*R*)-6-(Cyanomethyl)-4-hydroxy-5,5-dimethyltetrahydro-2*H*-pyran-2-carboxamide (4a), (2*S*,4*R*,6*S*)-6-(Cyanomethyl)-4-hydroxy-5,5-dimethyltetrahydro-2*H*-pyran-2-carboxamide (14a), and (2*S*,4*R*)-7-Cyano-2,4-dihydroxy-5,5-dimethylhept-6-enamide (6a): To a solution of lactone **5a** [(*E*)/(*Z*), 5:1; 72 mg, 0.37 mmol] in methanol (2 mL) was added ammonia (28% aqueous solution, 1 mL). After 16 h at room temp., silica (1 g) was added, and the solvent was removed in vacuo. Purification by column chromatography (silica, EtOAc) first afforded **4a** as a white solid (8.4 mg, 0.04 mmol, 11%) followed by **14a** as a white solid (10.5 mg, 0.05 mmol, 13%) and then **6a** as a white solid (23 mg, 0.108 mmol, 29%). Data for **4a**: M.p. 142–146 °C (MeOH). $[\alpha]_D^{29}$ = +81.1 (*c* = 0.19, MeOH, *l* = 2). ^1H NMR (400 MHz, CD_3OD): δ = 4.46 (dd, *J* = 5.9, 4.2 Hz, 1 H), 3.56 (dd, *J* = 9.2, 4.2 Hz, 1 H), 3.43 (dd, *J* = 9.8, 4.2 Hz, 1 H), 2.86 (dd, *J* = 17.1, 9.2 Hz, 1 H), 2.79 (dd, *J* = 17.1, 4.2 Hz, 1 H), 2.25 (dt, *J* = 13.5, 4.2 Hz, 1 H), 1.83 (ddd, *J* = 13.5, 9.8, 5.9 Hz, 1 H), 0.97 (s, 3 H), 0.91 (s, 3 H) ppm. ^{13}C NMR (100 MHz, CD_3OD): δ = 176.4 (C), 120.4 (C), 78.5 (CH), 73.2 (CH), 72.5 (CH), 39.2 (C), 30.8 (CH_2), 23.8 (CH_3), 19.6 (CH_2), 14.6 (CH_3) ppm. IR ($CHCl_3$): $\tilde{\nu}$ = 3467, 3346, 2974, 2919, 2880, 2844, 1677, 1592 cm^{-1}. MS (ESI+): *m*/*z* (%) = 235 (100) $[M + Na]^+$. HRMS (ESI+): calcd. for $C_{10}H_{16}N_2NaO_3$ $[M + Na]^+$ 235.1053; found 235.1056. Data for **14a**: M.p. 142–144 °C (MeOH). $[\alpha]_D^{29}$ = –140.0 (*c* = 0.15, MeOH, *l* = 2). ^1H NMR (400 MHz, $CDCl_3$): δ = 6.57 (br. s, 1 H), 5.52 (br. s, 1 H), 4.43 (dd, *J* = 12.5, 3.1 Hz, 1 H), 4.08, (dd, *J* = 9.3, 3.9 Hz, 1 H), 3.69 (t, *J* = 2.7 Hz, 1 H), 2.55 (dd, *J* = 16.8, 3.9 Hz, 1 H), 2.48 (dd, *J* = 16.8, 9.3 Hz, 1 H), 2.11 (app. dt, *J* = 14.6, 3.1 Hz, 1 H), 2.05 (br. s, 1 H), 1.95

(ddd, J = 16.8, 12.5, 2.7 Hz, 1 H), 0.99 (s, 3 H), 0.96 (s, 3 H) ppm. ^{13}C NMR (100 MHz, $CDCl_3$): δ = 174.2 (C), 118.2 (C), 75.1 (CH), 73.4 (C), 72.6 (CH), 37.0 (C), 32.7 (CH_2), 22.6 (CH_3), 19.5 (CH_2), 19.1 (CH_3) ppm. IR ($CHCl_3$): $\tilde{\nu}$ = 3465, 3350, 2958, 2923, 2864, 2840, 1674, 1590 cm^{-1}. MS (ESI+): m/z (%) = 235 (100) [M + Na]$^+$. HRMS (ESI+): calcd. for $C_{10}H_{16}N_2NaO_3$ [M + Na]$^+$ 235.1053; found 235.1055. Data for **6a**: M.p. 31–34 °C (EtOAc). ^{1}H NMR (400 MHz, CD_3OD): δ = 6.86 (d, J = 16.8 Hz, 1 H), 5.51 (d, J = 16.8 Hz, 1 H), 4.15 (dd, J = 7.6, 5.3 Hz, 1 H), 3.69 (dd, J = 10.4, 1.8 Hz, 1 H), 1.92 (ddd, J = 14.0, 5.3, 1.8 Hz, 1 H), 1.59 (ddd, J = 14.0, 10.4, 7.6 Hz, 1 H), 1.07 (s, 3 H), 1.06 (s, 3 H) ppm. ^{13}C NMR (100 MHz, CD_3OD): δ = 179.9 (C), 163.7 (CH), 118.9 (C), 99.1 (CH), 77.1 (CH), 72.3 (CH), 44.1 (C), 37.5 (CH_2), 22.6 (CH_3), 22.5 (CH_3) ppm. IR (CH_2Cl_2): $\tilde{\nu}$ = 3354, 2968, 2917, 2840, 2214, 1670, 1628, 1580 cm^{-1}. MS (ESI+): m/z (%) = 235 (100) [M + Na]$^+$. HRMS (ESI+): calcd. for $C_{10}H_{16}N_2NaO_3$ [M + Na]$^+$ 235.1053; found 235.1055.

(2*S*,4*R*)-7-Cyano-2,4-dihydroxy-5,5-dimethylhept-6-enamide (6a): To condensed ammonia (2 mL) at –78 °C under nitrogen was added a solution of lactone **5a** [(*E*)/(*Z*), 5:1; 62 mg, 0.32 mmol] in THF (2 mL). After 19 h at –78 °C followed by 4 h at –40 °C, the reaction mixture was warmed to room temp. and concentrated to give compound **6a** as a white solid (65 mg, 0.31 mmol, 97%). The ^{1}H NMR spectrum of this crude product showed it to be approximately a 6:1 mixture of (*E*)/(*Z*) isomers, which could be separated by column chromatography (silica, EtOAc). Data is reported above.

Ethyl (2*E*)-4-[(2*R*,4*S*)-4-Hydroxy-5-oxotetrahydrofuran-2-yl]-4-methylpent-2-enoate (5b): Ozone (1–2% in oxygen) was passed through a solution of lactone (3*S*,5*R*)-**10** (400 mg, 2.36 mmol) in CH_2Cl_2 (50 mL) at –78 °C until a blue color persisted (15 min). The mixture was purged with oxygen for 20 min, and then PPh_3 (1.24 g, 4.71 mmol) in CH_2Cl_2 (3 mL) was added. After 1 h at –78 °C, the solution was warmed to room temp. and concentrated in vacuo. The resulting oil was dissolved in acetonitrile (25 mL), and $Ph_3P{=}CHCO_2Et$ (871 mg, 2.5 mmol) was added. After heating to reflux under argon for 48 h, more ylide (617 mg, 1.77 mmol) was added. After heating to reflux for another 40 h, a third batch of ylide (411 mg, 1.18 mmol) was added followed by heating at reflux for an additional 20 h. The mixture was then cooled and concentrated in vacuo, and the resulting residue was purified by column chromatography (silica, Et_2O) to afford compound **5b** as a colorless oil (410 mg, 1.69 mmol, 72%). $[\alpha]_D^{26}$ = –26.0 (c = 0.15, MeOH, l = 2). ^{1}H NMR (400 MHz, $CDCl_3$): δ = 6.86 (d, J = 16.0 Hz, 1 H), 5.87 (d, J = 16.0 Hz, 1 H), 4.49 (dd, J = 7.9, 5.8 Hz, 1 H), 4.40 (ddd, J = 8.3, 6.0, 2.8 Hz, 1 H), 4.20 (q, J = 7.2 Hz, 2 H), 3.09 (d, J = 2.8 Hz, 1 H), 2.28 (ddd, J = 14.0, 8.3, 5.8 Hz, 1 H), 2.21 (ddd, J = 14.0, 7.9, 6.0 Hz, 1 H), 1.30 (t, J = 7.2 Hz, 3 H), 1.15 (s, 3 H), 1.13 (s, 3 H) ppm. ^{13}C NMR (100 MHz, $CDCl_3$): δ = 176.9 (C), 166.5 (C), 150.9 (CH), 121.8 (CH), 84.4 (CH), 67.8 (CH), 60.8 (CH_2), 40.5 (C), 31.7 (CH_2), 22.7 (2 CH_3), 14.4 (CH_3) ppm. MS (ESI+): m/z (%) = 265 (100) [M + Na]$^+$, 507 (50) [2 M + Na]$^+$. HRMS (ESI+): calcd. for $C_{12}H_{18}NaO_5$ [M + Na]$^+$ 265.1046; found 265.1047.

Ethyl (2*E*,5*R*,7*S*)-8-Amino-5,7-dihydroxy-4,4-dimethyl-8-oxooct-2-enoate (6b): To a solution of **4b** (493 mg, 2.04 mmol) in 1,4-dioxane (40 mL) was added ammonia (28% aqueous solution, 4 mL). After 2 h at room temp., additional ammonia (28% aqueous solution, 4 mL) was added. After 20 h, the reaction mixture was concentrated in vacuo, and the residue was purified by column chromatography (silica, 1–3% methanol/EtOAc) to afford compound **6b** as a viscous, colorless oil (485 mg, 1.87 mmol, 92%). $[\alpha]_D^{28}$ = +4.0 (c = 0.315, MeOH, l = 2). ^{1}H NMR (400 MHz, CD_3OD): δ = 7.03 (d, J = 16.1 Hz, 1 H), 5.81 (d, J = 16.1 Hz, 1 H), 4.17 (q, J = 7.1 Hz, 2 H), 4.15 (dd, J = 7.8, 5.0 Hz, 1 H), 3.70 (dd, J = 10.6, 2.0 Hz, 1 H), 1.93 (ddd, J = 14.2, 5.0, 2.0 Hz, 1 H), 1.55 (ddd, J = 14.2, 10.6, 7.8 Hz, 1 H), 1.28 (t, J = 7.1 Hz, 3 H), 1.08 (s, 3 H), 1.07 (s, 3 H) ppm. ^{13}C NMR (100 MHz, CD_3OD): δ = 180.0 (C), 168.6 (C), 156.9 (CH), 120.5 (CH), 77.8 (CH), 72.7 (CH), 61.6 (CH_2), 42.9 (C), 37.7 (CH_2), 23.6 (CH_3), 22.9 (CH_3), 14.7 (CH_3) ppm. IR (oil): $\tilde{\nu}$ = 3338, 2971, 1655, 1650, 1466, 1420 cm^{-1}. MS (ESI+): m/z (%) = 541 (25) [2 M + Na]$^+$, 282 (100) [M + Na]$^+$. HRMS (ESI+): calcd. for $C_{12}H_{21}NNaO_5$ [M + Na]$^+$ 282.1312; found 282.1310.

Ethyl [(2*R*,4*R*,6*S*)-6-Carbamoyl-4-hydroxy-3,3-dimethyltetrahydro-2*H*-pyran-2-yl]acetate (4b): To a solution of **5b** (300 mg, 1.16 mmol) in DMF (5 mL) was added DBU (528 mg, 3.47 mmol). After 24 h, the reaction mixture was concentrated in vacuo. The ^{1}H NMR spectrum of the crude residue indicated a dr of 14:1. Purification by column chromatography (silica, 80% EtOAc/petroleum ether) afforded compound **4b** as a white solid (220 mg, 0.85 mmol, 73%). M.p. 147–151 °C (CH_2Cl_2/petroleum ether). $[\alpha]_D^{28}$ = +93.2 (c = 0.28, MeOH, l = 2). ^{1}H NMR (400 MHz, CD_3OD): δ = 4.37 (dd, J = 6.9, 1.6 Hz, 1 H), 4.18 (q, J = 7.2 Hz, 1 H), 4.16 (q, J = 7.2 Hz, 1 H), 3.71 (dd, J = 10.7, 2.1 Hz, 1 H), 3.28 (dd, J = 11.9, 4.6 Hz, 1 H), 2.64 (dd, J = 17.2, 2.1 Hz, 1 H), 2.51 (dd, J = 17.2, 10.7 Hz, 1 H), 2.36 (ddd, J = 13.2, 4.6, 1.6 Hz, 1 H), 1.81 (ddd, J = 13.2, 11.9, 6.9 Hz, 1 H), 1.27 (t, J = 7.2 Hz, 3 H), 0.91 (s, 3 H), 0.88 (s, 3 H) ppm. ^{13}C NMR (100 MHz, CD_3OD): δ = 176.7 (C), 174.8 (C), 77.8 (CH), 74.7 (CH), 72.6 (CH), 62.0 (CH_2), 38.9 (C), 35.4 (CH_2), 30.3 (CH_2), 22.9 (CH_3), 14.5 (CH_3), 12.7 (CH_3) ppm. IR (solid): $\tilde{\nu}$ = 3453, 3405, 3332, 3304, 2994, 2978, 2966, 2957, 2877, 1730, 1674, 1650, 1594 cm^{-1}. MS (ESI+): m/z (%) = 541 (20) [2 M + Na]$^+$, 282 (100) [M + Na]$^+$. HRMS (ESI+): calcd. for $C_{12}H_{21}NNaO_5$ [M + Na]$^+$ 282.1312; found 282.1315. $C_{12}H_{21}NO_5$ (259.30): calcd. C 55.58, H 8.16, N 5.40; found C 55.32, H 8.19, N 5.12. For the X-ray crystal structure of **4b**, see Figure 1. CCDC-835923 contains the supplementary crystallographic data for this paper. These data can be obtained free of charge from The Cambridge Crystallographic Data Centre via www.ccdc.cam.ac.uk/data_request/cif.

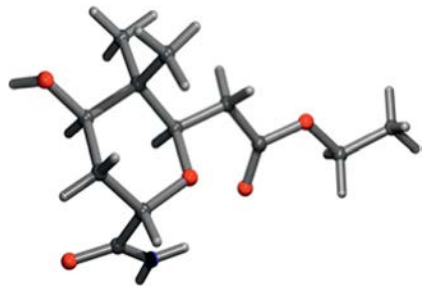

Figure 1. X-ray crystal structure of **4b**.

Supporting Information (see footnote on the first page of this article): Copies of spectra for all reported compounds.

Acknowledgments

We thank Pfizer, Engineering and Physical Sciences Research Council (EPSRC) and the European Regional Development Fund (ERDF) [Innovative Synthesis: Culture and Entrepreneurship in Chemistry (IS:CE) – Chem. & InterReg IVa program 4061] for financial support.

[1] D. Vuong, R. J. Capon, E. Lacey, J. H. Gill, K. Heiland, T. Friedel, *J. Nat. Prod.* **2001**, *64*, 640–642.

[2] a) S. Matsunaga, N. Fusetani, Y. Nakao, *Tetrahedron* **1992**, *48*, 8369–8376; b) S. Sakemi, T. Ichiba, S. Kohmoto, G. Saucy, T. Higa, *J. Am. Chem. Soc.* **1988**, *110*, 4851–4853.
[3] a) T. Matsumoto, M. Yanagiya, S. Maeno, S. Yasuda, *Tetrahedron Lett.* **1968**, *9*, 6297–6300; b) A. Furusaki, T. Watanabé, *Tetrahedron Lett.* **1968**, *9*, 6301–6304; c) C. Cardani, D. Ghiringhelli, R. Mondelli, A. Quilico, *Tetrahedron Lett.* **1965**, *6*, 2537–2545.
[4] a) R. H. Cichewicz, F. A. Valeriote, P. Crews, *Org. Lett.* **2004**, *6*, 1951–1954; b) G. R. Pettit, J. P. Xu, J. C. Chapuis, R. K. Pettit, L. P. Tackett, D. L. Doubek, J. N. A. Hooper, J. M. Schmidt, *J. Med. Chem.* **2004**, *47*, 1149–1152.
[5] A. Mayor in *Greek Fire, Poison Arrows and Scorpion Bombs*, The Overlook Press, New York, **2004**, p. 178.
[6] J. H. Frank, K. Kanamitsu, *J. Med. Entomol.* **1987**, *24*, 155–191.
[7] a) J. Piel, *Proc. Natl. Acad. Sci. USA* **2002**, *99*, 14002–14007; b) A. W. R. McCrae, S. A. Visser, *Ann. Trop. Med. Parasitol.* **1975**, *69*, 109–120.
[8] N. S. Burres, J. J. Clement, *Cancer Res.* **1989**, *49*, 2935–2940.
[9] For the syntheses of psymberin, see: a) X. Huang, N. Shao, A. Palani, R. Aslanian, A. Buevich, *Org. Lett.* **2007**, *9*, 2597–2600; b) X. Jiang, J. Garcia-Fortanet, J. K. De Brabander, *J. Am. Chem. Soc.* **2005**, *127*, 11254–11255; c) A. B. Smith III, J. A. Jurica, S. P. Walsh, *Org. Lett.* **2008**, *10*, 5625–5628; d) S. Ning, S. Kiren, L. J. Williams, *Org. Lett.* **2007**, *9*, 1093–1096; e) T. Watanabe, T. Imaizumi, M. Shibuya, N. Kanoh, Y. Iwabuchi, T. Chinen, Y. Nagumo, T. Usui, *Org. Lett.* **2010**, *12*, 1040–1043; f) M. T. Crimmins, J. M. Stevens, G. M. Schaaf, *Org. Lett.* **2009**, *11*, 3990–3993; g) N. Shao, X. Huang, A. Palani, R. Aslanian, A. Buevich, J. Piwinski, R. Huryk, C. Seidel-Dugan, *Synthesis* **2009**, *17*, 2855–2872; h) X. Jiang, N. Williams, J. K. De Brabander, *Org. Lett.* **2007**, *9*, 227–230.
[10] For the syntheses of pederin, see: a) F. Wu, M. E. Green, P. E. Floreancig, *Angew. Chem. Int. Ed.* **2011**, *50*, 1131–1134; *Angew. Chem.* **2011**, *123*, 1163–1166; b) J. C. Jewett, V. H. Rawal, *Angew. Chem.* **2007**, *119*, 6622–6624; *Angew. Chem. Int. Ed.* **2007**, *46*, 6502–6504; c) T. Takemura, Y. Nishii, S. Takahashi, J. Kobayashi, T. Nakata, *Tetrahedron* **2002**, *58*, 6359–6366; d) P. Kocienski, K. Jarowicki, S. Marczak, *Synthesis* **1991**, 1191–1200; e) T. M. Willson, P. Kocienski, K. Jarowicki, K. Isaac, P. M. Hitchcock, A. Faller, S. F. Campbell, *Tetrahedron* **1990**, *46*, 1767–1782; f) K. Jarowicki, P. Kocienski, S. Marczak, T. Willson, *Tetrahedron Lett.* **1990**, *31*, 3433–3436; g) F. Matsuda, N. Tomiyoshi, M. Yanagiya, T. Matsumoto, *Tetrahedron* **1988**, *44*, 7063–7080; h) T. Willson, P. Kocienski, A. Faller, S. Campbell, *J. Chem. Soc., Chem. Commun.* **1987**, 106–108; i) T. Nakata, S. Nagao, N. Mori, T. Oishi, *Tetrahedron Lett.* **1985**, *26*, 6461–6464; j) T. Nakata, S. Nagao, T. Oishi, *Tetrahedron Lett.* **1985**, *26*, 6465–6468; k) F. Matsuda, N. Tomiyoshi, M. Yanagiya, T. Matsumoto, *Tetrahedron Lett.* **1983**, *24*, 1277–1280; l) F. Matsuda, M. Yanagiya, T. Matsumoto, *Tetrahedron Lett.* **1982**, *23*, 4043–4046; m) M. Yanagiya, F. Matsuda, K. Hasegawa, T. Matsumoto, *Tetrahedron Lett.* **1982**, *23*, 4039–4042.
[11] For other approaches to the THP (tetrahydropyran) ring, see: a) X. Huang, N. Shao, A. Palani, R. Aslanian, R. Huryk, C. Seidel-Dugan, *Org. Lett.* **2009**, *11*, 867–870; b) S. Kiren, N. Shangguan, L. J. Williams, *Tetrahedron Lett.* **2007**, *48*, 7456–7459; c) D. Liu, J. Xue, Z. Xie, L. Wei, X. Zhang, Y. Li, *Synlett* **2008**, 1526–1528; d) N. Shangguan, S. Kiren, L. J. Williams, *Org. Lett.* **2007**, *9*, 1093–1096; e) J. C. Rech, P. E. Floreancig, *Org. Lett.* **2005**, *7*, 5175–5178; f) P. J. Kocienski, R. Narquizian, P. Raubo, C. Smith, F. T. Boyle, *Synlett* **1998**, 1432–1434; g) R. W. Hoffmann, A. Schlapbach, *Tetrahedron* **1992**, *48*, 1959–1968; h) T. Matsumoto, F. Matsuda, K. Hasegawa, M. Yanagiya, *Tetrahedron* **1984**, *40*, 2337–2344; i) P. Kocienski, T. M. Willson, *J. Chem. Soc., Chem. Commun.* **1984**, *15*, 1011–1012.
[12] a) L. De Luca, G. Giacomelli, A. Porcheddu, *Org. Lett.* **2001**, *3*, 3041–3043; b) C.-J. Jenny, B. Lohri, M. Schlageter, US Patent 5821374, **1998**.
[13] a) H. C. Brown, P. K. Jadhav, *Tetrahedron Lett.* **1984**, *25*, 1215–1218; b) H. C. Brown, M. C. Desai, P. K. Jadhav, *J. Org. Chem.* **1982**, *47*, 5065–5069; c) H. C. Brown, P. K. Jadhav, *J. Am. Chem. Soc.* **1983**, *105*, 2092–2093.
[14] For recent examples, see: a) Z. Tan, E.-I. Negishi, *Org. Lett.* **2006**, *8*, 2783–2785; b) A. L. Sewell, M. V. J. Villa, M. Matheson, R. Marquez, W. G. Whittingham, *Org. Lett.* **2011**, *13*, 800–803; c) A. C. Sivertsen, M. Gasior, M. Bejerring, S. U. Hansen, O. L. Lopez, N. C. Nielsen, M. Bols, *Eur. J. Org. Chem.* **2007**, 1735–1742; d) K. Kuramochi, S. Yukizawa, S. Ikeda, T. Sunoki, S. Arai, R. Matsui, A. Morita, Y. Mizushina, K. Sakaguchi, F. Sugawara, M. Ikekita, S. Kobayashi, *Bioorg. Med. Chem.* **2008**, *16*, 5039–5049.
[15] Oxa-Michael additions to α,β-unsaturated esters have been used extensively in the preparation of tetrahydropyrans; for examples, see: a) G. Sabitha, S. S. S. Reddy, J. S. Yadav, *Tetrahedron Lett.* **2011**, *52*, 2407–2409; b) J. Robertson, C. North, J. E. R. Sadig, *Tetrahedron* **2011**, *67*, 5011–5023; c) M. Kanematsu, M. Yoshida, K. Shishido, *Angew. Chem. Int. Ed.* **2011**, *50*, 2618–2620; *Angew. Chem.* **2011**, *123*, 2666–2668; d) K. L. Jackson, J. A. Henderson, H. Motoyoshi, A. J. Phillips, *Angew. Chem.* **2009**, *121*, 2382; *Angew. Chem. Int. Ed.* **2009**, *48*, 2346–2350; e) C.-G. Dong, J. A. Henderson, Y. Kaburagi, T. Sasaki, D.-S. Kim, J. T. Kim, D. Urabe, H. Guo, Y. Kishi, *J. Am. Chem. Soc.* **2009**, *131*, 15642–15646; f) S. H. Kang, S. Y. Kang, C. M. Kim, H.-w. Choi, H.-S. Jun, B. M. Lee, C. M. Park, J. W. Jeong, *Angew. Chem.* **2003**, *115*, 4927–4930; *Angew. Chem. Int. Ed.* **2003**, *42*, 4779–4782; g) H. Fuwa, N. Kainuma, K. Tachibana, M. Sasaki, *J. Am. Chem. Soc.* **2002**, *124*, 14983–14992; h) A. Fettes, E. M. Carreira, *Angew. Chem.* **2002**, *114*, 4272–4275; *Angew. Chem. Int. Ed.* **2002**, *41*, 4098–4101; i) K. C. Nicolaou, F. P. J. T. Rutjes, E. A. Theodorakis, J. Tiebes, M. Sato, E. Untersteller, *J. Am. Chem. Soc.* **1995**, *117*, 10252–10263 and references cited therein.
[16] M. Meot-Ner (Mautner), L. W. Sieck, *J. Am. Chem. Soc.* **1986**, *108*, 7525–7529.
[17] W. N. Olmstead, Z. Margolin, F. G. Bordwell, *J. Org. Chem.* **1980**, *45*, 3295–3299.
[18] X.-M. Zhang, F. G. Bordwell, M. Van Der Puy, H. E. Fried, *J. Org. Chem.* **1993**, *58*, 3060–3066.
[19] S. Hanessian, A. Tehim, P. Chen, *J. Org. Chem.* **1993**, *58*, 7768–7781.
[20] J. W. Burton, J. S. Clark, S. Derrer, T. C. Stork, J. G. Bendall, A. B. Holmes, *J. Am. Chem. Soc.* **1997**, *119*, 7483–7498.
[21] S. Monma, T. Sunazuka, K. Nagai, T. Arai, K. Shimoni, R. Matsui, S. Omura, *Org. Lett.* **2006**, *8*, 5601–5604.

Received: October 21, 2011
Published Online: January 11, 2012

BLESSED IS HE WHO EXPECTS NOTHING, FOR HE SHALL NEVER BE DISAPPOINTED.
ALEXANDER POPE

WE TEND TO MEET ANY NEW SITUATION BY REORGANIZING.
IT CAN BE A WONDERFUL METHOD FOR CREATING THE ILLUSION OF PROGRESS
WHILE PRODUCING CONFUSION, INEFFICIENCY, AND DEMORALIZATION.
ATTRIBUTED TO PETRONIUS ARBITER